

Dissertation zur Erlangung des Doktorgrades
der Fakultät für Chemie und Pharmazie
der Ludwig-Maximilians-Universität München

Synthesis of nitrogen heterocycles:
Total synthesis of *Lycopodium* alkaloids
and development of photoswitchable
glutamate derivatives

Felix Werner Wilhelm Hartrampf
aus München

2017

Erklärung

Diese Dissertation wurde im Sinne von § 7 der Promotionsordnung vom 28. November 2011 von Herrn Prof. Dr. Dirk Trauner betreut.

Eidesstattliche Versicherung

Diese Dissertation wurde eigenständig und ohne unerlaubte Hilfe erarbeitet.

München, den 31.05.2017

.....

Felix Hartrampf

Dissertation eingereicht am:	09. Juni 2017
1. Prüfer:	Prof. Dr. Dirk Trauner
2. Prüfer:	Dr. Thomas Magauer
Mündliche Prüfung am:	14. Juli 2017

To my family

To Nina

Acknowledgements

First of all, I would like to thank my PhD advisor, Prof. Dr. Dirk Trauner for giving me the opportunity to conduct my Bachelor's, Master's and finally my PhD thesis in his research group. I am very grateful for the freedom to pursue and develop my own ideas and projects. His passion for all aspects of total synthesis and commitment to an atmosphere of scientific excellence have helped me become a better chemist.

I would like to thank Dr. Thomas Magauer for agreeing to be the second reviewer for this PhD thesis as well as Prof. Dr. Franz Bracher, Prof. Dr. Konstantin Karaghiosoff, Dr. Dorian Didier and Prof. Dr. Anja Hoffmann-Röder for being on my PhD defense committee.

I would like to acknowledge the people that have helped to improve this PhD thesis with their excellent advice and careful proofreading: Philipp Leippe, Dr. Bryan Matsuura, Daniel Terwilliger, Nina Vrielink and Benjamin Williams.

Many of my projects were carried out in cooperation with other scientists, and every collaboration has helped me grow as a scientist. I would like to thank Dr. Takayuki Furukawa for the fun and fruitful time we spent in the early stages of the carbocyclization project. The NMDA-related projects were expertly run and managed by Dr. David Barber, Dr. Kevin Gottschling, Dr. Laura Laprell and Dr. Martin Sumser, from whom I learnt a lot about receptor physiology. The PPAR γ project was run in close cooperation with Dr. Johannes Broichhagen, Lisa Suwandhi and Philipp Leippe, which was a very enjoyable and instructive experience. Finally, I want to thank Bianca Eisel and Prof. Dr. Thomas Meier for the rapid evaluation of our resveratrol photoswitches.

I would like to thank the permanent staff, Carrie Louis, Aleksandra Grilc, Luis de la Osa de la Rosa and Dr. Martin Sumser, for keeping the group running. I am especially thankful to Heike Traub, who helped me out with organizational matters countless times, even after hours in her time off.

During my time as a PhD student, I had the opportunity to mentor a few very talented undergraduates, for whose contributions I am very grateful. These are, in order of appearance,

Morten Loehr, Christian Steinborn, Jonathon Ryan, Stephan Heß, Thomas Mies, Vanda Daskova and Laura Kqiku.

My time in the lab would have been much less enjoyable were it not for a bunch of people that are excellent chemists, but more importantly great colleagues and friends. As a long-standing member of the UV lab, I would like to thank my former colleagues Dr. Florian Löbermann, Dr. Nicolas Guimond, Dr. Henry Toombs-Ruane and Dr. Ahmed Ali as well as the most recent addition, Nils Winter for the nice lab atmosphere.

My biggest thanks go to the gang of three people that spent essentially my entire PhD time with me: David Konrad, Benjamin Williams and, of course, Daniel Terwilliger. I am very grateful for the support, friendship and great time we had in the most positive lab imaginable throughout these years.

Furthermore, I would like to thank, Dr. Daniel Hog, Dr. David Barber, Dr. Hong-Dong Hao, Dr. Bryan Matsuura, Dr. Nicolas Armanino, Dr. Julien Lefranc and Dr. Julius Reyes as well as Dr. Robin Meier, Dr. Cedric Hugelshofer, Dr. Klaus Speck, Katharina Hüll and Antonio Rizzo for all the good advice, chats, football tournaments, nights out and coffee breaks.

Apart from the Trauner group, many people helped, supported and motivated me through the good times as well as the rougher patches, most of all my family. I am eternally grateful for what my parents, Laura, Luisa, Clara and Moritz as well as my grandparents have done and made possible for me over the last decade of studies.

Last but not least, I would like to thank Nina. What an incredible ride the last seven years have been. Without you, I would have never made it this far, and I can't wait to see what the future holds for the two of us.

Publications and conference contributions

Parts of this thesis have been published in peer-reviewed journals

- “A Conia-Ene-type cyclization under basic conditions enables an efficient synthesis of (-)-lycposerramine R”, **F. W. W. Hartrampf**, T. Furukawa, D. Trauner, *Angew. Chem. Int. Ed.* **2017**, 56, 893.
- “Total synthesis of Lycopladine A and Carinatine A via a Base-Mediated Carbocyclization”, **F. W. W. Hartrampf**, D. Trauner, *J. Org. Chem.* **2017**, 82, 8206.
- Development of a photoswitchable antagonist of NMDA receptors”, **F. W. W. Hartrampf**, D. Barber, K. Gottschling, P. Leippe, M. Hollmann, D. Trauner, *Tetrahedron* **2017**, 73, 4905.
- “Optical control of NMDA receptors with a diffusible photoswitch”, L. Laprell, E. Repak, V. Franckevicius, **F. Hartrampf**, J. Terhag, M. Hollmann, M. Sumser, N. Rebola, D. DiGregorio, D. Trauner, *Nat. Commun.* **2015**, 6, 8076.

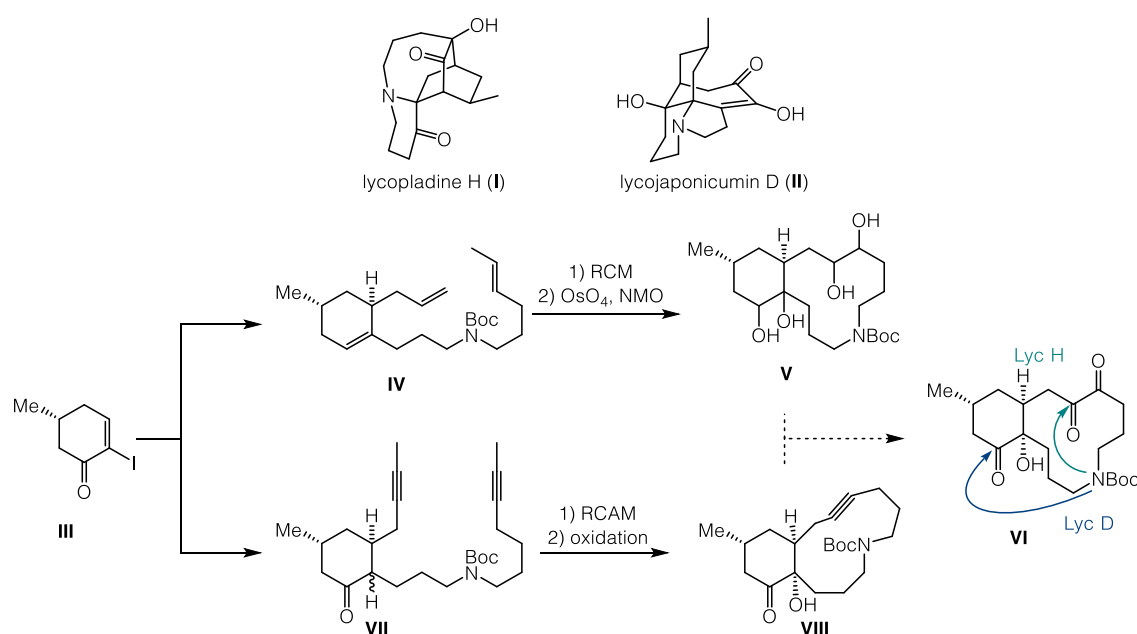
Parts of this thesis have been presented at scientific conferences:

- “A Conia-Ene-like carbocyclization for the total synthesis of *Lycopodium* alkaloids” F. Hartrampf, T. Furukawa, D. Trauner, **29. Irseer Naturstofftage**, Irsee, Germany, 2017.
- “A mild base-mediated cyclization for the synthesis of lycposerramine-R” F. Hartrampf, T. Furukawa, D. Trauner. **ORCHEM 2016**, Weimar, Germany, 2016.
- “A mild base-mediated cyclization for the synthesis of lycposerramine-R” F. Hartrampf, T. Furukawa, D. Trauner. **17th Tetrahedron Symposium**, Sitges, Spain, 2016.
- „A transannular Mannich strategy for the synthesis of Lycopladine H and Lycojaponicum D” F. Hartrampf, D. Trauner. **Tokyo LMU Symposium**, Munich, Germany, 2015.
- “A transannular Mannich strategy for the synthesis of lycopladine H” F. Hartrampf, D. Trauner. **24th International Symposium Synthesis in Organic Chemistry**, Cambridge, UK, 2015.
- “A transannular Mannich strategy for the synthesis of lycopladine H” F. Hartrampf, D. Trauner. **16th Tetrahedron Symposium**, Berlin, Germany, 2015.

Abstract

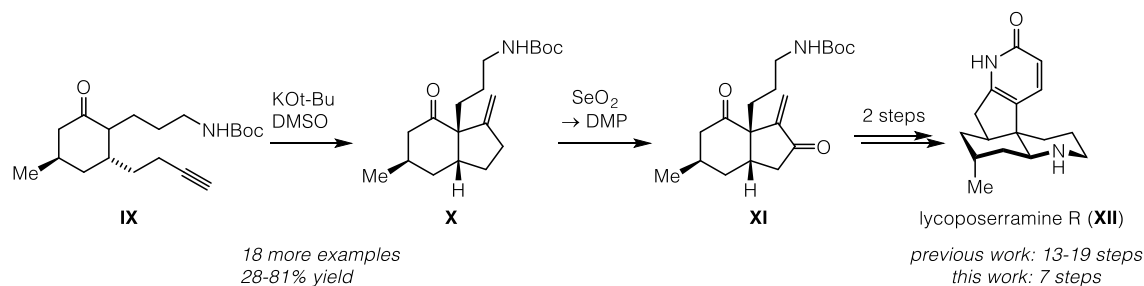
Part 1 – *Lycopodium* alkaloid total synthesis

The first part of this thesis describes efforts towards the *Lycopodium* alkaloids lycopladine H (**I**) and lycojaponicum D (**II**) and the chemistry developed in the course of these studies. We pursued a divergent transannular Mannich reaction approach for both from the same starting material (**VI**). Extensive screening to suppress dimerization of **IV**, prepared from iodoenone **III**, eventually led to a ring-closing metathesis protocol that allowed us to investigate the final steps of the synthesis. Tetraol **V** could be obtained, but we were unable to access triketone **VI** to investigate the final step.

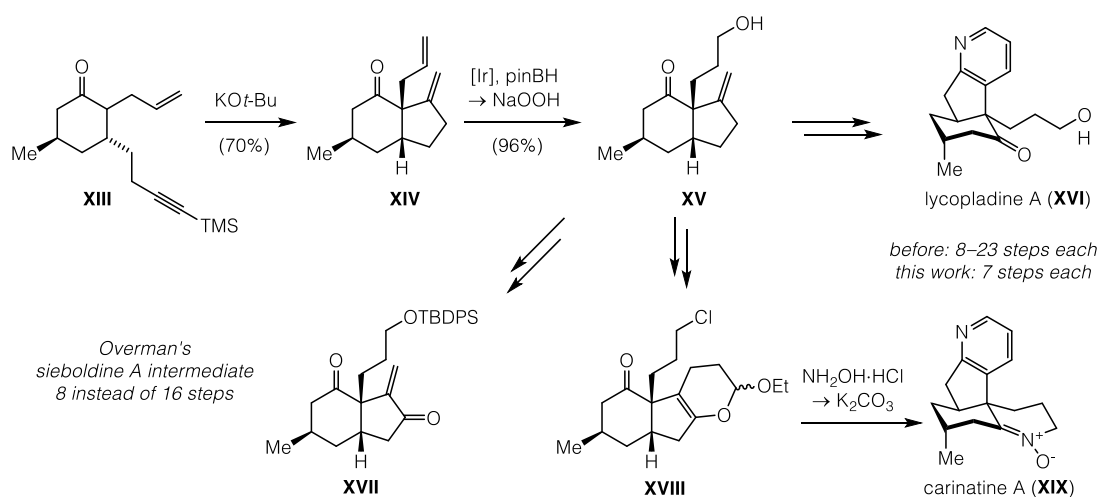


Investigations for a RCAM approach with bisalkyne **VII** using Fürstner's catalysts indeed yielded small quantities of **VIII**. While trying to more efficiently furnish the sidechain by basic isomerization of a butynyl moiety, we discovered a carbocyclization reaction which was the focus of the main part of this PhD work.

When trying to isomerize terminal alkynes like **IX** to the internal alkyne, we observed clean cyclization to hydrindanones like **X** bearing an all-carbon quaternary stereocenter. Further investigations revealed that potassium *tert*-butoxide in DMSO efficiently mediates the ring closure to form a range of 5-5- and 6-5-systems. We also realized that hydrindanones like **X** form the core of many *Lycopodium* alkaloids, such as the aromatic fawcettimine-type natural product lycoposerramine R (**XII**). Via allylic oxidation to enone **XI** and Kröhnke-type pyridone synthesis, we accessed (–)-Lycoposerramine R (**XII**) in 7 steps overall.

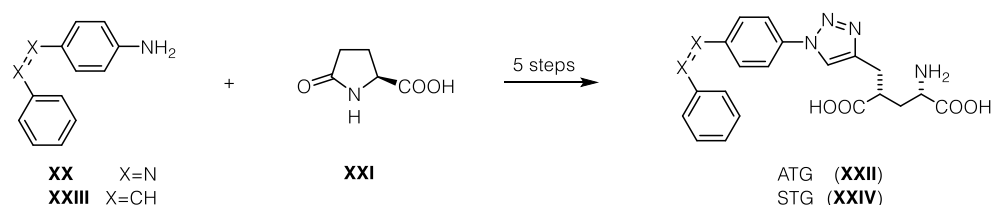


We were also able to apply similar chemistry to the other congeners lycoplamine A (**XVI**) and carinatine A (**XIX**): cyclization of TMS-protected alkyne **XIII** gave hydrindanone **XIV** in good yield on gram scale. From central building block **XV**, we were able to access intermediate **XVII** in 8 steps overall, which intercepts Overman's sieboldine A synthesis. Adapting the Ciufolini pyridine synthesis, the two pyridine-containing natural products lycoplamine A (**XVI**) and carinatine A (**XIX**) were accessed with the fastest syntheses to date, the latter through a newly developed telescoped biscyclization *via* chloride **XVIII**.

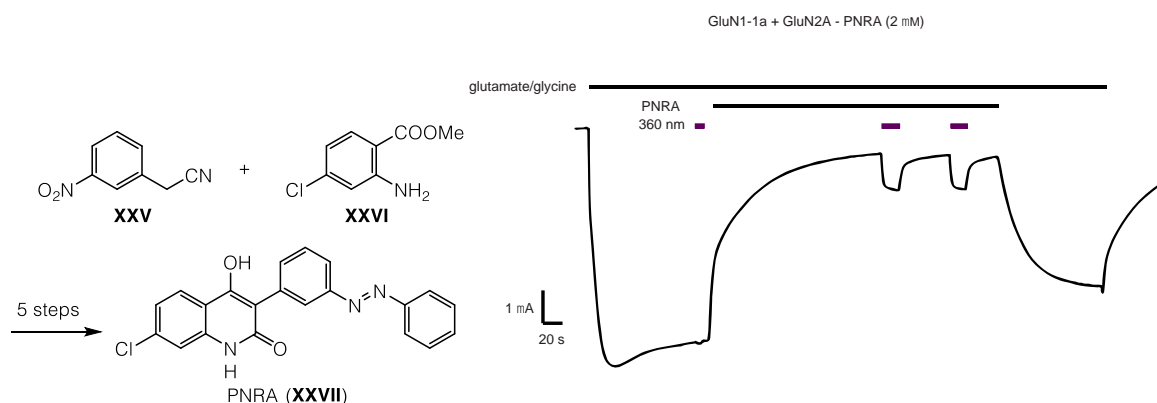


Part 2 – Photoswitchable glutamate derivatives

Glutamate is one of the most important neurotransmitters in neuroscience and deeply connected to all aspects of signal transduction, learning, behavior and memory. The latter is mainly associated with the NMDA receptor subtype. Based on previous SAR studies, we designed ATG (**XXII**), a selective agonist of NMDA receptors, which can be accessed from aniline **XX** and pyroglutamate (**XXI**). It can be switched into its active *cis* form using 740 nm light via two-photon irradiation. To further confirm its mode of action as a *cis*-agonist, a stilbene analog termed STG (**XXIV**) was also synthesized from **XXIII** and shown to be functionally equivalent. With these tools, NMDA receptors could be reversibly activated in *Xenopus* oocytes as well as murine brain slice preparations and retinae with the unmatched temporal and spatial precision of visible light.



As an extension, we also studied photoswitchable NMDA antagonists to complement ATG and STG. As various subtypes are well-defined in NMDA pharmacology, we aimed to address the different types of subunits with selective azobenzene-modified antagonists. After investigating a variety of azologization templates, we finally developed PNRA (**XXVII**), the first photoswitchable antagonist of NMDA receptors.



Glossary

18-c-6	1,4,7,10,13,16-hexaoxacyclooctadecane
9-BBN	9-borabicyclo[3.3.1]nonane
Å	Ångstrom
Ac	acetyl
acac	acetylacetonato
ACCN	1,1'-azobis(cyclohexanecarbonitrile)
ADDP	1,1'-(azodicarbonyl)dipiperidine
AIBN	azobisisobutyronitrile
AMPA	α -amino-3-hydroxy-5-methyl-4-isoxazolepropionic acid
Ar	unspecified aryl substituent
ATA	α -tertiary amine
ATR	attenuated total reflection (IR)
BAIB	bis(acetoxy)iodobenzene
BiPhePhos	6,6'-[(3,3'-di- <i>tert</i> -butyl-5,5'-dimethoxy-1,1'-biphenyl-2,2'-diyl)bis(oxy)]-bis-(dibenzo[d,f][1,3,2]dioxaphosphepin)
Bn	benzyl
Boc	<i>tert</i> -butyloxycarbonyl
Bobbitt salt	4-acetamido-2,2,6,6-tetramethyl-1-oxopiperidinium tetrafluoroborate
Bu	butyl
Bz	benzoyl
°C	degree(s) Celsius
CAN	cerium ammonium nitrate
catBH	catecholborane
Cbz	carboxybenzyl
CHD	1,4-cyclohexadiene
cod	1,5-cyclooctadiene

COSY	correlated spectroscopy (NMR)
cm	centimeter
Cp	cyclopentadienide
CSA	camphorsulfonic acid
Δ	heating
<i>d.r.</i>	diastereomeric ratio
dba	dibenzylideneacetone
DBU	1,8-diazabicyclo[5.4.0]undec-7-ene
DCB	1,2-dichlorobenzene
DCC	<i>N,N'</i> -dicyclohexylcarbodiimide
DCE	1,2-dichloroethane
DIBAL	diisobutylaluminum hydride
DIPEA	diisopropylethylamine
DMAP	4-(dimethylamino)pyridine
DMDO	dimethyldioxirane
DME	1,2-dimethoxyethane
DMF	dimethylformamide
DMP	Dess–Martin periodinane
DMSO	dimethylsulfoxide
DMTST	dimethyl(methylthio)sulfonium triflate
DPPA	diphenylphosphoryl azide
dppb	1,4-bis(diphenylphosphino)butane
dppe	1,2-bis(diphenylphosphino)ethane
dppf	1,1'-bis(diphenylphosphino)ferrocene
DTBPy	2,6-di- <i>tert</i> -butylpyridine
<i>E</i>	opposite (<i>trans</i>)
<i>ee</i>	enantiomeric excess
EI	electron impact ionization (mass spectrometry)
eq.	equivalent(s)
ESI	electron spray ionization (mass spectrometry)
Et	ethyl

fod	6,6,7,7,8,8,8-heptafluoro-2,2-dimethyl-3,5-octanedianato
g	gram(s)
G I	Grubbs first generation catalyst
G II	Grubbs second generation catalyst
h	hour(s)
Hantzsch ester	diethyl 1,4-dihydro-2,6-dimethyl-3,5-pyridine-dicarboxylate
HG II	Hoveyda–Grubbs second generation catalyst
HMBC	heteronuclear multiple-bond correlation spectroscopy
HMPA	hexamethylphosphoramide
HPLC	high performance liquid chromatography
HSQC	heteronuclear single-quantum correlation spectroscopy
Hz	Hertz (frequency)
IBX	2-iodoxybenzoic acid
iGluR	ionotropic glutamate receptor
Im	imidazole
Ipc	isopinocampheyl
IR	infrared
IUPAC	International Union of Pure and Applied Chemistry
J	coupling constant (NMR)
Jørgensen catalyst	(<i>S</i>)- α,α -bis[3,5-bis(trifluoromethyl)phenyl]-2-pyrrolidinemethanol trimethylsilyl ether
KHMDS	potassium hexamethyldisilazide
LDA	lithium diisopropylamide

LG	unspecified leaving group
LHMDS	lithium hexamethyldisilazide
M	molar
<i>m</i> -CPBA	<i>meta</i> -chloroperbenzoic acid
Me	methyl
mGluR	metabotropic glutamate receptor
min	minute(s)
mL	milliliter(s)
mmol	millimole(s)
Mp	melting point
MS	mass spectrometry or molecular sieves
MsCl	methanesulfonyl chloride
NBS	<i>N</i> -bromosuccinimide
NIS	<i>N</i> -iodosuccinimide
nm	nanometer(s)
NMDA	<i>N</i> -methyl- <i>D</i> -aspartic acid
NMO	<i>N</i> -morpholine <i>N</i> -oxide
NMR	nuclear magnetic resonance
NOESY	nuclear Overhauser effect correlation spectroscopy
Ns	2-nitrobenzenesulfonyl
Otera catalyst	tetrachloridooctabutylstannoxane
Oxone	potassium peroxy sulfate
<i>p</i>	<i>para</i>
<i>p</i> -TsOH	<i>para</i> -toluenesulfonic acid
PCC	pyridinium chlorochromate
PCL	photochromic ligand
PG	unspecified protecting group
Ph	phenyl
pin	2,3-dimethylbutane-2,3-diol

Piv	pivaloyl
PMP	<i>para</i> -methoxyphenyl
PPAR	peroxisome proliferator-activated receptor
ppm	parts per million
PPTS	pyridinium <i>para</i> -toluenesulfonate
PTL	photochromic tethered ligand
py	pyridine
R	unspecified substituent
RCAM	ring-closing alkyne metathesis
RCM	ring-closing metathesis
R _f	retardation factor
R _t	room temperature
RuPhos	2-dicyclohexylphosphino-2',6'- diisopropoxybiphenyl
SG II	Stewart–Grubbs second generation catalyst
SIMes	1,3-bis(2,4,6-trimethylphenyl)-4,5- dihydroimidazol-2-ylidene
SIPr	1,3-bis(2,6-diisopropylphenyl)-4,5- dihydroimidazol-2-ylidene
SPhos	2-dicyclohexylphosphino-2',6'- dimethoxybiphenyl
TBA	tetrabutylammonium
TBDPS	<i>tert</i> -butyldiphenylsilyl
TBHP	<i>tert</i> -butyl hydroperoxide
TBS	<i>tert</i> -butyldimethylsilyl
tbs	<i>N-tert</i> -butylsalicylaldiminato
TEMPO	(2,2,6,6-tetramethylpiperidin-1-yl)oxyl
TES	triethylsilyl
Tf	trifluoromethanesulfonyl
TFA	trifluoroacetic acid
TFAA	trifluoroacetic anhydride

TFE	2,2,2-trifluoroethanol
THF	tetrahydrofuran
TIPS	triisopropylsilyl
TLC	thin layer chromatography
TMS	trimethylsilyl
TPAP	tetrapropylammonium perruthenate
triphosgene	bis(trichloromethyl) carbonate
Ts	4-methylbenzenesulfonyl
TZD	thiazolidine-2,4-dione
Wilkinson catalyst	tris(triphenylphosphine)rhodium(I) chloride
wt%	weight percent
Z	together (cis)

Table of contents

ERKLÄRUNG	I
DEDICATION.....	II
ACKNOWLEDGEMENTS	III
PUBLICATIONS AND CONFERENCE CONTRIBUTIONS.....	V
ABSTRACT	VI
GLOSSARY	IX
TABLE OF CONTENTS.....	XV
1 TOTAL SYNTHESIS OF <i>LYCOPODIUM</i> ALKALOIDS	1
1.1 INTRODUCTION	1
1.1.1 <i>The Lycopodium alkaloids</i>	1
1.1.2 <i>Biosynthetic aspects</i>	3
1.1.3 <i>Synthetic approaches toward fawcettimine-type alkaloids</i>	5
1.1.4 <i>Synthetic approaches toward lycopodine-type alkaloids</i>	23
1.2 TOTAL SYNTHESIS OF FAWCETTIMINE ALKALOIDS	33
1.2.1 <i>Isolation, structure and previous efforts towards lycoposerramine R, lycopladine A and carinatine A</i>	33
1.2.2 <i>A Conia-Ene-type cyclization for the total synthesis of lycoposerramine R</i>	42
1.2.3 <i>Total Synthesis of Lycopladine A and Carinatine A via a Base-mediated Carbocyclization</i>	47
1.2.4 <i>Unpublished results</i>	55
1.2.5 <i>Summary and outlook</i>	62
1.3 TOWARD THE TOTAL SYNTHESIS OF LYCOPODINE-TYPE <i>LYCOPODIUM</i> ALKALOIDS.....	66
1.3.1 <i>Previous efforts towards lycopladine H and lycojaponicum D</i>	66
1.3.2 <i>The RCM route</i>	70
1.3.3 <i>The RCAM route</i>	82
1.3.4 <i>The alkylation route</i>	93
1.3.5 <i>Summary and outlook</i>	95
2 SYNTHESIS OF AZOBENZENES FOR THE CONTROL OF NMDA RECEPTORS.....	98
2.1 INTRODUCTION	98
2.1.1 <i>Photopharmacology</i>	98
2.1.2 <i>NMDA receptors as targets of high significance</i>	102
2.2 SYNTHESIS OF PHOTOSWITCHABLE GLUTAMATE DERIVATIVES	104

2.2.1	Synthesis of a photoswitchable glutamate agonist.....	104
2.2.2	Development of a photoswitchable antagonist of NMDA receptors.....	116
3	SYNTHESIS OF PHOTOSWITCHABLE PPARγ AGONISTS.....	127
4	EXPERIMENTAL SECTION	134
4.1	GENERAL EXPERIMENTAL SECTION.....	134
4.2	SUPPORTING INFORMATION FOR CHAPTER 1: LYCOPODIUM ALKALOIDS	135
4.2.1	Fawcettimine alkaloids	135
4.2.2	Additional cyclization precursors and products	171
4.2.3	Lycopladine H and Lycojaponicum D	185
4.3	SUPPORTING INFORMATION FOR CHAPTER 2: PHOTOSWITCHABLE GLUTAMATE DERIVATIVES	195
4.3.1	NMDA agonists.....	195
4.3.2	NMDA antagonists.....	209
4.4	SUPPORTING INFORMATION FOR CHAPTER 3: PHOTOSWITCHABLE PPAR γ AGONISTS	212
5	NMR SPECTRA	217
5.1	^1H AND ^{13}C NMR SPECTRA FOR CHAPTER 4.2.1.1.....	217
5.2	^1H AND ^{13}C NMR SPECTRA FOR CHAPTER 4.2.1.2.....	257
5.3	^1H AND ^{13}C NMR SPECTRA FOR CHAPTER 4.2.2.....	271
5.4	^1H AND ^{13}C NMR SPECTRA FOR CHAPTER 4.2.3.....	291
5.5	^1H AND ^{13}C NMR SPECTRA FOR CHAPTER 4.3.1.....	302
5.6	^1H AND ^{13}C NMR SPECTRA AND ADDITIONAL ELECTROPHYSIOLOGY DATA FOR CHAPTER 4.3.2..	311
5.7	^1H AND ^{13}C NMR SPECTRA FOR CHAPTER 4.4.....	324
6	BIBLIOGRAPHY.....	328

Part 1 – Total synthesis of *Lycopodium* alkaloids

1 Total synthesis of *Lycopodium* alkaloids

1.1 Introduction

1.1.1 The *Lycopodium* alkaloids

Lycopodium is the name of a genus of clubmoss, part of the *Lycopodiaceae* family, which comprises about a thousand vascular, terrestrial, flowerless plants. Their occurrence spans Africa, South America and Asia, but their use in folk medicine has been focused in Asia, where extracts are still commonly used as remedies in folk medicine for an eclectic array of conditions ranging from tissue inflammation and kidney disorders to cancer and memory loss.^[1-7] In most cases, biological activity is (tentatively) ascribed to a particular subset of nitrogen-containing small molecules named *Lycopodium* alkaloids. The best-known representative of a small molecule that is used in modern medicine (as opposed to whole-plant extracts) is huperzine A (**1.1**) from *Huperzia serrata* (Figure 1.1).^[8] This lycodine-type alkaloid (vide infra) is an inhibitor of acetylcholinesterase and as such currently evaluated for the treatment of early-stage Alzheimer's disease.^[8-11]

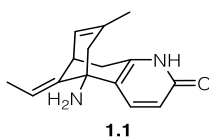


Figure 1.1. Structure of huperzine A (1.1).

The *Lycopodium* alkaloids are a structurally diverse family comprised of about 300 individual alkaloids. In 1881, Bödeker isolated the first family member, lycopodine, from *Lycopodium complanatum*.^[12] It wasn't until 1934 that Orechoff, followed by Muszynski, identified a high alkaloid content in *Lycopodium annotinum*.^[13-14] Since then, new members with a wide variety of skeletons are constantly identified and their structural connections investigated, pioneered by the Canadian school of Ayer and Manske from the 1940s until the 1970s and, nowadays, spearheaded by the Kobayashi group and a number of Chinese researchers.^[15-23] Interestingly, the alkaloids isolated so far stem from a rather small fraction (50 species) of the *Lycopodium* genus, hinting at a large untapped source of natural products. Historically, they have been categorized by two complementary systems. The simpler one ignores the skeletal connectivity and oxidation states, focusing solely on the number of carbon and nitrogen atoms in the skeleton. Additional methylation of heteroatoms is also ignored in the carbon count. By this nomenclature, most are C₁₆N and C₁₆N₂ alkaloids, but also C₂₇N₃ and other ratios are not

unheard of. In order to address the obvious shortcomings of this nomenclature, Ayer, one of the most eminent figures in *Lycopodium* alkaloid chemistry, introduced another system in the 1990s.^[20] He assigned each *Lycopodium* natural product to one of four classes, each named after a prominent member of increasing complexity. These classes are named after phlegmarine (**1.2**), lycodine (**1.3**), lycopodine (**1.4**) and fawcettimine (**1.5**), as depicted in Figure 1.2. The two-dimensional drawings in the first row stress the structural relations within the classes and the second row features the more commonly used three-dimensional representations.

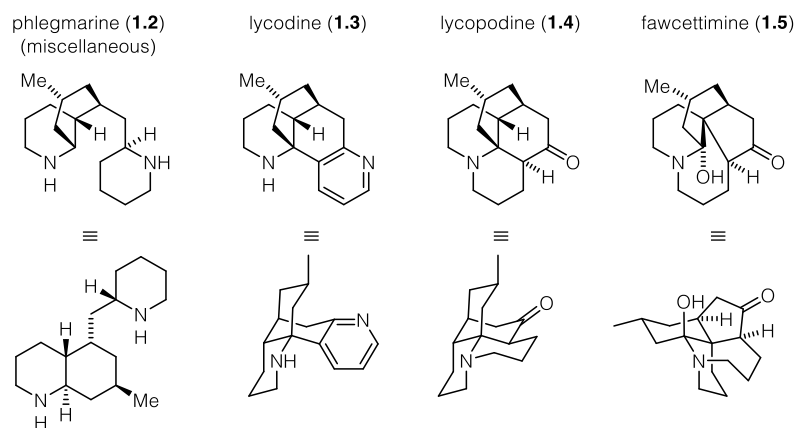


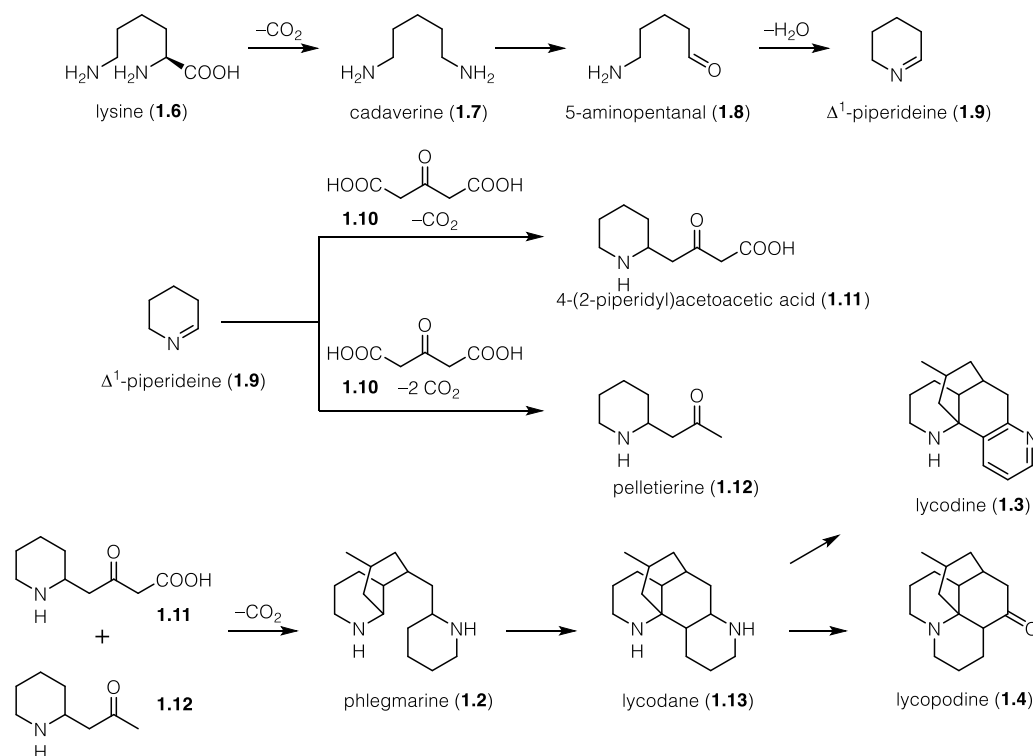
Figure 1.2. Two- and three-dimensional representations of the four major classes of *Lycopodium* alkaloids.

The phlegmarine (**1.2**) class contains the structurally least complex alkaloids that feature only three rings. Biosynthetically, most other *Lycopodium* alkaloids are thought to be derived from phlegmarine by a series of oxidations and rearrangements (chapter 1.1.2). In recent years, the phlegmarine class has also been named the “miscellaneous” class that holds all *Lycopodium* alkaloids that don’t clearly fit into any of the other three categories and thus arguably features the most structurally diverse set of natural products. The lycodine class is special insofar as all its members contain an aromatic moiety. It also features the medicinally most relevant *Lycopodium* alkaloid to date, huperzine A (**1.1**). The third class, the lycopodine (**1.4**) class, features the first family members ever to be isolated and is also the largest class. The fawcettimine (**1.5**) class, finally, is biosynthetically derived from the lycopodine class by oxidation and bond migration.

Given the fact that many *Lycopodium* alkaloids can be interconverted by rather straightforward skeletal rearrangements and oxidations, it is becoming increasingly difficult to unambiguously sort newly isolated alkaloids into one of the four existing classes. It is that reason that has led to discussions about whether these four classes should be divided according to further unique bond cleavages or formations.^[21]

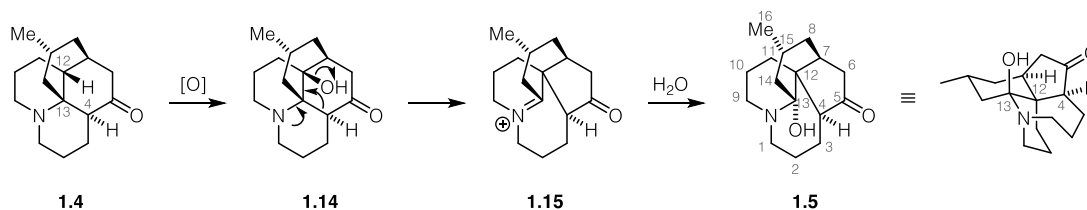
1.1.2 Biosynthetic aspects

Most *Lycopodium* species cannot be readily cultivated in a laboratory setting,^[24] reaching heights of only 15 cm after 5 or more years, thus complicating the investigation of their alkaloid biosynthesis. An early biosynthetic proposal suggested that phlegmarine, one of the most basic *Lycopodium* alkaloids, could be derived from connection of two coniine units,^[25] or from multiple aldol reactions of triketoctanoic acid.^[26] Others brought forth a biosynthesis that relied on sequential C₂ building block additions to Δ^1 -piperideine (**1.9**), as is established in the biosynthesis of other alkaloids.^[27] This cyclic imine is derived from lysine (**1.6**) *via* loss of carbon dioxide and water. It was Spenser who, over the course of three decades, established many important aspects of *Lycopodium* biosynthesis, some of which are summarized in Scheme 1.1.^[25, 28-32] Extensive field experiments with ¹³C and ¹⁴C-labeled building blocks injected into *Lycopodium tristachum* shoots established that the phlegmarine (**1.2**) and, by extension, lycopodine (**1.4**) skeleton are not formed by dimerization of two pelletierine (**1.12**) units.^[25, 28, 33] While one equivalent of pelletierine is completely incorporated as the C-9 to C-16 portion, the C-1 to C-8 portion has to be supplied by a compound similar but not identical to pelletierine. In the final installment of a series of publications, Spenser demonstrated that a very plausible synthetic equivalent is 4-(2-piperidyl)acetoacetate (**1.11**), resulting from nucleophilic attack of acetonedicarboxylic acid (**10**) or a coenzyme A-derived conjugate thereof on Δ^1 -piperideine (**1.9**).^[31-32] Piperideine is the product of decarboxylation of lysine (**1.6**) to cadaverine (**1.7**), which is then transaminated to **1.8** and finally condensed to **1.9**. Pelletierine (**1.12**), the electrophilic portion for the fragment union, is obtained by decarboxylation of **1.11**. A series of redox transformations and Mannich reactions leads to the phlegmarine skeleton, oxidation of which leads to the lycodane (**1.13**) skeleton. Though a few natural products feature this skeleton, lycodane mainly functions as a branching point between the lycodine (**1.3**) and lycopodine (**1.4**) classes. Direct aromatization yields lycodine-type alkaloids, whereas oxidation, piperidine ring rupture and reformation of a different piperidine ring leads to the lycopodine natural products.



Scheme 1.1. General biosynthesis of the *Lycopodium* alkaloids.

The lycopodine skeleton also serves as the starting point for the biosynthesis of the fawcettimine (**1.5**) skeleton (Scheme 1.2). Initial oxidation at C-12 to 12-hydroxylycopodine or lycodoline (**1.14**) gives a tertiary alcohol that is used as a leaving group in a 1,2-shift of the C-4-C-13 bond to form the quaternary center at C-12. This leaves an iminium ion **1.15** that is trapped to give the hemiaminal form of fawcettimine (**1.5**). This rearrangement removes one of the key structural elements of many *Lycopodium* alkaloids, the α -tertiary amine.^[34] Instead, a quaternary stereocenter two atoms further is established.

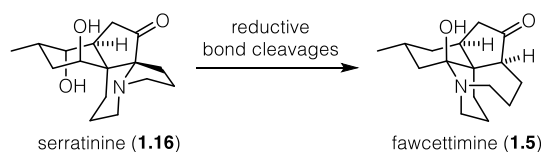


Scheme 1.2. The proposed biosynthetic rearrangement in the biosynthesis of lycopodine (**1.4**) to fawcettimine (**1.5**).

While these biosynthetic proposals, especially the steps from phlegmarine (**1.2**) to lycopodine (**1.4**), have been supported by feeding studies, there is still very limited information about the gene clusters and enzymes involved in the individual steps.

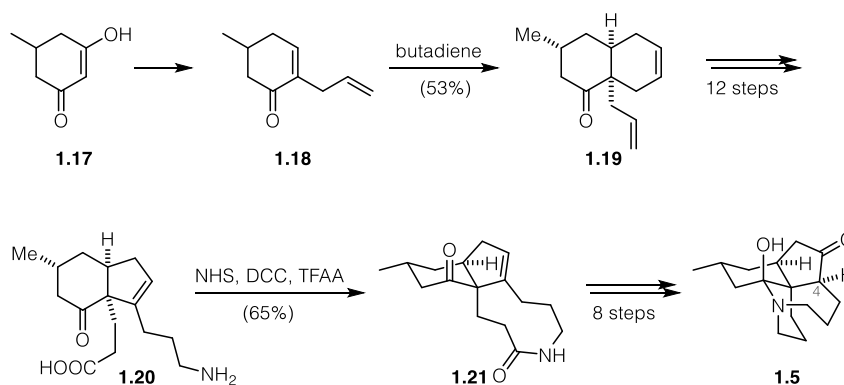
1.1.3 Synthetic approaches toward fawcettimine-type alkaloids

The first member of the fawcettimine family to be isolated was an alkaloid designated “Burnell Base A”, which was first discovered in the Blue Mountain Range in Jamaica in 1959 by Burnell.^[35] This compound was later renamed fawcettimine (**1.5**) and became the namesake for a group of *Lycopodium* alkaloids with now more than 80 members. After the initial isolation, it took a few years before the structure of fawcettimine was unambiguously proven in 1967 by chemical correlation with serratinine (**1.16**) (Scheme 1.3). Serratinine is a related alkaloid whose structure was elucidated by X-ray crystallography of its *p*-bromobenzoate derivative.^[36-37]



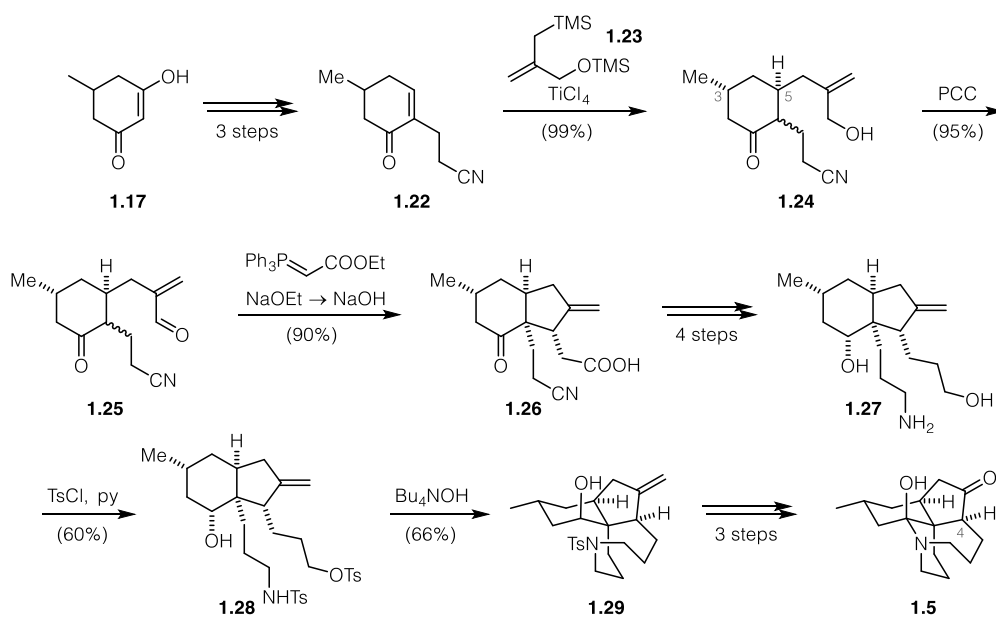
Scheme 1.3. Structure elucidation of fawcettimine (**1.5**) by multistep correlation with serratinine (**1.16**).

The first synthesis of a fawcettimine-type alkaloid was completed by Inubushi in 1979, furnishing fawcettimine (**1.5**) in 26 steps and confirming the structural assignment (Scheme 1.4).^[38] The last ambiguity regarding the configuration at C-4 and which of the two ketones is involved in the diketoamine-hemiaminal (or carbinolamine) tautomeric equilibrium was clarified by Heathcock’s classic synthesis in 1986 (Scheme 1.5).^[39-40] These two syntheses laid the foundation and served as a blueprint for a host of syntheses in the following decades. Inubushi’s synthesis started from dihydroorcinol (**1.17**), and the quaternary stereocenter was elaborated by a Diels–Alder reaction of cyclohexenone **1.18** and butadiene to give **1.19**. In a series of twelve steps, this decaline was transformed into hydrindane **1.20**, setting up the formation of the nine-membered ring by lactamization to **1.21**. A number of redox transformations, including a hydrogenation in the penultimate step, then led to the racemic first total synthesis of the natural product fawcettimine (**1.5**).



Scheme 1.4. Key steps of Inubushi’s seminal synthesis of fawcettimine (**1.5**).

The unselective hydrogenation and the resulting ambiguity regarding the C-4 stereochemistry were subsequently investigated by Heathcock. Using chemistry from his previous forays into *Lycopodium* alkaloid chemistry, he quickly accessed **1.24** by Sakurai allylation of **1.22** (made from dihydroorcinol **1.17**) with functionalized allylsilane reagent **1.23**.^[41] Interestingly, it was during Heathcock's classic lycopodine (Scheme 1.27) synthesis that he found the strong *trans*-diastereoselectivity of nucleophilic additions to 5-substituted cyclohexenones. As this quickly gives rise to the 3,5-*trans* stereochemical pattern (cyclohexane numbering) most commonly encountered in *Lycopodium* natural products, countless variants of this opening step have been and are being used in all types of *Lycopodium* alkaloid total synthesis.^[42]



Scheme 1.5. Heathcock's landmark synthesis of fawcettimine (**1.5**) via a tandem Wittig-Michael sequence of enal **1.25** to hydrindane **1.26**.

When the enal **1.25** was treated with a stabilized Wittig reagent, olefination was followed by selective 1,4-addition to give hydrindane **1.26** in accordance with Baldwin's rules. The last missing carbon was introduced by a three-step Arndt-Eistert homologation before global reduction yielded the aminodiol **1.27**. After extensive experimentation, selective bistosylation to **1.28** was achieved. Ring closure to **1.29** under mildly basic conditions and final redox adjustments then gave fawcettimine (**1.5**) in 15 steps from dihydroorcinol (**1.17**). In addition to vastly improving the overall efficiency of fawcettimine synthesis, he was also able to definitively clarify the configuration at the C-4 stereocenter and demonstrate that it need not be strictly controlled by synthesis as it very readily converts to the correct epimer under mild basic or acidic conditions. Heathcock's approach to introducing the central quaternary stereocenter with the pendant "C₃-amine equivalent" sidechain at an early stage of the synthesis has served

as a significant inspiration for later syntheses.^[43] Over the years, few methods have surpassed his method to access the nine-membered ring by alkylation of a sulfonamide or carbamate. It is for this reason that his 6-5-9 system has been coined the “Heathcock-type tricycle”(30) (Figure 1.3).^[44] In addition, as there is very little room to improve upon the endgame consisting of spontaneous condensation of an amine with a carbonyl, most research has focused on elegant and creative methods to furnish the 6-5-system.

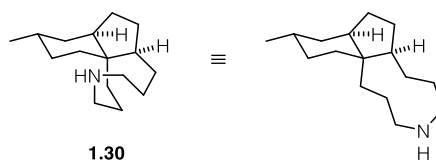
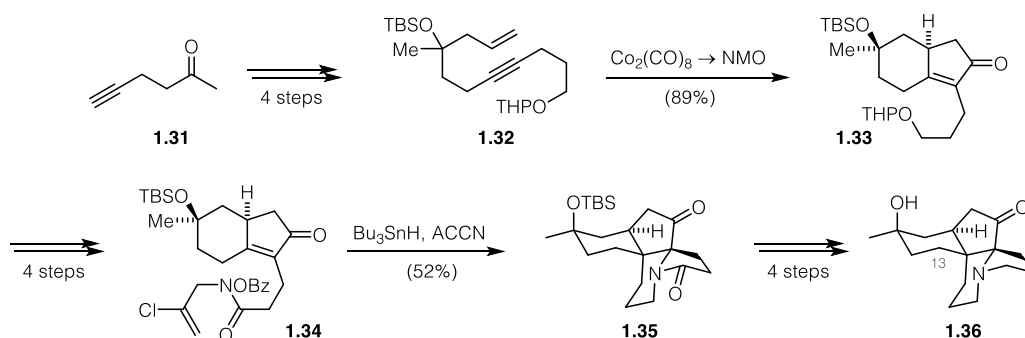


Figure 1.3. A generic representation of the “Heathcock tricycle” 1.30 in a fully reduced state.

The last roughly fifteen years have seen a large number of creative approaches towards fawcettimine-type alkaloids, various aspects of which have been reviewed.^[42, 44-47] After Heathcock’s fawcettimine synthesis, relatively little synthetic activity was recorded for about 20 years as most synthetic attention shifted towards lycopodine-type alkaloids. The next major contribution appeared in 2002, when Zard showcased his proprietary synthesis of *N*-heterocycles by addition of *N*-centered radicals across olefins in a synthesis of 13-deoxyserratine (1.36),^[48] a heavily modified fawcettimine-type compound related to serratinine that, unlike most others, features an α -tertiary amine (Scheme 1.6).^[34] Interestingly, his synthesis did not start from a methyl-substituted cyclohexanone derivative as the vast majority of syntheses do. Instead, the 6-5-system was obtained by a cobalt-catalyzed Pauson–Khand reaction, an approach extensively used by Takayama, Mukai and, most recently, Trauner.^[46, 49-54] Treating enyne 1.32, itself accessible in 4 steps from hex-5-yn-2-one (1.31), with dicobalt octacarbonyl and NMO gave the hydrindenedone 1.33 in very good yield.

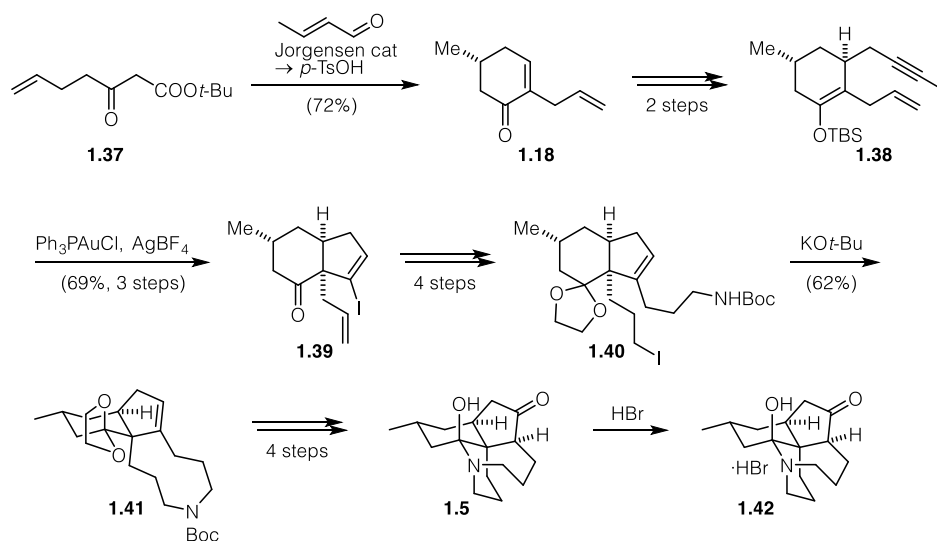


Scheme 1.6. The Zard synthesis of 13-deoxyserratine (36) via a radical cascade.

Another four steps established the substrate for his key step. Heating benzoylated hydroxamic acid derivative 1.34 with a radical starter and tributyltin hydride led to selective 5-*exo*-6-*endo*

cyclization. It is worth mentioning that the presence of the vinylic chloride was essential for the second ring closure to give **1.35**. Because of steric reasons, it successfully suppressed a 5-*exo*-5-*exo* reaction that became operational in its absence. With the tetracyclic skeleton assembled, all that remained was reduction of the lactam and deprotection to furnish (\pm)-13-deoxyserratine (**1.36**).

Shortly after, two total syntheses by the Toste group defined the first enantioselective approaches toward fawcettimine-type alkaloids (Scheme 1.7). The first, more methodology-oriented synthesis elegantly showcased Toste's gold-catalyzed 5-*endo*-cyclization of silyl enol ethers onto alkynes and is discussed in detail in chapter 1.2.1.^[55] The same methodology was subsequently utilized in the first enantioselective synthesis of fawcettimine itself (Scheme 1.7).^[56] After pre-installation of the sidechain oxygen or nitrogen—similar to the lycoplamine A synthesis (chapter 1.2.1, Scheme 1.42)—had failed, an organocatalytic Robinson annulation of **1.37** according to Jørgensen provided the six-membered ring of fawcettimine and delivered this key building block **1.18** on decagram scale in good yield and *ee* (88%).



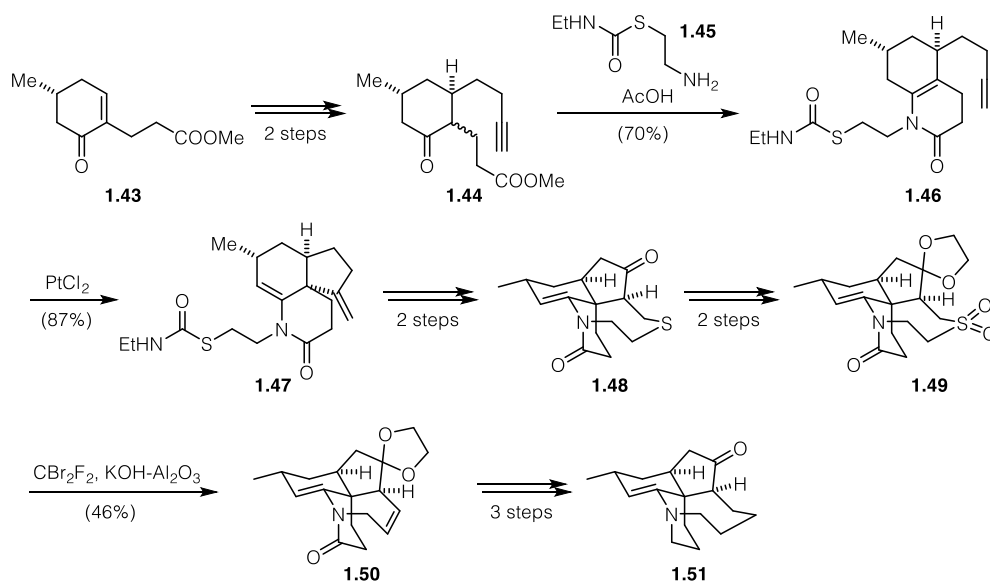
Scheme 1.7. The first enantioselective total synthesis of fawcettimine (**1.5**) by Toste through a gold-catalyzed 5-*endo*-cyclization of silyl enol ether **1.38**.

In this way, a scalemic version of Inubushi's classic building block **1.18** was made available. Two steps led to alkyne iodide **1.38**, which smoothly cyclized under gold catalysis to give hydrindane **1.39** in gram amounts. A sequence of four steps delivered the precursor **1.40** for the next key step, the formation of the nine-membered ring. The iodide **1.40** could be cyclized with potassium *tert*-butoxide whereas mesylate and tosylate only delivered complex product mixtures. With a Heathcock-type tricycle **1.41** (*vide supra*) in hand, the natural product **1.5** could be obtained in four more routine oxidation and deprotection steps. Additionally, the absolute

configuration of (+)-fawcettimine could be established by crystal structure analysis of the hydrobromide salt **1.42**.

At almost the same time as Toste's fawcettimine synthesis, Dake also utilized methodology developed in his own laboratories to furnish the quaternary stereocenter of a molecule closely related to fawcettimine called fawcettidine (**1.51**) (Scheme 1.8).^[57] The only difference between these two molecules is the presence of an enamine resulting from formal elimination of water from fawcettimine (**1.5**).

Like Toste in his lycoplidine A synthesis, Dake used a pulegone-derived building block to obtain the enone **1.43** in enantiomerically pure form.^[58] Addition of a C₄-alkyne building block delivered **1.44** as an inconsequential mixture of diastereomers. This δ -ketoester was heated with *S*-carbamoyl 2-thioethanolamine (**1.45**) to give a 10:1 mixture of regioisomeric enamides **1.46** (major isomer shown). This enamide served as the nucleophile in a platinum(II)-catalyzed annulation. Remarkably, the pendant thiocarbamate did not interfere with the cyclization to give the quaternary stereocenter in the tricyclic enamide **1.47**. The resulting *exo*-methylene group then was the handle for an allylic oxidation, yielding an enone before basic deprotection of the thiocarbamate led to hetero-Michael addition to yield **1.48**.

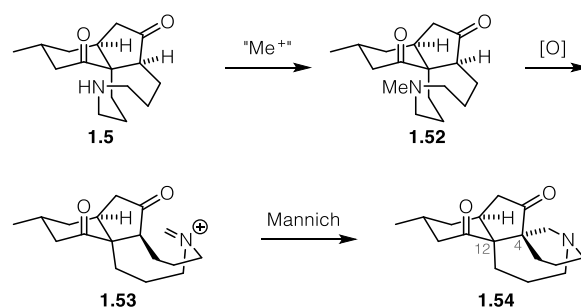


Scheme 1.8. Dake's synthesis of fawcettidine (**1.51**) via a platinum-catalyzed cyclization of enamide **1.47**.

At this stage, all that remained was to excise the sulfur atom and contract the ring. Protection, sulfide to sulfone oxidation and Ramberg-Bäcklund ring contraction of **1.49** using highly optimized conditions gave **1.50**, which could be transformed into fawcettidine (**1.51**) by standard redox manipulations. Dake's synthesis features a few notable aspects. First of all, by avoiding popular aldol-like reactions used in many other *Lycopodium* alkaloid syntheses, little

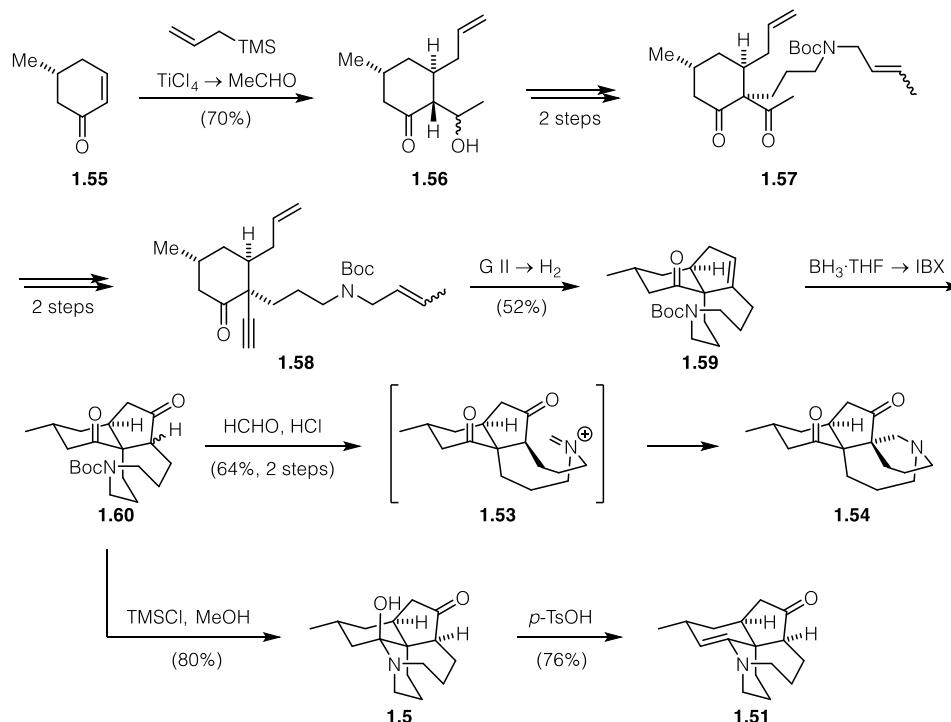
refunctionalization is needed for the cyclopentane ring. Second of all, his approach is the only one that furnishes the enamine functional group not by condensation of the azonane amine with the C-3 ketone, but introduces it very early on masked as a stable enamide. As a result, the six- and seven-membered heterocycles are constructed separately, and the cyclization occurs by *S*-alkylation rather than the conventional *N*-alkylation.

Another milestone in *Lycopodium* synthesis was Mulzer's approach toward a close relative of fawcettimine and fawcettidine, lycoflexine (**1.54**) (Scheme 1.9).^[59] This alkaloid was isolated in 1972 from *Lycopodium clavatum*.^[60] It most probably arises from fawcettimine by Mannich reaction between an iminium formed from the secondary amine and formaldehyde and the C-5 ketone. This results in a tetracyclic skeleton that is unique among fawcettimine alkaloids. Notably, it features two vicinal quaternary stereocenters at C-4 and C-12.



Scheme 1.9. The proposed biosynthesis of lycoflexine (**1.54**) from fawcettimine (**1.5**) through an intramolecular Mannich reaction.

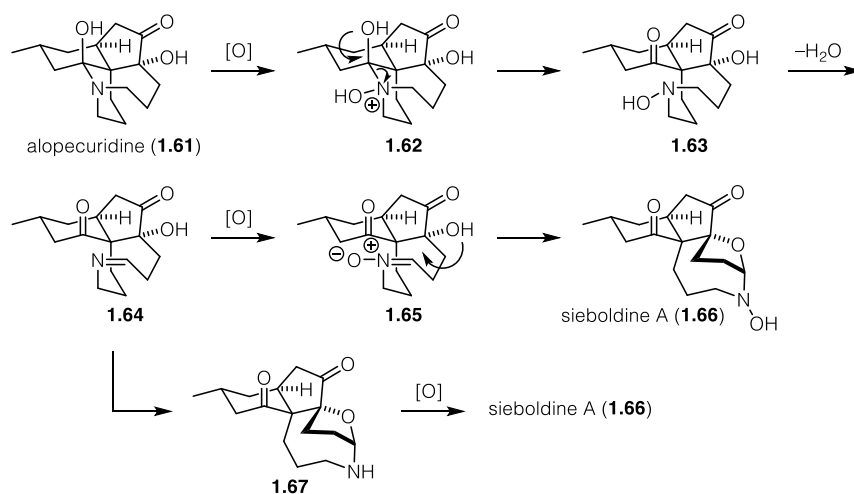
In 2010, Mulzer and coworkers decided to emulate this sequence from a rapidly assembled Heathcock tricycle (Scheme 1.10). A three-component coupling consisting of Sakurai allylation of pulegone-derived enone **1.55** and in-situ aldol reaction of the resulting titanium enolate gave adduct **1.56** as a mixture of diastereomers. This aldol was oxidized to the dicarbonyl and alkylated with a primary iodide to give **1.57**, setting the quaternary stereocenter of the fawcettimine alkaloids. In order to investigate their envisioned key step, the methyl ketone group was transformed into the alkyne by a high-yielding triflation-elimination sequence. With the dienyne **1.58** successfully assembled, the stage was set for the key biscyclization. Treatment with Grubbs II catalyst resulted in selective ring-closing enyne metathesis to first furnish the five-membered ring before closing the nine-membered heterocycle with a ring-closing metathesis (RCM) reaction.



Scheme 1.10. The Mulzer synthesis of lycoflexine (**1.54**), fawcettimine (**1.5**) and fawcettidine (**1.51**) through an enyne-RCM cascade starting from dienyne **1.58**.

As it was known that ruthenium-based metathesis catalysts can also serve as hydrogenation catalysts, the reaction mixture was purged with hydrogen and stirred until the more accessible disubstituted double bond was successfully reduced to finally yield **1.59**. This reaction cascade assembled the complete skeleton of fawcettimine (**1.5**), forming two rings at the same time. Hydroboration of the remaining double bond in **1.59** was followed by *in situ* treatment with IBX, a convenient replacement for the previously used chromium reagents, to yield Boc-protected fawcettimine **1.60**. At this stage, the synthesis branched. Simple treatment of **1.60** with methanolic HCl gave fawcettimine (**1.5**) by Boc deprotection and cyclization.^[61] Further acidic treatment with *p*-TsOH in toluene resulted in elimination to fawcettidine (**1.51**). If **1.60** was refluxed with dilute aqueous HCl and excess aqueous formaldehyde in EtOH, Boc deprotection was followed by formation of an iminium ion that was trapped in a Mannich reaction to give lycoflexine in 64% yield from **1.59**. The overall sequence yields fawcettimine and lycoflexine in only eight steps each from enone **1.55**, significantly raising the bar for the following syntheses. In 2003, Kobayashi reported the isolation of one of the most popular alkaloid targets of the following years, sieboldine A (**1.66**).^{[62] [63]} Alongside its isolation, Kobayashi proposed a biosynthesis starting from alopecuridine (**1.61**) (Scheme 1.11). *N*-oxidation of either the ketoamine or hemiaminal form of alopecuridine could give hydroxylamine **1.63** *via* the

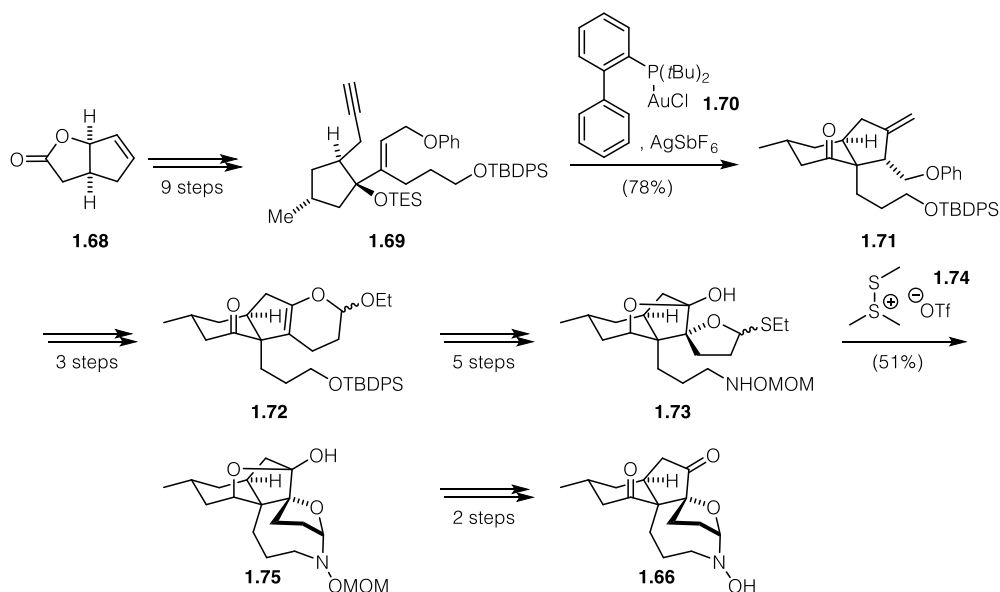
hydroxyammonium salt **1.62**. H₂O elimination would result in a presumably unstable imine **1.64**.



Scheme 1.11. Two proposed biosynthetic pathways *en route* to sieboldine A (**1.66**), both starting from alopecuridine (**1.61**).

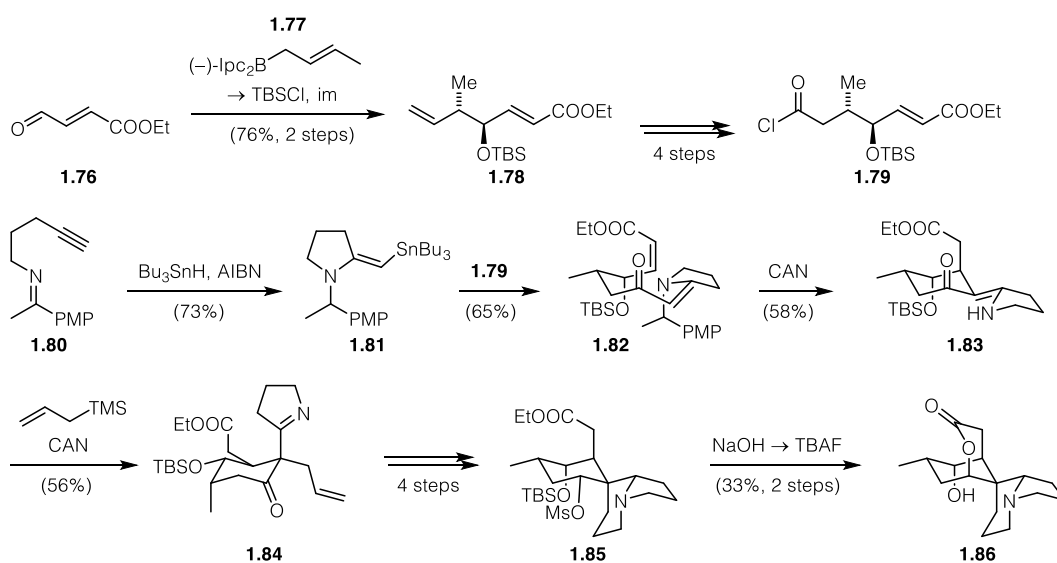
At this stage, two pathways can be envisaged. Another *N*-oxidation would yield a very electrophilic cyclic nitronium ion **1.65** that could be intercepted by the tertiary alcohol to directly yield sieboldine A (**1.66**). Alternatively, cyclization could occur directly at the imine stage to give the *N,O*-acetal **1.67**, oxidation of which would again give sieboldine A. Its most unusual feature is the THF ring that also contains an *N,O*-acetal formed from an hydroxylamine.

The Overman group published the first, enantioselective synthesis of the highly competitive *Lycopodium* alkaloid target in 2010 (Scheme 1.12).^{[64-65][66]} Apart from its intriguing biological activity, its interesting structure was attractive: it features a tetracyclic fawcettimine-type skeleton modified with an unusual additional tetrahydrofuran. Strategically very different from most other syntheses, Overman's starting compound did not contain any of the carbocycles of the final product. Instead, he elaborated the first key intermediate **1.69** from the known enantiopure lactone **1.68** in 9 steps. When this enyne was treated with the gold(I)-JohnPhos complex **1.70**, a pinacol-terminated cyclization developed in Overman's laboratories occurred,^[67] delivering hydrindane **1.71** featuring three of the natural product's stereocenters in good yield. A hetero-Diels–Alder reaction to add the missing C₂ unit gave **1.72** and a series of functional group interconversions furnished the thioglycoside **1.73**. Activation with DMTST salt **1.74** was uniquely suited for the glycosylation of the MOM-protected hydroxylamine to give the penultimate intermediate **1.75** *en route* to sieboldine A (**1.66**).



Scheme 1.12. The Overman synthesis of sieboldine A (1.66) through a gold-catalyzed pinacol-terminated cyclization of enyne 1.69 and a late-stage intramolecular glycosylation.

In 2009, Johnston disclosed the first synthesis of a heavily modified fawcettimine-type alkaloid called serratezomine A (1.86) (Scheme 1.13).^[68-69] Biosynthetically, this unusual tetracyclic alkaloid is probably derived from serratinine (1.16), also isolated from *Lycopodium serratum*, via a Polonovski-type fragmentation.^[70] The synthesis began with ethyl sorbate-derived aldehyde 1.76. The relative and absolute chemistry was set by a Brown crotylation with 1.77 to give secondary alcohol 1.78. Four more steps were needed to access acid 1.79. After activation as the acid chloride, it was coupled with a vinyl stannane 1.81 which was accessed by an interesting free radical-mediated aminostannylation of imine 1.80.^[71]

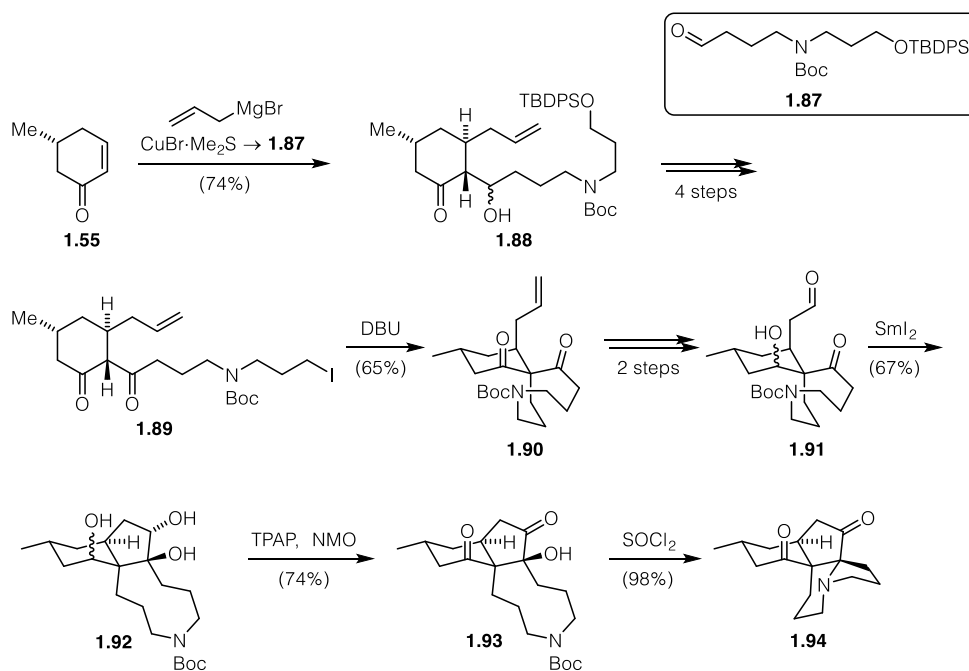


Scheme 1.13. Johnston's serratezomine A (1.86) synthesis through three radical-mediated transformations.

This vinylogous amide **1.82** could be deprotected under oxidative conditions, directly inducing intramolecular Michael addition to the unsaturated ester to yield **1.83**. The stereoselectivity was mainly guided by allylic strain of the nascent tetrasubstituted double bond, leading to a diaxial arrangement of the silyl ether and ethyl acetate substituents in **1.83**.^[72] The next key step was the introduction of the all-carbon stereocenter at C-12. Rather exotic oxidative conditions (cerium ammonium nitrate and allyltrimethylsilane) suppressed lactamization and allylated the vinylogous amide with high diastereoselectivity to the pyrroline **1.84**. At this stage, all atoms of the natural product were assembled. The imine **1.84** was transformed into the natural product serratezomine A (**1.86**) in six more steps, including a stereoselective iminium reduction and final lactone formation by nucleophilic substitution of equatorial mesylate **1.85**.

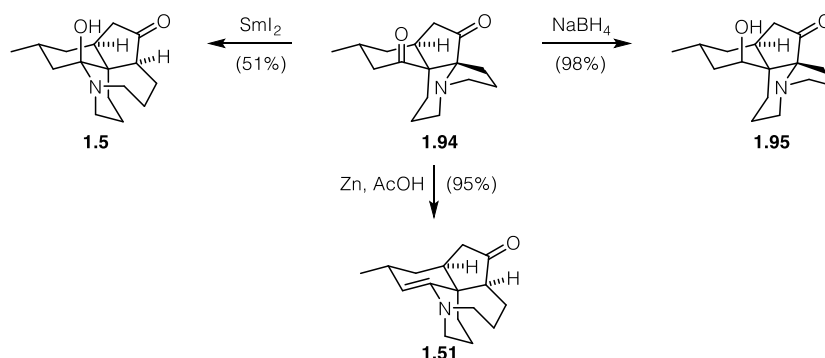
Since 2010, a few groups have not only introduced new concepts for *Lycopodium* alkaloid synthesis, but have also increasingly demonstrated the generality of their strategies by synthesizing multiple alkaloids using common building blocks. Prime examples are the recent efforts by the Lei and Tu groups, which will be discussed in the following. Other notable efforts were undertaken by the groups of Mukai, Williams, Zhao, Zhai and Taniguchi.^[52, 73-76]

Lei disclosed an interesting approach to fawcettimine (**1.5**) and fawcettidine (**1.51**) by way of a more complex congener, 13-dehydro-8-deoxyserratinine (**1.94**) (*vide supra* for Zard's very distinct approach to 13-deoxyserratine (**1.36**) in 2012 (Scheme 1.14).^[77] The synthetic sequence began with the same pulegone-derived enone **1.55** employed by Toste and Mulzer.^[55, 59] Similar to Mulzer's Sakurai-aldol sequence, Lei generated an enolate by conjugate addition of an allyl cuprate and trapped it with an aldehyde **1.87** that was made in three steps to give aldol **1.88**. Four steps converted it into diketone **1.89** that formed the quaternary stereocenter by intramolecular spirocyclization. Interestingly, the corresponding mesylate mainly gave *O*-alkylation under these conditions. Selective reduction and Lemieux-Johnson oxidation of **1.90** delivered ketoaldehyde **1.91** that underwent SmI₂-induced pinacol coupling to furnish **1.92**, the 6-5-9 ring system of fawcettimine-type alkaloids. This intermediate was converted into 13-dehydro-8-deoxyserratinine (**1.94**) by simple oxidation of the two secondary alcohols followed by treatment with thionyl chloride and triethylamine.



Scheme 1.14. Lei's synthesis of the key intermediate 13-dehydro-8-deoxyserratinine (**1.94**) through a *spiro* intermediate **1.90**.

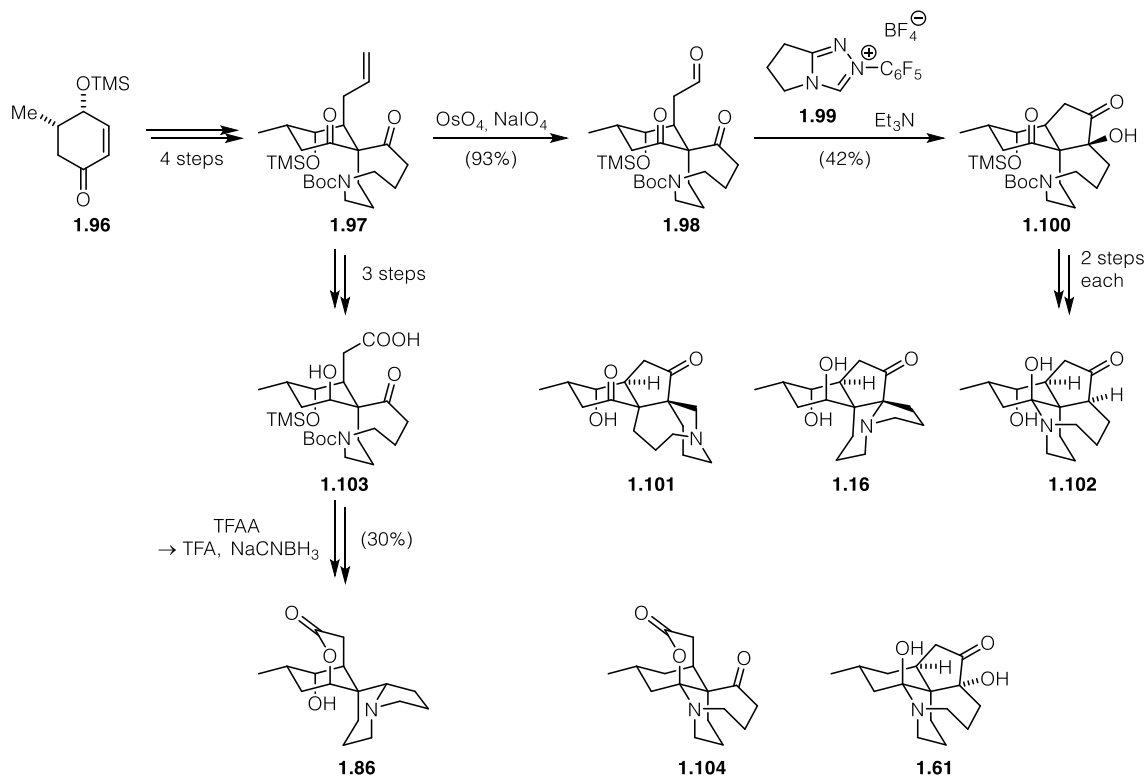
Presumably, the α -chloroketone generated with thionyl chloride is electrophilic enough that it can be attacked by the carbamate nitrogen in close proximity to give the α -tertiary ammonium ion from which the Boc group is readily removed *in situ*.^[78] Interestingly, efforts to alkylate the free secondary amine failed. From this common intermediate **1.94**, three *Lycopodium* alkaloids could be obtained by three distinct reductions (Scheme 1.15). Regio- and stereoselective ketone reduction with sodium borohydride yielded 8-deoxyserratinine (**1.95**). Reduction under acidic conditions and high temperature resulted in C-N cleavage followed by hemiaminal formation and water elimination to give fawcettidine (**1.51**).



Scheme 1.15. Late-stage diversification *via* reductive transformations to fawcettimine (**1.5**), 8-deoxyserratinine (**1.95**) and fawcettidine (**1.51**).

When **1.94** was reduced with SmI_2 , cleavage and aminal formation were observed without subsequent water elimination, yielding fawcettimine (**1.5**). In a follow-up study, Lei generalized

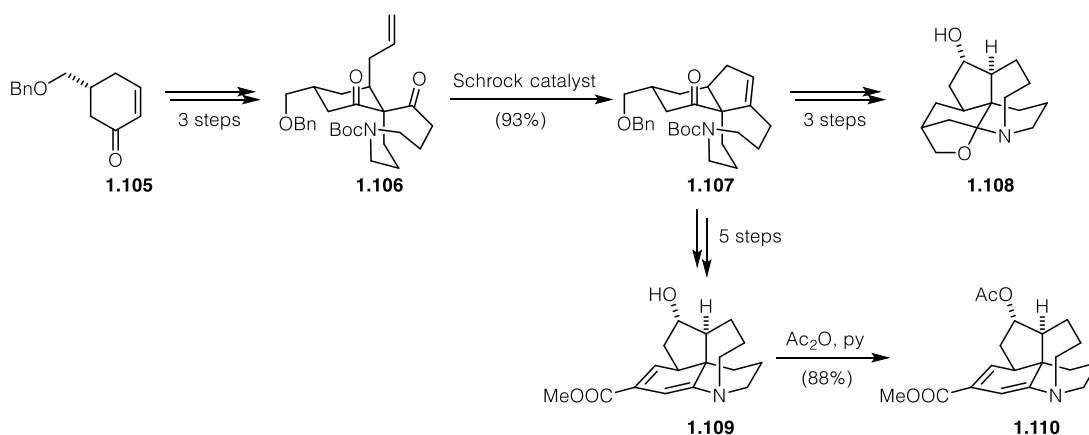
his approach in the context of diversity-oriented synthesis, accessing four more *Lycopodium* alkaloids together with a range of complex natural product-like scaffolds (Scheme 1.16).^[79] The starting point was the γ -hydroxylated enone **1.96**, allowing access to a host of C-8-hydroxylated fawcettimine alkaloids. Chemistry similar to that in Scheme 1.14 led to **1.97**, one of the key branching points.



Scheme 1.16. Lei's 2nd generation diversity-oriented synthesis approach towards numerous *Lycopodium* alkaloids. The key intermediate **1.97** again features a *spiro* stereocenter.

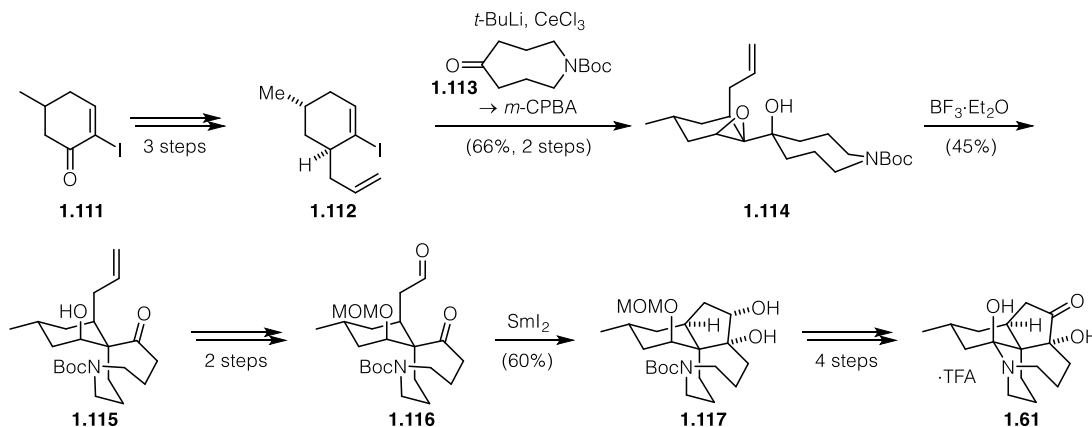
A benzoin reaction promoted by the NHC derived from triazolium salt **1.99** led to tricycle **1.100**, albeit with low yield due to poor selectivity between the two ketones. However, this circumvented the pinacol coupling-oxidation sequence previously used. From this Heathcock tricycle, three alkaloids were accessible, namely lycoposerramine U (**1.101**), serratinine (**1.16**) and 8-hydroxyfawcettimine (**1.102**). These natural products represent more oxidized versions of the alkaloids synthesized as shown in Scheme 1.14 and were made available by similar reductive methods. A completely different scaffold, however, could also be obtained from key intermediate **1.97**; Pinnick oxidation delivered δ -hydroxyacid **1.103**. When the acid was treated with trifluoroacetic anhydride followed by trifluoroacetic acid and sodium cyanoborohydride, a reductive amination occurred to yield serratezomine A (**1.86**), one of the more heavily modified fawcettimine-type *Lycopodium* alkaloids (*vide supra* for the Johnston approach). Another representative of the so-called “*seco*-fawcettimines” is lycojapodine A (**1.104**),^[80] which was

accessed together with alopecuridine (**1.61**) by Lei with a closely related “tautomer locking” approach,^[81] which was recently reviewed.^[47] The last installment was geared at the C-16-oxidized congeners huperzine Q (**1.108**) as well as lycopladine B (**1.109**) and C (**1.110**) (Scheme 1.17). Following their well-explored chemistry, the spirocyclic intermediate **1.106** was furnished, this time starting from a building block that only differed from methylcyclohexenone **1.55** in the oxidation of the stereogenic methyl group at C-16.^[82] This time, the cyclopentanone was furnished by an interesting carbonyl-olefin metathesis using Schrock’s catalyst as a reagent to give the key intermediate **1.107**. A deprotection-cyclization sequence led to huperzine Q (**1.108**) while an interesting late-stage bromofunctionalization then led to lycopladines B (**1.109**) and C (**1.110**). It is instructive to compare this strategy to Takayama’s synthesis of huperzine Q.^[51]



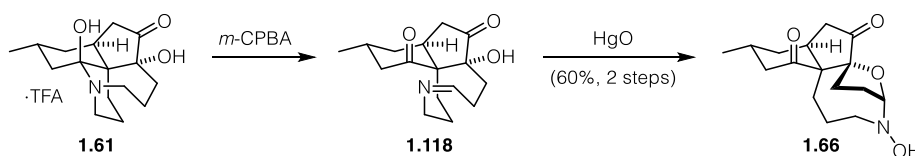
Scheme 1.17. Lei’s carbonyl-olefin metathesis approach for the synthesis of C-16-oxidized *Lycopodium* alkaloids huperzine Q (**1.108**), lycopladine B (**1.109**) and lycopladine C (**1.110**).

The Tu group published their efforts to alopecuridine (**1.61**) two years prior to Lei, in 2011 (Scheme 1.18).^[83] In three steps each, two building blocks **1.111** and **1.113** were furnished. The vinyl iodide **1.112** was synthesized from racemic **1.111** and not from pulegone, as the stereoinformation was lost in the following steps. Fragment coupling and epoxidation gave the epoxide **1.114**, which could be converted to **1.115** in a $\text{BF}_3 \cdot \text{Et}_2\text{O}$ -mediated semipinacol rearrangement to furnish **1.115** bearing the nine-membered ring of the *Lycopodium* alkaloids as well as the quaternary stereocenter. Two steps later, the cyclopentane portion was forged in a Sm(II)-mediated pinacol coupling of **1.116** to yield the Heathcock tricycle **1.117**. Interestingly, the stereochemistry of the C-4 tertiary alcohol could be defined by the stereochemistry of the C-13 alcohol, presumably depending on whether intramolecular coordination to samarium by the alcohol was possible or not. With the five-membered ring formed, all that remained was to remove the MOM group, oxidize the secondary alcohols and remove the nitrogen protecting group to furnish racemic alopecuridine (**1.61**)·TFA in 13 steps.



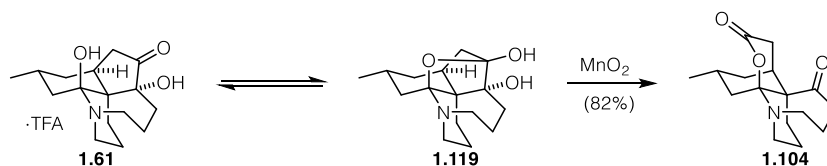
Scheme 1.18. Tu's semipinacol-rearrangement-based strategy for the synthesis of alopecuridine (1.61).

With a synthesis of alopecuridine completed, they were in a position to examine Kobayashi's proposed biosynthesis of sieboldine A (1.66) (see Scheme 1.11).^[62] Alopecuridine (1.61) was thus oxidized with $m\text{-CPBA}$ to the unstable $N\text{-oxide}$, which presumably either isomerizes to the free hydroxylamine or eliminates H_2O to give the imine proposed by Kobayashi (Scheme 1.19). Treatment of the crude mixture with mercury oxide in MeOH resulted in nitron formation and intramolecular cyclization to yield sieboldine A in 60% over two steps, validating the biosynthesis put forth.



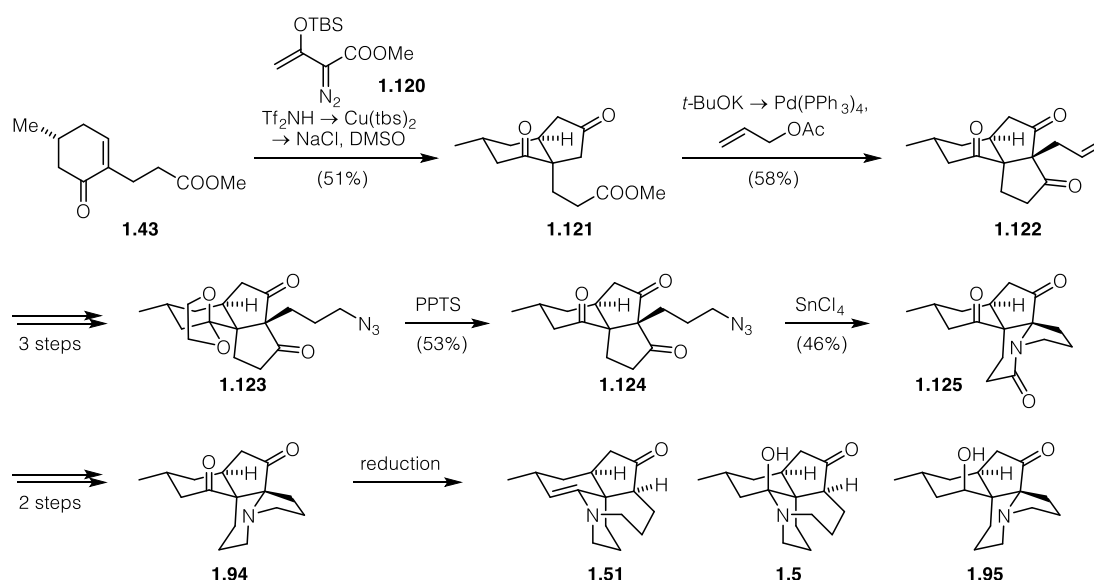
Scheme 1.19. A biomimetic synthesis of sieboldine A (1.66) through biomimetic oxidation of alopecuridine (1.61).

With a slightly more step-intensive approach, Tu's general synthesis could be rendered enantioselective and also extended to the synthesis of lycojapodine A (1.104) (Scheme 1.20).^[84] Zhao proposed that alopecuridine (1.61) could be in equilibrium with its hemiacetal form 1.119, oxidative diol cleavage of which would yield lycojapodine A (1.104).^[80] To their delight, treating alopecuridine TFA salt with manganese dioxide indeed yielded lycojapodine A in very good yield, validating their and Kobayashi's proposal (Scheme 1.20).



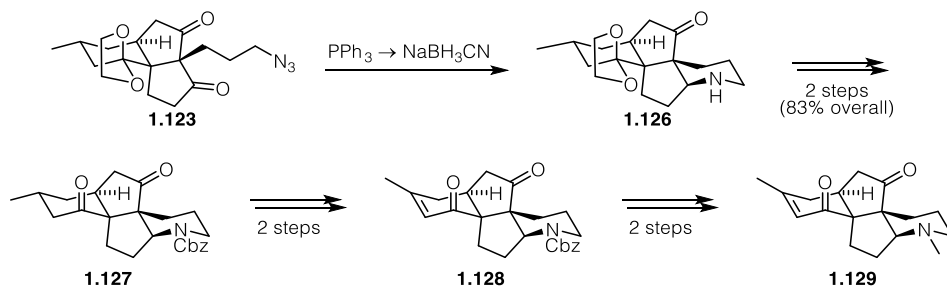
Scheme 1.20. A biomimetic synthesis of lycojapodine A (1.104) through oxidative cleavage of alopecuridine (1.61).

Tu also completed the first total synthesis of the recently isolated lycojaponicum C (**1.129**) from Dake's enone (**1.43**) and the donor-acceptor-substituted diazo compound **1.120**.^[85] In an impressive sequence consisting of Mukaiyama-aldol reaction, cyclopropanation/fragmentation and Krapcho decarboxylation, the hydrindane **1.121** could be forged on gram scale without the isolation of intermediates (Scheme 1.21). Indeed, the two-pot sequence was more efficient than isolating every intermediate.^[86] In another one-pot operation, Dieckmann condensation and allylation could be combined to forge the second quaternary stereocenter in the triketone **1.122**. The allyl group was transformed into the azide of **1.124** next, which, together with its C-13 ketal **1.123**, represented the key intermediates. Triketone **1.124** could be treated with tin(IV) chloride to trigger an Aubé-Schmidt rearrangement that furnished the tertiary α -tertiary amine **1.125** of the serratinine (**1.16**) class of alkaloids. In two more steps, it was transformed into **1.94**, the intermediate previously used by Lei to access fawcettimine (**1.5**), fawcettidine (**1.51**) and 8-deoxyserratinine (**1.95**) (Scheme 1.21).^[77]



Scheme 1.21. Tu's synthesis of two key intermediates **1.123** and **1.94** through a sequence of cascade reactions.

Alternatively, the ketal could be submitted to Staudinger reaction and reduction (to **1.126**), ketal hydrolysis and *N*-protection to yield tetracyclic intermediate **1.127** (Scheme 1.22). Two-step α,β -dehydrogenation to **1.128** was followed by hydrolysis and *N*-methylation to yield lycojaponicum C (**1.129**).



Scheme 1.22. Total synthesis of lycojaponicum C (**1.29**) from intermediate **1.123**.

Overall, the construction of the 9-membered ring by *N*-insertion into a 5-5 system offers great flexibility, arguably more so than the established Heathcock tricycles.

Given the maturation of the field, most of the synthetic attention has turned to more heavily modified fawcettimine-type alkaloids. This includes, for example the series of alkaloids where the C-15 methyl group is inverted or oxidized. As these are not easily obtained from pulegone or derivatives thereof, groups have devised very interesting strategies to access alkaloids like lycopalhine A (**1.130**) or palhinines A (**1.140**) and D (**1.141**).

Exemplary is Williams and Trauner's approach to the unusual hexacyclic *Lycopodium* alkaloid lycopalhine A (**1.130**),^[53] which was isolated recently from *Palhinhaea cernua*.^[87] At the time, it represented the first alkaloid to feature the C-6-C-16 linkage as well as C-9-N-2' (Figure 1.4, highlighted in bold), similar to its presumed biosynthetic precursor obscurinine (**1.131**),^[88] which was coisolated from the same sample by the Zhao group.

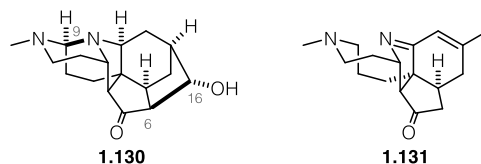
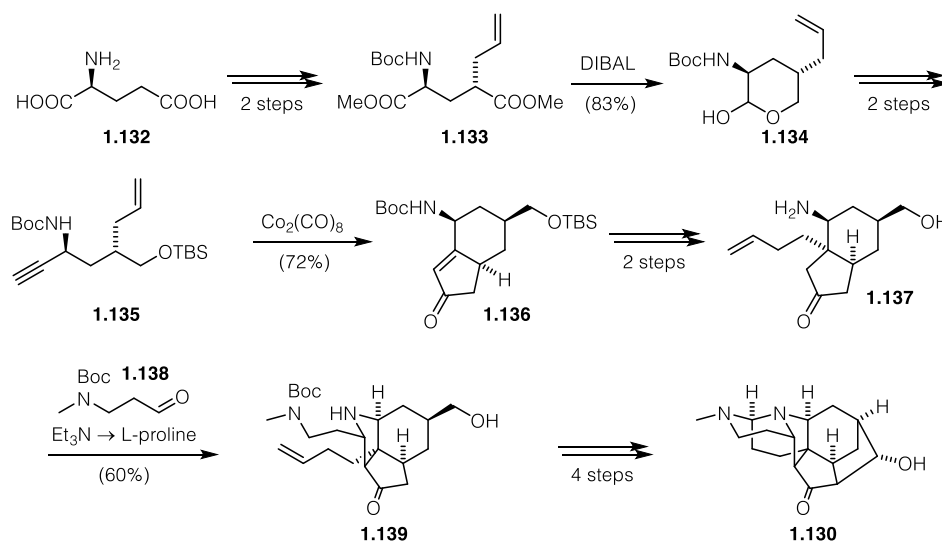


Figure 1.4. Two more heavily modified fawcettimine-type *Lycopodium* alkaloids, lycopalhine A (**1.130**) and obscurinine (**1.131**). Novel C-C linkages are highlighted in bold.

The retrosynthetic analysis led them back to a hydrindane system similar to the other fawcettimine alkaloids, but with an inverted and oxidized C-16 methyl group. Taking inspiration from the work of Zard,^[48] Mukai^[50, 52] and Takayama,^[51, 89] a Pauson–Khand retron was identified.^[46] Starting from the bulk chemical L-glutamate (**1.132**) that conveniently contains one of the required nitrogen atoms, the two ester functionalities in **1.33** could be differentiated *via* selective reduction to the lactol **1.134** (Scheme 1.23). Two more steps furnished the enyne **1.135**, which was transformed into the hydrindane **1.136** with very high diastereoselectivity, avoiding the adjustments at C-7 necessitated in Takayama's synthesis.^[89] After the quaternary stereocenter had been set by conjugate addition, a global deprotection to **1.137** and

condensation with aldehyde **1.138** resulted in an unusual 5-*endo-trig* Mannich reaction when L-proline was added. With the tricyclic core set, only the aminal and aldol bonds remained to be forged. In four steps, the natural product lycopalhine A (**1.130**) was obtained in good overall yield. Through this synthesis and deuteration studies, it was confirmed that lycopalhine A indeed exists in equilibrium with its C-16 epimer.



Scheme 1.23. The Trauner synthesis of lycopalhine A (**1.130**) through Pauson–Khand reaction of enyne **1.135** and an unusual intramolecular 5-*endo-trig* Mannich cyclization.

This notion was later confirmed by Fukuyama’s monumental 41 step synthesis that resulted in an identical 5.5:1 mixture.^[90-91]

Quite recently, a related natural product that also features an inverted and oxidized methyl group, palhinine A (**1.140**), was isolated.^[92] It was the first *Lycopodium* alkaloid of what is now a small family of natural products from *Palhinhaea cernua*, all bearing a highly functionalized isotwistane system, such as palhinine D (**1.141**) (Figure 1.5).^[92-95] A novel feature is the additional C-4-C-16 bond, resulting in two vicinal all carbon stereocenters at C-4 and C-12. It is not surprising that their caged, highly congested structures have garnered significant attention from the scientific community.^[96-101]

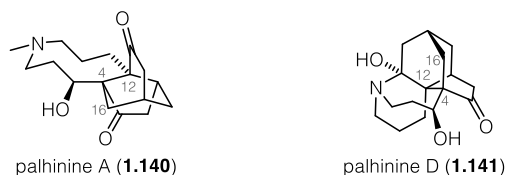
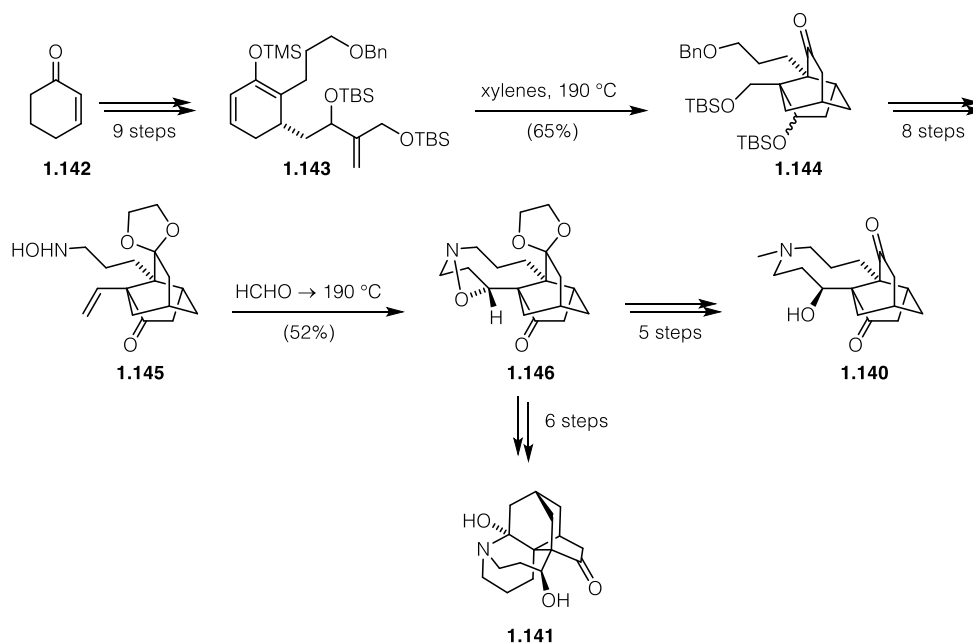


Figure 1.5. Structures of palhinine A (**1.140**) and palhinine D (**1.141**).

Very recently, Fan and coworkers reported the completion of the first, racemic total synthesis of palhinine-type natural products, namely palhinites A and D (Scheme 1.24).^[102] Starting from 2-cyclohexenone (**1.142**), nine steps gave the precursor **1.143** for an intramolecular Diels–Alder

reaction, a strategy also recognized by others as a means to construct isotwistane systems.^[99, 103-107] The reaction occurred at elevated temperatures without catalyst, giving the functionalized tricyclic **1.144**. Eight further steps were necessary to refunctionalize the core to the hydroxylamine **1.145**. When condensed with formaldehyde and subsequently heated in dichlorobenzene, an intramolecular (3+2)-nitron-alkene-cycloaddition took place to furnish **1.146** bearing the nine-membered ring of the fawcettimine-type *Lycopodium* alkaloids.



Scheme 1.24. The Fan synthesis of palhinine A (**1.140**) and D (**1.141**) via a ring-closing nitron cycloaddition. In this way, the medium-sized ring and the oxygenation at C-3 were introduced simultaneously, albeit with the wrong diastereoselectivity. This strategy was pursued because all standard techniques such as Mitsunobu alkylations using Fukuyama's method,^[108-110] simple alkylation methods^[39-40] and ring-closing metathesis failed. Reductive *N,O*-cleavage and alcohol inversion then led to the two natural products. It is interesting to see how the conformational restraints of the isotwistane core render many of the established methods ineffective, necessitating the development of creative new routes.

Somewhat distinct amongst the fawcettimine alkaloids are the magellanine alkaloids paniculatine (**1.147**), magellanine (**1.148**) and magellaninone (**1.149**) isolated from *Lycopodium magellanicum* (Figure 1.6). Probably derived from fawcettimine, they feature an additional C-C bond between C-5 and C-10. Because of the resulting unique diquinane substructure, quite different strategies have been employed for their synthesis, pioneered by the Overman and Paquette groups.^[111-113]

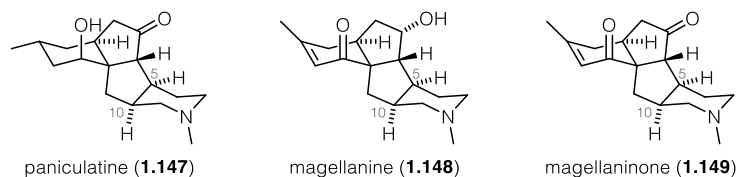
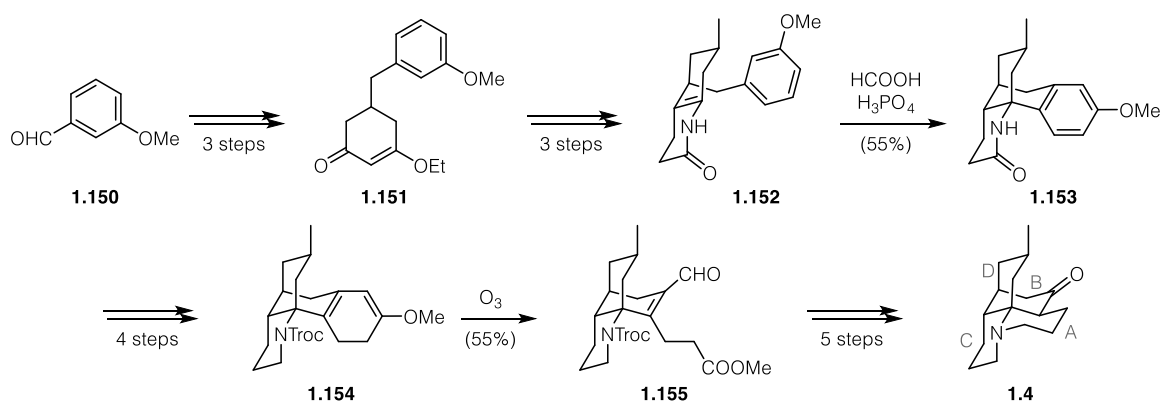


Figure 1.6. Structures of the three main alkaloids paniculatine (1.147), magellanine (1.148) and magellaninone (1.149) from *Lycopodium magellanicum*.

In recent years, multiple groups have significantly contributed with elegant approaches that can access multiple members of this subclass of *Lycopodium* alkaloids.^[49, 114-118] However, as they are of relatively little significance to this PhD thesis, they are not discussed in the context of this work.

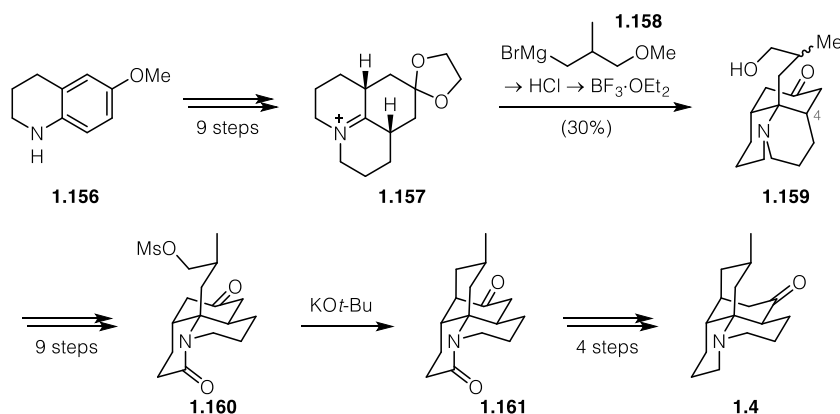
1.1.4 Synthetic approaches toward lycopodine-type alkaloids

The lycopodine family of *Lycopodium* alkaloids features the oldest member of the family, the namesake lycopodine (1.4), which was first isolated by Bödeker in 1881.^[12] After a few decades of constant isolation of new lycopodine-type alkaloids, the first synthesis of the lycopodane skeleton was put forth by Wiesner, who synthesized *epi*-lycopodine in 1967 (not shown).^[119-120] One year later, Ayer and Stork simultaneously completed the first syntheses of lycopodine itself.^[121-122] Through their and others' efforts, it quickly became apparent that one of the key challenges would be the efficient construction of the tertiary α -tertiary amine. The synthesis began with a three-step sequence to furnish vinylogous ester 1.151, the D-ring of lycopodine, from *p*-methoxybenzaldehyde (1.150) (Scheme 1.25). Three further steps set up the key step in Stork's synthesis, an *N*-acyliminium cyclization of 1.152 using a tethered anisole as the intramolecular nucleophile (Pictet–Spengler-like), to attach the B-ring of lycopodine and the α -tertiary amine to a bicyclic moiety, giving 1.153.



Scheme 1.25. Stork's *N*-acyliminium approach for the first total synthesis of lycopodine (1.4). Light grey letters indicate the common ring nomenclature.

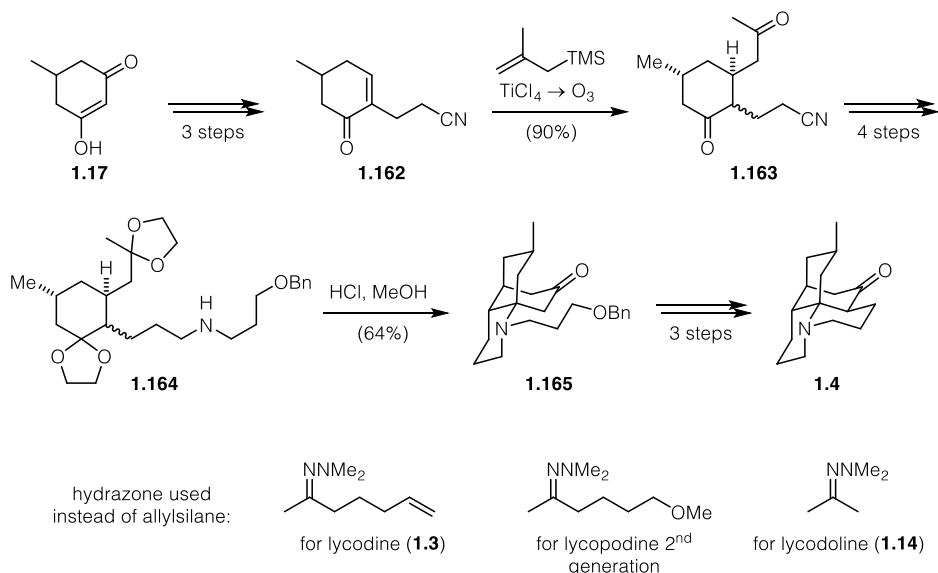
The anisole portion was reduced to diene **1.154**, which was cleaved *via* ozonolysis to reveal the C₃ chain of the lycopodine A-ring (**1.155**). Five more steps, including a Baeyer–Villiger oxidation to turn the enal into a ketone, then furnished synthetic lycopodine (**1.4**) for the first time. The success of the strategy (B-ring closure onto the D-ring) rendered this synthesis a blueprint for multiple later syntheses that followed similar general strategies. Ayer's synthesis also started from an anisole derivative **1.156**, but added the D-ring last (Scheme 1.26). Unfortunately, while the addition of Grignard reagent **1.158** to iminium ion **1.157** is a conceptually interesting approach, it resulted in the wrong stereochemistry at C-4, which required nine steps to correct. The last ring was finally closed by intramolecular alkylation of mesylate **1.160** to give **1.161** (no yield given). As the ketone was now at C-6 rather than C-5, tedious functional group interconversions were necessary and resulted in a rather lengthy synthesis (26 steps overall).



Scheme 1.26. Ayer's iminium addition approach toward the ATA of lycopodine (**1.4**).

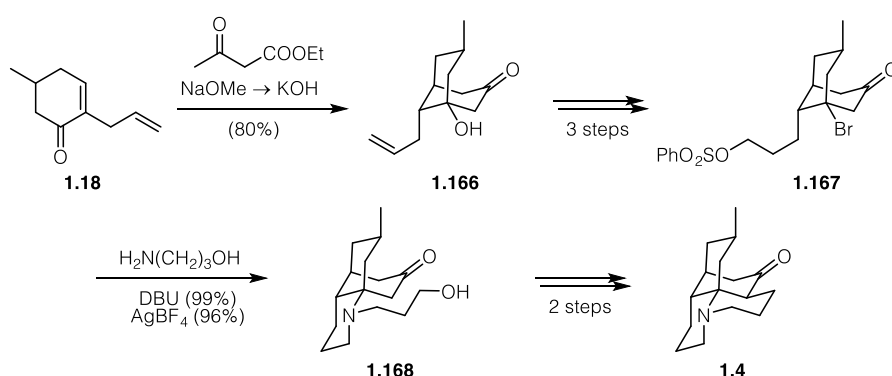
After these initial efforts, no significant synthesis efforts were published until Heathcock's landmark synthesis of lycopodine in 1978, followed by a second generation approach and syntheses of lycodoline (**1.14**) and lycodine (**1.3**) in 1982.^[41, 123] He was, surprisingly, the first to utilize the Mannich retron in the lycopodane skeleton (Scheme 1.27). Starting from dihydroorcinol (**1.17**), a three step sequence delivered enone **1.162**. Derivatives that bear different "head-groups" at the end of the C₃ chain have since seen a host of applications in both fawcettimine and lycopodine synthesis (*vide supra*). A C₃ unit was then attached either *via* allyl cuprate or, more efficiently, Sakurai addition to give **1.163** with perfect *anti* selectivity. The α -stereocenter was not controlled, which was of no consequence as both diastereomers converged at a later point. Five redox and protection steps then furnished the bisketal **1.164**. Upon heating in methanolic HCl for two weeks, smooth Mannich cyclization was observed, furnishing the almost complete lycopodine skeleton **1.165**. Debenzylation, a modified Oppenauer oxidation followed by aldol condensation and final reduction led to (\pm)-lycopodine

(**1.4**) in 13 steps, a vast improvement over previous approaches. A second generation synthesis further shortened the route by incorporating the C₃ A-ring unit into the hydrazone used for the conjugate addition (as the hydrazone azaenolate), arriving at one of the shortest and most efficient synthesis to date. Moreover, slight modifications resulted in very short syntheses of lycodine (**1.3**) (8 steps) and lycodoline (**1.14**) (11 steps).^[123]



Scheme 1.27. Heathcock's collective synthesis of lycopodine (**1.4**) and related alkaloids through a Mannich cyclization.

Unlike the fawcettimine-type alkaloids, the lycopodine-type alkaloids, especially lycopodine itself, remained popular synthesis targets over decades. In the 1980s, notable efforts came from Schumann (1982) and Kraus (1985).^[124-129] Kraus' synthesis used an acetoacetate addition to popular enone **1.18**, followed by Dieckmann cyclization to give the B-D system **1.166**. Functional group interconversion led to tertiary bromide **1.167** (Scheme 1.28).

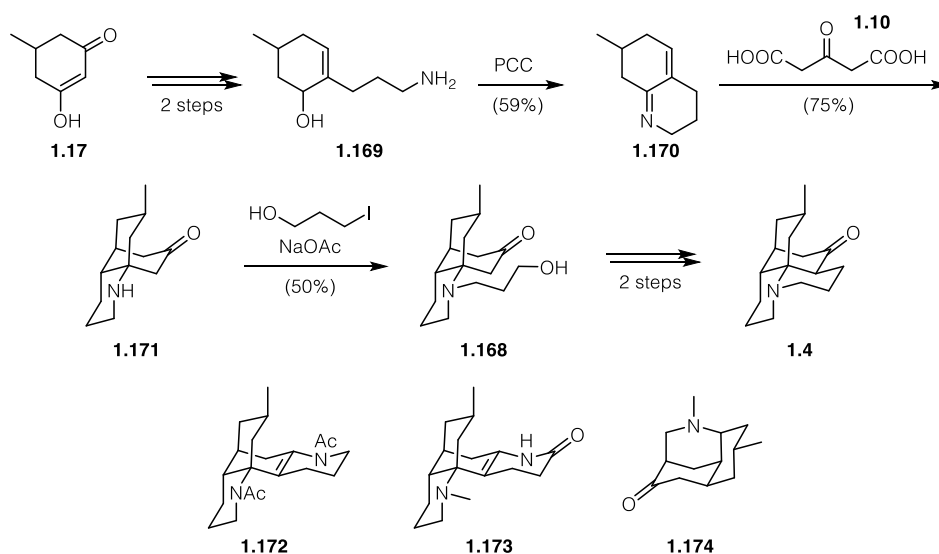


Scheme 1.28. Kraus' two syntheses of lycopodine (**1.4**) through either a Michael addition to an *anti*-Bredt enone (with DBU) or S_N1 addition to a tertiary cation (with AgBF₄).

This labile compound could be transformed to Heathcock's penultimate intermediate **1.168** very efficiently by double N-alkylation of 3-hydroxypropylamine under both acidic (AgBF₄) and

basic (DBU) conditions. Presumably, AgBF_4 leads to a $\text{S}_{\text{N}}1$ pathway whereas the basic conditions give a highly strained bridgehead enone and hetero-Michael addition.^[130]

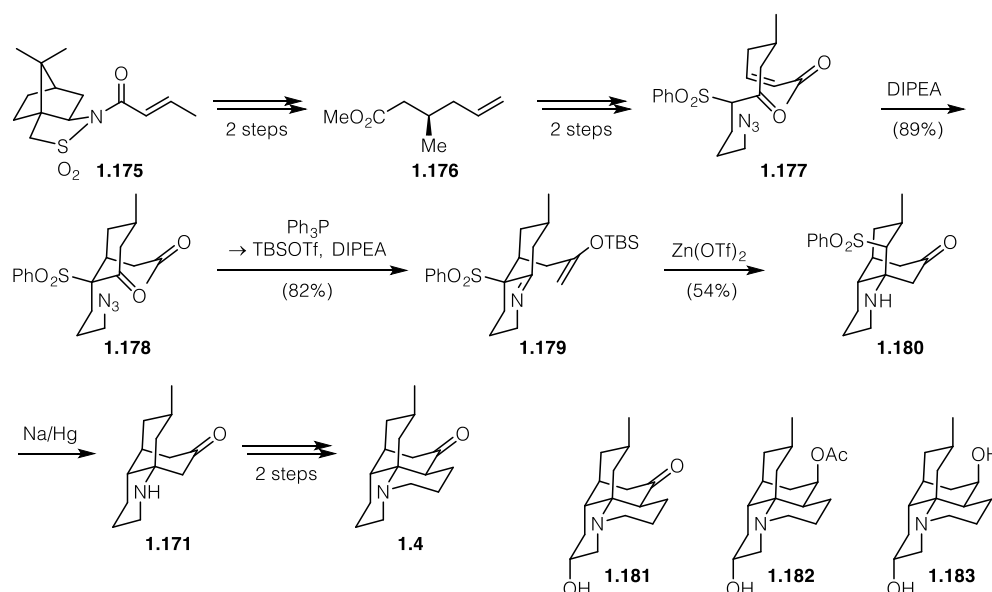
Schumann delivered a very straightforward synthesis of lycopodine (**1.4**) and, subsequently, a range of related alkaloids (Scheme 1.29).^[124-127] Starting from the same compound **1.17** as Heathcock, global reduction to **1.169** followed by allylic oxidation and condensation delivered a very sensitive α,β -unsaturated imine **1.170**. When this intermediate was heated with acetonedicarboxylic acid (**1.10**), conjugate addition was followed by decarboxylative Mannich reaction to give the B-C-D system **1.171** of lycopodine and a short (7 steps) formal synthesis of racemic lycopodine (**1.4**) after alkylation to **1.168**; the last two steps were performed according to Heathcock's method.^[41, 123] The α,β -unsaturated imine **1.170** was the cornerstone for the synthesis of other *Lycopodium* alkaloids of great structural variety, including acetylflabellidine (**1.172**),^[125] α -obscurine (**1.173**)^[126] and luciduline (**1.174**).^[127] The latter had previously been synthesized by Oppolzer in a succinct manner using a strategic nitron-alkene cycloaddition similar to the one used decades later in the total synthesis of palhinine A (**1.140**).^[102, 131-132]



Scheme 1.29. Schumann's use of a biomimetic double acetonedicarboxylic acid (**1.10**) addition to furnish the tricyclic core of lycopodine (**1.4**). Further alkaloids synthesized by this method are acetylflabellidine (**1.172**), α -obscurine (**1.173**) and luciduline (**1.174**).

It wasn't until 2008 that the first enantioselective synthesis of lycopodine was published by Carter, surprising given that enantiopure versions of many of the starting materials presented here were already available at the time.^[133-134] Carter's key transformation in essence represents a two-step variant of Heathcock's strategy that separates the closure of the C and B-rings (Scheme 1.30). In contrast to virtually all other syntheses that either started from cyclic materials or constructed them in the first step, Carter opted to install the crucial C-15 methyl stereocenter in **1.176** that subsequently directs all others *via* conjugate addition to a linear acylated Oppolzer

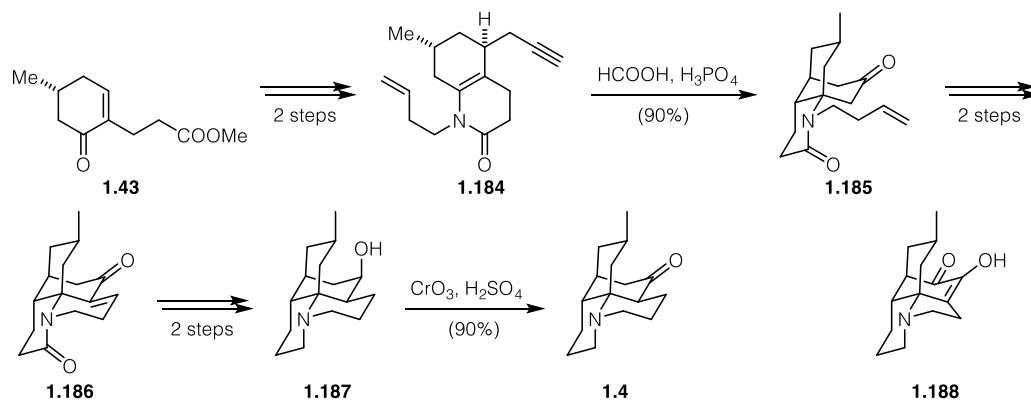
sultam **1.175**. Three more steps to add a C₄ chain and extend the alkene **1.176** to an enone gave an α -sulfonyl ketone **1.177** that underwent base-mediated diastereoselective Michael addition to the first cyclic intermediate **1.178**. Staudinger reduction and silyl enol ether formation set up the key Mannich reaction of **1.179**. Activation of the imine with zinc triflate gave tricycle **1.180** with concomitant phenyl sulfone 1,3-shift. After this key step, reductive desulfonation gave Heathcock's tricyclic intermediate **1.171** that was transformed to the natural product **1.4** with chemistry similar to Heathcock's. This general approach was subsequently used in the enantioselective synthesis of the more oxidized congeners 10-hydroxylycopodine (**1.181**) and (acetyl-)paniculine (**1.182** and **1.183**).^[135]



Scheme 1.30. First enantioselective lycopodine (**1.4**) synthesis by Carter using a two-step Mannich reaction. Other *Lycopodium* alkaloids (**1.181**–**1.183**) synthesized *via* this general method are shown in the right corner.

Since Carter's first enantioselective synthesis, only one further synthesis has been published. Very recently, in 2016, the She group employed an interesting amalgamation of the Stork and Heathcock approaches (Scheme 1.31).^[136] Starting from Dake's enone **1.43**, conjugate propargylation followed by condensation with homoallylamine furnished the bicyclic enamide **1.184**. Upon treatment with a mixture of formic and phosphoric acid, the *N*-acyliminium (similar to Stork's) was trapped in an alkyne-Prins cyclization reminiscent of Heathcock's Mannich reaction. With the tricycle **1.185** constructed in a very rapid fashion, the fourth ring was closed via aldol condensation to **1.186**. Redox adjustments delivered the natural product (–)-dihydrolycopodine (**1.187**) and by oxidation (–)-lycopodine (**1.4**). The group simultaneously published another paper detailing the identical construction of the tricyclic framework followed by a different oxidative endgame to arrive at (–)-lycospidine A (**1.188**).^[137] The most interesting facet of this natural product is its rare C₁₅N skeleton, as all except one other C₁₅ *Lycopodium*

alkaloids are of the C15N2 type, like huperzine A (**1.1**).^[138] Given that its skeleton can't be converted into one of the other four classes by skeletal rearrangements, it could be debated whether it should be considered the founding member of its own class and what the biosynthetic origin of this C-5-*nor*-alkaloid is.^[138]



Scheme 1.31. She's Stork-inspired *N*-acyliminium-Prins cyclization toward dihydrolycopodine (**1.187**), lycopodine (**1.4**) and lycospidine A (**1.188**).

Apart from lycopodine itself, many other lycopodine-type alkaloids have been targeted. This includes for example Evans' enantioselective total synthesis of clavolonine (**1.189**) or 8-hydroxylycopodine (Figure 1.7), which was isolated from *Lycopodium clavatum*.^[139]

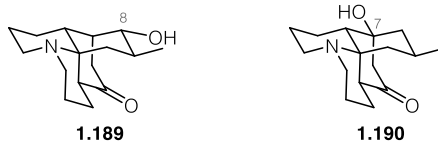
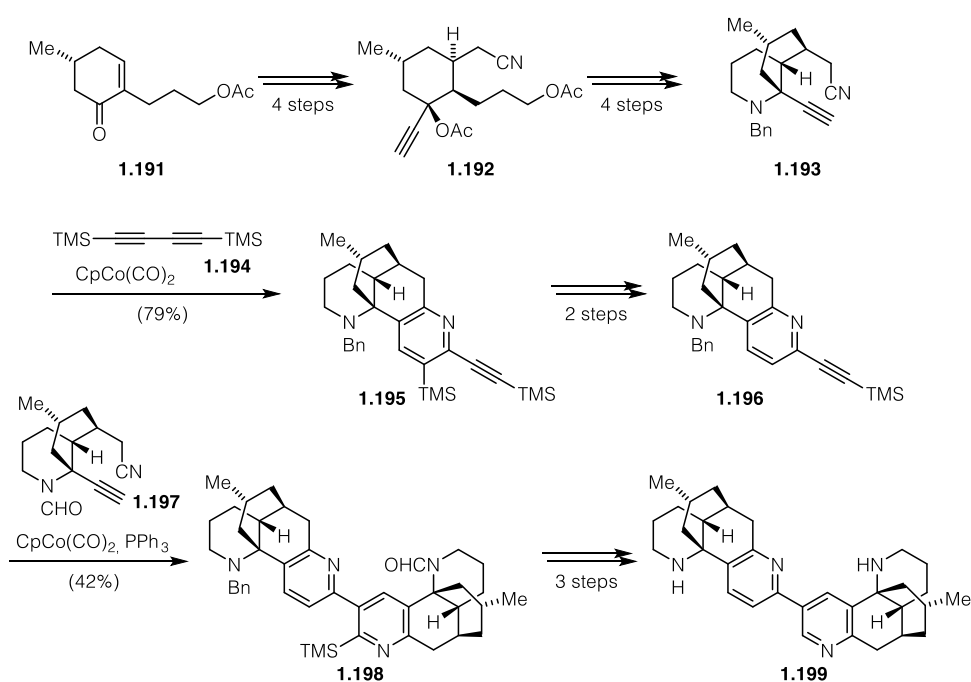


Figure 1.7. Structures of 8-hydroxylycopodine/clavolonine (**1.189**) and 7-hydroxylycopodine (**1.190**).

This followed the early efforts of Wenkert, who accessed clavolonine as part of a collective synthesis of six lycopodine-type alkaloids.^[140] Another noteworthy example are Breit's and Fujioka's enantioselective total synthesis of the same alkaloid to showcase Breit's directed hydroformylation and Fujioka's chiral acetal methodology, respectively.^[141-142] Like Evans, they opted for the *de novo* construction of all rings. This highlights the usefulness of non-chiral-pool-based approaches for enantioselective lycopodine-type *Lycopodium* alkaloid synthesis, allowing access to oxidation patterns not easily accessible from pulegone-derived building blocks. Another example for this is Snider's racemic 7-hydroxylycopodine (**1.190**) synthesis.^[143]

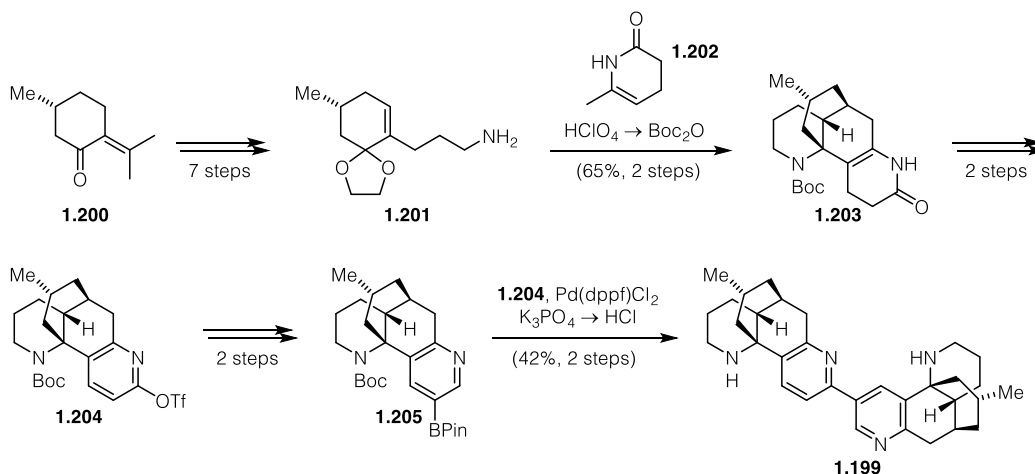
A few final examples which will be discussed in the following are lycodine-related *Lycopodium* alkaloids. Even though they are not part of the lycopodine class, some of the chemistry bears strong similarity and allows for very creative syntheses. In 2010, Siegel^[144] and Sarpong^[145] simultaneously disclosed their strategies for the total synthesis of complanadine A (**1.199**), a structurally interesting and highly bioactive^[146] dimeric *Lycopodium* alkaloid from *Lycopodium*

complanatum.^[147] It is worth noting that the natural product is not C_2 -symmetric because the pyridine units are connected at different positions. Siegel started with a pulegone-derived enone **1.191**^[58] that was transformed into a tertiary propargylic acetate **1.192** in four steps (Scheme 1.32). Another four steps delivered the bicyclic δ -cyanoalkyne **1.193**. When this compound was treated with bis-TMS-butadiyne (**1.194**) in the presence of a cobalt(I) catalyst, cyclization to the lycodine derivative **1.195** occurred. After a few manipulations, **1.196** could be coupled with δ -cyanoalkyne **1.197**, a differentially protected variant of **1.193**, in another cobalt-catalyzed cyclotrimerization to give arylsilane **1.198**. This bipyridine was converted to the natural product **1.199** in three more steps. The choice of *N*-protecting groups and solvents was crucial for regioselectivity in the cyclization.^[144, 148]



Scheme 1.32. Siegel's total synthesis of complanadine A (**1.199**) by two cobalt-catalyzed cyclotrimerization reactions.

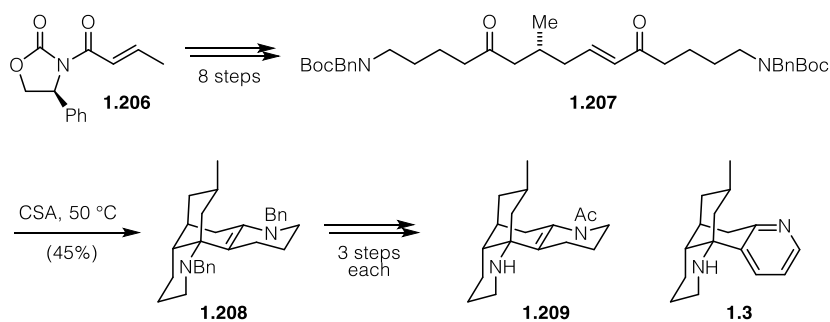
Sarpong used a very different approach, utilizing Schumann's method^[126] for the rapid construction of an obscurine derivative **1.203** (Scheme 1.33). However, by using the enantiopure amine **1.201** derived from pulegone (**1.200**), he was able to render the synthesis enantioselective. The dihydropyridone **1.202** efficiently condensed with **1.201**, which probably forms Schumann's imine **1.170** under the reaction conditions (see Scheme 1.29). With tetracyclic intermediate **1.203** available on multigram scale, it took three more steps to obtain the first coupling partner, pyridyl triflate **1.204**. Two more steps from this building block, including an iridium-mediated C-H borylation, yielded the second coupling partner, pyridylboronic ester **1.205**. Suzuki cross-coupling and deprotection gave the natural product complanadine A (**1.199**).^[145]



Scheme 1.33. Sarpong's approach using Schumann's chemistry to access an obscure derivative **1.203** as a platform for the rapid assembly of complanadine A (**1.199**).

A second study expanded this general approach to complanadine B, an oxidized congener.^[149-150] A related pyridine *N*-oxide arylation toward complanadines A and B was published by Hiram in 2013 (not shown).^[151] Their synthesis started from lycodine (**1.3**) itself, which was furnished by a distinct Diels–Alder- and Heck-based approach.^[152-153]

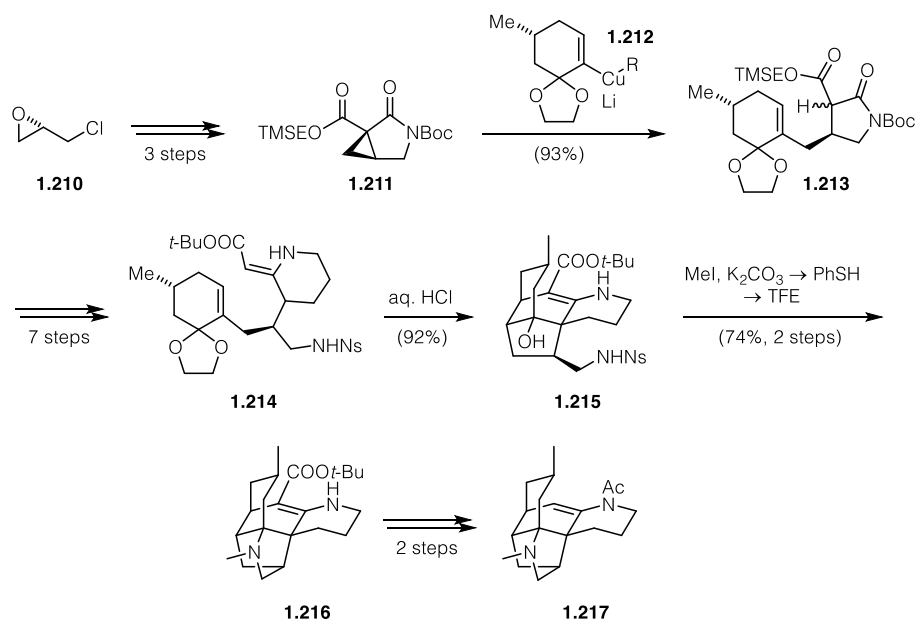
In 2014, Takayama disclosed a biogenetically inspired cascade cyclization that furnished (+)-flabellidine (**1.209**) and (–)-lycodine (**1.3**) (Scheme 1.34).^[154] Starting from acylated Evans' auxiliary **1.206**, the complete linear sidechain **1.207** was established in eight steps. When this linear molecule was heated with camphorsulfonic acid, a spectacular cyclization cascade occurred to furnish the complete lycodine skeleton (**1.208**) in one step. It presumably occurs *via* a series of Michael additions and a final Mannich reaction. Quite remarkably, the single methyl group stereocenter was sufficient to direct the correct conformation of the entire cascade. In three more steps each, flabellidine (**1.209**) and lycodine (**1.3**) were accessed.



Scheme 1.34. Takayama's remarkable cascade approach toward flabellidine (**1.209**) and lycodine (**1.3**).

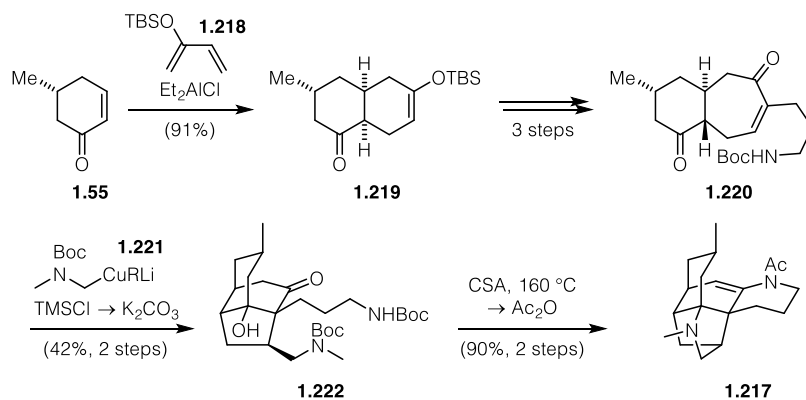
Similarly ambitious cyclization cascades were explored for the synthesis of fastigiatine (**1.216**), a lycodine-type *Lycopodium* alkaloid that features a rare C-4-C-10 bond, adding considerable strain and synthetic challenge to the molecule.^[155] The first synthesis was disclosed by the Shair

group 25 years after it was first isolated (Scheme 1.35).^[156] Starting from (*S*)-epichlorohydrin (**1.210**), the building block **1.211** was furnished in six steps, then coupled to the cuprate **1.212**, again derived from Cassell's building block, to give **1.213**.^[58] In seven steps, this intermediate was elaborated into the vinylogous carbamate **1.214**. In aqueous hydrochloric acid, the ketal was deprotected, unmasking an enone that was first attacked in a 1,4-addition followed by 1,2-attack to furnish the tetracyclic intermediate **1.215** featuring all rings but the pyrrolidine.



Scheme 1.35. Transannular Mannich chemistry used by Shair in the synthesis of fastigiatine (**1.217**).
R = 2-thienyl

After a one-pot nosyl-methyl exchange, a facile retro-Aldol reaction followed by intramolecular Mannich cyclization under neutral conditions gave the full ATA-bearing skeleton **1.216** and the natural product fastigiatine (**1.217**) after final protecting group manipulations. Subsequently, this approach was shown to be rather general for the total synthesis of five other seven-membered-ring-containing *Lycopodium* alkaloids such as lyconadin A and C.^[157] Especially lyconadin A^[158] and C^[159] had previously received significant synthetic attention as well.^[160-167]



Scheme 1.36. Rychnovsky's Mannich strategy for the synthesis of fastigiatine (**1.217**) via ring expansion and a retro-aldol-Mannich cascade, R = 1-hexynyl.

A related Aldol-Mannich cyclization cascade was used by Rychnovsky in his 2016 synthesis of fastigiatine (**1.217**) (Scheme 1.36).^[168] The Diels-Alder adduct **1.219** of enone **1.55** and diene **1.218** could be transformed into bicycle **1.220** through cyclopropanation followed by ring expansion. Conjugate addition of **1.221** followed by aldol addition yielded the tricyclic intermediate **1.222**. Similar to Shair's strategy, heating in acid, albeit at much higher temperature, brought about the double cyclization, yielding the natural product **1.217** after acetylation.

1.2 Total synthesis of fawcettimine alkaloids

1.2.1 Isolation, structure and previous efforts towards lycoposerramine R, lycopladine A and carinate A

Lycoposerramine R (**1.223**) is a fawcettimine-type alkaloid that was isolated in 2009 by Takayama from *Lycopodium serratum*, a prolific source of *Lycopodium* alkaloids.^[169] High-resolution mass spectroscopy in combination with UV-Vis and IR analysis suggested the presence of a pyridone moiety as part of a tetracyclic system that also features a piperidine unit. Extensive 2D NMR analysis finally allowed them to assign the structure of lycoposerramine as shown in Figure 1.8.

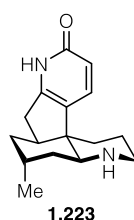


Figure 1.8. The structure of lycoposerramine R (**1.223**).

As far as the biosynthesis is concerned, three possible pathways were suggested. An unusual C-4-C-12 cyclization from a phlegmarine (**1.2**) skeleton could cyclize to give a fully reduced version **1.224** of the lycoposerramine R skeleton.

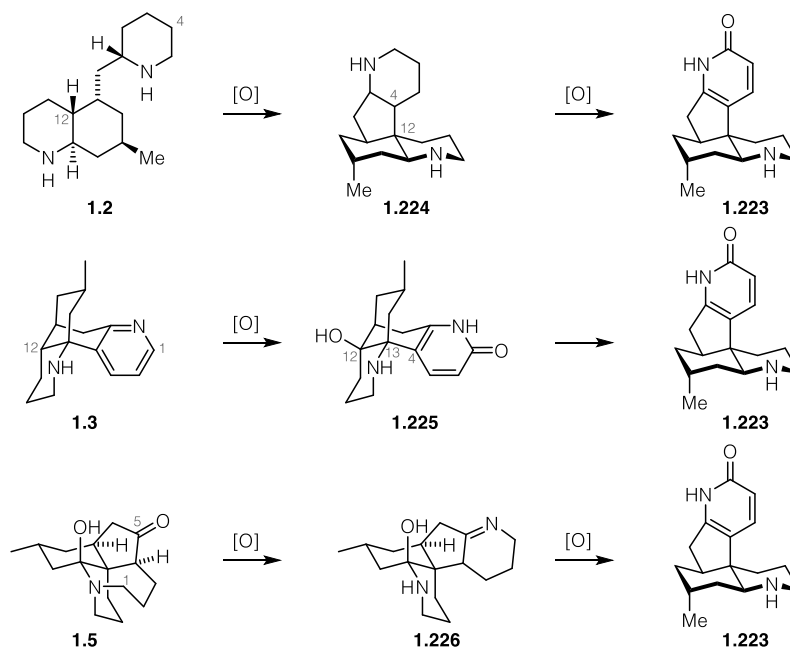
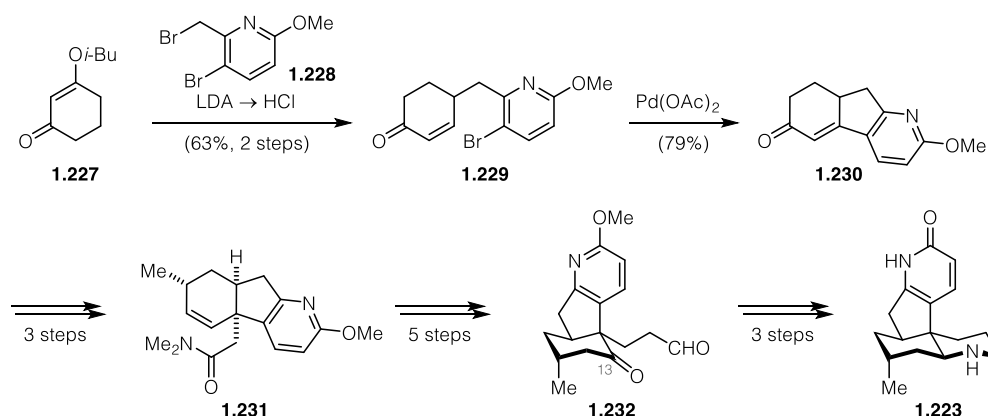


Figure 1.9. Proposed biosynthetic pathways for lycoposerramine R (**1.223**).

This would potentially occur through an oxidative coupling of two enamines. These oxidation states are known, but rare among the phlegmarine-type alkaloids.^[170-171] A second, more plausible pathway could be envisaged *via* lycodine (**1.3**): similar to the oxidation in the biosynthesis of lycopodine to fawcettimine, lycodine could be oxidized in the C-1 and C-12 positions, leading to C-12-oxygenated *N*-desmethyl- β -obscurine (**1.225**), a known *Lycopodium* alkaloid in its own right.^[172] A 1,2-shift followed by reduction of the resulting iminium ion would lead directly to lycoposerramine R. A third approach would start from fawcettimine (**1.5**) itself. N-C-1 bond scission followed by introduction of a second nitrogen atom and imine formation would lead to a compound like **1.226** that could give lycoposerramine R after redox manipulations.

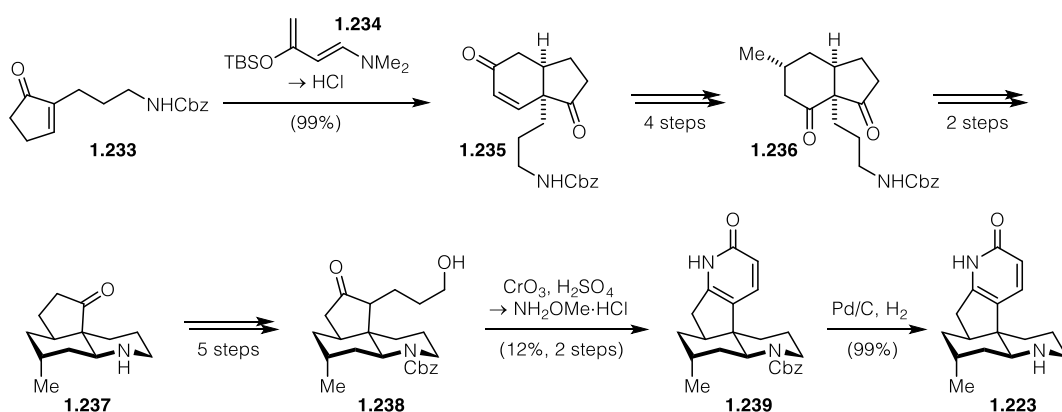
At the time of its isolation, lycoposerramine R (**1.223**) was the only fawcettimine-type alkaloid featuring a pyridone unit, a structural unit mostly limited to lycodine (**1.3**) natural products. It therefore came as no surprise that only one year after its publication, the first synthesis was documented by the Sarpong group.^[173] His approach was based on the realization that methoxypyridines serve as convenient synthetic equivalents of α -pyridones without the highly polar nature resulting from the strong hydrogen bonding, a concept previously explored in the context of the total synthesis of lyconadin A.^[162-163] In addition, methoxypyridines are aromatic and can therefore be used in reactions such as Heck couplings that are unavailable to α -pyridones. A Stork–Danheiser reaction between vinylogous ester **1.227** and pyridine **1.228** yielded enone **1.229**, setting up a Heck reaction that gave tricycle **1.230** in 79% yield.



Scheme 1.37. Sarpong's Heck- and Eschenmoser–Claisen-based approach to racemic lycoposerramine R (**1.223**).

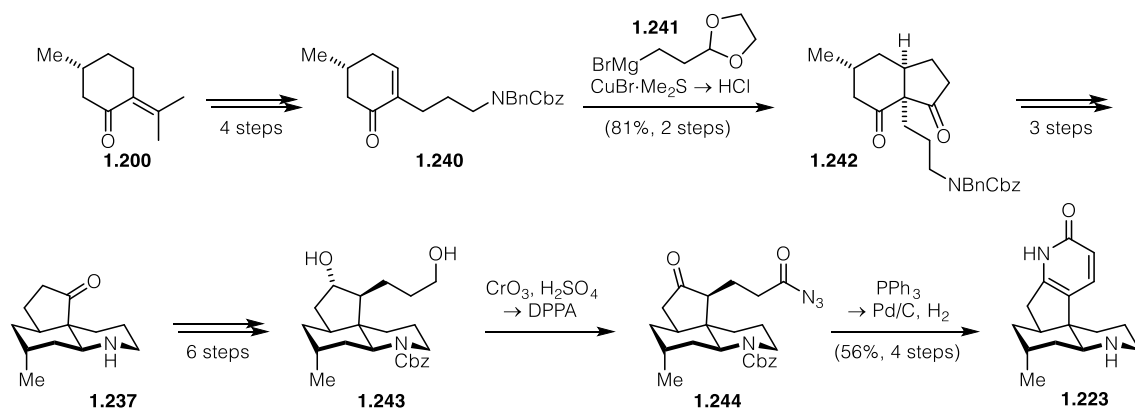
Three steps including a remarkably effective Eschenmoser–Claisen rearrangement were used to arrive at dimethylamide **1.231** bearing the quaternary stereocenter of lycoposerramine R. At that point, the side chain was homologated and the oxygenation at C-13 introduced over five steps. All that remained was a double reductive amination of ketoaldehyde **1.232** and final

methoxypyridine deprotection to complete the first synthesis of (\pm)-lycoposerramine R (**1.223**) in 13 steps from vinylogous ester **1.227**. Five years later, a second racemic and quite different synthesis of this alkaloid was published by the original isolation group.^[174] In contrast to Sarpong's approach, Takayama elected to construct the pyridone ring last and set the quaternary stereocenter in an intermolecular reaction. In a forward sense, enone **1.233** and Rawal diene **1.234** were reacted neat to give hydrindanone **1.235** after acid treatment. Wharton transposition followed by oxidation and conjugate addition of a methyl cuprate gave diketone **1.236**, bearing three of the four stereocenters present in lycoposerramine R (**1.223**).



Scheme 1.38. Takayama's first synthesis of lycoposerramine R (**1.223**) via Diels-Alder reaction.

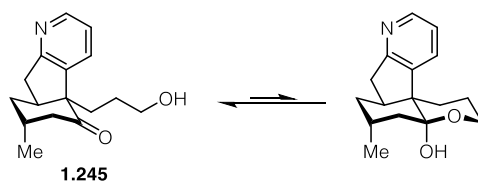
Interestingly, the following reductive amination was completely regio- and diastereoselective to give the tricyclic intermediate **1.237** featuring all the stereoinformation of the natural product. In order to append the pyridone, **1.237** was elaborated to δ -hydroxyketone **1.238**. Jones oxidation followed by heating the δ -ketoacid with *O*-methylhydroxylamine hydrochloride in acetic acid delivered the free pyridone **1.239** in low yield and, after Cbz deprotection, lycoposerramine R (**1.223**). Half a year later, Takayama published a second approach to the same target, delivering the first enantioselective synthesis of lycoposerramine R.^[175] While the general synthetic approach remained unchanged, the pyridone synthesis was revisited and the hydrindane was now supposed to be furnished by Helquist annulation. This cyclization had previously been established by Yang as an efficient entry into the fawcettimine series.^[176-178] Enone **1.240** was accessed in four steps from pulegone (**1.200**). Conjugate addition of Grignard reagent **1.241** followed by aqueous hydrochloric acid gave the hydrindane **1.242**. Four more steps including a reductive amination gave **1.237**, an intermediate of the racemic Takayama synthesis. Interestingly, the differentiation between the two ketones in the reductive amination was much less effective in this case, most probably a result of the slightly different protecting group pattern.



Scheme 1.39. Takayama's enantioselective second generation synthesis of lycoposerramine R (**1.223**).

Minor modifications of their previously reported procedures led to greater efficiency in the delivery of intermediate **1.243**. Given that the previous Knoevenagel-type pyridone synthesis had resulted in a very low yield, an interesting modification was made: the δ -ketoacid obtained by Jones oxidation was transformed into the acyl azide **1.244**, then submitted to Staudinger reduction to give a dihydropyridone that autooxidized during isolation. After deprotection, the absolute configuration of lycoposerramine R (**1.223**) could be established. With 54% over the final steps, this procedure provided a significant improvement.^[175]

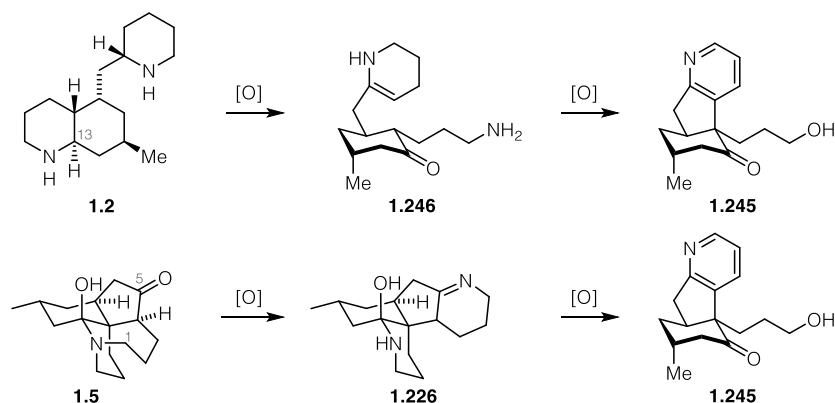
Three years before lycoposerramine R, lycopladine A (**1.245**) was isolated in Hokkaido from *Lycopodium complanatum* by Kobayashi and coworkers.^[179] Extensive 2D NMR and HRMS analysis suggested the presence of a disubstituted pyridine ring as well as 6-5-system bearing a primary alcohol and a ketone.



Scheme 1.40. Structure and ketone-hemiketal equilibrium of lycopladine A (**1.245**).

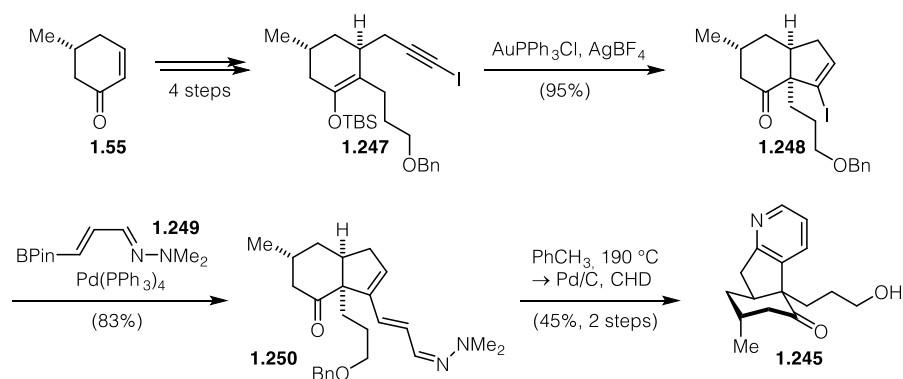
Careful analysis revealed a second minor compound in equilibrium with the main natural product. HMBC analysis of both compounds finally revealed that lycopladine A (**1.245**), whose structure is depicted in Scheme 1.40, occurs as a 7:1 mixture of open chain and hemiketal isomers. Biosynthetically, Kobayashi et al suggested a biosynthesis starting from phlegmarine (**1.2**) where the C-13-N bond is cleaved to **1.246** (Scheme 1.41). However, a detailed conversion of **1.246** into lycopladine A was not specified. One could also speculate about a biosynthesis that degrades the azonane ring of fawcettimine (**1.5**) by N-C-1 oxidation and

cleavage followed by transamination and condensation of the nitrogen with the C-5 carbonyl. Aromatization would yield the natural product.^[62]



Scheme 1.41. Plausible biosynthesis of lycopladine A (1.245).

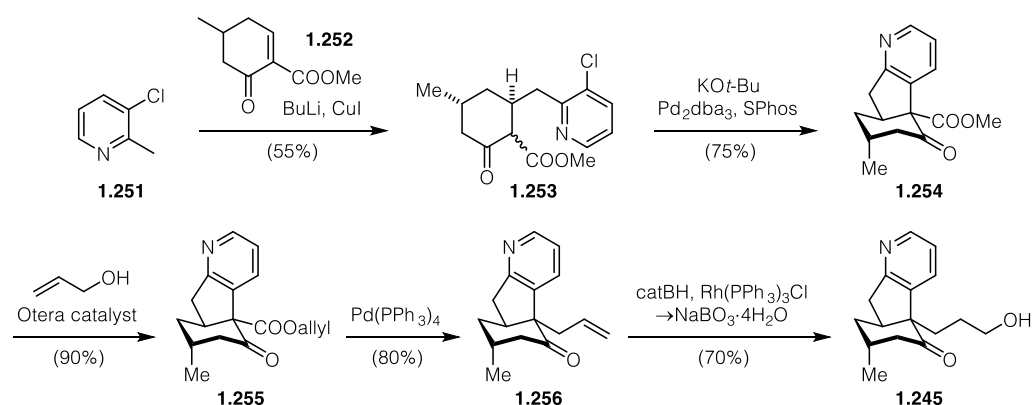
Remarkably, an enantioselective synthesis of lycopladine A was completed only three months later by Toste.^[55] Starting from Caine and Procter's popular pulegone-derived enantiopure enone **1.55**,^[58] three steps delivered iodoalkyne **1.247**, a substrate for a variation of the cyclization of enolate equivalents onto alkynes that Toste had previously developed.^[180-181] Treatment with $\text{AuPPh}_3\text{Cl}/\text{AgBF}_4$ delivered the hydrindane **1.248** in excellent yield within minutes, showcasing the ability of gold(I) to access different reaction manifolds than other d^{10} metals like $\text{Pd}(0)$. The reactivity of $\text{Pd}(0)$ was subsequently utilized for the synthesis of the pyridine ring by an interesting cascade. Cross-coupling with **1.249** gave hydrazone **1.250** which, upon heating to $190\text{ }^\circ\text{C}$, isomerized to the *cis*-isomer, then underwent 6π -electrocyclization followed by elimination of dimethylamine to furnish the pyridine moiety. Debenzylation under transfer hydrogenation conditions yielded (+)-lycopladine A (**1.245**) in 8 steps.



Scheme 1.42. Toste's use of a gold-catalyzed 5-*endo-trig* cyclization toward lycopladine A (1.245). CHD = 1,4-cyclohexadiene.

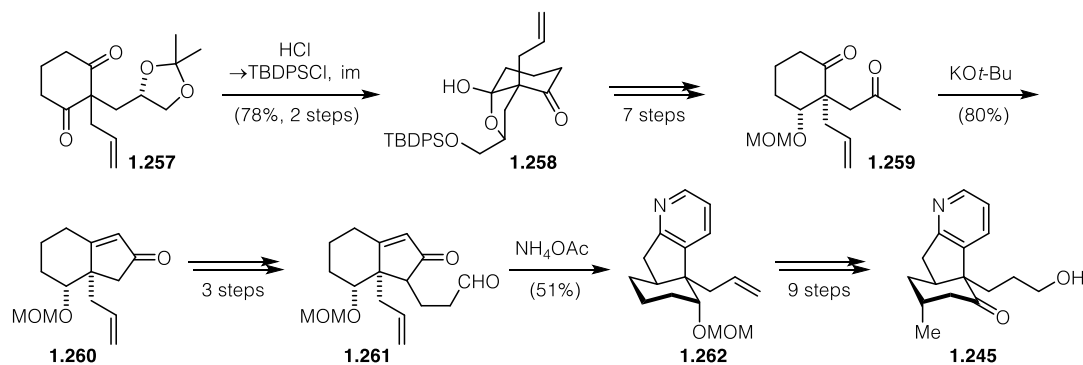
Four years later, Martin published the shortest synthesis of lycopladine A to date.^[182] Instead of building up the pyridine by aromatization from an aliphatic precursor, this fragment was

introduced by diastereoselective conjugate addition of a cuprate derived from 3-chloropicoline (**1.251**) to a known racemic enone (**1.252**) (Scheme 1.43). Treating the resulting with potassium tert-butoxide followed by a Pd-SPhos catalyst smoothly yielded the tricyclic core **1.254** of lycoplidine A. In order to introduce the quaternary stereocenter, a challenging transesterification was carried out and the resulting allyl ester **1.255** was submitted to decarboxylative allylation. In the last step of the synthesis, the double bond in **1.256** was hydroborated using catecholborane and Wilkinson's catalyst to yield (\pm)-lycoplidine A (**1.245**) in 5 steps from enone **1.252**.



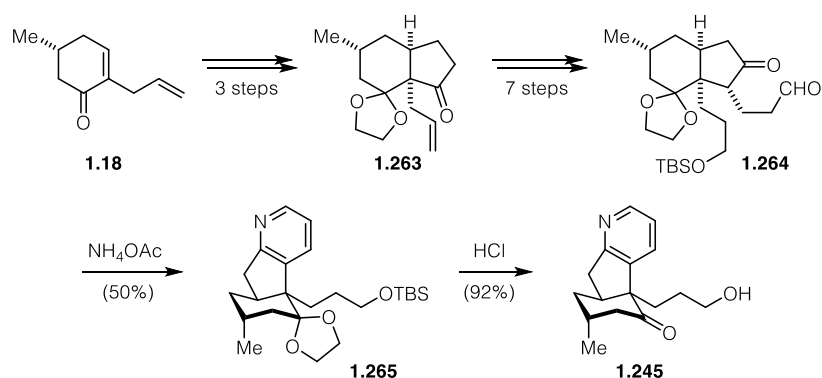
Scheme 1.43. Martin's enolate arylation strategy for a concise synthesis of lycoplidine A (**1.245**).

In 2011, a second asymmetric, methodology-based synthesis was described by the Hiroya group.^[183] The synthetic plan hinged on the differentiation of two carbonyls by diastereoselective ketalization.^[184] In the event, treatment of **1.257** with aqueous HCl led to almost exclusive formation of **1.258**. With the two groups differentiated, six further steps led to diketone **1.259**, which was cyclized to hydrindane **1.260** using potassium tert-butoxide. A number of steps delivered ketoaldehyde **1.261**, which delivered the pyridine **1.262** in a Kröhnke synthesis upon heating with NH₄OAc and spontaneous oxidation. Another eight steps were needed for introduction of the methyl group and functional group interconversions.



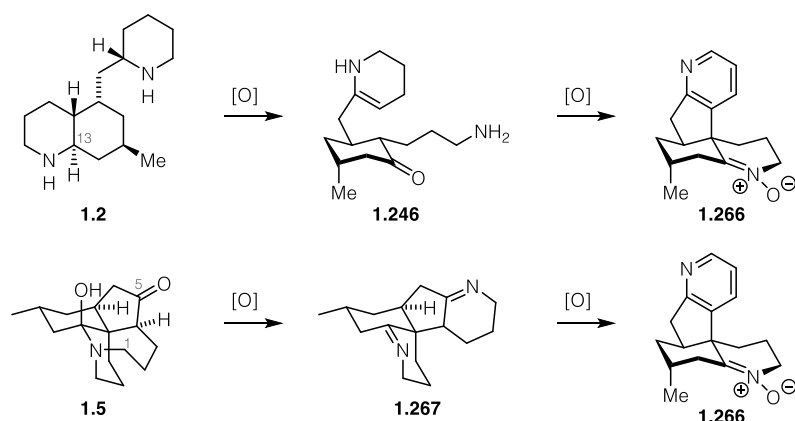
Scheme 1.44. A diastereomeric ketal differentiation used by Hiroya for lycoplidine A (**1.245**).

With 23 steps, it is the longest synthesis to date. Yang and coworkers published their approach toward (+)-lycopoladine A in 2013.^[185] A building block **1.263** that had previously been utilized in a (-)-8-deoxyserratinine synthesis served as the platform for their synthesis of lycopoladine A (**1.245**).^[177] With the quaternary stereocenter furnished by a Helquist annulation,^[176] most of the attention was focused on refunctionalizing the right-hand side. Seven steps furnished a ketoaldehyde **1.264** very similar to Hiroya's (**1.261**). Essentially identical conditions delivered the pyridine ring and, after global deprotection, lycopoladine A. This work highlights the challenges associated with refunctionalizing the five-membered ring.



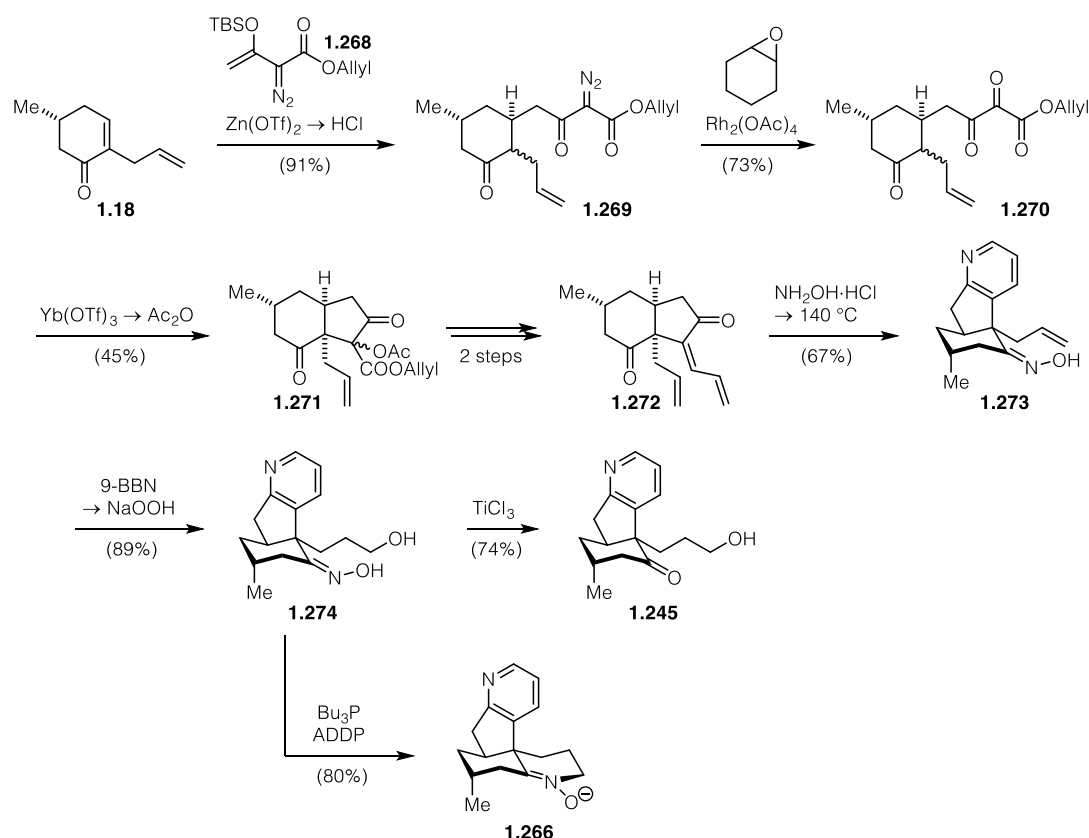
Scheme 1.45. Yang's Helquist annulation strategy to furnish the hydrindane of lycopoladine A (**1.245**).

Very recently, two very short syntheses have appeared. In 2016, Meng described a divergent enantioselective synthesis of (+)-lycopoladine A (**1.245**) and (-)-carinatine A (**1.266**), the first synthesis of this natural product (Scheme 1.47).^[186] Carinatine A was isolated in 2014 by Zhao from *Phlegmariurus carinatus*.^[187] Its fawcettimine-derived skeleton is remarkable insofar as it features both a pyridine and a cyclic nitron unit, structural elements otherwise most commonly found in phlegmarine- or lycodine-type *Lycopodium* alkaloids. Its biosynthesis is probably quite similar to lycopoladine A (Scheme 1.46). The first pathway would be identical to lycopoladine A (**1.245**) with the exception that the primary ring closes back on the C-13 ketone. A fawcettimine (**1.5**) pathway through C1-N fission followed by aromatization to the natural product is also plausible.



Scheme 1.46. Plausible biosynthetic pathways to carinatine A (1.266).

Starting from the same enone **1.18** as Yang, a Mukaiyama–Michael addition with **1.268** directly rendered **1.269** containing a functionalized sidechain. Rhodium-catalyzed oxidation of the diazo group gave a tricarbonyl **1.270** that could be aldolized and acetylated under Lewis-acidic conditions to **1.271**.

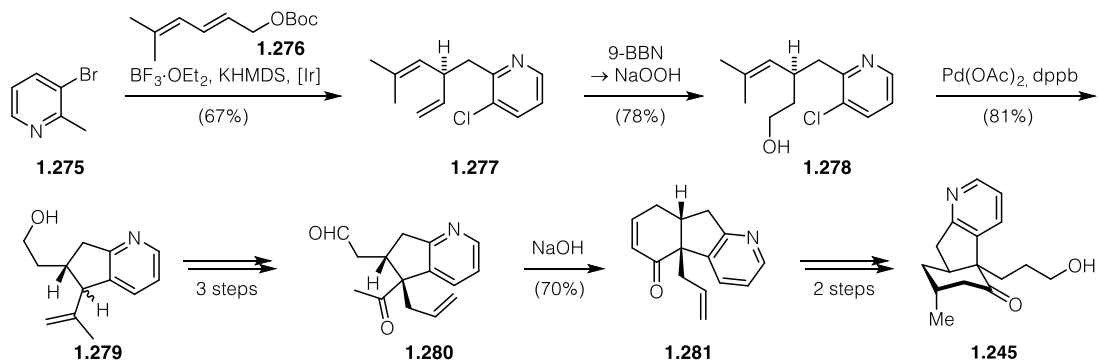


Scheme 1.47. Meng's late-stage divergent strategy for lycopladiene A (1.245) and carinatine A (1.266).

Strategically, the Yang and Meng syntheses bear some similarity, given the central quaternary stereocenter is formed *via* an aldol reaction that builds the hydrindane core of the targeted natural product. A decarboxylative allylation and elimination yielded dienone **1.272**, which was

then heated in a microwave with hydroxylamine, leading to 6π -electrocyclization and aromatization to **1.273**. Hydroboration-oxidation yielded the penultimate intermediate **1.274**. At this stage, a modified Mitsunobu reaction gave carinatine A (**1.266**) in good yield, whereas reductive oxime cleavage yielded lycopladine A (**1.245**). Meng's synthesis demonstrated how introducing an already functionalized sidechain can circumvent laborious functional group interconversions encountered in the Hiroya and Yang syntheses.

During the preparation of this thesis, another synthesis of lycopladine A, this time of the unnatural (-)-antipode, was disclosed by You.^[188] Conceptually quite different from all other syntheses, this methodology showcase is the only one to date that doesn't start with a functionalized cyclohexanone building block that serves as a template to forge all other rings. Instead, it starts with 3-bromopicoline (**1.275**) that acts as the nucleophile in an iridium-catalyzed enantioselective allylic substitution with allylic carbonate **1.276**. After hydroboration/oxidation of the terminal double bond to **1.278**, an intramolecular Heck reaction delivered the five-membered ring featuring an alkene (**1.279**) from which the ketone was liberated by ozonolysis. After the quaternary stereocenter had been set by allylation and the six-membered ring closed by aldol reaction, the tricyclic system **1.281** was complete.



Scheme 1.48. You's iridium chemistry for a conceptually different synthesis of lycopladine A (**1.245**).

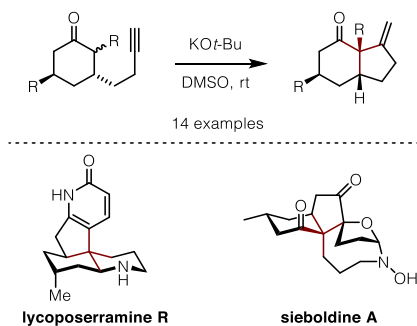
Finally, methylation and oxidation gave *ent*-lycopladine A (**1.245**) in 9 steps. It is remarkable that You's synthesis is the only catalytic enantioselective synthesis to date, as all others ultimately rely on enantiopure starting materials.

1.2.2 A Conia-Ene-type cyclization for the total synthesis of lycoposerramine R

Reprinted with permission from:

Felix W. W. Hartrampf, Takayuki Furukawa, Dirk Trauner, *Angew. Chem. Int. Ed.* **2017**, *56*, 893–896.

Copyright© 2017 John Wiley and Sons.



Total Synthesis

International Edition: DOI: 10.1002/anie.201610021
German Edition: DOI: 10.1002/ange.201610021

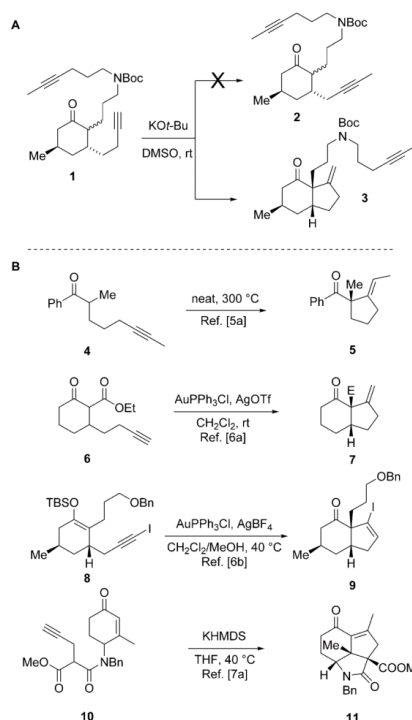
A Conia-Ene-Type Cyclization under Basic Conditions Enables an Efficient Synthesis of (–)-Lycoserramine R

Felix W. W. Hartrampf, Takayuki Furukawa, and Dirk Trauner*

Abstract: An enantioselective total synthesis of the Lycopodium alkaloid lycoserramine R is presented. It relies on a base-mediated cyclization that resembles the Conia-ene reaction of ynones and gold-catalyzed variants thereof. Thus, hydrindanones and other functionalized ring systems bearing an exocyclic alkene can be rapidly accessed at room temperature without noble metal catalysis or substrate preactivation.

Carbon–carbon triple bonds combine high enthalpies of formation and low steric hindrance with remarkable kinetic inertness, which can be overcome, however, through appropriate activation. As such, they are very useful functional groups for the construction of complex molecular frameworks in multistep syntheses.^[1] Indeed, alkynes have seen increasing use in synthesis, fueled by the development of transition-metal-catalyzed reactions that rely on the π -acidity of metals such as gold and platinum.^[2] Recently, alkyne metathesis reactions and stereoselective *trans*-additions to alkynes have further increased the synthetic value of these venerable functional groups.^[3]

Although their chemistry is now well developed, alkynes are occasionally found to react in unintended ways. During our studies towards the synthesis of lycopodium-type Lycopodium alkaloids, we sought to transform a terminal alkyne into an internal one under basic conditions.^[4] To this end, we treated compound **1** with three equivalents of potassium *tert*-butoxide in dimethyl sulfoxide and observed a clean reaction that went to completion within 30 minutes. The product, however, turned out to be *cis*-hydrindane **3** bearing an *exo*-methylene group instead of the intended internal alkyne **2** (Scheme 1 A). In essence, this cyclization represents a variant of the classic thermal Conia-ene reaction discovered in the 1970s (Scheme 1 B).^[5] This reaction occurs only under harsh thermal conditions (250–400 °C) due to the unfavorable equilibrium between the keto and enol tautomers. More recently, gold-catalyzed versions have emerged that require additional activation as a β -keto ester (**6**→**7**) or a silyl enol ether (**8**→**9**).^[6] Reports on transition metal free, base-



Scheme 1. Reaction discovery and previous related examples.

mediated carbocyclizations using unactivated alkynes are rare, with the notable exception of Dixon's study on *Daphniphyllum* alkaloids (**10**→**11**) and earlier work by Taguchi involving malonates.^[7] This prompted us to investigate our cyclization more systematically. We were also well aware that hydrindanes such as **3** would be of great interest for the synthesis of Lycopodium alkaloids, especially of the fawcettimine subclass.^[8]

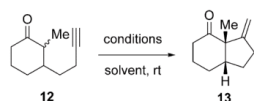
To identify the best conditions for the cyclization we chose ynone **12** as a model substrate. A screen of different bases in DMSO showed that potassium *tert*-butoxide was indeed the most efficient promoter of the reaction. Other bases such as potassium hydroxide, ethoxide, and hexamethyldisilazide provided the product in significantly lower yield (Table 1, entries 2–4) or gave rise to product mixtures. Other counterions proved inferior with respect to reaction times and yields

[*] F. W. W. Hartrampf, T. Furukawa, Prof. Dr. D. Trauner
Department of Chemistry
Ludwig-Maximilians-Universität München
Butenandtstrasse 5–13, 81377 München (Germany)
E-mail: dirk.trauner@lmu.de

T. Furukawa
Department of Applied Chemistry, Faculty of Engineering
Osaka University
Suita, Osaka 565-0871 (Japan)

Supporting information and the ORCID identification number for one of the authors of this article can be found under <http://dx.doi.org/10.1002/anie.201610021>.

Table 1: Reaction development.



Entry	Base	Equiv.	Solvent	Reaction time [h]	NMR yield [%] ^[a]
1	KO t -Bu	1.0	DMSO	0.5	71 (65)
2	KOEt	1.0	DMSO	0.5	65
3	KOH	1.0	DMSO	24	3
4	KHMDS	1.0	DMSO	5	57
5	NaO t -Bu	1.0	DMSO	2	47
6	LiO t -Bu	1.0	DMSO	16	0
7	KO t -Bu	0.2	DMSO	16	69
8	KO t -Bu ^[b]	0.2	DMSO	3	66
9	KO t -Bu	3.0	DMSO	0.5	56
10	KO t -Bu	1.0	DMF	16	18
11	KO t -Bu	3.0	THF	24	4
12	KO t -Bu	1.0	THF/DMSO (1:1)	1	70
13	KO t -Bu ^[c]	1.0	THF	16	6

[a] Yield of isolated product in brackets. [b] 0.2 equiv. 18-crown-6 was added. [c] 3.0 equiv. DMSO was added.

(entries 5 and 6), as did other solvents or solvent mixtures (entries 10–13). Substoichiometric amounts of base also led to clean product formation but did not improve the yields. The addition of 18-crown-6 improved the rate, but had little if any effect on the yield. Under all conditions surveyed, the *cis*-hydrindane **13** was the only diastereomer observable by ¹H NMR spectroscopy. To exclude possible catalysis from trace metals contained in the reagent or the substrate prepared via cuprate addition, we confirmed the absence of all metals commonly used in alkyne activation by ICP-AES.

With optimal conditions identified, we set out to investigate the scope and limitations of our method with a variety of substrates (Table 2). We typically used one equivalent of KO t -Bu in each case since it provided the cleanest reaction profile, unless stated otherwise. Cyclic ketones bearing various α -alkyl groups could be cyclized to afford compounds bearing a quaternary stereocenter (entries 1–5). As demonstrated in entries 4 and 5, both tertiary and secondary carbamates are tolerated. As an example of a nonterminal alkyne, alkynyl chloride **24** could be converted to the synthetically useful vinyl chloride **25**, which was obtained exclusively as the *cis* isomer. This matches Taguchi's analogous cyclization involving malonates.^[7b]

By substituting α -alkyl for α -aryl groups, benzylic quaternary stereocenters could be furnished as well (entries 8 and 9). Frameworks other than hydrindanes could also be accessed, such as the spiro compounds **23** and **31**. Notably, the pulegone-derived alkyne **22** cyclized smoothly to establish two adjacent quaternary carbons (entry 6) in good yield. We were also able to expand our method to heterocyclic systems. Oxindole **30** cleanly underwent the cyclization to give spiro compound **31**, whose single-crystal X-ray structure is shown in the Supporting Information. Tetrahydroquinolinone **32** was also a viable substrate, affording the functionalized tricycle **33**, albeit in moderate yield.

Table 2: Substrate scope.

Entry	Ynone	Product	Yield
1			62%
2			70%
3			61%
4			70%
5			62%
6			78% (1.3:1)
7			65%
8			28%
9			52%
10			75% ^[a]
11			40%

[a] 2.0 equiv. KO t -Bu was used. [b] NMR yield, preferably isolated as the Boc-protected oxindole. See the Supporting Information for details.

The reaction also worked well when cyclic ketones without α -substituents were used. In this case, the exocyclic double bonds isomerized under the basic conditions to yield conjugated enones, as had been observed previously by Dixon (Table 3).^[7a] Overall, this transformation is reminiscent of an

Table 3: Cyclization with concomitant double bond isomerization.

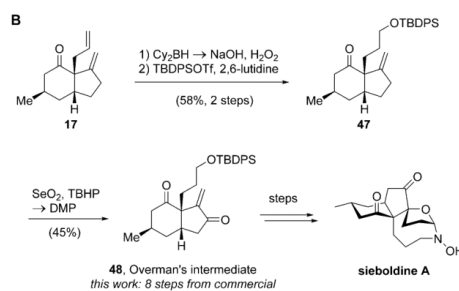
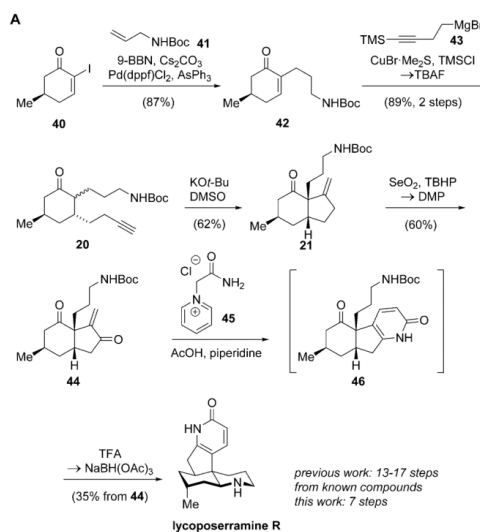
Entry	Ynone	Product	Yield
1			81% ^[a]
2			52%
3			62%

[a] 4:1 mixture of *exo/endo* isomers favoring the enone.

intramolecular aldol condensation, but it can be carried out with acid-sensitive substrates such as **34**.

With the insight gained from these substrates, we returned to our initial goal of developing a short synthesis of *Lycopodium* alkaloids. We deemed our hydrindanone synthesis well suited to access the fawcettimine family, in particular lycoposerramine R. This tetracyclic alkaloid, which bears four stereocenters including a quaternary one, was isolated by Takayama and co-workers from *Lycopodium serratum* in 2009.^[9] Due to its rather unusual structure, which also features an α -pyridone, it has attracted significant synthetic interest.^[10] This has so far resulted in racemic syntheses by the Sarpong^[10a] and Takayama^[10b] groups as well as an enantioselective synthesis by the latter.^[10c] The key quaternary stereocenter was set by Eschenmoser–Claisen, Diels–Alder, and alkylation reactions, respectively, in these studies. The total number of steps ranged from 13 for the shortest racemic synthesis to 17 for the enantioselective synthesis. We reasoned that our method would allow for a more rapid enantioselective synthesis starting from α -iodo ketone **40**, a popular building block in the synthesis of *Lycopodium* alkaloids.^[11] Our synthesis began with a *B*-alkyl Suzuki reaction of *N*-Boc-allylamine (**41**) and iodoenone **40**, delivering enone **42** in high yield.^[12] Cuprate addition of the known Grignard reagent **43** proceeded as planned, yielding the cyclization precursor **20** in very high overall yield after double desilylation (Scheme 2).

The ensuing cyclization furnished the desired hydrindanone **21** in 62% yield. Allylic oxidation of **21** to enone **44** could be carried out in a one-pot procedure using SeO₂/TBHP, followed by Dess–Martin oxidation. The transformation of the enone into an α -pyridone proved to be quite challenging due to competing decomposition under a variety of conditions.^[13] Eventually, a modification of the classic Kröhnke reaction gave the desired pyridone: heating enone **44** with acetamide derivative **45** for an extended time and at elevated temperature provided **46**, which was used directly in the ensuing steps.^[14] A Boc carbamate deprotection followed



Scheme 2. A) Total synthesis of lycoposerramine R; B) Synthesis of Overman's sieboldine A intermediate. See the Supporting Information for detailed procedures.

by reductive amination could be carried out as a one-pot procedure to give lycoposerramine R as a single diastereomer in 35% overall yield from enone **44**. Our synthetic compound was identical in all respects with the natural material isolated by Takayama.^[9] The key disconnection also proved useful in the synthesis of hydrindanone **17**, obtained with a route similar to **21**. Compound **17** was readily converted into enone **48** in three steps via hydrindanone **47**. This allowed us to intercept Overman's elegant route to sieboldine A,^[15] which hinges on Prins pinacol chemistry to furnish the hydrindane.^[16] With our route, intermediate **48** can be accessed in 8 steps from commercial starting materials, which compares favorably with the 16 steps of the original route.

In summary, a convenient base-mediated cyclization has been developed that gives access to useful polycyclic building blocks. The reaction is particularly well-suited for the construction of quaternary stereocenters next to carbonyl groups in a variety of ring systems. Notably, it occurs at room



temperature without the need for preactivation of the substrate or transition metal catalysis. The exact mechanism of this reaction remains to be determined and will be the subject of detailed analysis, both on the theoretical and the experimental level. We have successfully applied our methodology to the synthesis of lycoposerramine R, resulting in the most concise asymmetric synthesis to date (7 steps from a known iodoenone). In addition, an intermediate of Overman's sieboldine A synthesis was obtained, shortening the sequence significantly. Applications of this chemistry to the synthesis of other alkaloids are under investigation and will be reported in due course.

Acknowledgements

We thank Giulio Volpin, Nina Vrieling, Benjamin Williams, Dr. Bryan Matsuura and Dr. Hong-Dong Hao for helpful discussions during the preparation of this manuscript. We acknowledge Stephan Heß and Christian Steinborn for experimental assistance and JSPS for a JSPS Research Fellowship for Young Scientists for T. Furukawa.

Conflict of interest

The authors declare no conflict of interest.

Keywords: alkynes · Conia-ene reaction · hydrindanes · lycopodium alkaloids · total synthesis

How to cite: *Angew. Chem. Int. Ed.* **2017**, *56*, 893–896
Angew. Chem. **2017**, *129*, 912–915

- [1] a) B. Godoi, R. F. Schumacher, G. Zeni, *Chem. Rev.* **2011**, *111*, 2937–2980; b) U. Wille, *Chem. Rev.* **2013**, *113*, 813–853.
- [2] a) S. M. Abu Sohel, R.-S. Liu, *Chem. Soc. Rev.* **2009**, *38*, 2269–2281; b) R. Dorel, A. M. Echavarren, *Chem. Rev.* **2015**, *115*, 9028–9072.
- [3] a) A. Fürstner, *Angew. Chem. Int. Ed.* **2013**, *52*, 2794–2819; *Angew. Chem.* **2013**, *125*, 2860–2887; b) S. M. Rummelt, K. Radkowski, D.-A. Roşca, A. Fürstner, *J. Am. Chem. Soc.* **2015**, *137*, 5506–5519; c) B. M. Frost, Z. T. Ball, *Synthesis* **2005**, 853–887.
- [4] J. Chan, T. F. Jamison, *J. Am. Chem. Soc.* **2004**, *126*, 10682–10691.
- [5] a) R. Bloch, P. Le Perche, F. Rouessac, J. M. Conia, *Tetrahedron* **1968**, *24*, 5971–5989; b) J. M. Conia, P. Le Perche, *Synthesis* **1975**, *1975*, 1–19.
- [6] a) J. J. Kennedy-Smith, S. T. Staben, F. D. Toste, *J. Am. Chem. Soc.* **2004**, *126*, 4526–4527; b) S. T. Staben, J. J. Kennedy-Smith, D. Huang, B. K. Corkey, R. L. LaLonde, F. D. Toste, *Angew. Chem. Int. Ed.* **2006**, *45*, 5991–5994; *Angew. Chem.* **2006**, *118*, 6137–6140; c) D. Hack, M. Blumel, P. Chauhan, A. R. Philipps, D. Enders, *Chem. Soc. Rev.* **2015**, *44*, 6059–6093; for a related enamide cyclization in total synthesis, see: d) J. A. Kozak, G. R. Dake, *Angew. Chem. Int. Ed.* **2008**, *47*, 4221–4223; *Angew. Chem.* **2008**, *120*, 4289–4291.
- [7] a) C. Kourra, F. Klotter, F. Sladojevich, D. J. Dixon, *Org. Lett.* **2012**, *14*, 1016–1019; b) O. Kitagawa, T. Suzuki, H. Fujiwara, M. Fujita, T. Taguchi, *Tetrahedron Lett.* **1999**, *40*, 4585–4588; for other base-mediated reactions using alkynes, see: c) C. Koradin, A. Rodriguez, P. Knochel, *Synlett* **2000**, 1452–1454; d) K. Gao, J. Wu, *Org. Lett.* **2008**, *10*, 2251–2254; e) E. Dumez, A.-C. Durand, M. Guillaume, P.-Y. Roger, R. Faure, J.-M. Pons, G. Herbet, J.-P. Dulcère, D. Bonne, J. Rodriguez, *Chem. Eur. J.* **2009**, *15*, 12470–12488; f) S.-R. Li, C.-J. Shu, L.-Y. Chen, H.-M. Chen, P.-Y. Chen, E.-C. Wang, *Tetrahedron* **2009**, *65*, 8702–8707; g) B. A. Trofimov, E. Y. Schmidt, N. V. Zorina, E. V. Ivanova, I. A. Ushakov, *J. Org. Chem.* **2012**, *77*, 6880–6886; h) B. A. Trofimov, E. Y. Schmidt, I. A. Ushakov, N. V. Zorina, E. V. Skital'tseva, N. I. Protsuk, A. b. I. Mikhaleva, *Chem. Eur. J.* **2010**, *16*, 8516–8521; i) J. Weng, Y. Chen, B. Yue, M. Xu, H. Jin, *Eur. J. Org. Chem.* **2015**, 3164–3170.
- [8] R. A. Murphy, R. Sarpong, *Chem. Eur. J.* **2014**, *20*, 42–56.
- [9] K. Katakawa, N. Kogure, M. Kitajima, H. Takayama, *Helv. Chim. Acta* **2009**, *92*, 445–452.
- [10] a) V. Bisai, R. Sarpong, *Org. Lett.* **2010**, *12*, 2551–2553; b) H. Ishida, S. Kimura, N. Kogure, M. Kitajima, H. Takayama, *Tetrahedron* **2015**, *71*, 51–56; c) H. Ishida, S. Kimura, N. Kogure, M. Kitajima, H. Takayama, *Org. Biomol. Chem.* **2015**, *13*, 7762–7771.
- [11] a) D. Caine, K. Procter, R. A. Cassell, *J. Org. Chem.* **1984**, *49*, 2647–2648; b) T. L. Scott, B. C. G. Söderberg, *Tetrahedron* **2003**, *59*, 6323–6332; c) A. Carlone, M. Marigo, C. North, A. Landa, K. A. Jorgensen, *Chem. Commun.* **2006**, 4928–4930.
- [12] a) B. M. Trost, C. B. Lee, *J. Am. Chem. Soc.* **1998**, *120*, 6818–6819; for a review on B-alkyl Suzuki couplings, see: b) S. R. Chemler, D. Trauner, S. J. Danishefsky, *Angew. Chem. Int. Ed.* **2001**, *40*, 4544; *Angew. Chem.* **2001**, *113*, 4676.
- [13] a) T. Koshiba, S. Yokoshima, T. Fukuyama, *Org. Lett.* **2009**, *11*, 5354–5356; b) M. Fujii, T. Nishimura, T. Koshiba, S. Yokoshima, T. Fukuyama, *Org. Lett.* **2013**, *15*, 232–234; c) T. Nishimura, A. K. Unni, S. Yokoshima, T. Fukuyama, *J. Am. Chem. Soc.* **2013**, *135*, 3243–3247; d) R. Khajuria, P. Kannaboina, K. K. Kapoor, A. Gupta, G. Raina, A. K. Jassal, L. K. Rana, M. S. Hundal, P. Das, *Org. Biomol. Chem.* **2015**, *13*, 5944–5954; e) R. Boobalan, C. Chen, *Tetrahedron Lett.* **2016**, *57*, 1930–1934.
- [14] Y. Besidsky, K. Luthman, A. Claesson, C. J. Fowler, I. Csoregh, U. Hacksell, *J. Chem. Soc. Perkin Trans. 1* **1995**, 465–474.
- [15] Y. Hirasawa, H. Morita, M. Shiro, J. i. Kobayashi, *Org. Lett.* **2003**, *5*, 3991–3993.
- [16] a) S. M. Canham, D. J. France, L. E. Overman, *J. Am. Chem. Soc.* **2010**, *132*, 7876–7877; b) S. M. Canham, D. J. France, L. E. Overman, *J. Org. Chem.* **2013**, *78*, 9–34; for a different rearrangement-based approach towards sieboldine A, see: c) X.-M. Zhang, Y.-Q. Tu, F.-M. Zhang, H. Shao, X. Meng, *Angew. Chem. Int. Ed.* **2011**, *50*, 3916–3919; *Angew. Chem.* **2011**, *123*, 4002–4005; d) X.-M. Zhang, H. Shao, Y.-Q. Tu, F.-M. Zhang, S.-H. Wang, *J. Org. Chem.* **2012**, *77*, 8174–8181.

Manuscript received: October 13, 2016

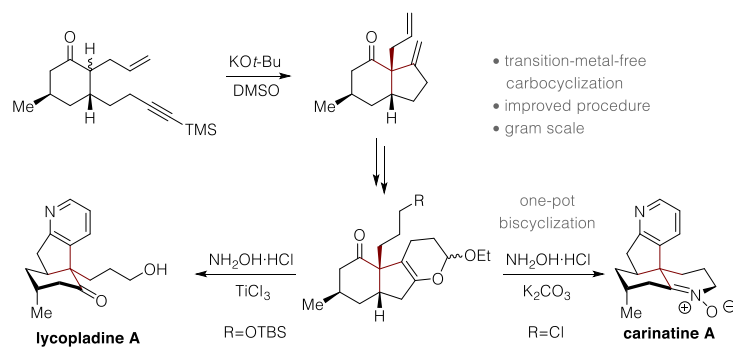
Final Article published: December 21, 2016

1.2.3 Total Synthesis of Lycopladine A and Carinatine A *via* a Base-mediated Carbocyclization

Reprinted with permission from:

Felix W. W. Hartrampf, Dirk Trauner, *J. Org. Chem.* **2017**, *82*, 8206–8212.

Copyright© 2017 American Chemical Society.



Total Synthesis of Lycopladine A and Carinatine A via a Base-Mediated Carbocyclization

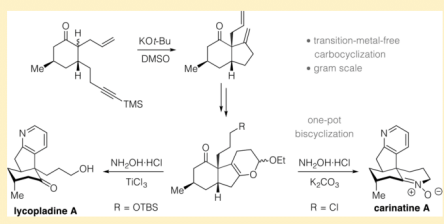
Felix W. W. Hartrampf[†] and Dirk Trauner^{*,†,‡}

[†]Department of Chemistry, Ludwig-Maximilians-Universität München, Butenandtstrasse 5-13, 81377 München, Germany

[‡]Department of Chemistry, New York University, 100 Washington Square East, Room 712, New York, New York 10003, United States

Supporting Information

ABSTRACT: A concise, enantioselective synthesis of lycopladine A and carinatine A is presented. Our synthetic approach hinges on the recently developed mild carbocyclization of yrones to furnish the hydrindane core of the alkaloids. Their pyridine ring was efficiently installed using the Ciufolini method. Both heterocycles of carinatine A, a rare naturally occurring nitrone, were formed in a single operation.



Club mosses, such as *Lycopodium complanatum* and *Lycopodium carinatum*, are a rich source of structurally attractive and bioactive alkaloids, a sample of which is shown in Figure 1.^{1–3} Lycposerramine R (1), which features a

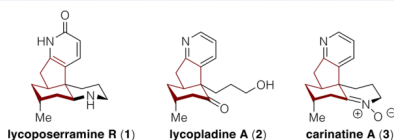


Figure 1. Alkaloids isolated from *Lycopodium serratum*, *L. complanatum*, and *L. carinatum*.

previously unknown skeleton with a pyridone and piperidine heterocycle, was isolated by Takayama and co-workers in 2009.⁴ Its simplified pyridine congener lycopladine A (2) was isolated from *L. complanatum* in 2006 and showed modest cytotoxicity against murine lymphoma cells.⁵ Carinatine A (3) was recently obtained from *L. carinatum*.⁶ Lycposerramine R (1), lycopladine A (2), and carinatine A (3) share a common carbocyclic core that consists of a *cis*-hydrindane with a methyl substituent and a three-carbon side chain. In lycposerramine R, this side chain is incorporated in the piperidine ring, which is oxidized to a nitrone in the case of carinatine A.

Because of their compact and beautiful structures, combined with some biological activity, these *Lycopodium* alkaloids have received a significant amount of attention from the synthetic community (Figure 2). Toste and co-workers⁷ accomplished the first synthesis of (+)-lycopladine A via a gold-catalyzed 5-*endo-dig* cyclization of a silyl enol ether onto an iodoalkyne. In 2010, Martin and co-workers⁸ accomplished the shortest

synthesis of (±)-lycopladine A via a palladium-catalyzed enolate arylation. In 2011, Hiroya et al.⁹ utilized a desymmetrization of a 1,3-cyclohexanedione via diastereoselective ketalization for an enantioselective synthesis. More recently, Yang and co-workers¹⁰ and Meng¹¹ developed aldol-based approaches to furnish the central quaternary stereocenter of (+)-lycopladine A. Because of the convergent nature of his approach, Meng was able to access the target in eight steps. The first synthesis of (+)-carinatine from a common intermediate was also reported, making use of a complex reaction cascade to furnish the pyridine ring from a dieneone. Very recently, Liu and You¹² published a conceptually different approach to (–)-lycopladine A. An Ir-catalyzed allylic substitution with a 2-methylpyridine nucleophile was utilized to set the first stereocenter. The five-membered ring was furnished with a Heck reaction, and finally, the six-membered ring was closed via aldol condensation.¹²

We now wish to report our own approach toward lycopladine A and carinatine A, which exploits the carbocyclization of yrones (4) recently developed in our laboratory (Scheme 1).¹³ Our method gives access to ring systems with a quaternary stereocenter next to a carbonyl group (5) and proceeds under mild basic conditions (KOt-Bu in DMSO at room temperature). It corresponds to the classic Conia–Ene reaction, which requires harsh thermal conditions, and modern transition metal-mediated variants thereof.^{14–18} As an initial demonstration of the utility of this cyclization, we completed a short enantioselective synthesis of the *Lycopodium* alkaloid lycposerramine R (1) as well as a formal synthesis of sieboldine A (6).^{4,19} The *exo*-alkene obtained in the key cyclization could be used to directly mount the pyridone

Received: April 15, 2017

Published: July 3, 2017

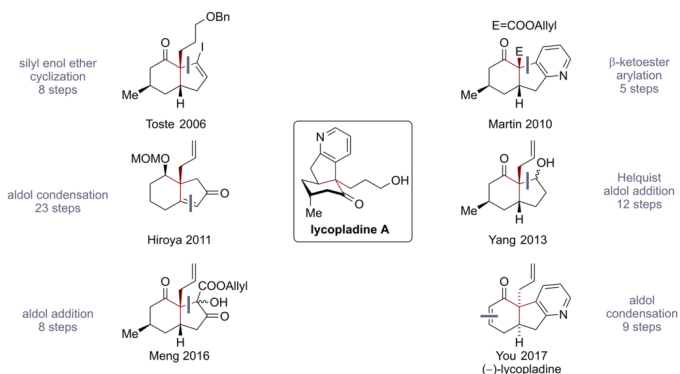
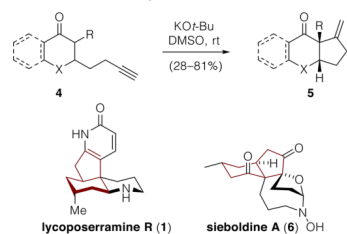


Figure 2. Previous approaches to the hydrindane core of lycopladine A with a total step count from known compounds.

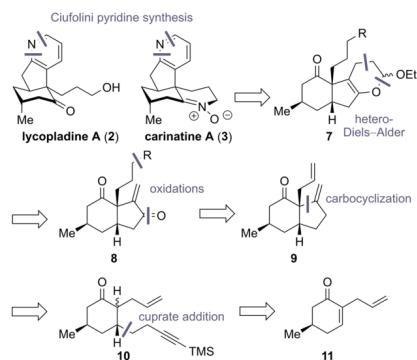
Scheme 1. Ynone Carbocyclization under Mild Conditions



moiety of lycoposerramine R, significantly reducing the total step count relative to those of earlier approaches.^{20–22}

Our retrosynthetic analysis of lycopladine A and carinatine A is shown in Scheme 2. We planned to furnish their characteristic pyridine ring using a Ciufolini pyridine synthesis involving an acetal 7, which could be obtained through a

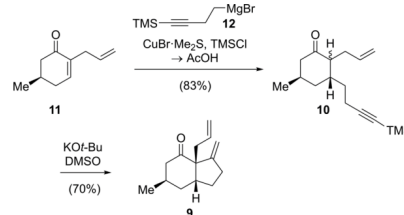
Scheme 2. Retrosynthetic Analysis of Lycopladine A and Carinatine A



hetero-Diels–Alder cycloaddition from an enone 8. The enone moiety would be installed through a selective allylic oxidation of hydrindane 9, which would be accessible via carbocyclization of 10.¹³ This compound, in turn, could be traced back to the known enone 11.^{23–25}

Hydrindanone 9, which had been previously described in the context of our formal synthesis of sieboldine A,¹³ was prepared on a gram scale using a shortened route (Scheme 3). Conjugate

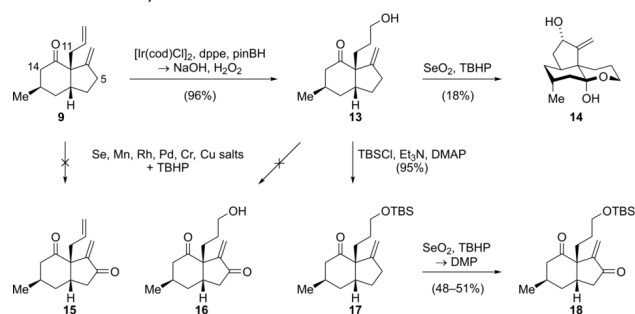
Scheme 3. Two-Step Procedure To Access Hydrindanone 9



addition of 12 followed by treatment with acetic acid gave TMS-protected alkyne 10. We reasoned that the cyclization conditions would rapidly remove the trimethylsilyl group. Therefore, we directly submitted 10 to the basic reaction conditions. Indeed, substoichiometric amounts of potassium *tert*-butoxide gave the desired product 9 in 70% yield. The hydrindanone core of the alkaloids featuring the central quaternary stereocenter could thus be obtained in two instead of three steps from enone 11.

To minimize protecting group manipulations, we first investigated whether direct allylic oxidation of this substrate was possible, anticipating the steric hindrance conferred by the quaternary stereocenter would lead to selective oxidation at C-5 over C-11 (Scheme 4). We subjected 9 to a wide range of allylic oxidation conditions but were never able to obtain more than traces of the desired product 15, which can be rationalized by competing Riley oxidation at C-14 or at the other allylic site (C-11). Since direct oxidation failed, we decided to reinvestigate the previously described hydroboration–oxidation

Scheme 4. Attempts To Oxidize the Cyclization Product 9

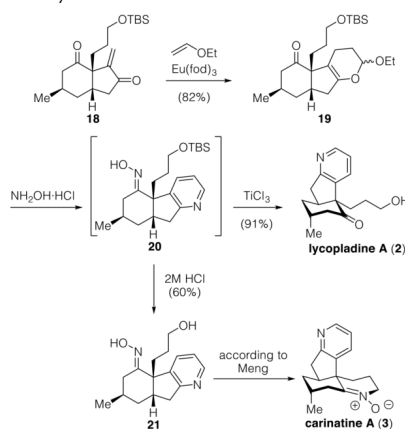


sequence to give **13**.¹³ While organoboranes such as Cy_2BH , Sia_2BH , $9-BBN$, $BH_3 \cdot SME_2$, and $BH_3 \cdot THF$ delivered the alcohol after oxidation with $NaOH/H_2O_2$ or sodium perborate, they proved to give low or variable yields on larger scale, as did reactions using Wilkinson's catalyst with catecholborane or pinacolborane. Eventually, we found that an iridium-based catalyst $\{[Ir(cod)Cl]_2/dppe\}$ in combination with pinacolborane²⁶ cleanly and rapidly gave an intermediate boronic ester (not isolated) that could be transformed to the alcohol in almost quantitative yield upon oxidative workup. Allylic oxidation of **13** using SeO_2 /*tert*-butyl hydroperoxide (TBHP) gave the tricyclic hemiacetal **14** in low yield. Interestingly, the cyclization occurred exclusively under these reaction conditions, whereas attempts to oxidize **13** to enone **16** with combinations of metal salts and TBHP mainly led to decomposition.

To our disappointment, we were unable to oxidize the allylic alcohol **14** further. Therefore, we decided to protect the hydroxy group in **13** as a silyl ether.²⁷ This transformation proved to be surprisingly difficult under standard conditions. Eventually, it was found that $TBSCl/Et_3N/DMAP$ in DMF at $-15^\circ C$ gave product **17** in excellent yield. After extensive screening of the subsequent allylic oxidation, we found that SeO_2 /TBHP furnished a mixture of allylic alcohol and ketone **18**, which was fully oxidized *in situ* using Dess–Martin periodinane (DMP). While the yield was moderate, it supplied ample material to finish our synthesis (Scheme 5). A hetero-Diels–Alder reaction with ethyl vinyl ether catalyzed by $Eu(fod)_3$ yielded acetal **19**,^{28,29} which was subsequently used to reach both lycopladiene A (**2**) and carinatine A (**3**). Treatment with hydroxylamine hydrochloride in refluxing acetonitrile furnished **20** *in situ*,²⁸ which was directly converted to lycopladiene A (**2**) through TBS deprotection and oxime cleavage with $TiCl_3$.³⁰ Our synthetic material, accessed in seven steps from enone **11**, was identical with the material obtained by isolation from natural sources in all respects.⁵

Having accomplished a total synthesis of lycopladiene A, we turned to the synthesis of carinatine A.⁶ When $TiCl_3$ was replaced with aqueous HCl, only the TBS group was removed to give **21** in moderate yield. This oxime could be converted to carinatine A (**3**) by Meng's method via a Mitsunobu-type reaction.¹¹ While this route provided a formal synthesis of the natural product, we wanted to probe a different, potentially more efficient route (Scheme 6). In an alternative end game, both the pyridine and the cyclic nitron would be closed in the

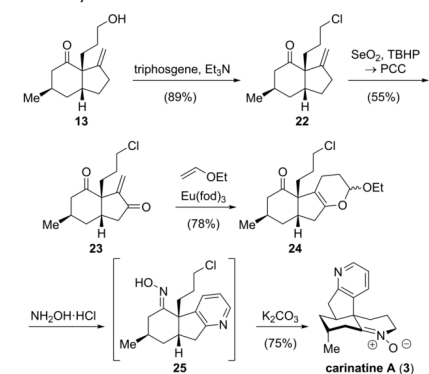
Scheme 5. End Game of the Lycopladine A Synthesis and Formal Synthesis of Carinatine A



same step. To this end, primary alcohol **13** was converted to chloride **22** using triphosgene and triethylamine,³¹ which outperformed classical $SOCl_2$ or Appel conditions. *In situ* oxidation of the allylic alcohol/enone mixture under our previously established conditions occurred in low yields when using DMP. However, pyridinium chlorochromate (PCC) smoothly gave the desired enone **23**.

With the enone in hand, we proceeded to the hetero-Diels–Alder reaction. Once more using ethyl vinyl ether and catalytic quantities of $Eu(fod)_3$, the enol acetal **24** was obtained in good yield. This enol acetal intermediate was then treated with hydroxylammonium chloride and refluxed in acetonitrile. After full conversion to the pyridine **25** had occurred, we added solid potassium carbonate and water.^{32,33} After 2 h at reflux, clean cyclization was observed and carinatine A (**3**) was isolated in 75% yield. Adding potassium carbonate from the start completely inhibited the pyridine synthesis, and very little oxime to nitron cyclization was observed in the absence of a base. In this way, we were able to access carinatine A in seven steps overall from enone **11**.

Scheme 6. Completion of the Synthesis of Carinatine A via Double Cyclization



In summary, we have used a recently developed carbocyclization reaction to access the two aromatic fawcettimine-type *Lycopodium* alkaloids, lycopladine A and carinatine A. In both cases, carefully choreographed reaction sequences that minimize protecting group manipulations allowed for the most concise, enantioselective routes to date. The Ciufolini method not only proved to be a powerful way to install the pyridine ring of the alkaloids but also was compatible with concomitant oxime hydrolysis and nitrone formation.

EXPERIMENTAL SECTION

All reactions were performed with standard Schlenk techniques under an atmosphere of nitrogen in oven-dried glassware (100 °C oven temperature) that was further dried using a heat gun (set to 650 °C) for all water-sensitive reactions. Tetrahydrofuran (THF) and diethyl ether (Et₂O) were distilled over sodium and benzophenone prior to use. Triethylamine (Et₃N) and dichloromethane (CH₂Cl₂) were distilled from calcium hydride. *N,N*-Dimethylformamide (DMF), acetonitrile (MeCN), and methanol (MeOH) were purchased from Acros Organics as "extra dry" reagents under an inert gas atmosphere and over molecular sieves. All other reagents were purchased from commercial sources and used without further purification. Reaction progress was monitored by analytical thin-layer chromatography (TLC), which was performed using precoated glass plates (silica gel 60 F₂₅₄) from Merck. Visualization was achieved by exposure to ultraviolet light (254 nm) where applicable followed by staining with a potassium permanganate solution. Flash column chromatography was performed using Merck silica gel (40–63 μm particle size). Proton nuclear magnetic resonance (¹H NMR) spectra were recorded on a Varian 400, Inova 400, or Varian 600 spectrometer. Chemical shifts (δ scale) are expressed in parts per million and calibrated using a residual protic solvent as an internal reference (CHCl₃, δ 7.26; CD₂HOD, δ 3.31). Data for ¹H NMR spectra are reported as follows: chemical shift (ppm) [multiplicity, coupling constants (hertz), integration]. Couplings are expressed as follows: s, singlet; d, doublet; t, triplet; q, quartet; m, multiplet; or combinations thereof. Carbon nuclear magnetic resonance (¹³C NMR) spectra were recorded on the same spectrometers at 100 and 150 MHz (±1 MHz variance). Carbon chemical shifts (δ scale) are also expressed in parts per million and are referenced to the central carbon resonances of the solvents (CDCl₃, δ 77.16; MeOH-*d*₄, δ 49.00). To assign the ¹H and ¹³C NMR spectra, a range of two-dimensional NMR experiments (COSY, HMQC, HMBC, and NOESY) was used as appropriate. Infrared (IR) spectra were recorded on a PerkinElmer Spectrum BX II instrument (FTIR

System) equipped with an attenuated total reflection (ATR) measuring unit. IR data are reported in frequency of absorption (inverse centimeters). Mass spectroscopy (MS) experiments were performed on a Thermo Finnigan MAT 95 (electron ionization double-focusing magnetic sector instrument, abbreviated as EI in this section) or on a Thermo Finnigan LTQ FT (electrospray ionization ion trap-based Fourier transform ion cyclotron resonance mass spectrometer, abbreviated as ESI in this section) instrument.

(5*R*)-2-Allyl-5-methyl-3-[4-(trimethylsilyl)but-3-yn-1-yl]-cyclohexan-1-one (10). Four drops of 1,2-dibromoethane were added to Mg chips (305 mg, 12.6 mmol, 4.00 equiv) in THF (20 mL), and the mixture was heated to reflux for 5 s. After the mixture had cooled to room temperature, (4-bromobut-1-yn-1-yl)trimethylsilane (1.61 g, 7.85 mmol, 2.5 equiv) was added dropwise. The reaction mixture was stirred at 50 °C for 1 h and then slowly cooled to –78 °C. CuBr·SMe₂ (132 mg, 0.63 mmol, 0.20 equiv) was added in one portion, and after the mixture had been stirred for 15 min, enone **11** (473 mg, 3.14 mmol, 1.00 equiv) in THF (12 mL), TMSCI (0.82 mL, 6.28 mmol, 2.0 equiv), and HMPA (1.10 mL, 6.28 mmol, 2.0 equiv) were added sequentially to the brown suspension. The reaction mixture was stirred for 2.0 h at –78 °C, then acetic acid (5 mL) was added and the cooling bath removed. The reaction mixture was stirred for 3 h before H₂O (20 mL) was added. The mixture was extracted with Et₂O (3 × 60 mL), and the combined organic layers were washed with saturated aqueous NaCl (30 mL), dried over MgSO₄, and concentrated. The obtained brown oil was purified by column chromatography (7:1 pentane:Et₂O) to give ketone **10** as a variable mixture of diastereomers (713 mg, 2.58 mmol, 83%); *R*_f = 0.66 (5:1 hexane:EtOAc); ¹H NMR (400 MHz, CDCl₃) δ 5.80–5.63 (m, 1H), 5.12–4.93 (m, 2H), 2.58–2.43 (m, 1H), 2.38 (t, *J* = 7.0, 2H), 2.34–2.18 (m, 3H), 2.18–1.88 (m, 4H), 1.72–1.58 (m, 2H), 1.53–1.41 (m, 1H), 1–0.99 (2 d, *J* = 5.9 and 5.7, 3H), 0.14 (s, 9H); ¹³C NMR (101 MHz, CDCl₃) δ 213.7, 136.4, 135.6, 116.9, 116.4, 106.5, 85.3, 54.4, 53.8, 50.3, 47.4, 37.4, 36.4, 34.5, 33.5, 32.1, 30.0, 29.6, 22.4, 21.7, 17.7, 0.3 (note that due to extensive signal overlap, the carbon count does not add up to two full sets of carbons); IR (ATR) 2956, 2926, 2174, 1710, 1641, 1456, 1334, 1249, 1003, 913, 841, 760 cm^{–1}; HRMS (ESI) *m/z* [M – H][–] calcd for C₁₇H₂₇O₂Si 275.1826, found 275.1826.

(3*S*,6*R*,7*aR*)-3*a*-Allyl-6-methyl-3-methylenecyclohexa-4*H*-inden-4-one (9). To KOt-Bu (406 mg, 3.60 mmol, 0.70 equiv) in DMSO (40 mL) was added **10** (1.43 g, 5.16 mmol, 1.00 equiv) in DMSO (20 mL) over 3 min. After 10 min, the dark-brown reaction mixture was diluted with Et₂O (50 mL) and cooled with an ice bath before pH 5.5 phosphate buffer (40 mL) was added dropwise. The phases were separated, and the aqueous phase was extracted with Et₂O (2 × 60 mL). The combined organic phases were washed with saturated aqueous NaCl (50 mL), dried over MgSO₄, and concentrated. The brown oil was purified by column chromatography (11:1 pentane:Et₂O) to give **9** (1.00 g, 3.62 mmol, 70%) as a yellow oil; *R*_f = 0.74 (5:1 hexane:EtOAc); ¹H NMR (400 MHz, CDCl₃) δ 5.71 (dddd, *J* = 19.9, 9.4, 8.1, 6.3, 1H), 5.08–5.03 (m, 1H), 5.03 (t, *J* = 2.1, 2H), 4.80 (t, *J* = 2.5, 1H), 2.64 (ddt, *J* = 13.9, 6.3, 1.1, 1H), 2.53 (dddd, *J* = 22.9, 11.5, 5.2, 2.8, 3H), 2.41 (ddd, *J* = 16.9, 9.5, 4.9, 2.3, 1H), 2.26–2.17 (m, 1H), 2.17–2.11 (m, 1H), 2.08 (ddd, *J* = 14.7, 6.4, 1.3, 1H), 1.92–1.78 (m, 1H), 1.69 (ddd, *J* = 12.6, 8.6, 3.8, 1H), 1.61–1.43 (m, 2H), 0.94 (d, *J* = 6.9, 3H); HRMS (EI) *m/z* [M]⁺ calcd for C₁₄H₂₀O 204.1509, found 204.1507. The analytical data were in good agreement with literature values.¹³

(3*S*,6*R*,7*aR*)-3*a*-(3-Hydroxypropyl)-6-methyl-3-methylenecyclohexa-4*H*-inden-4-one (13). To **9** (223 mg, 1.09 mmol, 1.00 equiv) in CH₂Cl₂ (12 mL) was added [Ir(cod)Cl]₂ (36 mg, 55 μmol, 0.05 equiv) followed by dppe (43 mg, 109 μmol, 0.10 equiv) to give a green solution. After 10 min, dropwise addition of pinBH (190 μL, 1.31 mmol, 1.20 equiv) gave a yellow solution. After further stirring for 25 min, the reaction mixture was cooled to 0 °C before 2 M NaOH (2.4 mL) and 30% aqueous H₂O₂ (2.4 mL) were added under vigorous stirring, resulting in a dark-gray suspension. After 1 h, the biphasic mixture was diluted with Et₂O (20 mL) and H₂O (10 mL), then saturated aqueous NH₄Cl (5 mL) was added. The aqueous phase was extracted with Et₂O (3 × 10 mL), and the combined organic

phases were washed with saturated aqueous NaCl (15 mL), dried over MgSO_4 , and concentrated. The greenish oil was purified by column chromatography (2:1 \rightarrow 1:1 pentane:Et₂O) to give the desired alcohol **13** (232 mg, 1.05 mmol, 96%) as a viscous colorless oil: $R_f = 0.44$ (1:1 hexane:EtOAc); ¹H NMR (600 MHz, CDCl₃) δ 5.00 (t, $J = 2.1$, 1H), 4.74 (t, $J = 2.4$, 1H), 3.66–3.56 (m, 2H), 2.58–2.34 (m, 4H), 2.25–2.18 (m, 1H), 2.07 (ddd, $J = 14.9$, 6.4, 1.4, 1H), 1.91–1.81 (m, 2H), 1.70 (ddd, $J = 13.8$, 8.5, 3.8, 1H), 1.64 (s, 1H), 1.60–1.46 (m, 5H), 0.96 (d, $J = 6.9$, 3H); ¹³C NMR (151 MHz, CDCl₃) δ 212.9, 153.9, 108.5, 63.2, 63.1, 46.0, 42.6, 34.3, 31.6, 30.3, 29.6, 29.0, 28.6, 20.2; IR (ATR) 3383, 2949, 2872, 1697, 1646, 1457, 1382, 1333, 1217, 1054, 886, 801 cm⁻¹; HRMS (ESI) m/z [M + H]⁺ calcd for C₁₄H₂₃O₂ 223.1693, found 223.1693; $[\alpha]_D^{20} = -21$ (c 0.7, CH₂Cl₂).

(4aS,7aS,9R,10aS)-9-Methyl-5-methylenecyclohexane-2H-cyclopentane[chromene-6,10a(5H)]-diol (14). To a solution of **13** (16 mg, 70 μmol , 1.0 equiv) in CH₂Cl₂ (0.7 mL) was added SeO₂ (7.8 mg, 70 μmol , 1.0 equiv) followed by TBHP (5.5 M in decane, 63 μL , 0.35 mmol, 5.0 equiv). The reaction mixture was stirred at room temperature for 15 h before H₂O (2 mL) was added. The aqueous phase was extracted with EtOAc (3 \times 5 mL), and the combined organic phases were washed with saturated aqueous Na₂S₂O₃ (5 mL), dried over MgSO₄, and concentrated. Purification of the yellow oil by flash column chromatography (3:1 pentane:Et₂O) yielded **14** as a colorless oil (3.0 mg, 13 μmol , 18%); $R_f = 0.60$ (1:1 hexane:EtOAc); ¹H NMR (400 MHz, CDCl₃) δ 4.99 (s, 1H), 4.75 (s, 1H), 4.41 (s, 1H), 3.85 (dd, $J = 12.1$, 5.2, 1H), 3.60 (td, $J = 12.4$, 2.7, 1H), 2.03 (q, $J = 7.5$, 5.6, 3.8, 2H), 1.94–1.83 (m, 3H), 1.77 (td, $J = 11.7$, 10.7, 1.8, 1H), 1.70–1.58 (m, 3H), 1.48 (dt, $J = 13.9$, 3.9, 1H), 1.44–1.36 (m, 1H), 1.11 (td, $J = 13.0$, 3.3, 1H), 0.96 (d, $J = 6.6$, 3H); ¹³C NMR (101 MHz, CDCl₃) δ 154.2, 103.8, 99.5, 64.0, 47.4, 38.0, 36.2, 34.7, 32.7, 24.3, 22.5, 21.8, 20.9; IR (ATR) 2982, 2958, 1718, 1646, 1465, 1367, 1294, 1257, 1176, 1152, 1095, 1032, 978, 774 cm⁻¹; HRMS (ESI) m/z [M – H₂O + H]⁺ calcd for C₁₄H₂₁O₂ 221.1536, found 221.1537; $[\alpha]_D^{20} = -10$ (c 0.2, CH₂Cl₂).

(3aS,6R,7aR)-3a-(3-[(tert-Butyldimethylsilyloxy)propyl]-6-methyl-3-methylenecyclohexane-4H-inden-4-one (17). To a solution of **13** (60 mg, 0.27 mmol, 1.0 equiv) in DMF (5 mL) at –15 °C was added Et₃N (46 μL , 0.34 mmol, 1.3 equiv) followed by DMAP (3.4 mg, 28 μmol , 0.10 equiv) and TBSCl (44 mg, 0.30 mmol, 1.1 equiv). After 15 min at –15 °C, the reaction mixture was diluted with Et₂O (5 mL) and 1 M HCl (2 mL). The aqueous phase was extracted with Et₂O (3 \times 15 mL), and the combined organic phases were washed with 10% aqueous LiCl (2 \times 10 mL) and saturated aqueous NaCl (10 mL), dried over MgSO₄, and concentrated to give the desired product **17** as a colorless oil (43 mg, 0.25 mmol, 95%). Note that the crude yield takes into account the presence of traces of DMF that did not hamper subsequent reactions. An analytically pure sample was obtained using column chromatography (11:1 pentane:Et₂O): $R_f = 0.76$ (5:1 hexane:EtOAc); ¹H NMR (600 MHz, CDCl₃) δ 5.03 (t, $J = 2.2$, 1H), 4.78 (t, $J = 2.5$, 1H), 3.63–3.52 (m, 2H), 2.55–2.42 (m, 3H), 2.40–2.33 (m, 1H), 2.19 (qt, $J = 7.6$, 4.5, 1H), 2.09 (ddd, $J = 14.6$, 7.7, 1.1, 1H), 1.85–1.75 (m, 2H), 1.71 (dddd, $J = 13.9$, 7.3, 3.9, 1.0, 1H), 1.60–1.44 (m, 5H), 0.97 (d, $J = 6.9$, 3H), 0.89 (s, 9H), 0.05–0.02 (m, 6H); ¹³C NMR (151 MHz, CDCl₃) δ 212.5, 153.5, 108.6, 63.5, 62.9, 46.4, 43.0, 34.1, 31.8, 30.5, 29.5, 28.7, 28.6, 26.1, 20.7, 18.5, –5.1; IR (ATR) 2952, 2928, 2362, 2340, 1702, 1647, 1472, 1462, 1384, 1254, 1208, 1097, 1006, 989, 938, 889, 834, 813, 775 cm⁻¹; HRMS (ESI) m/z [M + H]⁺ calcd for C₂₀H₃₇O₂Si 337.2557, found 337.2560; $[\alpha]_D^{20} = -2.0$ (c 2.5, CH₂Cl₂).

3a-(3-[(tert-Butyldimethylsilyloxy)propyl]-6-methyl-3-methylenecyclohexane-1H-indene-2,4-dione (18). SeO₂ (50 mg, 0.45 mmol, 2.5 equiv) and a TBHP solution (5.5 M in decane, 0.16 mL, 0.90 mmol, 5.0 equiv) were added to **17** (44 mg, 0.18 mmol, 1.0 equiv) in CH₂Cl₂ at 0 °C. The mixture was stirred at room temperature for 17 h. At this point, the reaction mixture was cooled to 0 °C before DMP (58 mg, 0.27 mmol, 1.5 equiv) was added to the reaction mixture. Stirring was continued for 1 h at the same temperature. Thereafter, a mixture (1:1, 2 mL) of saturated aqueous NaHCO₃ and saturated aqueous Na₂S₂O₃ was added, and the reaction mixture was stirred vigorously at room temperature. Afterward, H₂O

(5 mL) and CH₂Cl₂ (5 mL) were added and the phases separated. Following extraction of the aqueous phase with CH₂Cl₂ (2 \times 5 mL), the combined organic phases were washed with saturated aqueous NaCl (5 mL), dried over MgSO₄, and concentrated. The residue was purified by flash column chromatography (5:1 pentane:Et₂O) to yield **18** as a colorless oil (33 mg, 92 μmol , 51%); $R_f = 0.42$ (5:1 hexane:EtOAc); ¹H NMR (600 MHz, CDCl₃) δ 6.23 (s, 1H), 5.30 (s, 1H), 3.66–3.48 (m, 2H), 2.71 (p, $J = 6.8$, 1H), 2.56–2.42 (m, 2H), 2.26–2.11 (m, 3H), 1.93 (ddd, $J = 13.5$, 11.9, 4.7, 1H), 1.80–1.65 (m, 3H), 1.50 (m, 2H), 1.04 (d, $J = 6.3$, 3H), 0.88 (s, 9H), 0.03 (s, 6H); ¹³C NMR (151 MHz, CDCl₃) δ 210.6, 204.4, 146.6, 121.2, 62.9, 60.2, 46.0, 42.2, 36.7, 34.3, 32.1, 28.5, 28.3, 26.1, 21.0, 18.4, –5.2; IR (ATR) 2982, 2958, 1718, 1646, 1465, 1367, 1294, 1257, 1176, 1152, 1095, 1032, 978, 774 cm⁻¹; HRMS (ESI) m/z [M + H]⁺ calcd for C₂₀H₃₅O₃Si 351.2350, found 351.2351; $[\alpha]_D^{20} = 59$ (c 1.1, CH₂Cl₂).

(4bS,7R,8aS)-4b-(3-[(tert-Butyldimethylsilyloxy)propyl]-2-ethoxy-7-methyl-3,4,4b,6,7,8,8a,9-octahydroindeno[2,1-b]pyran-5(2H)-one (19). **18** (18 mg, 52 μmol , 1.0 equiv) was dissolved in 1,2-dichloroethane (0.5 mL) and ethyl vinyl ether (0.5 mL) before Eu(fod)₃ (5.0 mg, 5.2 μmol , 0.10 equiv) was added in one portion. The solution was stirred at 50 °C for 20 h, concentrated, and directly loaded on a florisil column (7:1 pentane:Et₂O) to give **19** (18 mg, 43 μmol , 82%) as a colorless oil: $R_f = 0.62$ (5:1 hexane:EtOAc); ¹H NMR (600 MHz, C₆D₆) δ 4.86 (ddd, $J = 13.1$, 3.8, 2.5, 1H), 3.87–3.74 (m, 1H), 3.66–3.49 (m, 2H), 3.43–3.30 (m, 1H), 2.61–2.43 (m, 1H), 2.41–2.02 (m, 4H), 1.93–1.71 (m, 5H), 1.67–1.43 (m, 2H), 1.35–1.24 (m, 1H), 1.18–1.02 (m, 5H), 1.00 (m, 9H), 0.69–0.62 (m, 3H), 0.09 (m, 6H) (note that due to extensive signal overlap, the integral sum is 41, not 42); ¹³C NMR (101 MHz, C₆D₆) δ 212.9, 212.3, 150.3, 150.0, 110.7, 110.3, 98.6, 63.9, 61.3, 47.2, 46.9, 39.1, 38.8, 37.3, 37.3, 37.1, 36.7, 31.7, 31.6, 28.3, 28.3, 27.3, 26.2, 25.9, 22.3, 22.2, 18.6, 16.7, 16.6, 15.6, 15.5, –5.0, –5.1 (note that due to extensive signal overlap, two full sets of signals could not be observed); IR (ATR) 2926, 2853, 1689, 1455, 1382, 1340, 1296, 1212, 1115, 1045, 968, 934, 849, 732 cm⁻¹; HRMS (ESI) m/z [M + H]⁺ calcd for C₂₄H₄₁O₅Si 423.2925, found 423.2927.

(4bS,7R,8aS,E)-4b-(3-Hydroxypropyl)-7-methyl-4b,6,7,8,8a,9-hexahydro-5H-indeno[2,1-b]pyridin-5-one Oxime (21). NH₂OH·HCl (9.4 mg, 0.14 mmol, 8.0 equiv) was added to a solution of **19** (7.0 mg, 17 μmol , 1.0 equiv) in MeCN (0.5 mL). The suspension was heated to 80 °C for 12 h, at which point it had turned into a dark-orange solution. The reaction mixture was cooled to room temperature, and 2 M HCl (0.5 mL) was added, turning the reaction mixture bright yellow. After 2 h, saturated aqueous NaHCO₃ (5 mL) was added, followed by EtOAc (10 mL). The aqueous phase was further extracted with EtOAc (2 \times 10 mL). The combined organic phases were washed with saturated aqueous NaCl (10 mL), dried over MgSO₄, and concentrated. The residue was purified by flash column chromatography (30:1:0.3 CH₂Cl₂:MeOH:NH₄OH) to yield **21** as a colorless oil (2.8 mg, 10 μmol , 60%); $R_f = 0.48$ (9:1 CH₂Cl₂:MeOH); ¹H NMR (400 MHz, CDCl₃) δ 8.23 (d, $J = 5.0$, 1H), 7.63 (d, $J = 7.6$, 1H), 7.18 (dd, $J = 7.7$, 5.1, 1H), 3.54 (td, $J = 6.5$, 2.4, 2H), 3.04–2.89 (m, 2H), 2.87–2.64 (m, 2H), 2.05–1.98 (m, 1H), 1.96–1.71 (m, 4H), 1.69–1.55 (m, 2H), 1.45–1.32 (m, 1H), 1.03 (d, $J = 5.6$, 3H); HRMS (ESI) m/z [M + H]⁺ calcd for C₁₆H₂₃N₂O₂ 275.1754, found 275.1758. The analytical data were in good agreement with literature values.¹¹

Lycopladine A (2). NH₂OH·HCl (17 mg, 0.24 mmol, 7.0 equiv) was added to a solution of **19** (15 mg, 34 μmol , 1.0 equiv) in MeCN (1.0 mL). The suspension was heated to 80 °C for 14 h, at which point it had turned into a dark-orange solution. The reaction mixture was cooled to room temperature, and TiCl₃ (~13% aqueous HCl solution, 0.2 mL) and acetone (0.2 mL) were added. The reaction mixture turned dark violet and then gradually back to light yellow. After 30 min, saturated aqueous NaHCO₃ (5 mL) was added, followed by EtOAc (10 mL) and filtration through a Celite pad. The aqueous phase was further extracted with EtOAc (2 \times 10 mL). The combined organic phases were washed with saturated aqueous NaCl (10 mL), dried over MgSO₄, and concentrated. The residue was purified by flash column chromatography (30:1:0.3 CH₂Cl₂:MeOH:NH₄OH) to yield lycopladine A (**2**) as a colorless solid (8.0 mg, 31 μmol , 91%); $R_f =$

0.52 (9:1 CH₂Cl₂:MeOH); ¹H NMR (400 MHz, CD₃OD) δ 8.30 (dd, *J* = 5.1, 1.4, 1H), 7.68 (dd, *J* = 7.8, 1.5, 1H), 7.25 (dd, *J* = 7.7, 5.1, 1H), 3.54 (td, *J* = 6.3, 1.8, 2H), 3.09 (dd, *J* = 16.1, 8.1, 1H), 3.02–2.92 (m, 1H), 2.83 (dd, *J* = 16.1, 8.9, 1H), 2.29 (d, *J* = 8.0, 2H), 2.18–2.00 (m, 2H), 1.94–1.77 (m, 3H), 1.62–1.50 (m, 1H), 1.41–1.30 (m, 1H), 1.09 (d, *J* = 6.5, 3H); ¹³C NMR (101 MHz, CD₃OD) δ 214.6, 164.3, 148.7, 140.0, 136.2, 123.1, 62.8, 62.7, 47.7, 43.5, 38.5, 34.7, 33.3, 29.6, 29.1, 22.0; IR (ATR) 2982, 2958, 1718, 1646, 1465, 1367, 1294 1257, 1176, 1152, 1095, 1032, 978, 774 cm⁻¹; HRMS (ESI) *m/z* [M + H]⁺ calcd for C₁₆H₂₂NO₂ 260.1645, found 260.1644; [α]_D²⁰ + 79 (c 1.0, CH₂Cl₂); [α]_D²⁰ + 110 (c 0.4, MeOH); mp 160 °C dec. The data were in full agreement with the literature (see also the Supporting Information).^{5,11}

3a-(3-Chloropropyl)-6-methyl-3-methylenooctahydro-4H-inden-4-one (22). 13 (44 mg, 0.20 mmol, 1.0 equiv) in CH₂Cl₂ (1.5 mL) was cooled to 0 °C before triethylamine (70 μL, 0.50 mmol, 2.5 equiv) was added. After 5 min, triphosgene (30 mg, 0.10 mmol, 0.5 equiv) was added in one portion. The reaction mixture quickly turned cloudy and was slowly warmed to room temperature. After 3 h, the reaction mixture was poured onto saturated aqueous NaHCO₃ (5 mL). The aqueous phase was extracted with CH₂Cl₂ (2 × 10 mL), and the combined organic phases were dried over MgSO₄ and concentrated. The residue was purified by flash column chromatography (12:1 pentane:Et₂O) to yield 22 as a colorless oil (43 mg, 0.18 mmol, 89%); *R*_f = 0.80 (5:1 hexane:EtOAc); ¹H NMR (400 MHz, CDCl₃) δ 5.02 (t, *J* = 2.2, 1H), 4.74 (t, *J* = 2.5, 1H), 3.61–3.42 (m, 2H), 2.60–2.49 (m, 2H), 2.49–2.36 (m, 2H), 2.28–2.16 (m, 1H), 2.06 (ddd, *J* = 14.8, 6.4, 1.3, 1H), 1.95–1.65 (m, 5H), 1.64–1.47 (m, 3H), 0.96 (d, *J* = 6.9, 3H); ¹³C NMR (101 MHz, CDCl₃) δ 212.3, 153.6, 108.8, 62.9, 46.0, 45.7, 42.7, 34.2, 32.9, 30.2, 29.6, 28.9, 28.6, 20.2; IR (ATR) 2953, 2924, 1697, 1646, 1458, 1443, 1333, 1310, 1246, 1133, 1048, 1015, 886 cm⁻¹; HRMS (ESI) *m/z* [M]⁺ calcd for C₁₄H₂₂ClO 240.1281, found 240.1274; [α]_D²⁰ – 43 (c 0.7, CH₂Cl₂).

3a-(3-Chloropropyl)-6-methyl-3-methylenhexahydro-1H-indene-2,4-dione (23). SeO₂ (50 mg, 0.45 mmol, 2.5 equiv) and a TBHP solution (5.5 M in decane, 0.16 mL, 0.90 mmol, 5.0 equiv) were added to 22 (44 mg, 0.18 mmol, 1.0 equiv) in CH₂Cl₂ at 0 °C. The mixture was stirred at room temperature for 17 h. At this point, the reaction mixture was cooled to 0 °C before PCC (58 mg, 0.27 mmol, 1.5 equiv) was added to the reaction mixture, turning it from bright orange to dark brown. Stirring was continued for 1 h at the same temperature. Thereafter, saturated aqueous NaHCO₃ (5 mL) was added, followed by dilution with H₂O (5 mL). After extraction with CH₂Cl₂ (3 × 8 mL), the combined organic phases were washed with saturated aqueous NaCl (5 mL), dried over MgSO₄, and concentrated. The brown residue was purified by flash column chromatography (5:1 pentane:Et₂O) to yield 23 as a colorless oil (35 mg, 99 μmol, 55%); *R*_f = 0.23 (5:1 hexane:EtOAc); ¹H NMR (400 MHz, CDCl₃) δ 6.22 (s, 1H), 5.27 (s, 1H), 3.63–3.42 (m, 2H), 2.70 (ddd, *J* = 13.0, 7.5, 5.5, 1H), 2.64–2.43 (m, 2H), 2.27–2.14 (m, 3H), 2.04–1.91 (m, 1H), 1.87–1.61 (m, 5H), 1.02 (d, *J* = 6.2, 3H); ¹³C NMR (101 MHz, CDCl₃) δ 210.2, 204.1, 146.5, 121.2, 59.8, 45.7, 45.1, 42.4, 36.3, 34.9, 33.2, 28.4, 28.2, 20.5; IR (ATR) 2953, 2925, 1727, 1705, 1638, 1457, 1384, 1289, 1257, 1129, 1095, 991, 951, 798 cm⁻¹; HRMS (ESI) *m/z* [M + H]⁺ calcd for C₁₄H₁₉ClO₂ 254.1074, found 254.1071; [α]_D²⁰ 12 (c 0.3, CH₂Cl₂).

(4bS,7R,8aS)-4b-(3-Chloropropyl)-2-ethoxy-7-methyl-3,4,4b,6,7,8,8a,9-octahydroindeno[2,1-b]pyran-5(2H)-one (24). 23 (24 mg, 94 μmol, 1.0 equiv) was dissolved in 1,2-dichloroethane (0.7 mL) and ethyl vinyl ether (0.7 mL) before Eu(fod)₃ (10 mg, 9.4 μmol, 0.10 equiv) was added in one portion. The yellow solution was stirred at 0 °C for 15 h, concentrated, and directly loaded on a florisil column (12:1 → 5:1 pentane:Et₂O) to give 24 (24 mg, 73 μmol, 78%) as a colorless oil and mixture of diastereomers; *R*_f = 0.43 (5:1 hexane:EtOAc); ¹H NMR (400 MHz, CDCl₃) δ 5.04 (t, *J* = 2.8, 1H), 3.91–3.74 (m, 1H), 3.65–3.44 (m, 3H), 2.75–2.56 (m, 1H), 2.56–2.40 (m, 2H), 2.24–2.06 (m, 2H), 2.01–1.54 (m, 8H), 1.46–1.29 (m, 1H), 1.27–1.15 (m, 4H), 0.97 (d, *J* = 6.7, 1H), 0.96 (d, *J* = 6.7, 2H) (note that due to extensive signal overlap, the integral sum is 26, not 27); ¹³C NMR (101 MHz, CDCl₃) δ 214.8, 214.4, 150.9, 150.6, 109.5,

109.3, 98.4, 98.4, 63.9, 63.9, 61.4, 61.3, 47.0, 46.7, 45.6, 45.6, 38.6, 38.5, 37.7, 37.5, 37.4, 37.3, 32.2, 32.0, 27.9, 27.7, 26.9, 26.9, 25.7, 25.6, 22.5, 22.4, 16.2, 16.1, 15.4, 15.3; IR (ATR) 2926, 2853, 1689, 1455, 1382, 1340, 1296, 1212, 1115, 1045, 968, 934, 849, 732 cm⁻¹; HRMS (ESI) *m/z* [M + H]⁺ calcd for C₁₈H₂₈ClO₃ 327.1721, found 327.1722.

Carinatine A (3). NH₄OH·HCl (25 mg, 0.37 mmol, 5.0 equiv) was added to a solution of 24 (24 mg, 73 μmol, 1.0 equiv) in MeCN (1.5 mL). The suspension was heated to 70 °C for 15 h, at which point it turned into a dark-orange solution. The reaction mixture was cooled to room temperature; K₂CO₃ (6.9 mg, 50 μmol, 0.7 equiv) and H₂O (0.5 mL) were added, and the mixture was heated to 80 °C. After 2 h, saturated aqueous NaHCO₃ (5 mL) was added, followed by CHCl₃ (10 mL). The aqueous phase was further extracted with CHCl₃ (4 × 8 mL). The combined organic phases were washed with saturated aqueous NaCl (10 mL), dried over MgSO₄, and concentrated. The residue was purified by flash column chromatography (19:1 → 9:1 CH₂Cl₂:MeOH) to yield carinatine A (3) as a slightly yellow oil (14 mg, 54 μmol, 75%); *R*_f = 0.40 (9:1 CH₂Cl₂:MeOH); ¹H NMR (400 MHz, CD₃OD) δ 8.40 (d, *J* = 5.0, 1H), 7.53 (d, *J* = 7.6, 1H), 7.28 (dd, *J* = 7.6, 5.1, 1H), 4.00 (m, 2H), 3.58 (dd, *J* = 17.3, 7.5, 1H), 3.04 (dd, *J* = 17.4, 6.8, 1H), 2.76 (q, *J* = 7.0, 1H), 2.70 (d, *J* = 17.5, 1H), 2.16–2.06 (m, 1H), 2.05–1.82 (m, 4H), 1.74–1.65 (m, 1H), 1.60 (dt, *J* = 14.1, 7.0, 1H), 1.45 (ddd, *J* = 13.8, 7.0, 3.2, 1H), 0.94 (d, *J* = 6.8, 3H); ¹³C NMR (101 MHz, CD₃OD) δ 165.0, 156.2, 149.5, 141.8, 134.2, 123.3, 59.1, 52.5, 45.3, 40.7, 38.5, 33.9, 32.9, 27.9, 20.1, 19.5; IR (ATR) 3374, 2919, 2484, 2074, 1655, 1592, 1427, 1180, 1117, 973, 937 cm⁻¹; HRMS (ESI) *m/z* [M + H]⁺ calcd for C₁₆H₂₁N₂O 257.1648, found 257.1647; [α]_D²⁰ – 60 (c 1.6, CH₂Cl₂); [α]_D²⁰ – 110 (c 0.4, MeOH). The data were in full agreement with the literature (see the Supporting Information).^{6,11}

■ ASSOCIATED CONTENT

Supporting Information

The Supporting Information is available free of charge on the ACS Publications website at DOI: 10.1021/acs.joc.7b00908.

Comparison of NMR data of isolated and synthetic lycoplidine A and carinatine A and ¹H and ¹³C spectra for all new compounds (PDF)

■ AUTHOR INFORMATION

Corresponding Author

*E-mail: dirktrauner@nyu.edu.

ORCID

Felix W. W. Hartrampf: 0000-0002-6748-5271

Dirk Trauner: 0000-0002-6782-6056

Notes

The authors declare no competing financial interest.

■ ACKNOWLEDGMENTS

The authors thank Dr. Julius Reyes, Dr. Bryan Matsuura, Benjamin Williams, and Nina Vrieling for assistance during the preparation of the manuscript.

■ REFERENCES

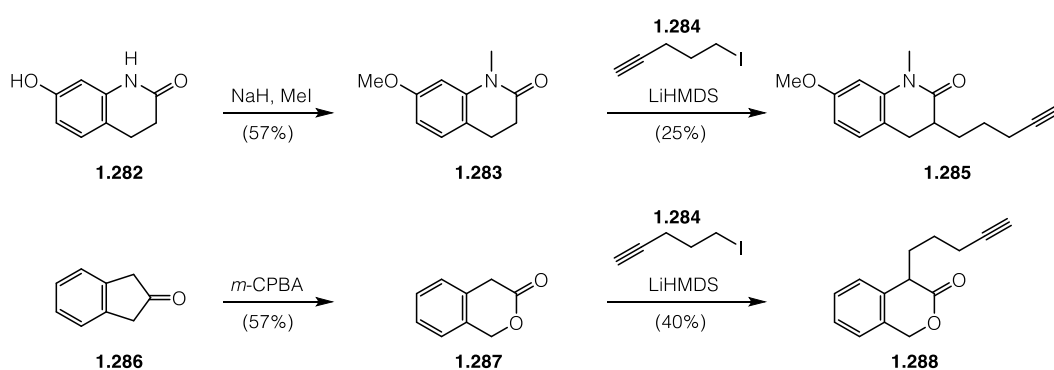
- (1) Ma, X.; Gang, D. *R. Nat. Prod. Rep.* 2004, 21, 752.
- (2) Hirasawa, Y.; Kobayashi, J.; Morita, H. *Heterocycles* 2009, 77, 679.
- (3) Siengalewicz, P.; Mulzer, J.; Rinner, U. In *The Alkaloids: Chemistry and Biology*; Hans-Joachim, K., Ed.; Academic Press: New York, 2013; Vol. 72, p 1.
- (4) Katakawa, K.; Kogure, N.; Kitajima, M.; Takayama, H. *Helv. Chim. Acta* 2009, 92, 445.
- (5) Ishiuchi, K. i.; Kubota, T.; Morita, H.; Kobayashi, J. I. *Tetrahedron Lett.* 2006, 47, 3287.
- (6) Liu, F.; Liu, Y.-C.; Jiang, W.-W.; He, J.; Wu, X.-D.; Peng, L.-Y.; Su, J.; Cheng, X.; Zhao, Q.-S. *Nat. Prod. Bioprospect.* 2014, 4, 221.

- (7) Staben, S. T.; Kennedy-Smith, J. J.; Huang, D.; Corkey, B. K.; LaLonde, R. L.; Toste, F. D. *Angew. Chem., Int. Ed.* **2006**, *45*, 5991.
- (8) DeLorbe, J. E.; Lotz, M. D.; Martin, S. F. *Org. Lett.* **2010**, *12*, 1576.
- (9) Hiroya, K.; Suwa, Y.; Ichihashi, Y.; Inamoto, K.; Doi, T. *J. Org. Chem.* **2011**, *76*, 4522.
- (10) Xu, T.; Luo, X.-L.; Yang, Y.-R. *Tetrahedron Lett.* **2013**, *54*, 2858.
- (11) Meng, L. *J. Org. Chem.* **2016**, *81*, 7784.
- (12) Liu, X.-J.; You, S.-L. *Angew. Chem., Int. Ed.* **2017**, *56*, 4002.
- (13) Hartrampf, F. W. W.; Furukawa, T.; Trauner, D. *Angew. Chem., Int. Ed.* **2017**, *56*, 893.
- (14) Conia, J. M.; Le Perche, P. *Synthesis* **1975**, 1975, 1.
- (15) Hack, D.; Blumel, M.; Chauhan, P.; Philipps, A. R.; Enders, D. *Chem. Soc. Rev.* **2015**, *44*, 6059.
- (16) Abu Sohail, S. M.; Liu, R.-S. *Chem. Soc. Rev.* **2009**, *38*, 2269.
- (17) Dénès, F.; Pérez-Luna, A.; Chemla, F. *Chem. Rev.* **2010**, *110*, 2366.
- (18) Dorel, R.; Echavarren, A. M. *Chem. Rev.* **2015**, *115*, 9028.
- (19) Hirasawa, Y.; Morita, H.; Shiro, M.; Kobayashi, J. *i. Org. Lett.* **2003**, *5*, 3991.
- (20) Bisai, V.; Sarpong, R. *Org. Lett.* **2010**, *12*, 2551.
- (21) Ishida, H.; Kimura, S.; Kogure, N.; Kitajima, M.; Takayama, H. *Org. Biomol. Chem.* **2015**, *13*, 7762.
- (22) Ishida, H.; Kimura, S.; Kogure, N.; Kitajima, M.; Takayama, H. *Tetrahedron* **2015**, *71*, 51.
- (23) Caine, D.; Procter, K.; Cassell, R. A. *J. Org. Chem.* **1984**, *49*, 2647.
- (24) Carlone, A.; Marigo, M.; North, C.; Landa, A.; Jorgensen, K. A. *Chem. Commun.* **2006**, 4928.
- (25) Linghu, X.; Kennedy-Smith, J. J.; Toste, F. D. *Angew. Chem., Int. Ed.* **2007**, *46*, 7671.
- (26) Yamamoto, Y.; Fujikawa, R.; Umemoto, T.; Miyaura, N. *Tetrahedron* **2004**, *60*, 10695.
- (27) A TBDPS protection followed by allylic oxidation of **13** would have led to an intermediate of Overman's sieboldine A synthesis as previously described.
- (28) Ciufolini, M. A.; Byrne, N. E. *J. Chem. Soc., Chem. Commun.* **1988**, 1230.
- (29) Bednarski, M.; Danishefsky, S. J. *Am. Chem. Soc.* **1983**, *105*, 3716.
- (30) Timms, G. H.; Wildsmith, E. *Tetrahedron Lett.* **1971**, *12*, 195.
- (31) Ayala, C. E.; Villalpando, A.; Nguyen, A. L.; McCandless, G. T.; Kartika, R. *Org. Lett.* **2012**, *14*, 3676.
- (32) Tanaka, T.; Kogure, N.; Kitajima, M.; Takayama, H. *J. Org. Chem.* **2009**, *74*, 8675.
- (33) Brandman, H. A.; Conley, R. T. *J. Org. Chem.* **1973**, *38*, 2236.

1.2.4 Unpublished results

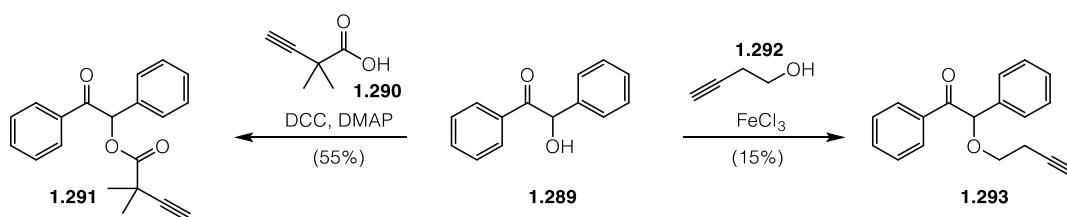
In addition to the results detailed in sections 1.2.2 and 1.2.3, a number of other cyclization precursors were assembled, which will be presented in the following.

We first wanted to explore the formation of other ring systems. More specifically, we were interested to see whether other substrate classes such as non-activated lactams or lactones could also act as nucleophiles in our carbocyclization reaction. Therefore, we first accessed lactam **1.283** and lactone **1.287** by double methylation and Baeyer–Villiger oxidation of **1.282** and **1.286**, respectively. The alkynylated compounds **1.285** and **1.288** were obtained by alkylation with 4-pentynyl iodide (**1.284**) in moderate yield.



Scheme 1.49. Preparation of lactam (**1.285**) and lactone (**1.288**) cyclization precursors.

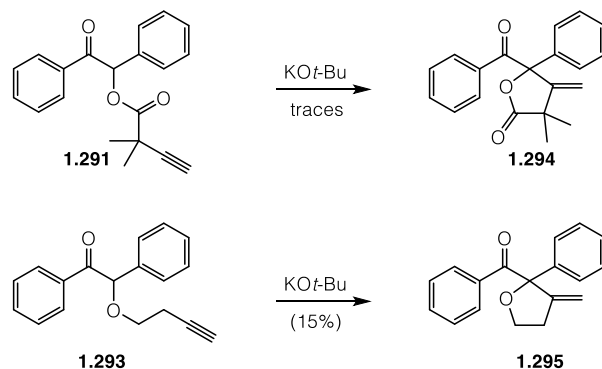
Furthermore, we wanted to extend our chemistry to linear substrates, which had proven reluctant to cyclize with propiophenone-derived material. We thus treated benzoin (**1.289**) with acid **1.290**^[189] or alcohol **1.292** to obtain cyclization substrates **1.291** and **1.293**. The low yield of the etherification can be explained by the competing oxidation of benzoin to benzil, which was isolated as the major product.



Scheme 1.50. Preparation of linear substrates **1.291** and **1.293** by esterification (left) or etherification (right).

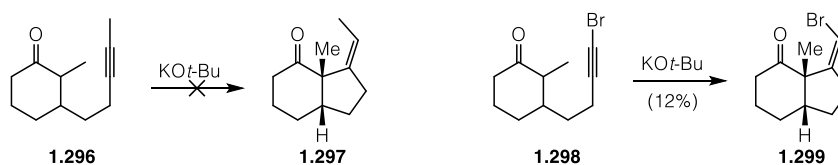
Under standard conditions, no conversion was observed for either one of the substrates. However, when treated with two equivalents of KO^tBu , **1.291** largely decomposed and only traces of **1.294** were observed. The cyclization of **1.293** indeed occurred, albeit with low efficiency, to give the five-membered heterocycle **1.295** (Scheme 1.51). Consistent with the

observations made with cyclic α -aryl ketones (chapter 1.2.2), this cyclization was significantly slower than those of α -alkyl ketones.



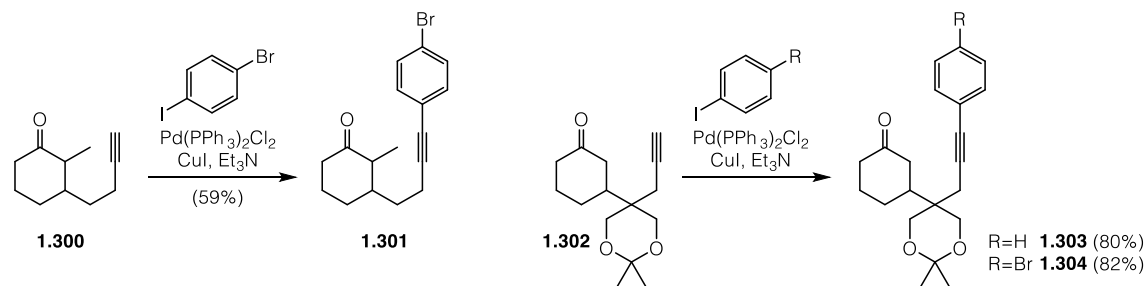
Scheme 1.51. Cyclization attempts of linear substrates **1.291** and **1.293**.

A major drawback of the preliminary substrate scope (chapter 1.2.2) was the absence of internal alkynes, with the notable exception of one chloroalkyne. We thus set out to prepare a range of substrates bearing various substituents on the alkyne. The methyl-capped alkyne **1.296** was prepared analogously to our general conjugate addition procedure. When submitted to our standard conditions, no reaction to **1.297** was observed. We next turned to bromoalkyne **1.298**, prepared by silver-catalyzed bromination. This substrate was of interest because the vinyl bromide resulting from a successful cyclization could serve as a synthetic handle for a range of follow-up transformations. Under our standard conditions, the bromide indeed cyclized to **1.299**, but the product was obtained in low yield (Scheme 1.52). The bulkier nature of the bromide (compared to the chloride) presumably precludes a more efficient cyclization.



Scheme 1.52. Attempts to cyclize internal alkynes **1.296** and **1.298**.

Furthermore, we accessed three arylated alkynes **1.301**, **1.303** and **1.304** by efficient Sonogashira couplings of the two alkynes **1.300** and **1.302** with iodobenzene and *p*-bromoiodobenzene.



Scheme 1.53. Preparation of aryl alkynes **1.301**, **1.303** and **1.304** via Sonogashira coupling of alkynes **1.300** and **1.302**.

The majority of substrates explored in chapters 1.2.2 and 1.2.3 were carbocyclic. We thus wanted to increase the structural span by exploring heteroatom-containing ring systems. More specifically, we reasoned that our method could be suitable for the synthesis of pyrrolizidines and indolizidines. Our method seemed well-suited for the preparation of the carbon skeleton of pyrrolizidine alkaloids like platynecine (**1.305**), turneforcidine (**1.306**) or hastanecine (**1.307**), which only differ in the stereochemistry at the tertiary and hydroxymethyl stereocenters (Figure 1.10). Other potential targets could be retronecanol (**1.308**) and the unusual natural product danaidone (**1.309**). All five compounds could arise from the cyclization product *via* simple redox manipulations.

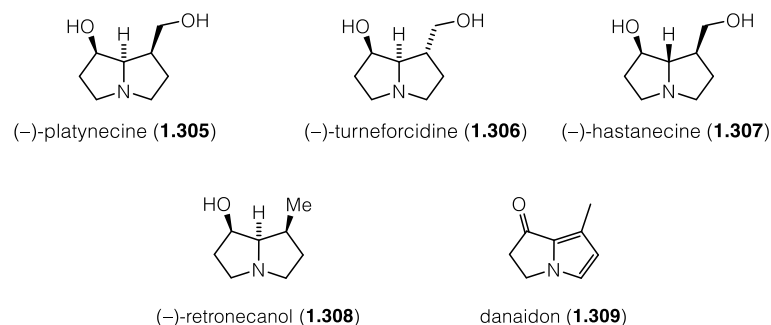
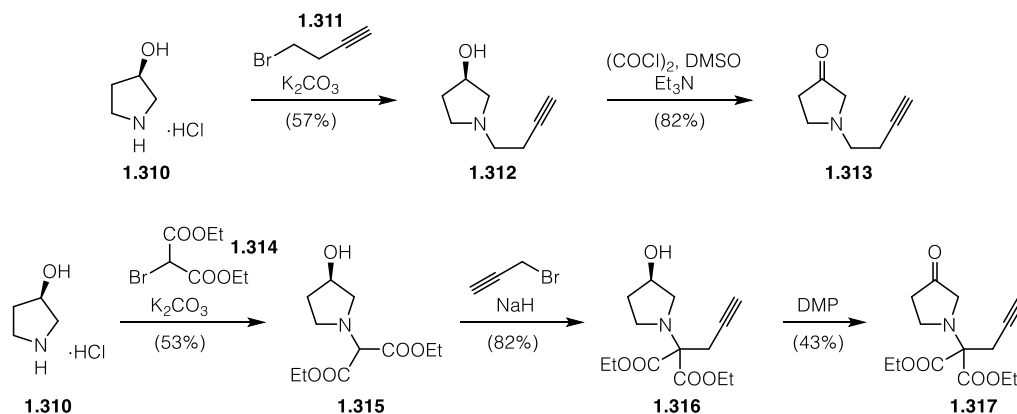


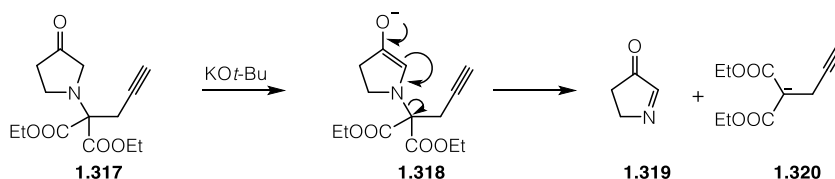
Figure 1.10. Structures of some representative necine alkaloids.

To this end, we prepared two substrates bearing nitrogen atoms at the ring junction (Scheme 1.54). Alkylation of 3-hydroxypyrrolidine hydrochloride (**1.310**) with 1-bromobut-4-yne (**1.311**) or diethyl bromomalonate (**1.314**) gave the corresponding tertiary amines **1.312** and **1.315**, the latter of which was propargylated to give **1.316**. After oxidation of the secondary alcohol, two ketones **1.313** and **1.317** were obtained.



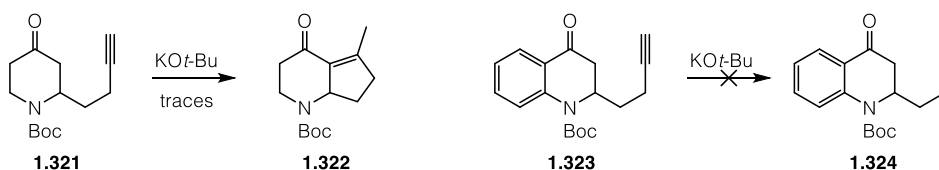
Scheme 1.54. Synthesis of α -aminoketone starting materials **1.313** and **1.317** by alkylation and oxidation.

When subjecting the two substrates to our carbocyclization conditions, both reactions indicated product formation. However, isolation of the products was not met with success so far. Interestingly, in the case of substrate **1.317**, one of the isolated products was diethyl 2-propargyl malonate, a possible mechanism for the formation of which is presented in Scheme 1.55. It was assumed that enolate formation occurred as intended (**1.318**). However, this was followed by β -elimination under extrusion of malonate **1.320** as well as imine **1.319**, which probably decomposed under the reaction conditions.



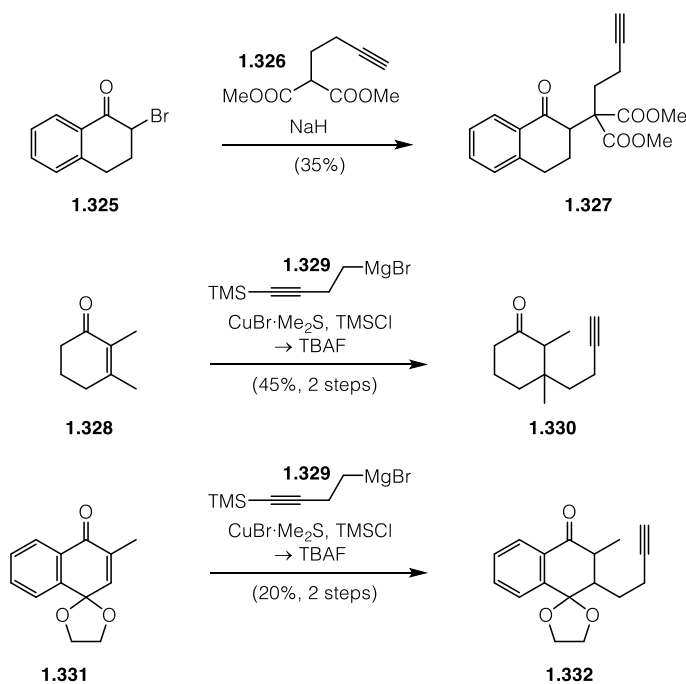
Scheme 1.55. Plausible β -elimination mechanism of malonate-derived cyclization substrate **1.317**.

In addition to these two nitrogen-bearing substrates, we also prepared the compounds **1.321** and **1.323** by conjugate addition to the corresponding vinylogous amides (not shown). An interesting aspect of this chemistry was to see whether the carbocyclization would outcompete the retro-Michael addition. When trying to cyclize **1.321** and **1.323**, mixed results were obtained. Piperidinone **1.321** gave the desired product **1.322**, albeit in low yield and purity. Substrate **1.323**, which is identical to one of the published substrates (see compound **32** in chapter 1.2.2) save the α -methyl group, did not react to **1.324**.



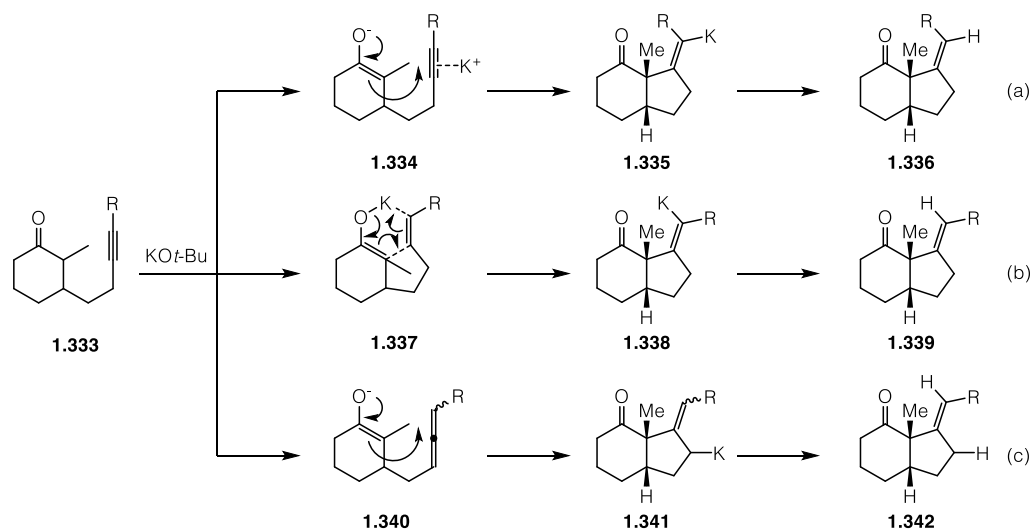
Scheme 1.56. Cyclization of β -aminosubstituted cyclic ketones **1.321** and **1.323**.

The last class of substrates contained those bearing quaternary stereocenters in the β or γ position to the ketone (Scheme 1.57). As a result, these would products bearing two (adjacent) quaternary stereocenters upon cyclization. The tetralone-derived building substrate **1.327** was prepared by malonate alkylation with bromide **1.325**, the ketones **1.330** and **1.332** were synthesized from **1.328** and **1.331** by our general method for the preparation of cyclization precursors.



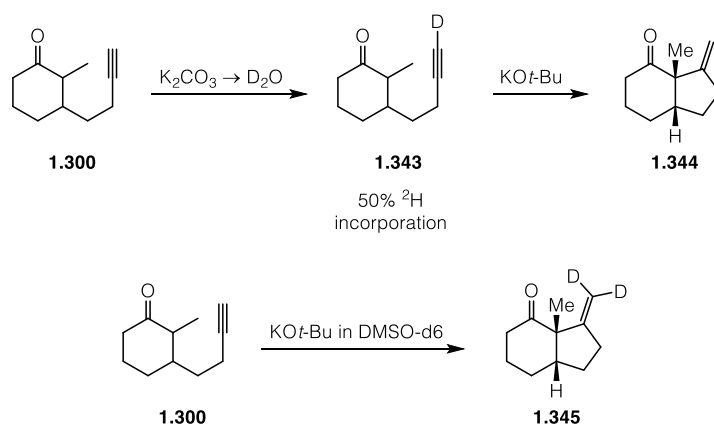
Scheme 1.57. Synthesis of substrates **1.327**, **1.330** and **1.332** bearing pre-existing β - or γ -quaternary carbons.

Finally, we undertook first steps of a mechanistic study. More specifically, we were interested to see whether the reaction occurs *via trans* addition or a concerted Conia–Ene-like cyclization (Scheme 1.58). The first pathway (a) from **1.333** would proceed *via* a coordination of the alkyne to a potassium ion (**1.334**) followed by attack of the nearby enolate. This would give vinylpotassium species **1.335** and finally product **1.336**. The second pathway (b) would be a concerted metalla-Conia–Ene reaction *via* **1.337**, resulting in vinylpotassium species **1.338** and product **1.339**. Of course, the two products **1.336** and **1.339** would be identical using a substrate where R = H, as was the case for most substrates investigated. A third plausible pathway (c) could consist of isomerization to an allene **1.340** followed by cyclization to an allylpotassium species **1.341** and protonation to **1.342**. In this case, determination of the double bond geometry is harder to predict. As detailed in chapter 1.2.2, most internal alkynes proved unreactive, but a cyclization using a chloroalkyne occurred in good yield and complete diastereoselectivity to give a product consistent with the *trans* addition pathway.



Scheme 1.58. Plausible mechanisms (a)–(c) for the carbocyclization reaction.

Aware that the chloro substituent might bias the outcome of this reaction, we decided to investigate deuterated substrates. First, we attempted the preparation of a deuterated alkyne **1.343**, which we wanted to prepare from our optimization substrate **1.300**. This was rendered more difficult than expected by the fact that basic conditions used for deuteration induced cyclization instead. Finally, Bew's method proved mild enough, providing about 50% deuterium incorporation (Scheme 1.59).^[190] When submitting this material to our standard conditions, we didn't observe any deuterium incorporation in the product **1.344**, hinting at a facile deprotonation of the alkyne. We next applied our standard cyclization conditions again, but used deuterated solvent. As expected, the reaction took place under our standard conditions. However, we isolated **1.345**, the product of double deuteration. This finding clarified that the alkynyl proton is readily exchanged under the reaction conditions.



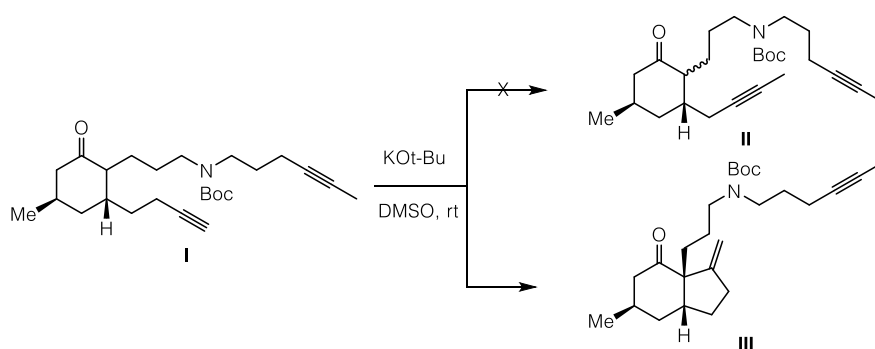
Scheme 1.59. Preparation and cyclization of deuterated substrate **1.343** (top) and preparation of deuterated analog **1.345** (bottom).

Furthermore, the resulting anionic species is protonated from the solvent, not another molecule of **1.300** or *t*-BuOH, both of which are more acidic than DMSO. The fact that no deuteration was observed in the allylic position of **1.345** speaks against an allene pathway, as the allylpotassium species would either be protonated directly or isomerize to the primary position first. This would result in an internal double bond, which could not be detected either.

1.2.5 Summary and outlook

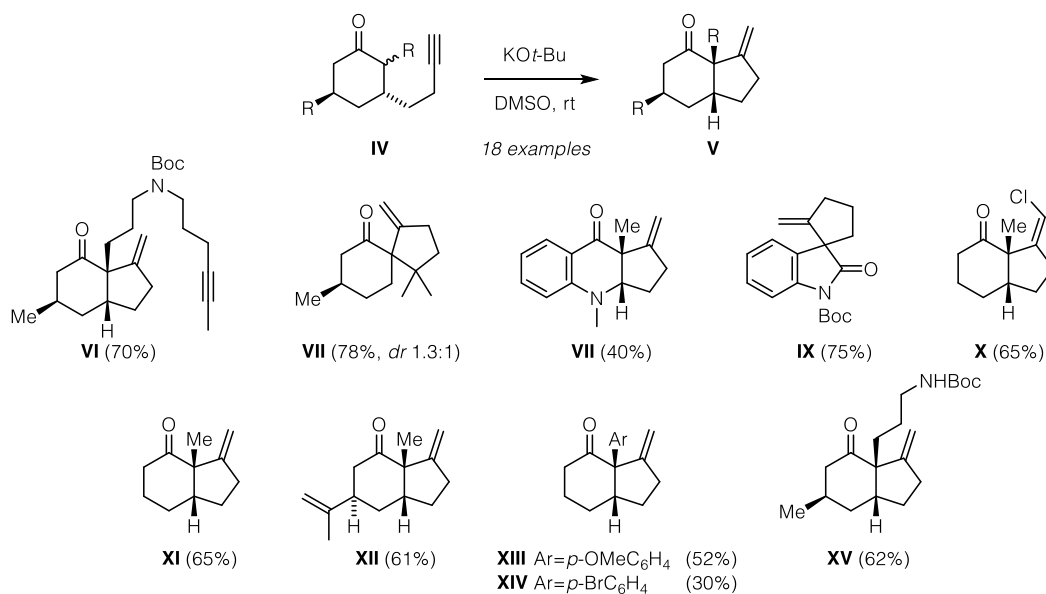
Note: As most of the compounds in the following section are published in peer-reviewed journals and additionally appear in other chapters, roman numerals are used in this section.

In summary, a new base-mediated carbocyclization has been developed and applied to *Lycopodium* alkaloid synthesis. After its serendipitous discovery (Scheme 1.60), systematic investigation of the reaction conditions allowed for the establishment of an efficient method to form five-membered rings in an intramolecular Conia–Ene-like carbocyclization reaction between ketones and alkynes.



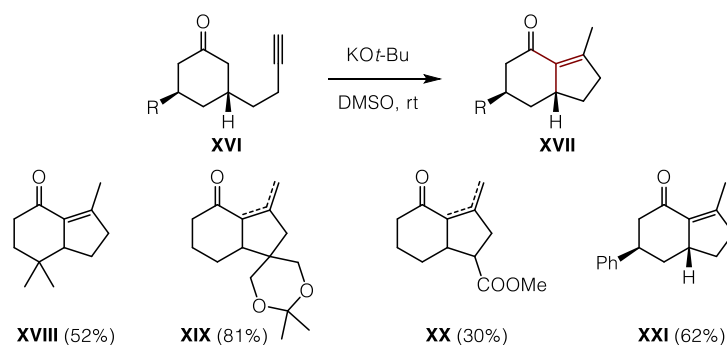
Scheme 1.60. Discovery of a carbocyclization reaction (I to III) under basic conditions.

Remarkably, it occurs in the absence of transition metal catalysts or carbonyl-activating groups such as (silyl) enol ethers or electron-withdrawing groups in the α -position. The carbocyclization was demonstrated on a range of substrates, delivering bi- and tricyclic



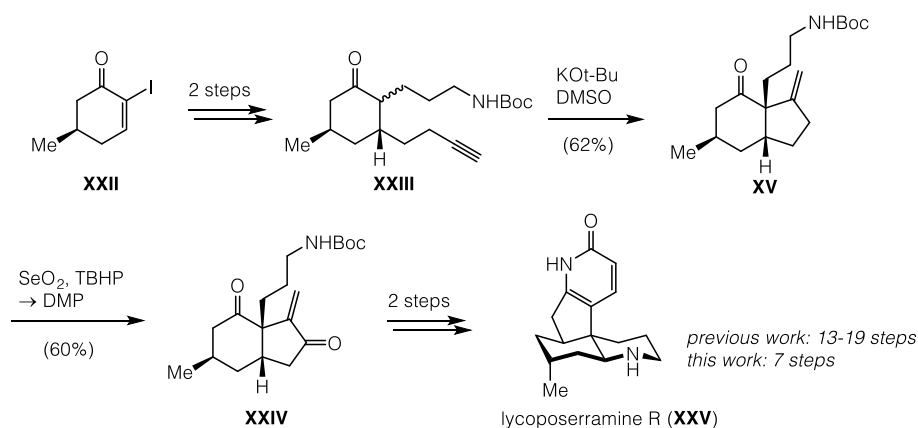
Scheme 1.61. Representative substrate scope of the carbocyclization reaction with substrates IV bearing α -substituents.

products in moderate to good yields (**VI–XV**, Scheme 1.61). While α -substituted cyclic ketones were the most thoroughly studied substrate class for our reaction, oxindoles and tetrahydroquinolinones were also viable. Aside from 6-5- and 5-5-fused systems, 6-5-spiroannulated systems like **VII** and **IX** could also be obtained. In addition, we were able to construct synthetically useful enones **XVII** bearing tetrasubstituted double bonds using our method (Scheme 1.62).



Scheme 1.62. Representative substrate scope regarding enone products **XVII**.

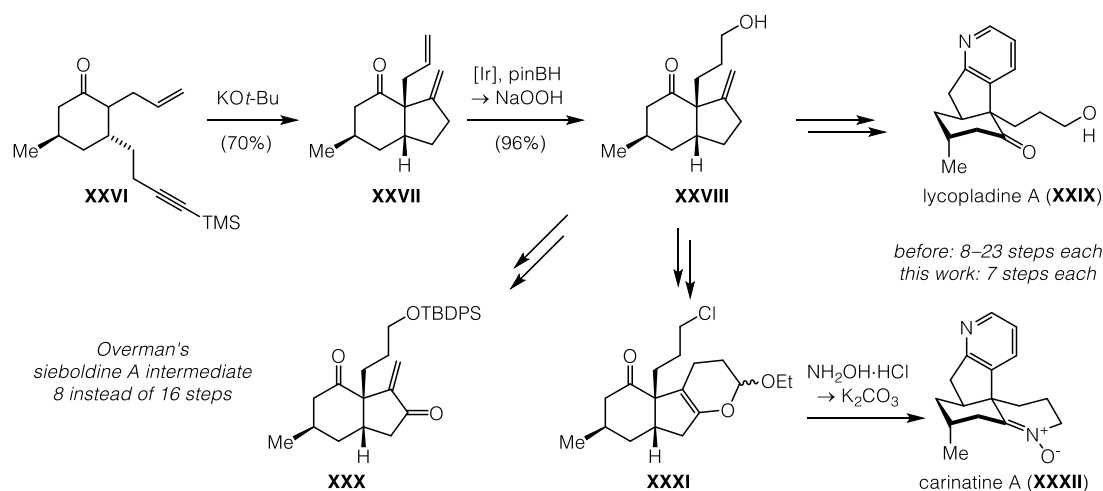
Having successfully demonstrated the viability of our methodology, we sought to employ it in natural product synthesis. Our synthesis of hydrindanes seemed especially suited for fawcettimine-type *Lycopodium* alkaloids and we first focused on the aromatic congeners lycoposerramine R (**XXV**).



Scheme 1.63. Total synthesis of lycoposerramine R (**XXV**) based on the newly developed carbocyclization.

We used the *exo*-methylene group of hydrindane building block (**XV**) resulting from the carbocyclization to quickly elaborate the aromatic portion by Kröhnke-type pyridone synthesis of enone **XXIV**, thus circumventing extensive functional group interconversions necessary in some other approaches. We next wanted to apply our carbocyclization to two other congeners, lycoplamine A (**XXIX**) and carinatine A (**XXXII**). For their total synthesis, we demonstrated that silylated alkynes like **XXVI** were just as efficient in the carbocyclization to as free alkynes,

further streamlining the reaction sequence. In order to furnish the aromatic portion of the two alkaloids, we used the Ciufolini pyridine synthesis, which in the case of carinatine A (**XXXII**) could nicely be telescoped to furnish both pyridine and cyclic nitron ring in one operation.



Scheme 1.64. Optimized carbocyclization procedure to access central intermediate **XXVIII**. Total synthesis of lycopladine A (**XXIX**), carinatine A (**XXXII**) and formal synthesis of sieboldine A through **XXX**.

With seven steps each from well-known building blocks, all three syntheses are the shortest enantioselective reported to date. Additionally, we demonstrated the suitability of our general approach to the “non-aromatic” fawcettimine-type alkaloids with a formal synthesis of sieboldine A (**1.66**) through intermediate **XXX**, reducing the step count for Overman's intermediate significantly. Future work will focus on further expanding the protocol. This would include, for example, synthesis of internal alkynes like **XXXIII** and **XXXIV**, and first positive results toward this end have been obtained. A very important extension to the carbocyclization will be the synthesis of other ring sizes. Research will focus on Thorpe–Ingold-modified sidechains such as in **XXXV** to enable the closure of six-membered rings and other yet unattainable motifs such as linear substrates **XXXVI** or unbiased esters or lactones like **XXXVII**.

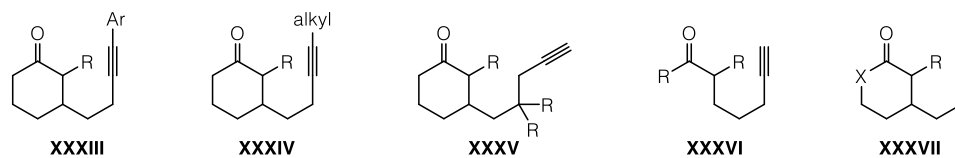


Figure 1.11. Generalized new motifs that are the topic of current and future research regarding the carbocyclization reaction.

Substrates belonging to these classes have been prepared and are currently being tested, as are deuterated substrates geared at elucidating the exact mechanism of the carbocyclization in combination with computational studies.

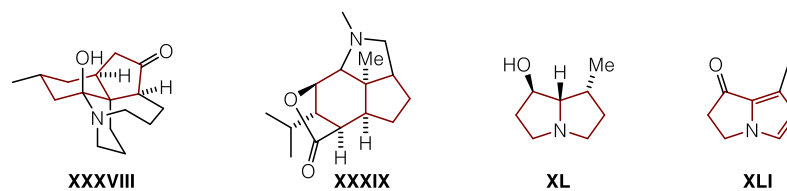


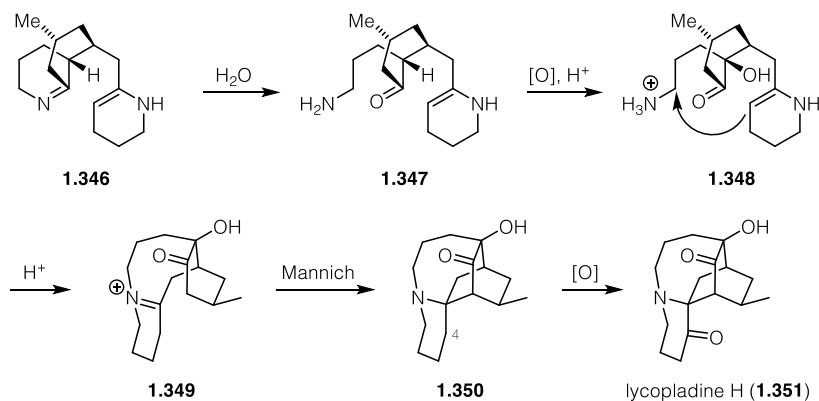
Figure 1.12. Possible future natural product targets. The 6-5- or 5-5-motif accessible *via* carbocyclization is highlighted in red.

Furthermore, we want to demonstrate the usefulness of our reaction for the synthesis of further *Lycopodium* natural products such as fawcettimine (**XXXVIII**) or other alkaloids, such as dendrobine (**XXXIX**) of the *Orchidaceae* family or the pyrrolizidine alkaloids retronecanol (**XL**) and danaidone (**XLI**).

1.3 Toward the total synthesis of lycopodine-type *Lycopodium* alkaloids

1.3.1 Previous efforts towards lycopladine H and lycojaponicum D

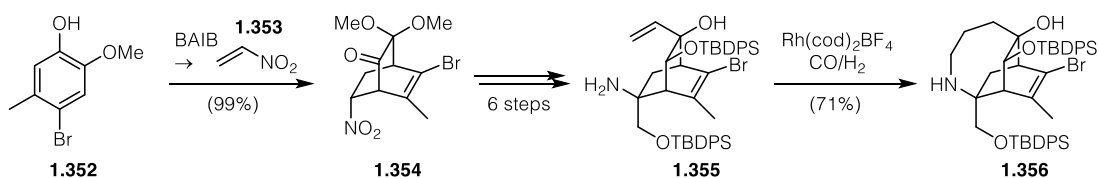
Lycopladine H (**1.351**) was isolated by the Kobayashi group from *Lycopodium complanatum* in 2009,^[191] sharing the natural source with lycopladine A (**1.245**). From a structural standpoint, however, it is not closely related to lycopladines A to G, as a matter of fact, its skeleton is unique amongst the *Lycopodium* alkaloids, bearing a very unusual C-6-C-14 bond. At this stage, no attempts to elucidate the biosynthesis have been reported, but a biogenesis starting from the phlegmarine (**1.2**) skeleton has been put forth. A phlegmarine-like imine **1.346** could be ring-opened to furnish a bicyclic intermediate **1.347**. α -Oxidation and activation of the resulting primary amine or alcohol would give an electrophile (**1.348**) for an intramolecular cyclization to an iminium species **1.349**. This iminium species could furnish the lycopladine H skeleton after a Mannich cyclization to **1.350**. Finally, oxidation of the C-4 position (lycopodine numbering) would yield lycopladine H (**1.351**). Interestingly, oxidation in this position is quite common amongst both fawcettimine and lycopodine alkaloids, albeit to the alcohol, not to the ketone oxidation stage.



Scheme 1.65. Proposed biosynthesis of lycopladine H (**1.351**) from a phlegmarine skeleton **1.346**.

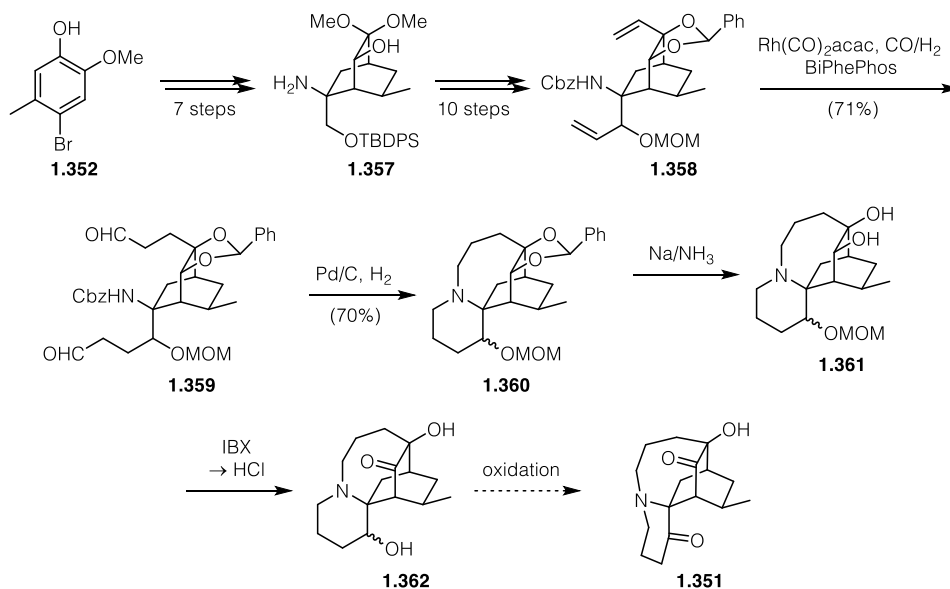
Its [2,2,2] core that bears all five stereocenters of the molecule makes lycopladine H a unique natural product amongst the *Lycopodium* alkaloids, even though it retains the classic C16N gross formula. In addition to its unusual core, it features two more rings: The first is a unique 3-piperidone spiro-fused to the [2,2,2] core, the second is an azocane unit. A final noteworthy structural feature is the sterically quite hindered tertiary α -tertiary amine that is characteristic of the lycopodine-type alkaloids.

Given its interesting and challenging structure, it is not surprising that efforts have been directed towards the total synthesis of lycoplamine H. The efforts of the Weinreb group have been documented in a sequence of three publications.^[192-194] Their retrosynthetic analysis remained unchanged throughout and always relied on the construction of the core **1.354** *via* a Diels–Alder reaction of an ortho-quinone ketal, obtained by oxidative dearomatization of phenol **1.352**, with the highly reactive dienophile nitroethene (**1.353**).^[192, 195] In six more steps, this adduct was elaborated into the amine **1.355**. The α -tertiary amine was introduced *via* nitroaldol reaction with formaldehyde, highlighting the need for strongly activated reaction partners to furnish α -tertiary amines in an intermolecular fashion. With the δ -vinylamine in hand, Weinreb and coworkers proceeded with their key step, an intramolecular hydroaminomethylation, in essence a hydroformylation followed by reductive amination. Using this reaction, a tricyclic intermediate **1.356** bearing the azocane moiety was furnished in eleven steps from isovanillin or eight steps from phenol **1.352**.^[193]



Scheme 1.66. Weinreb's opening steps to furnish the [2,2,2]-bicyclooctane core and the azocane ring.

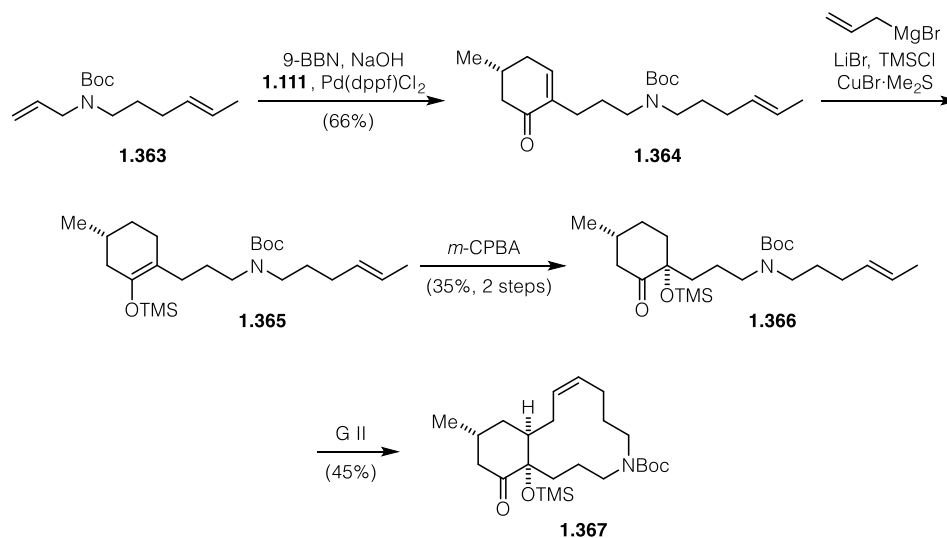
Two years later, the second approach was disclosed.^[194] This time, instead of aiming for sequential ring closures, the piperidine and azocane rings of lycoplamine H (**1.351**) were supposed to be furnished by simultaneous double hydroformylation and reductive amination. Again starting from phenol **1.352**, they accessed the [2,2,2] core **1.357** in seven steps, this time with the methyl stereocenter already set. Another ten steps delivered the diolefin **1.358**, which was hydroformylated twice when treated with a rhodium(I) catalyst under a H_2/CO atmosphere, giving dialdehyde **1.359**. Hydrogenolysis of the Cbz group also triggered the desired double reductive amination to finally give the tertiary amine **1.360**. At this stage, two protecting groups had to be removed and two secondary alcohols oxidized to the corresponding ketones to arrive at lycoplamine H (**1.351**). The benzylidene acetal of **1.360** could be removed under Birch conditions and the diol oxidized to the α -hydroxyketone, which was deprotected to **1.362**.



Scheme 1.67. Weinreb's double hydroformylation-reductive amination strategy to obtain the full carbon skeleton of lycopladiene H (**1.351**).

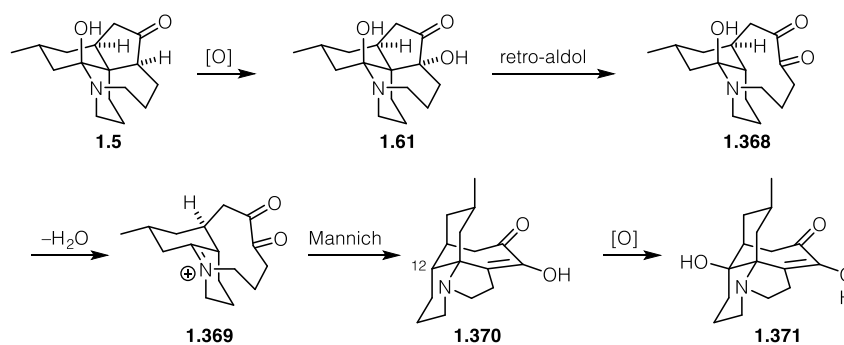
Unfortunately, this sequence was very low-yielding and only furnished minute amounts of intermediates that were not fully characterized. Attempts at oxidation of the secondary alcohol in **1.362** to lycopladiene H (**1.351**) were met with failure.

After the experimental work of this thesis had been concluded, another, strategically distinct approach toward the lycopladiene H skeleton was described in a Master's thesis.^[196] During a failed attempt to access the lycopodine (**1.4**) skeleton by transannular aza-Prins cyclization, it was realized that the same strategy with a more oxidized precursor could potentially give rise to lycopladiene H (**1.351**). Suzuki coupling of well-established α -iodoenone **1.111** with a C_{10} building block **1.363** gave enone **1.364**. Conjugate addition using an allyl cuprate gave unstable silyl enol ether **1.365** in moderate yield. The tertiary alcohol could be introduced by Rubottom oxidation with *m*-CPBA to give **1.366**, albeit in rather modest selectivity and yield. Under very high dilution conditions, the twelve-membered ring **1.367** could be furnished by ring-closing metathesis using second-generation Grubbs catalyst, even though the authors noted that the structure **1.367** was not firmly established yet. Oxidation of the *cis*-alkene **1.367** to a diketone could furnish the substrate for the desired transannular Mannich cyclization.



Scheme 1.68. The Wang approach toward the total synthesis of lycopladine H.

In addition to lycopladine H, another potential target was disclosed three years later; Lycojaponicum D (**1.371**) was identified as a minor component of *Lycopodium japonicum* by Shi-Shan Yu and coworkers.^[197] With its tetracyclic skeleton bearing a tertiary α -tertiary amine, it resembles the lycopodine-type alkaloids. It differs, however, by a formal 1,2-alkyl shift of the C-4-C13 bond to C-3, resulting in a 6-6-7-5 system instead of the common 6-6-6-6 system. Biosynthetically, it has been suggested that lycojaponicum D does not arise from oxidation of a lycopodine precursor, but instead from fawcettimine (**1.5**) or alopecuridine (**1.61**) (Scheme 1.69), where 1,2-diketones are not unheard of. Retroaldol rupture of the C-4-C-12 bond would lead to a diketone **1.368**, which could cyclize onto the iminium ion **1.369** in an intramolecular Mannich cyclization to give the carbon skeleton (**1.370**) of lycojaponicum D and the natural product **1.371** after oxidation of C-12.



Scheme 1.69. Proposed biosynthesis of lycojaponicum D (**1.371**) from fawcettimine (**1.5**) or alopecuridine (**1.61**).

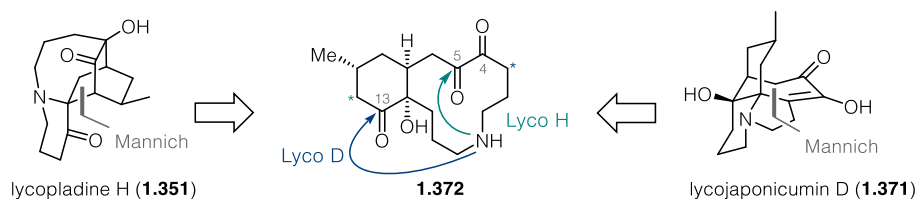
In summary, no complete total synthesis of lycopladine H (**1.351**) has been disclosed until now. However, the previous approaches showcase the challenges associated with its compact and

sterically encumbered structure. Surprisingly, no efforts toward lycojaponicum D have been disclosed this far.^[198]

The goal of this thesis was to develop an approach suitable for both alkaloids *via* a late-stage transannular Mannich cyclization and complete the first total synthesis of lycopladine H (**1.351**) and lycojaponicum D (**1.371**).

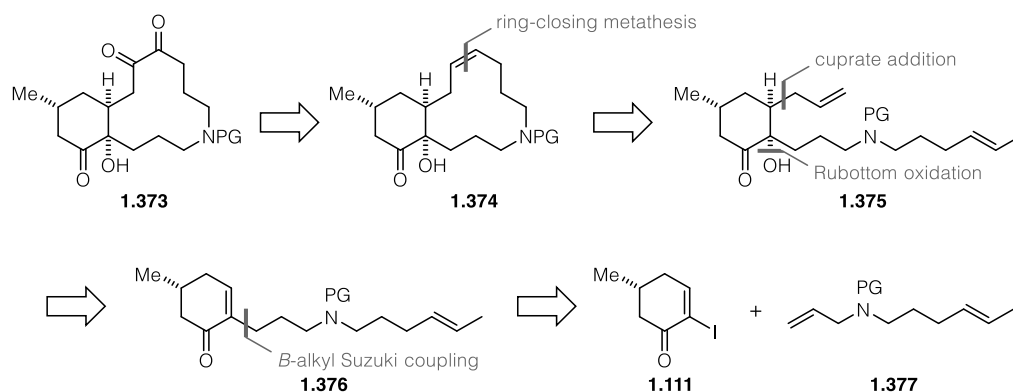
1.3.2 The RCM route

We envisioned a concise, convergent route to lycopladine H and lycojaponicum D that would rely on a late-stage Mannich reaction to furnish the skeleton of the two natural products (Scheme 1.70). We realized that disconnection of the Mannich retron in both cases led to a macrocycle **1.372** bearing an α -diketone and a secondary amine. The selectivity would mainly be governed by the reversible condensation of the secondary amine on either C-5 for lycopladine H or C-13 for lycojaponicum D. This would be followed by nucleophilic attack of the enol tautomer corresponding the C-13 ketone (lycopladine H) or C-4 ketone (lycojaponicum D), respectively.



Scheme 1.70. The Mannich retron in lycopladine H (**1.351**) and lycojaponicum D (**1.371**). The nucleophilic sites in **1.372** are indicated with an asterisk.

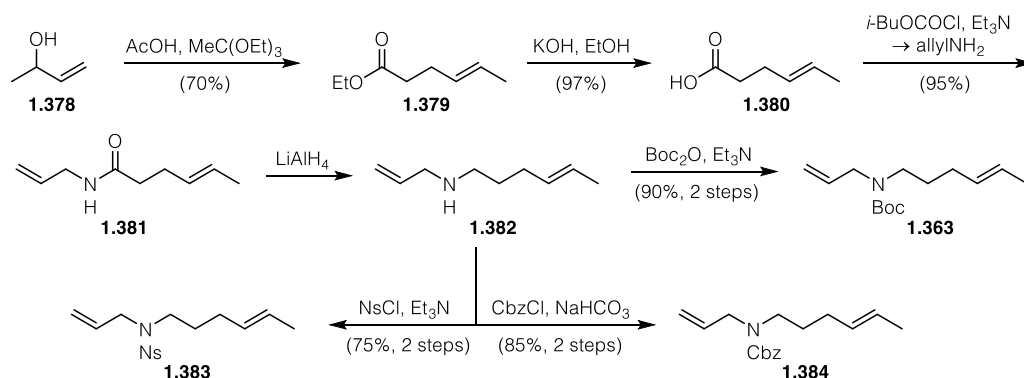
We were intrigued to investigate which cyclization mode would be favored and whether it could be influenced by choice of the reaction conditions. Therefore, we wanted to pursue an unprotected or minimally protected triketone as the penultimate intermediate.



Scheme 1.71. Retrosynthetic analysis of diketone **1.373**. PG = unspecified protecting group.

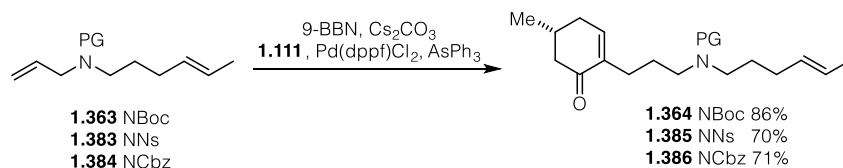
The presumably unstable α -diketone **1.373** was supposed to be furnished by a one- or two-step oxidation of a macrocyclic alkene **1.374** (Scheme 1.71). Given the advances over the last two decades, it seemed promising to furnish the twelve-membered macrocycle **1.374** by a ring-closing metathesis, even though examples for this particular ring size are scarce.^[199-201] Interestingly, alkene **1.374** and diketone **1.373** bear resemblance to a synthetic intermediate proposed by Heathcock in his seminal synthesis of lycopodine.^[123] However, Heathcock discarded this “most straightforward” disconnection, citing the lack of reliable synthetic methods to access an unsaturated macrocycle that was no less complex with regard to the natural product lycopodine (**1.4**). The bisalkene **1.375** necessary for the ring-closing metathesis could be obtained *via* conjugate addition or an equivalent process to append the allyl side chain to a suitable enone **1.376**. Ideally, trapping of the enolate would give a handle to introduce the tertiary alcohol of the two target alkaloids. Enone **1.376** could be obtained *via* a *B*-alkyl Suzuki coupling^[202] between two building blocks, **1.111** and **1.377**, both of which are accessible on multigram scale.^[203]

In the forward sense, we started with the fragment coupling of the Boc-protected side chain **1.364** to the known iodoenone (**1.111**).^[58] As disclosed previously,^[203] the side chain was available in gram quantities in five steps from but-3-en-2-ol (**1.378**) through a high-yielding sequence consisting of Johnson-Claisen rearrangement to **1.379**, ester hydrolysis to **1.380**, amide coupling with allylamine to **1.381**, reduction and Boc deprotection to finally give **1.363** (Scheme 1.72). Other protecting groups were easily introduced in the last step of the sequence.



Scheme 1.72. Gram scale synthesis of differentially protected sidechains **1.363**, **1.383** and **1.384**.

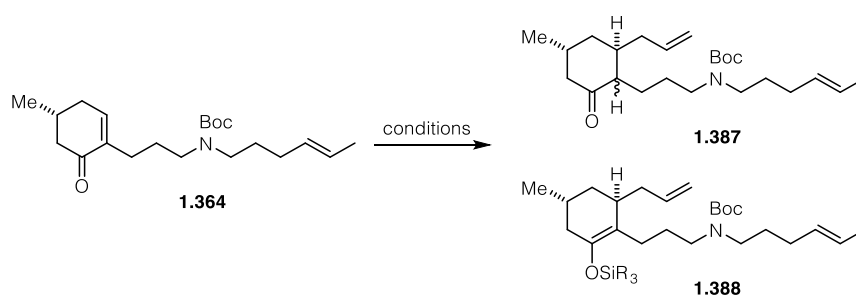
In this way, nosyl (Ns) and benzyl carbamate (Cbz) side chains **1.383** and **1.384** were accessed, giving some flexibility in the final protecting group manipulations of our synthesis. The *B*-alkyl Suzuki coupling gave the three enones **1.364**, **1.385** and **1.386** in good to very good yield (Scheme 1.73).



Scheme 1.73. *B*-alkyl Suzuki fragment coupling with different protecting groups on nitrogen.

However, to first probe the most rapid route, we explored the following steps with the Boc protected amine **1.364**. The next step, a conjugate addition of an allyl group turned out to be a major hurdle. Some representative results of the screening are shown in Table 1.1.

Table 1.1. Conjugate allylation of enone **1.364**.



entry	conditions	solvent, temperature	reaction outcome
1	allylSiMe ₃ , CH ₂ Cl ₂ , TiCl ₄	CH ₂ Cl ₂ , -78 °C	decomposition
2	allylSiMe ₃ , TMSCl, FeCl ₃	CH ₂ Cl ₂ , -78 °C	no reaction
3	allylSnBu ₃ , TMSCl	CH ₂ Cl ₂ , -78 to 0 °C	no reaction
4	allylSiMe ₃ , I ₂	CH ₂ Cl ₂ , rt	no reaction
5	In, InCl ₃ , CuI, allyl iodide	H ₂ O, 0 °C to rt	no reaction
6	allylMgBr, CuI, TMSCl	THF, -78 °C	23%
7	allylMgBr, CuBr·Me ₂ S, TMSCl	Et ₂ O, -78 °C	35%
8	allylMgBr, CuI	THF, -78 °C	no reaction
9	allylMgBr, CuI, LiCl	THF, -78 °C	low conversion
10	allylSnBu ₃ , TBSOTf	CH ₂ Cl ₂ , -78 °C	30%
11	allylSnBu ₃ , TESOTf, DTBPy	CH ₂ Cl ₂ , -78 °C	40–55%
12	allylSnBu ₃ , TBSOTf, DTBPy	CH ₂ Cl ₂ , -78 °C	55–65 ^[a]

[a] Allylation with Ns-protected enone **1.385** gave 58% yield (see supporting information).

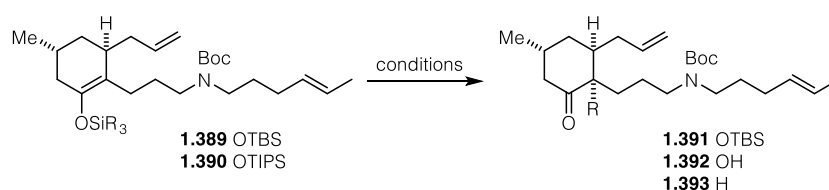
Sakurai's TiCl₄ conditions resulted in decomposition (entry 1).^[204–205] Milder Lewis acids like FeCl₃ in conjunction with TMSCl did not result in appreciable conversion (entry 2), even when the more reactive stannane was used (entry 3).^[206] I₂ was not sufficiently Lewis-acidic to induce

reaction (entry 4).^[207] Barbier-type radical addition did not work with an activated species like allyl iodide.^[208] Various copper-catalyzed methods (entries 6–9) were moderately successful only when TMSCl was present as a promoter.^[209–210] We then turned back to stannane-based methods and found some success with TBSOTf as the Lewis acid.^[211]

After extensive screening, a modification of an allylation-triflation methodology developed by Trauner originally in the context of a total synthesis of haouamine B^[212] proved to be most suitable for the synthesis of allylated silyl enol ether **1.388** (entries 11 and 12).^[213–214] In essence, simply exchanging the electrophilic component from triflic anhydride to *tert*-butyldimethylsilyl triflate allowed for the smooth synthesis of a silyl enol ether that was stable enough to be isolated by column chromatography; this stability is most probably conferred by its significant steric demand. NOE experiments revealed that the conjugate addition had occurred with complete (>20:1) *trans* selectivity, which is in line with earlier work on the related Sakurai allylations by Heathcock.^[205] With this activated carbonyl in hand, we proceeded to the introduction of the tertiary alcohol by Rubottom oxidation or a related method (Table 1.2).^[215–218] Treatment of TBS enol ether **1.389** with *m*-CPBA indeed resulted in slow conversion to the α -hydroxylated ketone **1.391**, alongside a significant amount of hydrolysis to the ketone **1.393** (entry 1). Modification of the solvent did not have a major influence on the reaction outcome (entries 2 and 3). Using purified *m*-CPBA (99%) and lowering the reaction temperature slightly improved the yield (entry 4). However, a major drawback was the modest diastereoselectivity, a 2.5:1 *d.r.* being the best result. In order to facilitate product isolation, we attempted the deprotection of the silyl ether obtained by Rubottom oxidation with tetrabutylammonium fluoride (TBAF) and the free α -hydroxyketone **1.392** was isolated in low yield (entry 5), which prompted us to investigate other oxidants. In the 1980s, Davis reported the use of (chiral) oxaziridines for the oxidation of electron-rich double bonds, mostly enamines and enolates.^[219] The use of these oxidants for silyl enol ethers is less common and requires higher temperatures than for enolates.^[220] In our case, this oxidant led to no conversion (entry 6). We therefore attempted Yu's enolate generation from silyl enol ethers with potassium ethoxide.^[221] Disappointingly, while clean deprotection was observed, no oxidation took place when Davis' oxaziridine was added (entry 7), and only ketone **1.393** was obtained. No oxidation was observed when the same enolate generation method was followed by treatment with an oxygen atmosphere and triethyl phosphite as a reducing agent (entry 8).^[222] We also briefly looked at TIPS enol ether **1.390**, but unsurprisingly, it was less reactive than its TBS counterpart **1.389** (entry 9).

An osmium tetroxide system was ineffective, as was the Sharpless AD system (entries 10 and 11).^[223] Remarkably, no oxidation of the two other double bonds in the substrate was observed under these conditions. Sarpong described the *in situ* generation of the highly electrophilic dimethyldioxirane (DMDO) in a biphasic medium.^[224] While clean conversion was observed, DMDO preferentially attacked the disubstituted double bond at room temperature and at 0 °C (entries 12 and 13). This came as a surprise given the highly electron-rich nature of the silyl enol ether. Using a preformed DMDO solution in dichloromethane/acetone did not result in appreciable conversion (entry 14).

Table 1.2. Rubottom and related oxidations of silyl enol ethers **1.389**.



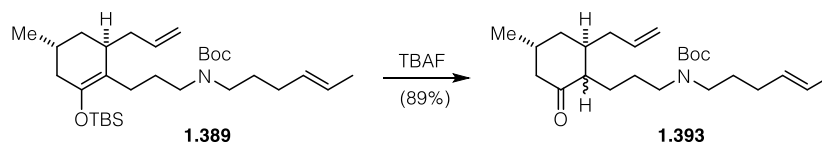
entry	oxidant	additives	solvent	yield [%]
1	<i>m</i> -CPBA (72%)	NaHCO ₃ (5 eq.)	CH ₂ Cl ₂ , 0 °C	27
2	<i>m</i> -CPBA (72%)	–	CH ₂ Cl ₂ , hex, 0 °C	22
3	<i>m</i> -CPBA (72%)	NaHCO ₃ (5 eq.)	toluene, –15 °C	31
4	<i>m</i> -CPBA (99%)	NaHCO ₃ (5 eq.)	CH ₂ Cl ₂ , –30 °C	40
5	<i>m</i> -CPBA (72%)→TBAF	NaHCO ₃ (5 eq.)	CH ₂ Cl ₂ , –15 °C to rt	decomposition
6	Cl ₂ -Davis oxaziridine	–	CH ₂ Cl ₂ , rt	no reaction
7	EtOK→ Cl ₂ -Davis	–	THF, 0 °C	1.393
8	EtOK→ P(OEt) ₂ , O ₂	–	THF, rt	1.393
9	<i>m</i> -CPBA (99%)	KHCO ₃ (10 eq.)	CH ₂ Cl ₂ , 0 °C	low conv. ^a
10	OsO ₄ , NMO	pyridine (1 eq.)	<i>t</i> -BuOH, H ₂ O	no reaction
11	Sharpless AD-mix α	MeSO ₂ NH ₂	<i>t</i> -BuOH, H ₂ O	low conv.
12	oxone, acetone	18-c-6, NaHCO ₃ (70 eq.)	CH ₂ Cl ₂ , H ₂ O, rt	– ^[a]
13	oxone, acetone	18-c-6, NaHCO ₃ (70 eq.)	CH ₂ Cl ₂ , H ₂ O, 0 °C	– ^[a]
14	DMDO	–	CH ₂ Cl ₂ , acetone, 0 °C	low conv.

[a] Oxidation of the disubstituted double bond.

At this point, it was evident that bulky enol ethers like **1.389** and **1.390** could not be oxidized with sufficient efficiency. It is perhaps not surprising that while a plethora of other oxidants is

available for Rubottom-like oxidations of silyl enol ethers, all of them utilize the much less hindered trimethylsilyl enol ethers.^[225-227]

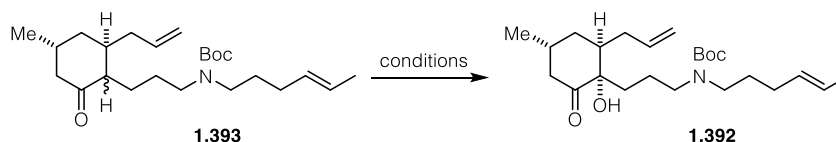
Alternatively, we explored the α -oxygenation from the ketone **1.393** obtained by straightforward TBAF treatment, hoping that the lower reactivity would be offset by the lower steric hindrance.



Scheme 1.74. Deprotection of TBS enol ether **1.389**.

To this end, we submitted the ketone to conditions originally developed by Moriarty (Table 1.3), which were completely ineffective (entries 1–3).^[228-229] We next explored Jiao's very simple hydroxylation conditions with cesium carbonate as a base and DMSO as the solvent (entry 4).^[230] Under these and Gardner's related conditions,^[222] partial conversion to the α -hydroxyketone was observed, but the isolated yield was low and the stereoselectivity poor, not exceeding 1.5–2:1 (entry 5).

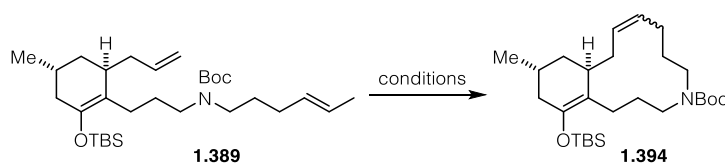
Table 1.3. Direct α -oxidation of ketone **1.393**.



entry	oxidant	additives	solvent	yield [%]
1	PhIO	NaOH	MeOH, 60 °C	no reaction
2	PhI(OAc) ₂	NaOH	MeOH, 60 °C	no reaction
3	2-iodosylbenzoic acid	NaOH	MeOH, 60 °C	no reaction
4	O ₂	Cs ₂ CO ₃ , P(OEt) ₃	DMSO, rt	20
5	O ₂	KOt-Bu	<i>t</i> -BuOH, DMF, rt	22

Given these mixed results, we reasoned that a bicyclic intermediate **1.394** could be better suited for selective oxidation due to its lower flexibility. We thus began to investigate the key ring-closing alkene metathesis to form a twelve-membered ring. We were aware that twelve-membered rings are amongst most difficult macrocycles to form due to their significant transannular strain.^[231-233] The results of our screening with the TBS enol ether **1.389** are summarized in Table 1.4.

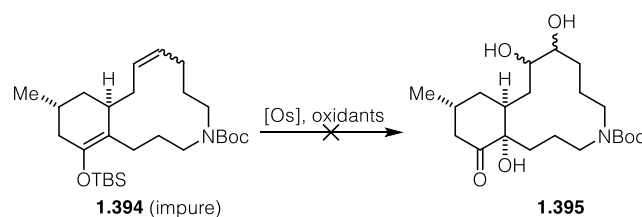
Table 1.4. Ring-closing metathesis of silyl enol ether **1.389**. All experiments were carried out with 15 mol% catalyst.



entry	catalyst, solvent	T [°C], t [h]	concentration [mM]	product, yield [%]
1	G II, CH ₂ Cl ₂	40, 7	10	product+dimer, 47
2	G II, CH ₂ Cl ₂	40, 7	10	product+dimer, 49
3	HG II, CH ₂ Cl ₂	40, 5.5	10	product+dimer, 65
4	HG II, PhMe	80, 5.5	6	product+dimer, 70
5	HG II, PhMe	80, 5.5	4	product+dimer, 46
6	Grela catalyst, PhMe	25, 7.5	3	product, 20
7	HG II, CH ₂ Cl ₂	25, 24	0.8	traces
8	G II, CH ₂ Cl ₂	25, 24	1	traces

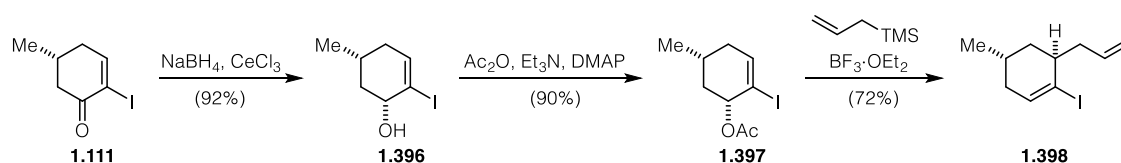
As can be seen from Table 1.4, the product **1.394** could be obtained with Grubbs 2nd generation and Hoveyda–Grubbs 2nd generation catalysts as well as the Grela catalyst.^[234–236] However, the product was consistently contaminated with compounds that could not be cleanly isolated, but were identified as dimers and trimers by high-resolution mass spectroscopy. Given that oligomers were obtained even at very high dilutions, we deemed the silyl enol ether **1.389** unsuitable for further experiments. As a testament to its stability, the silyl enol ether moiety was left untouched under all conditions and no hydrolysis was observed.

With these mixtures of desired product and oligomers, we wanted to investigate whether the silyl enol ether could be dihydroxylated in conjunction with the alkene obtained by RCM. While isolation of pure product was again unfeasible, we were able to identify that even with excess oxidizing agents, the disubstituted double bond had been dihydroxylated exclusively.



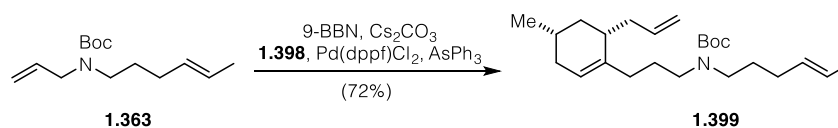
Scheme 1.75. Unsuccessful attempts at post-RCM α -oxidations.

Given these findings, we reevaluated our retrosynthesis. Postponing the oxidation of the silyl enol ether to the α -hydroxyketone to the post-metathesis stage did not render the reaction more efficient, and the metathesis itself had only yielded variable mixture of product and oligomers. Therefore, we next pursued an approach in which the oxidation pattern of the skeleton would be introduced from an almost fully reduced bicycle. Tracing it back the same way as before, this led to the identical side chain **1.363** and a cyclohexene building block **1.398**. This building block is readily available in racemic form,^[83] but enantioselective variants are available as well in a more step-intensive fashion.^[84]



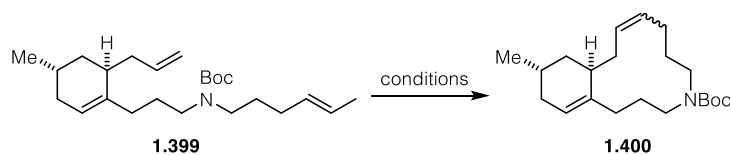
Scheme 1.76. Synthesis of vinyl iodide precursor **1.398**.

Starting from racemic iodoenone **1.111**, Luche reduction to **1.396** and acetylation gave the allylic acetate **1.397**. Even though these transformations were very clean, it was mandatory to purify the material *via* column chromatography at this stage to obtain a satisfactory yield in the next step. Treatment of allylic acetate **1.397** with excess allyltrimethylsilane and boron trifluoride diethyl etherate at elevated temperature gave vinyl iodide **1.398**, presumably *via* the *C*_s-symmetric cation. In accordance with the literature, the diastereoselectivity was 2.8–3.0:1, the desired *trans* diastereomer predominating.^[83] This building block was coupled to the side chain **1.363** under our previously established conditions to yield **1.399** in quantitative yield (*d.r.* 3.0:1). At this stage, the diastereomers could be separated, giving the desired diastereomer in 72% yield.



Scheme 1.77. *B*-alkyl Suzuki coupling of vinyl iodide **1.398** to sidechain **1.363**.

With this molecule in hand, we were in a position to reinvestigate our metathesis reaction with a less oxidized precursor (Table 1.5).

Table 1.5. Ring-closing metathesis of cyclohexene **1.399**. Experiments were carried out with 20 mol% catalyst.

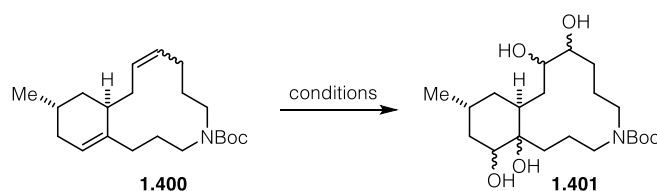
entry	catalyst, solvent	T [°C], t [h]	concentration [mM]	product, yield [%]
1	HG II, CH ₂ Cl ₂	40, 24	3	product+dimer, 44
2	<i>i</i> -Pr-HG II, CH ₂ Cl ₂	40, 48	3	product+dimer, 55
3	SG, PhMe	80, 24	3	dimer, 24
4	SG, CH ₂ Cl ₂	40, 26	3	dimer, 62
5	SG, CH ₂ Cl ₂ ^[a]	40, 24	3	dimer, 66
6	SG, C ₂ H ₄ Cl ₂	85, 48	3	dimer, 84
7	SG, C ₂ H ₄ Cl ₂	85, 48	0.2	dimer, 44
8	SG, CH ₂ Cl ₂	40, 48	0.2	traces
9	G I, CH ₂ Cl ₂	40, 48	3	dimer, 30
10	G I, CH ₂ Cl ₂	40, 48	0.2	60
11	G I, CH ₂ Cl ₂	40, 72	0.2	65
12	G I, CH ₂ Cl ₂	40, 72	1	36
13	G I, CH ₂ Cl ₂	40, 72	0.5	50
14	G I, CH ₂ Cl ₂ ^[b]	40, 72	0.2	62
15	G I (30%), CH ₂ Cl ₂ ^[b]	40, 72	0.2	70

[a] CH₂Cl₂ dried over molecular sieves was used; [b] CH₂Cl₂ was distilled from the reaction mixture and reused in subsequent RCM reactions without noticeable decrease in reaction efficiency.

It quickly became apparent that all second generation catalysts were not well-suited for this particular ring-closing metathesis. Also, compared to the screening in Table 1.4, all reactions in Table 1.5 were much slower. The Hoveyda–Grubbs catalyst gave a mixture of products that was not easily separated (entry 1), as did the isopropyl-Hoveyda–Grubbs variant that bears the SIPr NHC ligand instead of the regular SIMes NHC (entry 2).^[237] Reasoning that a less hindered variant could display different reactivity, we switched to the Stewart-Grubbs catalyst that contains *o*-tolyl instead of mesityl substituents on the NHC.^[237-238] After screening dichloromethane (HPLC grade or dry over molecular sieves), toluene and dichloroethane, we established dichloroethane as the best solvent, giving a single product in high yield (entries 3–

6). Unfortunately, after some experimentation, we found that the dimer had been formed in this and other reactions using second generation catalysts, even at extremely high dilution (entries 7 and 8). After this setback, we hoped that a very catalyst scaffold could furnish the desired twelve-membered ring. We thus turned to the NHC-free first generation Grubbs catalyst, which performed as poorly as the others at 3 mM, giving a moderate yield of multiple products (entry 9). However, upon careful optimization, it was found that lowering the concentration further to 0.2 mM, an acceptable yield could be obtained (entry 10), even slightly higher (and experimentally more convenient) concentrations were detrimental to the reaction yield (entries 12 and 13). Extending the reaction time was beneficial (entry 11). It was also found that vigorous degassing by freeze-pump-thaw was not necessary and sparging with argon was sufficient, as was using dichloromethane recycled from previous metathesis experiments (entry 14). Increasing the catalyst loading further to 30 mol%, added in three portions over three days (entry 15), slightly increased the yield to 70% (78% based on recovered starting material). Pleased to have finally closed the macrocycle, we immediately pressed on to the following oxidations (Table 1.6). Unfortunately, the twelve-membered ring **1.400** was obtained as a 1:1 mixture of *E* and *Z* alkene isomers that were inseparable at this stage.

Table 1.6 Double dihydroxylation of bisalkene **1.400** to tetraol **1.401**; all reactions carried out at room temperature.

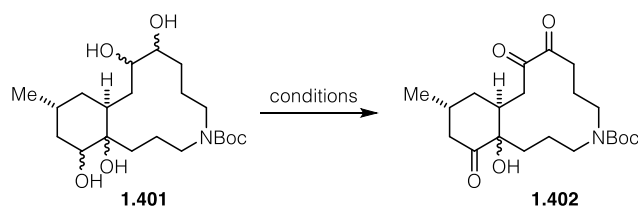


entry	oxidants (eq.)	additives (eq.)	solvent, reaction time [h]	yield [%]
1	OsO ₄ (0.1), NMO (2.4)	–	<i>t</i> -BuOH, H ₂ O, 24	35
2	OsO ₄ (0.2), NMO (2.4)	–	<i>t</i> -BuOH, H ₂ O, 16	80
3	OsO ₄ (0.2), NMO (2.4)	py (1.0)	<i>t</i> -BuOH, H ₂ O, 24	70 (impure)
4	OsO ₄ (0.2), NMO (2.0)	2,6-lutidine (1.0)	dioxane, acetone, H ₂ O, 16	65 (impure)
5	OsCl ₃ (0.1), K ₃ [Fe(CN) ₆] (6.0)	quinuclidine (0.5), MeSO ₂ NH ₂ (2.0)	<i>t</i> -BuOH, H ₂ O, 24	70
6	AD-mix α+β 1:1 (2.0)	MeSO ₂ NH ₂ (2.0)	<i>t</i> -BuOH, H ₂ O, 48	low conv.
7	AD-mix β (2.0)	MeSO ₂ NH ₂ (2.0)	<i>t</i> -BuOH, H ₂ O, 48	low conv.
8	AD-mix α (2.0)	MeSO ₂ NH ₂ (2.0)	<i>t</i> -BuOH, H ₂ O, 48	low conv.
9	RuCl ₃ (0.15), NaIO ₄ (3.0)	–	acetone, MeCN, H ₂ O, 6	– ^[a]

[a] oxidative cleavage was observed.

Osmium-based methods^[239] provided the desired tetraol in modest (entry 1) to good (entry 2) yield, with additives like pyridine^[240] and 2,6-lutidine^[241] (entries 3 and 4) giving worse results and intractable side products. An Os(III)-based system developed by Warren as a racemic Sharpless variant offered no benefit in terms of yield (entry 5).^[242] Sharpless' AD-mixes in different ratios provided low conversions (entries 6–8).^[243-244] A dihydroxylation using ruthenium trichloride resulted in oxidative cleavage of the disubstituted double bond (entry 9).^[245] While the transformations were generally rather clean, the identity of the product **1.401** could only be established by mass spectroscopy and LC-MS. ¹H NMR showed peaks that were plausible for a tetraol like **1.401**, but did not allow for analysis of diastereoselectivity. It was unclear whether this was a result of the *E/Z* mixture of isomers in the starting material or an inherent lack of selectivity in the double dihydroxylation. Nevertheless, we were pleased to have introduced the tertiary alcohol, which had been a major problem in the previous approach. Furthermore, we hoped that the mixture of diastereomers obtained in the oxidation would be inconsequential once the three secondary alcohols were oxidized to ketones. Our results for the oxidation are summarized in Table 1.7.

Table 1.7. Oxidation of tetraol **1.401** to triketone **1.402**.



entry	oxidant	additive (eq.)	solvent, temperature [°C],	yield [%]
1	DMP	–	CH ₂ Cl ₂ , rt	45, impure
2	DMP	NaHCO ₃	CH ₂ Cl ₂ , rt	42, impure
3	IBX	–	DMSO, THF, rt	60, impure
4	IBX	–	DMSO, EtOAc, rt	65, impure
5	NBS	py (1.0)	CCl ₄ , 70 °C	complex mixture
6	NMP·HBr ₃ , H ₂ O ₂	–	MeCN, 80 °C	α-bromination
7	MeReO ₃ , H ₂ O ₂	–	MeCN, 80 °C	decomposition
8	thiourea, TBHP	–	MeCN, 65 °C	decomposition
9	PhICl ₂ , TEMPO	py (12)	CHCl ₃ , 50 °C	decomposition
10	4-NHAc-TEMPO	p-TsOH·H ₂ O	CH ₂ Cl ₂ , 0 °C to rt	complex mixture
11	Bobbitt salt	–	CH ₂ Cl ₂ , 0 °C to rt	complex mixture

entry	oxidant	additive (eq.)	solvent, temperature [°C],	yield [%]
12	Bobbitt salt	silica (100 wt%)	CH ₂ Cl ₂ , 0 °C to rt	63, impure
13	IBX	–	acetone, EtOAc, 80 °C	65, impure
14	IBX	–	EtOAc, 80 °C	80, impure
15	IBX	–	MeCN, 80 °C	60, impure
16	IBX	–	acetone, 60 °C	70, impure

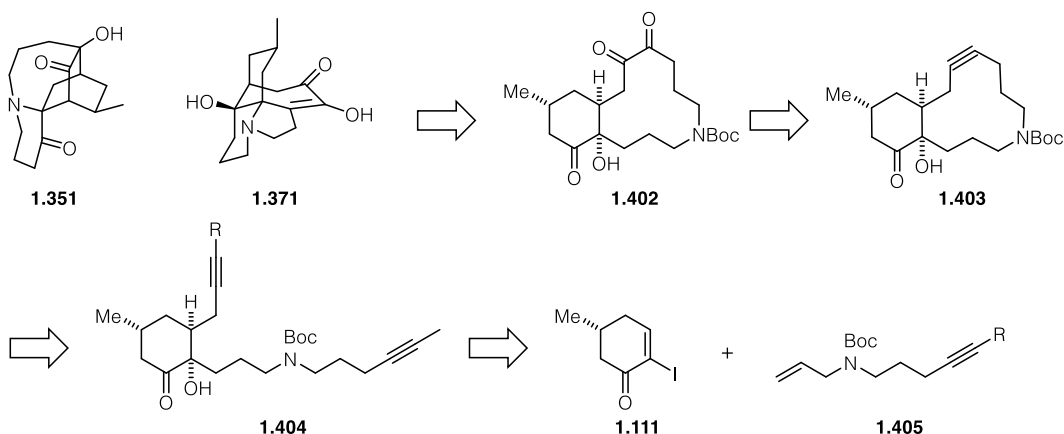
Initial experiments using Dess–Martin periodinane^[246] (entries 1 and 2) provided small amounts of material bearing the correct mass of triketone **1.402**, accompanied by C–C cleavage products. It was reported by Santagostino that the closely related IBX smoothly oxidizes 1,2-diols to the corresponding 1,2-diketones without C–C cleavage.^[247] The crucial insight was that IBX, which had previously only been used for the preparation of DMP due to its low solubility in virtually all organic solvents, is quite soluble in DMSO. Indeed, we obtained an improved yield and no side products originating from C–C cleavage (entries 3 and 4). Under all these conditions, we were unable to isolate a single reaction product, with ¹H NMR indicating the presence of at least three structurally similar products. We therefore investigated other procedures. A pyridine-NBS-based method (entry 5)^[248] resulted in a very complex mixture, possibly arising from partial formation of an enone by α -bromination and elimination. A much cleaner reaction profile was obtained using a NMP·HBr₃ in combination with hydrogen peroxide as the stoichiometric oxidant. However, the major product was again the enone (entry 6).^[249] Methyltrioxorhenium/H₂O₂^[250] as well as thiourea dioxide/TBHP mainly led to decomposition (entries 7 and 8).^[251] We next turned to oxoammonium-mediated or -catalyzed oxidations, which have more recently been developed as convenient and mild metal-free alternatives to most classic oxidations.^[252] We thus turned to Zhao's procedure utilizing stoichiometric amounts of iodobenzene dichloride in conjunction with TEMPO and pyridine (entry 9).^[253] Unfortunately, only decomposition was observed. Banwell's procedure for the *in situ* disproportionation of a TEMPO derivative under acidic conditions provided some product alongside various side products (entry 10).^[254] Reasoning that this disproportionation was not efficient enough, we turned to stoichiometric oxoammonium salts as described by Bobbitt.^[255], resulting in a complex mixture (entry 11). However, adding silica gel to the reaction mixture (entry 12) drastically improved the reaction (entry 12).^[256] Given that these oxidations also yielded various products all bearing the desired mass according to LC-MS, we returned once more to IBX-mediated procedures in the hope of getting a single identifiable product. Finney disclosed an oxidation protocol that makes use of its low solubility at room temperature.^[257] He found that IBX is

slightly soluble in a range of organic solvents at higher temperatures, thus combining the advantages of homogenous (fast reactions) and heterogeneous (easy workup by filtration) reactions. A small screening (entries 13–16) established ethyl acetate as the solvent of choice, giving the usual mixture in a good combined yield after simple filtration.

At this stage, we had performed three consecutive steps without complete assignment of structure. On the other hand, the putative product represented our final intermediate *en route* to lycoplamine H (**1.351**) and lycojaponicum D (**1.371**). Therefore, we submitted the mixture obtained by IBX oxidation to acidic conditions, expecting to induce the Mannich reaction after Boc deprotection. To our disappointment, neither trifluoroacetic acid^[56], amberlyst-15^[258] nor HCl in methanol^[41] or dioxane resulted in appreciable conversion, let alone natural product formation. This complete lack of reactivity shed serious doubt on the structural assignment. We therefore decided to explore a different, more stepwise approach that would allow for unambiguous establishment of all intermediates along the way.

1.3.3 The RCAM route

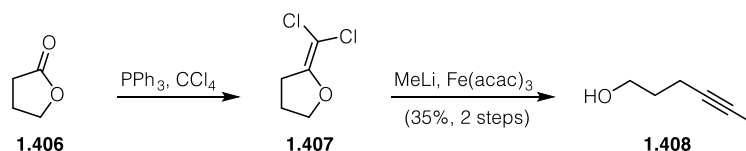
Given the problems with the oxidation steps in our previous approach to triketone **1.402** (chapter 1.3.2), we decided to pursue a slightly different tactic that would hopefully address its shortcomings. While the overall Mannich strategy from triketone **1.402** remained the same and the diketone would be furnished by oxidation,^[259] we wanted to close the challenging twelve-membered ring in **1.402** by a ring closing *alkyne* metathesis (RCAM). In recent years, alkyne metathesis has transitioned from a method primarily used for industrial interconversion of hydrocarbons to a powerful methodology to install triple bonds in highly functionalized molecules in completely orthogonal fashion to *alkene* metathesis.^[260-262] In particular, with the advent of Fürstner's silyloxy-substituted tungsten- and molybdenum-based catalysts, which are available as reasonably air- and moisture phenanthroline adducts (Figure 1.13), alkyne metathesis has become an increasingly attractive alternative to olefin metathesis for total synthesis purposes.^[263-264] We were aware that the ring strain induced by the two *sp*-hybridized atoms of an alkyne in a twelve-membered ring like **1.403** would be significantly higher compared to its *sp*²-hybridized alkene counterpart.^[265-266]



Scheme 1.78. Revised retrosynthesis based on RCAM chemistry. R = H, Me.

The remainder of the synthesis would be largely similar to the first RCM route, with the obvious difference that the conjugate allylation would be replaced with a conjugate propargylation to give **1.404** after α -oxidation.^[56, 267] It was not clear whether the alkyne introduced this way had to be methyl-capped or not.^[268-272] Furthermore, the synthesis of the side chain **1.405**, again thought to be coupled to iodoenone **1.111** *via* *B*-alkyl Suzuki coupling, would have to be revised to accommodate the necessary internal alkyne.

With a new retrosynthesis defined, we set out to synthesize the alkyne-bearing side chain **1.405** with R = H or Me. Treatment of γ -butyrolactone (**1.406**) with $\text{PPh}_3/\text{CCl}_4$ resulted in dichloromethylenation to **1.407**.^[273] Treatment of this compound with excess methyllithium and catalytic $\text{Fe}(\text{acac})_3$ according to Fürstner's method^[274] resulted in formation of hex-4-yn-1-ol (**1.408**) in moderate yield (Scheme 1.79).

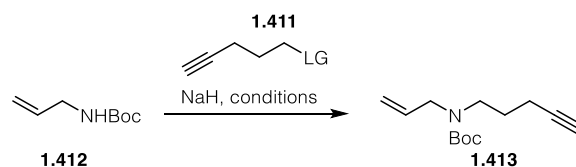


Scheme 1.79. Synthesis of hex-4-yn-1-ol (**1.408**) from γ -butyrolactone (**1.406**) *via* Suarez reaction and elimination.

Mainly because of the large amounts of PPh_3 and CCl_4 needed for larger scales, we decided to explore a more practical route where the methyl group would be introduced in the final step. To this end, pent-4-yn-1-ol was mesylated under standard conditions (MsCl , Et_3N) (**1.409**) and also transformed into the corresponding chloride **1.410** and iodide **1.284** by standard Appel conditions (not shown). With these alkylating agents **1.411** in hand, we proceeded with the alkylation of Boc-allylamine (**1.412**) (Table 1.8). The mesylate was unreactive when treated with the anion of **1.412** (entry 1), but a moderate yield was obtained in the presence of catalytic TBAI (entry 2). No reaction was observed when unprotected allylamine was reacted with **1.409**

(entry 3). The same trends were observed with chloride **1.410** (entries 4–6). The best yield was finally obtained with iodide **1.284**, which gave a good yield of **1.413**.

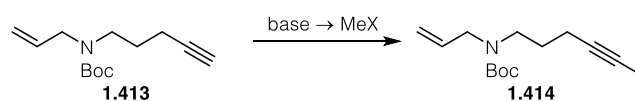
Table 1.8. Alkylation of Boc-allylamine (**1.412**) with a generic C₅ alkylating agent **1.411**.



entry	leaving group (eq.)	additive (eq.)	solvent, temperature [°C]	yield [%]
1	OMs 1.409 (1.5)	–	DMF, 0 → 50	–
2	OMs 1.409 (1.5)	TBAI (0.3)	DMF, 0 → 50	60
3	OMs 1.409 (1.5)	Et ₃ N/allylamine instead of NaH	THF, 23	no reaction
4	Cl 1.410 (1.3)		DMF, 0 → 50	35
5	Cl 1.410 (1.5)	Nal (0.1)	DMF, 0 → 50	64
6	Cl 1.410 (1.5)	TBAI (0.3)	DMF, 0 → 50	62
7	I 1.284 (1.2)		DMF, 0 → 50	80

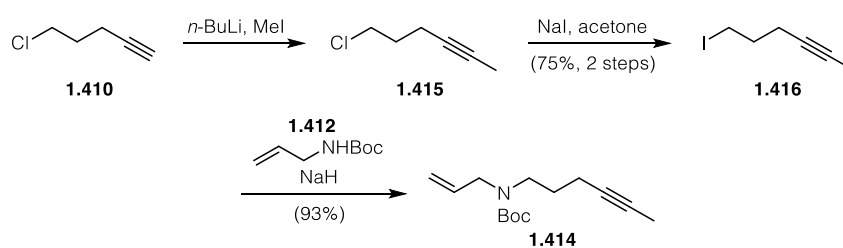
The methylation of the terminal alkyne in **1.413** was accomplished by deprotonation followed by quenching with the electrophilic methyl sources methyl iodide and methyl triflate to give the full side chain **1.414** (Table 1.9).

Table 1.9. Methylation of alkyne **1.413**.



entry	base (eq.)	alkylating agent (eq.)	solvent, temperature [°C]	yield [%]
1	<i>n</i> -BuLi (1.1)	Mel (1.2)	THF, –78 °C	25
2	<i>n</i> -BuLi (1.1)	Mel (1.5)	THF, –78 → –60 °C	35
3	LiHMDS (1.2)	Mel (1.5)	THF, –78 → –60 °C	30
4	<i>n</i> -BuLi (1.1)	Mel (1.2)	THF, HMPA–78 °C	40
5	<i>n</i> -BuLi (1.1)	MeOTf (1.2)	THF, –78 °C	45

Even though the synthetic sequence was short and appreciable amounts of the side chain **1.414** were obtained with MeI (entries 1–4) as well as MeOTf (entry 5), the low efficiency of this route and use of toxic methyl triflate rendered the sequence inconvenient on larger scale. Therefore, we decided to introduce the methyl group at an earlier stage. Using a slightly modified literature procedure, 5-chloro-1-pentyne (**1.410**) was methylated with methyl iodide to give 6-chlorohex-2-yne (**1.415**).^[275] The crude product was transformed into the iodide (**1.416**) under classic Finkelstein conditions in good overall yield (Scheme 1.80).



Scheme 1.80. Synthesis of the complete side chain **1.414**.

Under the conditions we had previously optimized for the alkylation of **1.412** with 5-iodopent-1-yne (**1.284**), we could access the full side chain **1.414** in very good yield on multi-gram scale. With the side chain in hand, the fragment coupling by *B*-alkyl Suzuki reaction could be investigated, the results of which are summarized in Table 1.10. In all cases, the side chain **1.414** was hydroborated with 1.2–1.5 equivalents 9-BBN in THF at room temperature or 40 °C, which had a negligible effect on the reaction outcome.

Table 1.10. *B*-alkyl Suzuki coupling of terminal alkene **1.414**.



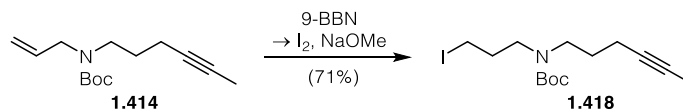
entry	palladium source (eq.), ligand (eq.)	base (eq.)	solvent, temperature [°C]	yield [%]
1	Pd(dppf)Cl ₂ (0.05), AsPh ₃ (0.1)	NaOH (3.0)	THF, DMF, rt	40
2	Pd(dppf)Cl ₂ (0.1)	NaOH (3.0)	THF, H ₂ O, 70	43
3	Pd(dppf)Cl ₂ (0.1)	NaOH (4.5)	THF, H ₂ O, 70	48
4	Pd(dppf)Cl ₂ (0.1)	NaOH (6.0)	THF, H ₂ O, 70	58
5	Pd(dppf)Cl ₂ (0.1)	K ₃ PO ₄ (1.2)	DMF, 50	42
6	Pd(dppf)Cl ₂ (0.1), AsPh ₃ (0.1)	Cs ₂ CO ₃ (4.0)	THF, DMF, 50	65 ^[a]
7	Pd(dppf)Cl ₂ (0.1), AsPh ₃ (0.1)	Cs ₂ CO ₃ (4.0)	THF, DMF, 50	49 ^[b]

entry	palladium source (eq.), ligand (eq.)	base (eq.)	solvent, temperature [°C]	yield [%]
8	Pd(dppf)Cl ₂ (0.1), AsPh ₃ (0.1)	Cs ₂ CO ₃ (4.0)	THF, DMF, 40	32 ^[c]
9	Pd(dppf)Cl ₂ (0.1)	Cs ₂ CO ₃ (3.0)	THF, 70	decomposition
10	Pd(dppf)Cl ₂ (0.1), AsPh ₃ (0.1)	NaOH (6.0)	THF, H ₂ O, 70	52
11	Pd(OAc) ₂ (0.05), RuPhos (0.1)	K ₃ PO ₄ (2.0)	THF, PhMe, 100	40
12	Pd(OAc) ₂ (0.1), RuPhos (0.12)	Cs ₂ CO ₃ (6.0)	THF, rt	70
13	Pd(OAc) ₂ (0.08), RuPhos (0.1)	Cs ₂ CO ₃ (6.0)	THF, rt	65 ^[b]
14	Pd G2 (0.05), SPhos (0.05)	Cs ₂ CO ₃ (2.0)	THF, DMF, 50	35
15	Pd G2 (0.08), SPhos (0.1)	Cs ₂ CO ₃ (6.0)	THF, DMF, 50	76 ^[e]

[a] 0.1 mmol scale; [b] 1.4 mmol scale; [c] the Cbz-protected amine was used; [d] the *B*-alkyl Suzuki partner was prepared separately by hydroboration with HBPIn; [e] 4.0 mmol scale.

Surprisingly, the seemingly minor modification within the side chain had a major impact on the coupling efficiency. Under the Trost conditions that had served us very well in the alkene series (86%),^[276] the target enone was obtained in only 50% yield (entry 1). Suzuki's original conditions, that were also previously used for similar *B*-alkyl Suzuki couplings in *Lycopodium* alkaloid total synthesis (entries 2–4),^[277–278] did not offer much improvement and were irreproducible on larger scale. Suzuki's protocol using potassium phosphate as base did not perform better, either.^[279] Modification of the reaction temperature improved the yield on small scale (entry 6), but offered no advantage in scalability (entry 7). We also prepared the Cbz-protected side chain, which performed worse than its Boc-protected counterpart (entry 8), and a BPin sidechain by iridium-catalyzed hydroboration,^[280] which only led to decomposition (entry 9). Combination of the conditions in entries 1 and 4) gave no improvement. However, switching to Buchwald's RuPhos ligands and Pd(OAc)₂ as the palladium source allowed for a much better reaction yield (entries 11–13).^[281] Finally, switching to Buchwald's 2nd generation precatalyst with added SPhos enabled an efficient coupling on 4 mmol scale (entries 14 and 15).^[282–284]

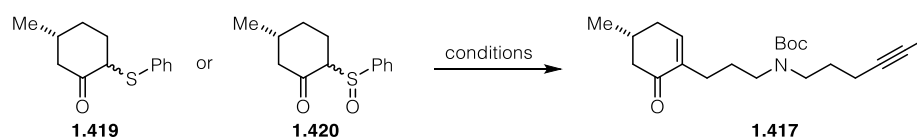
We also attempted the synthesis of enone **1.417** by alkylation of the known pulegone-derived ketone bearing an α -thiophenyl or α -phenylsulfinyl group. To this end, we prepared the unstable primary iodide **1.418** *via* Brown's hydroboration-iodination sequence.^[285–287]



Scheme 1.81. Anti-Markovnikov hydroiodination *via* hydroboration and oxidation of **1.414**.

Under conditions established by Dake,^[57] the sulfoxide was treated with DBU and iodide **1.418** at low temperature, followed by heating to induce sulfoxide elimination (entry 1) This resulted in decomposition, but a slower increase in temperature provided traces of the desired product with both DBU (entry 2) and NaH (entry 3) as base. Siegel's conditions for the alkylation were attempted next.^[144, 148] Using the sulfide **1.419**, no notable conversion was observed before decomposition of iodide **1.418** set in (entries 4–6).

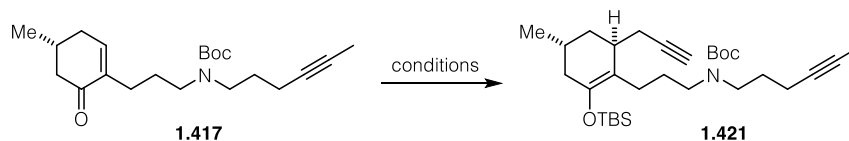
Table 1.11. The enolate alkylation approach toward enone **1.417**.



entry	ketone	base	solvent, temperature [°C]	yield [%]
1	sulfoxide 1.420	DBU	DMF, -40 to 40 °C	decomposition
2	sulfoxide 1.420	DBU	DMF, -40 to 0 to 40 °C	traces
3	sulfoxide 1.420	NaH	DMF, 0 to 40 °C	traces
4	sulfide 1.419	Cs ₂ CO ₃	DMF, 0 °C to rt	no conversion
5	sulfide 1.419	DBU	DMF, 0 °C to rt	no conversion
6	sulfide 1.419	DBU	DMF, 0 °C to rt	no conversion

Even though the alkylation approach was not successful, the Suzuki approach supplied ample material, so we proceeded to the conjugate propargylation (Table 1.12). Application of our previously established allylation conditions, using the technical grade allenyl- instead of the allylstannane, gave a small amount of the desired silyl enol ether **1.421** (entry 1).

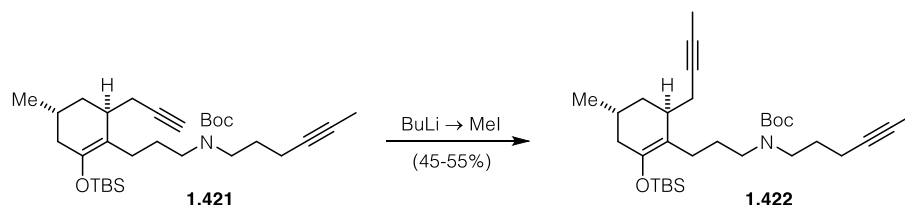
When fresh allenyltributylstannane prepared according to Torii's procedure was used,^[288] the yield was significantly improved compared to the commercially available stannane (entry 2). However, the reaction yield was highly variable, limiting effective material throughput. Under Haruta's original conditions without base and molecular sieves or at higher temperatures, decomposition was observed (entries 3 and 4).^[267]

Table 1.12. Conjugate propargylation of enone **1.417**.

entry	propargylating reagent	additives	solvent, temperature [°C]	yield [%]
1	allenylSnBu ₃ (80%)	TBSOTf, DTBPy, MS 4 Å	CH ₂ Cl ₂ , -78	15
2	allenylSnBu ₃ (pure)	TBSOTf, DTBPy, MS 4 Å	CH ₂ Cl ₂ , -78	20–58
3	allenylSnBu ₃ (pure)	TBSOTf	CH ₂ Cl ₂ , -78	decomposition
4	allenylSnBu ₃ (pure)	TBSOTf, DTBPy, MS 4 Å	CH ₂ Cl ₂ , 0	decomposition
5	allenylSnBu ₃ (pure)	TBSOTf, DTBPy, MS 4 Å	MeCN, -78	low conv.
6	allenylSnBu ₃ (pure)	TBSOTf, DTBPy, MS 4 Å	THF, -78	low conv.
7	In, propargyl bromide	TMSCl	THF, rt	decomposition
8	In, propargyl bromide	TBSOTf, Me ₂ S	THF, -78	decomposition
9	allenylSnPh ₃ (pure)	TBSOTf, DTBPy, MS 4 Å	CH ₂ Cl ₂ , -78 → -40	no reaction
10	allenylSnPh ₃ (pure)	TBSOTf, DTBPy, MS 4 Å	CH ₂ Cl ₂ , 0	no reaction
11	allenylSnPh ₃ (pure)	TiCl ₄	CH ₂ Cl ₂ , -78	decomposition
12	allenylSnBu ₃ (pure)	TiCl ₄	CH ₂ Cl ₂ , -78	decomposition
13	TMS-propargylMgBr	CuCN	THF, -78	1,2-addition, 40
14	TMS-propargylMgBr	CuI	THF, -78	1,2-addition, 85
15	propargylMgBr	CuI	THF, -78	no reaction
16	propargylMgBr	CuBr·Me ₂ S	THF, -78	no reaction

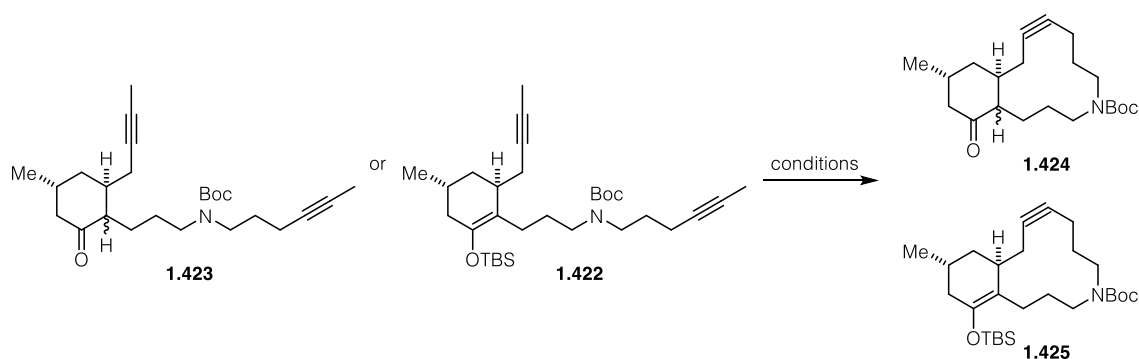
The two alternative solvents acetonitrile and THF provided low conversion (entries 5 and 6). Lee's conjugate propargylation under different Lewis-acidic conditions only resulted in decomposition (entries 7 and 8).^[289-290] Given the lack of reactivity with the indium-based reagents, we returned to allenylstannane reagents. To our disappointment, the allenyltriphenylstannane proved much less reactive than its tributyl counterpart (entries 9 and 10). We also attempted the synthesis of the propargylated ketone *via* TiCl₄ catalysis (entries 11 and 12), which resulted only in decomposition. Copper-catalyzed propargylations resulted in clean formation of the 1,2-adduct with TMS-protected propargyl Grignard (entries 13 and 14) and no reaction when propargylmagnesium bromide was used (entries 15 and 16). Cognizant of the limitations of our current approach, we wanted to press on to the RCAM step. Therefore, we

wanted to cap the terminal alkyne just introduced with a methyl group, even though some examples of alkyne metathesis reactions that are compatible with one terminal alkyne have recently surfaced.^[270-271] This was achieved with *n*-BuLi followed by treatment with methyl iodide to yield the 2-butynylated silyl enol ether **1.422** in moderate yield. LHMDS did not result in appreciable conversion.



Scheme 1.82. Methyl capping of the terminal alkyne in **1.421**.

At this point, we were in a position to attempt the ring-closing alkyne metathesis (Table 1.13). Reasoning that added conformational flexibility could be beneficial to forge the strained cyclododecyne ring, we also prepared the ketone **1.423** by simple TBAF deprotection and used it for initial investigations. The focus first was on protocols using the ill-defined molybdenum catalysts introduced by Mortreux in the 1974,^[291] which are experimentally convenient. They have undergone many rounds of improvement, mostly by empirical screening of additives and phenolic ligands.^[292-300] Under the original Mortreux conditions, only decomposition was observed (entry 1).^[291] Grela's 2-fluorophenol ligand provided traces of the desired ketone **1.424** (entry 2).^[296] Encouraged by this result, we investigated his more thoroughly optimized protocol,^[297] but this only resulted in very low conversion (entry 3). The addition of molecular sieves was not beneficial (entry 4).^[298] Bunz' conditions that are based on 4-chloro- or 4-trifluoromethylphenol as the ligand only gave starting and polymeric material (entries 5–7).^[292-295] At this point, we realized that these ill-defined complexes were not active enough for our challenging transformation. We therefore turned to the latest generation of Fürstner's catalysts that combine high catalytic performance with unmatched functional group tolerance (Figure 1.13).^[263-264, 301] The triphenylsilyloxy ligands play a crucial role in their reactivity profile, modulating the Lewis acidity of the Mo(VI) centers without compromising the reactivity of the alkylidyne unit.^[301]

Table 1.13. Ring-closing alkyne metathesis to furnish the twelve-membered bicycle **1.424**. R = H, Me.

entry	bisalkyne	catalyst system	solvent, temperature [°C]	reaction outcome
1	ketone 1.423	Mo(CO) ₆ , resorcinol	decalin, 130	decomposition
2	ketone 1.423	Mo(CO) ₆ , 2-F-phenol	PhCl, 130	traces of 1.424
3	ketone 1.423	Mo(CO) ₆ , 2-F-phenol, 3-hexyne, 1,2-MeOCH ₂	DCE, 85	low conversion
4	ketone 1.423	Mo(CO) ₆ , 2-F-phenol, 4 Å MS	PhCl, 130	traces of 1.424
5	ketone 1.423	Mo(CO) ₆ , 4-Cl-phenol	DCB, 130	low conversion
6	ketone 1.423	Mo(CO) ₆ , 4-CF ₃ -phenol	DCB, 125	low conversion
7	ketone 1.423	Mo(CO) ₆ , 4-Cl-phenol, 3-hexyne	DCB, 130	low conversion
8	ketone 1.423	1.428 , MnCl ₂ , MS 5 Å	PhMe, rt	no reaction
9	ketone 1.423	1.426 , MnCl ₂ , MS 5 Å	PhMe, 80	no reaction
10	enol ether 1.422	1.428 , MnCl ₂ , MS 5 Å	PhMe, rt	no reaction
11	enol ether 1.422	1.428 , MnCl ₂ , MS 5 Å	PhMe, 80	decomposition
12	enol ether 1.422	1.426 , MnCl ₂ , MS 5 Å	PhMe, 80	decomposition

Furthermore, it was found that one of the main drawbacks, the sensitivity towards moisture and air, could be addressed by simple complexation with 2,10-phenanthroline (**1.426** and **1.428**). These catalytically inactive adducts can be weighed in air and returned to their active state (**1.427** and **1.429**) by simple treatment with a mild Lewis acid like MnCl₂.^[264, 301] Unsurprisingly, these catalysts have largely supplanted Schrock's trialkoxytungsten(VI)-alkylidyne complex **1.430**^[302-303] or the more functional-group-compatible **1.431**^[304-305] in total synthesis applications.^[306-311]

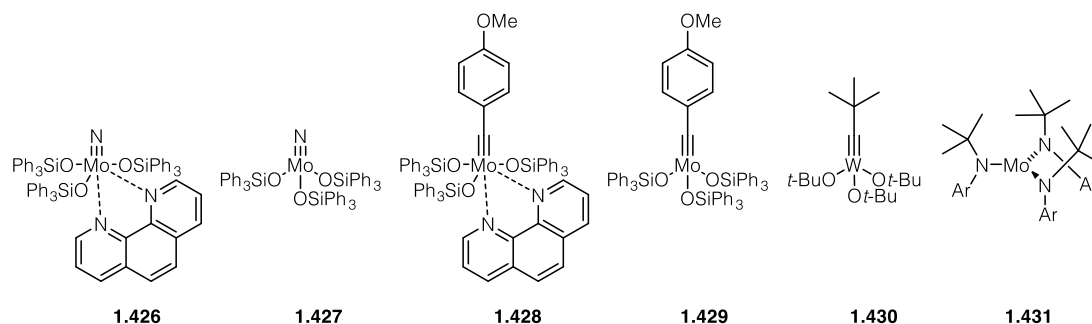
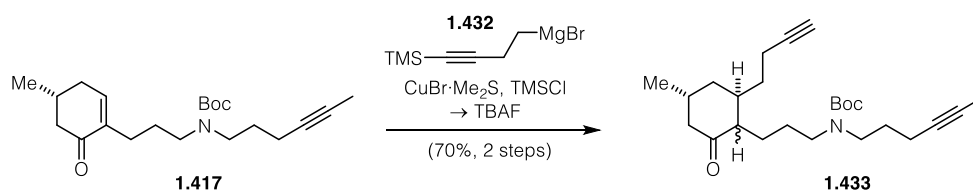


Figure 1.13. Structures of Fürstner's triphenylsilanol-substituted alkyne metathesis catalysts (**1.426–1.429**) and older high-valent metal alkylidyne catalysts **1.430** and **1.431**. **1.431** is transformed into the active alkylidyne with CH_2Cl_2 . Ar = 3,5-dimethylphenyl.

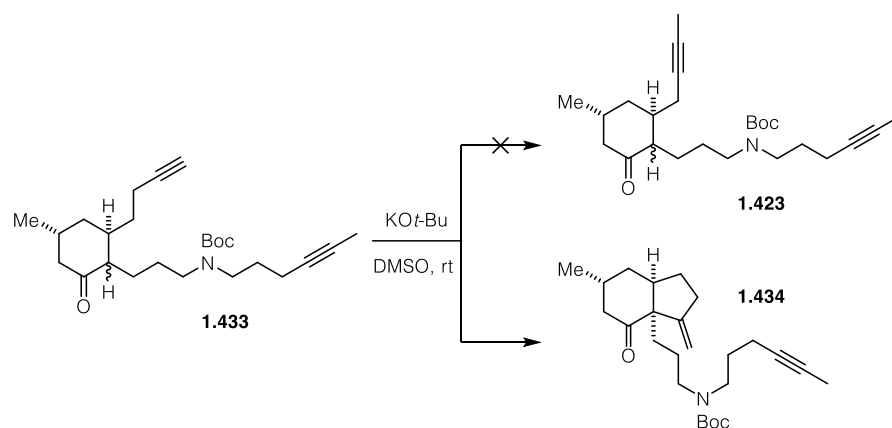
To our surprise, no reaction was observed with the two precatalysts (entries 8 and 9). We thus turned to the other possible substrate **1.422**, but realized it was unreactive at room temperature and not compatible with the active catalyst at elevated temperatures (entries 10–12).

At this stage, we were forced to reevaluate our synthetic route. While the enone **1.417** could be obtained in good yield after optimization of the Suzuki coupling, the propargylation and the methylation reactions were not reliable enough to supply sufficient material to screen the RCAM thoroughly. We therefore looked at alternative ways to introduce the 2-butynyl moiety. The introduction of a 3-butynyl chain followed by isomerization was identified as a viable option encouraged by reports from Taylor and Jamison.^[312-314] Again aiming for the ketone instead of the silyl enol ether first, we synthesized the 3-butynylated cyclohexenone **1.433** by copper-catalyzed addition of **1.432** followed by double TMS deprotection with TBAF (Scheme 1.83).



Scheme 1.83. Butynylation by cuprate addition to enone **1.417**.

When Jamison's conditions were applied to our ketone **1.433**, a rapid conversion to one product was observed. However, to our surprise, the isolated product was not the internal alkyne **1.423** resulting from isomerization to the internal alkyne; we isolated a hydrindane **1.434** bearing an *exo*-methylene group.

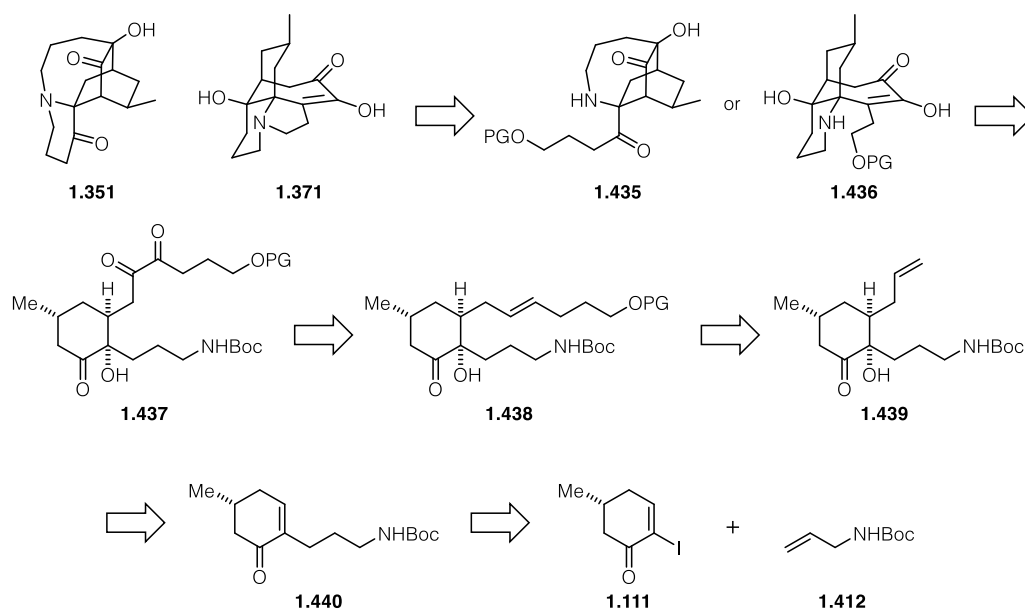


Scheme 1.84. An unexpected carbocyclization discovered during isomerization attempts of terminal alkyne **1.433** yields hydrindane **1.434**.

This finding inspired a research project exploring this largely unprecedented carbocyclization transformation and its application in *Lycopodium* alkaloid total synthesis.^[315] The results of this project are summarized in chapter 1.2.

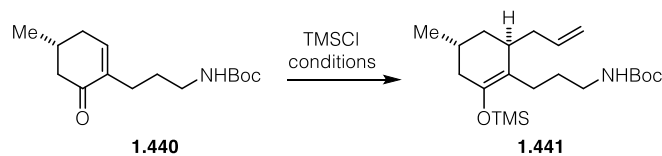
1.3.4 The alkylation route

As the two metathesis-based approaches did not furnish the desired cyclization precursor in pure form, we decided to change the order of ring-closing events. Instead of a late-stage Mannich cyclization to construct the piperidone and azocane rings, we decided to attempt the Mannich at an earlier stage. This would, in the case of lycoplamine H (**1.351**), lead to a tricyclic structure **1.435** or, in the case of lycojaponicum D (**1.371**), **1.436**. These intermediates would be obtained *via* divergent Mannich reactions of triketone **1.437** that, in turn, could be obtained from alkene **1.438**. Ultimately, it could be furnished *via* cross-metathesis and conjugate addition-oxidation to ketone **1.439**, which should be accessed from known and previously used enone building block **1.440** (see chapter 1.2.2). While more step-intensive, we expected this more conservative approach to be more reliable.



Scheme 1.85. Revised retrosynthetic analysis that avoids macrocyclizations. PG = unspecified protecting group.

With ample quantities of **1.440** in hand through a high-yielding *B*-alkyl Suzuki coupling (see chapter 1.2.2), we were in a position to screen the conjugate addition. Given our experience with the very sterically hindered TBS enol ethers **1.389** and **1.390** in the subsequent Rubottom oxidation, we wanted to focus on TMS enol ether **1.441**, expecting a more facile α -hydroxylation. We thus investigated cuprate additions as the most viable option, even though allyl additions to 2-substituted cyclohexenones are notoriously challenging.^[209-210]

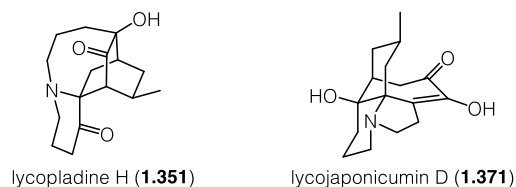
Table 1.14. Conjugate addition attempts for the synthesis of silyl enol ether **1.441**.

entry	allylating reagent (eq.)	copper source (eq.), ligand (eq.)	solvent, temperature [°C]	crude yield [%]
1	allylMgCl (3.0)	CuBr·Me ₂ S (0.3)	THF, -78	1,2-addition
2	allylMgBr (3.0)	CuBr·Me ₂ S (0.3), Me ₂ S (0.3)	THF, -78	1,2-addition
3	allylMgBr (1.5)	CuI (0.3)	THF, -78	1,2-addition
4	allylMgBr (1.5)	CuBr·Me ₂ S (1.6)	THF, -78	45
5	allylMgBr (1.5)	CuI (1.5)	THF, -78	40
6	allylMgBr (2.2)	CuBr·Me ₂ S (2.5)	THF, -100	50
7	allylMgBr (2.2)	CuBr·Me ₂ S (1.1)	THF, -78	low conversion
8	allylMgBr (3.4)	CuBr·Me ₂ S (1.7)	THF, -78	decomposition
9	allylMgBr (2.3)	CuBr·Me ₂ S (2.5)	THF, -78	70

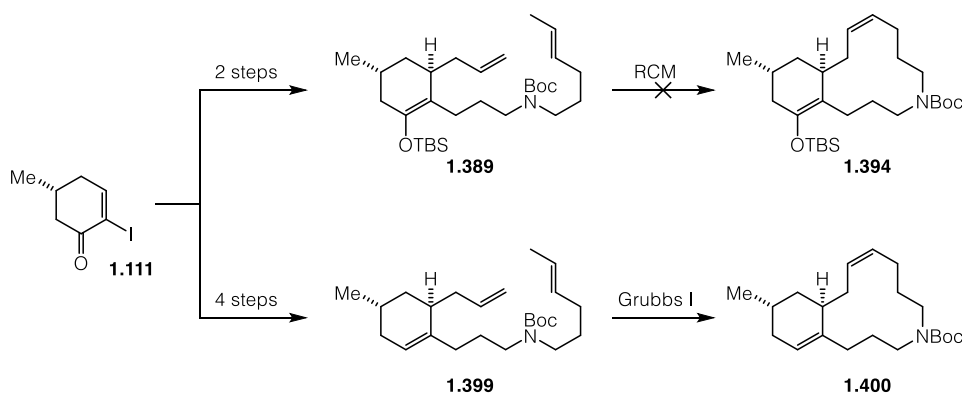
In our case, the major obstacle was to improve 1,4-selectivity over 1,2-addition which occurred with copper catalysis (entries 1–3). After screening various copper sources and reaction temperatures, it was established that only stoichiometric quantities of copper(I) bromide dimethyl sulfide complex gave the desired crude TMS enol ether **1.441** in appreciable quantities (entries 4 and 5). Conducting the reaction at -100 °C (entry 6) or with two equivalents Grignard reagent relative to copper (entry 7) did not improve the yield, and simply increasing the equivalents of organomagnesium reagent led to side products and partial hydrolysis of the silyl enol ether. The optimized conditions used 2.3 equivalents of allylmagnesium bromide and slightly more copper bromide dimethyl sulfide to ensure complete cuprate formation and suppress 1,2-addition. The crude reaction product was then used in the Rubottom oxidation without further purification. At this point, we faced the same diastereoselectivity issues first encountered in the RCM route (chapter 1.3.2): with *m*-CPBA, we obtained a 2.5:1 ratio of inseparable diastereomers and combined yield of 45%.

1.3.5 Summary and outlook

This section detailed our progress toward the *Lycopodium* alkaloids lycoplamine H (**1.351**) and lycojaponicum D (**1.371**).



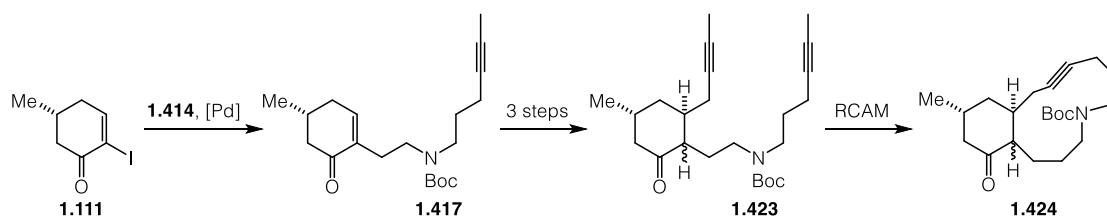
We were able to quickly furnish the first precursor to explore the key ring-closing metathesis *via* allylation conditions specifically developed for this purpose. A thorough screening revealed that silyl enol ether **1.389** was not suitable for the ring-closing metathesis to **1.394**, yielding a complex mixture of desired product as a mixture with dimers and decomposition products. Therefore, we next investigated an approach that would proceed through a reduced bicyclic system **1.399**.



Scheme 1.86. Synthesis of two RCM precursors and successful ring closure of **1.399** to **1.400**.

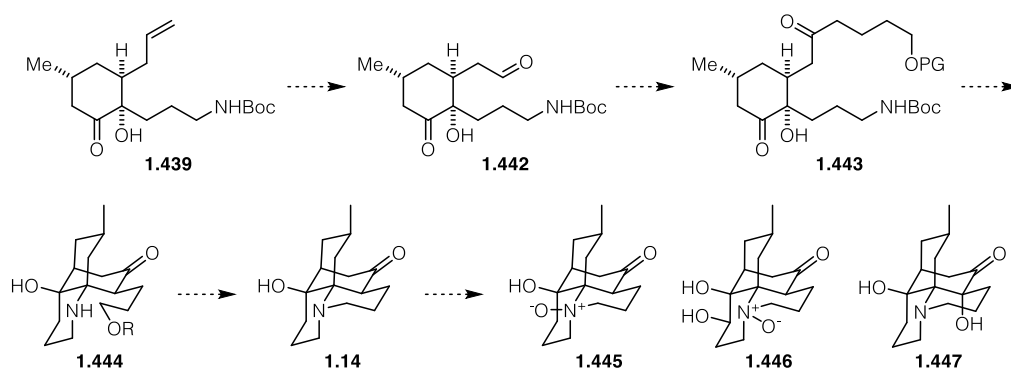
Extensive condition screening of this bisalkene revealed Grubbs' 1st generation catalyst to be optimal for the transformation to **1.400**, even though high catalyst loadings were necessary. The product, an inseparable mixture of *E* and *Z* isomers, was taken on to subsequent oxidation steps. While double dihydroxylation of the two alkenes to the tetraol **1.401** was possible, the resulting mixture of diastereomers rendered analysis at this stage very challenging. While the tetraol **1.401** could be oxidized to the triketone **1.402**, it could never be purified to unambiguously assign the structure or examine the key Mannich reaction.

We thus investigated an approach featuring RCAM for the macrocyclization. With the enone **1.417** in hand, we proceeded to the propargylation step, which turned out to be a major bottleneck due to reproducibility issues. With the product obtained *via* this route, we carried out preliminary investigations toward the key RCAM reaction.



Scheme 1.87. RCAM approach to furnish the macrocycle **1.424**.

While investigations indicated the presence of the desired macrocyclic alkyne **1.424**, these results could not be confirmed due to paucity of material. It was during efforts to streamline the precursor synthesis that we found a base-mediated carbocyclization, which was subsequently investigated as the main topic of this thesis (chapter 1.2). A future approach could consist of a monocyclic precursor for the key Mannich cyclization. Ideally, this would result in a tricyclic intermediate for the two *Lycopodium* alkaloids with only a five- or six-membered ring closure remaining. First steps to this end were undertaken and have yielded promising results (chapter 1.3.4).



Scheme 1.88. Proposed general approach to C-12-oxidized lycopodine-type *Lycopodium* alkaloids with some representative derivatives **1.445**–**1.447**. PG = unspecified protecting group.

We also realized that a compound like **1.439** could serve as a branching point toward many other *Lycopodium* C-4 and C-6-oxidized lycopodine derivatives (Scheme 1.88). Replacing the metathesis with an oxidative cleavage would give an aldehyde **1.442** that could be attacked by a bifunctional nucleophilic reagent to yield a ketone **1.443** after oxidation. This would circumvent potential problems associated with regioselective oxidation of the double bond. Lycodoline itself could serve as a platform to access a range of C-12-oxidized *Lycopodium* alkaloids, such as obscurumine A (**1.445**), diphaladine A (**1.446**) and lycoposerramine G (**1.447**), none of which have been synthesized to date.

Part 2 – Synthesis of azobenzenes for the control of
NMDA receptors

2 Synthesis of azobenzenes for the control of NMDA receptors

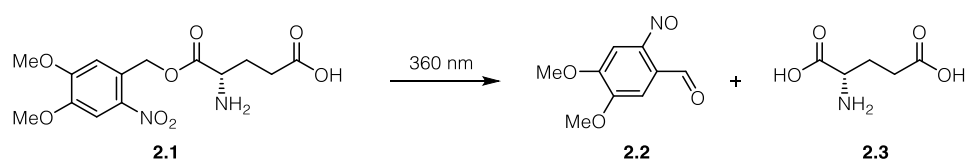
2.1 Introduction

2.1.1 Photopharmacology

The study of neuronal networks is one of the most important frontiers in today's medical, biological and chemical research.^[316] In order to address questions of high relevance for medicinal research, it is crucial to first gain a detailed understanding of the fundamental principles and dynamics of neuronal transmission and related processes. Remarkable progress has been achieved in elucidating the basic mechanisms of signal transduction in terms of molecular interactions. Yet many processes remain poorly understood in detail, such as temporal and spatial requirements for the precise and exact integration of signal cascades. To study these highly regulated processes in more detail, a large number of techniques have been explored. One method consists of genetically silencing some components, allowing the subsequent study of the effect by their absence. Another method is the genetical engineering of components to study their basic mode of action. Complementary to these biological approaches, conventional pharmacology has produced a vast variety of drugs, agonists and antagonists specifically for many types of receptors, to non-invasively study a wide variety of targets.^[317] All these methods have their specific scope of application, yet they share one main disadvantage, namely their global application: they affect whole cell composites, organs or organisms. Accordingly, there is a need for novel tools that are able to modulate and control biological function in a more spatiotemporally precise manner. One approach to resolve this issue is the combination of non-invasive light as an activating agent, chemistry and genetics. This new way of manipulating biological targets is called "photopharmacology".^[318-320]

A promising method to achieve dynamic control of receptors is the use of molecular photoswitches in combination with light.^[321] Light as the inducer of switching has the unique advantage that it can be applied with unmatched spatial and temporal precision.^[322-323] Furthermore, visible light is non-invasive and not inherently toxic. As a matter of fact, significant efforts have been devoted to shifting the absorption spectrum of all types of photoswitches to the red in order to increase tissue penetration and decrease the harmful effects of short-wavelength light, both by chemical and biochemical methods.^[324-334] With light, the desired signal can be generated in a dosed fashion by varying the intensity and exposure time at the exact location by simply focusing with an illumination device. In addition, most biological systems are not

inherently sensitive to light, therefore a light pulse does not interfere with the system itself. One approach to confer light sensitivity is to use “caged” compounds, biologically inactive molecules such as **2.1** that are activated by the removal of a photoreactive protecting group **2.2** to reveal the target molecule **2.3** (Scheme 2.1).^[335] This method has, for example, allowed in-depth studies of the kinetics of glutamate receptors using caged glutamate and the dissection of neuronal circuitry.^[336] One drawback of this method is the irreversible nature of the uncaging process, thus necessitating the addition of more substrate and clearance of the uncaged active agent to repeat the uncaging process. Furthermore, the cleaved protecting group can be toxic or have undesired side effects.^[337]



Scheme 2.1. A caged, inactive glutamate derivative **2.1** is converted to glutamate **2.3** by irradiation with $\lambda = 360$ nm light.

In the last decade, a novel class of photosensitive compounds has emerged to control biological function with light. In contrast to caged compounds, these reversible photoswitches feature a photosensitive moiety that can be switched back and forth with discrete and orthogonal wavelengths of light. Apart from inherently photosensitive proteins, such as channel- and halorhodopsins that use retinal as the photoswitchable unit, azobenzene photoswitches have attracted considerable attention.^[338] These synthetic photoswitches can be divided in two classes according to the nature of their interaction with the target protein (Figure 2.1).

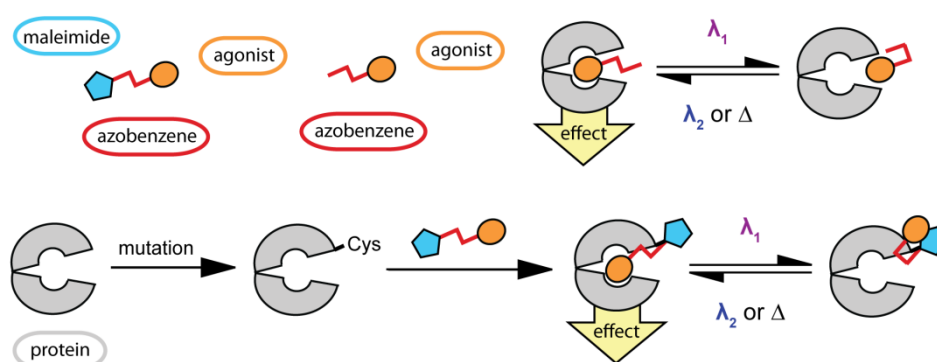
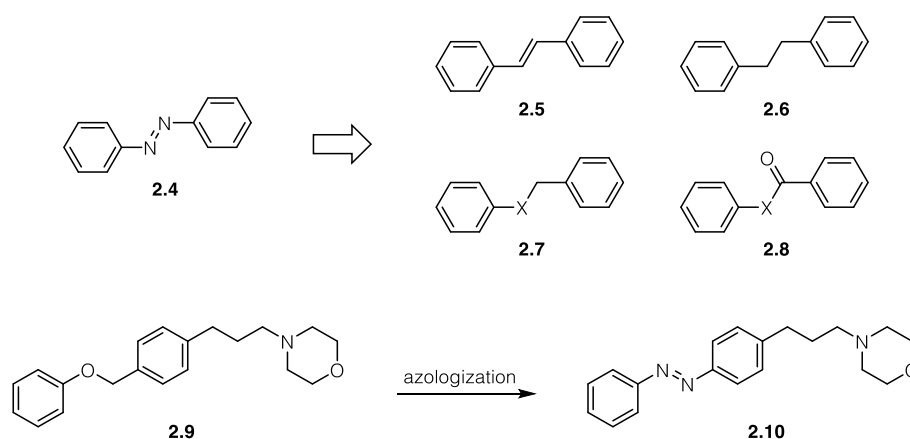


Figure 2.1. The PCL (top) and PTL (bottom) approaches for the control of proteins (grey clamshell). A photoswitch consisting of a ligand (yellow) and an azobenzene (red) can bind to wild-type proteins (PCL) or, with an added linking group (blue), to cysteine groups in engineered proteins (PTL). Application of light with different wavelengths allows for the reversible regulation of protein activity.

The first class consists of so-called **photochromic ligands (PCLs)**, which are freely diffusible azobenzene units connected to ligands for specific targets that can bind to wild-type proteins. The

second class are so-called **photochromic tethered ligands (PTLs)**, which follow a different design principle. A maleimide moiety (blue) covalently attaches the photoswitch to the protein of interest *via* residual or, more commonly, genetically engineered cysteine moieties (Figure 2.1). In both cases, their azobenzene portion (red) can be isomerized back and forth between its *cis*- and *trans*-state using light with two different wavelengths. In terms of photopharmacology, the conformational change reduces or enhances the efficacy of the ligand (PCL) or allows the ligand to be unleashed towards or withdrawn from its binding site (PTL), thus modulating the activity of the protein under investigation.

It is key to the success of a photoswitch to determine the correct position of the photochromic moiety within the ligand. Looking at the available ligands, one has to identify compounds that could fit the guidelines laid out in the so-called “azologization” concept (Scheme 2.2).^[339] In short, this entails the identification of motifs within known bioactive compounds that could be replaced with an azo unit (**2.4**). Ideally, properties like shape and size of the molecule are not drastically changed by this modification, the obvious exception being the introduction of a light-sensitive unit that can subsequently be used to change the drug’s efficacy with light. These “azosteric” units include for example stilbenoid compounds **2.5** and diphenylethanes **2.6**, benzyl (thio-)ethers and amines **2.7** as well as diaryl (thio-)esters and amides **2.8**. The first example for this approach was the azologization of the channel blocker fomocaine (**2.9**) to the photoswitchable fotocaine (**2.10**).^[339]



Scheme 2.2. Examples for the azologization concept using a generic azobenzene (top) and application to the development of a photoswitchable version **2.10** of the ion channel blocker fomocaine (**2.9**) (bottom). X = O, S, NR.

In the absence of an obvious azologization site, one can take to structure-activity relationship studies in order to identify positions that could accommodate an additional bulky hydrophobic azobenzene moiety protruding from the ligand. This complementary approach is referred to as azo-extension.^[319, 340-341]

This approach was applied by the Trauner group to several biological systems *in vitro* and *in vivo*, showing the versatility of this method. Using a glutamate-based PTL approach, control of an ionotropic glutamate receptor (iGluR6) could be achieved, turning a “blind” receptor into the light-gated, photosensitive receptor “LiGluR” (Figure 2.2).^[342]

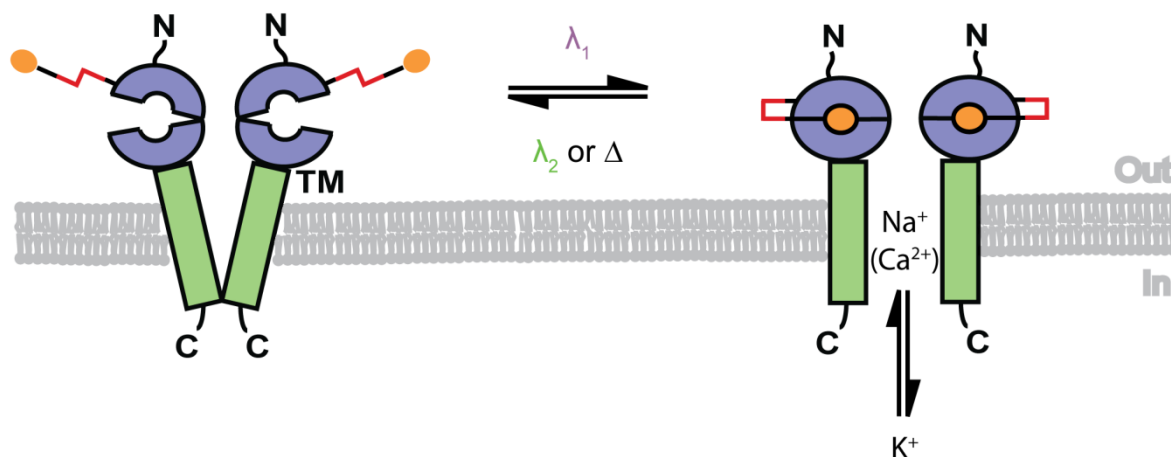


Figure 2.2. The PTL approach for a light-gated ionotropic glutamate receptor (LiGluR). Upon irradiation, the bound ligand in its *cis*-conformation causes ion flow through the membrane (right), while in its *trans*-conformation the ligand cannot reach the active site (left) (N: N-terminal domain; C: C-terminal domain; TM: transmembrane domain).

Upon irradiation with $\lambda = 380$ nm, the azobenzene is converted to its *cis*-state, moving the glutamate portion in proximity of the ligand-binding domain, which causes binding and subsequent pore opening. Irradiation with $\lambda = 500$ nm reverses this process and therefore closes the pore. Recently, this concept has been extended to three metabotropic receptors (mGluRs).^[343] The most thoroughly characterized “LimGluR2” was used, *inter alia*, to control the escape reflex in zebrafish larvae. More recently, the sometimes capricious cysteine-maleimide combination^[344-345] was replaced with the SnAP-Tag methodology.^[346]

Apart from glutamate receptors, the azobenzene photoswitch concept has been successfully applied to the development of PCL and PTL potassium channel blockers with implications for vision restoration in mice models.^[347-350] Other notable applications include the inhibition of bacterial survival and the reversible blocking of P2X channels, with other targets constantly being added.^[318, 320, 338, 351-354] While these examples clearly show the potential of azobenzenes and related photoswitches, some receptors of high interest have remained untouched until recently. One example is another class of glutamate receptors which play a highly important role in the brain, namely the NMDA receptors (NMDARs).

2.1.2 NMDA receptors as targets of high significance

In the last decades, one main field of research has been the biology and chemistry of glutamate receptors.^[355] Throughout the nervous system and especially the brain, the amino acid glutamate (**2.3**) mediates the majority of excitatory neurotransmission as it acts on two main types of membrane receptors, metabotropic and ionotropic glutamate receptors. The iGluRs are cation-permeable ion channels, divided into three subclasses, each named after a selective synthetic agonist: α -Amino-3-hydroxy-5-methyl-4-isoxazolepropionic acid (**2.11**, AMPA receptors), kainic acid (**2.12**, kainate receptors) and *N*-Methyl-D-aspartic acid (**2.13**, NMDA receptors), as shown in Figure 2.3.^[355-356]

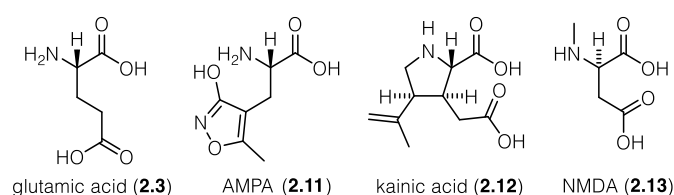


Figure 2.3. Structures of the most common agonists of glutamate channels.

Sequence similarity suggests they all share the same overall structure, consisting of four semiautonomous domains: the extracellular *N*-terminal domain (ATD), the extracellular ligand-binding domain (LBD), the transmembrane domain (TMD) and the intracellular *C*-terminal domain.^[357-358] The recently published first crystal structure of a full NMDA receptor with all four subunits is shown in Figure 2.4.^[359] NMDARs have kept fascinating neuroscientists due to their central role in the functioning of the central nervous system.^[355] They possess the unique feature of being both voltage- and ligand-gated ion channels and are so-called coincidence detectors. The NMDA receptors are essential for the induction and maintenance of synaptic plasticity, in the process of learning and memory, but also in neurological diseases, where they play an important role in excitotoxicity.^[360] In this process, an excess of glutamate release results in overexcitation of neurons, eventually inducing cell death by a large influx of calcium ions.^[361] Therefore, it comes as no surprise that treatments for a wide variety of neurological and psychiatric disorders are focused on the modulation of NMDA receptors.

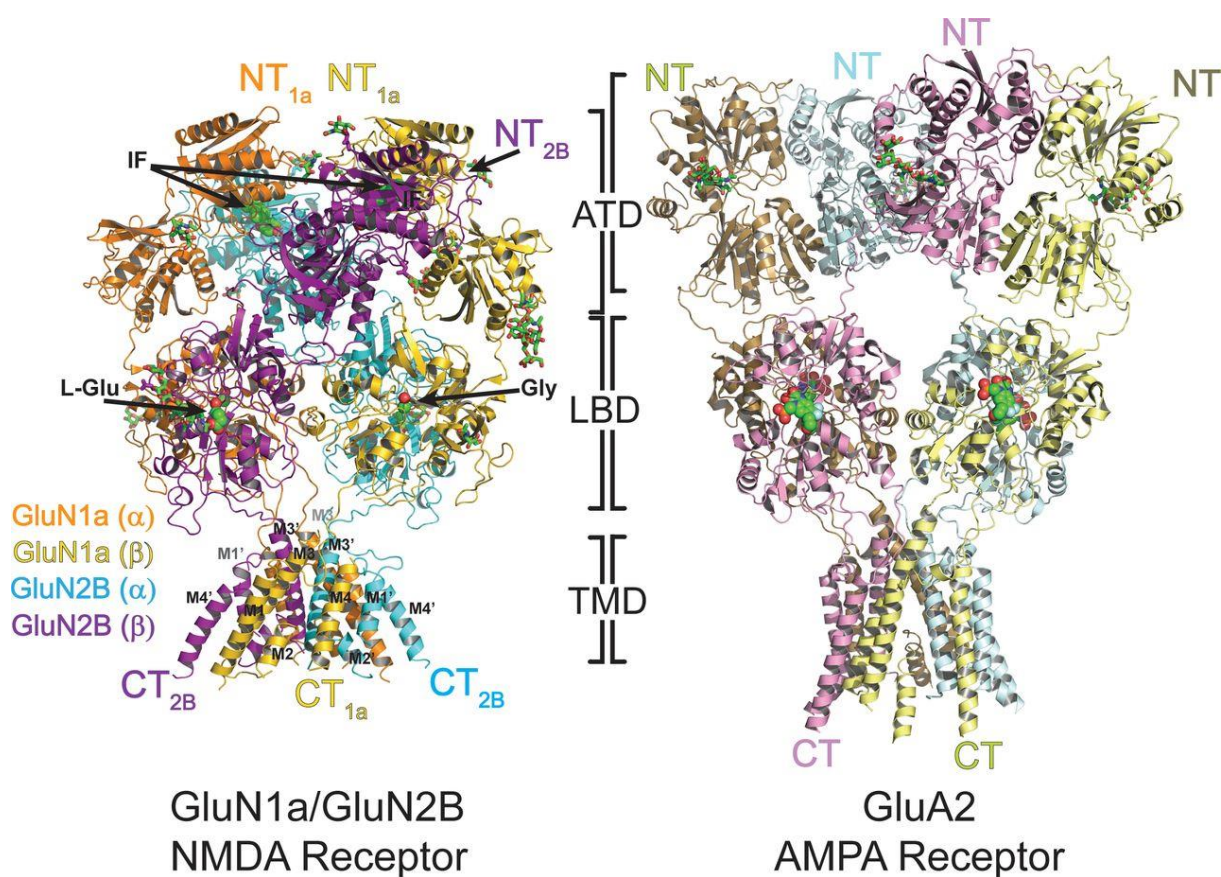


Figure 2.4: Overall structure of iGluRs exemplified by the NMDA receptor GluN1a/GluN2B (left) and the AMPA receptor GluA2 (right (modified from Karakas *et al*).

These include widespread neurodegenerative conditions such as Alzheimer's, Huntington's and Parkinson's diseases, but also acute clinical conditions such as stroke.^[362-364] The development of selective antagonists is a complex and challenging task due to the multitude of binding sites and the structural diversity of NMDA receptors. All NMDARs are tetrameric complexes that are composed of several homologous subunits, the NR1 subunit with eight splice variants (NR1a-h), the NR2 subunit with four subtypes (NR2A-D) encoded by four different genes and the NR3 subunit with two subtypes NR3A and NR3B that are encoded by two separate genes.^[357, 365] Functional NMDARs consist of at least one NR1 subunit bearing the glycine-binding site and one NR2 subunit bearing the glutamate binding site. The composition of the NMDARs varies depending on the location within the nervous system, but also as a function of age, yielding receptors with a wide pharmacological variety.^[357, 365] Therefore, it would be highly beneficial to selectively control NMDA activity with photopharmacology in order to further study these important channels in a reversible manner. This would lead to deeper insights into their function, ultimately paving the way to understand their role in health and disease.

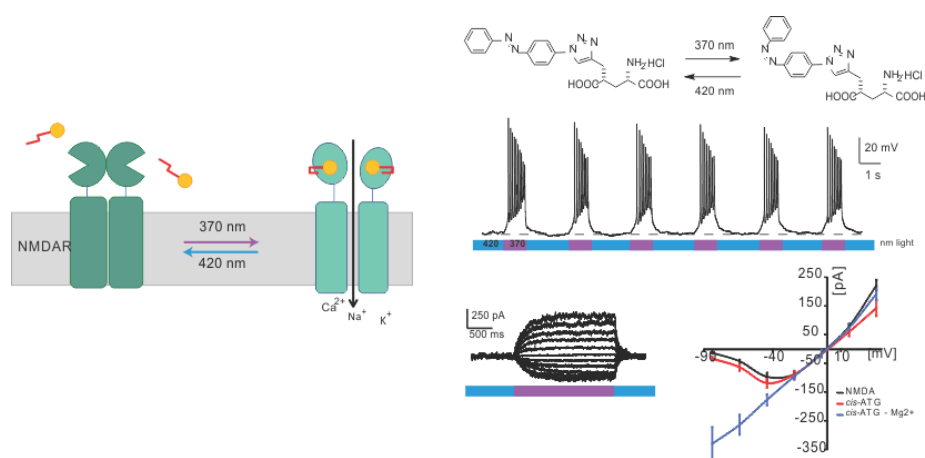
2.2 Synthesis of photoswitchable glutamate derivatives

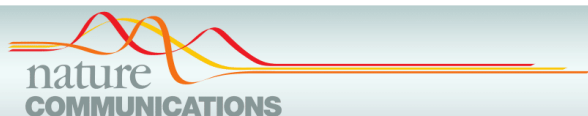
2.2.1 Synthesis of a photoswitchable glutamate agonist

Reprinted with permission from:

Laura Laprell, Emilienne Repak, Vilius Franckevicius, Felix Hartrampf, Jan Terhag, Michael Hollmann, Martin Sumser, Nelson Rebola, David A. DiGregorio and Dirk Trauner, *Nat. Commun.* **2015**, *6*, 8076.

Copyright© 2015 Nature Publishing Group.





ARTICLE

Received 28 Aug 2014 | Accepted 13 Jul 2015 | Published 27 Aug 2015

DOI: 10.1038/ncomms9076

OPEN

Optical control of NMDA receptors with a diffusible photoswitch

Laura Laprell^{1,*}, Emilienne Repak^{2,3,*}, Vilius Franckevicius¹, Felix Hartrampf¹, Jan Terhag⁴, Michael Hollmann⁴, Martin Sumser¹, Nelson Rebola^{2,3}, David A. DiGregorio^{2,3} & Dirk Trauner¹

N-methyl-D-aspartate receptors (NMDARs) play a central role in synaptic plasticity, learning and memory, and are implicated in various neuronal disorders. We synthesized a diffusible photochromic glutamate analogue, azobenzene-triazole-glutamate (**ATG**), which is specific for NMDARs and functions as a photoswitchable agonist. **ATG** is inactive in its dark-adapted *trans*-isoform, but can be converted into its active *cis*-isoform using one-photon (near UV) or two-photon (740 nm) excitation. Irradiation with violet light photo-inactivates **ATG** within milliseconds, allowing agonist removal on the timescale of NMDAR deactivation. **ATG** is compatible with Ca²⁺ imaging and can be used to optically mimic synaptic coincidence detection protocols. Thus, **ATG** can be used like traditional caged glutamate compounds, but with the added advantages of NMDAR specificity, low antagonism of GABAR-mediated currents, and precise temporal control of agonist delivery.

¹Department of Chemistry and Pharmacology, Ludwig-Maximilians-Universität, München, and Center for Integrated Protein Science, Munich 81377, Germany. ²Institut Pasteur, Unit of Dynamic Neuronal Imaging, 25 rue du Dr Roux, Paris Cedex 15 75724, France. ³CNRS UMR 3571, Genes, Synapses, and Cognition, Institut Pasteur, 25 rue du Dr Roux, Paris Cedex 15 75724, France. ⁴Ruhr-Universität-Bochum, Department of Biochemistry, Bochum 44780, Germany. * These authors contributed equally to this work. Correspondence and requests for materials should be addressed to D.D. (email: david.digregorio@pasteur.fr) or to D.T. (email: dirk.trauner@lmu.de).

I onotropic glutamate receptors mediate fast excitatory synaptic transmission and are ubiquitously expressed in the central nervous system. They can be separated into three major classes: α -amino-3-hydroxy-5-methyl-4-isoxazolepropionic acid receptors (AMPA receptors), kainate receptors and *N*-methyl-D-aspartate receptors (NMDARs). The latter are involved in the induction of synaptic plasticity, the cellular correlate of learning and memory¹. NMDARs, of which a functional tetrameric receptor structure has been reported lately^{2,3}, have also been implicated in a variety of neurological diseases and dysfunctions including ischaemia-related cell death, Alzheimer's, Huntington's and Parkinson's Diseases, as well as schizophrenia and autism spectrum disorders¹. NMDARs are heterotetramers whose subunit composition varies based upon brain region, maturation and synaptic activity. Subunit differences result in variations in receptor kinetics, which confer different computational properties on the receptors^{1,4}. Such variations in kinetic behaviour of NMDAR subunits have been examined on extrasynaptic and recombinant receptors using outside-out patch clamp recordings and fast application of agonist^{5,6}.

The study of glutamate receptors in their native environment has been facilitated by the development of optical tools, namely light-sensitive caged agonists and antagonists, which take advantage of the temporal and spatial precision that light provides. Compounds including caged glutamate, caged NMDA and caged MK-801 have proven very useful for finely tuned, non-invasive studies of NMDARs^{7–11}. For example, MNI-glutamate uncaging in a diffraction-limited laser illumination volume enables synaptic-like activation of both AMPARs and NMDARs^{12–15}. Larger illumination volumes can be used to quantify activation and desensitization kinetics of synaptic receptors¹⁵. However, the study of deactivation of receptors must be done following rapid removal of agonist, a feat not possible with caged glutamate because of slow clearance by diffusion or uptake¹⁵. This is particularly challenging in functional networks within brain tissue.

Molecular photoswitches provide an interesting alternative to caged compounds since they can be rapidly and repeatedly switched on and off and do not generate photochemical byproducts. Over the past decade, several photoswitches have been developed including both photoswitchable tethered ligands and freely diffusible photochromic ligands (PCL) that allow for the optical control of transmembrane receptors and, by extension, neural systems¹⁶. **GluAzo** is a photochromic version of glutamate that functions as a PCL for the kainate receptors GluK1 and GluK2¹⁷, and **ATA-3** is a PCL selective for AMPARs¹⁸ (Fig. 1a). Both **GluAzo** and **ATA-3** are active in the thermally relaxed, dark-adapted state, thus their use with networks of neurons is challenging as the whole preparation must be illuminated to prevent tonic activity.

We now report a unique photochromic agonist that targets a different family of glutamate receptors. This compound, azobenzene-triazole-glutamate (**ATG**), complements **ATA-3** and **GluAzo** since it selectively activates NMDARs (Fig. 1b). In addition, it possesses an important functional advantage that distinguishes it from our previously developed PCLs: it is inactive in the dark-adapted *trans*-isoform, but quickly converts into its active *cis*-isoform when irradiated with ultra-violet (UV) light (370 nm). As such, it is not excitotoxic when applied to neural networks in the absence of light, and it becomes an agonist of NMDARs with millisecond precision when irradiated. In addition, we show that **ATG** is the first diffusible PCL that can be precisely controlled with two-photon excitation (740 nm).

Results

Synthesis and Photophysical Characterization of ATG. **ATG** was synthesized in a few steps from the known glutamate

derivative 4(*R*)-propargyl glutamate (**1**) using click chemistry (Fig. 1c). In brief, **1** was treated with azobenzene azide **2** in the presence of a copper catalyst to afford triazole **3**. Global deprotection then yielded **ATG**. A thermally stable stilbene analogue of *cis*-**ATG**, termed *cis*-**STG**, was synthesized in a similar fashion by treating **1** with **4** and deprotecting the resultant triazole **5** (Fig. 1d). Details of the synthesis and full characterization can be found in Supplementary Fig. 10, Supplementary Note 1 and in the Supplementary Methods.

ATG behaves as a regular azobenzene that can be converted to its *cis*-isoform with UV-A light. Conversion into the thermodynamically favourable *trans*-isoform requires irradiation with violet light (Fig. 1 and Supplementary Fig. 1a). Thermal relaxation into the *trans*-isoform is very slow in physiological buffer solution in accordance with the 'regular azobenzene' nature of **ATG** (Supplementary Fig. 1b).

Photopharmacology of ATG. To evaluate **ATG** as a photo-switchable agonist in neurons, we performed electrophysiological recordings in mouse layer 2/3 cortical neurons in acute coronal slices, while continuously perfusing 200 μ M **ATG** in artificial cerebrospinal fluid (ACSF) (Fig. 2, Supplementary Fig. 2a,b). Using the whole-cell voltage-clamp configuration, we examined the spectral sensitivity of *cis*-**ATG**-evoked currents from 350 to 410 nm (Fig. 2a, Supplementary Fig. 2a). Maximal **ATG**-elicited currents were observed in response to 360 nm light, (3.75 mW mm⁻²; Supplementary Fig. 2c), whereas above 390 nm *cis*-**ATG**-mediated currents were negligible (< -10 pA). This action spectrum corresponds to the maximal conversion to *cis*-**ATG** after 365 nm irradiation, as determined by UV-VIS spectroscopy (Supplementary Fig. 1a). Switching back to *trans*-**ATG** was fastest using 425 nm light ($\tau_{\text{off}} = 0.17 \text{ s} \pm 0.03$; $n = 16$, Fig. 2b and Supplementary Fig. 2b). According to these data, **ATG** is *cis*-active, which is in sharp contrast to other photoswitchable glutamate receptor agonists previously developed^{17,18}. Using our illumination system, the dose-response curve of **ATG** indicated an EC₅₀ value of 185 μ M under 370 nm light (Fig. 2c). In whole cell current-clamp recordings of mouse cortical layer 2/3 neurons, **ATG** triggered action potential (AP) firing under 370 nm light (Fig. 2d). Using 420 nm light, AP-firing could be quickly silenced. Thus, **ATG** photoswitching can be used to control neural activity with light.

We examined *cis*-**ATG**-mediated currents in the presence of various antagonists of ionotropic glutamate receptors (iGluRs) to identify the molecular targets of **ATG**. Application of NBQX (25 μ M), an AMPAR-selective antagonist, had no effect on light-evoked currents (Supplementary Fig. 3). By contrast, D-AP5 (40 μ M), a competitive NMDAR-selective antagonist, and MK-801 (50 μ M), a use-dependent pore blocker that preferentially acts on NMDARs, completely abolished *cis*-**ATG**-mediated AP firing and currents, respectively (Fig. 2e and Supplementary Fig. 3)¹⁹.

Using heterologous expression strategies we next examined whether *cis*-**ATG** can activate NMDA receptors containing different isoforms. *Cis*-**ATG**-mediated currents were not detectable in HEK cells expressing different subunit combinations. In *Xenopus* oocytes, however, the high level of receptor expression facilitated the detection of *cis*-**ATG**-mediated currents (Supplementary Fig. 4). To normalize for different expression levels we compared the steady-state amplitude of *cis*-**ATG**-mediated currents in oocytes expressing recombinant dimeric NMDARs with those evoked by saturating NMDA concentrations (1 mM, Supplementary Fig. 4). We found that photoactivation of **ATG** is able to activate all subunit combinations between GluN1-1a and either GluN2A, B, C or D. The observation that *cis*-**ATG**-mediated currents were smaller

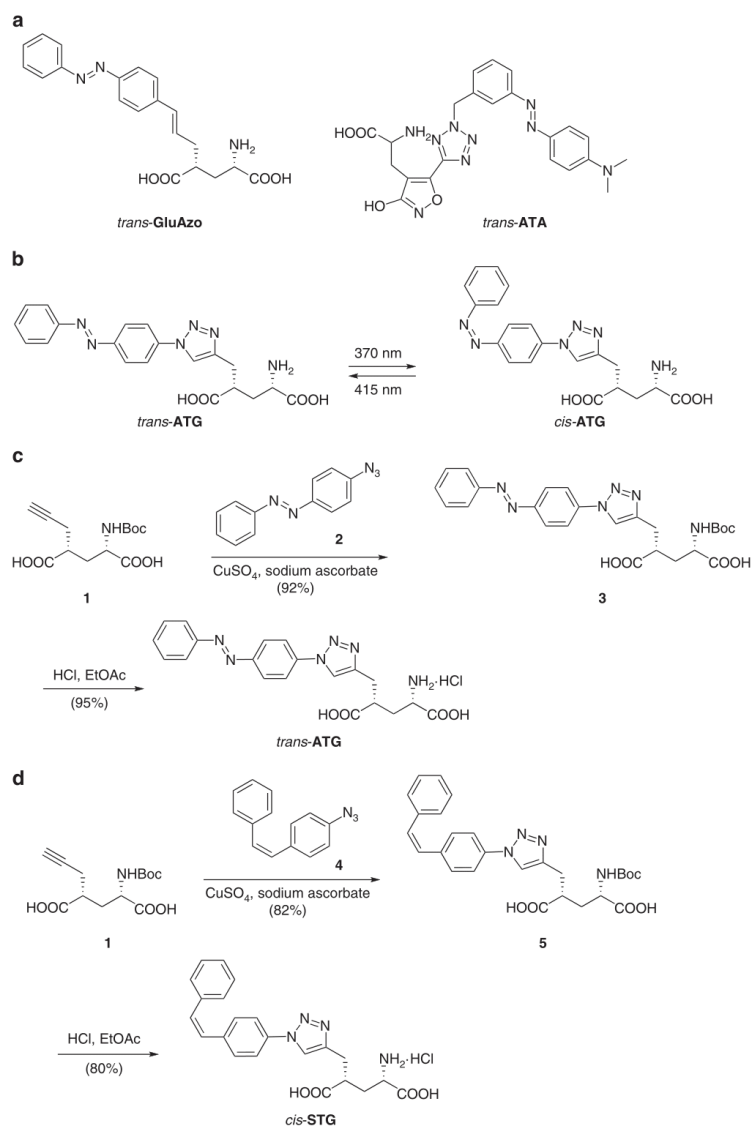


Figure 1 | Design and synthesis of ATG. (a) Structures of **GluAzo**, a photochromic agonist of kainate receptors, and **ATA**, a photochromic agonist of AMPA receptors in their respective *trans* isoform. (b) Structure and photophysical properties of **ATG**. The molecule consists of a photoswitchable azobenzene, a triazole and a glutamate moiety. The *trans*- and *cis*-configuration of **ATG** are shown. (c) Synthesis of the azobenzene **ATG** using click chemistry. (d) Synthesis of the stilbene **STG** using click chemistry.

than those elicited by superfusion of NMDA (<5%), may be because of increased light absorption resulting in incomplete photoconversion in the oocyte setup.

To further demonstrate the selectivity of **ATG** for NMDARs, we recorded current–voltage (*I*–*V*) relationships comparing NMDA (200 μM) puff application with **ATG** photoswitching (Fig. 2f). Because of their magnesium sensitivity, NMDARs are

partially blocked at resting membrane potentials, imparting a J-shaped *I*–*V* relationship²⁰ (Fig. 2f, right, black), which we observed for both NMDA application and *cis*-**ATG**-mediated currents (Fig. 2f). As expected for non-selective cation channels, the reversal potential was close to 0 mV. In the absence of external Mg²⁺ the *I*–*V* relationship was found to be linear, as expected for NMDARs (Fig. 2f, right, blue).

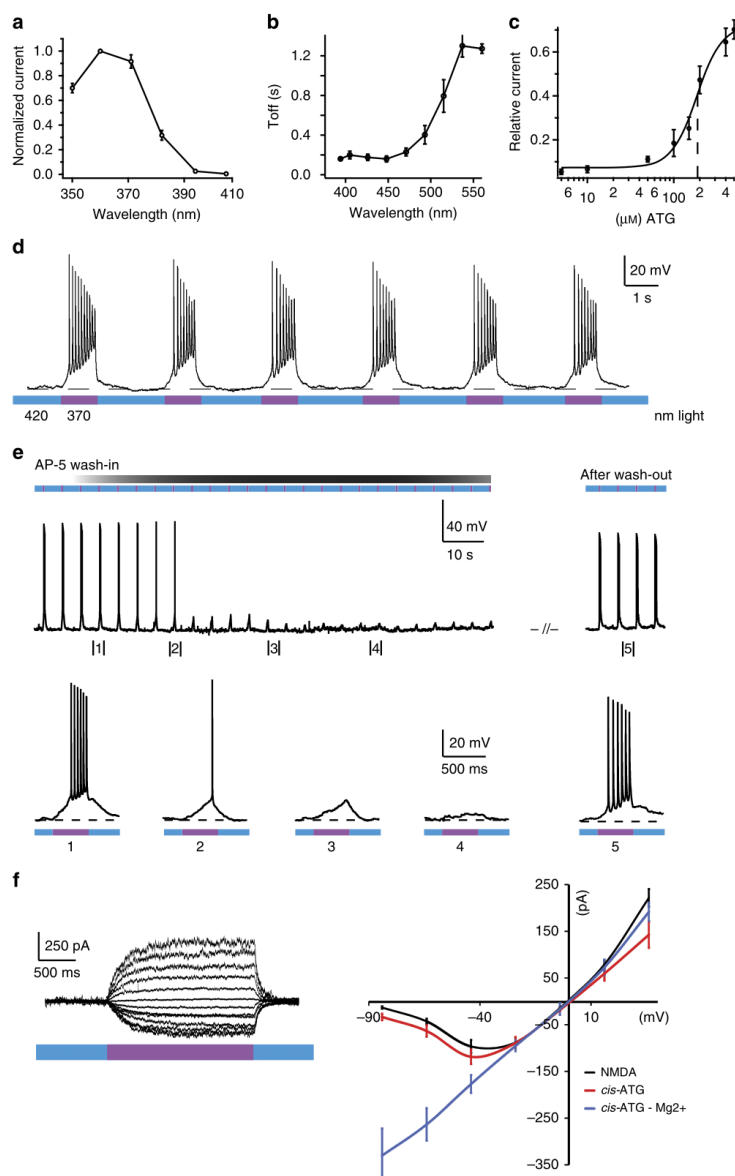


Figure 2 | Photopharmacology of ATG. (a) Action spectrum of ATG recorded in layer 2/3 cortical neurons in an acute slice preparation in presence of 200 μ M ATG in ACSF. Current amplitude was measured after 5 s light stimulation with the respective wavelength and normalized to the maximal current amplitude at 360 nm. (b) Wavelength screening for τ_{off} kinetics of ATG-mediated currents between 400 and 560 nm light. Best τ_{off} kinetics were achieved at 400–450 nm light. (c) Dose–response relationship of ATG-mediated currents in cortical slice preparations. Concentrations from 1 to 500 μ M were tested. The EC_{50} is 185 μ M (black dashed line) and was calculated using the Hill-equation. (d) Current-clamp recording of a layer 2/3 cortical neuron. Irradiation with 370 nm light (purple) induces robust action potential firing that is terminated by irradiation with 420 nm light (blue). (e) Washing in D-AP-5 (40 μ M), an NMDA-specific antagonist, blocks the ATG-mediated light-dependent action potential firing. (f) Current–voltage relationships indicative of NMDARs as targets for ATG. Black; current–voltage relationship of puff-applied NMDA (200 μ M) currents ($n = 12$ cells). Red; current–voltage relationship of ATG-mediated currents under 370 nm light ($n = 10$ cells). Blue; current–voltage relationship of ATG-mediated currents in the absence of Mg^{2+} ions ($n = 10$ cells). Error bars indicate s.e.m.

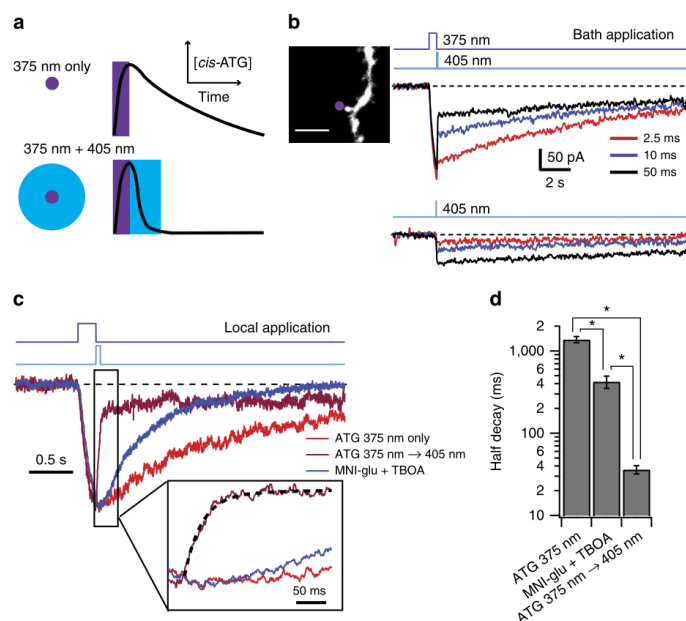


Figure 3 | Dendritic NMDAR currents evoked by rapid laser-mediated photoswitching of ATG. (a) Schematic diagram showing putative sculpting of NMDAR gating by ATG photoswitching. A near-diffraction-limited spot of 375 nm light switches ATG to an active *cis*-conformation (top) that can activate the NMDAR transiently. When the 375 nm laser light is followed quickly by a brief 405 nm laser pulse focused over a larger volume, ATG is converted to the inactive *trans*-conformation (bottom), eliminating *cis*-ATG-mediated current more quickly than via diffusional clearance of *cis*-ATG. (b) Upper traces show light-evoked NMDAR currents recorded in CA1 pyramidal neurons while bath applying 200 μ M ATG, in response to a 500 ms 375 nm laser pulse immediately followed by various durations of 405 nm laser pulses. Lower traces show smaller currents evoked by 405 nm pulses alone. Inset: confocal image of dendrite stimulated in these recordings. Purple dot indicates targeted point of ATG stimulation. Scale bar 3 μ m (c) Normalized population averages of NMDAR currents evoked by 375 nm laser pulse (100 ms) alone (red; $n = 9$ cells), or 375 nm followed by 405 nm laser pulse (50 ms; magenta; $n = 9$ cells) when locally applying ATG (100 μ M) with a patch pipette. Blue trace represents uncaging-evoked NMDAR responses when locally applying MNI-glutamate (100 μ M; $n = 5$ cells). Dotted line on the magenta trace in the inset indicates the double exponential decay function. (d) Bar graph shows half-decay of NMDAR currents from cells in c. Error bars indicate s.e.m. * $P < 0.05$ for all three comparisons (Steel Dwass all pairs nonparametric multiple comparison test).

We further examined whether the thermally stable *cis*-ATG analogue (*cis*-STG, Fig. 1d), which does not photoswitch, has similar pharmacology and specificity for NMDARs. When puff applied, the stilbene *cis*-STG indeed elicited APs in mouse layer 2/3 cortical neurons (Supplementary Fig. 5a). The J-shaped I-V relationship (Supplementary Fig. 5b) indicates that *cis*-STG also targets NMDARs. As such, *cis*-STG represents a new structural class of agonist for these receptors.

One drawback of traditional caged glutamate compounds is that they are often antagonists of GABA_AR-mediated synaptic currents²¹. We therefore tested the effect of *trans*-ATG on GABA_AR-mediated inhibitory postsynaptic currents (IPSCs) in hippocampal CA1 pyramidal neurons. Using 400 μ M bath application of ATG, we observed no detectable alteration of spontaneous IPSCs, but observed a $38 \pm 6\%$ ($n = 10$ cells) block of evoked IPSCs and an increase in coefficient of variation, consistent with a presynaptic target (Supplementary Fig. 6). Nevertheless, this is less than the 50% block by RuBi-glutamate (300 μ M²¹), the 55% block by CDNI-glutamate (400 μ M²²) and the 83% block by the commonly used MNI-glutamate (300 μ M²¹).

ATG-mediated photoswitching of NMDAR gating. We next considered the possibility that ATG photoswitching could be used

to perform temporally precise agonism of NMDARs. We used fast digitally controlled diode lasers at 375 nm to switch to *cis*-ATG and 405 nm to preferentially switch to *trans*-ATG (Fig. 3a). The 375 nm laser light was focused to a near-diffraction-limited spot (full-width half-maximum (FWHM): 300 nm; Supplementary Fig. 7) and the 405 nm laser beam was adjusted to form a 4 μ m spot (full-width half-maximum; Supplementary Fig. 7). NMDAR currents were recorded from CA1 pyramidal neuron dendrites within 100 μ m of the soma at a holding potential of -30 mV. In the first set of experiments, 200 μ M ATG was bath-applied (Fig. 3b). Laser illumination of 100 ms at 375 nm (~ 150 μ W) was required to see significant *cis*-ATG-mediated currents (average peak response: -87 ± 12 pA; $n = 6$ cells). Illumination for 5 s with 375 nm laser light resulted in large currents (-494 ± 56 pA, $n = 18$ cells) that rose over the light pulse duration (Supplementary Fig. 8a) and decayed over tens of seconds (Supplementary Fig. 8a,b). The reduction in *cis*-ATG-mediated current was maximal when using 50 ms illumination of 405 nm laser light (11 mW), but incomplete ($56 \pm 3\%$ reduction, $n = 14$ cells; Fig. 3b). The residual current was similar in amplitude to that when delivering a 50 ms 405 nm light pulse alone ($P = 0.35$; Wilcoxon-matched pair signed rank test). The UV-VIS spectra indicate that irradiation with 405 nm light produces a

ARTICLE

NATURE COMMUNICATIONS | DOI: 10.1038/ncomms9076

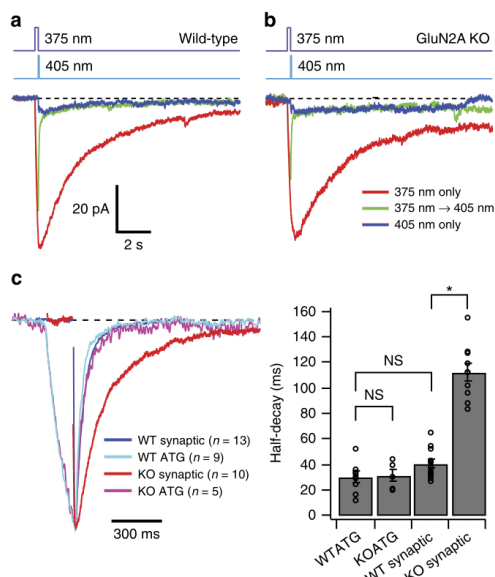


Figure 4 | Comparison of ATG photoswitching responses between wild-type and GluN2A KO animals. (a) Population averages of light-evoked currents from WT CA1 pyramidal cells in response to 375 nm (100 ms) only, 375 nm followed by 405 nm (50 ms), and 405 nm only when locally applying ATG (100 μ M) with a patch pipette ($n = 9$ cells). (b) Population averages of photoswitching currents from GluN2A KO animals under same conditions as (a) ($n = 5$ cells). (c) (left) Normalized currents in response to 375-405 nm photoswitching from (a) and (b) and population averages of NMDAR EPSCs in wild-type ($n = 13$ cells) and KO animals ($n = 10$ cells). Traces were aligned on their peaks and electrical artifacts from presynaptic stimulation have been blanked. Right: Bar graph of half-decays. Error bars indicate s.e.m. * $P < 0.05$ and NS indicates comparisons that are not significantly different (Steel Dwass all pairs nonparametric multiple comparison test).

small but measurable amount of *cis*-ATG (Supplementary Fig. 1a). This could explain why 405 nm illumination reduces current following 375 nm illumination, but evokes current when not preceded by 375 nm illumination (Fig. 3b).

When we examined the spatial dependence of *cis*-ATG-mediated currents, we saw little change in the peak amplitude even if the 375 nm laser was positioned up to 100 μ m away from the dendrite. This finding, along with the slow rise and decay times, led us to the hypothesis that we had a very large effective photoactivation volume because of ATG photoswitching out-of-focus—an effect observed for bath application of caged compounds²³. To further improve the kinetics of the NMDAR response, we tested local perfusion of ATG at 100 μ M. Under these conditions, the decay of light-evoked *cis*-ATG-mediated currents was accelerated over sixfold, and we observed a halving of the peak current at only 5 μ m away from the dendrite (Supplementary Fig. 8d). Local perfusion also permitted the use of higher concentrations of ATG to improve the activation time of NMDAR currents to <100 ms, similar to that of the widely used caged compound MNI-glutamate at similar concentrations (Supplementary Fig. 9a). Additionally, local application of ATG

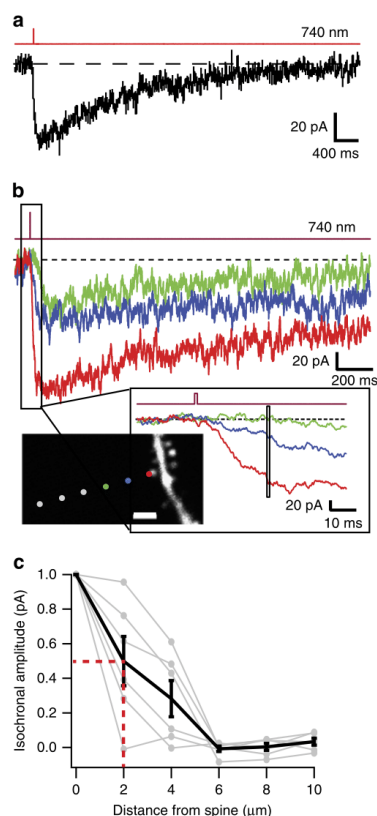


Figure 5 | Localized two-photon activation of ATG. (a) *Cis*-ATG-mediated current evoked by two-photon illumination (1 ms, 740 nm) in a CA1 pyramidal cell while bath applying 400 μ M ATG. (b) 2P-evoked *cis*-ATG-mediated currents with illumination spot parked at 0.5, 2 and 4 μ m away from spine head. Illumination duration was 1 ms, and the wavelength set at 740 nm. (inset) Enlarged view of distance-dependent ATG evoked responses. Box over traces illustrates the time window over which spatial dependence was estimated for isochronal amplitude plots in (c) (Scale bar 2 μ m). This was chosen to correspond to the time point at which the largest current reached 75% of its amplitude. (c) Normalized isochronal plots for six cells, with the average in black (half-width half-maximum = 2.0 μ m, red dotted lines). Error bars indicate s.e.m.

resulted in an enhanced fractional reduction of *cis*-ATG-mediated currents upon 405 nm light illumination (Fig. 3c and Supplementary Fig. 9b), up to 77 \pm 3% reduction, 100 μ M ($n = 9$ cells). Finally, and most importantly, local application of ATG resulted in faster decay of NMDAR currents following 405 nm illumination (ATG_{off}): the half-decay of 33 ± 4 ms ($n = 9$ cells; Fig. 3d) was over 12 times faster than NMDAR current decays recorded in response to MNI-glutamate uncaging (422 ± 72 ms, $n = 5$ cells, $P = 0.01$). Interestingly, the weighted decay time constant of ATG_{off} (τ_{weighted} of 102 ± 42 ms; $n = 9$ cells; see example fit in Fig. 3c inset) was intermediate to the decay values for recombinant receptors containing either GluN1/GluN2A ($\tau_{\text{weighted}} = 29$ ms) and GluN1/GluN2B ($\tau_{\text{weighted}} = 193$ ms)²⁴.

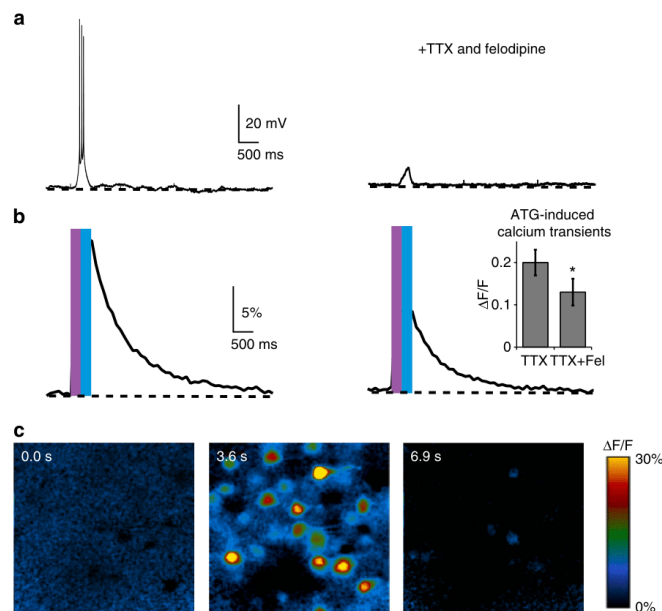


Figure 6 | Calcium imaging using ATG in acute hippocampal slices. (a) *Cis*-ATG-mediated (200 μ M) electrical signals in ACSF (left) and in the presence of 40 μ M felodipine (Fel) and 1 μ M TTX (right), elicited with 370 nm light and terminated with 420 nm (250 ms light pulse for each wavelength). (b) Calcium transients from responsive cells in the field of view corresponding to *cis*-ATG-mediated recording presented in (a). Bar graph: quantification of calcium transients (ATG + TTX: $n=18$ experiments and ATG + TTX + felodipine: $n=10$ experiments). * $P < 0.05$, Wilcoxon rank-sum test. Error bars indicate s.e.m. (c) Changes in fluorescence ($\Delta F/F$) at different time points of the calcium transient; prior to light stimulation, immediately after illumination and after returning to basal calcium levels.

We therefore considered the possibility that the rapid ATG_{off} decay could be used to estimate relative contributions of GluN2A and GluN2B to dendritic NMDAR activation.

In mature CA1 pyramidal neurons (> P21), NMDARs are mostly comprised of tri-heteromers of GluN1, GluN2A and GluN2B^{4,25} whose kinetics are dominated by the rapid deactivation of GluN2A^{26,27}. We therefore compared the decay of ATG_{off} in WT and GluN2A KO mice. To get a better estimate of the ATG_{off} kinetics without contamination of 405 nm-induced *cis*-ATG-mediated currents, we subtracted a scaled curve fit to the 405 nm-induced current of each individual cell (Fig. 4a,b). The half-decay of subtracted ATG_{off} currents was 30 ± 4 ms ($n=9$ cells) similar to the decay of NMDAR EPSCs recorded at the same age (40 ± 3 , $n=13$ cells; $P=0.18$; Steel Dwass all pairs nonparametric multiple comparison test; Fig. 4c). To determine whether the decay of ATG_{off} currents was influenced by GluN2A expression, we examined ATG_{off} decays in GluN2A KO mice (P29-P55). Surprisingly, the decay of ATG_{off} remained largely unaltered (KO half-decay: 31 ± 5 ms, $n=5$, $P=0.99$ Steel Dwass all pairs nonparametric multiple comparison test), but the evoked synaptic responses were nearly three times slower (KO half-decay: 113 ± 7 ms, $n=10$, $P=0.0004$, Steel Dwass all pairs nonparametric multiple comparison test; Fig. 4c), confirming the kinetic influence of GluN2A expression. Thus, the ATG_{off} decay is insensitive to subunit composition of NMDARs that are known to alter channel deactivation²⁸.

Two-photon activation of ATG. One strategy to achieve very localized photoactivation is to use two-photon (2P) excitation.

We found that, during bath application of 400 μ M ATG, femtosecond pulsed-laser illumination at 725–740 nm evoked detectable *cis*-ATG-mediated currents when using illumination durations as brief as 250 μ s, which is much more efficient than one-photon activation of ATG (Fig. 5a), and similar to illumination durations required to evoke NMDAR currents using MNI-glutamate^{29–32}. One millisecond duration pulses (740 nm) produced an average *cis*-ATG-mediated current of -48 ± 7 pA (rise time (10–90%) = 44 ± 4 ms, $n=16$ spines), larger than the published values for single spine activation using caged-glutamate^{29–31}. Nevertheless, spatial dependence of the amplitude of 2P-evoked *cis*-ATG-mediated currents indicated a local activation within 2 μ m of the spine head (Fig. 5b,c).

Combining ATG photoactivation with Ca^{2+} imaging. The calcium permeability of NMDARs links their activity to post-synaptic biochemical alterations, such as spine morphology and glutamate receptor expression, which are associated with synaptic plasticity²⁰. Since ATG specifically acts on NMDARs, we examined the possibility of imaging its effect with a Ca^{2+} -sensitive fluorescent dye (Fig. 6). To this end, we incubated hippocampal slices with Quest Fluo-8-AM, a membrane-permeable Ca^{2+} indicator that is compatible with the activation wavelength of ATG because of its excitation wavelength of 490 nm (Fig. 6b). We applied tetrodotoxin citrate (TTX) (1 μ M) and felodipine (40 μ M), which prevents opening of voltage-gated Ca^{2+} channels to limit the response to NMDAR-mediated calcium entry (Fig. 6 right half). Indeed, upon irradiation with 370 nm in the presence of ATG,

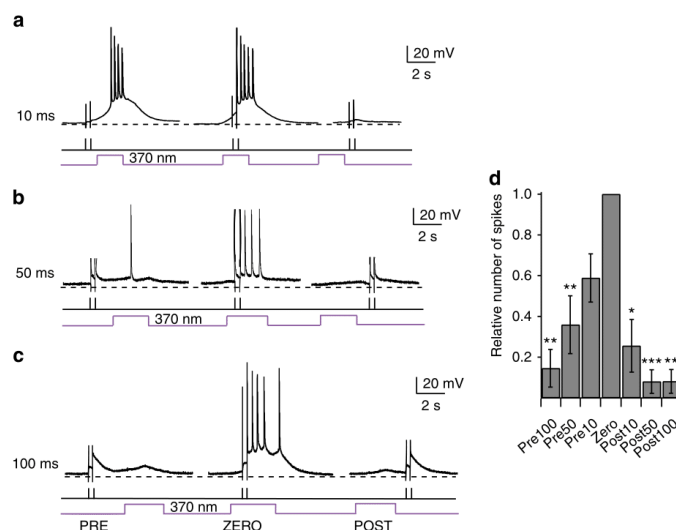


Figure 7 | Coincidence detection using ATG in layer 2/3 cortical neurons. Coincidence detection of *cis*-ATG mediated current (200 μ M) paired with antidromic stimulation. **(a)** Antidromic stimulation (black bars) of the postsynaptic cell 10 ms before, during and 10 ms after the light stimulation (purple trace). **(b)** As in **(a)**, but with 50 ms intervals. **(c)** As in **(a)**, but with 100 ms intervals. **(d)** Quantification of coincidence detection. Relative number of spikes compared with condition ZERO, when both stimuli were applied together ($n=11$ cells). Statistics were calculated using the Wilcoxon rank-sum test (* $P<0.05$, ** $P<0.01$, *** $P<0.001$).

we observed light-evoked *cis*-ATG-mediated Ca^{2+} transients (Fig. 6b; $\Delta F/F=20 \pm 3\%$, $n=18$) which decreased in amplitude in the presence of blockers ($\Delta F/F=13 \pm 3\%$, $n=10$). We attributed the remaining Ca^{2+} transient to the influx through ATG-mediated NMDAR opening.

Mimicking synaptic coincidence detection with ATG. One of the most intriguing properties of NMDARs is their voltage-sensitive Mg^{2+} block at resting membrane potential. Accordingly, the presence of a neurotransmitter and concomitant postsynaptic depolarization are required to activate the ion channel, rendering NMDARs coincidence detectors of pre- and postsynaptic activity³³. To test whether *cis*-ATG-mediated NMDAR activation can replace the synaptic stimulation necessary for coincidence detection, we designed a stimulus protocol, which couples antidromic stimulation (electrical stimulus of the axon hillock; Fig. 7, black line) of the postsynaptic cell with light activation (Fig. 7, purple line) of NMDARs at defined intervals. The electric stimuli were given at subthreshold intensities and did not induce AP firing by themselves. By varying the interval between the two stimuli, we showed that only coincident activation with light and current injection led to suprathreshold signals that generated APs. If the stimuli did not coincide or the delay between stimuli was too long, the number of spikes generated was significantly reduced (Fig. 7d).

Discussion

To circumvent the limitations of traditional irreversible caged agonists, we synthesized a novel photo-reversible glutamate receptor agonist, ATG. This compound has functional features that make it unique and useful to neurobiological research: It is inactive in the dark, selectively targets NMDARs, can be quickly activated by irradiation with 360–375 nm light (or 725–740 nm

light, 2P activation) and quickly deactivated with 405–460 nm light. Using rapid laser illumination, we demonstrated the unique photoswitching between a *cis*-active and *trans*-inactive compound, which enabled activation and deactivation of NMDARs on the timescale of their intrinsic gating properties. We also demonstrated that ATG is amenable to combination with other optical techniques, namely Ca^{2+} imaging. Finally, we showed that ATG could be used to mimic synaptic activation in coincidence detection protocols.

In the absence of detailed structural data and molecular dynamics calculations, it is difficult to explain why *cis*-ATG is the active form and why it is selective for NMDARs. Structure-activity relationship studies indicate that the pharmacological space available for ATG is relatively narrow, which makes it a challenge to develop red-shifted derivatives (D. Trauner, unpublished results). As the physiological activity of the stilbene analogue *cis*-STG indicates, the diazene unit ($\text{N}=\text{N}$ bond) is not essential for ligand binding and is probably not engaged in hydrogen-bonding interactions to the ligand-binding domain. This is also apparent in a recent X-ray structure of GluAzo bound to the GluK2 ligand binding domain³⁴. Attempts to red-shift the action spectrum of ATG by substituting it with strongly electron-donating substituents, such as a diethylamino group, in the 4'-position have so far yielded inactive compounds, indicating that substituents in this position clash with the ligand-binding domain in its closed state. Other ways to red-shift, for example, with heterocyclic azobenzenes, can be imagined and are under active investigation. Finally, *cis*-ATG and *cis*-STG represent a new class of agonists (and potentially antagonists) for ionotropic glutamate receptors that can be rapidly assembled using click-chemistry.

Herein, we show that ATG photoswitching and light-dependent NMDAR activation can be achieved with a monochromator, LEDs or laser light source. In principle, simple LEDs or standard light sources used in fluorescence imaging could also

be used. It should be taken into account, however, that the kinetics of photoswitching are strongly dependent on the applied light intensities. ATG exhibits a high molar extinction coefficient ($48,778 \text{ cm}^{-1} \text{ M}^{-1}$ at 330 nm). Although such a feature enables efficient light absorption, it also reduces the light intensity at the focal point as a consequence of Lambert-Beer's law²³. We circumvented this limitation by performing local perfusion of ATG to limit the optical path length in which photoswitching occurred. Two-photon excitation also provides a solution to the problem of out-of-focus light absorption while in parallel improving depth penetration in scattering tissue and providing intrinsic localization, properties well-suited for activation of single spines with a PCL. Deactivation at longer wavelengths can still be performed by large 1P illumination areas, which is advantageous for switching any molecules that have diffused out of the diffraction-limited illumination volume. Although the 2P cross-section has not been estimated, the ability of brief laser illumination durations (<1 ms) to evoke synaptic-like NMDAR current amplitudes could render ATG a useful complement to MNI-glutamate. Very recently, MAG_{2p}, a derivative of glutamate that can be activated with 2P absorption, has been introduced^{35,36}. This compound, however, is covalently attached to the receptor and not freely diffusible like ATG.

Because diffraction-limited illumination volumes are much larger than a single synaptic vesicle fusion event, the photolysis of caged neurotransmitter in diffraction-limited spots (by one- or two-photon excitation) is unlikely to mimic the rapid decay of neurotransmitter clearance¹⁵. PCL compounds, however, are ideally suited to overcome this diffusion-limited problem because photoisomerization of azobenzenes can occur on a picosecond timescale, sufficient for photo-inactivation of an agonist before it diffuses away. It remains to be determined if the switching speed is similar when *cis*-ATG is bound to the receptor. Nevertheless, we were able to demonstrate that ATG photoswitching can accelerate NMDAR current decays which, when using classical caged agonists, would have been limited by diffusional clearance. This requires that the inactive *trans*-ATG have an affinity low enough to be effectively a non-agonist. Consistent with the relative low-affinity of *trans*-ATG, the ATG_{off} decays are nearly thirty times faster than the decay of *cis*-ATG currents. *Trans*-ATG also appears to unbind NMDARs more rapidly than glutamate, as the half-decay is over twelve times faster than that achieved by glutamate uncaging (Fig. 3). We demonstrate, for the first time, the fundamental ability to switch 'off' channel agonism, thereby speeding the decay of NMDAR currents.

We were surprised that the ATG_{off} decay was not altered in GluN2A KO mice, especially since faster unbinding rates of glutamate are thought to underlie the faster deactivation rates of GluN2A-containing channels³⁴. One possible interpretation of these results is that the affinity of *trans*-ATG is so low that photoconversion reveals a ligand-independent closing transition. To confirm this, future experiments would be required, especially to confirm rapid switching of *cis*-ATG when bound to the NMDAR.

Our results show that ATG is a powerful tool that permits precise temporal control of NMDAR gating not otherwise achieved with state-of-the-art caged compounds. They extend the reach of photopharmacology to an important subtype of glutamate receptors and demonstrate that photoswitchable neurotransmitters that are inactive in the dark can be synthesized and used to precisely control receptor activation in their native environment.

Methods

UV-Vis spectra. ATG was dissolved to a concentration of 50 μM in buffer containing (in mM) 138 NaCl, 1.5 KCl, 2.5 CaCl₂, 1.2 MgCl₂, 10 Glucose and 5

HEPES, adjusted to pH 7.4. UV-VIS spectra were taken in a 100 μl cuvette with the switching light (monochromator) introduced through a glass fibre from the top of the cuvette, perpendicular to the light path of the spectrometer (Varian, Cary 50). The kinetics of the *trans*- to *cis*-conversion were recorded at the maximal absorption wavelength of *trans*-ATG (330 nm). To achieve fast switching rates, we used high power LEDs at 365 and 460 nm (Prizmatix) for *trans*-*cis* and *cis*-*trans* isomerization, respectively.

Cortical slice preparation and external solutions. Cortical coronal slices were prepared from C57Bl6/J mice (postnatal day 10–15, both male and female animals were used without known experimenter bias). Following decapitation, the brain was rapidly removed and transferred to an ice-cold saline solution composed of (in mM) 2.5 KCl, 1.25 NaH₂PO₄, 25 NaHCO₃, 0.5 CaCl₂, 7 MgCl₂, 25 glucose, 75 sucrose saturated with carbogen (95% O₂/5% CO₂). Slices (300 μm thick) were made using a Campden vibratome 7,000 smz-2 (NPI Electronic). Slices were incubated at 34 °C for 30 min in ACSF composed of (in mM) 125 NaCl, 2.5 KCl, 1.25 NaH₂PO₄, 26 NaHCO₃, 2 CaCl₂, 1 MgCl₂, 20 glucose saturated with carbogen (95% O₂ and 5% CO₂). After incubation, slices were stored at room temperature from 30 min to five hours before being recorded. Experiments were carried out at room temperature. Unless stated otherwise, ATG was added from a 200 mM dimethyl sulfoxide stock to the ACSF to yield a final concentration of 200 μM . The ACSF was heated to 40 °C to improve the solubility of the ATG stock. The solution was not filtered because ATG adheres to filter materials.

For the identification of target receptors and calcium imaging experiments, the iGluR antagonists NBQX (25 μM) and D-AP-5 (40 μM), and the channel blockers TTX (1 μM) and flunitrazepam (40 μM) were bath-applied, whereas MK-801 (50 μM) (all from Abcam) was loaded into the patch pipette. NMDA (1 mM, Sigma-Aldrich) and *cis*-STG (200 μM) were puff-applied through a glass pipette using a pressure ejection system (PDES, NPI Electronic). For voltage-clamp recordings, TTX was added to the ACSF.

Patch clamp recordings of cortical layer 2/3 neurons. Pyramidal neurons were patched using fire-polished glass electrodes with a resistance of 6–9 M Ω . Current-clamp recordings were carried out using the following intracellular solution (in mM): 140 K-gluconate, 10 HEPES, 12 KCl, 4 NaCl, 4 Mg-ATP, 0.4 Na₂-GTP. For whole-cell voltage-clamp recordings, we used (in mM) 110 Cs-gluconate, 15 NaCl, 10 HEPES, 5 TEA, 0.16 EGTA, 4 Mg-ATP, 0.4 Na₂-GTP. Recordings were made with an EPC 10 USB amplifier, controlled by the Patchmaster software (HEKA). Data was filtered at 2.9–10 kHz and digitized at 50 kHz. Holding potential was corrected for a 14 mV liquid junction potential. Cells were rejected if leak currents were >200 pA or series resistance >25 M Ω . Data was analysed using the Patcher's Power Tools (MPI Göttingen) and routines written in IgorPro (Wavemetrics).

For antidromic stimulation, glass electrodes (5 M Ω) filled with ACSF were placed within 20 μm of the axon hillock and the stimulus pulse was applied through an isolated stimulation unit (A-M Systems). The stimulation intensity was set to be subthreshold. The temporal pattern of the antidromic and ATG light stimuli were controlled through the Patchmaster software (HEKA).

Hippocampal slice preparation and external solutions. Hippocampal coronal slices were prepared from C57Bl6/J mice (Janvier Labs) (postnatal day 15–55, both male and female animals were used without known experimenter bias) following decapitation and rapid removal of the brain³⁷. A Leica VT1200S vibratome was used to make 250 μm thick slices while the brain was immersed in an ice-cold saline solution composed of (in mM) 2.5 KCl, 1.25 NaH₂PO₄, 25 NaHCO₃, 0.5 CaCl₂, 8 MgCl₂, 25 glucose, 230 sucrose and 0.5 ascorbic acid saturated with 95% O₂/5% CO₂. After 30 min incubation at 33 °C in solution composed of (in mM) 125 NaCl, 2.5 KCl, 1.25 NaH₂PO₄, 25 NaHCO₃, 2 CaCl₂, 1 MgCl₂, 25 glucose and 0.5 ascorbic acid saturated with 95% O₂/5% CO₂, slices were stored at room temperature from 30 min to 5 h in the same solution before being recorded. NMDAR currents were recorded in the presence of (in μM) 10 SR95531 (Abcam Biochemicals) to block GABARs, 0.3 strychnine (Sigma-Aldrich) to block glycine receptors, 5 2,3-Dioxo-6-nitro-1,2,3,4-tetrahydrobenzo[*f*]quinoxaline-7-sulfonamide (NBQX) (Abcam Biochemicals) to block AMPARs, and 1 TTX (Abcam Biochemicals) to minimize spontaneous activity. 50 μM D-serine (Sigma-Aldrich) was also included in the bath solution to saturate the co-agonist binding site of NMDAR. GABAR currents were isolated through the addition of (in μM) 0.3 strychnine, 5 NBQX, 10 D-(-)-2-Amino-5-phosphonopentanoic acid (Abcam Biochemicals) and 20 7-chlorokynurenic acid (Abcam Biochemicals). ATG or 4-methoxy-7-nitroindolyl-caged L-glutamate (MNI-glutamate; Tocris Bioscience) was perfused locally using a 3–6 μm tip-diameter patch pipette. The ATG and MNI-glutamate perfusion solutions contained (in mM) 110 NaCl, 2.5 KCl, 2 NaHCO₃, 1.25 NaH₂PO₄, 30 HEPES, 10 Glucose, 2 CaCl₂, 1 MgCl₂, 0.05 Alexa Fluor 488 (Life Technologies), 0.01 SR95531, 0.0003 strychnine, 0.005 NBQX, 0.001 TTX, 0.05 D-serine, and where noted, 0.05–0.1 D, L-threo- β -Benzyloxyspartic acid (Tocris Bioscience, Bristol, UK). Alexa Fluor 488 was used to visualize the perfusion and ensure its regularity over the course of the experiment. The pH of the final perfusion solution was adjusted to 7.3 after dilution. As ATG is not readily soluble in water, a stock solution (10 mM) was prepared in 0.1N NaOH.

ARTICLE

NATURE COMMUNICATIONS | DOI: 10.1038/ncomms9076

Patch clamp recordings in hippocampal CA1 pyramidal neurons. Whole-cell voltage-clamp was performed from visually identified hippocampal CA1 pyramidal cells at 32 °C using an Axopatch 700B, Molecular Devices. Fire-polished patch electrodes had a tip resistance of 4–6 MΩ, and contained a Cs-methanesulfonate-based internal solution composed of (in mM) 105 CsCH₃O₃S, 10 EGTA, 3 CaCl₂, 4 MgCl₂, 10 Hepes, 4 NaCl, 4 NaATP, 0.4 NaGTP and 5 phosphocreatine for recording NMDAR currents. To record GABA_AR currents, we used a similar solution except that we did not use NaCl and we added (in mM) 70 CsCl and 35 CsCH₃O₃S. 40–100 μM Alexa Fluor 594 was also added to the solution to visualize dendritic morphology during whole-cell experiments for all experiments except GABA_AR recordings. Extracellular stimulation of EPSCs and IPSCs was performed at 0.1 Hz using a constant voltage stimulator (20–60 V, 50 μs, Digitimer) and a 4 MΩ resistance pipette. We recorded IPSCs for 10 min in ACSF, then 20 min in ACSF plus 400 μM ATG. Currents were filtered at 4–10 kHz then digitized at 100 kHz (NI PCI-6052E, National Instruments) using the software Neuroomatic (www.neuroomatic.thinkrandom.com/). Offline, traces were filtered between 4–10 kHz. Holding potentials were corrected for a –7 mV liquid junction potential (JP_{CalcW}), and then set at –30 mV, except for GABA_AR currents which were recorded at –70 mV.

Photoswitching of ATG and calcium imaging. A Poly-V monochromator (FEI Systems) controlled through the Patchmaster software was used to toggle between *trans*- and *cis*-ATG at varying wavelengths (370 and 420 nm unless otherwise indicated). During calcium imaging experiments, the monochromator was controlled by the Live Analysis software (FEI). The calcium indicator Quest-Fluo-8-AM (50 μM MoBiTec) was added to the ACSF, and acute hippocampal slices were incubated for at least 20 min at 37 °C to facilitate uptake of the indicator. Calcium changes were recorded at 480 nm, digitized at 10 Hz, background corrected and the $\Delta F/F_0$ ratio was calculated using IgorPro routines and ImageJ (NIH).

Laser-mediated photoswitching and uncaging. Visually guided patch experiments were performed using differential interference contrast or Dodt contrast. Dendrites were visualized using either a confocal (592 nm excitation of Alexa Fluor 594) or a 2P imaging system (810 nm, Ultima, Prairie Technologies). We coupled a 405 nm diode laser (Model PhoxX 405-120, Omicron Laserage) and a 375 nm diode laser (Model PhoxX 375, Omicron Laserage) into the photoactivation galvanometers of the scanhead (for rapid spot positioning) using single-mode optical fibres (Part QPMJ-A3S-A3S-400-3/125-3-2-1, Oz Optics). For one-photon photoswitching, we used 150 μW (bath application) or 375 μW (local application) of 375 nm and 10.5 mW of 405 nm, measured after the objective. For two-photon photoactivation, a pulsed Ti:Sapphire laser (Chameleon Ultra II, Coherent) tuned to either 725 nm or 740 nm was directed into a photoactivation path. Photoactivation was performed on proximal dendrites within 100 μm of the soma to minimize possible effects of dendritic filtering. Illumination spots were typically placed <0.5 μm from the tip of the spine head, except when longer duration pulses were used (>500 ms), in which case the spot was placed 1 μm away.

In vitro transcription and preparation of cRNA. For expression in *Xenopus laevis* oocytes, clones (derived from *Rattus norvegicus*) of GluN1-1a (genebank accession number: U08261), GluN2A (AF001423), GluN2B (U11419.1), GluN2C (U08259.1) and GluN2D (U08260.1), each in the *X. laevis* oocyte expression vector pSGEM, were transcribed to cRNA *in vitro* using the T7 mMESSAGE mMACHINE Kit (Ambion) according to the protocol provided. Transcribed cRNA was isolated with a spin-column kit (Clean & Concentrator 25, Zymo) and cRNA integrity was checked via denaturing agarose gel electrophoresis. RNA concentration was determined photometrically with a NanoPhotometer (Implen) and the concentrations of all samples were adjusted to 200 ng μl⁻¹ with nuclease-free water.

Expression and two-electrode recordings in *Xenopus* oocytes. Frog oocytes were surgically removed from the ovaries of *X. laevis* (Nasco) anesthetized with ethyl 3-aminobenzoate methanesulfonate (2.3 g l⁻¹; Sigma). The lumps of oocytes were incubated with 300 U ml⁻¹ (10 mg ml⁻¹) collagenase type I (Worthington Biochemicals) for 3 h at 21 °C in Ca²⁺-free Barth's solution (in mM) 88 NaCl, 1.1 KCl, 2.4 NaHCO₃, 0.8 MgSO₄, 15 HEPES, pH adjusted to 7.6 with NaOH) with slow agitation to remove the follicular cell layer, and then washed extensively with Barth's solution (in mM) 88 NaCl, 1.1 KCl, 2.4 NaHCO₃, 0.8 MgSO₄, 0.4 CaCl₂, 0.3 Ca(NO₃)₂, 15 HEPES, pH adjusted to 7.6 with NaOH). Oocytes were maintained in Barth's solution supplemented with 100 μg ml⁻¹ gentamycin, 40 μg ml⁻¹ streptomycin and 63 μg ml⁻¹ penicillin. Intact oocytes of stages V or VI were selected and cRNA was injected with a Nanoliter 2010 injector (WPI) within 8 h after surgery. For expression of GluN1/GluN2 heteromers, 20 nl (4 ng) of cRNA for each subunit were injected. Electrophysiological recordings were carried out 5 days after injection. Two-electrode voltage clamping was performed using a TurboTec-10CX amplifier (npi electronic) controlled by Pulse software (HEKA). For photoswitching experiments, the recording chamber was illuminated using LEDs (365 and 460 nm, Prizmatix) coupled to a light guide, which was placed directly above the oocyte. LEDs were controlled via the TTL outputs of the

ADC/DAC (ITC-16, Instrutech). Borosilicate glass capillaries (Harvard Instruments) were pulled to resistances of 0.1–1 MΩ with a vertical puller (PIPS, HEKA) and filled with 3 M KCl.

Oocytes were clamped at –70 mV. All recordings were performed in continuously superfused with Barium Ringer (BaR, in mM) 115 NaCl, 2.5 KCl, 1.8 BaCl₂, 10 HEPES-NaOH, pH 7.2). When a stable holding current was attained, the recording protocol was started. To further prevent opening of calcium-induced chloride channels, niflumic acid (NFA, 250 μM) was added to the BaR. All agonist solutions contained 10 μM glycine. In addition, the BaR used for recording photo-currents was supplemented with ATG (200 μM). For recording of *cis*-ATG mediated currents, the microscope light was switched-off and the photoswitching recording sequence was started. A 5 s pulse of blue light (460 nm) was followed by 5 s of UV light (365 nm) and, again, 5 s of blue light. These protocols were carried out first in the absence of ATG to control for possible artifacts, and then repeated in the presence of 200 μM ATG. For the recording of NMDA-induced currents, 1 mM NMDA in BaR supplemented with 10 μM glycine was perfused. After steady-state currents were achieved, the NMDA was washed out until a stable baseline was reached. The application of 1 mM NMDA was repeated until two consecutive applications resulted in similar steady-state amplitudes. For analysis, light-induced ATG-independent currents were subtracted from *cis*-ATG-mediated currents. The steady-state amplitude of the corrected *cis*-ATG-mediated currents were then normalized to steady-state amplitude of NMDA-induced currents.

Data analysis. Data analysis was performed using the Neuroomatic analysis package and custom routines within the IgorPro environment (Wavemetrics). Cells were rejected from analysis if the leak current was > –100 pA at –30 mV holding potential or the series resistance was over 15 MΩ, except for the GluN2A KO animals in which larger leak currents were accepted. *Cis*-ATG-mediated current peak amplitudes from one-photon photoswitching were measured over a 1 ms window around the peak. Error bars are presented as the mean ± s.e.m. unless otherwise indicated. Current decays were estimated from a fit with a double exponential equation $y = A_1 \exp\left\{-\left(x - x_0\right) / \tau_1\right\} + A_2 \exp\left\{-\left(x - x_0\right) / \tau_2\right\}$. The weighted decay time constant (τ_{weighted}) was calculated as $\left(\frac{A_1}{A_1 + A_2}\right) * \tau_1 + \left(\frac{A_2}{A_1 + A_2}\right) * \tau_2$. Isochronal amplitudes represent averages of the currents in a 200 μs window centred at the time point at which the on-spine response had reached 75% of its peak value.

To better estimate the NMDAR current decay following 405 nm illumination without contamination from partial *cis*-activation of ATG, we performed a subtraction protocol. 405 nm-induced currents were fit to an empirical function that describes the rising phase and dual exponential decay²⁸:

$$I(t) = A_1 \left(1 - \exp\left(-\frac{t - t_0}{\tau_{\text{rise}}}\right)\right)^n \times \left(A_2 \exp\left(-\frac{t - t_0}{\tau_{\text{decay1}}}\right) + (1 - A_2) \exp\left(-\frac{t - t_0}{\tau_{\text{decay2}}}\right)\right)$$

The fits of each individual cell were scaled by eye to maximally overlay the slow decay component of 405 nm only and 375/405 nm-induced currents. We justified such a scaling because the population traces overlapped (Fig. 4a,b). The scaled fits for each cell were then subtracted from the associated average current trace induced by 375 nm illumination followed by 405 nm illumination. Cells were only analysed if three or more recordings were performed under each illumination condition (375 nm only, 375 nm followed by 405 nm, 405 nm only).

GABAR spontaneous events (Supplementary Fig. 6) were detected using an event detection algorithm within the Neuroomatic analysis software based on initial 10 pA threshold detection. Events were refined using two additional search features: (1) event onset detection using a 1.5 ms backward sliding window to ensure the point of threshold detection was 7 × s.d. of background noise; and (2) event peak detection using a 0.2 ms forward sliding window to ensure the event peaked within 2 ms of the time point of event threshold detection with a current greater than that of the point of event threshold by at least 2 × s.d. of background noise. Parameters were determined empirically, but were held constant for all analysis.

Peak amplitudes of IPSCs (Supplementary Fig. 6) were estimated from a 200 μs window centred at the time point of the peak value of the average of all events for a particular condition (number of events were typically between 50 and 300 per cell). Each synaptic current peak amplitude was corrected for series resistance error, as well as for a slight (~5%) decay in peak amplitude of IPSCs over the duration of the recording, which was not due to ATG activity (estimated from sham experiments, $n = 5$ cells). The coefficient of variation of the GABAR IPSCs was calculated as $\frac{\sigma_{\text{peak}}}{\text{peak}} = \frac{\sigma_{\text{background}}}{\text{peak}}$ where σ represents the s.d. over a 200 μs window. Background variance was measured as the standard deviation over a 200 μs window immediately before the stimulation pulse.

Statistical analyses requiring multiple comparisons were first examined with a nonparametric one-way analysis of variance (Kruskal–Wallis) followed by nonparametric tests between specific values. We considered comparisons to be significantly different if P -values were <0.05.

References

- Paoletti, P., Bellone, C. & Zhou, Q. NMDA receptor subunit diversity: impact on receptor properties, synaptic plasticity and disease. *Nat. Rev. Neurosci.* **14**, 383–400 (2013).
- Karakas, E. & Furukawa, H. Crystal structure of a heterotetrameric NMDA receptor ion channel. *Science* **344**, 992–997 (2014).
- Lee, C. H. *et al.* NMDA receptor structures reveal subunit arrangement and pore architecture. *Nature* **511**, 191–197 (2014).
- Tovar, K. R., McGinley, M. J. & Westbrook, G. L. Triheteromeric NMDA receptors at hippocampal synapses. *J. Neurosci.* **33**, 9150–9160 (2013).
- Lester, R. A., Clements, J. D., Westbrook, G. L. & Jahr, C. E. Channel kinetics determine the time course of NMDA receptor-mediated synaptic currents. *Nature* **346**, 565–567 (1990).
- Banke, T. G. & Traynelis, S. F. Activation of NR1/NR2B NMDA receptors. *Nat. Neurosci.* **6**, 144–152 (2003).
- Gee, K. R., Niu, L., Schaper, K., Jayaraman, V. & Hess, G. P. Synthesis and photochemistry of a photolabile precursor of N-methyl-D-aspartate (NMDA) that is photolyzed in the microsecond time region and is suitable for chemical kinetic investigations of the NMDA receptor. *Biochemistry* **38**, 3140–3147 (1999).
- Maier, W., Corrie, J. E., Papageorgiou, G., Laube, B. & Grever, C. Comparative analysis of inhibitory effects of caged ligands for the NMDA receptor. *J. Neurosci. Methods* **142**, 1–9 (2005).
- Rodríguez-Moreno, A. *et al.* Presynaptic induction and expression of timing-dependent long-term depression demonstrated by compartment-specific photorelease of a use-dependent NMDA receptor antagonist. *J. Neurosci.* **31**, 8564–8569 (2011).
- Kramer, R. H., Fortin, D. L. & Trauner, D. New photochemical tools for controlling neuronal activity. *Curr. Opin. Neurobiol.* **19**, 544–552 (2009).
- Thompson, S. M. Flashy science: controlling neural function with light. *J. Neurosci.* **25**, 10358–10365 (2005).
- Matsuzaki, M. *et al.* Dendritic spine geometry is critical for AMPA receptor expression in hippocampal CA1 pyramidal neurons. *Nat. Neurosci.* **4**, 1086–1092 (2001).
- Carter, A. G. & Sabatini, B. L. State-dependent calcium signaling in dendritic spines of striatal medium spiny neurons. *Neuron* **44**, 483–493 (2004).
- Bagal, A. A., Kao, J. P. Y., Tang, C. M. & Thompson, S. M. Long-term potentiation of exogenous glutamate responses at single dendritic spines. *Proc. Natl Acad. Sci. USA* **102**, 14434–14439 (2005).
- DiGregorio, D. A., Rothman, J. S., Nielsen, T. A. & Silver, R. A. Desensitization properties of AMPA receptors at the cerebellar mossy fiber granule cell synapse. *J. Neurosci.* **27**, 8344–8357 (2007).
- Fehrentz, T., Schonberger, M. & Trauner, D. Optochemical genetics. *Angew. Chem. Int. Ed. Engl.* **50**, 12156–12182 (2011).
- Volgraf, M. *et al.* Reversibly caged glutamate: a photochromic agonist of ionotropic glutamate receptors. *J. Am. Chem. Soc.* **129**, 260–261 (2007).
- Stawski, P., Sumsner, M. & Trauner, D. A photochromic agonist of AMPA receptors. *Angew. Chem. Int. Ed. Engl.* **51**, 5748–5751 (2012).
- Coan, E. J., Saywood, W. & Collingridge, G. L. MK-801 blocks NMDA receptor-mediated synaptic transmission and long term potentiation in rat hippocampal slices. *Neurosci. Lett.* **80**, 111–114 (1987).
- Dingledine, R. B. K., Bowie, D. & Traynelis, S. F. The glutamate receptor ion channels. *Pharmacol. Rev.* **51**, 7–61 (1999).
- Fino, E., Araya, R., Peterka, D. S., Salierno, M., Etchenique, R. & Yuste, R. RuBi-glutamate: two-photon and visible-light photoactivation of neurons and dendritic spines. *Front. Neural Circuits* **3**, 2 doi: 10.3389/neuro.04.002.2009 (2009).
- Amatrudo, J. M. *et al.* Wavelength-selective one- and two-photon uncaging of GABA. *ACS Chem. Neurosci.* **5**, 64–70 (2014).
- Trigo, F. F., Corrie, J. E. T. & Ogden, D. Laser photolysis of caged compounds at 405nm: photochemical advantages, localisation, phototoxicity and methods for calibration. *J. Neurosci. Methods* **180**, 9–21 (2009).
- Bidoret, C., Ayon, A., Barbour, B. & Casado, M. Presynaptic NR2A-containing NMDA receptors implement a high-pass filter synaptic plasticity rule. *Proc. Natl Acad. Sci. USA* **106**, 14126–14131 (2009).
- Gray, J. A. *et al.* Distinct modes of AMPA receptor suppression at developing synapses by GluN2A and GluN2B: single-cell NMDA receptor subunit deletion *in vivo*. *Neuron* **71**, 1085–1101 (2011).
- Hansen, K. B., Ogden, K. K., Yuan, H. & Traynelis, S. F. Distinct functional and pharmacological properties of triheteromeric GluN1/GluN2A/GluN2B NMDA receptors. *Neuron* **81**, 1084–1096 (2014).
- Stroebel, D., Carvalho, S., Grand, T., Zhu, S. & Paoletti, P. Controlling NMDA receptor subunit composition using ectopic retention signals. *J. Neurosci.* **34**, 16630–16636 (2014).
- Makara, J. K. & Magee, J. C. Variable dendritic integration in hippocampal CA1 pyramidal neurons. *Neuron* **80**, 1438–1450 (2013).
- Sobczyk, A. & Svoboda, K. Activity-dependent plasticity of the NMDA-receptor fractional Ca²⁺ current. *Neuron* **53**, 17–24 (2007).
- Busetto, G., Higley, M. J. & Sabatini, B. L. Developmental presence and disappearance of postsynaptically silent synapses on dendritic spines of rat layer 2/3 pyramidal neurons. *J. Physiol.* **586**, 1519–1527 (2008).
- Noguchi, J., Matsuzaki, M., Ellis-Davies, G. C. R. & Kasai, H. Spine-neck geometry determines NMDA receptor-dependent Ca²⁺ signaling in dendrites. *Neuron* **46**, 609–622 (2005).
- Nevian, T. Single spine Ca²⁺ signals evoked by coincident EPSPs and backpropagating action potentials in spiny stellate cells of layer 4 in the juvenile rat somatosensory barrel cortex. *J. Neurosci.* **24**, 1689–1699 (2004).
- Reiter, A., Skerra, A., Trauner, D. & Schiefner, A. A photoswitchable neurotransmitter analogue bound to its receptor. *Biochemistry* **52**, 8972–8974 (2013).
- Erreger, K., Dravid, S. M., Banke, T. G., Wyllie, D. J. & Traynelis, S. F. Subunit-specific gating controls rat NR1/NR2A and NR1/NR2B NMDA channel kinetics and synaptic signalling profiles. *J. Physiol.* **563**, 345–358 (2005).
- Izquierdo-Serra, M. *et al.* Two-photon neuronal and astrocytic stimulation with azobenzene-based photoswitches. *J. Am. Chem. Soc.* **136**, 8693–8701 (2014).
- Carroll, E. C. *et al.* Two-photon brightness of azobenzene photoswitches designed for glutamate receptor optogenetics. *Proc. Natl Acad. Sci. USA* **112**, E776–E785 (2015).
- Bischofberger, J., Engel, D., Li, L., Geiger, J. R. P. & Jonas, P. Patch-clamp recording from mossy fiber terminals in hippocampal slices. *Nat. Protoc.* **1**, 2075–2081 (2006).
- Nielsen, T. A., DiGregorio, D. A. & Silver, R. A. Modulation of glutamate mobility reveals the mechanism underlying slow-rising AMPAR EPSCs and the diffusion coefficient in the synaptic cleft. *Neuron* **42**, 757–771 (2004).

Acknowledgements

This study was supported by an ERC Advanced Grant (No. 268795 to D.T.), the Centre National de la Recherche Scientifique through the Actions Thématiques et Initiatives sur Programme, Fondation Fyssen, Fondation pour la Recherche Médicale, Fédération pour la Recherche sur le Cerveau, Agence Nationale de la Recherche (ANR-07-NEUR-008 and ANR-2010-BLANC-1411), NeRF Equipment Mi-lourd 2010 and Ecole des Neurosciences de Paris to D.D. E.R. was supported by the Ecole des Neurosciences de Paris and the Fondation de la Recherche Médicale (FDT20130928054). We thank Pierre Paoletti and his laboratory for providing us with the GluN2A KO animals. We thank Gaël Moneron for helpful advice on optical design. We also thank Florian Rückerl and GM for their help in constructing and aligning the uncaging system used in the 2P photoactivation experiments.

Author contributions

V.F. and F.H. designed and synthesized the compounds. L.L. carried out electrophysiology for basic characterization of ATG and *cis*-STG, calcium imaging experiments and coincidence detection in collaboration with M.S. E.R. performed single dendrite ATG photoswitching and control synaptic experiments. E.R. and N.R. performed synaptic experiment on GluN2A KO. N.R. performed two-photon activation experiments in collaboration with E.R. J.T. performed oocyte experiments in collaboration with M.S. and L.L. which were directed by M.H. and L.L. All authors contributed to writing the manuscript. D.T. and D.D. directed the study.


Additional information

Supplementary Information accompanies this paper at <http://www.nature.com/naturecommunications>

Competing financial interests: The authors declare no competing financial interests.

Reprints and permission information is available online at <http://npg.nature.com/reprintsandpermissions/>

How to cite this article: Laprell, L. *et al.* Optical control of NMDA receptors with a diffusible photoswitch. *Nat. Commun.* **6**:8076 doi: 10.1038/ncomms9076 (2015).

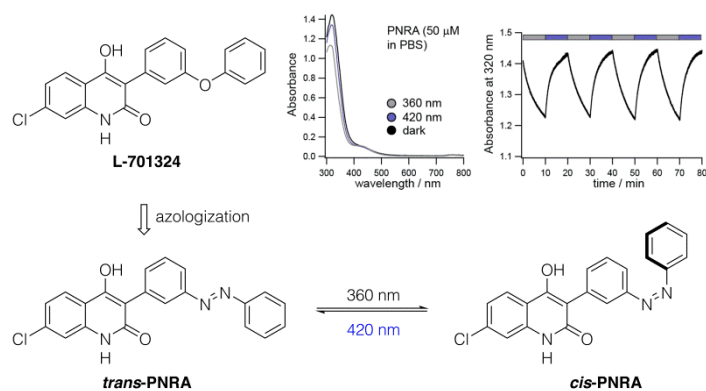
 This work is licensed under a Creative Commons Attribution 4.0 International License. The images or other third party material in this article are included in the article's Creative Commons license, unless indicated otherwise in the credit line; if the material is not included under the Creative Commons license, users will need to obtain permission from the license holder to reproduce the material. To view a copy of this license, visit <http://creativecommons.org/licenses/by/4.0/>

2.2.2 Development of a photoswitchable antagonist of NMDA receptors

Reprinted with permission from:

Felix W. W. Hartrampf, David M. Barber, Kevin Gottschling, Philipp Leippe, Michael Hollmann and Dirk Trauner, *Tetrahedron* **2017**, 73,4905–4912.

Copyright© 2017 Elsevier.



Tetrahedron 73 (2017) 4905–4912



Contents lists available at ScienceDirect

Tetrahedron

journal homepage: www.elsevier.com/locate/tet

Development of a photoswitchable antagonist of NMDA receptors

Felix W.W. Hartrampf^a, David M. Barber^a, Kevin Gottschling^b, Philipp Leippe^a,
Michael Hollmann^b, Dirk Trauner^{a, c, *}^a Department of Chemistry and Pharmacy, Ludwig-Maximilians-Universität, München, and Center for Integrated Protein Science, Munich, 81377, Germany^b Ruhr University Bochum, Department of Biochemistry I – Receptor Biochemistry, Bochum, 44780, Germany^c Department of Chemistry, New York University, New York, NY, 10003, USA

ARTICLE INFO

Article history:

Received 15 May 2017

Received in revised form

26 June 2017

Accepted 27 June 2017

Available online 28 June 2017

Keywords:

glutamate receptor

Antagonist

Azobenzene

Photopharmacology

Photoswitch

ABSTRACT

N-methyl-D-aspartate receptors (NMDARs) are vital for neurological processes such as learning, memory, and synaptic plasticity. As such, small molecules that modulate their function are of interest in the study of numerous neurological diseases. We have synthesized a small library of photoswitches that modulate NMDAR function. The most efficient photoswitch to date is based on a known ligand of the glycine binding site and shows significant subtype selectivity.

© 2017 Published by Elsevier Ltd.

1. Introduction

Ionotropic glutamate receptors are the workhorses of fast synaptic transmission and are therefore ubiquitously expressed throughout the nervous system.^{1,2} The ionotropic glutamate receptors are commonly divided into three classes, each named after a selective agonist mimicking glutamate (1) itself (Fig. 1): the kainate (2) receptors, the AMPA receptors (α -amino-3-hydroxy-5-methyl-4-isoxazolepropionic acid, 3) and the NMDA receptors (*N*-methyl-D-aspartate, 4). Each type is marked by specific pharmacology: kainate receptors are thought to have more of a supporting and modulatory role, AMPA receptors are responsible for the majority of excitatory synaptic transmission. NMDA receptors are both ligand- and voltage-sensitive and play a major role in coincidence detection related to postsynaptic depolarization and synaptic glutamate release.^{3–6} As such, they are of key importance in synaptic plasticity, the molecular basis of memory and learning, as well as in a range of neurodegenerative disorders such as Alzheimer's disease and Parkinson's disease. In order to study the molecular

underpinnings of glutamatergic neuronal networks with the high spatial and temporal precision of light, numerous optical tools have been developed, most of which are caged variants of either glutamate itself or well-established (ant-)agonists like MK-801 or NMDA.^{7–10} A long-standing goal of our and other groups is the application of synthetic photoswitches to the optical control of various targets with light,^{11–16} with a special focus on reversibly controlling glutamate receptors using either freely diffusible or covalently linked ligands.^{17–21} To date, all three receptor subclasses have been addressed using freely diffusible photoswitchable agonists.^{22–24} Most recently, we developed a photochromic agonist of NMDA receptors named ATG that could be used for precise two-photon activation upon irradiation with 740 nm light.²⁴ While these agonists represent powerful tools, they create conditions that are not always physiological (e.g. anomalous overexcitation) and thus may render the analysis of neuronal networks more complicated. It is therefore advantageous to develop photoswitchable antagonists of glutamatergic signaling.²⁵ Herein, we present the design and synthesis of a small library of photoswitchable NMDA antagonists using the concepts of azologization²⁶ and azo-extension as well as their biological evaluation in *Xenopus* oocytes, which demonstrated the viability of azo-L-701324 as a reversible antagonist of NMDA receptors.

* Corresponding author. Department of Chemistry, New York University, New York, NY, 10003, USA.

E-mail address: dirktrauner@nyu.edu (D. Trauner).

<http://dx.doi.org/10.1016/j.tet.2017.06.056>

0040-4020/© 2017 Published by Elsevier Ltd.

4906

F.W.W. Hartrampf et al. / Tetrahedron 73 (2017) 4905–4912

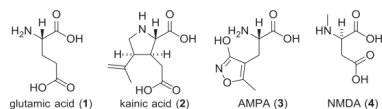


Fig. 1. Structure of glutamate and selective agonists of different classes of glutamate receptors.

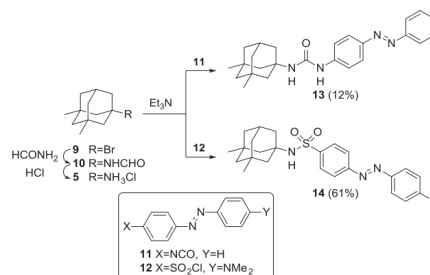
2. Results and discussion

2.1. Chemistry

We first identified NMDA antagonists that would be amenable to azologization, i.e. the replacement of structural units such as diaryl ethers or stilbenes with azobenzenes, or azo-extension, the appendage of an azobenzene unit to existing biologically active compounds. Ideally, these would cover the various known binding sites of NMDA receptors identified through classical pharmacology, as a crystal structure of a full tetrameric NMDA receptor was not published until very recently.^{27,28} A survey of NMDA antagonists with well-established structure-activity relationship (SAR) studies yielded four scaffolds that featured sites tolerant of substitution with large hydrophobic residues (Fig. 2). Specifically, these were the α -tertiary amines memantine hydrochloride (**5**) and amantadine (**6**), two channel blockers approved for the treatment of Alzheimer's disease, *cis*-PPDA (**7**), a glutamate site antagonist,²⁹ and finally L-701324 (**8**),³⁰ a hydroxyquinolone targeting the glycine binding site. It was known that the primary amine of memantine could be coupled to bulky sulfonamides like dansyl chloride without significantly compromising the binding ability.³¹ A range of derivatives of *cis*-PPDA were investigated, all of them bearing very bulky aromatic residues such as phenanthrene, biphenyl or anthracene.²⁹ For L-701324, studies established that the phenyl ether moiety could be exchanged for substituted benzyl or aniline groups.^{30,32,33}

We started the synthesis of photoswitchable memantine derivatives from 1-bromo-3,5-dimethyl-adamantane (**9**), which could be aminated to formamide **10** and hydrolyzed to memantine hydrochloride (**5**) in two steps according to a literature procedure (Scheme 1).³⁴ A more direct C,H-activation Ritter-type reaction did not reproducibly yield the desired product.³⁵

Under standard conditions, it was coupled to *p*-azobenzene isocyanate (**11**) to yield the first NMDA receptor antagonist candidate **13**. A second derivative was obtained by condensation of **5** with commercially available dansyl chloride (**12**), yielding the corresponding photoswitchable sulfonamide **14**. Two more derivatives were accessed through alkylation of the slightly less hindered adamantylamine (amantadine, **6**) with *p*-nitrobenzyl bromide (**15**) to give the secondary amine **16** (Scheme 2). Reduction



Scheme 1. Synthesis of azo-amantadine derivatives via diversification of an aniline building block.

of the nitro group with tin in ethanolic HCl gave aniline **17**. At this point, straightforward Mills coupling with nitrosobenzene gave azobenzene **18**, whilst azo coupling with diethylaniline resulted in substituted red-shifted azobenzene **19**.

For the synthesis of azo-PPDA derivatives, we utilized precedent from the original paper, in which *cis*-2,3-piperazinedicarboxylic acid (**21**) was coupled under Schotten–Baumann conditions (Scheme 3).²⁹ When trying to couple this building block to the azobenzene carboxylic acid chloride derived from **20**, only traces of product **22** could be obtained. We thus switched to an alkylation approach. To this end, we started with known *cis*-piperazinedicarboxylic acid dimethyl ester (**23**).²⁹ This *meso* compound could be alkylated with 1-(4-(bromomethyl)phenyl)-2-phenyldiazene (**24**)³⁶ to give the racemic diester **25**. This compound could then be saponified with aqueous LiOH to afford *cis*-PPDA derivative **26**, “azo-PPDA”.

In order to access a photoswitchable version of our fourth azologization template, L-701324, we prepared the amide **27** according to a modified literature procedure.³² More precisely, benzylic nitrile **27** was hydrolyzed to **28** in quantitative yield with sulfuric acid/hydrochloric acid in acetic acid. After activation of the carboxylic acid as the acid chloride, coupling with methyl 4-chloroanthranilate (**29**) gave amide **30** in good overall yield (Scheme 4). Under the reduction conditions described by Magata, we isolated aniline **31** in low yield and purity (Table 1).³²

Using sodium sulfide, we only isolated small amounts of product. We therefore attempted reduction under palladium catalysis, which resulted in ester hydrolysis and decomposition. We thus

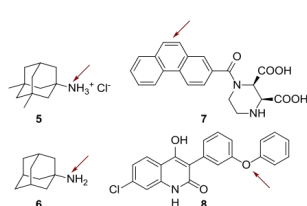
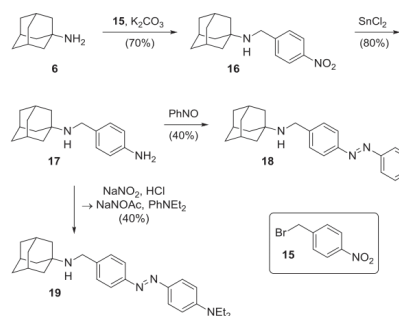
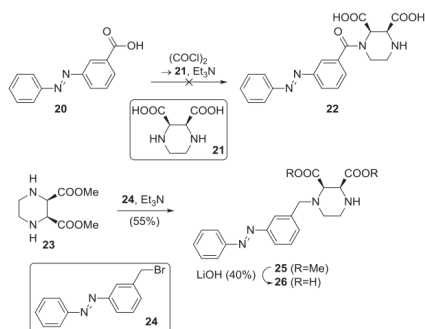


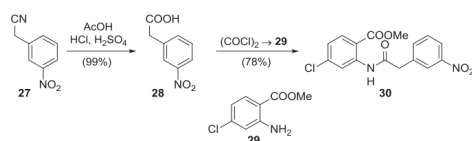
Fig. 2. Diversification sites identified by SAR studies. Red arrows indicate the azo- or azo-extension site.



Scheme 2. Synthesis of azo-memantine derivatives **18** and **19**.



Scheme 3. Failed acylation attempts toward azo-PPDA (top) and successful alkylation approach (bottom) to racemic bisaminoacid azo-PPDA (**26**).



Scheme 4. Synthesis of nitroaryl **30** through amide coupling of arylacetic acid **28** with anthranilate **29**.

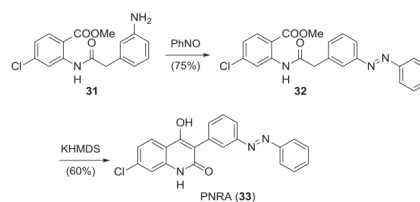
turned to metal reductants such as tin and zinc, which offered a small improvement. Finally, we found that zinc in ethanol with CaCl_2 as a mild Lewis acid gave the desired product in good yield and sufficient purity.

When we attempted to cyclize compound **31** using base (K_2CO_3 or KHMDS) to the hydroxyquinolone as a platform for diversification, intractable mixtures of highly polar compounds were found. We thus changed our approach and first coupled aniline **31** to nitrosobenzene in a Mills reaction. With azobenzene **32** in hand, the cyclization occurred in moderate yield to give azo-L-701324 (**33**), which we termed PNRA (Photoswitchable NMDA Receptor Antagonist) (Scheme 5).

With a set of compounds in hand, we determined their photoswitching properties using UV–Vis spectroscopy. The data obtained indicated that the azoswitches behaved like regular, “unbiased” azobenzenes with optimal *trans/cis* switching wavelengths between 340 and 360 nm (see Fig. 3 for the characterization of PNRA).

Table 1
Reduction of the nitro group in **30** to aniline **31**.

Reductant	Reaction conditions	Yield %
Fe	AcOH , 80 °C	27
Na_2S	dioxane, H_2O , 80 °C	25
Na_2S	dioxane, H_2O , 100 °C	35
Pd/C , $\text{N}_2\text{H}_4 \cdot \text{H}_2\text{O}$	CH_2Cl_2 , EtOH , rt	decomposition
Sn	10% HCl , EtOH , 80 °C	39
Zn	10% HCl , EtOH , 80 °C	50
Zn, CaCl_2	EtOH , H_2O , 80 °C	73



Scheme 5. Synthesis of PNRA (**33**) via Mills reaction and cyclization.

The exceptions were azo-memantine **14**, whose optimal switching wavelength was strongly red-shifted (450 nm) due to its push-pull system, and the amantadine derivative **19**, which switched at 440 nm.³⁷ For the characterization of all other azoswitches, see the supporting information (Fig. S2).

2.2. Biological evaluation

Having established the switching wavelengths for our compounds, we set out to investigate whether they would act as functional mimics of their parent compounds and, more importantly, whether they would do so in a light-dependent manner. As the test system, we chose *Xenopus* oocytes, as they had served us well in the biological evaluation of photoswitchable NMDA receptor agonists as well as AMPA receptor antagonists due to the high level of heterologous expression.^{24,25} Furthermore, we wanted to probe the effect on different receptor subunit combinations using two-electrode voltage clamp electrophysiology. Solutions of compounds were washed in under ambient light (where all are predominantly in the *trans*-state), then irradiated with 360 or 415 nm light to induce switching to the *cis*-state.

We first examined the action of our photoswitchable channel blockers **13**, **14**, **18** and **19**. The first memantine-derived antagonist was the unsymmetrical urea **13**. Whilst it acted as an antagonist at 20 μM , the overall block was only about 10% with a light-dependent current change of only roughly 5%. Dabsyl-conjugated memantine **14** showed very modest block of $\text{GluN1-1a} + \text{GluN2A}$ and hardly any of $\text{GluN1-1a} + \text{GluN2B}$ at 50 μM , neither of which was influenced by light. We thus turned to the amantadine derivatives **18** and **19**, each at a concentration of 50 μM . In *Xenopus* oocytes, **18** showed around 15% block that was not abridged with light. Essentially the same outcome was observed with the red-shifted variant **19** that was switched with 410 nm light. Interestingly, while all channel blockers performed poorly overall, some selectivity of $\text{GluN1-1a} + \text{GluN2A}$ over $\text{GluN1-1a} + \text{GluN2B}$ was obtained in all cases. At this point, we decided to pursue ligands of other binding sites. The next compound tested was azo-PPDA (**26**),

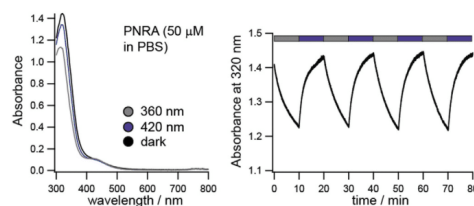


Fig. 3. Photoswitching of PNRA in PBS buffer. $\tau_{(420 \text{ nm})} = 2.868 \pm 0.00674 \text{ min}$; $\tau_{(360 \text{ nm})} = 2.868 \pm 0.00674 \text{ min}$.

whose bisamino acid portion binds to the glutamate site of NMDA receptors. Originally designed by Monaghan and coworkers,²⁹ *cis*-PPDA (**7**) was developed as a subtype-selective antagonist that would show a different selectivity profile. At the time, most antagonists preferentially bound to GluN2A > GluN2B > GluN2C ≈ GluN2D (high to low affinities) whereas *cis*-PPDA showed the opposite affinity pattern (GluN2C/GluN2D over GluN2A/GluN2B). However, our *azo*-modified version of *cis*-PPDA showed different selectivity, with little antagonistic effect observed in the case of NMDA receptors bearing GluN2A/GluN2B subunits, and no affinity to GluN2C, each at a concentration of 100 μM. Our final compound, PNRA (**33**), was investigated next. To our delight, it was shown to be a strong antagonist of GluN1-1a + GluN2A at 2 μM, blocking 80% of the glutamate/glycine-induced current, which could be restored once perfusion of the compound was stopped (Fig. 4). A possible explanation for the moderately light-dependent antagonism could be the known tolerance for modification on the right-hand side of L-701324-like antagonists, hinting at a large binding pocket able to accommodate both isomers of PRNA.³²

Furthermore, the block of the NMDA current caused by *trans*-PNRA could be reversibly reduced when exposed to 360 nm light (Fig. 4). The same was true for GluN1-1a + GluN2C, albeit with a lower (60%) initial block (Fig. S1c). Interestingly, heterologously expressed GluN1-1a + GluN2B and GluN1-1a + GluN2D were blocked with much lower efficiency (30%), although the reduction in antagonism upon illumination with 360 nm light was rather similar (Figs. S1b and S1d). This selectivity profile is rather unusual, as alluded to before. To the best of our knowledge, PNRA is the first NMDA antagonist displaying higher affinity for GluN2A and GluN2C over GluN2B and GluN2D. As such, it could be used as a starting point for the development of other, even more subtype-specific NMDAR antagonists.

3. Conclusion

In summary, we have synthesized and characterized a series of azobenzene photoswitches for the optical control of NMDA receptors and evaluated them *in vitro*. From this work, *azo*-L-701324 or PNRA (**35**) emerged as a viable photochromic antagonist of NMDA receptors that shows subtype selectivity for GluN2A and GluN2C over GluN2B and GluN2D. It is an active blocker in its dark-adapted *trans*-state and can be switched into its less active *cis*-state using near-UV light. Future research will focus on the development of red-shifted and other variants to increase the light-dependent current change, enabling the study of NMDA receptors in more advanced biological settings like acute mouse brain slices and

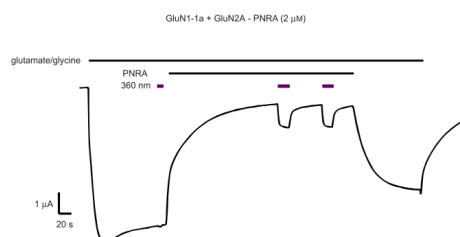


Fig. 4. Two-electrode voltage clamp electrophysiology of *Xenopus* oocytes expressing GluN1-1a + GluN2A channels. Evaluation of PNRA (**33**) (2 μM) revealed that it can modulate NMDA receptor currents in a light-dependent fashion in the presence of glutamate (100 μM) and glycine (10 μM). Trace representative of *n* = 5 oocytes.

whole-cell patch-clamp electrophysiology of hippocampal CA1 neurons.

4. Experimental section

4.1. Chemical methods and materials

All reactions were performed with standard Schlenk techniques under an atmosphere of nitrogen in oven-dried glassware (100 °C oven temperature) that was further dried using a heatgun (set to 650 °C) for all water-sensitive reactions. Tetrahydrofuran (THF) and diethyl ether (Et₂O) were distilled prior to use from sodium and benzophenone, triethylamine (Et₃N), and dichloromethane (CH₂Cl₂) were distilled from calcium hydride. N,N-dimethylformamide (DMF), acetonitrile (MeCN), and methanol (MeOH) were purchased from Acros Organics as 'extra dry' reagents under inert gas atmosphere and over molecular sieves. All other reagents were purchased from commercial sources and used without further purification. Reaction progress was monitored by analytical thin-layer chromatography (TLC), which was carried out using pre-coated glass plates (silica gel 60 F₂₅₄) from Merck. Visualization was achieved by exposure to ultraviolet light (254 nm) where applicable followed by staining with potassium permanganate solution. Flash column chromatography was performed using Merck silica gel (40–63 μm particle size). Proton nuclear magnetic resonance (¹H NMR) spectra were recorded on a Varian 400, Inova 400, Varian 600 or Varian 800 spectrometer. Chemical shifts (δ scale) are expressed in parts per million (ppm) and are calibrated using residual protic solvent as an internal reference (CHCl₃: δ = 7.26 ppm, CD₂HOD: δ = 3.31 ppm, DMSO-d₆: δ = 2.50 ppm, HOD: δ = 4.79 ppm). Data for ¹H NMR spectra are reported as follows: chemical shift (ppm) (multiplicity, coupling constants (Hz), integration). Couplings are expressed as: a = apparent, s = singlet, d = doublet, t = triplet, q = quartet, m = multiplet, or combinations thereof. Carbon nuclear magnetic resonance (¹³C NMR) spectra were recorded on the same spectrometers at 100, 150 or 200 MHz (±1 MHz variance). Carbon chemical shifts (δ scale) are also expressed in parts per million (ppm) and are referenced to the central carbon resonances of the solvents (CDCl₃: δ = 77.16 ppm, MeOH-d₄: δ = 49.00 ppm). In order to assign the ¹H and ¹³C NMR spectra, a range of 2D-NMR experiments (COSY, HMQC, HMBC, NOESY) was used as appropriate. Infrared (IR) spectra were recorded on a Perkin Elmer Spectrum BX II (FTIR System) equipped with an attenuated total reflection (ATR) measuring unit. IR data are reported in frequency of absorption (cm⁻¹). Mass spectroscopy (MS) experiments were performed on a Thermo Finnigan MAT 95 (electron ionization, EI) or on a Thermo Finnigan LTQ FT (electrospray ionization, ESI) instrument. (2*S*,3*R*)-piperazine-2,3-dicarboxylic acid (**21**), dimethyl (2*S*,3*R*)-piperazine-2,3-dicarboxylate (**23**) and 1-(3-(bromomethyl)phenyl)-2-phenyldiazene (**24**) were prepared according to literature procedures.^{29,36}

4.2. Biological methods

cRNA was synthesized from cDNA clones of GluN1-1a (GenBank accession number U08261), GluN2A (NM_012573), GluN2B (U11419), GluN2C (NM_012575), GluN2D (NM_022797), GluA1(Q) flip (P19490.2), GluA1(Q) flop (P19490.1), GluA2(R) flip (P19491.2), and GluK2(P42260) subcloned in the *Xenopus laevis* oocyte expression vector pSGEM using the T7 mMESAGE mMACHINE Kit (Ambion). Synthesized cRNA was isolated via the Clean & Concentrator 25 kit (Zymo), the quality of the cRNA controlled via denaturing agarose gel electrophoresis and the concentration, after photometrical determination, adjusted to 400 ng μL⁻¹ with

nuclease-free water. All animal procedures were performed in accordance with the Tierschutzgesetz (TierSchG) and the Tierschutz-Versuchstierverordnung (TierSchVersV). *Xenopus* oocytes of stages V or VI were obtained by surgical removal of the ovaries of a *Xenopus laevis* frog previously anesthetized with ethyl 3-aminobenzoate methanesulfonate (2.3 g L⁻¹; Sigma). The ovaries were cut and under constant shaking incubated with 300 U mL⁻¹ (10 mg mL⁻¹) collagenase type I 44 (Worthington Biochemicals) for 3 h at 21 °C in Ca²⁺-free Barth's solution (in mM: 88 NaCl, 1.1 KCl, 2.4 NaHCO₃, 0.8 MgSO₄, 15 HEPES, pH adjusted to 7.6 with NaOH). The Ca²⁺-sensitive collagenase reaction was stopped by rinsing with Barth's solution with (in mM: 88 NaCl, 1.1 KCl, 2.4 NaHCO₃, 0.8 MgSO₄, 0.4 CaCl₂, 0.3 Ca(NO₃)₂, 15 HEPES, pH adjusted to 7.6 with NaOH). Oocytes were kept in Barth's medium supplemented with 100 µg mL⁻¹ gentamycin, 40 µg mL⁻¹ streptomycin, and 63 mg mL⁻¹ penicillin. Oocytes of stages V or VI were selected and injected with cRNA within 8 h after surgery using a Nanoliter 2010 injector (WPI). For the expression of the heteromeric NMDA receptors, 4 ng (10 nL) GluN1-1a cRNA were coinjected with one of the following: 7 ng (17 nL) GluN2A, or 6 ng (15 nL) GluN2B, or 5 ng (13 nL) GluN2C, or 5 ng (13 nL) GluN2D. Electrophysiological recordings were performed on days 4–7. Two-electrode voltage clamping was performed using a TurboTec-10CX amplifier (npi electronic) controlled by Pulse software (HEKA). Borosilicate glass capillaries (Harvard Instruments) were pulled to resistances of 0.1–1.0 MΩ and filled with 3 M KCl. Oocytes were clamped at 70 mV. All recordings were performed in barium Ringer's solution (BaR, in mM: 115 NaCl, 2.5 KCl, 1.8 BaCl₂, 10 HEPES-NaOH, pH 7.2) supplemented with 250 mM niflumic acid (NFA) to prevent the opening of endogenous calcium-induced chloride channels. For the recording of the NMDA receptor currents 100 µM glutamate and 10 µM glycine were used. The photoswitches were irradiated with high-power fiber-coupled Prizmatix LED (360 and 415 nm) after wash-in. All compounds were handled under ambient light conditions without precautions to exclude light.

4.3. Synthetic procedures and characterization data

4.3.1. (1*r*,3*R*,5*S*,7*r*)-3,5-dimethyladamantan-1-aminium chloride (memantine hydrochloride) (**5**)

Bromide **9** (4.03 g, 16.6 mmol, 1.00 eq) was dissolved in formamide (17 mL) and heated to 125 °C for 14 h, at which point GC-MS indicated full conversion, then cooled to room temperature. The mixture was diluted with H₂O (50 mL), then extracted with CH₂Cl₂ (2 × 80 mL). The combined organic phases were washed with concentrated aqueous NaCl (100 mL), then dried and concentrated to give a yellow oil that was directly taken on to the next step. Crude **10** was dissolved in concentrated aqueous HCl (35 mL) and heated to 100 °C, resulting in the slow formation of a voluminous precipitate. After 5 h, the mixture was cooled to room temperature and concentrated. The residue was washed with ice-cold Et₂O (60 mL) and dried to give **5** as a colorless solid (2.28 g, 10.6 mmol, 64% over two steps). ¹H NMR (400 MHz, CDCl₃) δ = 2.29–2.19 (m, 1H), 1.72 (d, J = 3.3, 2H), 1.50 (q, J = 12.0, 11.4, 3H), 1.42 (ad, J = 2.8, 4H), 1.23 (aq, J = 13.5, 12.7, 2H), 0.93 (s, 6H). Analytical data matched the literature values.³⁴

4.3.2. 1-((1*r*,3*R*,5*S*,7*r*)-3,5-dimethyladamantan-1-yl)-3-(4-(phenyldiazenyl)phenyl)urea (**13**)

4-(phenyldiazenyl)aniline (197 mg, 1.00 mmol, 1.00 eq) was dissolved in dry CH₂Cl₂ and the solution was cooled to 0 °C before Et₃N (420 µL, 3.00 mmol, 3.00 eq) and triphosgene (148 mg, 500 µmol, 0.50 eq) were added. The reaction mixture was stirred for 6 h. In a separate vial, a solution containing memantine hydrochloride (**5**) (215 mg, 1.00 mmol, 1.00 eq) and Et₃N (420 µL,

3.00 mmol, 3.00 eq) in dry CH₂Cl₂ was prepared and cooled to 0 °C. The second solution was added dropwise to the first containing *p*-azobenzene isocyanate (**11**) and the resulting reaction mixture was stirred for 17 h. The solvent was removed by rotary evaporation and the residue was redissolved in EtOAc (40 mL). The organic phase was washed with H₂O (15 mL) and saturated aqueous NaCl (25 mL), dried over MgSO₄ and the solvent was removed by rotary evaporation. Two purifications by column chromatography (pentane:EtOAc 7:1 and 15:1) yielded urea **13** (50 mg, 0.12 mmol, 12%) as an orange solid. *R*_f 0.49 (hexanes:EtOAc 5:1). ¹H NMR (400 MHz, CDCl₃) δ = 7.98 (d, J = 8.6, 2H), 7.94–7.87 (m, 4H), 6.76 (d, J = 8.9, 2H), 4.52 (s, 1H), 3.12 (s, 5H), 2.10–2.02 (m, 1H), 1.64–1.60 (m, 2H), 1.55–1.38 (m, 4H), 1.30–1.16 (m, 4H), 1.07 (s, 2H), 0.78 (s, 6H). ¹³C NMR (101 MHz, CDCl₃) δ = 153.7, 152.8, 148.2, 142.1, 130.7, 129.2, 124.4, 122.8, 119.4, 53.4, 50.7, 48.3, 42.8, 40.9, 32.6, 30.2. IR (ATR) 3324, 2900, 1746, 1652, 1541, 1454, 1303, 1220, 1142, 1098, 1017, 843, 763, 685. HRMS (ESI) Calculated for C₂₆H₃₄N₄O₂S 466.2402, found 466.2393. *Mp* 184–185 °C.

4.3.3. *N*-((1*r*,3*R*,5*S*,7*r*)-3,5-dimethyladamantan-1-yl)-4-(4-(dimethylamino)phenyl)diazanyl-benzenesulfonamide (**14**)

Memantine hydrochloride (**5**) (43 mg, 0.20 mmol, 1.0 eq) was dissolved in CH₂Cl₂ (3 mL) and Et₃N (84 µL, 0.60 mmol, 3.0 eq) was added before the reaction mixture was cooled to 0 °C. Dabsyl chloride (**12**) (68 mg, 0.21 mmol, 1.05 eq) was added, whereupon the reaction mixture turned dark red. After 30 min, the solution was warmed to room temperature and stirred for 14 h. At this point CH₂Cl₂ (15 mL) was added and the organic phase was washed with H₂O (15 mL), saturated aqueous NaHCO₃ (15 mL) and saturated aqueous NaCl (15 mL). The organic phase was dried over MgSO₄ and the solvent was removed by rotary evaporation. Purification by column chromatography (pentane:EtOAc 5:1) yielded sulfonamide **14** as a dark red solid (57 mg, 0.12 mmol, 61%). *R*_f 0.28 (hexanes:EtOAc 3:1). Dark-red solid. ¹H NMR (400 MHz, CDCl₃) δ = 7.98 (d, J = 8.6, 2H), 7.94–7.87 (m, 4H), 6.76 (d, J = 8.9, 2H), 4.52 (s, 1H), 3.12 (s, 5H), 2.10–2.02 (m, 1H), 1.64–1.60 (m, 2H), 1.55–1.38 (m, 4H), 1.30–1.16 (m, 4H), 1.07 (s, 2H), 0.78 (s, 6H). ¹³C NMR (101 MHz, CDCl₃) δ = 155.3, 153.2, 143.7, 143.5, 128.0, 125.8, 122.5, 111.6, 56.9, 50.3, 49.4, 42.3, 41.5, 40.5, 32.8, 30.2, 30.0. IR (ATR) 3473 w, 3288 w, 2958 m, 2928 m, 2358 w, 1815 w, 1690 s, 1478 m, 1454 m, 1416 m, 1366 m, 1299 m, 1247 m, 1166 m, 1056 w, 889 w. HRMS (ESI) Calculated for C₂₆H₃₄N₄O₂S 466.2402, found 466.2393. *Mp* 178–180 °C.

4.3.4. (3*s*,5*s*,7*s*)-*N*-(4-nitrobenzyl)adamantan-1-amine (**16**)

To adamantylamine (**6**) (302 mg, 2.00 mmol, 1.00 eq) in MeCN (2.5 mL) was added K₂CO₃ (373 mg, 2.70 mmol, 1.35 eq) and *p*-nitrobenzyl bromide (**15**) (389 mg, 1.80 mmol, 0.90 eq). The resulting suspension was stirred at 80 °C for 24 h before it was cooled to room temperature and filtered through a plug of celite. The solution was concentrated and purified by column chromatography (hexanes:EtOAc 5:1) to yield **16** (363 mg, 1.27 mmol, 70%) as an off-white solid. *R*_f 0.11 (hexanes:EtOAc 5:1). Off-white solid. ¹H NMR (400 MHz, CDCl₃) δ = 8.16 (d, J = 8.7, 2H), 7.53 (d, J = 8.4, 2H), 3.87 (s, 2H), 2.09 (d, J = 4.4, 3H), 1.74–1.58 (m, 12H). HRMS (ESI): Calculated for C₁₇H₂₃N₂O₂ 287.1754, found 287.1754. The data matched literature values.³⁸

4.3.5. (3*s*,5*s*,7*s*)-*N*-(4-aminobenzyl)adamantan-1-amine (**17**)

Nitroaryl **16** (0.14 g, 0.50 mmol, 1.0 eq) was dissolved in EtOH (5 mL) before tin(II) chloride (95 mg, 0.80 mmol, 1.6 eq) and aqueous HCl (2 M, 4.5 mL) were added, turning the colorless solution bright yellow. After stirring at 80 °C for 15 h, the mixture was cooled to room temperature before saturated aqueous NaHCO₃ (10 mL) was added. The solution was extracted with CH₂Cl₂

(3 × 15 mL), then washed with saturated aqueous NaCl (15 mL), dried over MgSO₄ and concentrated. The off-white solid **17** (0.10 g, 0.40 mmol, 80%) thus obtained was deemed pure enough for further transformations. ¹H NMR (400 MHz, CDCl₃) δ = 7.14 (d, *J* = 7.9, 2H), 6.64 (d, *J* = 8.2, 2H), 3.66 (s, 2H), 3.59 (s, 2H), 2.09 (s, 3H), 1.77–1.60 (m, 12H). The data matched literature values.³⁸

4.3.6. (3*s*,5*s*,7*s*)-*N*-(4-(phenyldiazenyl)benzyl)-adamantan-1-amine (**18**)

Amine **17** (51 mg, 0.20 mmol, 1.0 eq) was dissolved in CH₂Cl₂ (0.5 mL) in an open flask. Glacial AcOH (0.5 mL) and nitrosobenzene (23 mg, 0.21 mmol, 1.0 eq) were added. The flask was sealed with a septum and the solution was heated to 40 °C, whereupon it turned dark brown. After 20 h the reaction was cooled to room temperature, the solvent was removed by rotary evaporation and the crude product was purified by column chromatography (CH₂Cl₂:MeOH 12:1). Further purification by preparative TLC (CH₂Cl₂:MeOH 7:1) yielded azobenzene **18** (17 mg, 50 mmol, 40%) as an orange solid. *R*_f 0.29 (hexanes:EtOAc 5:1). ¹H NMR (400 MHz, CDCl₃) δ = 7.94–7.78 (m, 4H), 7.57–7.41 (m, 5H), 3.86 (s, 2H), 2.10 (t, *J* = 3.3, 3H), 1.76 (d, *J* = 2.8, 6H), 1.73–1.58 (m, 7H). ¹³C NMR (101 MHz, CDCl₃) δ = 152.7, 151.7, 130.9, 129.1, 128.8, 123.0, 122.8, 120.9, 120.4, 44.7, 42.3, 36.6, 29.6. IR (ATR) 2900, 2848, 1453, 1356, 1308, 1137, 828, 685. HRMS (ESI) Calculated for C₂₃H₂₉N₃ 346.2278, found 346.2275. *Mp* 110–112 °C.

4.3.7. (3*s*,5*s*,7*s*)-*N*-(4-((4-diethylamino)-phenyl)diazenyl)benzyl)adamantan-1-amine (**19**)

Amine **17** (52 mg, 0.20 mmol, 1.0 eq) was dissolved in MeOH (0.5 mL) and H₂O (0.5 mL) and cooled to 0 °C before concentrated HCl (63 μL, 0.60 mmol, 3.0 eq) was added. NaNO₂ (15 mg, 0.22 mmol, 1.1 eq) dissolved in H₂O (0.1 mL) was then added dropwise, turning the reaction mixture bright yellow. After 40 min at 0 °C, NaOAc (98 mg, 1.2 mmol, 6.0 eq) was added, followed by *N,N*-diethylaniline (25 μL, 0.20 mmol, 1.0 eq). At this point, the reaction was slowly warmed to room temperature. After 15 h, EtOAc (10 mL) was added and the phases were separated. The organic phase was washed with H₂O (5 mL), NaOH (2 M, 5 mL) and concentrated aqueous NaCl (5 mL), dried over MgSO₄ and concentrated. The crude product was purified by column chromatography (pentane:EtOAc 1:1) to yield azobenzene **19** (17 mg, 50 mmol, 40%) as an orange solid.

*R*_f 0.39 (CH₂Cl₂:MeOH 9:1). ¹H NMR (600 MHz, CDCl₃) δ = 7.84 (d, *J* = 9.2, 2H), 7.78 (d, *J* = 8.4, 2H), 7.47–7.39 (m, 2H), 6.75–6.67 (m, 2H), 3.82 (s, 2H), 3.45 (q, *J* = 7.1, 4H), 2.10 (q, *J* = 2.9, 3H), 1.73 (d, *J* = 2.8, 6H), 1.72–1.61 (m, 7H), 1.23 (t, *J* = 7.1, 6H). ¹³C NMR (151 MHz, CDCl₃) δ = 152.2, 150.0, 143.1, 128.7, 125.1, 122.2, 110.9, 44.9, 44.7, 42.9, 36.7, 29.6, 12.6. IR (ATR) 2972, 2899, 2845, 1597, 1513, 1393, 1349, 1137, 1096, 1008, 823, 812. HRMS (ESI) Calculated for C₂₇H₃₆N₄ 416.2934, found 416.2931. *Mp* 172–174 °C.

4.3.8. 3-(phenyldiazenyl)benzoic acid (**20**)

3-aminobenzoic acid (274 mg, 2.0 mmol, 1.0 eq) was dissolved in MeOH (10 mL). AcOH (0.34 mL, 6.0 mmol, 3.0 eq) and nitrosobenzene (214 mg, 2.0 mmol, 1.0 eq) were added, turning the reaction mixture dark brown. After heating to 50 °C for 22 h, the solvent was removed and the residue was redissolved in EtOAc (40 mL). The organic phase was washed with H₂O (2 × 10 mL), HCl (1 M, 20 mL), NaOH (1 M, 20 mL), H₂O (15 mL) and saturated aqueous NaCl (15 mL). The solvent was removed and the crude product was purified by column chromatography (CH₂Cl₂:MeOH 49:1 to 9:1) to give **20** (227 mg, 1.00 mmol, 50%) as an orange solid. *R*_f 0.44 (hexanes:EtOAc 9:1). ¹H NMR (400 MHz, CDCl₃) δ = 8.66 (s, 1H), 8.24 (d, *J* = 7.6, 1H), 8.18 (d, *J* = 7.7, 1H), 7.97 (d, *J* = 7.6, 2H), 7.65 (t, *J* = 7.8, 1H), 7.59–7.49 (m, 3H). ¹³C NMR (151 MHz, CDCl₃)

δ = 170.8, 152.8, 152.5, 132.3, 131.7, 130.4, 129.5, 129.3, 127.9, 124.9123.2. IR (ATR) 2822, 2563, 1889, 1676, 1585, 1421, 1308, 1211, 1160, 1077, 917, 762, 680. HRMS (EI) Calculated for C₁₃H₁₁N₂O₂ 226.0742, found 226.0729. *Mp* 169–170 °C. The data matched literature values.³⁶

4.3.9. Dimethyl *cis*-1-(3-(phenyldiazenyl)benzyl)piperazine-2,3-dicarboxylate (**25**)

To a solution of dimethyl *cis*-piperazine-2,3-dicarboxylate (**24**) in THF (1.0 mL) was added Et₃N (20 μL, 0.15 mmol, 1.0 eq) at 0 °C. 1-(3-(Bromomethyl)phenyl)-2-phenyldiazene in THF (0.50 mL) was subsequently added dropwise and the mixture was stirred for 30 min at this temperature before the cooling bath was removed. The mixture was stirred for 16 h before it was concentrated *in vacuo*. The residue was redissolved in EtOAc (25 mL), then washed with H₂O (5 mL) and concentrated aqueous NaCl (5 mL), dried over MgSO₄ and concentrated. The crude product was purified by column chromatography (pentane:EtOAc 1:1 to 0:1) to yield azobenzene **25** (33 mg, 83 μmol, 55%) as a red oil. *R*_f 0.50 (CH₂Cl₂:MeOH 9:1). ¹H NMR (400 MHz, CDCl₃) δ = 7.96–7.86 (m, 3H), 7.85–7.78 (m, 1H), 7.56–7.42 (m, 5H), 4.00–3.83 (m, 4H), 3.73 (s, 3H), 3.73 (s, 3H), 3.12–3.00 (m, 1H), 2.96–2.81 (m, 2H), 2.60–2.48 (m, 1H), 2.17 (s, 1H). ¹³C NMR (101 MHz, CDCl₃) δ = 171.1, 171.0, 153.0, 152.7, 139.9, 131.3, 131.1, 129.2, 123.1, 122.9, 121.8, 62.1, 60.8, 60.0, 52.3, 51.5, 46.6, 45.4. IR (ATR) 3349, 2950, 1738, 1600, 1434, 1357, 1200, 1148, 1076, 1034, 1013, 910, 797, 764, 660. HRMS (ESI) Calculated for C₂₁H₂₅N₄O₄ 397.1870, found 397.1875.

4.3.10. *Cis*-1-(3-(phenyldiazenyl)benzyl)piperazine-2,3-dicarboxylate (**26**)

To a solution of **25** in THF (1.0 mL) was added LiOH (41 mg, 0.96 μmol, 12 eq) in H₂O (0.5 mL) at room temperature. The orange solution was stirred for 36 h before it was treated with aqueous HCl (2 M, 0.5 mL) until pH ≈ 3. The mixture was concentrated to half volume, diluted with H₂O (2 mL), and concentrated to half volume again. The suspension was filtered and the orange residue washed with ice-cold water and Et₂O to yield azobenzene **26** (14 mg, 38 μmol, 40%) as an orange-red solid.

¹H NMR (400 MHz, MeOH-*d*₄) δ = 8.03–7.80 (m, 4H), 7.65–7.43 (m, 5H), 4.34 (d, *J* = 3.9, 1H), 4.22 (d, *J* = 4.0, 1H), 4.19 (d, *J* = 13.7, 1H), 3.94 (d, *J* = 13.7, 1H), 3.37 (d, *J* = 12.6, 1H), 3.22 (td, *J* = 12.4, 4.0, 1H), 2.93 (dd, *J* = 13.4, 3.6, 1H), 2.82 (td, *J* = 12.9, 3.0, 1H). ¹³C NMR (101 MHz, MeOH-*d*₄) δ = 171.5, 168.7, 154.2, 153.9, 140.4, 132.9, 132.4, 130.5, 130.3, 124.2, 123.8, 123.2, 60.3, 60.0, 58.0, 44.6, 44.0. IR (ATR) 3079, 2925, 2339, 1748, 1643, 1459, 1380, 1240, 1203, 1159, 1107, 1056, 998, 905, 829, 771, 694. HRMS (ESI) Calculated for C₁₉H₂₁N₄O₄ 369.1557, found 369.1561. *Mp* 180–188 °C.

4.3.11. 2-(3-nitrophenyl)acetic acid (**28**)

2-(3-nitrophenyl)acetonitrile (**27**) (1.95 g, 12.0 mmol, 1.00 eq) was dissolved in H₂O (7 mL) before concentrated H₂SO₄ (7 mL) and AcOH (7 mL) were added dropwise. The solution was stirred at 110 °C for 5 h. After cooling to room temperature, H₂O (40 mL) was added carefully. The solution was extracted with EtOAc (3 × 50 mL), then washed with H₂O (90 mL) and saturated aqueous NaCl (90 mL), dried over MgSO₄ and concentrated. The off-white solid **28** (2.15 g, 11.9 mmol, 99%) thus obtained was pure enough for further transformations. ¹H NMR (400 MHz, CDCl₃) δ = 8.17 (d, *J* = 7.0, 2H), 7.63 (d, *J* = 7.6, 1H), 7.58–7.48 (m, 1H), 3.79 (s, 2H). The data matched literature values.³⁹

4.3.12. Methyl 4-chloro-2-(2-(3-nitrophenyl)-acetamido)benzoate (**30**)

2-(3-nitrophenyl)acetic acid (**28**) (1.62 g, 9.00 mmol, 2.00 eq) was dissolved in CH₂Cl₂ (28 mL) and cooled to 0 °C before oxalyl

chloride solution (2 M, 5.90 mL, 11.7 mmol, 2.60 eq) was added dropwise over 30 min, followed by addition of DMF (70 μ L, 0.90 mmol, 0.20 eq) over 2 min. The solution was warmed to room temperature and stirred for 5 h. After this time, the solvent was removed in a nitrogen stream. The residue was redissolved in 1,2-dichloroethane (30 mL) and methyl 2-amino-4-chlorobenzoate (**29**) (835 mg, 4.50 mmol, 1.00 eq) was added in one portion. The dark-yellow solution was stirred at 80 °C for 15 h, then cooled to room temperature. Saturated aqueous NaHCO₃ (20 mL) was added and the solution was extracted with CH₂Cl₂ (3 \times 60 mL), then washed with H₂O (50 mL) and saturated aqueous NaCl (90 mL), dried over MgSO₄ and concentrated. The residue was purified by column chromatography (hexanes:EtOAc 4:1) to yield **30** (1.18 g, 3.38 mmol, 75%) as a white solid. **R_f** 0.38 (hexanes:EtOAc 3:1) ¹H NMR (400 MHz, CDCl₃) δ = 11.32 (s, 1H), 8.79 (d, *J* = 2.1, 1H), 8.25 (d, *J* = 2.0, 1H), 8.19 (dt, *J* = 8.2, 1.5, 1H), 7.94 (d, *J* = 8.6, 1H), 7.72 (d, *J* = 7.6, 1H), 7.56 (t, *J* = 7.9, 1H), 7.07 (dd, *J* = 8.6, 2.1, 1H), 3.89 (s, 3H), 3.88 (s, 2H). The data matched literature values.^{32,39}

4.3.13. Methyl 2-(2-(3-aminophenyl)acetamido)-4-chlorobenzoate (**31**)

Methyl 2-(2-(3-aminophenyl)acetamido)-4-chlorobenzoate (**30**) (736 mg, 2.11 mmol, 1.00 eq) was dissolved in EtOH (85 mL) and H₂O (28 mL) before zinc powder (4.12 g, 63.0 mmol, 30.0 eq) and a CaCl₂·6H₂O (468 mg, 4.22 mmol, 2.00 eq) were added in one portion. The suspension was stirred at 80 °C for 3 h, then cooled to room temperature and filtered over a plug of celite with EtOAc (50 mL). The filtrate was diluted with H₂O (50 mL) and the phases were separated. The aqueous phase was extracted with EtOAc (3 \times 60 mL). The combined organic phases were washed with saturated aqueous NaCl (90 mL), dried over MgSO₄ and concentrated. The residue was purified by column chromatography (hexanes:EtOAc 2:1) to yield **31** (1.18 g, 3.38 mmol, 75%) as a white solid. **R_f** 0.37 (hexanes:EtOAc 1:1) ¹H NMR (400 MHz, CDCl₃) δ = 11.06 (s, 1H), 8.82 (d, *J* = 2.1, 1H), 7.91 (d, *J* = 8.6, 1H), 7.15 (t, *J* = 7.8, 1H), 7.03 (dd, *J* = 8.6, 2.1, 1H), 6.76 (ddd, *J* = 7.5, 1.7, 1.0, 1H), 6.71 (t, *J* = 2.0, 1H), 6.62 (ddd, *J* = 8.0, 2.4, 0.9, 1H), 3.87 (s, 3H), 3.65 (s, 2H). The data matched literature values.³²

4.3.14. Methyl 4-chloro-2-(2-(3-(phenyldiazenyl)phenyl)acetamido)benzoate (**32**)

To a solution of **31** (0.16 g, 0.50 mmol, 1.0 eq) in MeOH (2.5 mL) was added acetic acid (2.5 mL) followed by nitrosobenzene (59 mg, 0.55 mmol, 1.1 eq) at room temperature. The mixture was stirred at 50 °C for 24 h, at which point, LC-MS analysis showed full conversion and saturated aq. NaHCO₃ (5 mL) was added at room temperature after dilution with EtOAc (10 mL). After extraction of the aqueous phase with EtOAc (3 \times 10 mL), the combined organic phases were washed with saturated aqueous NaCl (15 mL), dried and evaporated to give a red oil that was purified by column chromatography (hexanes:EtOAc 6:1) to give **32** as an orange solid (0.13 g, 0.32 mmol, 63%).

R_f 0.51 (hexanes:EtOAc 5:1). ¹H NMR (400 MHz, CDCl₃) δ = 11.22 (s, 1H), 8.84 (d, *J* = 2.0, 1H), 8.01–7.81 (m, 5H), 7.64–7.38 (m, 5H), 7.04 (dd, *J* = 8.7, 2.0, 1H), 3.88 (s, 2H), 3.84 (s, 3H). ¹³C NMR (101 MHz, CDCl₃) δ = 169.8, 168.0, 153.1, 152.7, 142.3, 141.0, 135.2, 132.1, 131.9, 131.2, 129.7, 129.2, 123.8, 123.1, 123.0, 122.5, 120.4, 113.5, 52.6, 45.6. IR (ATR) 3246 w, 3119 w, 2918 w, 1693 s, 1580 s, 1512 m, 1252 s, 1236 s, 1098 m, 759 s, 690 s. HRMS (ESI) Calculated for C₂₂H₁₉ClN₃O₃ 408.1109, found 408.1118. **Mp** 89–92 °C.

4.3.15. 7-chloro-4-hydroxy-3-(3-(phenyldiazenyl)phenyl)quinolin-2(1H)-one, PNRA (**33**)

To a solution of **32** (62 mg, 0.15 mmol, 1.0 eq) in THF (1.0 mL) was added KHMDS (0.5 M in PhMe, 0.90 mL, 0.45 mmol, 3.0 eq)

dropwise at 0 °C, turning the solution dark-red. The cooling bath was removed and the mixture was stirred at room temperature. After 2.5 h, MeOH (2 mL) was added, followed by careful addition of TFA until pH = 8 and EtOAc (20 mL). The organic phase was washed with concentrated aqueous NaCl (10 mL), dried and evaporated to give a red oil that was purified by column chromatography (hexanes:EtOAc 2:1 to 1:2) to give **33** as an orange solid (39 mg, 0.96 μ mol, 63%). **R_f** 0.18 (hexanes:EtOAc 2:1). ¹H NMR (800 MHz, DMSO-*d*₆) δ = 11.65 (s, 1H), 7.99 (d, *J* = 8.6, 1H), 7.94–7.91 (m, 3H), 7.88 (dt, *J* = 7.9, 1.6, 1H), 7.64 (d, *J* = 7.8, 1H), 7.63–7.57 (m, 5H), 7.36 (d, *J* = 2.1, 1H), 7.25 (dd, *J* = 8.6, 2.1, 1H). ¹³C NMR (201 MHz, DMSO-*d*₆) δ = 163.0, 158.0, 152.4, 152.1, 139.5, 135.6, 134.9, 134.8, 131.9, 130.0, 129.3, 125.8, 125.6, 123.0, 122.2, 121.8, 114.9, 114.6, 112.4. IR (ATR) 3025 w, 2928 w, 1642 s, 1599 m, 1500 w, 1365 m, 1270 m, 1149 m, 880 m, 795 s, 688 s. HRMS (ESI) Calculated for C₂₁H₁₅ClN₃O₂ 376.0847, found 376.0847. **Mp** > 275 °C.

Acknowledgments

D. M. B. gratefully acknowledges the European Commission for a Marie Skłodowska-Curie Intra-European Fellowship (PIEF-GA-2013-627990). D. T. thanks the Munich Center for Integrated Protein Science (CIPSM) and the European Research Council (Advanced Grant 268795).

Appendix A. Supplementary data

Supplementary data related to this article can be found at <http://dx.doi.org/10.1016/j.tet.2017.06.056>.

References

- Gereau RW, Swanson G. *The Glutamate Receptors*. New York: Humana Press; 2008.
- Traynelis SF, Wollmuth LP, McBain CJ, et al. *Pharmacol Rev*. 2010;62:405–496.
- VanDongen AM. *Biology of the NMDA Receptor*. CRC Press; 2008.
- Hunt DL, Castillo PE. *Curr Opin Neurobiol*. 2012;22:496–508.
- Bannerman DM, Sprengel R, Sanderson DJ, et al. *Nat Rev Neurosci*. 2014;15:181–192.
- Paoletti P, Bellone C, Zhou Q. *Nat Rev Neurosci*. 2013;14:383–400.
- Ellis-Davies GCR, Matsuzaki M, Paukert M, Kasai H, Bergles DE. *J Neurosci*. 2007;27:6601–6604.
- Ellis-Davies GCR. *Nat Meth*. 2007;4:619–628.
- Palma-Cerda F, Auger C, Crawford DJ, et al. *Neuropharmacology*. 2012;63:624–634.
- Palmer LM, Shai AS, Reeve JE, Anderson HL, Paulsen O, Larkum ME. *Nat Neurosci*. 2014;17:383–390.
- Gorostiza P, Isacoff EY. *Science*. 2008;322:395–399.
- Fehrentz T, Schönberger M, Trauner D. *Angew Chem Int Ed*. 2011;50:12156–12182.
- Szymański W, Beierle JM, Kistemaker HAV, Velema WA, Feringa BL. *Chem Rev*. 2013;113:6114–6178.
- Velema WA, Szymański W, Feringa BL. *J Am Chem Soc*. 2014;136:2178–2191.
- Broichhagen J, Frank JA, Trauner D. *Acc Chem Res*. 2015;48:1947–1960.
- Lerch MM, Hansen MJ, van Dam GM, Szymański W, Feringa BL. *Angew Chem Int Ed*. 2016;55:10978–10999.
- Izquierdo-Serra M, Gascón-Moya M, Hirtz JJ, et al. *J Am Chem Soc*. 2014;136:8693–8701.
- Pittolo S, Gómez-Santacana X, Eckelt K, et al. *Nat Chem Biol*. 2014;10:813–815.
- Rovira X, Trapero A, Pittolo S, et al. *Cell Chem Biol*. 2016;23:929–934.
- Izquierdo-Serra M, Bautista-Barrufet A, Trapero A, et al. *Nat Commun*. 2016;7:12221.
- Gómez-Santacana X, Pittolo S, Rovira X, et al. *ACS Cent Sci*. 2017;3:81–91.
- Volgraf M, Gorostiza P, Szobota S, Helix MR, Isacoff EY, Trauner D. *J Am Chem Soc*. 2006;129:260–261.
- Stawski P, Sumser M, Trauner D. *Angew Chem Int Ed*. 2012;51:5748–5751.
- Laprell L, Repak E, Franckevicius V, et al. *Nat Commun*. 2015;6:8076.
- Barber DM, Liu S-A, Gottschling K, Sumser M, Hollmann M, Trauner D. *Chem Sci*. 2017;8:611–615.
- Schoenberger M, Damijonaitis A, Zhang Z, Nagel D, Trauner D. *ACS Chem Neurosci*. 2014;5:514–518.
- Karakas E, Furukawa H. *Science*. 2014;344:992–997.
- Lee C-H, Lu W, Michel JC, et al. *Nature*. 2014;511:191–197.
- Morley RM, Tse H-W, Feng B, Miller JC, Monaghan DT, Jane DE. *J Med Chem*. 2005;48:2627–2637.

4912

F.W.W. Hartrampf et al. / Tetrahedron 73 (2017) 4905–4912

30. Kulagowski JJ, Baker R, Curtis NR, et al. *J Med Chem.* 1994;37:1402–1405.
31. Joubert J, Dyk SV, Green IR, Malan SF. *Bioorg Med Chem.* 2011;19:3935–3944.
32. Fuchigami T, Haradahira T, Fujimoto N, et al. *Bioorg Med Chem.* 2009;17:5665–5675.
33. Brameld, K. A.; Verner, E. WO2014182829 A1, 2014.
34. Reddy JM, Prasad G, Raju V, Ravikumar M, Himabindu V, Reddy GM. *Org Process Res Dev.* 2007;11:268–269.
35. Madhra MK, Sharma M, Khanduri CH. *Org Process Res Dev.* 2007;11:922–923.
36. Fatás P, Longo E, Rastrelli F, et al. *Chem Eur J.* 2011;17:12606–12611.
37. Dong M, Babalhavaeji A, Samanta S, Beharry AA, Woolley GA. *Acc Chem Res.* 2015;48:2662–2670.
38. Wang J, Ma C, Wang J, et al. *J Med Chem.* 2013;56:2804–2812.
39. Kreimeyer A, Laube B, Sturgess M, Goeldner M, Foucaud B. *J Med Chem.* 1999;42:4394–4404.

Part 3 – Synthesis of photoswitchable PPAR γ agonists

3 Synthesis of photoswitchable PPAR γ agonists¹

As part of a research program related to the photopharmacology of nuclear receptors, we became interested in the so-called peroxisome proliferator-activated receptors (PPARs).^[366-367] These are ligand-activated nuclear receptors that function as transcription factors and share a high degree of structural homology with many other nuclear hormone receptors such as retinoid X receptors, with which they form obligate heterodimers.^[368] PPARs play a vital role in many metabolic pathways that reaches far beyond the stimulation of peroxisome proliferation for which they were initially named.^[369] There are three PPAR isotypes called PPAR α , PPAR β/δ and PPAR γ . These receptors are widely expressed across many tissue types, but the expression level of the three subtypes depends strongly on the tissue. PPAR α is mostly expressed in tissues with high fatty acid metabolism; PPAR β/δ features a much broader and variable expression pattern, depending on the extent of cell proliferation and differentiation. Metabolic functions of this subtype were assigned in the gut, skin and brain, amongst others.

PPAR γ is found in most tissues except muscles, but its main functions are in adipose tissue and the large intestine. PPAR γ plays a key role in the regulation of genes related to adipogenesis, energy balance, and lipid biosynthesis.^[370-372] Physiologically, the ligands for PPAR γ are fatty acids such as arachidonic acid and derivatives like the prostaglandins. Given the implication of this nuclear receptor in a variety of fatty acid-related diseases like obesity and diabetes, it comes as no surprise that significant attention has been devoted to the development of synthetic ligands for PPAR γ . A particularly well-developed class of ligands, whose members act as insulin sensitizers, is the thiazolidinedione (TZD) family.^[373] While quite diverse in structure, all members of the TZD class bear this polar head group (see 3.1–3.4, Figure 3.1). Attached to this moiety is a benzyl unit, from which a diverse set of spacers and other substituents protrude.^[374] In many cases, the linker is a short (C₁–C₃) alkyl chain connected to another aromatic portion, often a *N*-heterocycle.

We were attracted to this class of nuclear hormone receptors because of the side effects associated with TZD^[375-376] and the potential benefits of photoswitchable derivatives thereof. Furthermore, in a more general sense, photoswitchable TZDs hold promise as general tools for the optical control of gene expression. A third reason is that X-ray crystal structure of the

¹*In vitro* assays in HEK cells were performed by Dr. Johannes Broichhagen and Philipp Leippe; *in vitro* assays in preadipocytes were performed by Lisa Suwandhi, PhD student in the Ussar group at the Helmholtz Zentrum München.

PPAR γ ligand binding domain possesses a large binding pocket, explaining the large structural variety of ligands and increasing the probability of a photoswitch to be accommodated.^[377]

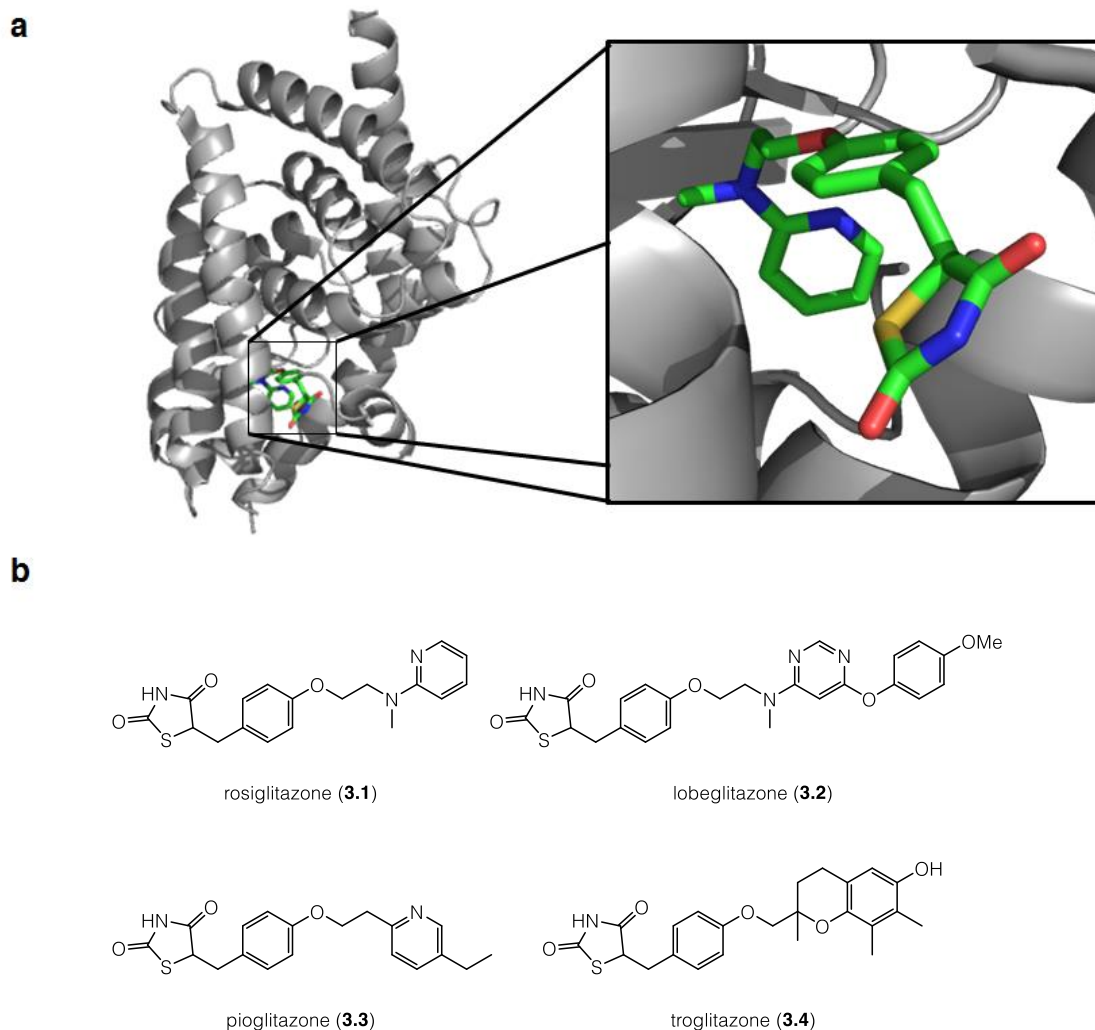
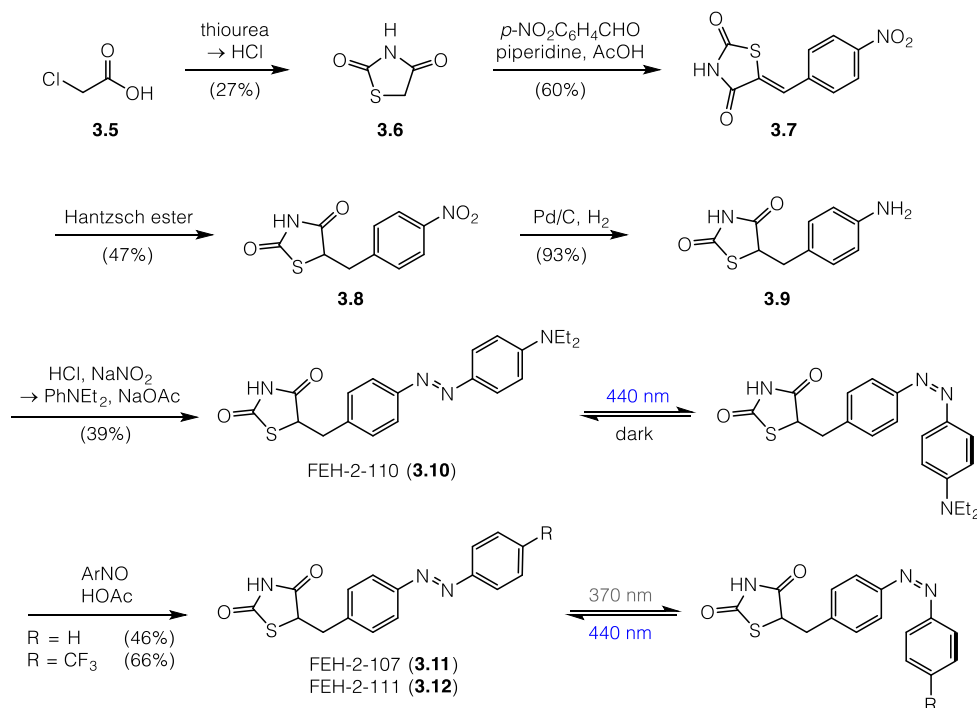


Figure 3.1. a) Binding mode of rosiglitazone (**3.1**) in the ligand-binding pocket with the aliphatic chain in a *cis* alignment; b) Four representatives **3.1**–**3.4** of the TZD family showcasing the similarities in the polar head group and diversity in linker length and lipophilic aromatic unit.

Following our azologization rationale,^[339] we reasoned that rosiglitazone (**3.1**), an FDA-approved insulin sensitizer, would represent a good template for the incorporation of an azobenzene unit (Scheme 2.2). The synthesis of our derivatives was straightforward: Following a modified literature procedure, aniline **3.9** was accessed in four steps.^[378] Thiazolidine-2,4-dione (**3.6**) was obtained by condensation of chloroacetic acid (**3.5**) with thiourea, then condensed with *p*-nitrobenzaldehyde in a Knoevenagel-like reaction to give **3.7**. A range of reduction conditions were explored to reduce the alkene and nitro group in one step, and ultimately, we settled for a 1,4-reduction using Hantzsch ester to give nitroaryl **3.8** followed by palladium-catalyzed hydrogenation to the aniline **3.9**. With this intermediate in hand, three azologs of rosiglitazone (**3.1**), FEH-2-107 (**3.11**), FEH-2-110 (**3.10**) and FEH-2-111 (**3.12**), were

obtained by azo or Mills coupling in moderate yields. These azobenzenes showed regular UV-Vis absorption spectra: the unsubstituted and CF₃-substituted compounds were most efficiently isomerized to the *cis*-isomer with 340 nm light and relaxed thermally to the *trans*-isomer within 10 min in the dark, the NEt₂-substituted photoswitch isomerized to the *cis*-form at 420 nm and relaxed back to the *trans* form within seconds.



Scheme 3.1. Synthesis of photoswitchable PPAR γ agonists through diversification of a common intermediate aniline **3.9**.

With a regular (**3.11**), an electron-poor (**3.12**) and electron-rich (**3.10**) azobenzene in hand, we evaluated our compounds using a PPAR γ luciferase reporter assay in transfected HEK293T cells to see whether our compounds were able to activate PPAR γ *in vitro*. As can be seen in Figure 3.2, all three compounds are functional mimics of rosiglitazone (**3.1**), which served as the positive control (not shown). From this first assay, FEH-2-110 (**3.10**) emerged as the most promising candidate, showing the largest difference between dark and irradiation even though it was irradiated at a wavelength quite distant from its absorption maximum. FEH-2-107 (**3.11**) and FEH-2-111 (**3.12**) showed activation at higher concentrations, but the effect was much less pronounced and we reasoned that the 370 nm irradiation needed would be problematic in long-term *in vivo* applications. Therefore, we investigated FEH-2-110 further using 435 nm light. As can be seen in Figure 3.3, the photoswitch acts an activator at nanomolar concentrations under blue light whereas negligible activation is observed in the dark even at higher concentrations. The azologization template rosiglitazone (**3.1**) thus is about one magnitude more potent.

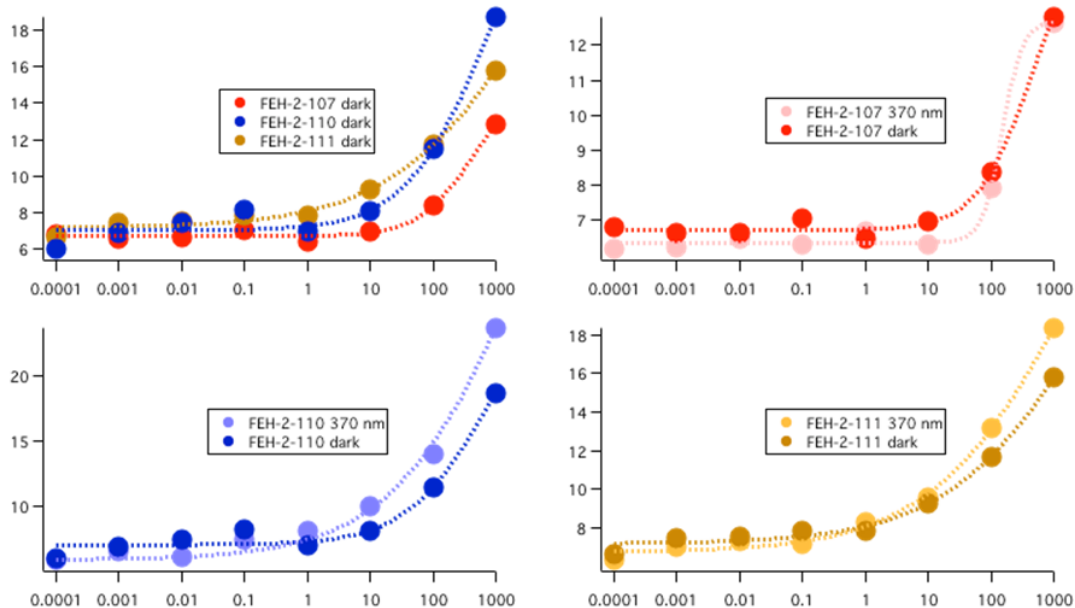


Figure 3.2. Evaluation of azobenzenes 3.10–3.12 using an *in vitro* assay in the dark (darker shades) and under irradiation with 370 nm light (lighter shades). Concentrations are nanomolar.

Therefore, our assumption guided by crystal structure analysis that an azobenzene in its *cis* state could act as a functional mimic rosiglitazone was confirmed.

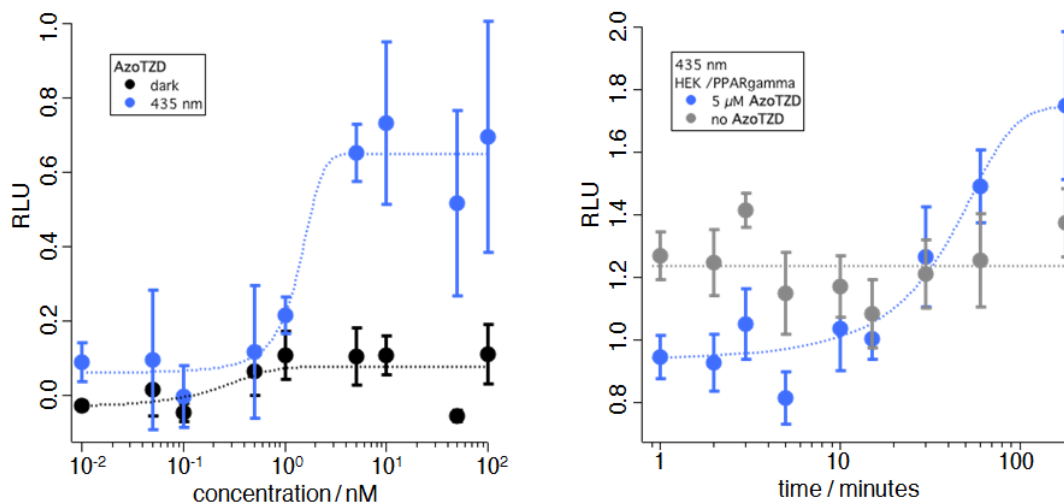


Figure 3.3. Left: Dose-response relationship of azo-TZD FEH-2-110 (3.10) upon irradiation with 435 nm light (blue dots) or in the dark (black dots). Right: PPAR γ activation as a function of light exposure length.

Given these encouraging results, we were interested in investigating our lead compound FEH-2-110 in a more advanced *in vitro* setting. An intriguing application would be the regioselective induction of cell differentiation, which is caused *inter alia* by PPAR γ activation, with light. We thus tested whether our compounds could induce the differentiation of

preadipocytes into adipocytes with an Oil red O staining assay, which is commonly carried out with rosiglitazone. Here, it served as positive control. Oil red O is a lipophilic reagent which stains triglycerides and other lipids, which are enriched in adipocytes. The optical density recorded thus serves as a measure of preadipocyte differentiation.

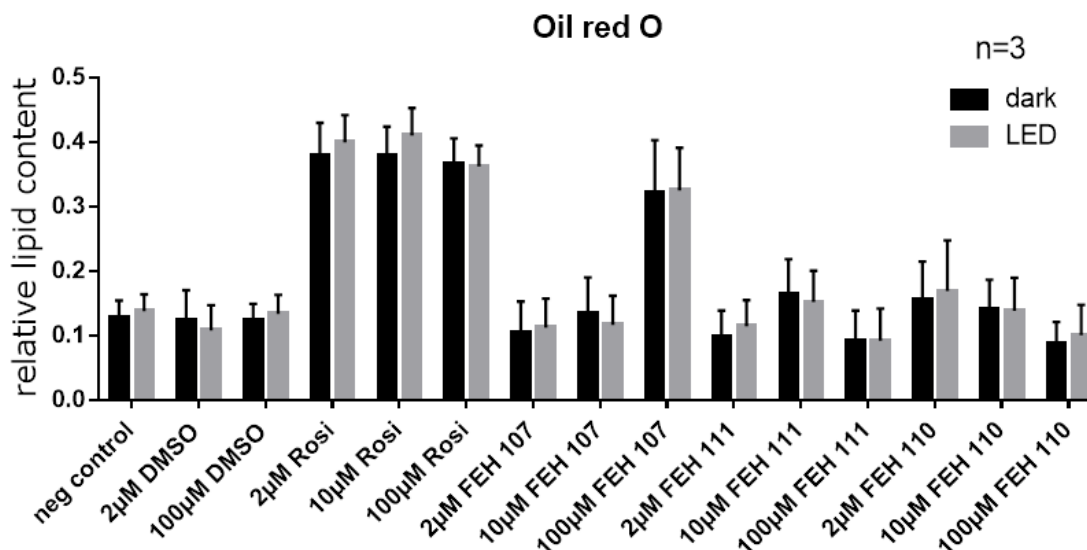
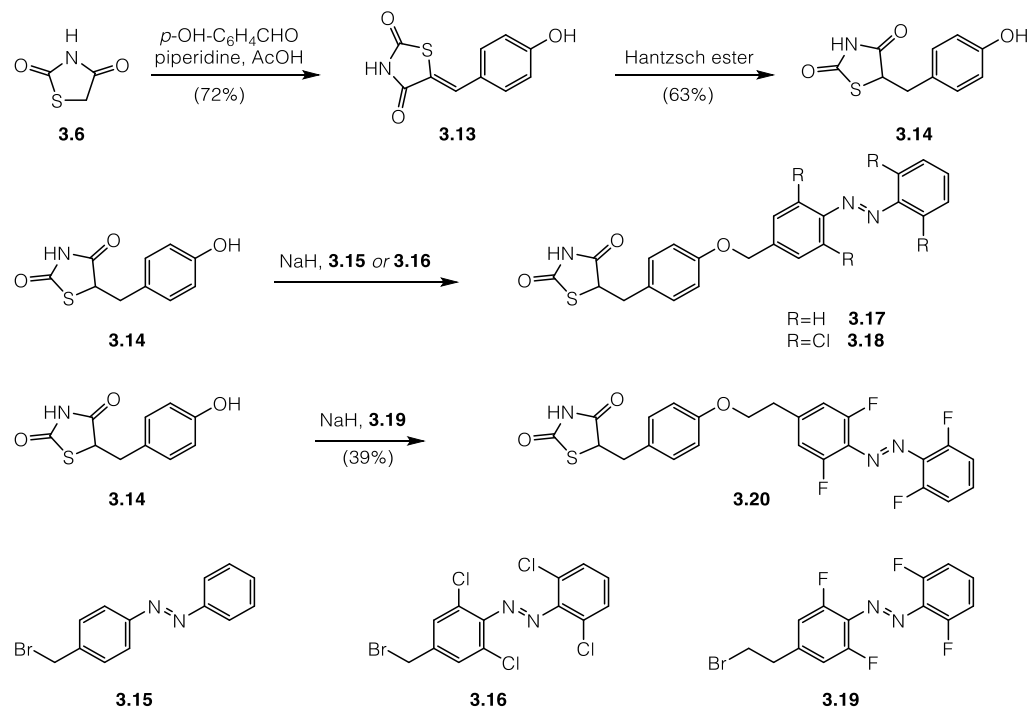


Figure 3.4. Preadipocyte differentiation assay with Oil Red O stain.

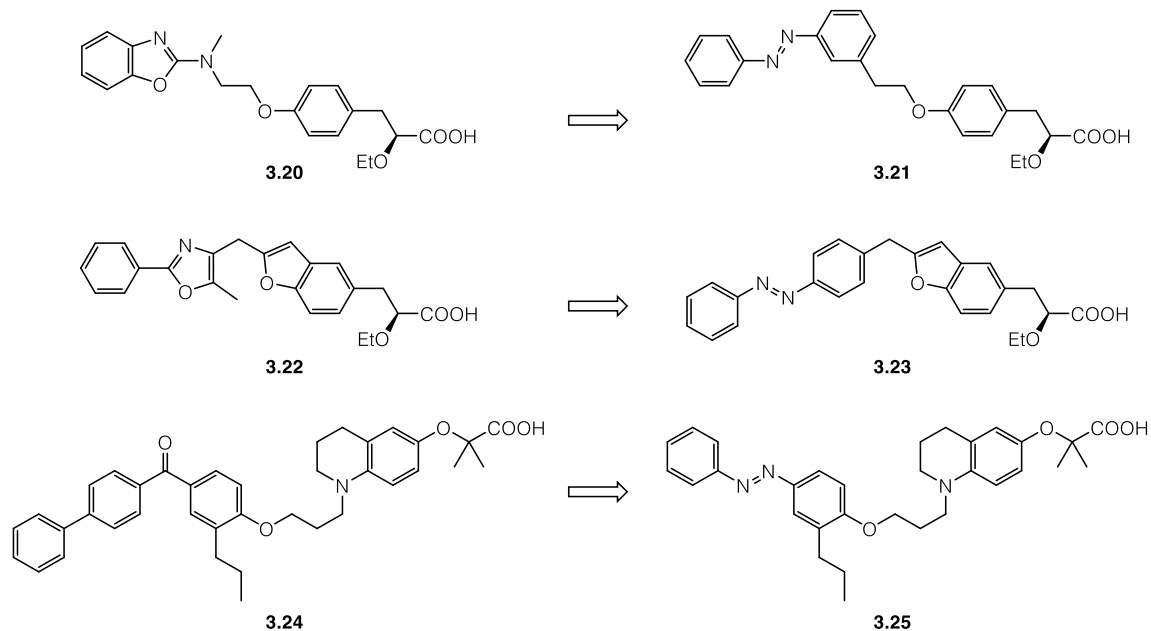
To our disappointment, none of the compounds showed significant induction of cell differentiation in a light-dependent manner. FEH-2-107 (**3.11**), the azo-TZD bearing an unsubstituted azobenzene, was the only compound to induce cell differentiation at 100 μ M. Rosiglitazone (**3.1**), the positive control, induced differentiation at 2 μ M.

At this stage, it became apparent that the present compounds **3.10–3.12** were not suitable for this more advanced *in vitro* assay. Possible reasons include reductive cleavage by azobenzene reductase^[379] Hence, two more azo-TZD were prepared for future testing.^[380] In this series, we decided to keep the phenol commonly used in TZD synthesis and etherify it with three azobenzene-containing electrophiles. Their synthesis is depicted in Scheme 3.2. Again starting from TZD (**3.6**), condensation with *p*-hydroxybenzaldehyde gave **3.13**, which was reduced to phenol **3.14** with Hantzsch ester. The phenol was then treated with two alkyl bromides **3.15** and **3.16** to yield the two photoswitches **3.17** and **3.18** connected to the benzyl-TZD unit with a C₂ chain. A third photoswitch **3.20** was obtained with a similar method using electrophile **3.19**. All three need to be purified further before they can be evaluated in *in vitro* or *in vivo* assays.



Scheme 3.2. Synthesis of red-shifted PPAR γ agonist candidates **3.17**, **3.18** and **3.20** with C₂ or C₃ tethers.

In addition to these TZD-based PPAR γ activators, future work will consist of exploring azobenzenes based on other scaffolds, some of which are depicted in Scheme 3.3.^[380-381]



Scheme 3.3. Non-glitazone-based targets **3.20**, **3.22** and **3.24** for PPAR γ activation and possible azologization thereof.

All three compounds are part of the fibrate class. Fibrates have long been used in combination with statins to reduce the risk of cardiovascular events, mainly by lowering triglyceride levels

and reducing insulin resistance.^[382-385] In general, these compounds feature a carboxylic acid thought to be a bioisostere of the TZD heterocycle on one side of the molecule and bulky aromatic moieties on the other side. With an aliphatic linker inbetween, they are thought to bind to PPAR similarly to the thiazolidines (Figure 3.5).

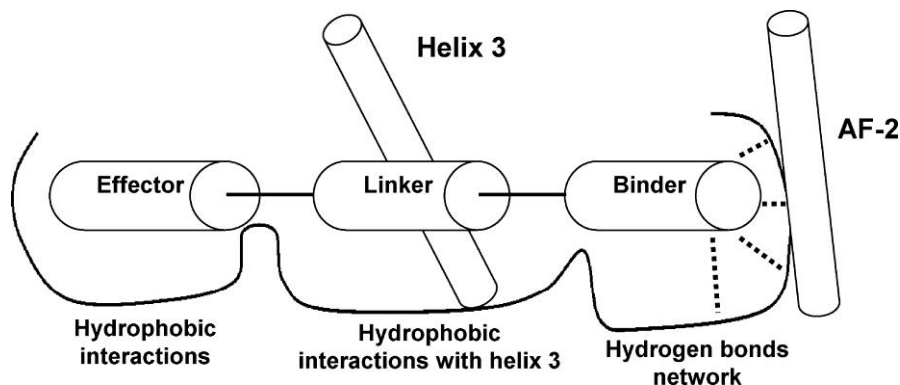


Figure 3.5. Conceptualized representation of the agonist binding mode of TZD and fibrate PPAR γ agonists. Adapted with permission from *J. Med. Chem.* 2012, 55, 4027. Copyright © 2017 American Chemical Society.

In both cases, the polar head group is thought to be involved in a hydrogen bond network, the central section shows hydrophobic interaction with helix 3 of PPAR and the large hydrophobic section mainly occupies the large cavity of the binding pocket.^[377] Although they also act on PPAR, most fibrates activate PPAR α rather than PPAR γ .^[386] However, **3.20**,^[387] **3.22**^[388] and **3.24**^[389] were found to be powerful activators of PPAR γ . An added advantage of these compounds over TZD-based agonists would be the possibility to prepare them as single enantiomers. It was shown that only one enantiomer of rosiglitazone (**3.1**) acts as an agonist of PPAR γ , but it is administered as a racemate due to rapid isomerization under physiological conditions.^[390] In the cases of molecules like **3.20** or **3.22**, the homobenzylic position is much less prone to racemization.

4 Experimental section

4.1 General experimental section

Unless stated otherwise, all reactions were performed with standard Schlenk techniques under an atmosphere of nitrogen in oven-dried glassware (100 °C oven temperature) that was further dried using a heat gun (set to 650 °C) for all water-sensitive reactions. Tetrahydrofuran (THF) and diethyl ether (Et₂O) were distilled prior to use from sodium and benzophenone, triethylamine (Et₃N), and dichloromethane (CH₂Cl₂) were distilled from calcium hydride. *N,N*-dimethylformamide (DMF), acetonitrile (MeCN), and methanol (MeOH) were purchased from Acros Organics as 'extra dry' reagents under inert gas atmosphere and over molecular sieves. All other reagents were purchased from commercial sources and used without further purification. Reaction progress was monitored by analytical thin-layer chromatography (TLC), which was carried out using pre-coated glass plates (silica gel 60 F₂₅₄) from Merck. Visualization was achieved by exposure to ultraviolet light (254 nm) where applicable followed by staining with potassium permanganate solution. Flash column chromatography was performed using Merck silica gel (40–63 μm particle size). Proton nuclear magnetic resonance (¹H NMR) spectra were recorded on a Varian 400, Inova 400, Varian 600 or Varian 800 spectrometer. Chemical shifts (δ scale) are expressed in parts per million (ppm) and are calibrated using residual protic solvent as an internal reference (CHCl₃: δ = 7.26 ppm, CD₂HOD: δ = 3.31 ppm, DMSO-*d*₆: δ = 2.50 ppm). Data for ¹H NMR spectra are reported as follows: chemical shift (ppm) (multiplicity, coupling constants (Hz), integration). Couplings are expressed as: s = singlet, d = doublet, t = triplet, q = quartet, m = multiplet, or combinations thereof. Carbon nuclear magnetic resonance (¹³C NMR) spectra were recorded on the same spectrometers at 100, 150 and 200 MHz (±1 MHz variance). Carbon chemical shifts (δ scale) are also expressed in parts per million (ppm) and are referenced to the central carbon resonances of the solvents (CDCl₃: δ = 77.16 ppm, CD₃OD: δ = 49.00 ppm). In order to assign the ¹H and ¹³C NMR spectra, a range of 2D-NMR experiments (COSY, HMQC, HMBC, NOESY) was used as appropriate. Infrared (IR) spectra were recorded on a Perkin Elmer Spectrum BX II (FTIR System) equipped with an attenuated total reflection (ATR) measuring unit. IR data are reported in frequency of absorption (cm⁻¹). Mass spectroscopy (MS) experiments were performed on a Thermo Finnigan MAT 95 (electron ionization, EI) or on a Thermo Finnigan LTQ FT (electrospray ionization, ESI) instrument.

4.2 Supporting information for chapter 1: *Lycopodium* alkaloids

4.2.1 Fawcettimine alkaloids

4.2.1.1 A Conia-Ene-type cyclization for the total synthesis of lycoserramine R

General procedure A: substrate preparation by cuprate addition.

Three drops of dibromoethane were added to Mg chips (49.0 mg, 2.00 mmol, 4.00 eq.) in THF (5 mL). After short heating the reaction mixture was cooled back to room temperature and (4-bromobut-1-yn-1-yl)trimethylsilane (308 mg, 1.50 mmol, 3.00 eq.) was added dropwise. The reaction mixture was stirred at 50 °C for 1.5 h, then slowly cooled down to -78 °C. CuBr·SMe₂ (21 mg, 0.10 mmol, 0.20 eq.) was added in one portion. After stirring for 15 min, the enone (0.50 mmol, 1.0 eq.) in THF (1.0 mL), TMSCl (126 μL, 1.00 mmol, 2.0 eq.) and HMPA (174 μL, 1.00 mmol, 2.0 eq.) were added sequentially to the brownish suspension. The reaction was stirred until judged complete by TLC analysis, then quenched with saturated aqueous NH₄Cl (4 mL), warmed to room temperature, diluted with H₂O (4 mL) and extracted with ether (3×5 mL). The combined organic layers were washed with H₂O (10 mL) and saturated aqueous NaCl (10 mL), dried over MgSO₄ and concentrated by vacuum evaporation. The residue was dissolved in THF (5 mL) and cooled to 0 °C. After dropwise addition of TBAF (1M in THF, 1.50 mL, 1.50 mmol, 3.00 eq.), the reaction mixture was allowed to warm to room temperature and stirred until TLC analysis indicated full conversion. Saturated aqueous NH₄Cl (10 mL) and H₂O (5 mL) were added, followed by extraction with ether (3×15 mL). The combined organic layers were washed with H₂O (10 mL) and saturated aqueous NaCl (20 mL), dried over MgSO₄ and concentrated by vacuum evaporation. The obtained brown oil was purified by column chromatography (pentane:Et₂O) to give the ketone as an inconsequential mixture of diastereomers.

General procedure B: KO^t-Bu-mediated cyclization reaction.

To a solution of KO^t-Bu (11 mg, 0.10 mmol, 1.0 eq.) in degassed DMSO (3.0 mL), ynone (0.10 mmol) in degassed DMSO (1.0 mL) was added dropwise. The mixture was stirred at room temperature, monitoring by TLC. After 30 min, pH 5.5 phosphate buffer (1.0 mL) and H₂O (10 mL) were added and the aqueous phase was extracted with Et₂O (3×15 mL). The combined organic phases were washed with H₂O (10 mL) and saturated aqueous NaCl (15 mL), dried over

MgSO₄ and concentrated by vacuum evaporation. After purification by column chromatography over silica gel (pentane:Et₂O 20:1), analytically pure products were obtained.

Preparation of starting materials

Non-commercial starting materials were prepared according to literature procedures unless specified otherwise. Spectral data obtained matched literature values.

(R)-2-iodo-5-methylcyclohex-2-en-1-one: *Chem. Commun.* **2006**, 4928

2-methyl-2-cyclohexen-1-one: *J. Org. Chem.* **1990**, *55*, 4995

(4-bromobut-1-yn-1-yl)trimethylsilane: *Chem. Commun.* **2013**, *49*, 4012

2-methyl-3-(4-(trimethylsilyl)but-3-yn-1-yl)cyclohexan-1-one: *J. Am. Chem. Soc.* **1988**, *110*, 3315.

tert-butyl 4-oxo-3,4-dihydropyridine-1(2H)-carboxylate: *J. Am. Chem. Soc.* **2011**, *133*, 14566.

1-methylquinolin-4(1H)-one: *Chem. Eur. J.* **2015**, *21*, 2339.

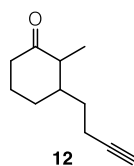
4'-methoxy-4,5-dihydro-[1,1'-biphenyl]-2(3H)-one: *J. Org. Chem.* **2005**, *70*, 8575.

4'-bromo-4,5-dihydro-[1,1'-biphenyl]-2(3H)-one: *J. Org. Chem.* **2005**, *70*, 8575.

(R)-2-allyl-5-methylcyclohex-2-en-1-one: *Angew. Chem. Int. Ed.* **2007**, *46*, 7671.

dimethyl 2-(3-oxocyclohexyl)-2-(prop-2-yn-1-yl)malonate: *Angew. Chem. Int. Ed.* **2005**, *44*, 5273.

Note: In the following, the numbering corresponds to the numbering in the manuscript reprinted in chapter 1.2.2.

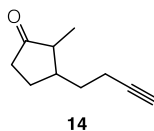


3-(but-3-yn-1-yl)-2-methylcyclohexan-1-one (12). Compound **12** was prepared according to general procedure A in 79% yield.

R_f 0.50 (hexanes:EtOAc 5:1). Colorless liquid.

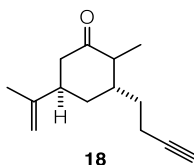
¹H NMR (599 MHz, CDCl₃) δ = 2.64–2.57 (m, 1H), 2.45–2.38 (m, 1H), 2.34–2.24 (m, 2H), 2.24–2.11 (m, 2H), 2.06 (ddq, *J* = 13.6, 6.0, 3.8, 1H), 2.02–1.96 (m, 1H), 1.96–1.94 (m, 1H), 1.88 (dtd, *J* = 13.6, 8.2, 3.5, 1H), 1.83–1.75 (m, 1H), 1.75–1.69 (m, 1H), 1.69–1.62 (m, 1H), 1.62–1.54 (m, 2H), 1.50–1.42 (m, 1H), 1.39 (dddd, *J* = 15.3, 9.5, 4.6, 2.2, 1H), 1.08 (dd, *J* = 6.6, 0.6, 3H), 1.03 (dd, *J* = 7.1, 0.6, 1H).

¹³C NMR	(151 MHz, CDCl ₃) δ = 214.4, 213.1, 84.0, 83.8, 68.9, 68.8, 50.0, 48.7, 44.6, 41.5, 41.0, 39.8, 32.8, 29.9, 27.8, 26.6, 25.8, 24.0, 16.2, 15.8, 12.2, 11.6.
IR	(ATR): 3290 w, 2934 m, 2866 w, 1708 s, 1457 w, 1445 w, 1312 w, 1220 w.
HRMS	(EI): calculated for C ₁₁ H ₁₆ O 164.1201, found 164.1199.



3-(but-3-yn-1-yl)-2-methylcyclopentan-1-one (14). Compound **14** was prepared according to general procedure A in 79% yield.

R_f	0.48 (hexanes:EtOAc 5:1). Colorless liquid.
¹H NMR	(599 MHz, CDCl ₃) δ = 2.41–2.31 (m, 2H), 2.29–2.23 (m, 1H), 2.22–2.16 (m, 1H), 2.16–2.08 (m, 1H), 1.98–1.92 (m, 2H), 1.84–1.76 (m, 1H), 1.77–1.69 (m, 1H), 1.53–1.46 (m, 1H), 1.42–1.33 (m, 1H), 1.08 (d, <i>J</i> = 6.8, 3H). major isomer.
¹³C NMR	(151 MHz, CDCl ₃) δ = 220.75, 84.04, 68.92, 50.36, 43.86, 37.48, 33.38, 26.99, 16.55, 12.80. major isomer.
IR	(ATR): 3292 w. 2932 w, 2873 w, 1735 s, 1653 w, 1558 w, 1456 w, 1163 w, 1036 w.
HRMS	(EI): calculated for C ₁₀ H ₁₄ O 150.1045, found 150.1051



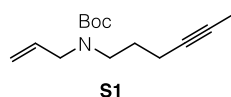
(3*R*,5*R*)-3-(but-3-yn-1-yl)-2-methyl-5-(prop-1-en-2-yl)cyclohexan-1-one (18). Compound **18** was prepared according to general procedure A in 81% yield.

R_f	0.56 (hexanes:EtOAc 5:1). Pale-yellow oil.
¹H NMR	(599 MHz, CDCl ₃) δ = 4.83 (d, <i>J</i> = 1.3, 1H), 4.79 (t, <i>J</i> = 1.5, 1H), 4.76–4.74 (m, 1H), 4.72–4.70 (m, 1H), 2.71–2.65 (m, 1H), 2.65–2.61 (m, 1H), 2.61–2.55 (m, 1H), 2.50 (td, <i>J</i> = 12.0, 6.0, 1H), 2.44 (ddd, <i>J</i> = 13.3, 4.5, 1.9, 2H), 2.39 (ddt, <i>J</i> = 14.3, 5.3, 1.1,

1H), 2.34–2.19 (m, 4H), 2.19–2.15 (m, 1H), 2.15–2.09 (m, 2H), 2.04 (dddd, $J = 13.8$, 7.6, 4.0, 1.2, 1H), 2.01–1.96 (m, 1H), 1.95 (t, $J = 2.6$, 1H), 1.87–1.75 (m, 2H), 1.75 (s, 3H), 1.63 (m, 2H), 1.48 (dddd, $J = 13.6$, 8.7, 7.5, 6.0, 1H), 1.25–1.17 (m, 1H), 1.15 (d, $J = 6.9$, 3H), 1.03 (d, $J = 6.8$, 3H).

¹³C NMR (151 MHz, CDCl₃) $\delta = 213.6$, 212.6, 147.4, 146.9, 111.6, 110.3, 83.8, 83.6, 69.0, 49.6, 48.5, 46.4, 43.8, 41.1, 40.6, 39.9, 39.2, 32.8, 32.3, 30.8, 25.7, 21.6, 20.8, 16.4, 16.1, 14.4, 11.8.

HRMS (EI): calculated for C₁₄H₂₀O 204.1514, found 204.1516.



Tert-butyl allyl(hex-4-yn-1-yl)carbamate (S1). Sodium hydride (60%, 312 mg, 7.80 mmol, 1.30 eq.) was added in one portion to Boc-protected allylamine (943 mg, 6.00 mmol, 1.00 eq.) in dry DMF (21 mL) at 0 °C to give an orange suspension. After 20 min, 4-hexynyl iodide (1.87 g, 9.00 mmol, 1.50 eq.) was added dropwise at 0 °C. After the addition was complete, the ice bath was removed and the reaction was stirred at room temperature for 22 h. When the reaction was judged complete by TLC, saturated aqueous NH₄Cl (15 mL) and H₂O (10 mL) were added carefully. The aqueous phase was extracted with Et₂O (3×30 mL), then the combined organic phases were washed with saturated aqueous NaCl (30 mL), dried, filtered and evaporated to give a yellow residue that was purified by column chromatography (hexanes:EtOAc 15:1) to give the desired product **S1** as a colorless oil (1.33 g, 5.60 mmol, 93%).

R_f 0.67 (hexanes:EtOAc 5:1). Colorless oil.

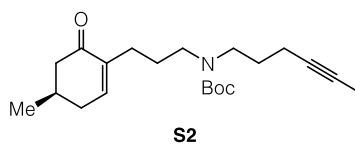
NMR spectra were obtained at 353 K due to extensive rotamer line broadening.

¹H NMR (400 MHz, DMSO-*d*₆) $\delta = 5.84$ – 5.73 (m, 1H), 5.16– 5.06 (m, 2H), 3.78 (dt, $J = 5.7$, 1.5, 2H), 3.21 (t, $J = 7.2$, 2H), 2.09 (tq, $J = 7.2$, 2.5, 2H), 1.73 (t, $J = 2.6$, 3H), 1.64 (p, $J = 7.1$, 2H), 1.42 (s, 9H).

¹³C NMR (101 MHz, DMSO-*d*₆) $\delta = 154.2$, 134.2, 115.4, 78.0, 75.1, 48.8, 45.3, 27.6, 27.2, 15.3, 2.4. *Note: one alkyne carbon could not be observed.*

IR (ATR): 3617 w, 3081 w, 2975 m, 2921 w, 1690 s, 1644 w, 1462 m, 1407 m, 1365 m, 1245 m, 1162 s, 1099 m, 997 w, 916 m, 772 m.

HRMS (EI): calculated for $C_{10}H_{15}NO_2$ (-tBu) 181.1103 found 181.1082, Calculated for $C_9H_{14}N$ (-Boc) 136.1126 found 136.1131.



***Tert*-butyl (*R*)-hex-4-yn-1-yl(3-(4-methyl-6-oxocyclohex-1-en-1-yl)propyl)carbamate (S2).**

To a solution of **S1** (855 mg, 3.60 mmol, 1.00 eq.) in THF (5 mL) at 0 °C was added a 9-BBN solution (0.5 M in THF, 8.60 mL, 4.30 mmol, 1.20 eq.) dropwise. After 30 min at 0 °C, the mixture was warmed to room temperature and stirred for 2.5 h. In a separate flask, SPhos-Pd G2 (108 mg, 0.15 mmol, 0.04 eq.), SPhos (62 mg, 0.15 mmol, 0.04 eq.) and cesium carbonate (1.95 g, 6.00 mmol, 2.00 eq.) were dissolved in a degassed mixture of DMF (27 mL) and H₂O (3 mL) before the contents of the first flask were cannulated in (rinsed with 1 mL to quantitate transfer). The now cloudy reaction mixture was then heated to 50 °C for 3 h, at which point TLC indicated full conversion. The reaction was treated with saturated aqueous NH₄Cl (20 mL), extracted with EtOAc (3×30 mL), washed with saturated aqueous NaCl (2×20 mL), then dried filtered and concentrated. The brown residue was purified by column chromatography (pentane:Et₂O 6:1) to give **S2** as a brown oil (788 mg, 2.28 mmol, 76%).

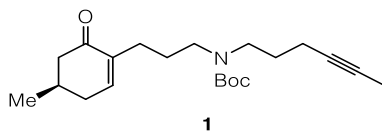
R_f 0.37 (hexanes:EtOAc 5:1) Brown oil.

¹H NMR (599 MHz, CDCl₃) δ = 6.69 (s, 1H), 3.22 (d, *J* = 7.2, 2H), 3.15 (d, *J* = 23.9, 3H), 2.50–2.43 (m, 1H), 2.39 (d, *J* = 18.3, 1H), 2.14 (t, *J* = 8.0, 2H), 2.12–2.04 (m, 2H), 2.05–1.98 (m, 1H), 1.76 (t, *J* = 2.6, 3H), 1.70–1.63 (m, 2H), 1.65–1.56 (m, 2H), 1.43 (s, 9H), 1.03 (d, *J* = 6.5, 3H).

¹³C NMR (151 MHz, CDCl₃) δ = 199.7, 155.7, 144.9, 144.4, 138.9, 79.3, 78.5, 76.0, 47.5, 46.8, 46.4, 34.5, 30.8, 29.8, 28.6, 28.2, 27.8, 27.1, 26.9, 21.3, 16.4, 3.6.

IR (ATR): 3486 w, 2954 m, 2923 m, 2360 w, 1690 s, 1675 s, 1470 m, 1455 m, 1365 m, 1298 m, 1251 m, 1167 s, 1122 m, 922 w, 889 w, 773 w.

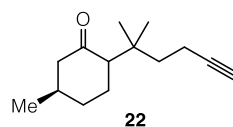
HRMS (ESI): calculated for $C_{21}H_{34}NO_3$ + 348.2533, found 348.2533.



***Tert*-butyl (*R*)-hex-4-yn-1-yl(3-(4-methyl-6-oxocyclohex-1-en-1-yl)propyl)carbamate (**1**).**

Compound **1** was prepared according to general procedure A in 65% yield.

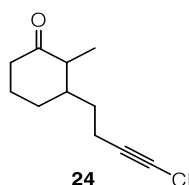
R_f	0.31 (hexanes:EtOAc 5:1). Pale-yellow oil.
¹H NMR	(599 MHz, CDCl ₃) δ 3.27–3.12 (m, 4H), 2.49 (d, <i>J</i> = 22.0, 1H), 2.36 (d, <i>J</i> = 11.6, 1H), 2.21 (d, <i>J</i> = 8.7, 2H), 2.15–2.08 (m, 4H), 2.01–1.98 (m, 1H), 1.94 (td, <i>J</i> = 2.7, 1.2, 1H), 1.77 (t, <i>J</i> = 2.5, 5H), 1.68 (dq, <i>J</i> = 14.6, 6.3, 5.2, 7H), 1.45 (s, 15H), 1.19–1.13 (m, 1H), 1.01 (d, <i>J</i> = 5.9, 3H), 0.99 (d, <i>J</i> = 6.3, 2H).
¹³C NMR	(151 MHz, CDCl ₃) δ = 211.9, 155.5, 83.5, 79.2, 78.4, 75.9, 68.8, 54.5, 53.5, 50.2, (46.9, 46.3), 39.2, 36.2, 33.4, 31.9, 30.0, 29.7, 29.5, 28.4, 28.0, 27.7, 26.7, 26.2, (25.6, 25.4), 23.4, 23.3, 22.2, 21.7, 16.3, 16.2, 3.5. (not all peaks of both isomers can be observed, some peaks are doublets due to rotamers),
IR	(ATR): 3473 w, 3288 w, 2958 m, 2928 m, 2358 w, 1815 w, 1690 s, 1478 m, 1454 m, 1416 m, 1366 m, 1299 m, 1247 m, 1166 m, 1056 w, 889 w.
HRMS	(ESI): calculated for C ₂₅ H ₄₀ NO ₂ 402.3003, found 402.3004.



(5*R*)-5-Methyl-2-(2-methylhex-5-yn-2-yl)cyclohexan-1-one (22**).** Compound **22** was prepared according to general procedure A in 84% yield.

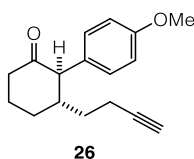
R_f	0.69 (hexanes:EtOAc 5:1). Colorless liquid.
¹H NMR	(800 MHz, CDCl ₃) δ = 2.29 (ddd, <i>J</i> = 12.3, 4.1, 2.2, 1H), 2.20 (ddd, <i>J</i> = 13.1, 4.8, 1.2, 1H), 2.15–2.11 (m, 3H), 2.04 (td, <i>J</i> = 12.5, 1.3, 1H), 1.96–1.90 (m, 2H), 1.90–1.83 (m, 2H), 1.63–1.57 (m, 1H), 1.48 (qd, <i>J</i> = 13.1, 3.3, 1H), 1.39–1.31 (m, 1H), 1.03–1.01 (m, 6H), 0.98 (s, 3H).

¹³C NMR	(201 MHz, CDCl ₃) = 211.9, 85.5, 77.4, 68.1, 57.4, 52.7, 38.9, 36.6, 34.9, 28.4, 24.9, 24.4, 22.5, 13.6.
IR	(ATR): 3312 w, 2954 m, 1709 s, 1559 w, 1457 w, 1364 w.
HRMS	(EI): calculated for C ₁₃ H ₁₉ O (-Me) 191.1436, found 191.1443.



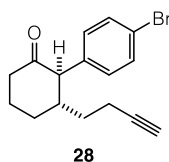
3-(4-Chlorobut-3-yn-1-yl)-2-methylcyclohexan-1-one (24). To 2-methyl-3-(4-(trimethylsilyl)but-3-yn-1-yl)cyclohexan-1-one (95 mg, 0.40 mmol, 1.0 eq.), NCS (107 mg, 0.80 mmol, 2.0 eq.) and AgNO₃ (20 mg, 0.12 mmol, 0.30 eq.) suspended in MeCN (2 mL) was added a TBAF solution (1.0 M in THF, 0.24 mL, 0.24 mmol, 0.60 eq.) dropwise at 0 °C under exclusion of light. After 20 h, the suspension was concentrated and directly purified by column chromatography (pentane:Et₂O 7:1) to give **24** as a colorless oil (70 mg, 0.35 mmol, 88%).

R_f	0.54 (hexanes:EtOAc 5:1), colorless oil.
¹H NMR	(800 MHz, CDCl ₃) δ 2.63–2.56 (m, 1H), 2.44–2.38 (m, 1H), 2.32–2.26 (m, 2H), 2.23–2.08 (m, 3H), 2.06 (ddq, <i>J</i> = 13.6, 6.0, 3.8, 1H), 1.98–1.94 (m, 1H), 1.92–1.83 (m, 1H), 1.82–1.76 (m, 1H), 1.75–1.69 (m, 1H), 1.68–1.62 (m, 1H), 1.55–1.52 (m, 1H), 1.48–1.31 (m, 2H), 1.07 (d, <i>J</i> = 6.6, 3H), 1.02 (d, <i>J</i> = 7.0, 1H).
¹³C NMR	(201 MHz, CDCl ₃) δ = 214.1, 212.8, 69.0, 68.8, 57.7, 57.7, 49.8, 48.5, 44.5, 41.3, 40.9, 39.6, 32.6, 29.8, 27.7, 26.5, 25.6, 23.8, 16.5, 16.1, 12.0, 11.4.
IR	(ATR): 2935 m, 2866 w, 2241 w, 1708 s, 1447m, 1430 m, 1313 w, 1219 w, 1082 w, 957 w.
HRMS	(EI): calculated for C ₁₁ H ₁₅ ClO 198.0811, found 198.0824.



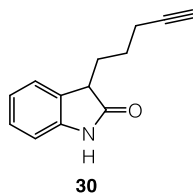
3-(But-3-yn-1-yl)-2-(4-methoxyphenyl)cyclohexan-1-one (26). Compound **26** was prepared according to general procedure A in 75% yield.

R_f	0.22 (hexanes:EtOAc 5:1). colorless liquid.
¹H NMR	(800 MHz, CDCl ₃) δ = 6.99 (d, <i>J</i> = 8.7, 2H), 6.88 (d, <i>J</i> = 8.7, 2H), 3.80 (s, 3H), 3.24 (d, <i>J</i> = 12.2, 1H), 2.57–2.51 (m, 1H), 2.43 (tdd, <i>J</i> = 13.7, 5.9, 1.1, 1H), 2.20–2.11 (m, 4H), 2.11–2.05 (m, 1H), 1.89 (t, <i>J</i> = 2.6, 1H), 1.83–1.76 (m, 1H), 1.55–1.46 (m, 2H), 1.32–1.25 (m, 1H).
¹³C NMR	(201 MHz, CDCl ₃) δ = 210.2, 158.7, 130.4, 129.1, 114.1, 83.9, 68.8, 62.9, 55.4, 44.1, 42.0, 33.4, 30.7, 25.9, 16.0.
IR	(ATR): 3289 w, 2937 w, 2863 w, 1710 s, 1612 w, 1513 s, 1444 w, 1284 w, 1247 s, 1179 m, 1034 m, 818 w.
HRMS	(EI): calculated for C ₁₇ H ₂₀ O ₂ 256.1463, found 256.1467.



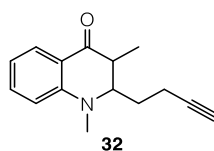
2-(4-Bromophenyl)-3-(but-3-yn-1-yl)cyclohexan-1-one (28). Compound **28** was prepared according to general procedure A in 70% yield.

R_f	0.33 (hexanes:EtOAc 5:1). colorless liquid.
¹H NMR	(599 MHz, CDCl ₃) δ = 7.47 (d, <i>J</i> = 7.6, 2H), 6.95 (d, <i>J</i> = 8.0, 2H), 3.27 (d, <i>J</i> = 11.8, 1H), 2.59–2.51 (m, 1H), 2.44 (td, <i>J</i> = 13.6, 5.8, 1H), 2.24–2.04 (m, 7H), 1.90 (td, <i>J</i> = 2.5, 0.7, 1H), 1.85–1.74 (m, 1H), 1.59–1.40 (m, 3H), 1.33–1.24 (m, 1H).
¹³C NMR	(151 MHz, CDCl ₃) δ = 209.2, 136.1, 131.7, 131.3, 121.2, 83.6, 69.0, 63.2, 43.9, 42.0, 33.3, 30.6, 25.9, 16.0.
IR	(ATR): 3296 w, 2941 w, 2863 w, 1709 s, 1488 s, 1446 w, 1406 w, 1313 w, 1271 w, 1159 w, 1072 m, 1010 s, 805 s.
HRMS	(EI): calculated for C ₁₇ H ₂₀ O ₂ 304.0461, found 304.0463.



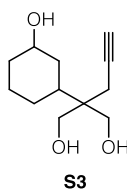
3-(pent-4-yn-1-yl)indolin-2-one (30). To oxindole (0.13 g, 1.0 mmol, 2.0 eq.) and TMEDA (0.30 mL, 2.0 mmol, 4.0 eq.) in THF (5.0 mL) was added *n*-BuLi (0.81 mL, 2.0 mmol, 4.0 eq.) dropwise at $-78\text{ }^{\circ}\text{C}$ to give an orange solution. After 30 min, pentynyl iodide (97 mg, 0.50 mmol, 1.0 eq.) was added dropwise at $-78\text{ }^{\circ}\text{C}$. After 1 h at $-78\text{ }^{\circ}\text{C}$, the mixture was warmed to room temperature over 1 h and stirred for a further 2 h. After addition of saturated aqueous NH_4Cl (10 mL), the layers were separated and the aqueous phase was extracted with Et_2O (3 \times 20 mL). The combined organic phases were dried and evaporated and the residue was purified by column chromatography (hexanes:EtOAc 6:1 \rightarrow 3:1) to give **30** as an off-white solid (61 mg, 0.31 mmol, 61%).

R_f	0.51 (hexanes:EtOAc 1:1), off-white solid.
¹H NMR	(400 MHz, CDCl_3) δ = 7.77 (s, 1H), 7.26–7.19 (m, 2H), 7.04 (td, J = 7.5, 1.0, 1H), 6.87 (d, J = 7.7, 1H), 3.50 (t, J = 6.0, 1H), 2.22 (td, J = 7.1, 2.7, 2H), 2.12–2.04 (m, 2H), 1.95 (t, J = 2.6, 1H), 1.73–1.52 (m, 2H).
¹³C NMR	(101 MHz, CDCl_3) δ = 179.4, 141.4, 129.5, 128.1, 124.4, 122.6, 109.6, 83.9, 68.9, 45.5, 29.8, 24.8, 18.6.
IR	(ATR): 3288 w, 3091 w, 2865 w, 1699 s, 1619 m, 1470 m, 1337 w, 1218 w, 1102 w, 750 w.
HRMS	(EI): calculated for $\text{C}_{13}\text{H}_{13}\text{NO}$ 199.0997, found 199.0985.
Mp.	101–103 $^{\circ}\text{C}$.



2-(But-3-yn-1-yl)-1,3-dimethyl-2,3-dihydroquinolin-4(1H)-one (32). Compound **32** was prepared according to general procedure A in 38% yield.

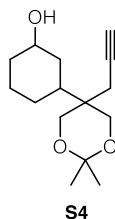
R_f	0.40 (hexanes:EtOAc 5:1), fluorescent yellow oil.
¹H NMR	(400 MHz, CDCl ₃) δ = 7.66 (dd, <i>J</i> = 7.8, 1.8, 1H), 7.22 (ddd, <i>J</i> = 8.7, 7.0, 1.8, 1H), 6.51 (t, <i>J</i> = 7.2, 1H), 6.43 (d, <i>J</i> = 8.5, 1H), 3.30–3.24 (m, 1H), 2.96 (s, 3H), 2.33 (qd, <i>J</i> = 7.3, 1.8, 1H), 2.07–2.01 (m, 2H), 1.84 (t, <i>J</i> = 2.6, 1H), 1.69 (dt, <i>J</i> = 13.9, 6.9, 1H), 1.49 (dt, <i>J</i> = 13.9, 6.7, 1H), 1.07 (d, <i>J</i> = 7.2, 3H).
¹³C NMR	(101 MHz, CDCl ₃) δ = 197.0, 148.7, 135.8, 128.2, 117.0, 116.2, 112.7, 82.9, 69.7, 65.6, 44.3, 39.0, 27.9, 16.2, 15.3.
IR	(ATR): 3260 w, 2980 w, 2920 w, 2333 w, 1685 s, 1600 m, 1479 m, 1360 m, 1268 m, 1233 w, 1160 s, 1115 m, 1047 w, 768 m.
HRMS	(ESI): calculated for C ₁₅ H ₁₈ NO 228.1383, found 228.1383.



2-(3-hydroxycyclohexyl)-2-(prop-2-yn-1-yl)propane-1,3-diol (S3). Dimethyl 2-(3-oxocyclohexyl)-2-(prop-2-yn-1-yl)malonate (1.84 g, 6.93 mmol, 1.00 eq.) in THF (24 mL) was cannulated into a suspension of LiAlH₄ (1.05 g, 27.7 mmol, 4.00 eq.) in THF (5 mL) cooled to 0°C. The cooling bath was directly replaced with an oil bath and the mixture was heated to 45 °C for 5 h. After full conversion was observed by TLC, the mixture was cooled to 0 °C. Subsequently, the suspension was diluted with Et₂O (20 mL) before sequential addition of water (1 mL), 2M NaOH (1 mL) and again H₂O (3 mL). After stirring for 15 min at room temperature, the reaction was dried over MgSO₄, filtered over celite and concentrated by vacuum evaporation. The residue can be used directly in the next step or purified by column chromatography (hexanes:EtOAc 1:1 → 0:1) to give triol **S3** (1.18 g, 5.54 mmol, 80%) as a highly viscous colorless oil contaminated with EtOAc (9%).

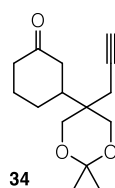
R_f	0.14 (hexanes:EtOAc 1:2), viscous colorless oil.
¹H NMR	(400 MHz, CDCl ₃) δ = 3.84–3.71 (m, 4H), 3.58 (ddd, <i>J</i> = 14.8, 10.0, 4.0, 1H), 2.34 (d, <i>J</i> = 2.7, 2H), 2.29–2.20 (m, 2H), 2.02 (t, <i>J</i> = 2.7, 1H), 1.98 (td, <i>J</i> = 4.4, 2.0, 1H), 1.83 (dq, <i>J</i> = 12.9, 3.2, 1H), 1.70 (tt, <i>J</i> = 12.8, 2.9, 2H), 1.52 (s, 1H), 1.35–0.92 (m, 5H).

¹³C NMR	(101 MHz, CDCl ₃) δ = 81.5, 71.3, 71.0, 67.0, 66.9, 43.1, 38.0, 36.5, 35.7, 25.9, 24.2, 20.2.
IR	(ATR): 3295 (s), 2932 (s), 2858 (m), 2361 (w), 1450 (m), 1362 (m), 1045 (s), 964 (m).
HRMS	(EI): calculated for C ₁₂ H ₂₀ O ₃ 212.1412, found 212.1408.



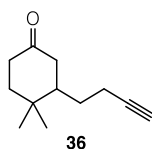
3-(2,2-Dimethyl-5-(prop-2-yn-1-yl)-1,3-dioxan-5-yl)cyclohexan-1-ol (S4). To triol **S3** (1.55 g, 7.30 mmol, 1.00 eq.) in CH₂Cl₂ (50 mL) was added PPTS (92 mg, 0.37 μmol, 0.050 eq.) and 2-methoxypropene (3.50 mL, 36.0 mmol, 5.00 eq.). The reaction mixture was stirred for 2 h. The reaction was diluted with EtOAc (50 mL), washed with sat. NaHCO₃ (20 mL) and saturated aqueous NaCl (20 mL), dried over MgSO₄ and concentrated by vacuum evaporation. The crude product was purified by column chromatography (pentane:Et₂O 1:1) to give alcohol **S4** (1.79 g, 7.09 mmol, 97%) as a yellow oil.

R_f	0.57 (hexanes:EtOAc 1:2), yellow oil.
¹H NMR	(400 MHz, CDCl ₃) δ = 3.84–3.81 (m, 2H), 3.71–3.52 (m, 3H), 2.51–2.49 (m, 2H), 2.05–1.93 (m, 3H), 1.84 (dt, <i>J</i> = 12.8, 3.2 Hz, 1H), 1.70–1.54 (m, 3H), 1.40 (s, 6H), 1.32–1.19 (m, 1H), 1.18–0.96 (m, 3H).
¹³C NMR	(101 MHz, CDCl ₃) δ = 98.4, 81.6, 71.3, 65.3, 38.9, 37.3, 36.3, 35.8, 26.9, 25.7, 24.3, 21.1, 21.0.
IR	(ATR): 3299 (m), 2936 (vs), 2860 (m), 2360 (m), 2341 (m), 1451 (s), 1372 (m), 1261 (m), 1196 (s), 1161 (m), 1067 (m), 830 (m).
HRMS	(ESI): calculated for C ₁₄ H ₂₁ O ₃ 237.1491 (-Me), found 237.1490.



3-(2,2-Dimethyl-5-(prop-2-yn-1-yl)-1,3-dioxan-5-yl)cyclohexan-1-one (34). PDC (1.09 g, 2.89 mmol, 1.50 eq.) was added in one portion to alcohol **S4** (487 mg, 1.93 mmol, 1.00 eq.) in CH₂Cl₂ (30 mL) at 0 °C. The reaction was allowed to warm to room temperature. After 15 h of stirring, TLC indicated full conversion. The reaction was diluted with hexanes (10 mL) and Et₂O (10 mL) and filtered through celite. After removing the solvent by vacuum evaporation, the crude product was submitted to column chromatography (hexanes:EtOAc 3:1) to give ketone **34** (358 mg, 1.43 mmol, 74%) as a yellow oil.

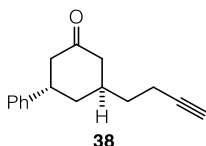
R_f	0.25 (hexanes:EtOAc 3:1), colorless oil.
¹H NMR	(400 MHz, CDCl ₃) δ = 3.79–3.71 (m, 2H), 3.71–3.65 (m, 2H), 2.50–2.48 (m, 2H), 2.46–2.21 (m, 4H), 2.19–2.09 (m, 1H), 2.05–2.03 (m, 1H), 2.01–1.84 (m, 1H), 1.65–1.49 (m, 2H), 1.41–1.40 (m, 2H), 1.39 (s, 3H).
¹³C NMR	(101 MHz, CDCl ₃) δ = 210.9, 98.4, 80.9, 71.7, 65.4, 65.0, 42.8, 41.8, 41.3, 37.3, 25.4, 21.3, 20.8.
IR	(ATR): 3281 (w), 2990 (w), 2941 (m), 1710 (s), 1452 (w), 1372 (m), 1265 (m), 1229 (m), 1197 (s), 828 (m).
HRMS (EI):	Calculated for C ₁₅ H ₂₃ O ₃ 251.1602, found 251.1630.



3-(but-3-yn-1-yl)-4,4-dimethylcyclohexan-1-one (36). Compound **36** was prepared according to general procedure A in 83% yield.

R_f	0.38 (hexanes:EtOAc 5:1). Colorless liquid.
¹H NMR	(800 MHz, CDCl ₃) δ = 2.47–2.38 (m, 2H), 2.35–2.24 (m, 2H), 2.13–2.02 (m, 2H), 1.95 (t, <i>J</i> = 2.6, 1H), 1.87–1.80 (m, 1H), 1.74–1.66 (m, 2H), 1.63 (td, <i>J</i> = 13.4, 4.9, 1H), 1.28–1.22 (m, 1H), 1.06 (s, 3H), 1.01 (s, 3H).
¹³C NMR	(201 MHz, CDCl ₃) δ = 211.73, 83.92, 69.02, 45.70, 42.50, 40.43, 38.42, 32.93, 29.71, 28.82, 19.79, 16.69.

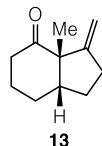
- IR** (ATR): 3292 w, 2956 m, 2867 m, 1712 s, 1470 w, 1430 w, 1418 w, 1390 w, 1251 w, 1146 w.
- HRMS** (EI): calculated for C₁₂H₁₈O 178.1358, found 178.1359.



3-(but-3-yn-1-yl)-5-phenylcyclohexan-1-one (38). Compound **38** was prepared according to general procedure A in 72% yield.

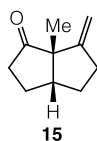
- R_f** 0.56 (hexanes:EtOAc 5:1), colorless oil.
- ¹H NMR** (400 MHz, CDCl₃) δ = 7.35–7.30 (m, 2H), 7.25–7.16 (m, 3H), 3.32–3.30 (m, 1H), 2.64–2.55 (m, 3H), 2.34–2.17 (m, 4H), 2.10 (ddd, *J* = 13.7, 9.6, 3.9, 1H), 1.99–1.95 (m, 1H), 1.91 (t, *J* = 2.7, 1H), 1.62–1.57 (m, 2H).
- ¹³C NMR** (101 MHz, CDCl₃) δ = 211.1, 144.1, 128.8, 127.0, 126.8, 83.5, 69.1, 47.7, 46.3, 39.7, 36.9, 33.5, 32.5, 16.3.
- IR** (ATR): 3288 (m), 2922 (m), 1708 (vs), 1495 (m), 1444 (m), 1229 (m), 1040 (m), 748 (m), 700 (m).
- HRMS** (EI): calculated for C₁₆H₁₈O 226.1358, found 226.1349.

Preparation and characterization of cyclized substrates



3a-Methyl-3-methyleneoctahydro-4H-inden-4-one (13). Compound **13** was prepared according to general procedure B.

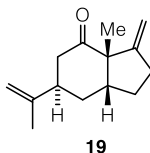
R_f	0.60 (hexanes:EtOAc 5:1). Colorless oil.
¹H NMR	(800 MHz, CDCl ₃) δ = 4.92 (t, <i>J</i> = 2.1, 1H), 4.70 (t, <i>J</i> = 2.5, 1H), 2.56 (dtt, <i>J</i> = 17.6, 9.0, 2.4, 1H), 2.48 (ddd, <i>J</i> = 17.5, 9.7, 3.3, 2.2, 1H), 2.39 (ddd, <i>J</i> = 14.7, 12.1, 5.4, 1H), 2.31 (dtd, <i>J</i> = 14.7, 4.4, 1.7, 1H), 2.13 (ddt, <i>J</i> = 12.2, 5.9, 2.7, 1H), 1.96–1.90 (m, 2H), 1.75 (dtdd, <i>J</i> = 14.0, 5.3, 3.3, 1.7, 1H), 1.69–1.63 (m, 1H), 1.59–1.55 (m, 2H), 1.46 (dddd, <i>J</i> = 13.9, 11.5, 10.5, 3.5, 1H), 1.19 (s, 3H).
¹³C NMR	(201 MHz, CDCl ₃) δ = 213.1, 155.6, 107.5, 60.1, 50.5, 38.9, 29.3, 29.0, 28.3, 24.8, 23.5.
IR	(ATR): 2925 w, 2855 m, 1705 s, 1653 m, 1457 w, 1370 w, 1257 w, 1085 w, 891 w.
HRMS	(EI): calculated for C ₁₁ H ₁₆ O 164.1201, found 164.1198.



6a-Methyl-6-methylenehexahydropentalen-1(2H)-one (15). Compound **15** was prepared according to general procedure B.

R_f	0.56 (hexanes:EtOAc 5:1). Colorless oil.
¹H NMR	(599 MHz, CDCl ₃) δ = 5.02 (t, <i>J</i> = 2.3, 1H), 4.98 (t, <i>J</i> = 2.1, 1H), 2.49–2.45 (m, 2H), 2.45–2.40 (m, 1H), 2.40–2.36 (m, 1H), 2.23 (ddd, <i>J</i> = 18.8, 9.2, 8.3, 1H), 2.04–1.90 (m, 2H), 1.65–1.51 (m, 2H), 1.16 (s, 3H).
¹³C NMR	(151 MHz, CDCl ₃) δ = 220.1, 154.0, 108.5, 59.7, 50.0, 37.0, 31.5, 29.0, 24.2, 22.8.

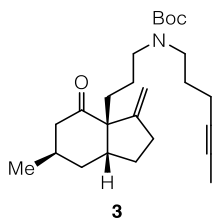
- IR** (ATR): 2924 m, 1736 s, 1700 w, 1684 w, 1653 w, 1635 w, 1558 w, 1540 w, 1521 w, 1506 w, 1457 w, 894 w.
- HRMS** (EI): calculated for C₁₀H₁₄O 150.1045, found 150.1036.



(3a*S*,6*R*,7a*R*)-3a-Methyl-3-methylene-6-(prop-1-en-2-yl)octahydro-4H-inden-4-one (19).

Compound **19** was prepared according to general procedure B. Spectral data matched literature values.

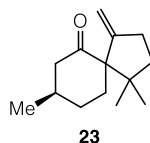
- R_f** 0.74 (hexanes:EtOAc 5:1). Colorless oil.
- ¹H NMR** (400 MHz, CDCl₃) δ = 5.02 (t, *J* = 2.2, 1H), 4.84–4.80 (m, 2H), 4.71–4.66 (m, 1H), 2.63 (q, *J* = 6.2, 1H), 2.58–2.35 (m, 4H), 2.18–2.09 (m, 1H), 1.94–1.75 (m, 3H), 1.75 (dt, *J* = 1.4, 0.6, 3H), 1.51 (ddd, *J* = 12.9, 6.4, 2.9, 1H), 1.24 (s, 3H).
- IR** (ATR): 3080 w, 2932 m, 2360 w, 2252 w, 1700 s, 1646 m, 1449 m, 1377 m, 1220 w, 906 s, 776 s, 647 s.
- HRMS** (EI): calculated for C₁₄H₂₀O 204.1514, found 204.1516.



***Tert*-butyl hex-4-yn-1-yl(3-((3a*S*,6*R*,7a*R*)-6-methyl-3-methylene-4-oxooctahydro-3aH-inden-3a-yl)propyl)carbamate (3).** Compound **3** was prepared according to general procedure B in 70% yield.

- R_f** 0.70 (hexanes:EtOAc 5:1). Colorless liquid.

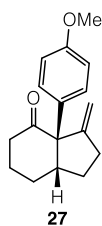
- ¹H NMR** (599 MHz, CDCl₃) δ = 5.01 (t, *J* = 2.0, 1H), 4.75 (t, *J* = 2.5, 1H), 3.23 (d, *J* = 8.9, 3H), 3.16–3.09 (m, 2H), 2.56–2.42 (m, 3H), 2.38 (dt, *J* = 14.2, 6.9, 1H), 2.19 (s, 1H), 2.14–2.09 (m, 3H), 2.08–2.01 (m, 1H), 1.83 (ddt, *J* = 13.2, 9.1, 6.8, 1H), 1.77 (t, *J* = 2.5, 4H), 1.55 (dt, *J* = 13.5, 6.5, 1H), 1.51–1.45 (m, 2H), 1.44 (s, 12H), 0.96 (d, *J* = 6.9, 3H).
- ¹³C NMR** (151 MHz, CDCl₃) δ = 212.4, 155.7, 153.7, 108.5, 79.3, 78.5, 76.0, 63.0, (48.0, 47.4), (46.6, 46.4), 46.2, 42.8, 34.2, 32.8, 32.7, 30.4, 29.5, 28.9, 28.6, 28.2, 27.8, (24.6, 24.0), 20.5, 16.4, 3.6. (carbons next to the NBoc moiety form rotamers, indicated by parentheses)
- IR** (ATR): 2952 s, 2833 m, 2360 m, 2340 m, 1691 s, 1680 s, 1510 m, 1422 m, 1367 m, 1251 m, 1165 s, 773 s, 1001 m.
- HRMS** (ESI): calculated for C₂₅H₄₀NO₃ 402.3003, found 402.3005.



(8*R*)-1,1,8-Trimethyl-4-methylenespiro[4.5]decan-6-one (23). Compound **23** was prepared according to general procedure B.

- R_f** 0.70 (hexanes:EtOAc 5:1). Colorless liquid.
- ¹H NMR** (800 MHz, CDCl₃) δ = 5.18 (t, *J* = 2.4, 1H), 5.05 (t, *J* = 2.2, 1H), 5.02 (t, *J* = 2.1, 1H), 4.87 (t, *J* = 2.5, 1H), 2.56 (ddd, *J* = 14.9, 4.4, 1.7, 1H), 2.52 (dtd, *J* = 12.1, 4.7, 2.3, 1H), 2.44–2.39 (m, 1H), 2.39–2.32 (m, 2H), 2.31–2.24 (m, 2H), 2.23–2.18 (m, 1H), 2.10–2.05 (m, 2H), 2.05–1.99 (m, 1H), 1.97 (ddd, *J* = 14.2, 4.4, 3.8, 1H), 1.92–1.86 (m, 2H), 1.85–1.75 (m, 3H), 1.75–1.69 (m, 1H), 1.62–1.57 (m, 1H), 1.57–1.50 (m, 1H), 1.45 (ddd, *J* = 12.8, 8.7, 4.4, 1H), 1.38 (ddd, *J* = 12.2, 9.4, 3.5, 1H), 1.07–0.99 (m, 15H), 0.80 (s, 3H).
- ¹³C NMR** (201 MHz, CDCl₃) δ = 213.4, 211.7, 157.6, 156.8, 109.0, 108.4, 64.4, 64.3, 50.5, 48.4, 45.6, 45.3, 38.3, 36.9, 32.8, 32.3, 31.9, 31.5, 30.4, 30.3, 30.2, 29.9, 26.7, 26.4, 25.8, 22.4, 22.2, 22.1.
- IR** (ATR): 2952 s, 2870 m, 1698 s, 1646 w, 1457 m, 1385 w, 1364 w, 1202 w, 1126 w, 882 w.

HRMS (EI): calculated for C₁₃H₂₀O 191.1436, found 191.1433.



(3aS,7aS)-3a-(4-Methoxyphenyl)-3-methyleneoctahydro-4H-inden-4-one (27). Compound **27** was prepared according to general procedure B in 52% yield.

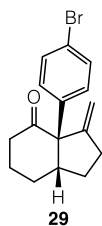
R_f 0.42 (hexanes:EtOAc 5:1). colorless liquid.

¹H NMR (800 MHz, CDCl₃) δ = 7.09 (d, *J* = 8.8, 2H), 6.86 (d, *J* = 8.8, 2H), 5.23 (t, *J* = 2.2, 1H), 4.71 (t, *J* = 2.5, 1H), 3.79 (s, 3H), 2.82 (ddd, *J* = 11.0, 9.4, 5.2, 1H), 2.64–2.58 (m, 1H), 2.47 (dddd, *J* = 14.8, 9.6, 5.1, 2.7, 2H), 2.41 (dddd, *J* = 14.7, 6.3, 4.7, 1.3, 1H), 2.07–2.01 (m, 1H), 1.90–1.81 (m, 1H), 1.65–1.59 (m, 2H), 1.58–1.53 (m, 2H).

¹³C NMR (201 MHz, CDCl₃) δ = 211.9, 158.4, 152.8, 133.3, 129.1, 113.9, 111.5, 70.1, 55.3, 50.2, 39.6.

IR (ATR): 2938 m, 1703 s, 1609 w, 1510 s, 1457 w, 1295 w, 1249 s, 1182 m, 1036 m, 823 m.

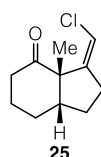
HRMS (EI): calculated for C₁₇H₂₀O 256.1463, found 256.1459.



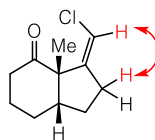
3a-(4-Bromophenyl)-3-methyleneoctahydro-4H-inden-4-one (29). Compound **29** was prepared according to general procedure B in 28% yield.

R_f 0.68 (hexanes:EtOAc 5:1). colorless liquid.

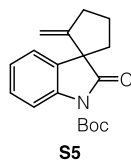
¹H NMR	(400 MHz, CDCl ₃) δ = 7.48–7.38 (m, 2H), 7.09–6.98 (m, 2H), 5.28 (t, <i>J</i> = 2.2, 1H), 4.76 (t, <i>J</i> = 2.6, 1H), 2.76 (dq, <i>J</i> = 10.0, 4.9, 1H), 2.63 (dt, <i>J</i> = 17.3, 8.5, 2.3, 2H), 2.56–2.33 (m, 3H), 2.12–1.98 (m, 1H), 1.91–1.76 (m, 2H), 1.67–1.54 (m, 2H).
¹³C NMR	(101 MHz, CDCl ₃) δ = 211.3, 151.9, 140.7, 131.5, 130.0, 112.3, 70.5, 50.7, 39.4, 29.4, 27.8, 27.2, 24.7.
IR	(ATR): 2929 m, 2885 m, 2360 m, 1701 s, 1488 m, 1457 w, 1395 w, 1245 w, 1140 w, 1010 m, 811 m.
HRMS	(EI): calculated for C ₁₆ H ₁₇ BrO 304.0463, found 304.0462.



(3a*S*,7a*S*,*Z*)-3-(Chloromethylene)-3a-methyloctahydro-4H-inden-4-one (25). Compound **25** was prepared according to general procedure B in 65% yield. The configuration of the double bond was assigned using NOESY experiments as indicated below:



R_f	0.56 (hexanes:EtOAc 5:1), colorless oil.
¹H NMR	(400 MHz, CDCl ₃) δ = 5.91 (t, <i>J</i> = 2.2, 1H), 2.72 (dtd, <i>J</i> = 17.7, 9.0, 2.2, 1H), 2.60–2.47 (m, 2H), 2.39 (dtd, <i>J</i> = 12.3, 4.0, 1.6, 1H), 2.17–2.07 (m, 1H), 2.07–1.92 (m, 2H), 1.76–1.63 (m, 2H), 1.63–1.56 (m, 1H), 1.56–1.41 (m, 1H), 1.25 (s, 3H).
¹³C NMR	(101 MHz, CDCl ₃) δ = 213.1, 147.9, 110.8, 60.4, 53.7, 40.2, 29.5, 29.5, 28.8, 27.1, 19.6.
IR	(ATR): 2933 m, 2863 w, 2363 w, 1711 s, 1640 w, 1445 w, 1372 w, 1316 w, 1256 w, 1080 w, 1015 w, 806 m.
HRMS	(EI): calculated for C ₁₁ H ₁₅ ClO 198.0811, found 198.0809.

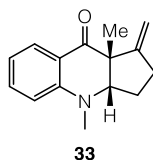


Tert-butyl 2-methylene-2'-oxospiro[cyclopentane-1,3'-indoline]-1'-carboxylate (S5).

Compound **S5** was prepared according to general procedure B with the following modification: Instead of an aqueous workup, EtOAc (5 mL) was added, stirred for 5 min, then evaporated under reduced pressure to give crude **31**. The yellow solution was diluted with CH₂Cl₂ (1 mL) and Et₃N (14 μL, 0.10 mmol, 1.0 eq.) as well as DMAP (2.5 mg, 20 μmol, 0.20 eq.) were added. The solution was cooled to 0 °C and Boc₂O (33 mg, 0.15 mmol, 1.5 eq.) was added. The mixture was warmed to room temperature and stirred for 3 h. When full conversion was observed by TLC, it was diluted with Et₂O (10 mL) and H₂O (10 mL) and the aqueous phase was extracted with Et₂O (3×15 mL). The combined organic phases were washed with 10% aqueous LiCl solution (20 mL) and saturated aqueous NaCl (20 mL), then dried, filtered and concentrated to give a yellow oil that was purified by column chromatography (pentane:Et₂O 9:1) to give **31** colorless crystals (15 mg, 50 μmol, 50% over 2 steps).

Note: A crude NMR using 1,1,2,2-tetrachloroethane as an internal standard indicated a 75% yield for the cyclization and exclusive formation of the exo-isomer.

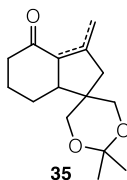
R_f	0.75 (hexanes:EtOAc 5:1).
¹H NMR	(400 MHz, CDCl ₃) δ = 7.86 (dt, <i>J</i> = 8.2, 0.8, 1H), 7.33–7.25 (m, 1H), 7.15 (td, <i>J</i> = 7.5, 1.0, 1H), 7.15–7.06 (m, 2H), 5.79 (d, <i>J</i> = 1.6, 1H), 5.01 (t, <i>J</i> = 2.1, 1H), 4.43 (t, <i>J</i> = 2.3, 1H), 2.85–2.72 (m, 1H), 2.70–2.53 (m, 2H), 2.38 (ddd, <i>J</i> = 12.6, 7.2, 5.6, 1H), 2.32–2.13 (m, 1H), 2.07 (dt, <i>J</i> = 12.5, 7.4, 1H), 2.01–1.87 (m, 1H), 1.65 (s, 3H), 1.64 (s, 9H), 1.38 (d, <i>J</i> = 1.8, 1H). <i>4:1 mixture of exo/endo olefin isomers.</i>
¹³C NMR	(101 MHz, CDCl ₃) δ = 178.8, 178.1, 155.0, 149.7, 149.5, 140.3, 139.8, 139.4, 133.7, 132.4, 130.7, 128.3, 128.1, 124.9, 124.8, 123.3, 123.1, 114.9, 114.9, 109.7, 84.4, 84.3, 64.1, 58.8, 39.7, 38.1, 33.8, 31.6, 28.3, 24.3, 13.2. <i>4:1 mixture of exo/endo olefin isomers.</i>
IR	(ATR): 2980 w, 2360 w, 1764 s, 1730 s, 1607 w, 1479 m, 1348 s, 1290 s, 1250 m, 1148 s, 1099 m, 754 m.
HRMS	(ESI): calculated for C ₁₈ H ₂₁ NO ₃ 299,1521, found 299.1512.



4,9a-Dimethyl-1-methylene-1,2,3,3a,4,9a-hexahydro-9H-cyclopenta[b]quinolin-9-one (33).

Compound **33** was prepared according to general procedure B in 40% yield.

R_f	0.48 (hexanes:EtOAc 5:1), fluorescent yellow oil.
¹H NMR	(600 MHz, CDCl ₃) δ = 7.89 (dt, <i>J</i> = 7.9, 1.5, 1H), 7.40 (ddt, <i>J</i> = 8.7, 7.2, 1.6, 1H), 6.69 (ddt, <i>J</i> = 8.0, 7.0, 1.2, 1H), 6.66 (dd, <i>J</i> = 8.5, 1.2, 1H), 3.41–3.33 (m, 1H), 3.08 (d, <i>J</i> = 1.2, 3H), 2.49–2.41 (m, 1H), 2.33–2.24 (m, 1H), 1.94–1.87 (m, 1H), 1.74–1.62 (m, 1H), 1.31 (s, 3H).
¹³C NMR	(151 MHz, CDCl ₃) δ = 195.0, 150.5, 149.0, 135.8, 129.1, 117.3, 116.5, 113.0, 110.7, 71.8, 55.8, 38.3, 27.4, 23.6, 21.5.
IR	(ATR): 2925 m, 2830 w, 2333 w, 1700 s, 1600 m, 1460 m, 1360 m, 1268 m, 1233 w, 1160 s, 1115 m, 1047 w, 778 m.
HRMS	(ESI): calculated for C ₁₅ H ₁₈ NO 228.1383, found 228.1382.

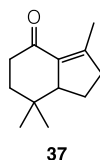


2',2',3-Trimethyl-5,6,7,7a-tetrahydrospiro[indene-1,5'-[1,3]dioxan]-4(2H)-one (35). Compound **35** was prepared according to general procedure B.

R_f	0.16 (hexanes:EtOAc 5:1). Colorless oil.
¹H NMR	(400 MHz, CDCl ₃) δ = 3.88 (dd, <i>J</i> = 11.3, 6.8, 2H), 3.66 (dd, <i>J</i> = 11.4, 1.6, 1H), 3.52 (dd, <i>J</i> = 11.5, 1.6, 1H), 2.71–2.60 (m, 1H), 2.50–2.34 (m, 4H), 2.20 (ddd, <i>J</i> = 17.5, 13.1, 6.2, 1H), 2.06–2.04 (m, 3H), 2.03 (dt, <i>J</i> = 3.8, 2.0, 1H), 1.76–1.54 (m, 2H), 1.43 (s, 3H), 1.42 (s, 3H). <i>major isomer quoted.</i>
¹³C NMR	(151 MHz, CDCl ₃) δ = 200.4, 150.6, 133.6, 98.1, 69.3, 65.3, 52.8, 47.6, 42.4, 41.1, 26.5, 24.2, 16.4. <i>major isomer quoted.</i>

IR (ATR): 3451 w, 2991 m, 2938 m, 2862 m, 2169 w, 1707 m, 1677 s, 1617 s, 1453 m, 1433 m, 1383 m, 1371 s, 1255 s, 1213 s, 1198 s, 1155 m, 1078 s, 1066 s, 1030 m, 932 w, 840 m, 830 m.

HRMS (ESI): calculated for C₁₅H₂₃O₃ 251.1642, found 251.1643.



3,7,7-trimethyl-1,2,5,6,7,7a-hexahydro-4H-inden-4-one (37). Compound **37** was prepared according to general procedure B.

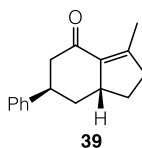
R_f 0.60 (hexanes:EtOAc 5:1). Pale-yellow liquid.

¹H NMR (400 MHz, CDCl₃) δ = 2.76 (ddq, *J* = 10.2, 5.3, 2.6, 1H), 2.46–2.23 (m, 3H), 2.10 (dt, *J* = 2.4, 1.2, 3H), 1.88 (dtd, *J* = 12.7, 8.1, 2.2, 1H), 1.74–1.47 (m, 3H), 0.97 (s, 3H), 0.83 (s, 3H).

¹³C NMR (101 MHz, CDCl₃) δ = 200.7, 154.9, 133.6, 56.6, 39.1, 38.7, 37.6, 32.9, 29.1, 24.5, 19.2, 16.5.

IR (ATR): 3440 s, 2966 s, 2359 m, 1708 s, 1371 m, 1440 m, 1229 w.

HRMS (EI): calculated for C₁₂H₁₈O 178.1358, found 178.1359.



3-Methyl-6-phenyl-1,2,5,6,7,7a-hexahydro-4H-inden-4-one (39). Compound **39** was prepared according to general procedure B.

R_f 0.74 (hexanes:EtOAc 5:1). Pale-yellow liquid.

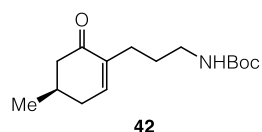
¹H NMR (400 MHz, CDCl₃) δ = 7.40–7.04 (m, 5H), 3.48 (dq, *J* = 5.9, 4.5 Hz, 1H), 2.78–2.68 (m, 1H), 2.64 (dd, *J* = 17.2, 6.0 Hz, 1H), 2.47–2.34 (m, 1H), 2.35–2.14 (m, 2H), 2.14

(dt, $J = 2.4, 1.1$ Hz, 3H), 2.02 (dtd, $J = 12.2, 7.4, 1.4$ Hz, 1H), 1.82–1.71 (m, 1H), 1.47 (ddt, $J = 12.3, 11.0, 9.6$ Hz, 1H), 1.28–1.19 (m, 1H).

¹³C NMR (101 MHz, CDCl₃) $\delta = 200.4, 154.6, 144.7, 135.3, 128.5, 127.4, 126.3, 45.7, 41.4, 39.7, 38.9, 38.8, 31.8, 16.6$.

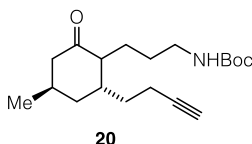
IR (ATR): 3026 (w), 2923 (m), 2857 (m), 1673 (s), 1617 (s), 1449 (m), 1430 (m), 1259 (m), 1133 1133 (m), 785 (m), 699 (s).

HRMS (EI): calculated for C₁₆H₁₈O 226.1358, found 226.1351.

Total synthesis of lycoposerramine R

Tert-butyl (R)-(3-(4-methyl-6-oxocyclohex-1-en-1-yl)propyl)carbamate (42). To a solution of **41** (1.41 g, 9.00 mmol, 1.50 eq.) in THF (30 mL) at 0 °C was added a 9-BBN solution (0:5 M in THF, 36 mL, 18.0 mmol, 3.00 eq.) dropwise. After 30 min at 0 °C, the mixture was warmed to room temperature and stirred for 4.5 h. At this point a degassed aqueous solution of cesium carbonate (3.00 M, 4.00 mL, 12.0 mmol, 2.00 eq.) was added, followed by DMF (27 mL), AsPh₃ (147 mg, 0.48 mmol, 0.08 eq.) and **40** (1.41 g, 6.00 mmol, 1.00 eq.). This mixture was degassed by sparging with nitrogen for 5 min before Pd(dppf)Cl₂ (351 mg, 0.48 mmol, 0.08 eq.) was added. After stirring at room temperature for 18 h, the mixture was poured on aqueous NH₄Cl (40 mL) and the phases were separated. The aqueous phase was extracted with Et₂O (3×70 mL), then washed with 10% aqueous LiCl (100 mL) and saturated aqueous NaCl (100 mL), then dried, filtered and concentrated. The resulting black oil was purified by column chromatography (hexanes:EtOAc 8:1→4:1) to give **42** (1.39 g, 5.20 mmol, 87%) as a yellow oil.

R_f	0.18 (hexanes:EtOAc 5:1). Yellow oil.
¹H NMR	(400 MHz, CDCl ₃) δ = 6.70 (dd, <i>J</i> = 5.8, 2.6, 1H), 4.69 (s, 1H), 3.07 (q, <i>J</i> = 6.6, 2H), 2.51–2.44 (m, 1H), 2.40 (dt, <i>J</i> = 18.3, 4.6, 2H), 2.19 (t, <i>J</i> = 7.6, 3H), 2.02 (ddt, <i>J</i> = 10.2, 7.8, 2.1, 1H), 1.57 (p, <i>J</i> = 7.2, 2H), 1.43 (s, 9H), 1.04 (d, <i>J</i> = 6.3, 3H).
¹³C NMR	(100 MHz, CDCl ₃) δ = 199.9, 156.0, 145.3, 138.6, 79.0, 46.6, 39.9, 34.4, 30.6, 29.0, 28.4, 26.5, 21.2.
IR	(ATR): 3356 w, 2928 w, 1699 s, 1673 s, 1521 m, 1456 w, 1389 w, 1365 m, 1251 m, 1171 s.
HRMS	(EI): calculated for C ₁₅ H ₂₆ NO ₃ 268.1907, found 268.1910.
[α]_D²⁰	–34 (0.6, CH ₂ Cl ₂).

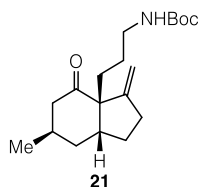


***Tert*-butyl (3-((2*R*,4*R*)-2-(but-3-yn-1-yl)-4-methyl-6-oxocyclohexyl)propyl)carbamate (20).**

Three drops of dibromoethane were added to Mg chips (490 mg, 20.3 mmol, 4.50 eq.) in THF (30 mL). After short heating the reaction mixture was cooled back to room temperature and **43** (3.23 g, 15.8 mmol, 3.5 eq.) was added dropwise. The reaction mixture was stirred at 50 °C for 1.5 h, then slowly cooled down to -78 °C. CuBr·SMe₂ (185 mg, 0.90 mmol, 0.20 eq.) was added in one portion and after stirring for 15 min, enone **42** (1.20 mg, 4.50 mmol, 1.00 eq.) in THF (15 mL), TMSCl (1.14 mL, 9.00 mmol, 2.0 eq.) and HMPA (1.60 mL, 9.00 mmol, 2.0 eq.) were added sequentially to the brownish suspension. The reaction was stirred for 2.5 h, then was quenched with saturated aqueous NaHCO₃ (40 mL), warmed to room temperature and extracted with Et₂O (3 × 60 mL). The combined organic layers were washed with saturated aqueous NH₄Cl (30 mL) and saturated aqueous NaCl (30 mL), dried over MgSO₄ and concentrated by vacuum evaporation. The yellow residue was dissolved in THF (12 mL) and cooled to 0 °C. After dropwise addition of TBAF (1M in THF, 11.3 mL, 11.3 mmol, 2.50 eq.), the now bright red reaction mixture was allowed to warm to room temperature and stirred for 35 min. H₂O (25 mL) was added, followed by extraction with Et₂O (3 × 30 mL). The combined organic layers were washed with H₂O (25 mL) and saturated aqueous NaCl (30 mL), dried over MgSO₄ and concentrated by vacuum evaporation. The obtained brown oil was purified by column chromatography (pentane:Et₂O 2:1) to give the ketone **20** as an inconsequential mixture of diastereomers (1.29 g, 4.00 mmol, 89% over 2 steps).

R_f	0.24 (hexanes:EtOAc 5:1). Pale-yellow oil.
¹H NMR	(400 MHz, CDCl ₃) δ = 4.60 (br, 1H), 3.09–3.07 (m, 2H), 2.52–2.42 (m, 1H), 2.39–2.25 (m, 2H), 2.23–2.18 (m, 2H), 2.15–1.96 (m, 3H), 1.96–1.94 (m, 1H), 1.91–1.61 (m, 3H), 1.61–1.47 (m, 2H), 1.43 (s, 9H), 1.36–1.01 (m, 2H), 1.02–0.95 (m, 3H) (<i>mixture of both diastereomers and rotamers</i>).
¹³C NMR	(100 MHz, CDCl ₃) δ = 214.2, 212.4, 156.1, 154.2, 133.0, 122.8, 84.7, 83.6, 80.2, 79.3, 69.1, 68.5, 54.6, 53.7, 50.4, 45.0, 40.6, 40.5, 38.4, 34.5, 34.3, 33.8, 32.3, 32.1, 30.8, 30.1, 29.6, 28.6, 28.1, 27.6, 26.5, 25.6, 25.2, 24.1, 23.5, 22.4, 21.8, 21.3, 19.9, 17.0, 16.3 (<i>mixture of both diastereomers and rotamers</i>).
IR	(ATR): 3306 w, 2927 w, 1700 s, 1521 w, 1507 w, 1456 w, 1364 w, 1172 w.

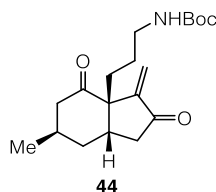
HRMS (EI): calculated for C₁₉H₃₂NO₃ 322.2377, found 322.2344.
[α]_D²⁰ -3.6 (0.56, CH₂Cl₂).



tert-butyl (3-((3a*S*,6*R*,7a*R*)-6-methyl-3-methylene-4-oxooctahydro-3a*H*-inden-3a-yl)propyl) carbamate (21). A solution of KO*t*-Bu (247 mg, 2.20 mmol, 1.10 eq.) in degassed DMSO (12 mL) was added dropwise to a solution of **20** (643 mg, 2.00 mmol, 1.00 eq.) in degassed DMSO (24 mL). The mixture was stirred at room temperature, monitoring by TLC. After 1.5 h, the reaction was diluted with Et₂O (25 mL) and cooled to 0 °C before phosphate buffer (pH = 5.5, 30 mL) was added. The aqueous phase was extracted with Et₂O (3 × 40 mL). The combined organic phases were washed with 10% aqueous LiCl (3 × 30 mL) and saturated aqueous NaCl (15 mL), dried over MgSO₄ and concentrated by vacuum evaporation. After purification by column chromatography over silica gel (pentane:Et₂O 5:1), **21** was obtained as pale yellow liquid (398 mg, 1.24 mmol, 62%).

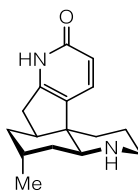
*Note: in this reaction, the yield varied between 52% and 62%, depending on the purity of KO*t*-Bu.*

R_f 0.24 (hexanes:EtOAc 5:1). Pale-yellow liquid.
¹H NMR (800 MHz, CDCl₃) δ = 5.02 (t, *J* = 2.2, 1H), 4.75 (t, *J* = 2.5, 1H), 4.67–4.62 (m, 1H), 3.16–3.06 (m, 2H), 2.59–2.51 (m, 2H), 2.49–2.45 (m, 1H), 2.45–2.39 (m, 1H), 2.27–2.18 (m, 1H), 2.07 (ddd, *J* = 14.8, 6.4, 1.4, 1H), 1.90–1.84 (m, 1H), 1.82–1.77 (m, 1H), 1.71 (ddd, *J* = 13.9, 8.5, 3.8, 1H), 1.60–1.55 (m, 1H), 1.55–1.49 (m, 1H), 1.49–1.41 (m, 12H), 0.97 (d, *J* = 6.9, 3H).
¹³C NMR (201 MHz, CDCl₃) δ = 212.6, 156.2, 153.9, 108.6, 79.2, 63.1, 46.1, 42.6, 41.1, 34.3, 32.7, 30.3, 29.6, 29.0, 28.6, 25.8, 20.3.
IR (ATR): 3364 w, 2952 m, 1699 w, 1521 m, 1457 w, 1365 w, 1272 w, 1248 w, 1173 m, 887 w.
HRMS (EI): calculated for C₁₉H₃₂NO₃ 322.2377, found 322.2383.
[α]_D²⁰ -13 (0.26, CH₂Cl₂).



***Tert*-butyl (3-((3*aS*,6*R*,7*aS*)-6-methyl-3-methylene-2,4-dioxooctahydro-3*aH*-inden-3*a*-yl)propyl)carbamate (44).** To a turbid solution of *tert*-butyl hydroperoxide (5.5 M solution in anhydrous decane, 80 μ L, 0.40 mmol, 2.0 eq.) and SeO₂ (11 mg, 0.10 mmol, 0.5 eq.) in CH₂Cl₂ (1.0 mL) was added a solution of **21** (64 mg, 0.20 mmol, 1.0 eq.) in CH₂Cl₂ (0.50 mL) at room temperature. The mixture was stirred at room temperature for 24 h before TLC analysis showed full conversion and NaHCO₃ (34 mg, 0.40 mmol, 2.0 eq.) as well as Dess-Martin periodinane (102 mg, 0.24 mmol, 1.2 eq.) were added sequentially at room temperature. The colorless suspension was stirred at room temperature for 3 h before TLC analysis indicated full conversion. A 1:1 mixture of saturated aqueous NaHCO₃ and 10% aqueous Na₂S₂O₃ (8 mL) was added and the biphasic mixture was stirred vigorously until two clear phases formed (ca. 30 min). Extraction with Et₂O (3 \times 15 mL) and washes with H₂O (20 mL) and saturated aqueous NaCl (20 mL) gave a yellow oil. Column chromatography (pentane:Et₂O 2:1) yielded **44** as a colorless oil (41 mg, 0.12 mmol, 61% over two steps).

R_f	0.32 (hexanes:EtOAc 2:1). Colorless oil.
¹H NMR	(800 MHz, CDCl ₃) δ = 6.19 (s, 1H), 5.24 (s, 1H), 4.61 (s, 1H), 3.16–3.02 (m, 2H), 2.68 (tq, J = 9.5, 4.8, 3.9, 1H), 2.59–2.51 (m, 1H), 2.49 (dd, J = 18.1, 7.8, 1H), 2.23–2.10 (m, 3H), 1.93–1.81 (m, 1H), 1.78–1.52 (m, 3H), 1.52–1.45 (m, 1H), 1.43 (s, 9H), 1.01 (d, J = 6.4, 3H).
¹³C NMR	(101 MHz, CDCl ₃) δ = 210.3, 204.1, 155.9, 146.5, 120.8, 59.9, 45.6, 42.3, 40.6, 36.0, 34.8, 32.9, 28.4, 25.6, 20.4.
IR (ATR):	3373 w, 2956 m, 2956 m, 2360 w, 1697 s, 1519 m, 1455 w, 1365 w, 1250 w, 1168 s, 737 w.
HRMS	(ESI): calculated for C ₁₉ H ₃₀ NO ₄ 336.2169, found 336.2170.
[α]_D²⁰	34 (0.6, CH ₂ Cl ₂).

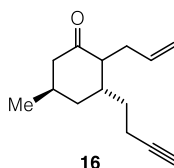
**lycoposerramine R**

Lycoposerramine R. To a solution of **44** (56 mg, 0.16 mmol, 1.0 eq.) in *n*-BuOH (1.6 mL) were added acetic acid (38 μ L, 0.66 mmol, 4.0 eq.), piperidine (66 μ L, 0.66 mmol, 4.0 eq.) and piperidinium salt **45** (83 mg, 0.48 mmol, 3.0 eq.) at room temperature. The mixture was stirred at 115–120 °C for 48 h before TLC analysis showed full conversion and H₂O (5 mL) was added after cooling to room temperature. After extraction with CH₂Cl₂:MeOH (19:1, 3 \times 10 mL), the combined organic phases were dried and evaporated to give a brown oil that was passed over a short column with 1:1 acetone:CH₂Cl₂. Half of the residue obtained was dissolved in CH₂Cl₂ (1.2 mL) and TFA (60 μ L, 0.80 mmol, 20 eq.) was added dropwise at room temperature and stirred for 2 h before LC-MS analysis indicated full conversion. All volatiles were evaporated and the residue was redissolved in THF (0.8 mL). After addition of AcOH (4 μ L, 72 μ mol, 2.0 eq.) and NaBH(OAc)₃ (15 mg, 72 μ mol, 2.0 eq.), the mixture was stirred at room temperature for 2.5 h, at which time LC-MS analysis showed full conversion. The reaction was basified using 1M NaOH (2 mL) and the aqueous phase was extracted with CH₂Cl₂ (3 \times 8 mL). The combined organic phases were washed with saturated aqueous NaHCO₃ (5 mL), then dried over K₂CO₃ and concentrated to give a yellow oil. Column chromatography (CH₂Cl₂:MeOH 19:1 + 0.5% aqueous NH₃) gave **lycoposerramine R** as a slightly yellow oil (7.2 mg, 28 μ mol, 35% over three steps).

R_f	0.09 (CH ₂ Cl ₂ :MeOH 9:1). Slightly yellow oil.
¹H NMR	(400 MHz, CDCl ₃) δ = 8.32 (d, <i>J</i> = 9.1, 1H), 6.34 (d, <i>J</i> = 9.1, 1H), 3.20 (dd, <i>J</i> = 16.9, 6.9, 2H), 2.90 (dd, <i>J</i> = 12.1, 4.8, 1H), 2.79 (td, <i>J</i> = 11.3, 3.1, 1H), 2.33 (d, <i>J</i> = 16.8, 1H), 2.19 (dd, <i>J</i> = 6.5, 1H), 1.82–1.73 (m, 1H), 1.71–1.64 (m, 1H), 1.65–1.55 (m, 1H), 1.55–1.38 (m, 6H), 1.29–1.14 (m, 2H), 0.96 (d, <i>J</i> = 7.0, 2H).
¹³C NMR	(101 MHz, CDCl ₃) δ = 166.2, 150.5, 143.5, 124.6, 114.9, 57.3, 49.5, 48.1, 41.9, 38.2, 36.2, 36.1, 34.9, 25.8, 22.9, 20.7.
IR	(ATR): 3292 w, 2923 s, 2850 m, 2799 m, 1650 s, 1598 m, 1462 m, 1333 m, 1093 w, 832 w.
HRMS	(ESI): calculated for C ₁₆ H ₂₃ NO ₂ 259.1805, found 259.1805.
[α]_D²⁰	–21 (0.05, CHCl ₃).

Comparison of natural and synthetic Lycposerramine R

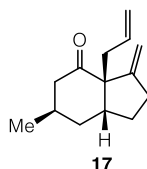
	¹ H NMR (400 MHz, δ in ppm, J in Hz)		¹³ C NMR (101 MHz, δ in ppm)	
	Natural	Synthetic	Natural	Synthetic
1			165.8	166.2
2	6.34 (d, <i>J</i> = 9.2)	6.34 (d, <i>J</i> = 9.1)	115.0	114.9
3	8.33 (d, <i>J</i> = 9.2)	8.32 (d, <i>J</i> = 9.1)	143.3	143.5
4			124.5	124.6
5			150.4	150.5
6a	3.17–3.23 (m)	3.20 (dd, <i>J</i> = 16.9, 6.9)	36.2	36.2
6b	2.33 (d, <i>J</i> = 17.0)	2.33 (d, <i>J</i> = 16.8)		
7	2.19 (ddd, <i>J</i> = 6.9, 6.9, 6.9)	2.19 (dd, <i>J</i> = 6.5, 1H)	42.0	41.9
8a	1.47–1.55 (m)		36.0	36.1
8b	1.20–1.25 (m)			
9a	3.17–3.23 (m)	3.20 (dd, <i>J</i> = 16.9, 6.9)	47.8	48.1
9b	2.80 (td, <i>J</i> = 11.6, 3.0)	2.79 (td, <i>J</i> = 11.3, 3.1)		
10a	1.41–1.59 (m)	1.55–1.38 (m)	22.7	22.9
10b	1.41–1.59 (m)	1.55–1.38 (m)		
11a	1.66–1.69 (m)	1.71–1.64 (m)	38.1	38.2
11b	1.39–1.50 (m)	1.55–1.38 (m)		
12			49.4	49.4
13	2.92 (dd, <i>J</i> = 12.1, 4.8)	2.90 (dd, <i>J</i> = 12.1, 4.8)	57.1	57.3
14a	1.42–1.50 (m)	1.55–1.38 (m)	34.6	34.9
14b	1.20–1.25 (m)			-
15	1.72–1.79 (m)	1.82–1.73 (m)	25.6	25.8
16	0.96 (d, <i>J</i> = 6.9, 3 H)	0.96 (d, <i>J</i> = 7.0)	20.6	20.7

Formal total synthesis of sieboldine A

(3R,5R)-2-Allyl-3-(but-3-yn-1-yl)-5-methylcyclohexan-1-one (16). Three drops of dibromoethane were added to Mg chips (263 mg, 10.8 mmol, 4.00 eq.) in THF (25 mL). After short heating the reaction mixture was cooled back to room temperature and (4-bromobut-1-yn-1-yl)trimethylsilane (1.66 g, 3.54 mmol, 3.00 eq.) was added dropwise. The reaction mixture was stirred at 50 °C for 1.5 h, then slowly cooled down to -78 °C. CuBr·SMe₂ (111 mg, 0.54 mmol, 0.20 eq.) was added in one portion and after stirring for 15 min, (406 mg, 2.70 mmol, 1.00 eq.) in THF (5.0 mL) and TMSCl (680 μL, 5.40 mmol, 2.00 eq.) were added simultaneously to the yellow suspension, followed by HMPA (950 μL, 5.40 mmol, 2.00 eq.) to give an orange suspension. After 2.5 h at -78 °C, the reaction was quenched with saturated aqueous NaHCO₃ (20 mL), warmed to room temperature, diluted with H₂O (10 mL) and extracted with Et₂O (3×30 mL). The combined organic layers were washed with saturated aqueous NaCl (20 mL), dried over MgSO₄ and concentrated. The residue was dissolved in THF (15 mL) and cooled to 0 °C. After dropwise addition of TBAF (1M in THF, 8.10 mL, 8.10 mmol, 3.00 eq.), the reaction mixture was allowed to warm to room temperature. After 1 h, H₂O (10 mL) was added, followed by extraction with Et₂O (2 × 30 mL). The combined organic layers were washed with saturated aqueous NaCl (20 mL), dried and concentrated. The brown residue was purified by column chromatography (pentane:Et₂O 6:1) to yield **16** as a yellow oil (397 mg, 1.94 mmol, 72% over two steps).

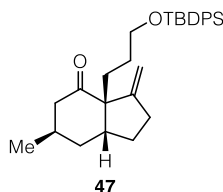
R_f	0.63 (hexanes:EtOAc 5:1). yellow oil.
¹H NMR	(400 MHz, CDCl ₃) δ = 5.79–5.66 (m, 1H), 5.09–4.98 (m, 2H), 2.60–1.89 (m, 10H), 1.94 (t, <i>J</i> = 2.6, 1H), 1.75–1.43 (m, 2H), 1.23–1.12 (m, 1H), 1.02 (t, <i>J</i> = 6.1, 2H), 1.00 (d, <i>J</i> = 6.2, 3H).
¹³C NMR	(101 MHz, CDCl ₃) δ = 213.6, 211.8, 136.4, 135.5, 116.9, 116.4, 83.7, 83.7, 68.9, 54.4, 53.8, 50.3, 47.3, 38.5, 37.6, 36.4, 34.7, 33.6, 32.0, 30.5, 30.0, 29.6, 25.4, 22.4, 21.7, 16.3.

IR	(ATR): 3297 w, 2953 m, 2926 w, 2870 w, 2360 w, 2118 w, 1707 s, 1641 w, 1456 m, 1333 w, 1234 w, 995 w, 914 m.
HRMS	(EI): calculated for C ₁₃ H ₁₇ O (-Me): 189.1279, found 189.1289.
[α]_D²⁰	8 (0.1, CH ₂ Cl ₂).



(3a*S*,6*R*,7a*R*)-3a-Allyl-6-methyl-3-methyleneoctahydro-4H-inden-4-one (17). A slightly yellow solution of KO*t*-Bu (218 mg, 1.94 mmol, 1.00 eq.) in degassed DMSO (10 mL) was cannulated into a solution of ketone **16** (397 mg, 1.94 mmol, 1.00 eq.) in degassed DMSO (20 mL), resulting in a dark-red solution within seconds. After stirring at room temperature for 10 min, the mixture was diluted with Et₂O (25 mL) and pH 5.5 phosphate buffer solution (35 mL) was added dropwise at 0 °C. The aqueous phase was extracted with Et₂O (2 × 50 mL) and the combined organic phases were washed with 10% aqueous LiCl solution (30 mL) and saturated aqueous NaCl (20 mL), dried over MgSO₄ and concentrated. The resulting yellow oil was purified by column chromatography (pentane:Et₂O 15:1) to give hydrindanone **17** as a colorless oil (281 mg, 1.38 mmol, 71%).

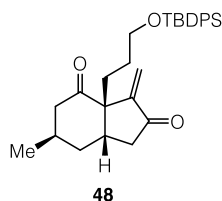
R_f	0.74 (hexanes:EtOAc 5:1). Colorless oil.
¹H NMR	(400 MHz, CDCl ₃): δ = 5.71 (dddd, <i>J</i> = 19.9, 9.4, 8.1, 6.3, 1H), 5.08–5.03 (m, 1H), 5.03 (t, <i>J</i> = 2.1, 2H), 4.80 (t, <i>J</i> = 2.5, 1H), 2.64 (ddt, <i>J</i> = 13.9, 6.3, 1.1, 1H), 2.53 (dddd, <i>J</i> = 22.9, 11.5, 5.2, 2.8, 3H), 2.41 (dddt, <i>J</i> = 16.9, 9.5, 4.9, 2.3, 1H), 2.26–2.17 (m, 1H), 2.17–2.11 (m, 1H), 2.08 (ddd, <i>J</i> = 14.7, 6.4, 1.3, 1H), 1.92–1.78 (m, 1H), 1.69 (ddd, <i>J</i> = 12.6, 8.6, 3.8, 1H), 1.61–1.43 (m, 2H), 0.94 (d, <i>J</i> = 6.9, 3H).
¹³C NMR	(101 MHz, CDCl ₃): δ = 212.1, 153.6, 135.1, 117.8, 108.7, 62.8, 46.1, 42.2, 40.5, 34.1, 30.3, 29.7, 28.7, 20.1.
IR	(ATR): 3075 (w), 2952 (s), 1699 (s), 1645 (m), 1459 (w), 1431 (w), 1383 (w), 1332 (w), 1282 (w), 1229 (w), 912 (m), 890 (m).
HRMS	(EI): calculated for C ₁₄ H ₂₀ O 204.1509, found 204.1507.
[α]_D²⁰	−9.4 (0.17, CH ₂ Cl ₂).



(3a*S*,6*R*,7a*R*)-3a-(3-((*Tert*-butyldiphenylsilyl)oxy)propyl)-6-methyl-3-methyleneoctahydro-4*H*-inden-4-one (47). $\text{BH}_3 \cdot \text{Me}_2\text{S}$ (24 μL , 0.25 mmol, 2.5 eq.) was added to a solution of cyclohexene (56 μL , 0.55 mmol, 5.5 eq.) in THF (1 mL) at 0 °C, which resulted in the formation of a precipitate after 1 h. After 2.5 h, a solution of hydrindanone **17** (20 mg, 0.10 mmol, 1.0 eq.) in THF (1 mL) was added dropwise, then the ice bath was removed. After stirring at room temperature for 2 h, aqueous NaOH (2 M, 1.0 mL) and aqueous H_2O_2 (30%, 1.0 mL) were added. The mixture was stirred at room temperature for 2 h before H_2O (10 mL) was added and the aqueous phase was extracted with EtOAc (3 \times 15 mL). The combined organic phases were washed with saturated aqueous NaCl (20 mL), dried over MgSO_4 and concentrated by vacuum evaporation. The crude alcohol was taken on directly to the next step. To a solution of crude alcohol in CH_2Cl_2 (0.8 mL), TBDPSOTf (37 μL , 0.12 mmol, 1.2 eq.) and 2,6-lutidine (23 μL , 0.20 mmol, 2.0 eq.) were added at 0 °C. The mixture was stirred for 2 h at 0 °C before H_2O (2 mL) and CH_2Cl_2 (5 mL) were added. The aqueous phase was extracted with CH_2Cl_2 (2 \times 10 mL) and the combined organic layers were washed with saturated aqueous NaCl (5 mL), dried over MgSO_4 and concentrated by vacuum evaporation. Column chromatography (pentane:Et₂O 15:1) gave TBDPS-protected alcohol **47** as a colorless oil (27 mg, 0.058 mmol, 58% over 2 steps).

R_f	0.90 (hexanes:EtOAc 5:1). Colorless liquid.
¹H NMR	(400 MHz, CDCl_3): δ = 7.69–7.62 (m, 4H), 7.45–7.33 (m, 6H), 5.03 (t, J = 2.2, 1H), 4.77 (t, J = 2.5, 1H), 3.71–3.57 (m, 2H), 2.55–2.28 (m, 4H), 2.23–2.12 (m, 1H), 2.08 (ddd, J = 14.2, 8.0, 1.0, 1H), 1.79 (ddd, J = 12.6, 9.5, 6.8, 2H), 1.70 (dddd, J = 14.0, 7.1, 3.8, 1.0, 1H), 1.59–1.46 (m, 5H), 1.04 (s, 9H), 0.96 (d, J = 6.7, 3H).
¹³C NMR	(101 MHz, CDCl_3): δ = 212.5, 153.3, 135.7, 134.1, 129.7, 127.7, 108.7, 64.2, 62.8, 46.4, 43.1, 33.9, 31.6, 30.5, 29.5, 28.6, 28.3, 27.0, 20.8, 19.4.
IR	(ATR): 3071 w, 2953 s, 2950 m, 2857 m, 2360 w, 1701 s, 1458 m, 1428 m, 1386 w, 1207 w, 1111 s, 997 w, 888 w, 823 m, 740 m, 702 s.
HRMS	(ESI): calculated for $\text{C}_{30}\text{H}_{41}\text{O}_2\text{Si}$ 461.2870, found 461.2876.

$[\alpha]_{D^{20}}$ 25 (0.10, CH₂Cl₂).



(3a*S*,6*R*,7a*S*)-3a-(3-((*Tert*-butyldiphenylsilyl)oxy)propyl)-6-methyl-3-methylenehexahydro-1*H*-indene-2,4-dione (48). To a suspension of SeO₂ (5.3 mg, 48 μmol, 1.7 eq.) and TBHP (5.5 M in decane, 28 μL, 0.14 mmol, 5.0 eq.) in CH₂Cl₂ (0.5 mL), TBDPS-protected alcohol **47** (12.9 mg, 0.028 mmol, 1.0 eq.) in CH₂Cl₂ (0.5 mL) was added dropwise at room temperature. After stirring for 16 h, DMP (14 mg, 34 μmol, 1.2 eq.) and NaHCO₃ (3.0 mg, 34 μmol, 2.0 eq.) were added at room temperature and the mixture was stirred for 3 h. Saturated aqueous NaHCO₃ solution (0.5 mL) and saturated aqueous Na₂O₃ solution (0.5 mL) were added and the biphasic mixture was vigorously stirred for 0.5 h. The aqueous phase was extracted with CH₂Cl₂ (3 × 10 mL) and the combined organic phases were washed with saturated aqueous NaCl (5 mL), dried over MgSO₄ and concentrated by vacuum evaporation. Purification by column chromatography (pentane:Et₂O 7:1) gave diketone **7** as a colorless oil (6.0 mg, 13 μmol, 45%).

R_f 0.46 (hexanes:EtOAc 5:1). Colorless oil.

¹H-NMR (400 MHz, CDCl₃): δ = 7.68–7.57 (m, 4H), 7.39 (ddd, *J* = 14.0, 7.6, 6.0, 6H), 6.22 (s, 1H), 5.27 (s, 1H), 3.73–3.54 (m, 2H), 2.64 (ddd, *J* = 13.4, 7.6, 5.7, 1H), 2.53–2.38 (m, 2H), 2.24–2.08 (m, 3H), 1.92 (ddd, *J* = 13.8, 12.0, 4.7, 1H), 1.78–1.63 (m, 3H), 1.63–1.40 (m, 2H), 1.04 (s, 9H), 1.02 (d, *J* = 6.4, 3H).

¹³C-NMR (101 MHz, CDCl₃): δ = 210.5, 204.3, 146.5, 135.7, 133.8, 129.8, 127.8, 121.3, 63.7, 60.1, 46.1, 42.1, 36.9, 34.1, 32.1, 28.5, 28.0, 27.0, 21.0, 19.3.

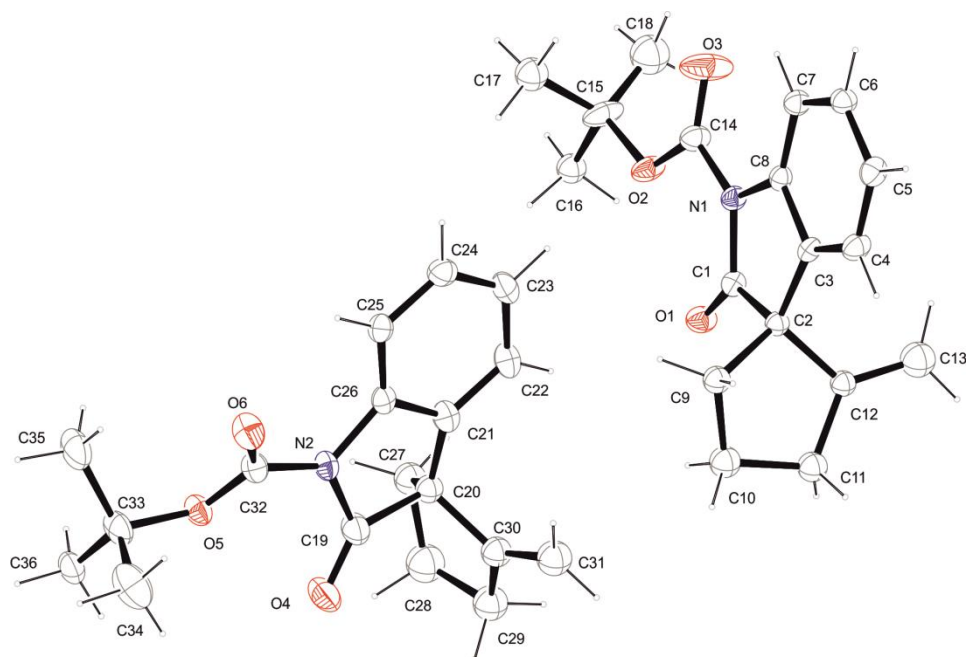
IR (ATR) 3007 w, 2954 s, 2857 m, 1727s, 1705 s, 1458 m, 1425 m, 1111 s, 880 m.

HRMS (ESI): calculated for C₃₀H₃₈O₃SiNa 497.2488, found, 497.2481.

$[\alpha]_{D^{20}}$ 27.4 (0.1, CH₂Cl₂).

All data obtained are in full agreement with those by Overman.

Crystal structure of oxindole S5



net formula	$C_{18}H_{21}NO_3$
$M_r/g\ mol^{-1}$	299.36
crystal size/mm	$0.100 \times 0.070 \times 0.040$
T/K	100.(2)
radiation	MoK α
diffractometer	'Bruker D8 Venture TXS'
crystal system	orthorhombic
space group	'P 21 21 21'
$a/\text{\AA}$	14.0471(8)
$b/\text{\AA}$	14.6566(8)
$c/\text{\AA}$	15.7115(9)
$\alpha/^\circ$	90
$\beta/^\circ$	90
$\gamma/^\circ$	90
$V/\text{\AA}^3$	3234.7(3)
Z	8
calc. density/ $g\ cm^{-3}$	1.229
μ/mm^{-1}	0.083
absorption correction	Multi-Scan
transmission factor range	0.8890–0.9580
refls. measured	43436
R_{int}	0.0550
mean $\sigma(I)/I$	0.0357

θ range	3.135–25.394
observed refls.	5074
x, y (weighting scheme)	0.0458, 2.4112
hydrogen refinement	constr
Flack parameter	0.5
refls in refinement	5914
parameters	394
restraints	0
$R(F_{\text{obs}})$	0.0569
$R_w(F^2)$	0.1400
S	1.087
shift/error _{max}	0.001
max electron density/e \AA^{-3}	0.358
min electron density/e \AA^{-3}	-0.241

4.2.1.2 Total synthesis of lycopladine A and carinatine A

Comparison of natural and synthetic lycopladine A

	¹ H NMR (400 MHz, δ in ppm, <i>J</i> in Hz)		¹³ C NMR (101 MHz, δ in ppm)	
	Natural	Synthetic	Natural	Synthetic
1	8.30 (dd, <i>J</i> = 5.0, 1.4)	8.30 (dd, <i>J</i> = 5.1, 1.4)	148.8	148.7
2	7.67 (dd, <i>J</i> = 7.7, 1.4)	7.68 (dd, <i>J</i> = 7.8, 1.5)	136.1	136.2
3	7.24 (dd, <i>J</i> = 7.7, 5.0)	7.25 (dd, <i>J</i> = 7.7, 5.1)	123.0	123.1
4	--	--	140.0	140.0
5	--	--	164.3	164.3
9	3.53 (m)	3.54 (td, <i>J</i> = 6.3, 1.8)	62.8	62.8
6a	3.09 (dd, <i>J</i> = 16.5, 8.2)	3.09 (dd, <i>J</i> = 16.1, 8.1)	38.6	38.5
6b	2.83 (dd, <i>J</i> = 16.5, 9.1)	2.83 (dd, <i>J</i> = 16.1, 8.9)	62.8	62.8
7	2.97 (m)	3.02–2.92 (m)	43.5	43.5
12	--	--	62.7	62.7
13	--	--	214.6	214.6
14	2.29 (m)	2.29 (d, <i>J</i> = 8.0)	47.7	47.7
15	2.12 (m)	2.18–2.00 (m)	29.5	29.6
11a	2.06 (ddd, <i>J</i> = 13.6, 13.6, 4.6)	2.18–2.00 (m)	43.5	43.5
11b	1.90, 1.88, 1.83 (m)	1.94–1.77 (m)	43.5	43.5
8a	1.90, 1.88, 1.83 (m)	1.94–1.77 (m)	34.8	34.7
8b	1.90, 1.88, 1.83 (m)	1.94–1.77 (m)	34.8	34.7
10a	1.56 (m)	1.62–1.50 (m)	29.1	29.1
10b	1.35 (m)	1.41–1.30 (m)	29.1	29.1
16	1.08 (d, <i>J</i> = 6.5)	1.09 (d, <i>J</i> = 6.5)	22.0	22.0

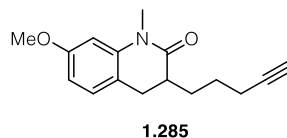
All data obtained are in full agreement with those by Takayama.

Comparison of natural and synthetic carinatine A

	¹ H NMR (400 MHz, δ in ppm, <i>J</i> in Hz)		¹³ C NMR (101 MHz, δ in ppm)	
	Natural	Synthetic	Natural	Synthetic
1	8.30 (dd, <i>J</i> = 5.1, 1.3)	8.40 (d, <i>J</i> = 5.0)	149.5	149.5
2	7.18 (dd, <i>J</i> = 7.7, 5.1)	7.28 (dd, <i>J</i> = 7.6, 5.1)	123.3	123.3
3	7.43 (dd, <i>J</i> = 7.7, 1.3)	7.53 (d, <i>J</i> = 7.6)	134.2	134.2
4	–	–	141.8	141.8
5	–	–	165.0	165.0
6a	3.48 (dd, <i>J</i> = 17.3, 7.1)	3.58 (dd, <i>J</i> = 17.3, 7.5)	40.7	40.7
6b	2.60 (dd, <i>J</i> = 17.3, 7.1)	2.70 (d, <i>J</i> = 17.5)	40.7	40.7
7	2.66 (q, <i>J</i> = 7.1)	2.76 (q, <i>J</i> = 7.0)	45.3	45.3
8a	1.50 (dt, <i>J</i> = 14.0, 7.1)	1.50 (dt, <i>J</i> = 14.0, 7.1)	38.5	38.5
8b	1.36 (ddd, <i>J</i> = 14.0, 7.1, 3.1)	1.45 (ddd, <i>J</i> = 13.8, 7.0, 3.2)	38.5	38.5
9	3.90 (m)	4.00 (m)	59.0	59.1
10	1.92, 1.91, 1.83, 1.75 (m)	2.05–1.82 (m)	19.5	19.5
11	1.92, 1.91, 1.83, 1.75 (m)	2.05–1.82 (m)	32.9	32.9
12	–	–	52.6	52.5
13	–	–	156.2	156.2
14a	2.94 (dd, <i>J</i> = 17.1, 7.1)	3.04 (dd, <i>J</i> = 17.4, 3.8)	33.9	33.9
14b	2.01 (m)	2.16–2.06 (m)	33.9	33.9
15	1.60 (m)	1.74–1.65 (m)	27.9	27.9
16	0.84 (d, <i>J</i> = 6.8)	0.94 (d, <i>J</i> = 6.8)	20.1	20.1

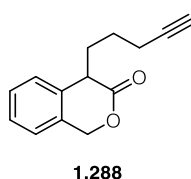
All data obtained are in full agreement with those by Takayama and Meng, who observed the same minor differences in the ¹H NMR spectrum.

4.2.2 Additional cyclization precursors and products



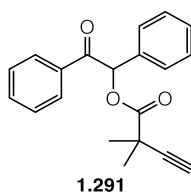
7-Methoxy-1-methyl-3-(pent-4-yn-1-yl)-3,4-dihydroquinolin-2(1H)-one (1.285). To **1.283** (0.12 g, 0.60 mmol, 1.00 eq.) in THF (4 mL) was added *n*-BuLi (0.44 mL, 1.2 mmol, 2.0 eq.) dropwise at $-78\text{ }^{\circ}\text{C}$ to give a yellow solution. After 30 min, the solution was warmed to room temperature for 35 min, then cooled back to $-78\text{ }^{\circ}\text{C}$. 4-Pentynyl iodide (**1.284**) (0.13 g, 0.66 mmol, 1.1 eq.) was added dropwise at $-78\text{ }^{\circ}\text{C}$. After 1 h at $-78\text{ }^{\circ}\text{C}$, the mixture was warmed to room temperature overnight. After addition of saturated aqueous NH_4Cl (10 mL), the layers were separated and the aqueous phase was extracted with Et_2O ($3 \times 20\text{ mL}$). The combined organic phases were washed with saturated aqueous NaCl (20 mL), dried and evaporated to give a yellow oil that was purified by column chromatography (hexanes:EtOAc 6:1 to 3:1) to give **1.285** as a yellow oil (37 mg, 0.14 mmol, 25%).

R_f	0.58 (hexanes:EtOAc 2:1), yellow oil.
¹H NMR	(400 MHz, CDCl_3) δ = 7.05 (d, J = 8.9, 1H), 6.56–6.51 (m, 2H), 3.81 (s, 3H), 3.32 (s, 3H), 2.92 (dd, J = 15.0, 5.2, 1H), 2.63 (dd, J = 15.0, 9.3, 1H), 2.56–2.48 (m, 1H), 2.21 (tdd, J = 6.9, 4.1, 2.7, 2H), 1.93 (t, J = 2.6, 1H), 1.88 (ddt, J = 12.1, 10.0, 3.4, 1H), 1.75–1.45 (m, 3H).
¹³C NMR	(101 MHz, CDCl_3) δ = 172.6, 159.3, 141.3, 128.6, 117.7, 106.5, 102.4, 84.2, 68.7, 55.6, 40.6, 30.0, 29.9, 29.0, 26.2, 18.5.
IR	(ATR): 3290 w, 2934 m, 2837 w, 2115 w, 1167 s, 1612 s, 1590 s, 1513 s, 1467 m, 1356 m, 1272 s, 1225 m, 1120.
HRMS	(EI): calculated for $\text{C}_{16}\text{H}_{19}\text{NO}_2$ 257.1416, found 257.1409.



4-(Pent-4-yn-1-yl)isochroman-3-one (1.288). To **1.287** (0.12 g, 0.75 mmol, 1.0 eq.) and 4-pentynyl iodide (**1.284**) (0.15 g, 0.75 mmol, 1.00 eq.) in THF (4 mL) and HMPA (0.2 mL) was added KHMDS (1.5 mL, 0.75 mmol, 1.0 eq.) dropwise at room temperature to give a yellow solution. After 13 h at room temperature, H₂O (5 mL) was added. The layers were separated and the aqueous phase was extracted with Et₂O (3 × 15 mL). The combined organic phases were washed with aqueous HCl (1 M, 15 mL) and saturated aqueous NaCl (20 mL), dried with MgSO₄ and evaporated to give a yellow oil that was purified by column chromatography (hexanes:EtOAc 6:1 to 3:1) to give the desired product **1.288** (37 mg, 0.17 mmol, 23%) as a yellow oil contaminated with 10% of the double alkynylation product.

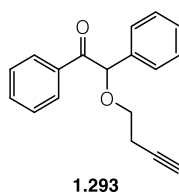
R_f	0.78 (hexanes:EtOAc 1:1), yellow oil.
¹H NMR	(400 MHz, CDCl ₃) δ = 7.37 (td, <i>J</i> = 7.4, 1.5, 1H), 7.31 (td, <i>J</i> = 7.4, 1.6, 1H), 7.26–7.21 (m, 2H), 5.48–5.38 (m, 1H), 5.27 (d, <i>J</i> = 14.2, 1H), 3.64 (t, <i>J</i> = 7.2, 1H), 2.32–2.25 (m, 2H), 2.22–1.99 (m, 3H), 1.97 (t, <i>J</i> = 2.7, 1H), 1.82–1.64 (m, 2H), 1.48–1.20 (m, 1H).
¹³C NMR	(101 MHz, CDCl ₃) δ = 172.6, 134.6, 131.3, 128.9, 127.4, 126.7, 124.9, 83.6, 69.7, 69.2, 45.5, 29.1, 25.9, 18.3.
IR	(ATR): 3290, 2938, 2044, 1736, 1609, 1546, 1492, 1461, 1390, 1334, 1240, 1185, 1157, 1126, 1079, 1047, 1033, 889, 756, 697.
HRMS	(EI): calculated for C ₁₄ H ₁₅ O ₂ 215.1067, found 215.1071.



2-Oxo-1,2-diphenylethyl 2,2-dimethylbut-3-ynoate (1.291). DCC (0.10 g, 0.50 mmol, 1.0 eq.) was added to a solution of benzoin (**1.289**) (0.10 g, 0.50 mmol, 1.0 eq.), 2,2-dimethylbut-3-ynoic acid (**1.290**) (62 mg, 0.55 mmol, 1.1 eq.) and DMAP (6.1 mg, 50 μmol, 0.10 eq.) in CH₂Cl₂ (3 mL) at room temperature. After stirring for 20 h, additional DCC (52 mg, 0.25 mmol, 0.50 eq.) was added. After stirring for 8 h, the mixture was diluted with EtOAc (80 mL) and filtrated over a silica plug. The organic phase was washed sequentially with hydrochloric acid (1 M, 10 mL), saturated aqueous NaHCO₃ solution (10 mL) and saturated aqueous NaCl (10 mL), dried over

MgSO₄ and concentrated. Purification by column chromatography (pentane:Et₂O 6:1) gave the desired product **1.291** as a colorless solid (85 mg, 0.28 mmol, 55%).

R_f	0.49 (hexanes:EtOAc 5:1), colorless amorphous solid.
¹H NMR	(400 MHz, CDCl ₃) δ = 7.97–7.89 (m, 2H), 7.55–7.50 (m, 1H), 7.48 (dd, <i>J</i> = 7.7, 1.9, 2H), 7.44–7.32 (m, 6H), 6.82 (s, 1H), 2.28 (s, 1H), 1.59 (s, 3H), 1.57 (s, 3H).
¹³C NMR	(101 MHz, CDCl ₃) δ = 193.7, 173.0, 133.5, 133.3, 129.2, 129.0, 128.8, 128.6, 128.3, 78.3, 70.3, 38.2, 27.1, 27.0.
IR (ATR):	3292 (w), 3065 (w), 2986 (w), 2939 (w), 2359 (w), 1738 (s), 1696 (s), 1598 (m), 1449 (m), 1387 (w), 1249 (s), 1141 (s), 969 (m), 761 (w), 696 (s).
HRMS	(EI): calculated for C ₁₈ H ₁₈ O ₃ 306.1256, found 306.1250.

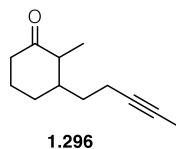


2-(But-3-yn-1-yloxy)-1,2-diphenylethan-1-one (1.293). To benzoin (**1.289**) (425 mg, 2.00 mmol, 1.00 eq.) in THF (6 mL) were added anhydrous FeCl₃ (81 mg, 0.50 mmol, 0.25 eq.) and 3-butyn-1-ol (**1.292**) (4.20 mL, 56.0 mmol, 28.0 eq.) to give a deep-red solution. After nitrogen sparging for 15 min, the mixture was heated to 80 °C for 18 h, at which point no further conversion was observed. by GC-MS analysis. After filtration over a silica plug with CH₂Cl₂ (20 mL), all volatiles were removed in vacuo at 50 °C and the residue was purified by column chromatography (pentane:Et₂O 15:1 to 13:1) to give the desired product **1.293** as a fluorescent yellow oil (81 mg, 0.30 mmol, 15%) as well as benzil (15%) and recovered starting material (25%).

R_f	0.48 (hexanes:EtOAc 5:1), fluorescent yellow oil.
¹H NMR	(400 MHz, Chloroform- <i>d</i>) δ = 8.01 (dd, <i>J</i> = 8.5, 1.4, 2H), 7.49–7.44 (m, 2H), 7.41–7.30 (m, 5H), 5.66 (s, 1H), 3.77–3.60 (m, 2H), 2.55 (dddd, <i>J</i> = 7.4, 6.8, 2.7, 1.9, 2H), 1.97 (t, <i>J</i> = 2.7, 1H).
¹³C NMR	(101 MHz, CDCl ₃) δ = 197.2, 136.2, 135.0, 133.4, 130.1, 129.4, 129.2, 129.0, 128.7, 128.6, 127.6, 85.6, 81.1, 69.8, 68.0, 20.1.

IR (ATR): 3296 w, 3064 w, 2730 w, 1688 s, 1598 m, 1583 w, 1450 m, 1274 s, 1213 m, 1112 m, 1026 m, 708 s.

HRMS (ESI): calculated for C₁₅H₁₈NO 228.1383, found 228.1382.



2-Methyl-3-(pent-3-yn-1-yl)cyclohexan-1-one (1.296). Compound **1.296** was prepared according to general procedure A (chapter 4.2.1.1) in 82% yield.

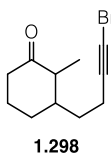
R_f 0.46 (hexanes:EtOAc 5:1). Colorless liquid.

¹H NMR (599 MHz, Chloroform-*d*) δ = 2.34–2.27 (m, 1H), 2.22–2.10 (m, 2H), 2.09–1.97 (m, 2H), 1.97–1.92 (m, 1H), 1.86 (dq, *J* = 13.0, 3.7, 1.5, 1H), 1.76–1.68 (m, 1H), 1.66 (t, *J* = 2.6, 3H), 1.56–1.51 (m, 1H), 1.48–1.39 (m, 1H), 1.35–1.25 (m, 2H), 0.96 (d, *J* = 6.6, 3H).

¹³C NMR (151 MHz, cdcl₃) δ = 213.37, 78.73, 76.09, 50.09, 44.78, 41.58, 33.47, 29.99, 25.90, 16.18, 12.22, 3.63.

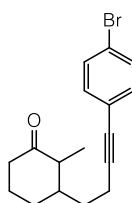
IR (ATR): 2920 m, 2862 w, 1709 s, 1445 w, 1312 w, 1218 w, 1035 w, 956 w.

HRMS (EI): calculated for C₁₂H₁₈O 178.1358, found 178.1332.



3-(4-Bromobut-3-yn-1-yl)-2-methylcyclohexan-1-one (1.298). AgNO₃ (38 mg, 0.23 mmol, 0.25 eq.) was added to a solution of 2-methyl-3-(4-(trimethylsilyl)but-3-yn-1-yl)cyclohexan-1-one (75 mg, 0.90 mmol, 1.0 eq.) and NBS (0.24 g, 1.4 mmol, 1.5 eq.) in dry acetone (3 mL). After stirring for 16 h at room temperature under exclusion of light, the crude mixture was passed over a plug of silica to give an orange oil that was concentrated and purified by column chromatography (pentane:Et₂O 8:1) to give bromide **1.298** as a colorless oil (174 mg, 0.72 mmol, 80%).

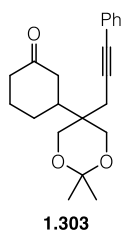
R_f	0.52 (hexanes:EtOAc) 5:1, colorless oil.
¹H NMR	(400 MHz, CDCl ₃) δ = 2.47–2.01 (m, 6H), 2.00–1.20 (m, 6H), 1.07 (d, <i>J</i> = 6.6, 2H), 1.02 (d, <i>J</i> = 7.1, 1H).
¹³C NMR	(101 MHz, CDCl ₃): = 214.2, 213.1, 84.0, 83.8, 79.7, 79.5, 68.8, 49.9, 48.6, 44.6, 41.5, 41.1, 41.0, 39.8, 38.5, 38.4, 32.8, 32.6, 29.9, 27.8, 27.7, 26.6, 25.7, 23.9, 17.5, 17.1, 16.2, 15.8, 12.1, 11.6.
IR	(ATR): 3301 (w), 2933 (m), 2865 (w), 1708 (s), 1447 (m), 1429 (m), 1378 (w), 1219 (w), 1082 (w), 957 (w), 848 (w).
HRMS	(EI): calculated for C ₈ H ₁₄ NO 242.0306, found 242.0297.

**1.301**

3-(4-(4-Bromophenyl)but-3-yn-1-yl)-2-methylcyclohexan-1-one (1.301). Pd(PPh₃)₂Cl₂ (28 mg, 40 μmol, 0.05 eq.) was added to a solution of ketone **1.300** (0.13 g, 0.80 mmol, 1.0 eq.), 1-bromo-4-iodobenzene (0.25 g, 0.88 mmol, 1.1 eq.), copper iodide (15 mg, 80 μmol, 0.10 eq.) and triethylamine (0.44 mL, 3.2 mmol, 4.0 eq.) in THF (8 mL) at room temperature. After stirring for 23 h, saturated aqueous NH₄Cl solution (1 mL) was added and the aqueous phase was extracted with EtOAc (3 × 10 mL). The combined organic phases were washed with saturated aqueous NaCl (5 mL), dried over MgSO₄ and the solvent was removed by vacuum evaporation. Purification by column chromatography (pentane:Et₂O 6:1) gave the desired product **1.301** (150 mg, 0.47 mmol, 59%) as a brown oil.

R_f	0.53 (hexanes:EtOAc 5:1), yellow solid.
¹H NMR	(400 MHz, CDCl ₃) δ = 7.40 (d, <i>J</i> = 8.2, 2H), 7.22 (d, <i>J</i> = 8.2, 2H), 2.69–1.87 (m, 8H), 1.85–1.36 (m, 5H), 1.07 (2 d, <i>J</i> = 6.8, 3H).
¹³C NMR	(101 MHz, CDCl ₃) δ = 214.4, 213.1, 133.1, 133.1, 131.6, 122.8, 121.9, 90.9, 90.7, 80.2, 80.1, 50.0, 48.7, 44.8, 41.5, 41.4, 39.8, 32.9, 30.0, 28.0, 26.7, 25.8, 24.0, 17.3, 16.9, 12.2, 11.6.

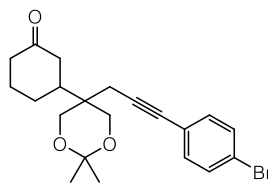
IR	(ATR): 3377, 2944, 2866, 2220, 1703, 1585, 1485, 1447, 1393, 1331, 1283, 1224, 1166, 1098, 1070, 1011, 955, 844, 820, 742.
HRMS	(EI): calculated for C ₁₇ H ₁₉ OBr 318.0619, found 318.0615.
Mp.	130–132 °C.



3-(2,2-Dimethyl-5-(3-phenylprop-2-yn-1-yl)-1,3-dioxan-5-yl)cyclohexan-1-one (1.303).

Pd(PPh₃)₂Cl₂ (21 mg, 30 μmol, 0.05 eq.) was added to a solution of cyclohexanone derivative **1.302** (0.15 g, 0.59 mmol, 1.0 eq.), iodobenzene (65 μL, 0.59 mmol, 1.0 eq.), copper iodide (5.6 mg, 30 μmol, 0.05 eq.) and triethylamine (0.33 mL, 2.4 mmol, 4.0 eq.) in THF (1.5 mL) at room temperature. After stirring for 23 h, saturated aqueous NH₄Cl solution (1 mL) was added and the aqueous phase was extracted with EtOAc (3 × 10 mL). The combined organic phases were washed with saturated aqueous NaCl (5 mL), dried over MgSO₄ and the solvent was removed by vacuum evaporation. Purification by column chromatography (pentane:Et₂O 2:1) gave the desired product **1.303** as a brown oil (0.16 g, 0.48 mmol, 82%).

R_f	0.70 (hexanes:EtOAc 1:1), colorless oil.
¹H NMR	(400 MHz, CDCl ₃) δ = 7.39–7.35 (m, 2H), 7.30–7.27 (m, 3H), 3.81 (dd, <i>J</i> = 11.9, 3.6, 2H), 3.78–3.73 (m, 2H), 2.70 (s, 2H), 2.49 (ddd, <i>J</i> = 11.7, 4.6, 2.4, 1H), 2.46–2.39 (m, 2H), 2.28 (td, <i>J</i> = 13.5, 6.4, 1H), 2.14 (ddd, <i>J</i> = 12.4, 6.1, 3.2, 1H), 2.06–1.93 (m, 2H), 1.70–1.56 (m, 2H), 1.43 (s, 3H), 1.41 (s, 3H).
¹³C NMR	(101 MHz, CDCl ₃) δ = 211.2, 131.6, 128.4, 128.1, 123.5, 98.5, 86.6, 83.8, 65.8, 65.4, 43.0, 42.1, 41.5, 37.9, 26.1, 25.8, 25.7, 21.9, 21.7.
IR	(ATR): 2990 (m), 2941 (m), 2866 (m), 1708 (s), 1490 (m), 1443 (m), 1372 (m), 1261 (m), 1197 (s), 1120 (m), 934 (w), 829 (m), 758 (s), 692 (s).
HRMS	(EI): calculated for C ₂₁ H ₂₆ O ₃ 326.1882, found 326.1871.

**1.304****3-(5-(3-(4-Bromophenyl)prop-2-yn-1-yl)-2,2-dimethyl-1,3-dioxan-5-yl)cyclohexan-1-one**

(1.304). Pd(PPh₃)₂Cl₂ (21 mg, 30 μmol, 0.05 eq.) was added to a solution of ketone **1.302** (0.15 g, 0.59 mmol, 1.0 eq.), 1-bromo-4-iodobenzene (0.17 g, 0.59 mmol, 1.0 eq.), copper iodide (5.6 mg, 30 μmol, 0.05 eq.) and triethylamine (0.33 mL, 2.4 mmol, 4.0 eq.) in THF (1.5 mL) at room temperature. After stirring for 23 h, saturated aqueous NH₄Cl solution (1 mL) was added and the aqueous phase was extracted with EtOAc (3 × 10 mL). The combined organic phases were washed with saturated aqueous NaCl (5 mL), dried over MgSO₄ and the solvent was removed by vacuum evaporation. Purification by column chromatography (pentane:Et₂O 3:1 to 5:2) gave the desired product **1.304** as a brown oil (192 mg, 0.47 mmol, 80%).

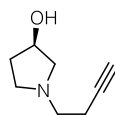
R_f 0.71 (hexanes:EtOAc 1:1), brown oil.

¹H NMR (400 MHz, CDCl₃) δ = 7.43–7.40 (m, 2H), 7.25–7.20 (m, 2H), 3.84–3.78 (m, 2H), 3.73 (d, *J* = 11.9, 2H), 2.70 (d, *J* = 2.6, 2H), 2.47 (ddt, *J* = 13.6, 4.1, 2.1, 1H), 2.39 (t, *J* = 13.3, 2H), 2.28 (td, *J* = 13.4, 6.6 Hz, 1H), 2.18–2.11 (m, 1H), 2.04–1.91 (m, 2H), 1.67–1.56 (m, 2H), 1.42 (s, 3H), 1.41 (s, 3H).

¹³C NMR (101 MHz, CDCl₃) δ = 211.0, 133.1, 131.7, 122.5, 122.2, 98.6, 88.0, 82.8, 65.7, 65.3, 43.0, 42.2, 41.5, 38.0, 26.3, 25.8, 25.7, 21.9, 21.4.

IR (ATR): 2989 (m), 2940 (m), 2866 (m), 1708 (s), 1485 (m), 1450 (m), 1371 (m), 1263 (m), 1195 (s), 1159 (m), 1069 (s), 1010 (m), 934 (w), 822 (m), 734 (s).

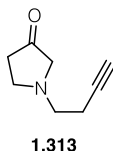
HRMS (EI): calculated for C₂₁H₂₅O₃Br 404.0987, found 404.0975.

**1.312**

(R)-1-(But-3-yn-1-yl)pyrrolidin-3-ol (1.312). To a suspension of (*R*)-pyrrolidin-3-ol hydrochloride (**1.310**) (124 mg, 1.00 mmol, 1.00 eq.) and K₂CO₃ (553 mg, 4.00 mmol, 4.00 eq.) in

acetonitrile (2.5 mL), was added 4-bromo-1-butyne (**1.311**) (113 μ L, 1.20 mmol, 1.20 eq.) dropwise. After stirring at 50 °C for 15 h, the mixture was cooled to room temperature and H₂O (5 mL) was added. The aqueous phase was extracted with Et₂O (3 \times 10 mL) and the combined organic phases were washed with saturated aqueous NaCl (10 mL) and dried over MgSO₄. Removal of the solvent by vacuum evaporation yielded alkylated pyrrolidinol **1.312** as a yellow oil (80 mg, 0.57 mmol, 57%). The product was used in subsequent steps without further purification.

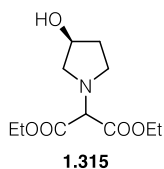
R_f	0.14 (CH ₂ Cl ₂ :MeOH 9:1).
¹H NMR	(400 MHz, CDCl ₃) δ = 4.34 (ddt, J = 7.3, 4.9, 2.3, 1H), 2.91 (td, J = 8.6, 5.1, 1H), 2.73–2.69 (m, 1H), 2.67 (t, J = 7.6, 2H), 2.56 (dd, J = 10.0, 5.2, 1H), 2.39 (td, J = 7.5, 2.6, 2H), 2.33 (td, J = 8.9, 6.4, 1H), 2.28 (s, 1H), 2.18 (dddd, J = 13.9, 8.7; 7.1, 5.2, 1H), 1.98 (t, J = 2.7, 1H), 1.78–1.70 (m, 1H).
¹³C NMR	(151 MHz, CDCl ₃) δ = 82.5, 71.1, 69.0, 62.8, 54.4, 52.2, 34.8, 18.4.
IR	(ATR): 3305, 3290, 2946, 2812, 2361, 2118, 1653, 1479, 1435, 1382, 1336, 1242, 1144, 1123, 1095, 999, 880.
HRMS	(EI): calculated for C ₈ H ₁₄ NO 140.1070, found 140.1069.



1-(But-3-yn-1-yl)pyrrolidin-3-one (1.313). To a solution of oxalyl chloride (2 M in CH₂Cl₂, 0.15 mL, 0.30 mmol, 2.0 eq.) in CH₂Cl₂ (1 mL), DMSO (42 μ L, 0.60 mmol, 4.0 eq.) was added dropwise at -78 °C. After 25 min, alkylated pyrrolidinol **1.312** (21 mg, 0.15 mmol, 1.0 eq.) in CH₂Cl₂ (0.5 mL) was added dropwise. The solution was stirred at -78 °C for 10 min before triethylamine (0.17 mL, 1.2 mmol, 8.0 eq.) was added dropwise. After further stirring for 30 min at -78 °C, the mixture was allowed to warm to room temperature and stirred for additional 1.5 h. H₂O (5 mL) was added and the aqueous phase was extracted with CH₂Cl₂ (3 \times 10 mL). The combined organic phases were sequentially washed with saturated aqueous NaHCO₃ solution (10 mL) and saturated aqueous NaCl (10 mL), dried over MgSO₄ and concentrated by vacuum evaporation to give pyrrolidinone **1.313** as a brown oil (17 mg, 0.12 mmol, 82%).

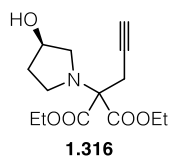
R_f	0.55 (CH ₂ Cl ₂ :MeOH 9:1).
¹H NMR	(400 MHz, CDCl ₃) δ = 3.00 (s, 2H), 2.95 (t, <i>J</i> = 7.0, 2H), 2.74 (t, <i>J</i> = 7.2, 2H), 2.45–2.35 (m, 4H), 2.00 (t, <i>J</i> = 2.7, 1H).
¹³C NMR	(101 MHz, CDCl ₃) δ = 213.9, 82.3, 69.5, 61.6, 55.2, 51.6, 38.0, 18.1.
IR	(ATR): 3496, 3282, 2926, 2809, 1754, 1478, 1430, 1378, 1340, 1267, 1246, 1188, 1134, 1030, 923, 865, 751.
MS	(ESI): calculated for C ₈ H ₁₂ NO 138.09, found 138.10. (<i>high resolution mass could not be obtained</i>)

Note: This compound decomposes at room temperature, but is stable for at least three months at –20 °C. It was therefore usually used directly in subsequent reactions.



Diethyl (S)-2-(3-hydroxypyrrolidin-1-yl)malonate (1.315). To a suspension of (*R*)-pyrrolidin-3-ol hydrochloride (**1.310**) (247 mg, 2.00 mmol, 1.00 eq.) and K₂CO₃ (332 mg, 2.40 mmol, 1.20 eq.) in DMF (2 mL), diethyl bromomalonate (**1.314**) (340 μL, 2.00 mmol, 1.00 eq.) was added dropwise. After the mixture was stirred for 24 h at room temperature, a solution of concentrated aqueous NH₃ and NH₄Cl (3:2, 15 mL) was added. The aqueous phase was extracted with EtOAc (3 × 30 mL) and the combined organic phases were washed with concentrated aqueous NaCl (20 mL), dried over MgSO₄ and concentrated. Purification by column chromatography (hexanes:EtOAc 1:1 to 1:2) gave **1.315** as a slightly yellow oil (301 mg, 1.06 mmol, 53%).

R_f	0.10 (hexanes:EtOAc 1:1), yellow oil.
¹H NMR	(400 MHz, CDCl ₃) δ = 4.34–4.27 (m, 1H), 4.26–4.15 (m, 5H), 3.11 (dd, <i>J</i> = 10.5, 5.0, 1H), 3.03 (q, <i>J</i> = 8.1, 1H), 2.90–2.82 (m, 2H), 2.05 (dtd, <i>J</i> = 14.0, 8.3, 5.7, 1H), 1.86–1.77 (m, 1H), 1.26 (t, <i>J</i> = 7.2, 6H).
¹³C NMR	(101 MHz, CDCl ₃) δ = 167.9, 167.6, 71.5, 67.7, 61.7, 58.9, 48.9, 34.9, 14.2.
IR	(ATR): 3402 (br), 2981 (w), 2941 (w), 1728 (s), 1446 (m), 1391 (m), 1299 (m), 1209 (s), 1150 (s), 1095 (s), 1025 (s), 860 (w), 733 (w).
HRMS	(ESI): calculated for C ₁₁ H ₂₀ NO ₅ 246.1336, found 246.1330.



Diethyl (R)-2-(3-hydroxypyrrolidin-1-yl)-2-(prop-2-yn-1-yl)malonate (1.316). Alkylated pyrrolidinol **1.315** (0.25 g, 1.0 mmol, 1.0 eq.) in DMF (1.5 mL) was added dropwise to a suspension of NaH (60% dispersion in mineral oil, 40 mg, 1.0 mmol, 1.0 eq.) in DMF (1 mL) at 0 °C. After the suspension was stirred for 80 min at 0 °C, propargyl bromide (80 wt.% in toluene, 0.17 mL, 1.5 mmol, 1.5 eq.) was added dropwise. The mixture was stirred at 0 °C for 6 h and additional 14 h at room temperature. A solution of concentrated aqueous NH₃ and NH₄Cl (3:2, 5 mL) was added dropwise at 0 °C and the aqueous phase was extracted with Et₂O (3 × 20 mL). The combined organic phases were washed with concentrated aqueous NaCl (10 mL), dried over MgSO₄ and the solvent was removed by vacuum evaporation. Purification by column chromatography (pentane:Et₂O 1:2 to 1:3) yielded alkynylated pyrrolidinol derivative **1.316** (0.23 g, 0.81 mmol, 81%) as a yellow oil.

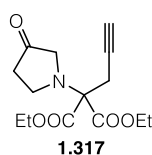
R_f 0.18 (hexanes:EtOAc 1:1), yellow oil.

¹H NMR (400 MHz, CDCl₃) δ 4.30 (s, 1H), 4.26 (q, *J* = 7.1, 4H), 3.21–3.09 (m, 2H), 3.05 (d, *J* = 10.5, 1H), 2.98 (d, *J* = 2.7, 2H), 2.93 (td, *J* = 8.6, 3.6, 1H), 2.54 (d, *J* = 7.7, 1H), 2.07 (t, *J* = 2.7, 1H), 2.07–1.94 (m, 1H), 1.84 (dddt, *J* = 12.9, 7.2, 3.6, 1.7, 1H), 1.29 (t, *J* = 7.1, 6H).

¹³C NMR (101 MHz, CDCl₃) δ = 168.6, 168.5, 78.9, 72.0, 71.5, 71.2, 61.8, 57.1, 45.8, 34.4, 25.9, 14.1.

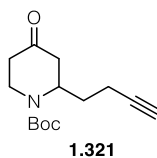
IR (ATR): 3428, 3281, 2981, 2872, 2360, 1724, 1466, 1446, 1391, 1368, 1232, 1194, 1096, 1039, 1018, 944, 857.

HRMS (ESI): calculated for C₁₄H₂₂NO₅ 284.1492, found 284.1491.



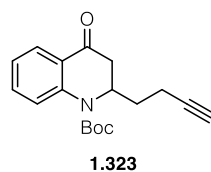
Diethyl 2-(3-oxopyrrolidin-1-yl)-2-(prop-2-yn-1-yl)malonate (1.317). DMP (0.13 g, 0.30 mmol, 1.5 eq.) was added in one portion to a solution of **1.316** (48 mg, 0.20 mmol, 1.0 eq.) in CH₂Cl₂ (1 mL) and MeCN (1 mL) at room temperature. After stirring for 2.5 h, Et₂O (5 mL) and then saturated aqueous Na₂S₂O₃ solution (1 mL) were added. After stirring for 30 min, H₂O (5 mL) was added. The aqueous phase was extracted with Et₂O (3 × 10 mL) and the combined organic phases were washed with concentrated aqueous NaCl (10 mL), dried over MgSO₄ and concentrated. The crude product was dry loaded on a chromatography column (pentane:Et₂O 2:1) to yield alkynylated pyrrolidinone **1.317** (24 mg, 90 μmol, 43%) as a colorless oil.

R_f	0.75 (hexanes:EtOAc 1:1), colorless oil.
¹H NMR	(400 MHz, CDCl ₃) δ = 4.34–4.22 (m, 4H), 3.46 (s, 2H), 3.29 (t, <i>J</i> = 7.1, 2H), 3.02 (d, <i>J</i> = 2.7, 2H), 2.49 (t, <i>J</i> = 7.1, 2H), 2.10 (t, <i>J</i> = 2.7, 1H), 1.30 (t, <i>J</i> = 7.1, 6H).
¹³C NMR	(101 MHz, CDCl ₃) δ = 213.2, 167.6, 78.2, 72.1, 72.1, 62.1, 56.4, 45.9, 37.7, 24.9, 14.3.
IR	(ATR): 3279, 2983, 2966, 1758, 1729, 1446, 1368, 1235, 1192, 1129, 1041, 857.
HRMS	(ESI): calculated for C ₁₄ H ₂₀ NO ₅ 282.1336 Found 282.1338.



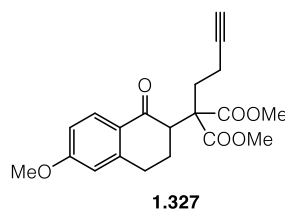
Tert-butyl 2-(but-3-yn-1-yl)-4-oxopiperidine-1-carboxylate (1.321). Compound **1.321** was prepared according to general procedure A (chapter 4.2.1.1) in 59% yield.

R_f	0.18 (hexanes:EtOAc 5:1). Pale-yellow liquid.
¹H NMR	(599 MHz, CDCl ₃) δ = 4.72 (s, 1H), 4.40, (br s, 1H), 3.14 (br, 2H), 2.66 (ddd, <i>J</i> = 14.5, 6.8, 1.0, 1H), 2.52–2.40 (m, 1H), 2.34–2.25 (m, 2H), 2.22–2.12 (m, 2H), 1.94 (t, <i>J</i> = 2.6, 1H), 1.81–1.72 (m, 1H), 1.69–1.60 (m, 1H), 1.48 (s, 9H).
¹³C NMR	(151 MHz, CDCl ₃) δ = 207.92, 154.80, 83.10, 80.86, 69.19, 51.58, 45.48, 41.4, 40.84, 31.33, 28.55, 15.40.
IR	(ATR): 3276 w, 2975 w, 2931 w, 1719 m, 1690 s, 1412 m, 1366 m, 1240 w, 1160 s, 1115 w.
HRMS	(EI): calculated for C ₁₀ H ₁₄ NO ₃ 196.0968 (<i>-t</i> -Bu), found 196.0969.



Tert-butyl 2-(but-3-yn-1-yl)-4-oxo-3,4-dihydroquinoline-1(2H)-carboxylate (1.323). Compound **1.323** was prepared according to general procedure A (chapter 4.2.1.1) in 20% yield.

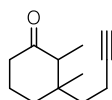
R_f	0.75 (hexanes:EtOAc 1:1), yellow oil.
¹H NMR	(400 MHz, CDCl ₃) δ = 7.05 (d, <i>J</i> = 8.9, 1H), 6.56–6.51 (m, 2H), 3.81 (s, 3H), 3.32 (s, 3H), 2.92 (dd, <i>J</i> = 15.0, 5.2, 1H), 2.63 (dd, <i>J</i> = 15.0, 9.3, 1H), 2.56–2.48 (m, 1H), 2.21 (tdd, <i>J</i> = 6.9, 4.1, 2.7, 2H), 1.93 (t, <i>J</i> = 2.6, 1H), 1.88 (ddt, <i>J</i> = 12.1, 10.0, 3.4, 1H), 1.75–1.45 (m, 3H).
¹³C NMR	(101 MHz, CDCl ₃) δ = 193.3, 153.1, 141.4, 134.4, 126.9, 125.1, 124.8, 124.0, 83.1, 82.4, 69.2, 53.0, 43.3, 30.5, 28.4, 15.8.
IR	(ATR): 3294 w, 2977 w, 2931 w, 2338 w, 1704 s, 1688 s, 1600m, 1479 m, 1459 m, 1368 m, 1347 m, 1233 w, 1159 s, 1135 m, 1047 w, 768 m.
HRMS	(ESI): calculated for C ₁₈ H ₂₀ NO ₃ 298.1449, found 298.1449.



Dimethyl 2-(but-3-yn-1-yl)-2-(6-methoxy-1-oxo-1,2,3,4-tetrahydronaphthalen-2-yl)malonate (1.327). Propargylated dimethyl malonate **1.326** (0.13 g, 0.67 mmol, 1.0 eq.) in DMF (2 mL) was added to a suspension of NaH (30 mg, 0.74 mmol, 1.1 eq.) in DMF (4 mL) at 0 °C. After stirring for 1.5 h, brominated tetralone **1.325** (0.23 g, 0.87 mmol, 1.3 eq.) was added dropwise at 0 °C and the mixture was allowed to warm to room temperature. After 14 h, the solvent was removed by vacuum evaporation and the residue was directly purified by column chromatography (pentane:Et₂O 7:1) to give tetralone **1.327** as a yellow oil (94 mg, 0.26 mmol, 39%).

R_f 0.78 (hexanes:EtOAc 1:1), yellow oil.

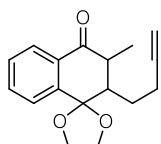
- ¹H NMR** (400 MHz, CDCl₃) δ = 7.99 (dd, *J* = 8.8, 4.1, 1H), 6.82 (dd, *J* = 8.8, 2.5, 1H), 6.68 (d, *J* = 2.4, 1H), 3.85 (s, 3H), 3.80 (s, 3H), 3.71 (s, 3H), 3.26 (dd, *J* = 13.5, 4.1, 1H), 3.11–2.98 (m, 1H), 2.95 (dt, *J* = 16.6, 3.5, 1H), 2.55–2.10 (m, 5H), 2.02 (td, *J* = 13.0, 4.4, 1H), 1.96 (t, *J* = 2.6, 1H).
- IR** (ATR): 3287 (w), 2951 (m), 2842 (w), 1730 (s), 1674 (s), 1599 (s), 1495 (w), 1434 (m), 1249 (s), 1201 (m), 1097 (m), 1028 (m).
- HRMS** (EI): calculated for C₂₀H₂₂O₆ 358.1416, found 358.1411.



1.330

3-(But-3-yn-1-yl)-2,3-dimethylcyclohexan-1-one (1.330). Compound **1.330** was prepared according to the general procedure A (chapter 4.2.1.1) and obtained in 45% yield.

- R_f** 0.57 (hexanes:EtOAc 5:1), colorless oil.
- ¹H NMR** (400 MHz, CDCl₃) δ = 2.44–2.15 (m, 7H), 2.11–2.04 (m, 1H), 1.95 (dt, *J* = 12.4, 2.7, 2H), 1.90–1.68 (m, 3H), 1.66 (t, *J* = 8.2, 2H), 1.62–1.35 (m, 4H), 1.02–0.93 (m, 7H), 0.76 (s, 3H).
- ¹³C NMR** (101 MHz, CDCl₃) δ = 213.3, 84.5, 84.4, 68.4, 68.3, 55.4, 52.3, 41.3, 40.9, 40.8, 40.3, 40.1, 35.3, 34.4, 32.4, 25.3, 22.2, 22.0, 19.6, 13.1, 12.8, 8.8, 8.3.
- IR** (ATR): 3248 (w), 2941 (m), 2874 (w), 1705 (vs), 1452 (m), 1385 (m), 1070 (m), 939 (m), 695 (m)
- HRMS** (EI): calculated for C₁₂H₁₈O 178.1358, found 178.1342.



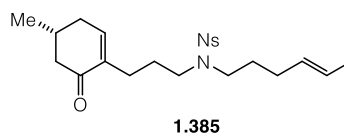
1.332

2-(But-3-yn-1-yl)-3-methyl-2,3-dihydro-4H-spiro[naphthalene-1,2'-[1,3]dioxolan]-4-one (1.332).

Compound **1.332** was prepared according to the general procedure A (chapter 4.2.1.1) in 20% yield.

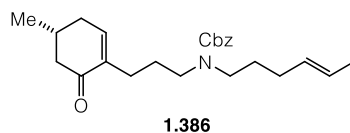
R_f	0.25 (hexanes:EtOAc 9:1), colorless oil.
¹H NMR	(400 MHz, CDCl ₃) δ = 7.66 (dd, <i>J</i> = 8.0, 3.7, 1H), 7.26 (d, <i>J</i> = 7.4, 2H), 7.20–7.06 (m, 1H), 4.06–3.99 (m, 1H), 3.90 (q, <i>J</i> = 7.0, 1H), 3.84–3.75 (m, 2H), 3.12 (dtd, <i>J</i> = 10.9, 7.1, 4.1, 1H), 2.13 (q, <i>J</i> = 5.2, 1H), 2.03 (tdd, <i>J</i> = 17.1, 8.2, 5.5, 2H), 1.63 (dt, <i>J</i> = 5.6, 2.8, 1H), 1.20–1.12 (m, 2H), 1.11–1.07 (m, 1H), 0.97 (d, <i>J</i> = 6.8, 2H).
¹³C NMR	(101 MHz, CDCl ₃) δ = 200.1, 199.4, 142.9, 141.2, 133.9, 133.4, 132.1, 131.6, 129.3, 129.2, 127.6, 126.6, 126.1, 124.6, 109.1, 108.1, 84.4, 84.2, 68.9, 68.8, 66.5, 66.4, 64.7, 64.3, 47.7, 47.4, 45.2, 44.5, 28.1, 25.3, 18.5, 17.8, 16.5, 12.7.
IR	(ATR): 3292 (w), 2956 (w), 2889 (w), 1686 (s), 1600 (m), 1463 (w), 1364 (m), 1297 (m), 1245 (s), 1224 (m), 1155 (m), 1118 (m), 1069 (s), 992 (s), 948 (s), 889 (w), 796 (w), 763 (s), 699 (w).
HRMS	(EI): calculated for C ₁₇ H ₁₈ O ₃ 270.1243, found 207.1256.

4.2.3 Lycopladiene H and Lycojaponicum D



(*R,E*)-N-(Hex-4-en-1-yl)-N-(3-(4-methyl-6-oxocyclohex-1-en-1-yl)propyl)-2-nitrobenzenesulfonamide (1.385). Amine **1.383** (47 mg, 0.30 mmol, 1.5 eq.) was dissolved in THF (2.5 mL) and 9-BBN (0.5 M in THF, 0.80 mL, 0.40 mmol, 2.0 eq.) was added dropwise at room temperature. After 8 h, TLC analysis showed full conversion. H₂O (0.1 mL) was degassed with Ar for 20 min, then added to the solution, immediately followed by addition of Cs₂CO₃ (98 mg, 0.30 mmol, 1.5 eq.). After 50 min at room temperature, AsPh₃ (9.0 mg, 30 μmol, 0.15 eq.), vinyl iodide **1.111** (47 mg, 0.20 mmol, 1.0 eq.) and DMF (2 mL) were added sequentially. The mixture was sparged with Argon for 20 min before Pd(dppf)Cl₂ (7.3 mg, 10 μmol, 0.05 eq.) was added and the reaction was stirred at room temperature for 16 h. During this time, the reaction mixture turned from slightly yellow to dark red. The mixture was then poured on saturated aqueous NH₄Cl solution (20 mL) and diluted with Et₂O (20 mL). The aqueous phase was further extracted with Et₂O (2 × 20 mL) and the organic phases were combined. After washing with H₂O (2 × 25 mL) and saturated aqueous NaCl (25 mL), the organic phase was dried with MgSO₄, filtered and concentrated to give a brown residue that was purified by column chromatography (pentane:EtOAc 3:1) to yield **1.385** (61 mg, 0.14 mmol, 70%) as a yellow oil.

R_f	0.15 (hexanes:EtOAc 5:1). Slightly yellow oil.
¹H NMR	(400 MHz, CDCl ₃) δ = 8.04–7.90 (m, 1H), 7.69–7.65 (m, 2H), 7.62–7.59 (m, 1H), 6.70 (ddd, <i>J</i> = 5.4, 2.6, 1.3, 1H), 5.45–5.27 (m, 2H), 3.30–3.23 (m, 4H), 2.50–2.45 (m, 1H), 2.45–2.35 (m, 1H), 2.17–2.10 (m, 3H), 2.10–1.88 (m, 4H), 1.70–1.50 (m, 8H), 1.04 (d, <i>J</i> = 6.3, 3H).
¹³C NMR	(101 MHz, CDCl ₃) δ = 199.7, 148.2, 145.6, 138.2, 133.8, 133.4, 131.6, 130.8, 129.8, 126.1, 124.2, 47.1, 46.9, 46.7, 34.5, 30.7, 29.6, 28.0, 27.2, 26.9, 21.3, 18.1.
IR	(ATR): 2953, 2927, 1670, 1545, 1454, 1439, 1373, 1348, 1297, 1264, 1204, 1161, 1125, 1060, 967, 851, 779.
HRMS	(EI): calculated for C ₂₂ H ₃₁ N ₂ O ₅ S 435.1948 found 435.1953.



Benzyl (R,E)-hex-4-en-1-yl(3-(4-methyl-6-oxocyclohex-1-en-1-yl)propyl)carbamate (1.386).

Amine **1.384** (0.41 mg, 0.15 mmol, 1.5 eq.) was dissolved in THF (1 mL) and 9-BBN (0.5 M in THF, 0.40 mL, 0.20 mmol, 2.0 eq.) was added dropwise at room temperature. After 8 h, TLC analysis showed full conversion. H₂O (0.1 mL) was degassed with Ar for 20 min, then added to the solution, immediately followed by addition of Cs₂CO₃ (65 mg, 0.2 mmol, 2.0 eq.). After 30 min at room temperature, AsPh₃ (3.0 mg, 10 μmol, 0.10 eq.), iodide **1.111** (24 mg, 0.10 mmol, 1.0eq.) and DMF (1 mL) were added sequentially. The mixture was sparged with Argon for 20 min before Pd(dppf)Cl₂ (6.0 mg, 8 μmol, 0.08 eq.) was added and the reaction was stirred at room temperature for 16 h. During this time, the reaction mixture turned from slightly yellow to dark red. The mixture was then poured on saturated aqueous NH₄Cl solution (20 mL) and diluted with Et₂O (20 mL). The aqueous phase was further extracted with Et₂O (2 × 20 mL) and the organic phases were combined. After washing with H₂O (2 × 25 mL) and saturated aqueous NaCl (25 mL), the organic phase was dried with MgSO₄, filtered and concentrated to give a brown residue that was purified by column chromatography (pentane:Et₂O 6:1) to yield **1.386** (27 mg, 71 μmol, 71%) as a yellow oil.

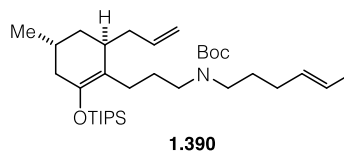
R_f 0.25 (hexanes:EtOAc 5:1). Colorless oil.

¹H NMR (400 MHz, CDCl₃) δ = 7.32–7.16 (m, 2H), 6.57 (2 d, *J* = 4.1, 1H), 5.31 (dt, *J* = 17.2, 4.9, 2H), 5.03 (s, 2H), 3.14 (q, *J* = 8.4, 4H), 2.38 (t, *J* = 12.9, 1H), 2.31–2.16 (m, 1H), 2.13–1.80 (m, 6H), 1.61–1.44 (m, 6H), 0.95 (2 d, *J* = 6.5, 3H). *Note: 3 Cbz protons are obscured by the solvent signal. Due to extensive rotamer line broadening, not all integrals match.*

¹³C NMR (101 MHz, CDCl₃) δ = 199.7, 199.5, 156.1, 156.1, 144.9, 144.6, 138.6, 137.0, 130.4, 130.3, 128.4, 127.8, 127.7, 125.5, 125.4, 66.8, 47.2, 46.7, 46.5, 34.4, 34.3, 30.6, 29.9, 29.8, 28.4, 27.9, 27.5, 26.9, 26.7, 21.2, 17.9. *Note: due to rotamers, almost two complete sets of peaks were observed.*

IR (ATR): 2954, 2926, 2858, 1694, 1472, 1416, 1366, 1288, 1255, 1225, 1169, 1054, 974, 934, 894, 837, 777, 676.

HRMS (EI): calculated for C₂₄H₃₃NO₃ 384.2460, found 383.2447.



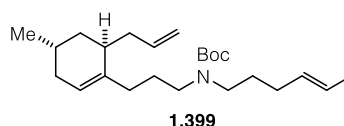
Tert-butyl (3-((4R,6R)-6-allyl-4-methyl-2-((triisopropylsilyl)oxy)cyclohex-1-en-1-yl)propyl)((E)-hex-4-en-1-yl)carbamate (1.390). Enone **1.385** (35 mg, 0.10 mmol, 1.0 eq.) was dissolved in CH₂Cl₂ (0.8 mL) and cooled to -78 °C before DTBPy (33 μL, 0.15 mmol, 1.5 eq) was added. After 15 min, TIPSOTf (32 μL, 0.12 mmol, 1.2 eq) was added dropwise, rendering a yellow solution to which allylSnBu₃ (37 μL, 0.11 mmol, 1.1 eq) was added another 10 min later. After 2 h at -78 °C, the reaction was diluted with CH₂Cl₂ (10 mL) and warmed to room temperature before saturated aqueous NaHCO₃ (5 mL) and H₂O (2 mL) were added. The aqueous phase was extracted with CH₂Cl₂ (3 × 8 mL) and the combined organic phases were washed with saturated aqueous NaCl (5 mL), dried with MgSO₄ and concentrated. The resulting yellow oil was purified using column chromatography (pentane:EtOAc 30:1 + 1% Et₃N) to give **1.390** (26 mg, 45 μmol, 45%) as a colorless oil.

R_f 0.20 (hexanes:EtOAc 30:1). Colorless oil.

¹H NMR (400 MHz, CDCl₃) δ = 5.75 (dddd, *J* = 15.5, 11.0, 8.1, 6.0, 1H), 5.49–5.32 (m, 2H), 5.00 (d, *J* = 6.8, 1H), 4.96 (s, 1H), 3.21–3.01 (m, 4H), 2.42 (ddd, *J* = 13.1, 10.1, 6.2, 1H), 2.27 (ddd, *J* = 15.3, 5.8, 3.1, 1H), 2.19–2.12 (m, 1H), 2.06 (dd, *J* = 15.9, 5.0, 1H), 2.01–1.81 (m, 3H), 1.79–1.66 (m, 2H), 1.63 (d, *J* = 3.5, 3H), 1.62–1.46 (m, 3H), 1.44 (s, 9H), 1.10 (s, 1H), 1.10–1.06 (m, 18H), 0.93 (d, *J* = 6.4, 3H).

¹³C NMR (101 MHz, CDCl₃) δ = 155.5, 144.4, 138.3, 130.6, 125.2, 116.4, 115.5, 78.8, 47.4, 46.7, 39.0, 37.8, 35.8, 34.3, 30.0, 29.7, 28.5, 28.1, 25.3, 24.6, 21.9, 18.2, 17.9, 13.4.

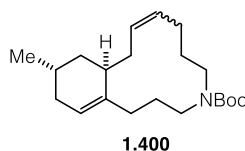
HRMS (EI): calculated for C₃₃H₆₂NO₃Si 548.4493, found 548.4503.



Tert-butyl (3-((4S,6R)-6-allyl-4-methylcyclohex-1-en-1-yl)propyl)((E)-hex-4-en-1-yl)carbamate (1.399). Amine **1.363** (0.41 g, 0.15 mmol, 1.5 eq.) was dissolved in THF (6 mL) and 9-BBN (0.5 M in THF, 4.5 mL, 2.3 mmol, 2.0 eq.) was added dropwise at room temperature. After 8 h, TLC

analysis showed full conversion and a degassed aqueous solution Cs_2CO_3 (3 M, 1.2 mL, 3.4 mmol, 3.0 eq.) was added. After 30 min, iodide **1.398** (0.30 g, 1.1 mmol, 1.0 eq.) in degassed DMF (6 mL) and AsPh_3 (35 mg, 0.11 mmol, 0.10 eq.) were added. After 10 min, $\text{Pd}(\text{dppf})\text{Cl}_2$ (43 mg, 56 μmol , 0.05 eq.) was added, turning the reaction mixture dark brown within 2 min. After 15 h at room temperature, saturated aqueous NH_4Cl (20 mL) and H_2O (10 mL) were added. The heterogeneous mixture was extracted with Et_2O (3×40 mL), the combined organic phases were washed with saturated aqueous NaCl (30 mL), dried with MgSO_4 and concentrated to give a brown oil. Purification by column chromatography (pentane: EtOAc 30:1) gave **1.399** (0.32 g, 0.87 mmol, 72%) as a colorless oil.

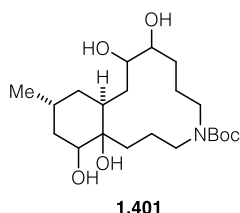
- R_f** 0.77 (hexanes: EtOAc 5:1). Colorless oil.
- ¹H NMR** (400 MHz, CDCl_3) δ = 5.82–5.67 (m, 1H), 5.48–5.39 (m, 2H), 5.41–5.36 (m, 1H), 5.06–4.96 (m, 2H), 3.14 (br s, 4H), 2.36–2.22 (m, 1H), 2.08–2.03 (m, 2H), 2.03–1.90 (m, 5H), 1.76–1.69 (m, 1H), 1.64 (d, J = 4.3, 4H), 1.59–1.52 (m, 4H), 1.44 (d, J = 1.8, 9H), 1.19 (td, J = 12.4, 5.4, 1H), 0.91 (t, J = 6.7, 3H). *Due to extensive rotamer line broadening, not all integrals match.*
- ¹³C NMR** (101 MHz, CDCl_3) δ = 155.7, 139.6, 138.2, 137.0, 130.7, 125.4, 123.2, 121.8, 116.2, 115.8, 79.1, 47.3, 46.9, 38.3, 37.7, 37.6, 37.4, 36.7, 34.8, 34.6, 34.3, 32.5, 32.0, 30.1, 29.1, 28.7, 28.3, 27.1, 26.9, 23.6, 22.3, 22.1, 18.1. *Note: due to rotamers, almost two complete sets of peaks were observed.*
- IR** (ATR): 2925, 2868, 1693, 1468, 1455, 1414, 1365, 1300, 1255, 1165, 1155, 1060, 994, 965, 908, 808, 772, 733.
- HRMS** (EI): calculated for $\text{C}_{24}\text{H}_{42}\text{NO}_2$ 376.3210 found 376.3217.



***Tert*-butyl (10a*S*,12*S*)-12-methyl-2,3,5,6,7,10,10a,11,12,13-decahydrobenzo-[e][1]-azacyclododecine-4(1*H*)-carboxylate (1.400)**. Alkene **1.399** (144 mg, 0.40 mmol, 1.0 eq.) was dissolved in CH_2Cl_2 (1.9 L) and the solution was degassed with argon for 20 min. At this point, Grubbs I (33 mg, 40 μmol , 0.10 eq.) was added and the mixture was heated to 40 °C. After 24 and 48 h, additional Grubbs I (two times 32 mg, 40 μmol , 0.10 eq.) was added. After 72 h, the solvent was

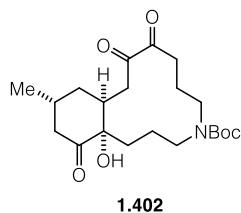
removed and the residue purified by column chromatography (pentane:EtOAc 30:1) to give **1.400** (92 mg, 0.28 mmol, 70%) as a colorless oil.

R_f	0.70 (hexanes:EtOAc 5:1). Colorless oil.
¹H NMR	(400 MHz, CDCl ₃) δ = 5.68–5.58 (m, 1H), 5.54–5.43 (m, 2H), 5.42–5.32 (m, 3H), 3.80 (s, 4H), 3.42–3.25 (m, 1H), 3.27–2.99 (m, 4H), 2.95–2.79 (m, 3H), 2.45 (q, <i>J</i> =13.2, 12.6, 1H), 2.39–2.30 (m, 1H), 2.29–1.43 (m, 12H), 1.40 (d, <i>J</i> =1.5, 22H), 1.17 (d, <i>J</i> =12.1, 4H), 0.92–0.82 (m, 7H). <i>Due to extensive rotamer line broadening, not all integrals match.</i>
¹³C NMR	(101 MHz, CDCl ₃) δ = 157.1, 156.9, 140.7, 140.5, 130.5, 130.1, 129.8, 129.1, 122.5, 122.4, 79.3, 79.2, 49.5, 49.1, 48.9, 48.5, 41.8, 41.0, 40.2, 39.4, 38.7, 36.4, 34.6, 34.4, 34.3, 32.1, 31.9, 31.1, 30.5, 29.6, 29.4, 28.7, 28.6, 24.7, 24.4, 24.2, 23.5, 22.3, 22.3. <i>Note: due to rotamers, almost two complete sets of peaks were observed.</i>
IR	(ATR): 2947, 2924, 1694, 1459, 1414, 1365, 1300, 1282, 1240, 1171, 1121, 1058, 978, 866, 769, 721.
HRMS	(EI): calculated for C ₂₁ H ₃₅ NO ₂ 333.2668 found 333.2662.



Tert-butyl (10a*S*,12*R*)-8,9,14,14a-tetrahydroxy-12-methyltetradecahydrobenzo[*e*][1]-azacyclododecine-4(1*H*)-carboxylate (1.401).

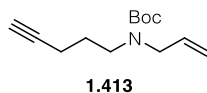
R_f	0.55 (CH ₂ Cl ₂ :MeOH:AcOH:H ₂ O 90:10:0.6:0.6). Colorless foam.
IR	(ATR): 3451, 3417, 3404, 2950, 2926, 1690, 1666, 1480, 1464, 1417, 1366, 1311, 1249, 1167, 1095, 1044, 982, 866, 757, 684.
HRMS	(ESI): calculated for C ₂₁ H ₄₀ NO ₆ 402.2850 found 402.2859.



Tert-butyl (10*aS*,12*R*)-14*a*-hydroxy-12-methyl-8,9,14-trioxotetradecahydrobenzo-
[e][1]azacyclo-dodecine-4(1*H*)-carboxylate (**1.402**).

R_f 0.25 (hexanes:EtOAc 1:1). Colorless foam.

HRMS (ESI): calculated for C₂₄H₃₄NO₃ 396.2381 found 396.2390.



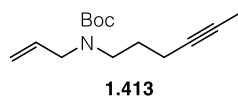
Tert-butyl allyl(pent-4-yn-1-yl)carbamate (**1.413**). Sodium hydride (60%, 24 mg, 0.60 mmol, 1.2 eq.) was added in one portion to Boc-protected allylamine **1.412** (79 mg, 0.50 mmol, 1.0 eq.) in dry DMF (1.5 mL) at 0 °C to give an orange suspension. After 20 min, 4-pentynyl iodide (**1.284**) (0.15 g, 0.75 mmol, 1.50 eq.) was added dropwise at 0 °C. After the addition was complete, the ice bath was removed and the reaction was stirred at room temperature for 22 h. When the reaction was judged complete by TLC, saturated aqueous NH₄Cl (15 mL) and H₂O (10 mL) were added carefully. The aqueous phase was extracted with Et₂O (3 × 30 mL), then the combined organic phases were washed with saturated aqueous NaCl (30 mL), dried, filtered and evaporated to give a yellow residue that was purified by column chromatography (hexanes:EtOAc 15:1) to give the desired product **1.413** as a colorless oil (89 mg, 0.40 mmol, 80%).

R_f 0.62 (hexanes:EtOAc 5:1). Colorless oil.

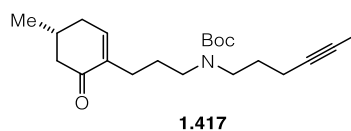
¹H NMR (400 MHz, CDCl₃) δ = 5.75 (ddt, *J* = 16.3, 10.6, 5.7, 1H), 5.09 (d, *J* = 11.4, 2H), 3.79 (d, *J* = 18.3, 2H), 3.25 (t, *J* = 7.1, 2H), 2.17 (td, *J* = 7.1, 2.6, 2H), 1.93 (t, *J* = 2.7, 1H), 1.72 (t, *J* = 7.2, 2H), 1.43 (s, 9H).

¹³C NMR (101 MHz, CDCl₃) δ = 155.6, 152.4, 134.3, 116.6, 116.1, 83.8, 82.4, 79.6, 68.8, 50.2, 49.6, 45.9, 45.7, 28.5, 27.4, 27.2, 16.1. (3 peaks were strongly broadened due to rotamers).

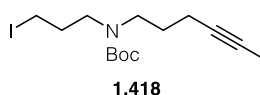
- IR** (ATR): 3309, 3255, 2976, 2932, 1688, 1463, 1408, 1365, 1273, 1246, 1162, 1137, 992, 916, 772, 630.
- HRMS** (EI): calculated for $C_{14}H_{22}NO_2$ 224.1645 found 224.1645.



Tert-butyl allyl(hex-4-yn-1-yl)carbamate (1.413). Full characterization for compound **1.413** can be found in section 4.2.1.1 (compound **S1**).



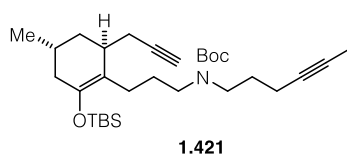
Tert-butyl (R)-hex-4-yn-1-yl(3-(4-methyl-6-oxocyclohex-1-en-1-yl)propyl)-carbamate (1.417). Full characterization for compound **1.417** can be found in section 4.2.1.1 (compound **S2**).



Tert-butyl hex-4-yn-1-yl(3-iodopropyl)carbamate (1.418). 9-BBN (0.5 M in THF, 2.2 mL, 1.1 mmol, 1.2 eq.) was added dropwise to terminal alkene **1.413** (0.22 g, 0.90 mmol, 1.0 eq.) in THF (3 mL) at 0 °C. After stirring for 30 min at 0 °C and 3 h at room temperature, a solution of NaOMe in MeOH (0.72 mL, 3.9 mmol, 4.3 eq.), followed by I₂ (0.82 g, 3.3 mmol, 3.6 eq.) in MeOH, (4 mL) were added via cannula. The resulting mixture was stirred at room temperature for 3 h, then diluted with saturated aqueous Na₂S₂O₃ (10 mL) and extracted with EtOAc (3 × 15 mL). The organic extracts were washed with aqueous HCl (1 M, 10 mL), saturated aqueous NaCl (15 mL) and dried over MgSO₄. The yellow solution was filtrated over a short silica plug and concentrated in vacuo to give **1.418** (0.23 g, 0.64 mmol, 71%) as a slightly yellow oil.

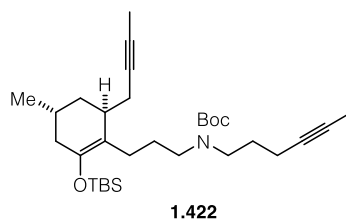
R_f	0.37 (hexanes:EtOAc 5:1) Brown oil.
¹H NMR	(400 MHz, CDCl ₃) δ = 3.30–3.23 (m, 4H), 3.15 (t, <i>J</i> = 6.9, 2H), 2.13 (ddt, <i>J</i> = 7.0, 4.5, 2.5, 1H), 2.06 (d, <i>J</i> = 7.8, 3H), 1.78 (t, <i>J</i> = 2.5, 3H), 1.70 (d, <i>J</i> = 8.8, 2H), 1.45 (s, 9H).
¹³C NMR	(151 MHz, CDCl ₃) δ = 155.9, 80.0, 78.6, 48.4, 47.3, 32.8, 28.8, 28.5, 16.6, 3.9, 3.5, 3.3.

Note: This primary iodide decomposes quickly at room temperature, but is stable for at least three days at -20 °C.



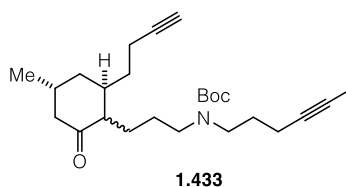
***Tert*-butyl (3-((4*R*,6*S*)-2-((*tert*-butyldimethylsilyl)oxy)-4-methyl-6-(prop-2-yn-1-yl)cyclohex-1-en-1-yl)propyl)(hex-4-yn-1-yl)carbamate (1.421).** Enone **1.417** (35 mg, 0.10 mmol, 1.0 eq.) was dissolved in CH₂Cl₂ (0.8 mL) and cooled to -78 °C. 2,6-Di-*tert*-butylpyridine (22 μL, 0.10 mmol, 1.0 eq.) and TBSOTf (29 μL, 0.12 mmol, 1.2 eq.) were added sequentially in one portion at -78 °C, at which point the reaction turned bright yellow. After 10 min, allenyltributyltin (39 mg, 0.12 mmol, 1.2 eq.) was added dropwise over 10 min. The reaction was stirred at -78 °C for 5 h, then saturated aqueous NaHCO₃ solution (3 mL) was added. The biphasic mixture was allowed to warm to room temperature and was extracted with Et₂O (3 × 15 mL). The organic phases were dried with MgSO₄ and concentrated to give a colorless oil that was submitted to column chromatography (pentane:Et₂O 12:1) to yield a colorless oil **1.421** (25 mg, 50 μmol, 50%)

R_f	0.70 (hexanes:EtOAc 5:1). Colorless oil.
¹H NMR	(400 MHz, C ₆ D ₆) δ = 3.47–3.02 (m, 5H), 2.58–2.28 (m, 3H), 2.21–1.93 (m, 6H), 1.90–1.63 (m, 6H), 1.59 (s, 3H), 1.49 (s, 9H), 1.28 (dt, <i>J</i> = 11.9, 6.2, 1H), 1.02 (s, 9H), 0.87 (d, <i>J</i> = 6.4, 3H), 0.12 (s, 6H).
¹³C NMR	(101 MHz, C ₆ D ₆) δ = 155.3, 145.2, 83.9, 78.9, 78.7, 75.9, 69.8, 48.0, 47.7, 46.8, 39.3, 36.2, 35.3, 28.6, 27.6, 26.2, 25.5, 25.1, 23.4, 21.8, 18.5, 16.7, 3.5, -3.4, -3.4.
IR	(ATR): 3312, 2954, 2928, 2858, 2349, 1694, 1471, 1414, 1365, 1288, 1253, 1223, 1170, 1053, 933, 890, 837, 777, 626.
HRMS	(EI): calculated for C ₃₀ H ₅₁ NO ₃ Si 501.3638, found 501.3630.

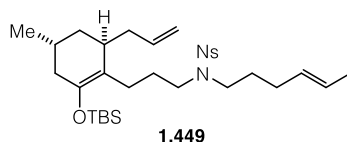


Tert-butyl (3-((4*R*,6*S*)-6-(but-2-yn-1-yl)-2-((tert-butyldimethylsilyl)oxy)-4-methylcyclohex-1-en-1-yl)propyl)(hex-4-yn-1-yl)carbamate (1.422). Silyl enol ether **1.421** (10 mg, 19 μ mol, 1.0 eq.) was dissolved in THF (0.7 mL) and cooled to -78 $^{\circ}$ C before *n*-BuLi (2.28 M, 10 μ L, 21 μ mol, 1.1 eq.) was added dropwise, giving a bright yellow solution. After 35 min, methyl iodide (5 μ L (1 drop), 29 μ mol, 1.50 eq.) was added at -78 $^{\circ}$ C, immediately decolorizing the solution. After 1.5 h, the cooling bath was removed and the reaction was stirred for another 3 h. The reaction mixture was evaporated to give a yellow residue that was purified by column chromatography (hexanes:Et₂O 12:1) to give the desired product **1.422** as a colorless oil (7 mg, 12 μ mol, 63%).

R_f	0.75 (hexanes:EtOAc 5:1). Colorless oil.
¹H NMR	(400 MHz, CDCl ₃) δ = 3.21 (br s, 3H), 3.09 (br s, 2H), 2.37–2.21 (m, 3H), 2.11 (s, 2H), 2.04 (dd, <i>J</i> = 16.5, 5.8, 1H), 1.86 (d, <i>J</i> = 12.0, 2H), 1.77 (2s, 6H), 1.74–1.58 (m, 3H), 1.44 (s, 9H), 1.32–1.15 (m, 2H), 0.96 (d, <i>J</i> = 6.5, 3H), 0.93 (s, 9H), 0.12 (s, 6H).
¹³C NMR	(101 MHz, C ₆ D ₆) δ = 155.5, 144.8, 79.0, 78.5, 76.0, 75.7, 46.3, 39.0, 36.3, 34.8, 28.5, 25.9, 24.7, 23.2, 21.8, 18.2, 16.3, 3.6, 3.5, -3.5, -3.6.
IR	(ATR): 2954, 2926, 2858, 1694, 1472, 1416, 1366, 1288, 1255, 1225, 1169, 1054, 974, 894, 837, 777, 676.
HRMS	(EI): calculated for C ₃₀ H ₅₁ NO ₃ Si 515.3795, found 515.3789.



Tert-butyl (3-((2*R*,4*R*)-2-(but-3-yn-1-yl)-4-methyl-6-oxocyclohexyl)propyl)-(hex-4-yn-1-yl)-carbamate (1.433). Full characterization for this compound can be found in section 4.2.1.1 (compound 1).



N-(3-((4*R*,6*R*)-6-Allyl-2-((tert-butyldimethylsilyl)oxy)-4-methylcyclohex-1-en-1-yl)propyl)-N-((*E*)-hex-4-en-1-yl)-2-nitrobenzenesulfonamide (1.449). Enone **1.385** (43 mg, 0.10 mmol, 1.0 eq.) was dissolved in CH₂Cl₂ (0.8 mL) and cooled to -78 °C before DTBPy (33 μL, 0.15 mmol, 1.5 eq) and molecular sieves 4 Å (50 mg, powdered) were added. After 15 min, TBSOTf (28 μL, 0.12 mmol, 1.2 eq) was added dropwise, rendering a yellow solution to which allylSnBu₃ (37 μL, 0.11 mmol, 1.1 eq) was added 10 min later. After 3 h at -78 °C, the reaction was diluted with CH₂Cl₂ (10 mL) and warmed to room temperature before saturated aqueous NaHCO₃ (5 mL) and H₂O (2 mL) were added. The aqueous phase was extracted with CH₂Cl₂ (3 × 10 mL) and the combined organic phases were washed with saturated aqueous NaHCO₃ (5 mL), dried with MgSO₄ and concentrated. The resulting yellow oil was purified by column chromatography (pentane:EtOAc 15:1 to 10:1) to give **1.449** (34 mg, 58 μmol, 58%) as a colorless oil.

R_f 0.58 (hexanes:EtOAc 5:1). Colorless oil.

¹H NMR (400 MHz, C₆D₆) δ = 7.79 (dd, *J* = 7.9, 1.2, 1H), 6.76–6.65 (m, 2H), 6.54 (td, *J* = 7.7, 1.3, 1H), 5.74 (dtd, *J* = 17.8, 8.3, 6.0, 1H), 5.30 (p, *J* = 5.7, 2H), 5.13–4.97 (m, 2H), 3.46–3.14 (m, 4H), 2.43 (ddd, *J* = 14.0, 9.8, 6.8, 1H), 2.29 (dt, *J* = 14.1, 4.7, 1H), 2.15 (dd, *J* = 9.3, 4.9, 1H), 2.07 (dd, *J* = 15.9, 5.2, 1H), 1.98–1.91 (m, 1H), 1.91–1.60 (m, 7H), 1.58–1.52 (m, 5H), 1.16 (td, *J* = 12.3, 5.5, 1H), 1.02 (s, 9H), 0.88 (d, *J* = 6.4, 3H), 0.13 (s, 6H).

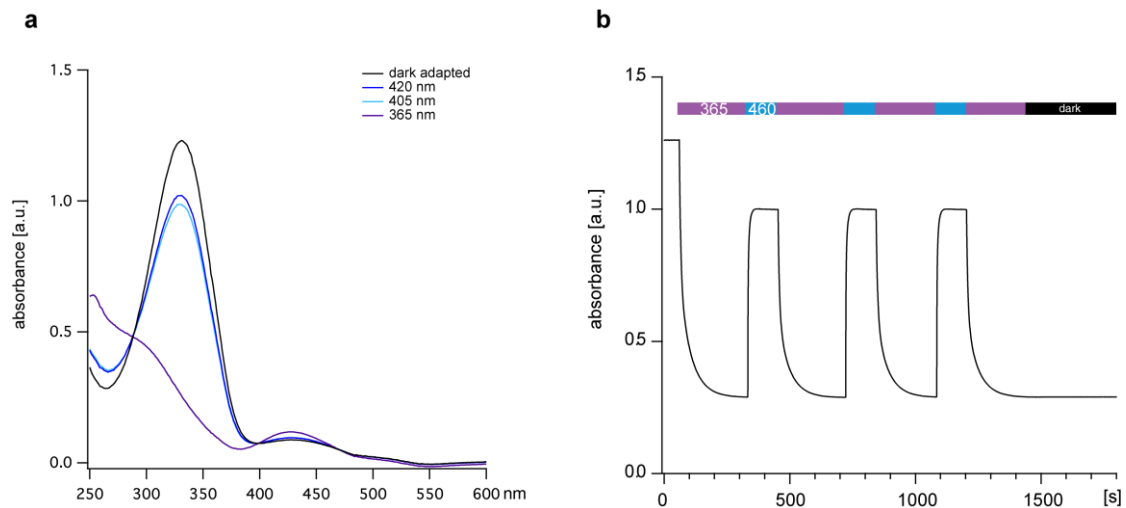
¹³C NMR (101 MHz, C₆D₆) δ = 148.5, 144.9, 138.4, 134.3, 132.7, 130.9, 130.8, 130.3, 125.9, 123.9, 117.2, 116.0, 47.6, 47.2, 39.3, 38.3, 36.3, 34.7, 29.9, 28.4, 27.1, 26.2, 25.5, 25.0, 22.0, 18.5, 18.1, -3.3, -3.4.

IR (ATR): 2951, 2928, 2856, 1709, 1671, 1639, 1544, 1471, 1461, 1439, 1370, 1350, 1252, 1199, 1160, 1124, 1059, 966, 850, 836, 776, 736, 704.

HRMS (EI): calculated for C₂₄H₄₅N₂O₅SSi (-allyl) 549.2818 found 549.2866.

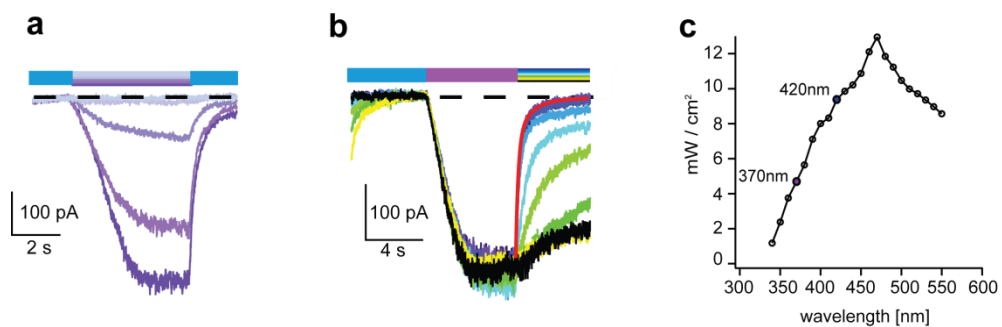
4.3 Supporting information for chapter 2: Photoswitchable glutamate derivatives

4.3.1 NMDA agonists



Supplementary Figure 1. UV-Vis spectra and thermal stability of ATG.

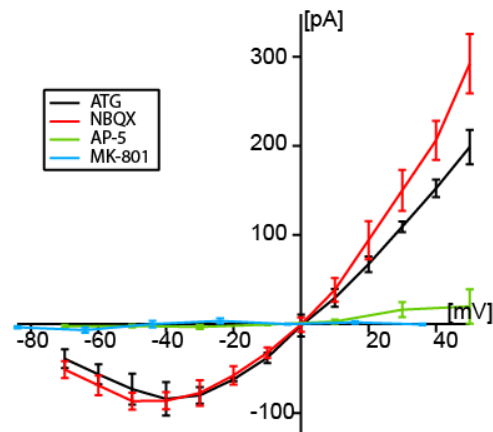
(a) UV-Vis spectra of ATG in the dark-adapted state and during illumination with 370, 405 and 420 nm light in physiological buffer. (b) Kinetics of the conversion of *trans*- to *cis*-ATG during illumination with 460 and 365 nm light (high power LEDs) measured at the maximal absorption wavelength of *trans*-ATG (330 nm).



Supplementary Figure 2. Action spectrum, kinetics and dose-response curve recorded in layer 2/3 cortical neurons.

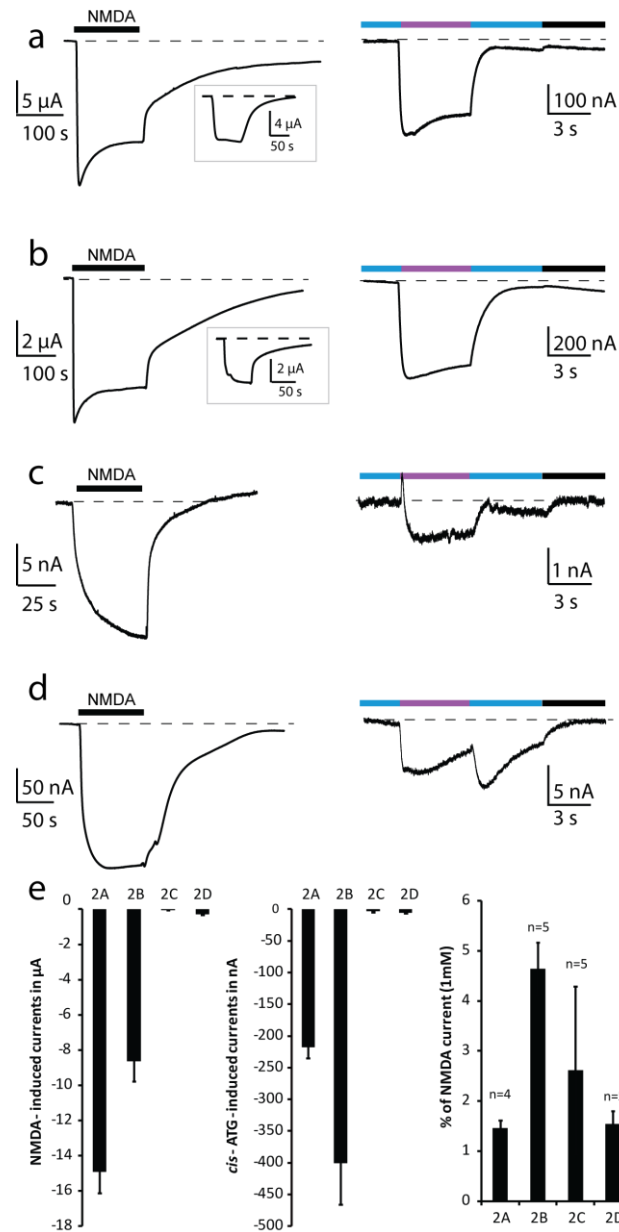
(a) Wavelength screening for activation of ATG-mediated (200 μ M) currents. Left: Raw data traces for 5 s light stimulation from 360 nm to 410 nm light (dark to light violet). Right: Current amplitude was measured after 5 s light stimulation with the respective wavelength and normalized to the maximal current amplitude at 360 nm. (b) Wavelength screening for τ_{off} kinetics of ATG-mediated currents. Left: Raw data traces showing the off-kinetics after a 5 s

light-stimulation with 370 nm. Best τ_{off} kinetics were achieved at 425–450 nm light (red trace: exponential fit). Right: Measurement of τ_{off} kinetics for wavelengths between 400 nm and 540 nm light. (c) Relative light intensities depending on wavelengths used. Light intensity for *trans-cis* isomerization (370 nm) approx. 5 mW cm⁻² and for *cis-trans* isomerization approx. 9.5 mW cm⁻².



Supplementary Figure 3. ATG targets NMDARs

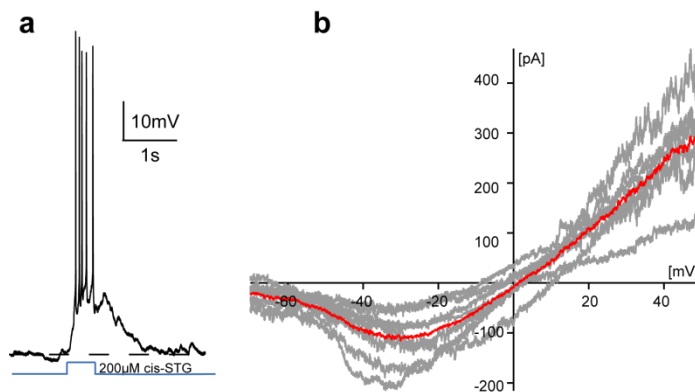
Current-voltage relationship of ATG-mediated currents measured after 3 s of illumination (370 nm) in the presence of NMDAR and AMPAR antagonists in layer 2/3 cortical neurons of acute brain slices. 200 μM ATG was used for all experiments. Black: control Red: 25 μM NBQX (n=8 cells), a selective AMPAR antagonist. Green: 40 μM D-AP-5, a selective NMDAR antagonist (n=3 cells). Blue: 50 μM MK-801, a selective NMDAR blocker (n=5 cells). Single data points represent mean \pm SEM.



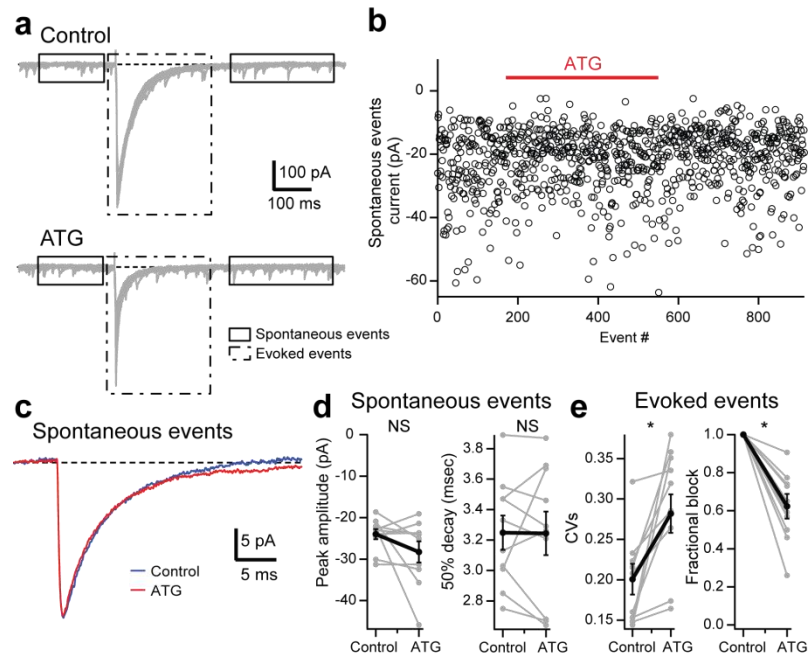
Supplementary Figure 4. ATG activates different NMDA receptor compositions in *Xenopus* oocytes.

NMDA- and *cis*-ATG-mediated currents in oocytes heterologously expressing NMDA receptor subunit combinations in the presence of 1.8 mM barium, 250 µM NFA and 10 µM glycine. Representative current traces in response to transient bath perfusion of 1 mM NMDA (left) and light-mediated currents (365 nm LED illumination, pink) in presence of 200 µM ATG (right) for the NMDA receptor combinations GluN1-1a and (a) GluN2A, (b) GluN2B, (c) GluN2C, and (d) GluN2D. Blue bar indicates 460 nm LED illumination. The insets in (a) and (b) show currents in response to non-saturating NMDA concentrations (10 µM), ruling out the presence of a calcium-induced chloride currents. 460 nm-evoked currents were present for GluN2C and 2D

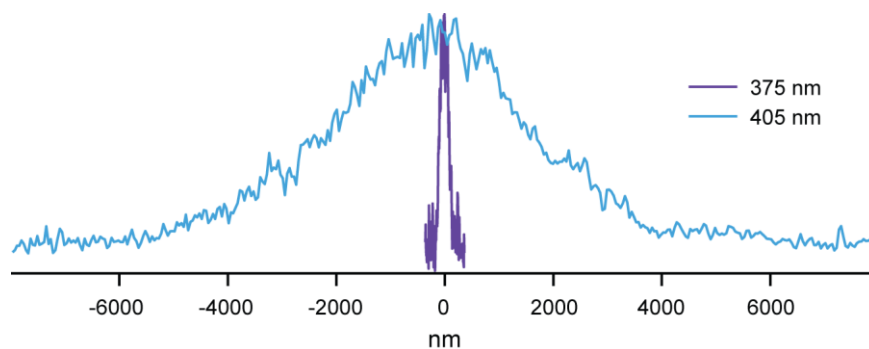
containing receptors. (e) Summary plots showing average steady-state current amplitudes induced by 1 mM NMDA (left) and by 200 μ M *cis*-ATG (center) for all subtype combinations shown in (a). Summary plot of the average within-cell ratio of *cis*-ATG-mediated currents in relation to saturating NMDA-induced currents (right). Average NMDA-evoked currents were larger (GluN1-1a/2A = $-14.93 \pm 1.21 \mu$ A, GluN1-1a/2B = $-8.65 \pm 1.13 \mu$ A, GluN1-1a/2C = $-0.06 \pm 0.01 \mu$ A and GluN1-1a/2D = $-0.29 \pm 0.05 \mu$ A) than *cis*-ATG-mediated currents (GluN1-1a/2A = -217.6 ± 17.5 nA, GluN1-1a/2B = -400.9 ± 65.4 nA, GluN1-1a/2C = -3.46 ± 1.69 nA and GluN1-1a/2D = -5.91 ± 0.57 nA).



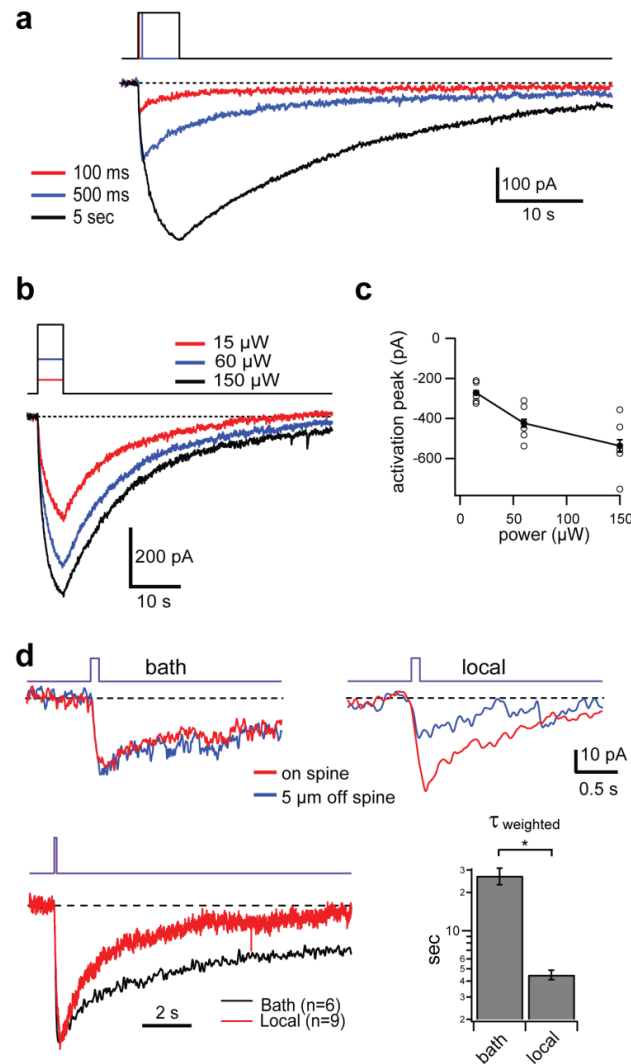
Supplementary Figure 5. Characterization of *cis*-STG in layer 2/3 cortical neurons. (a) Current-clamp recording in layer 2/3 cortical neuron with *cis*-STG. Puff-application of 200 μ M *cis*-STG for 500 ms result in robust action potential firing. (b) Current-voltage relationship of *cis*-STG in cortical neurons. Ramps were performed between -70 mV and 50 mV. Single cell recording are depicted in grey ($n=5$), average trace of all experiments is shown in red.



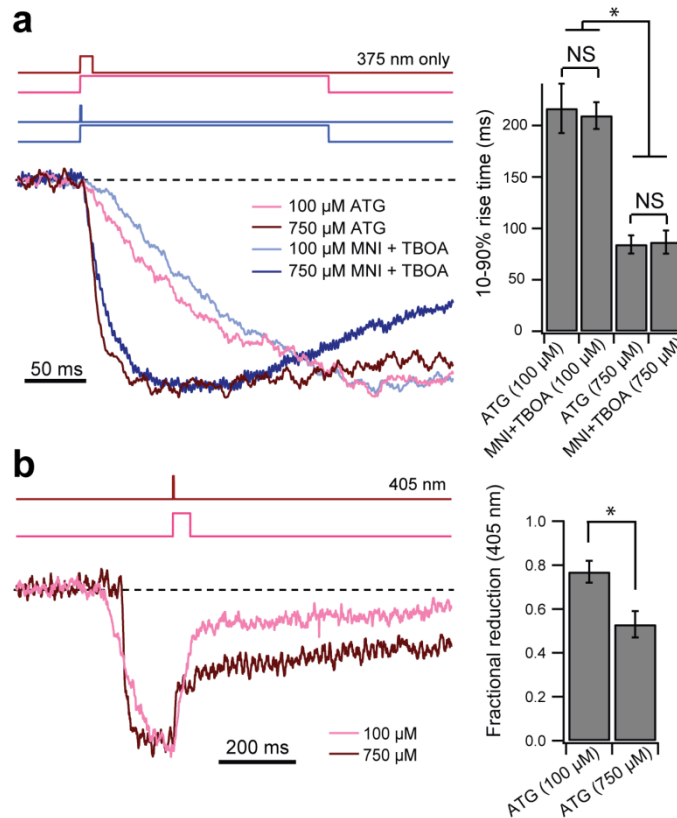
Supplementary Figure 6. Impact of ATG on GABA_A-mediated currents. (a) Spontaneous iGABA_AR currents and evoked IPSCs (elicited with 0.1 Hz stimulation) recorded from a CA1 pyramidal cell from an acute brain slice. (b) Peak amplitude of spontaneous events. After 10 minutes of recording, ATG (400 μ M) was washed in for twenty minutes, and then subsequently washed out. (c) Average spontaneous event currents from example cell shown in a) in control conditions and in the presence of 400 μ M ATG. (d) Summary plots showing the time at which spontaneous IPSCs decayed by 50% in control and in 400 μ M ATG (n=10 cells). (e) Summary plots showing the coefficient of variation and fractional block of IPSCs by 400 μ M ATG (n=10). *, P<0.05, NS indicates comparisons that are not significantly different (Wilcoxon matched pairs signed rank test).



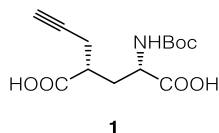
Supplementary Figure 7. One-photon 375 nm and 405 nm laser spot sizes. Relative intensity profile resulting from scanning 100 nm green fluorescence with 375 nm (FWHM = 300 nm) or 405 nm (FWHM = 4.25 μ m) laser illumination.



Supplementary Figure 8. NMDAR currents evoked in hippocampal CA1 pyramidal neurons in acute brain slices by one-photon activation of bath applied ATG. (a) Representative *cis*-ATG-mediated currents in response to 100 ms, 500 ms, and 5 s 375 nm laser illumination of dendrites in the presence of 200 μM ATG. (b) *cis*-ATG-mediated currents were evoked with 5 s 375 nm laser pulses of 15 μW, 60 μW, and 150 μW. (c) The dependence of ATG-evoked peak response on activating laser power for 5 cells. Increasing the power from 50 to 150 μW produces a sublinear increase in *cis*-ATG-mediated current amplitudes, suggesting responses are maximal, potentially due to saturation of ATG conversion or NMDAR occupancy. (d) Top: Distance dependence of *cis*-ATG-mediated responses evoked by 100 ms, 375 nm light pulses using bath and local ATG application (100 μM). A more localized response is achieved using local application of ATG. Traces are averages of 3 trials. Bottom: Decay kinetics of *cis*-ATG-mediated responses (100 ms illumination) in bath and local application. Summary bar graph shows weighted decay time constants (τ_{weighted}) for bath (27.1 ± 4.0 s, n = 6 cells) and local perfusion (local, 4.5 ± 0.4 s, n = 9 cells).*, $P < 0.05$, (Wilcoxon matched pairs signed rank test).

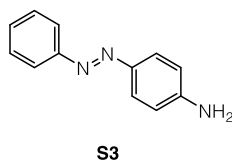


Supplementary Figure 9. Concentration dependence of activation and fractional reduction of CA1 pyramidal cell NMDAR currents for ATG and MNI-glutamate. (a) NMDAR currents evoked by activation of locally applied ATG and uncaging of MNI-glutamate (ATG: 100 μ M (n = 9 cells), and 750 μ M (n = 12); MNI-glutamate: 100 μ M (n = 5), 750 μ M (n = 5)). MNI-glu experiments were performed in TBOA (500 μ M)). There is no significant difference between rise times of NMDAR currents evoked by MNI-glu uncaging and ATG activation for the same concentration. (b) Comparison 405 nm- mediated reduction in NMDAR currents following 375 nm activation at different concentrations $77 \pm 5\%$ for 100 μ M (n = 8 cells) and $53 \pm 6\%$ for 750 μ M (n = 6). Fractional reduction was calculated as $1 - \frac{50 \text{ ms average immediately after } 405 \text{ nm pulse}}{50 \text{ ms average immediately before } 405 \text{ nm pulse}}$. *P<0.05 (Steel Dwass all pairs nonparametric multiple comparison test). The fractional reduction in NMDAR currents by 405 nm light was most effective when working at the lower ATG concentrations, 100 μ M.



(2S,4R)-2-(tert-Butoxycarbonylamino)-4-(prop-2-ynyl)pentanedioic acid (1). To a solution of propargylated pyroglutamate **S1** (528 mg, 1.79 mmol) in THF (50 mL) cooled to 0 °C was added aqueous LiOH (1 M, 50 mL). The resulting mixture was allowed to warm to room temperature and stirred at this temperature for 30 min. The solution was acidified to pH = 1 with aqueous HCl (1 N, 100 mL) and extracted with EtOAc (2 x 200 mL). The combined organic phase was washed with concentrated aqueous NaCl (400 mL), then dried (MgSO₄) and concentrated *in vacuo*. Column chromatography (CH₂Cl₂:MeOH:AcOH:H₂O 90:10:0.6:0.6) afforded diacid **1** (510 mg, 1.79 mmol, 99%) as a white foam.

R_f	0.23 (CH ₂ Cl ₂ :MeOH:AcOH:H ₂ O 90:10:0.6:0.6);
¹H NMR	(400 MHz, CD ₃ OD) δ = 4.21 (dd, <i>J</i> = 10.6, 4.2, 1H), 2.72–2.63 (m, 1H), 2.55–2.48 (m, 2H), 2.35–2.31 (m, 1H), 2.31–2.24 (m, 1H), 1.84 (ddd, <i>J</i> = 14.2, 10.7, 4.0, 1H), 1.44 (s, 9H).
¹³C NMR	(101 MHz, CD ₃ OD) δ = 176.9, 175.8, 158.1, 81.5, 80.5, 71.6, 53.2, 42.2, 33.9, 28.7, 22.5.
IR	(ATR): 3296, 2979, 2934, 2556 (br), 1706, 1515.
HRMS	(ESI): calculated for C ₁₃ H ₁₉ NO ₆ 284.1140, found 284.1147.
[α]_D²²	-12.0 (3.1, MeOH).
Mp.	47–49 °C.

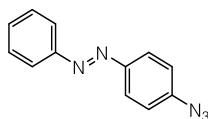


(E)-4-(Phenyldiazenyl)aniline (S3). To a solution of nitrosobenzene (749 mg, 7.0 mmol) in acetic acid (50 mL) was added 1,4-phenylenediamine (**S2**) (756 mg, 7.0 mmol) as a solid and the resulting mixture was stirred at 40 °C for 15 h. The dark solution was allowed to cool to room temperature, then diluted with H₂O (300 mL) and extracted with EtOAc (3 x 300 mL). The combined organic phase was washed further with concentrated aqueous NaCl (2 x 500 mL),

then dried (MgSO_4) and concentrated *in vacuo*. Column chromatography (dry-loaded, hexanes:EtOAc 4:1) afforded (*E*)-4-(phenyldiazenyl)aniline (**S3**) (510 mg, 2.59 mmol, 37%) as an orange solid.

R_f	0.24 (hexanes:EtOAc 4:1).
¹H NMR	(400 MHz, CDCl_3) δ = 7.87–7.80 (m, 4H), 7.49 (t, J = 7.5, 2H), 7.41 (t, J = 7.4, 1H), 6.75 (d, J = 8.9, 2H), 4.04 (br s, 2H).
¹³C NMR	(101 MHz, CDCl_3) δ = 152.9, 149.5, 145.5, 129.8, 128.9, 125.1, 122.3, 114.6.
IR	(ATR): 3348, 1616, 1596.
HRMS	(EI): calculated for $\text{C}_{12}\text{H}_{11}\text{N}_3$ 197.0947, found 197.0954.
Mp.	116–119 °C.

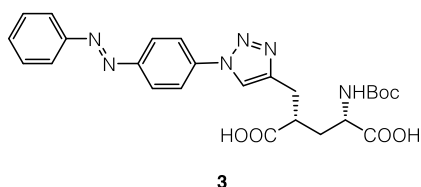
(*E*)-4-(Phenyldiazenyl)aniline can also be prepared *via* a modified literature procedure.² To a suspension of aniline **S2** (9.34 g, 100 mmol) in H_2O (200 mL) was added solid sodium carbonate (5.30 g, 50 mmol) and the mixture was cooled to 0 °C. A solution of sodium nitrite (7.40 g, 107 mmol) in H_2O (100 mL), half-concentrated aqueous HCl (40 mL), and a solution of aniline (9.34 g, 100 mL) in acetic acid (6 mL) were all slowly added in a sequential manner with careful monitoring of the temperature. The mixture was stirred at 0 °C for 30 min, at which point aqueous NaOH (12%, 100 mL) was added, resulting in the formation of an orange solid. The mixture was allowed to warm to room temperature and vigorously stirred at this temperature for 2 h. The suspension was diluted with concentrated aqueous NaCl (200 mL) and extracted with CH_2Cl_2 (500 mL). The organic phase was dried (MgSO_4) and concentrated *in vacuo*. Column chromatography (dry-loaded, hexanes:EtOAc 9:1 to 4:1) afforded (*E*)-4-(phenyldiazenyl)aniline (**S3**) (5.72 g, 30 mmol, 30%) as an orange solid.

**2**

(*E*)-1-(4-Azidophenyl)-2-phenyldiazene (2). To a solution of (*E*)-4-(phenyldiazenyl)aniline (99 mg, 0.50 mmol) in MeCN at 0 °C was added *tert*-butyl nitrite (89 μL , 0.75 mmol) followed by trimethylsilyl azide (97%, 80 μL , 0.60 mmol). The mixture was allowed to warm to room temperature and stirred at this temperature for 1 h, then concentrated *in vacuo*. Flash column

chromatography (dry-loaded, hexanes:CH₂Cl₂ 9:1) afforded azide **2** (98 mg, 88%) as an orange solid.

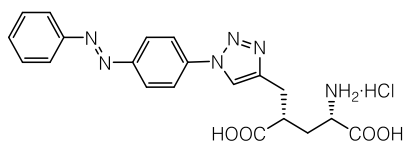
R_f	0.20 (hexanes:CH ₂ Cl ₂ 9:1).
¹H NMR	(400 MHz, CDCl ₃) δ = 7.95 (d, <i>J</i> = 9.0, 2H), 7.91 (dd, <i>J</i> = 8.3, 1.5, 2H), 7.55–7.44 (m, 3H), 7.16 (d, <i>J</i> = 9.0, 2H).
¹³C NMR	(100 MHz, CDCl ₃) δ = 152.6, 149.8, 142.6, 131.0, 129.1, 124.6, 122.8, 119.5.
IR	(ATR): 2107, 1592.
HRMS	(EI): calculated for C ₁₂ H ₉ N ₅ 223.0852, found 223.0858.
Mp.	90–91 °C.



(2*S*,4*S*)-2-(*tert*-Butoxycarbonylamino)-4-((1-(4-((*E*)-phenyldiazenyl)phenyl)-1*H*-1,2,3-triazol-4-yl)methyl)pentanedioic acid (3**).** Alkyne **1** (215 mg, 0.75 mmol) and azide **2** (168 mg, 0.75 mmol) were dissolved in a mixture of MeOH (12 mL) and DMSO (4 mL) by means of ultrasound. Copper(II) sulfate pentahydrate (38 mg, 0.15 mmol), sodium ascorbate (37 mg, 0.19 mmol) and H₂O (4 mL) were added, and the resulting suspension was stirred at room temperature for 24 h. The reaction was allowed to cool to room temperature, then quenched with aqueous HCl (1 N, 50 mL) and extracted with EtOAc (3 x 50 mL). The combined organic phase was washed with aqueous LiCl (10%, 3 x 100 mL) and concentrated aqueous NaCl (100 mL), dried (MgSO₄) and concentrated *in vacuo*. Column chromatography (CH₂Cl₂:MeOH:AcOH:H₂O 90:10:0.6:0.6) afforded the Boc-protected amine **3** (353 mg, 0.69 mmol, 92%) as an orange solid.

R_f	0.26 (CH ₂ Cl ₂ :MeOH:AcOH:H ₂ O 90:10:0.6:0.6).
¹H NMR	(400 MHz, CD ₃ OD, major <i>E</i> isomer quoted) δ = 8.37 (s, 1H), 8.04 (d, <i>J</i> = 9.1, 2H), 7.98 (d, <i>J</i> = 9.1, 2H), 7.92–7.88 (m, 2H), 7.56–7.50 (m, 3H), 4.25 (dd, <i>J</i> = 10.6, 3.9, 1H), 3.21–3.12 (m, 1H), 3.07–2.93 (m, 2H), 2.29 (ddd, <i>J</i> = 13.5, 9.7, 3.9, 1H), 1.89 (ddd, <i>J</i> = 13.6, 10.7, 3.3, 1H), 1.43 (s, 9H).

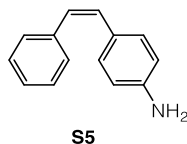
¹³C NMR	(100 MHz, CD ₃ OD, major <i>E</i> isomer quoted) δ = 177.5, 175.8, 158.1, 153.8, 153.3, 147.1, 139.9, 132.8, 130.3, 125.3, 124.0, 122.2, 121.9, 80.5, 53.3, 43.3, 34.4, 29.3, 28.7.
HRMS	(ESI): calculated for C ₂₅ H ₂₈ N ₆ O ₆ 509.2143, found 509.2145.
IR	(ATR): 2978, 2930, 2508 (br), 1700, 1603, 1507.
[α]_D²²	+4.9 (1.63, MeOH).
Mp.	136 °C (decomposition).

*trans*-ATG

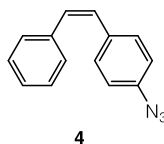
(2*S*,4*S*)-2-Amino-4-((1-(4-((*E*)-phenyldiazenyl)phenyl)-1*H*-1,2,3-triazol-4-

yl)methyl)pentanedioic acid hydrochloride (*trans*-ATG). To solid Boc-protected amine **3** (338 mg, 0.67 mmol) was added concentrated HCl solution in EtOAc (20 mL), prepared by bubbling HCl gas through EtOAc for 1 h, and the resulting mixture was vigorously stirred at room temperature for 3 h. The suspension was diluted with Et₂O (100 mL). The solid was separated, then washed with Et₂O (2 x 50 mL) and dried *in vacuo* to afford amine hydrochloride *trans*-ATG (281 mg, 95%) as an orange solid.

¹H NMR	(600 MHz, CD ₃ OD) δ = 8.48 (s, 1H), 8.13 (d, <i>J</i> = 8.7, 2H), 8.06 (d, <i>J</i> = 8.9, 2H), 7.96 (dd, <i>J</i> = 8.1, 1.5, 2H), 7.60–7.53 (m, 3H), 4.15 (dd, <i>J</i> = 8.1, 6.0, 1H), 3.30–3.22 (m, 1H), 3.20–3.12 (m, 2H), 2.48–2.41 (m, 1H), 2.05 (ddd, <i>J</i> = 14.7, 8.1, 4.6, 1H).
¹³C NMR	(150 MHz, CD ₃ OD) δ = 176.5, 171.4, 153.9, 153.6, 146.5, 139.9, 132.8, 130.4, 125.3, 124.0, 122.7, 122.0, 52.4, 42.4, 32.7, 28.5.
IR	(ATR): 2903 (br), 2612 (br), 1726, 1596, 1507.
HRMS	(ESI): calculated for C ₂₀ H ₂₀ N ₆ O ₄ 409.1619, found 409.1618.
[α]_D²²	+20.2 (0.27, MeOH).
Mp.	171 °C (decomposition).
UV/Vis	λ_{\max} = 331 nm. (5% DMSO in H ₂ O).

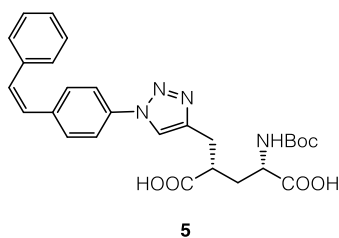


(Z)-4-styrylaniline (S5). (Z)-1-nitro-4-styrylbenzene (**S4**)⁵ (225 mg, 1.00 mmol) was dissolved in EtOH (6.0 mL) and CH₂Cl₂ (6.0 mL), followed by addition of Pd/C (20 mg) and cooling to 0 °C. N₂H₄·H₂O (85%, 38 μL, 1.00 mmol) was then added dropwise under vigorous stirring and the resulting mixture was warmed to room temperature overnight. After 15 h, the mixture was filtered through a pad of celite with CH₂Cl₂ (30 mL). Concentration *in vacuo* gave (Z)-4-styrylaniline **S5** (196 mg, 1.00 mmol, 100%) as a yellow oil. The spectral data matched the one provided in the literature.⁶



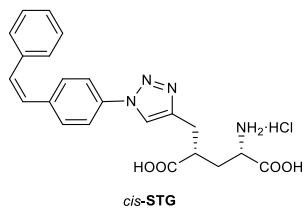
(Z)-1-azido-4-styrylbenzene (4). Amine **S5** (293 mg, 1.50 mmol) was dissolved in MeCN (4 mL) and cooled to 0 °C before *t*-butyl nitrite (267 μL, 2.25 mmol) was added dropwise, immediately followed by trimethylsilyl azide (239 μL, 1.80 mmol). The reaction mixture was stirred at 0 °C for 1 h, then warmed to room temperature and concentrated *in vacuo* to give a dark-red oil. Column chromatography (hexanes:EtOAc 50:1) gave azide **4** (203 mg, 0.92 mmol, 61%) as a yellow oil.

R_f	0.35 (hexanes:EtOAc 9:1).
¹H NMR	(400 MHz, C ₆ D ₆) δ = 7.23–7.19 (m, 2H), 7.08–7.04 (m, 2H), 7.03 (m, 2H), 7.01 (m, 2H), 6.52 (d, <i>J</i> = 8.5, 2H), 6.44 (d, <i>J</i> = 12.2, 1H), 6.33 (d, <i>J</i> = 12.1, 1H)
¹³C NMR	(101 MHz, C ₆ D ₆) δ = 139.2, 137.6, 134.2, 130.7, 130.6, 129.6, 129.2, 128.7, 127.6, 126.9, 119.5.
IR	(ATR): 3213 (w), 3054 (w), 2924 (m), 2412 (w), 2093 (s), 1599 (m), 1503 (s), 1285 (s), 1244 (s), 1181 (m), 832 (s), 696 (s).
HRMS	(EI): calculated for C ₁₄ H ₁₁ N ₃ 221.0953 found 221.0957.



(2S,4S)-2-((tert-Butoxycarbonyl)amino)-4-((1-(4-((Z)-styryl)phenyl)-1H-1,2,3-triazol-4-yl)methyl)pentanedioic acid (5). Alkyne **1** (57 mg, 0.20 mmol) and azide **4** (44 mg, 0.20 mmol) were dissolved in a mixture of MeOH (3 mL), H₂O (1 mL) and DMSO (1 mL) to give a yellow solution. Copper(II) sulfate pentahydrate (10 mg, 0.04 mmol) and sodium ascorbate (10 mg, 0.05 mmol) were added in one portion, and the resulting suspension was stirred at room temperature for 72 h, then quenched with aqueous HCl (1 M, 10 mL) and extracted with EtOAc (3 x 40 mL). The organic phase was washed with aqueous LiCl (10%, 3 x 70 mL) and concentrated aqueous NaCl (100 mL), then dried (MgSO₄), filtered and concentrated *in vacuo* to give a colorless foam. Column chromatography (CH₂Cl₂:MeOH:AcOH:H₂O 90:10:0.6:0.6) gave **5** (82 mg, 0.16 mmol, 81%) as a colorless oil, along with 10% reisolated starting materials.

R_f	0.34 (CH ₂ Cl ₂ :MeOH:AcOH:H ₂ O 90:10:0.6:0.6).
¹H NMR	(400 MHz, CD ₃ OD) δ = 8.26 (s, 1H), 7.77–7.62 (m, 2H), 7.42–7.32 (m, 2H), 7.29–7.15 (m, 5H), 6.73 (d, <i>J</i> = 12.2, 1H), 6.65 (d, <i>J</i> = 12.2, 1H), 4.25–4.10 (m, 1H), 3.13 (dt, <i>J</i> = 11.0, 5.4, 1H), 3.09–2.89 (m, 2H), 2.25 (ddd, <i>J</i> = 13.8, 9.5, 3.8, 1H), 1.85 (ddd, <i>J</i> = 13.5, 10.3, 3.7, 1H), 1.42 (s, 9H), 1.35–1.21 (m, 1H).
¹³C NMR	(101 MHz, CD ₃ OD) δ = 177.8, 176.1, 158.1, 146.9, 139.4, 138.3, 137.0, 132.8, 131.3, 129.9, 129.8, 129.5, 128.5, 122.1, 121.1, 80.5, 53.4, 43.4, 34.5, 29.3, 28.7.
IR	(ATR): 3213 (w), 3054 (w), 2924 (m), 2515 (w), 1702 (s), 1516 (m), 1446 (s), 1231 (s), 1161 (s), 1023 (m), 783 (s), 699 (s).
HRMS	(ESI): calculated for C ₂₇ H ₂₉ N ₄ O ₆ 505.2093, found 505.2084.
[α]_D²²	+8.5 (1.4, MeOH).



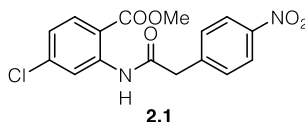
(1S,3S)-1,3-Dicarboxy-4-(1-(4-((Z)-styryl)phenyl)-1H-1,2,3-triazol-4-yl)butan-1-aminium

chloride (*cis*-STG). Boc-Protected *cis*-STG (**5**) (21 mg, 41 μ mol) in EtOAc (0.5 mL) was treated with a solution of concentrated HCl in EtOAc (2 mL), prepared by bubbling HCl gas through anhydrous EtOAc for 40 min. The turbid solution was stirred for 2 h at room temperature. Upon addition of ice-cold Et₂O (5 mL), a colorless precipitate formed, which was centrifuged with Et₂O (3 x 10 mL) and dried *in vacuo* to give *cis*-STG (14 mg, 31 μ mol, 80%) as a colorless solid.

R_f	0.45 (MeCN:H ₂ O 5:1).
¹H NMR	(400 MHz, CD ₃ OD) δ = 8.41 (s, 1H), 7.70 (d, <i>J</i> = 8.6 Hz, 2H), 7.41 (d, <i>J</i> = 8.5 Hz, 2H), 7.31–7.13 (m, 5H), 6.76 (d, <i>J</i> = 12.2 Hz, 1H), 6.68 (d, <i>J</i> = 12.2 Hz, 1H), 4.14 (dd, <i>J</i> = 8.0, 5.9 Hz, 1H), 3.28–3.21 (m, 1H), 3.21–3.05 (m, 2H), 2.42 (ddd, <i>J</i> = 14.6, 8.5, 6.0 Hz, 1H), 2.02 (ddd, <i>J</i> = 14.6, 8.2, 4.3 Hz, 1H).
¹³C NMR	(101 MHz, CD ₃ OD) δ = 176.4, 171.3, 146.0, 139.8, 138.2, 136.7, 133.0, 131.4, 129.9, 129.7, 129.5, 128.5, 123.0, 121.3, 121.2, 52.4, 42.4, 32.6.
IR	(ATR): 3376 (br), 2922 (s), 2515 (br), 1918 (br w), 1720 (s), 1599 (m), 1513 (s), 1446 (m), 1222 (br s), 832 (s), 698 (s).
HRMS	(ESI): calculated for C ₂₂ H ₂₂ N ₄ O ₄ Na: 429.1533 [M+Na] ⁺ found 429.1539 [M+Na] ⁺ .
[α]_D²²	+17.9 (0.96, MeOH).

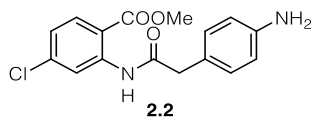
4.3.2 NMDA antagonists

Note: The following compounds were prepared in addition to the compounds described in chapter 2.2.2 and don't appear in the main text.



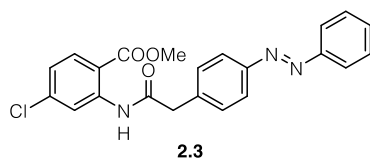
Methyl 4-chloro-2-(2-(4-nitrophenyl)acetamido)benzoate (2.1). 2-(4-nitrophenyl)acetic acid (362 mg, 2.00 mmol, 2.40 eq.) was dissolved in CH₂Cl₂ (7 mL) and cooled to 0 °C before oxalyl chloride solution (2M, 1.30 mL, 2.60 mmol, 3.10 eq.) was added dropwise over 30 min, followed by DMF (2 drops). The solution was warmed to room temperature and stirred for 5 h. After this time, the solvent was removed in a nitrogen stream. The residue was redissolved in CH₂Cl₂ (4 mL) and methyl 2-amino-4-chlorobenzoate (155 mg, 0.83 mmol, 1.00 eq.) was added in one portion. The dark-yellow solution was stirred at room temperature or 15 h. Saturated aqueous NaHCO₃ (5 mL) was added and the solution was extracted with CH₂Cl₂ (3 × 20 mL), then washed with H₂O (15 mL) and saturated aqueous NaCl (15 mL), dried over MgSO₄ and concentrated. The residue was purified by column chromatography (hexanes:EtOAc 2:1) to yield **2.1** (260 mg, 0.75 mmol, 90%) as an off-white solid.

R_f	0.18 (hexanes:EtOAc 2:1). Off-white solid.
¹H NMR	(400 MHz, CDCl ₃) δ = 11.30 (s, 1H), 8.78 (d, <i>J</i> = 1.9, 1H), 8.24 (d, <i>J</i> = 8.3, 2H), 7.94 (d, <i>J</i> = 8.6, 1H), 7.55 (d, <i>J</i> = 8.3, 2H), 7.07 (dd, <i>J</i> = 8.6, 2.0, 1H), 3.89 (s, 3H), 3.87 (s, 2H).
¹³C NMR	(101 MHz, CDCl ₃) δ = 168.3, 168.1, 147.4, 142.0, 141.4, 141.1, 131.9, 130.4, 124.0, 123.3, 120.2, 113.2, 52.6, 45.2.
IR	(ATR): 2956, 2924, 1695, 1692, 1581, 1521, 1431, 1347, 1313, 1254, 1104, 778.
HRMS	(ESI): calculated for C ₁₆ H ₁₂ ClN ₂ O ₅ 347.0440, found 347.0439.
Mp	159–163 °C.



Methyl 2-(2-(4-aminophenyl)acetamido)-4-chlorobenzoate (2.2). Methyl 2-(2-(4-aminophenyl)acetamido)-4-chlorobenzoate (**2.1**) (45 mg, 0.13 mmol, 1.0 eq.) was dissolved in EtOH (4 mL) and H₂O (2 mL) before zinc powder (0.26 g, 3.9 mmol, 30 eq.) and CaCl₂·6H₂O (29 mg, 0.26 mmol, 2.0 eq.) were added in one portion. The suspension was stirred at 80 °C for 3 h, then cooled to room temperature and filtered over a plug of celite with EtOAc (30 mL). The filtrate was diluted with H₂O (10 mL) and the phases were separated. The aqueous phase was extracted with EtOAc (3 × 20 mL). The combined organic phases were washed with saturated aqueous NaCl (30 mL), dried over MgSO₄ and concentrated. The residue was purified by column chromatography (hexanes:EtOAc 2:1) to yield **2.2** (1.18 g, 3.38 mmol, 75%) as a yellow solid.

R_f	0.18 (hexanes:EtOAc 1:1). Yellow solid.
¹H NMR	(400 MHz, CDCl ₃) δ = 11.01 (s, 1H), 8.82 (d, <i>J</i> = 1.9, 1H), 7.90 (d, <i>J</i> = 8.5, 1H), 7.15 (d, <i>J</i> = 8.1, 2H), 7.01 (dd, <i>J</i> = 8.6, 2.0, 1H), 6.69 (d, <i>J</i> = 8.0, 2H), 3.85 (s, 3H), 3.76–3.64 (br s, 2H), 3.64 (s, 2H).
¹³C NMR	(101 MHz, CDCl ₃) δ = 171.1, 167.9, 145.8, 142.4, 140.9, 131.9, 130.5, 123.9, 122.8, 120.4, 115.6, 113.4, 52.5, 45.1.
IR	(ATR): 3362, 3259, 2923, 1688, 1599, 1579, 1513, 1437, 1412, 1252, 1104, 776.
HRMS	(ESI): calculated for C ₁₆ H ₁₆ ClN ₂ O ₃ 319.0844, found 319.0845.
Mp	116–120 °C.

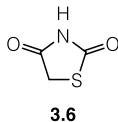


Methyl 4-chloro-2-(2-(4-(phenyldiazenyl)phenyl)acetamido)benzoate (2.3). To a solution of **2.2** (32 mg, 0.10 mmol, 1.0 eq) in MeOH (0.8 mL) was added acetic acid (0.8 mL) followed by nitrosobenzene (16 mg, 0.15 mmol, 1.5 eq) at room temperature. The mixture was stirred at 45 °C for 24 h, at which point LC-MS analysis showed full conversion. Saturated aqueous NaHCO₃ (5 mL) was added at room temperature after dilution with EtOAc (10 mL). After

extraction of the aqueous phase with EtOAc (3×10 mL), the combined organic phases were washed with saturated aqueous NaCl (15 mL), dried and evaporated to give a red oil that was purified by column chromatography (hexanes:EtOAc 6:1) to give **32** (35 mg, 86 μ mol, 86%) as an orange solid.

R_f	0.35 (hexanes:EtOAc 5:1). orange solid.
¹H NMR	(400 MHz, CDCl ₃) δ = 11.22 (s, 1H), 8.83 (d, J = 2.1, 1H), 7.99–7.85 (m, 5H), 7.58–7.43 (m, 5H), 7.04 (dd, J = 8.6, 2.1, 1H), 3.86 (s, 3H), 3.84 (s, 2H). (<i>10:1 mixture of isomers, major isomer quoted</i>).
¹³C NMR	(101 MHz, CDCl ₃) δ = 168.0, 152.7, 152.0, 142.3, 141.1, 137.2, 132.0, 131.1, 130.3, 129.2, 123.5, 123.1, 123.0, 120.4, 113.4, 52.6, 45.7.
IR	(ATR): 3257, 3060, 2926, 1688, 1579, 1513, 1413, 1312, 1251, 1103, 1016, 836, 775, 688.
HRMS	(ESI): calculated for C ₂₂ H ₁₉ ClN ₃ O ₃ 408.1109, found 408.1114.

4.4 Supporting information for chapter 3: Photoswitchable PPAR γ agonists

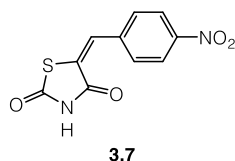


Thiazolidine-2,4-dione (3.6). Thiazolidine-2,4-dione (**3.6**) was prepared according to a literature procedure in 27% yield. Recrystallization from EtOH yielded colorless crystals suitable for X-ray diffraction. The data are in good agreement with the literature.^[378]

¹H NMR (400 MHz, DMSO-*d*₆) δ = 12.03 (s, 1H), 4.14 (s, 2H).

¹³C NMR (101 MHz, DMSO) δ = 174.0, 173.2, 35.9.

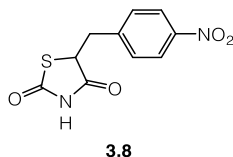
HRMS (EI): calculated for C₃H₃NO₂S 116.9879, found 116.9846.



(E)-5-(4-Nitrobenzylidene)thiazolidine-2,4-dione (3.7). 4-Nitrobenzaldehyde (1.2 g, 8.0 mmol, 1.0 eq.) and thiazolidine-2,4-dione (0.94 g, 8.0 mmol, 1.0 eq.) were dissolved in absolute EtOH (16 mL) before piperidine (80 μ L, 0.80 mmol, 0.10 eq.) and AcOH (46 μ L, 0.80 mmol, 0.10 eq.) were added. The mixture was stirred at 80 °C for 24 h, then cooled to 0 °C, filtered and the residue washed with toluene (20 mL) to give **3.7** (1.2 g, 4.8 mmol, 60%) as a yellow solid. The data are in good agreement with the literature.^[378]

R_f 0.40 (hexanes:EtOAc 2:1). Yellow solid.

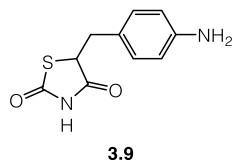
¹H NMR (400 MHz, DMSO-*d*₆) δ = 12.8 (s, 1H), 8.34 (d, *J* = 8.7, 2H), 7.90 (s, 1H), 7.87 (d, *J* = 8.7, 2H).



(E)-5-(4-Aminobenzylidene)thiazolidine-2,4-dione (3.8). Thiazolidinedione **3.7** (90 mg, 0.36 mmol, 1.0 eq.) was dissolved in toluene (5 mL) before oven-dried silica gel (0.36 g) and Hantzsch ester (0.12 g, 0.47 mmol, 1.3 eq.) were added. The mixture was stirred at 100 °C for 24 h, then cooled to room temperature, filtered over Celite with EtOAc (30 mL). The solution was washed with 1 M HCl (2 × 10 mL) and saturated aqueous NaCl (20 mL), dried with MgSO₄ and concentrated to give a yellow oil which was purified by column chromatography (hexanes:EtOAc 4:1) to give **3.8** (43 mg, 0.17 mmol, 47%) as an off-white solid. The data are in good agreement with the literature.^[378]

R_f 0.40 (hexanes:EtOAc 2:1). Off-white solid.

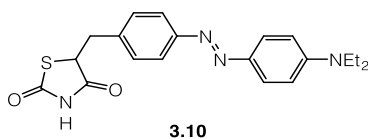
¹H NMR (400 MHz, CD₃OD) δ = 8.20 (d, *J* = 8.2, 2H), 7.54 (d, *J* = 8.2, 2H), 4.84 (dd, *J* = 8.5, 4.5, 1H), 3.56 (dd, *J* = 14.1, 4.6, 1H), 3.35 (dd, *J* = 14.2, 8.6, 1H).



5-(4-aminobenzyl)thiazolidine-2,4-dione (3.9). 5-(4-Nitrobenzyl)thiazolidine-2,4-dione (**3.8**) (43 mg, 0.17 mmol, 1.0 eq) was dissolved in MeOH (1.5 mL) and DMSO (0.5 mL) before Pd/C (10wt%, spatula tip) was added. The headspace was purged with hydrogen three times and the suspension was stirred for 16 h. The reaction mixture was filtered over Celite with EtOAc (30 mL). The solution was washed with 10% aqueous LiCl (4 × 10 mL), dried with MgSO₄ and concentrated to give **3.9** (35 mg, 0.16 mmol, 93%) a yellow oil. The data are in good agreement with the literature.^[378]

R_f 0.10 (hexanes:EtOAc 2:1). Yellow oil.

¹H NMR (400 MHz, DMSO-d₆) δ = 11.98 (br s, 1H), 6.88 (d, *J* = 7.9, 2H), 6.48 (d, *J* = 7.8, 2H), 4.79 (dd, *J* = 9.3, 4.0, 1H), 3.19 (dd, *J* = 14.2, 4.3, 1H), 2.91 (dd, *J* = 14.0, 9.1, 1H).



5-(4-((4-(Diethylamino)phenyl)diazenyl)benzyl)thiazolidine-2,4-dione (3.10). To a solution of **3.9** (22 mg, 0.10 mmol, 1.0 eq.) in MeOH (0.5 mL) was added NaNO₂ (8.3 mg, 0.12 mmol, 1.2 eq.) in H₂O (0.5 mL), followed by 1 M HCl (0.3 mL, 0.3 mmol). The resulting faintly yellow mixture was stirred at 0 °C for 1 h before NaOAc·3H₂O (41 mg, 0.3 mmol, 3.0 eq.) and *N,N*-diethylaniline (19 μL, 0.12 mmol, 1.2 eq.) were added sequentially. The cloudy yellow solution was stirred at room temperature for 15 h. The resulting dark-red suspension was diluted with EtOAc (20 mL). The organic layer was washed with saturated aqueous NH₄Cl (10 mL), saturated aqueous NaCl (10 mL), then dried with MgSO₄ and concentrated *in vacuo*. The resulting red solid was purified *via* column chromatography (CH₂Cl₂:acetone 100:0.5) to afford **3.10** (15 mg, 39 μmol, 39%) as an orange solid.

R_f 0.69 (hexanes:EtOAc 1:1). Orange solid.

¹H NMR (400 MHz, CDCl₃) δ = 7.87–7.82 (m, 3H), 7.78 (d, *J* = 8.0, 3H), 7.33 (d, *J* = 8.0, 2H), 6.72 (d, *J* = 8.8, 2H), 4.58 (dd, *J* = 9.8, 3.9, 1H), 3.59 (dd, *J* = 14.1, 3.9, 1H), 3.46 (q, *J* = 7.1, 4H), 3.21 (dd, *J* = 14.0, 9.7, 1H), 1.23 (t, *J* = 7.0, 6H).

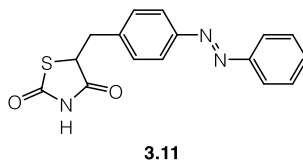
¹³C NMR (101 MHz, CDCl₃) δ = 173.4, 169.6, 152.8, 150.3, 143.1, 136.5, 129.9, 125.4, 122.5, 110.9, 53.3, 44.7, 38.4, 12.7.

IR (ATR): 3198, 3061, 2973, 2927, 1754, 1697, 1599, 1515, 1397, 1354, 1271, 1125, 1077, 822.

HRMS (EI): calculated for C₂₀H₂₂N₄O₂S 382.1463, found 382.1457.

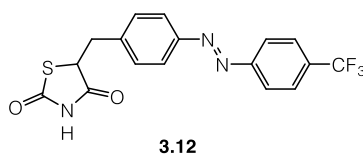
Mp. 158–161 °C.

UV-Vis (50 μM in DMSO): λ_{max} = 440 nm.



5-(4-(Phenyldiazenyl)benzyl)thiazolidine-2,4-dione (3.11). To a solution of **3.9** (35 mg, 0.16 mmol, 1.0 eq.) in AcOH (0.8 mL) and MeOH (0.8 mL) was added nitrosobenzene (19 mg, 0.18 mmol, 1.1 eq.). The resulting mixture was stirred at room temperature for 16 h, during which it turned from light-green to dark-red. The dark-red solution was concentrated and the residue diluted with EtOAc (25 mL). The organic layer was washed with saturated aqueous NaHCO₃ (8 mL), saturated aqueous NaCl (10 mL), then dried with MgSO₄ and concentrated *in vacuo*. The resulting yellow oil was purified *via* column chromatography (CH₂Cl₂:acetone 100:0.5) to afford **3.11** (23 mg, 74 μmol, 46%) as an orange solid.

R_f	0.30 (hexanes:EtOAc 2:1). Yellow-orange solid.
¹H NMR	(400 MHz, CDCl ₃) δ = 8.23 (s, 1H), 7.96–7.85 (m, 4H), 7.56–7.48 (m, 3H), 7.39 (d, <i>J</i> = 8.0, 2H), 4.60 (dd, <i>J</i> = 9.6, 4.0, 1H), 3.61 (dd, <i>J</i> = 14.1, 4.0, 1H), 3.26 (dd, <i>J</i> = 14.1, 9.5, 1H).
¹³C NMR	(101 MHz, CDCl ₃) δ = 173.6, 169.8, 152.6, 152.1, 138.6, 131.2, 130.1, 129.1, 123.3, 122.9, 53.0, 38.4.
IR	(ATR): 3179, 3059, 2810, 1756, 1675, 1326, 1155.
HRMS	(EI): calculated for C ₁₆ H ₁₃ N ₃ O ₂ S 311.0728, found 311.0721.
Mp.	149–152 °C.
UV-Vis	(50 μM in DMSO): λ _{max} (<i>trans</i> -π-π*) = 326 nm, λ _{max} (<i>trans</i> -n-π*) = 438 nm.



5-(4-((4-(Trifluoromethyl)phenyl)diazenyl)benzyl)thiazolidine-2,4-dione (3.12). To a solution of **3.9** (22 mg, 0.10 mmol) in AcOH (0.5 mL) and MeOH (0.5 mL) was added 1-nitroso-4-(trifluoromethyl)benzene (19 mg, 0.18 mmol, 1.8 eq.). The resulting mixture was stirred at 35 °C for 23 h, during which it turned from light-green gradually to dark-red. The dark-red solution was concentrated and the residue diluted with EtOAc (20 mL). The organic phase was washed

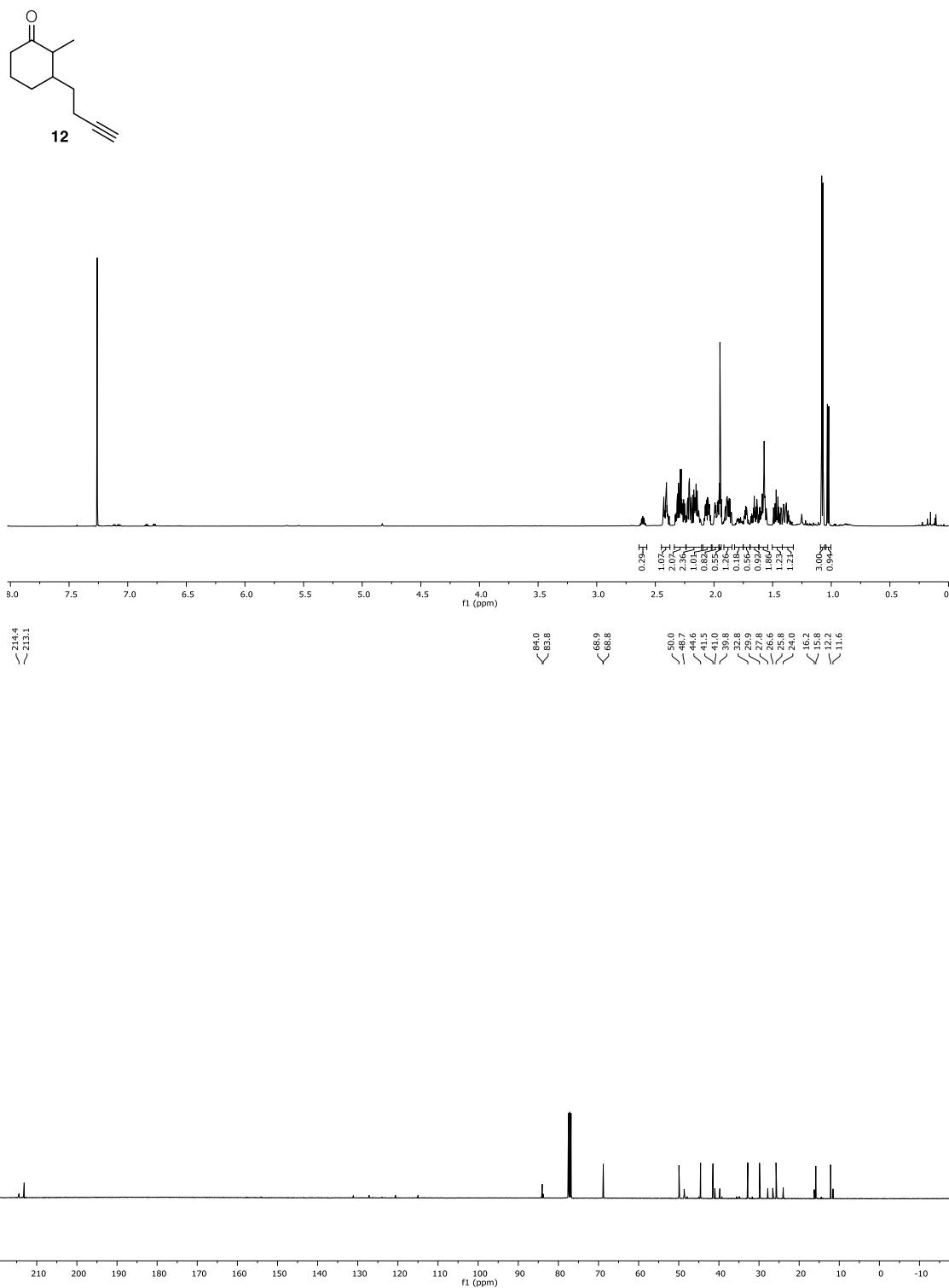
with saturated aqueous NaHCO₃ (6 mL), H₂O (6 mL), saturated aqueous NaCl (6 mL), then dried with MgSO₄ and concentrated *in vacuo*. The resulting orange oil was purified *via* column chromatography (CH₂Cl₂:acetone 100:0.5 to 100:1) to afford **3.12** (25 mg, 66%) as an orange solid.

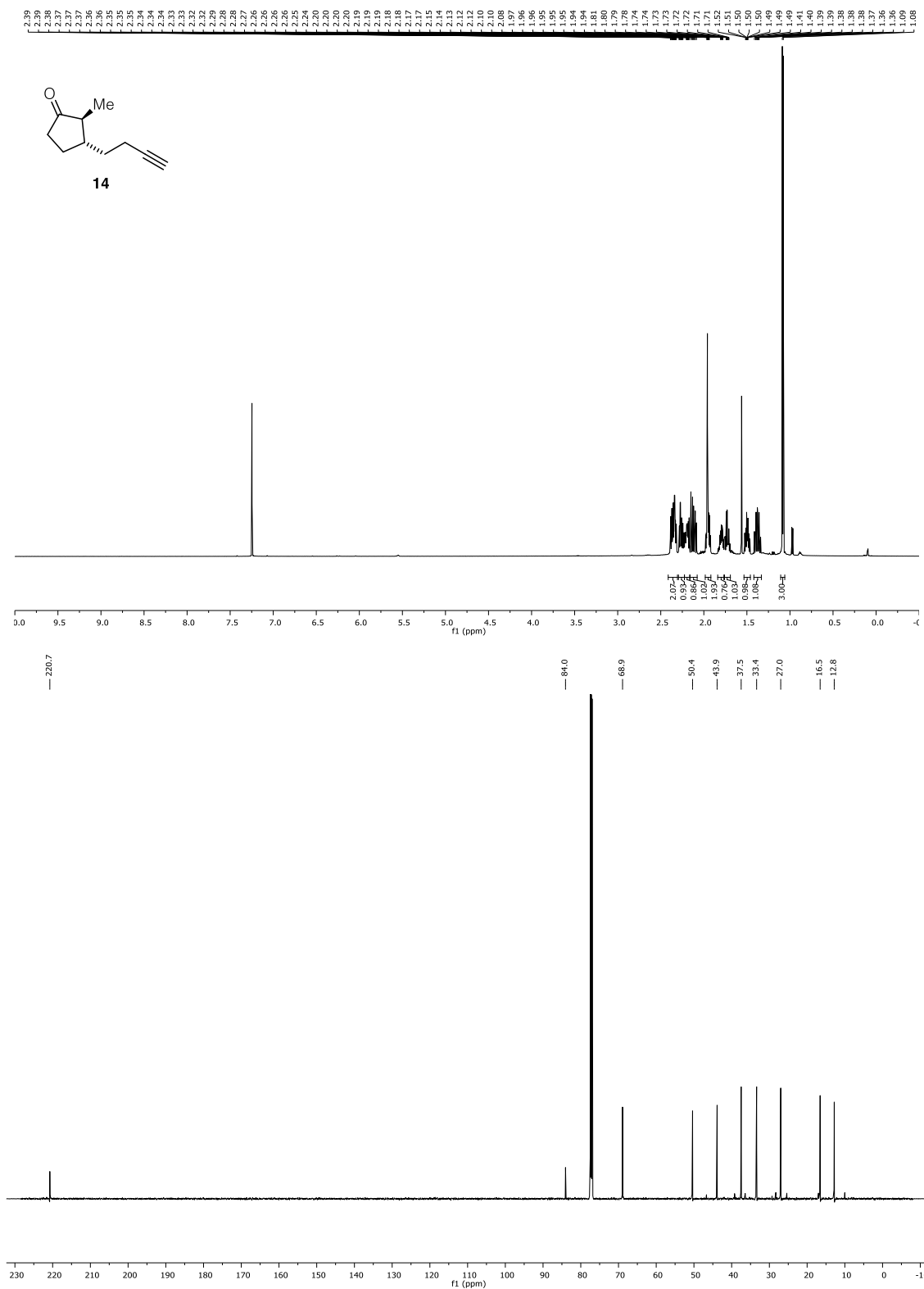
R_f	0.73 (hexanes:EtOAc 1:1). Yellow-orange solid.
¹H NMR	(400 MHz, CDCl ₃) δ = 8.29–8.15 (m, 1H), 8.00 (d, <i>J</i> = 8.2, 2H), 7.93 (d, <i>J</i> = 7.9, 2H), 7.79 (d, <i>J</i> = 8.1, 2H), 7.42 (d, <i>J</i> = 8.0, 2H), 4.61 (dd, <i>J</i> = 9.4, 3.9, 1H), 3.61 (dd, <i>J</i> = 14.2, 4.0, 1H), 3.28 (dd, <i>J</i> = 14.1, 9.4, 1H).
¹³C NMR	(101 MHz, CDCl ₃) δ = 173.7, 169.8, 154.5, 151.9, 139.6, 133.8 (q, <i>J</i> = 32.2), 130.3, 126.5 (q, <i>J</i> = 3.6), 124.1 (q, <i>J</i> = 270.1), 123.8, 123.2, 53.0, 38.5.
¹⁹F NMR	(400 MHz, CDCl ₃) δ = -62.58.
IR	(ATR): 3196, 3059, 2925, 2759, 1758, 1675, 1661, 1500, 1414, 1328, 1160, 1125, 1064.
HRMS	(EI): calculated for C ₁₇ H ₁₂ F ₃ N ₃ O ₂ S 379.0602, found 379.0601.
Mp	136–140 °C.
UV-Vis	(50 μM in DMSO): λ _{max} (<i>trans</i> -π-π*) = 332 nm, λ _{max} (<i>trans</i> -n-π*) = 435 nm.

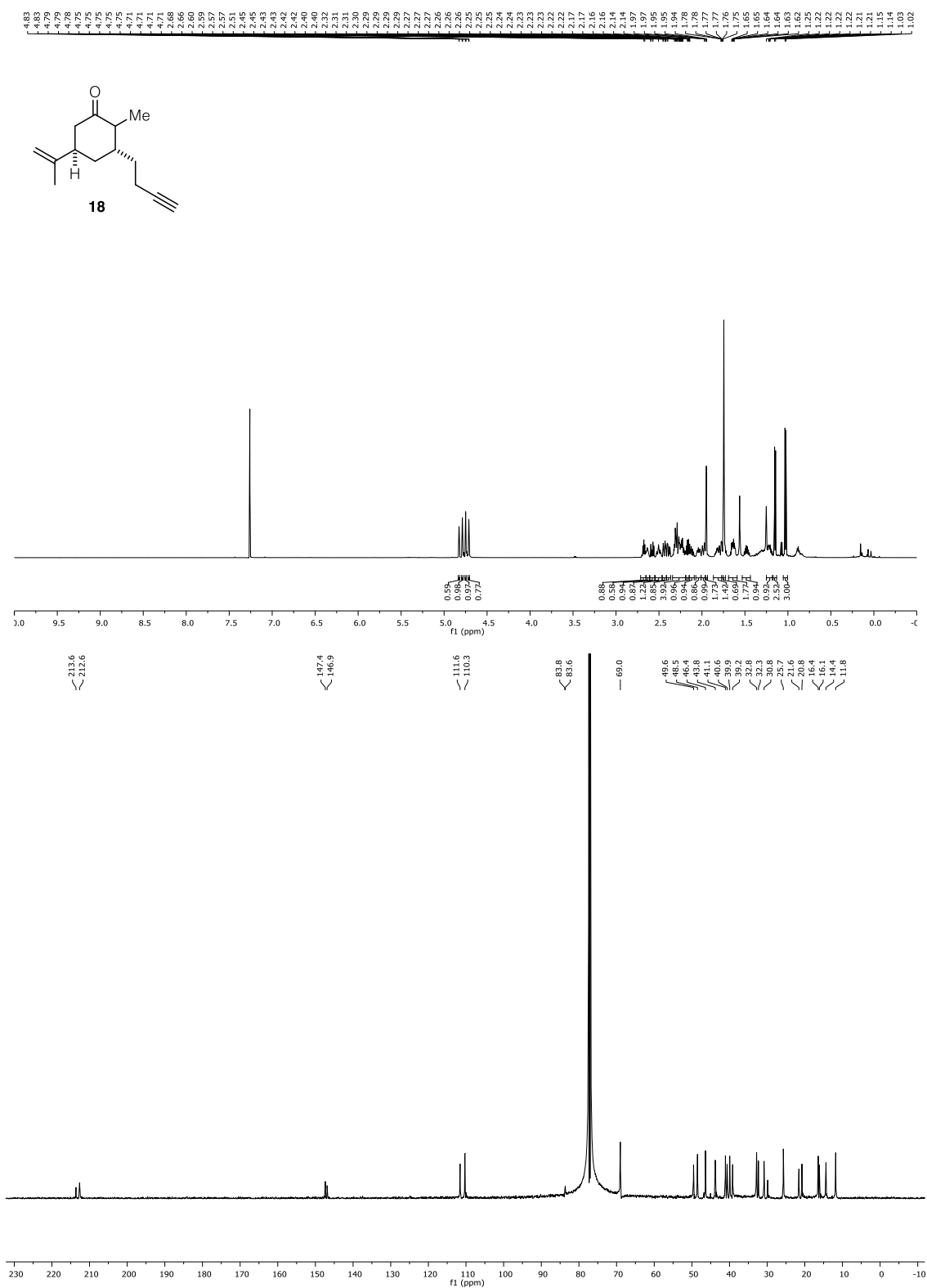
5 NMR spectra

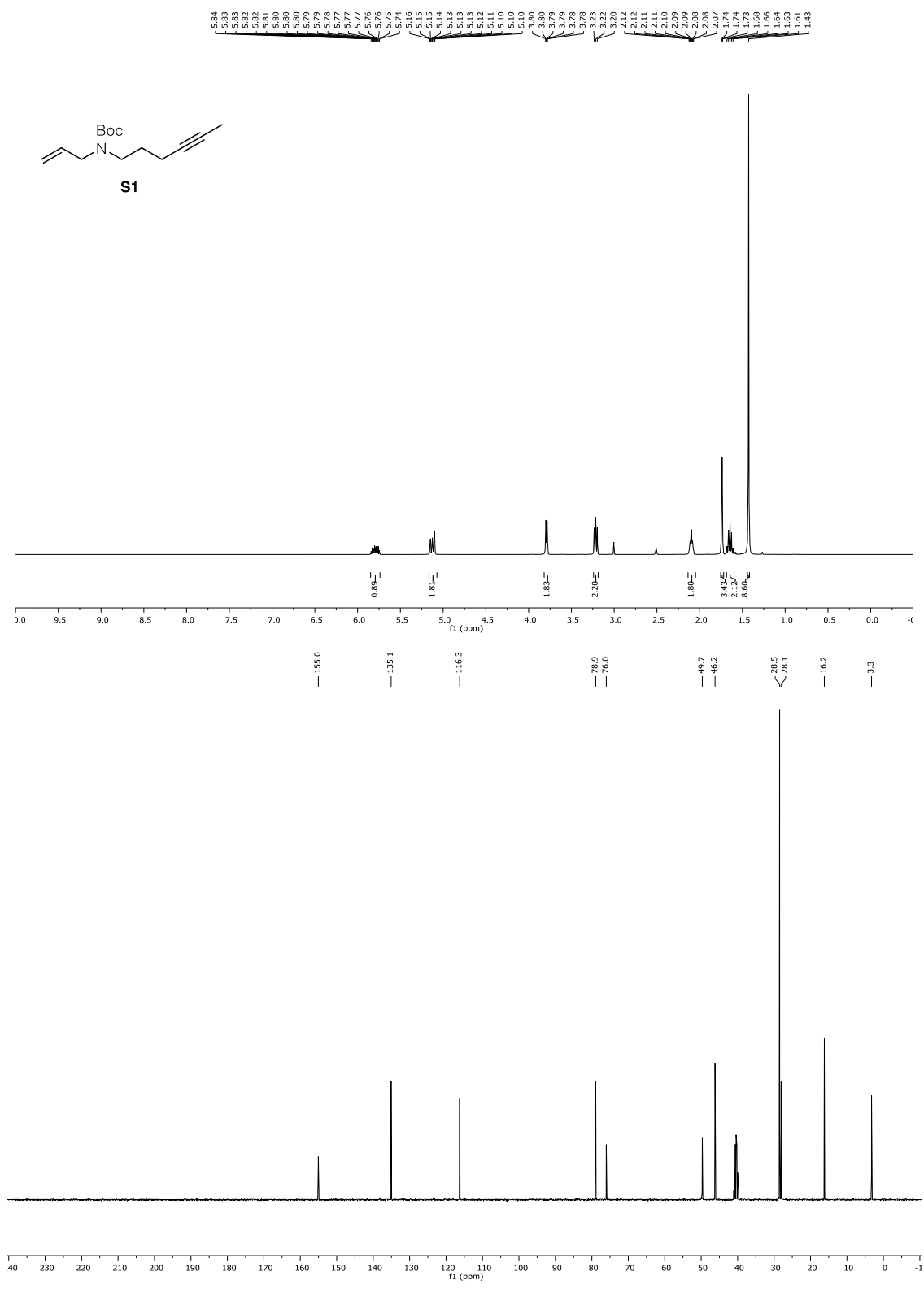
The spectra are numbered and ordered as they appear in the main text. In the case of published manuscripts, the numbering is adapted from the manuscript.

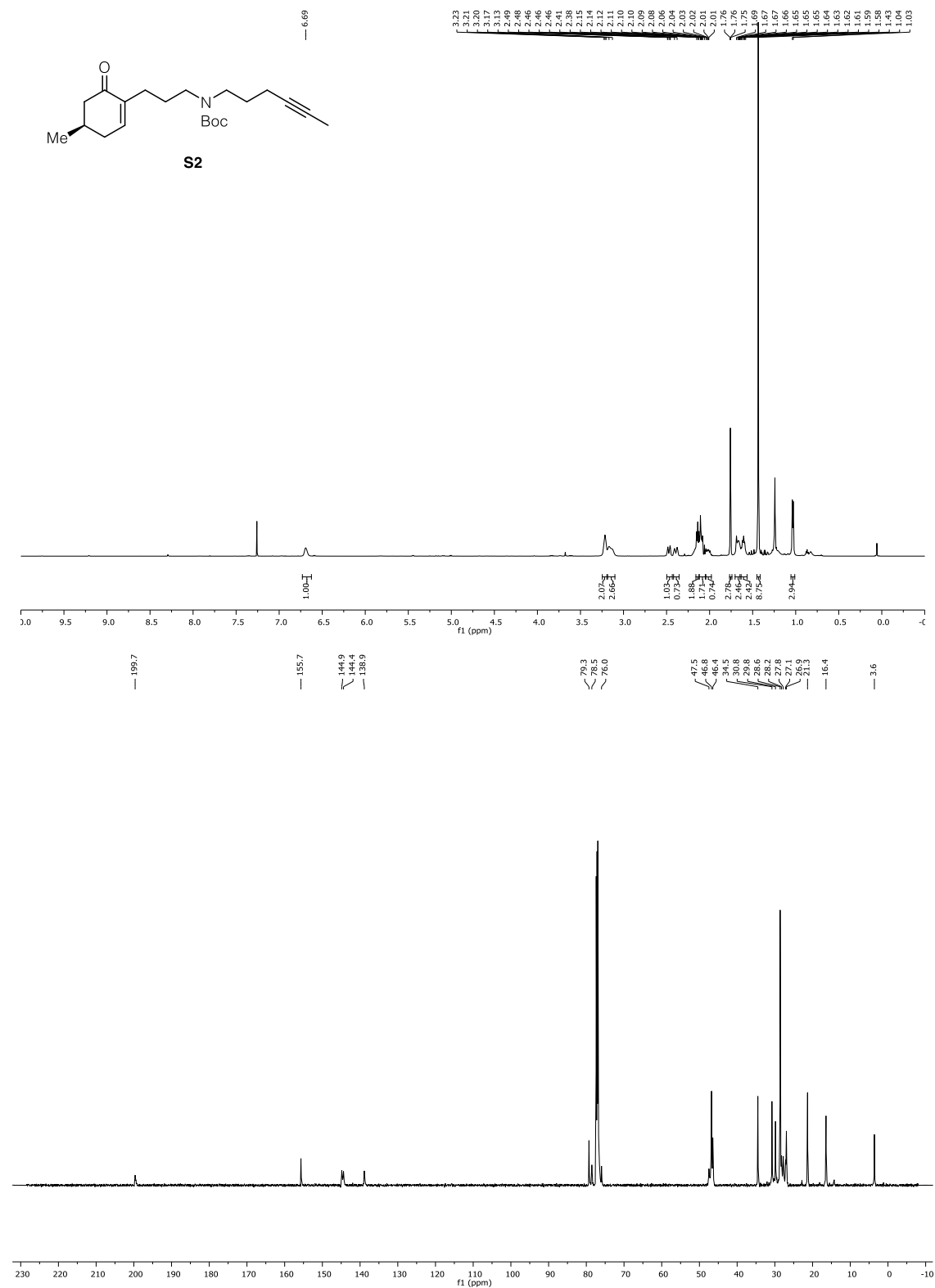
5.1 ^1H and ^{13}C NMR spectra for chapter 4.2.1.1

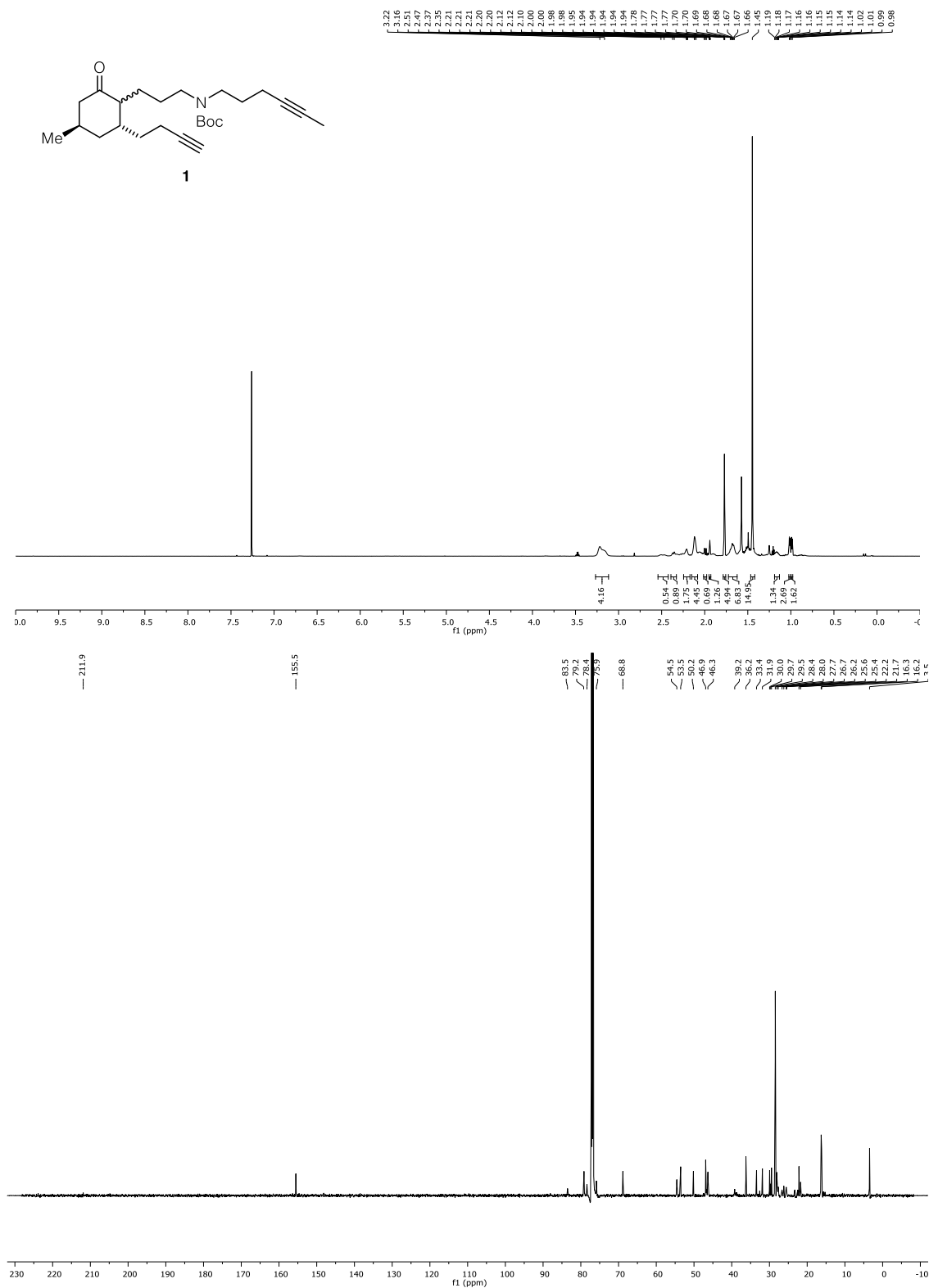


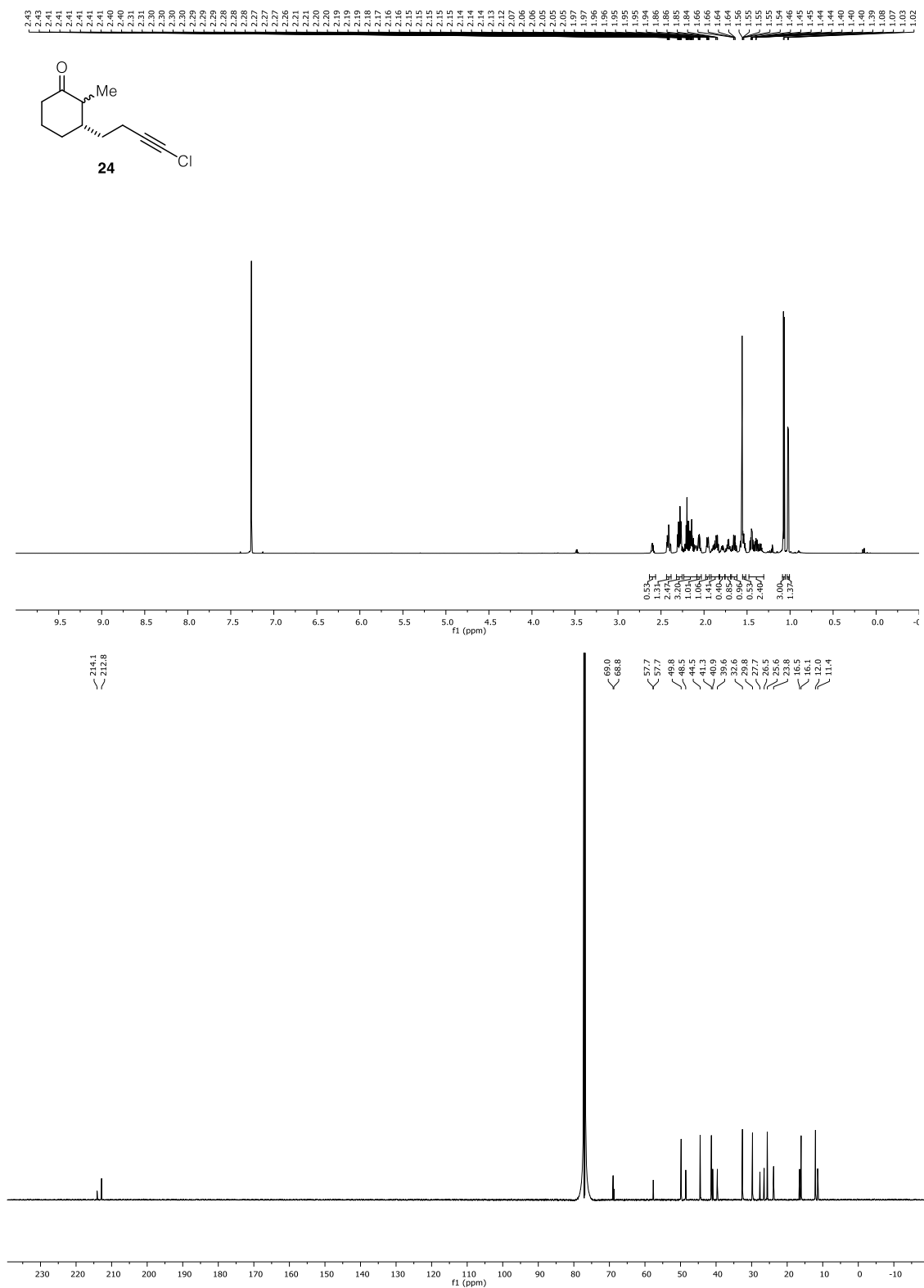


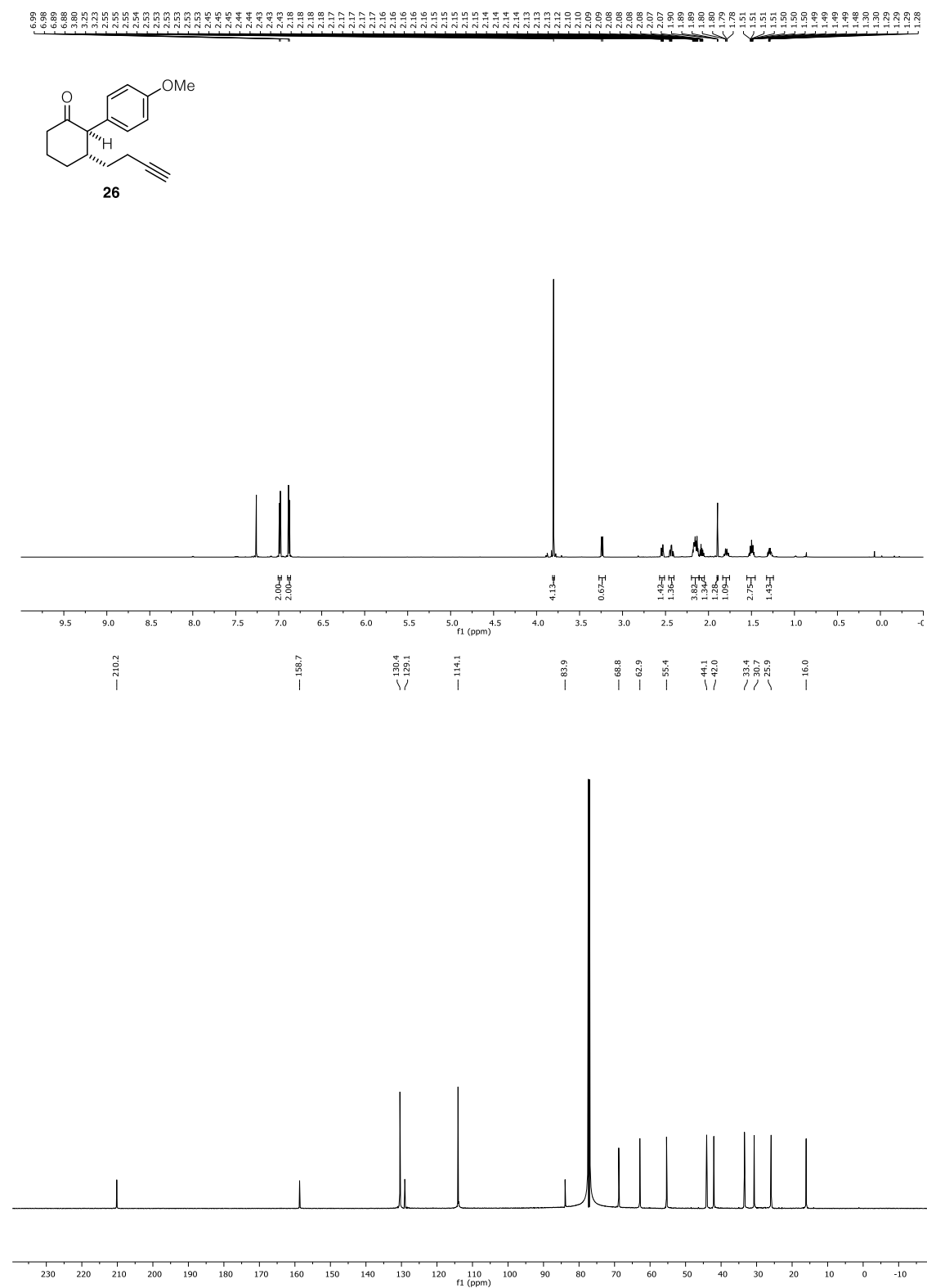




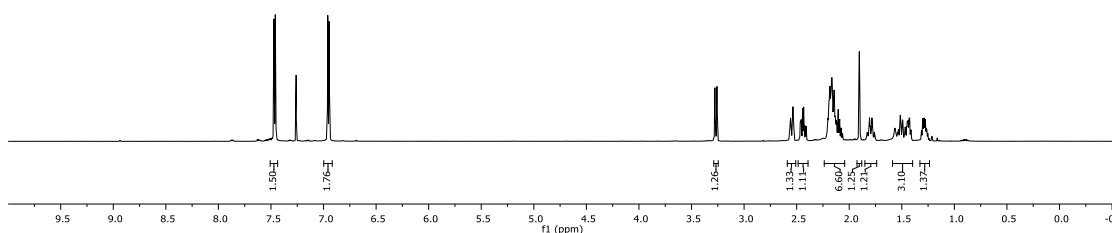
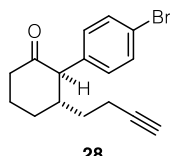




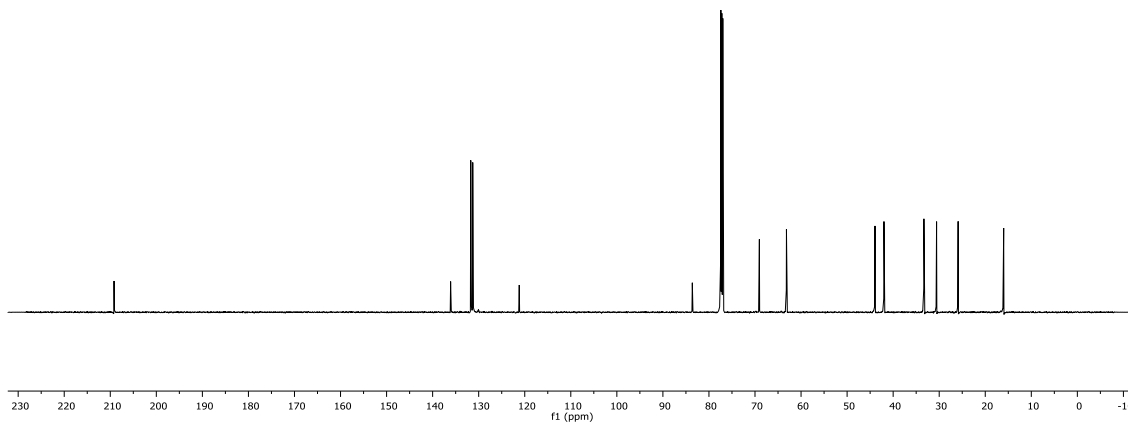


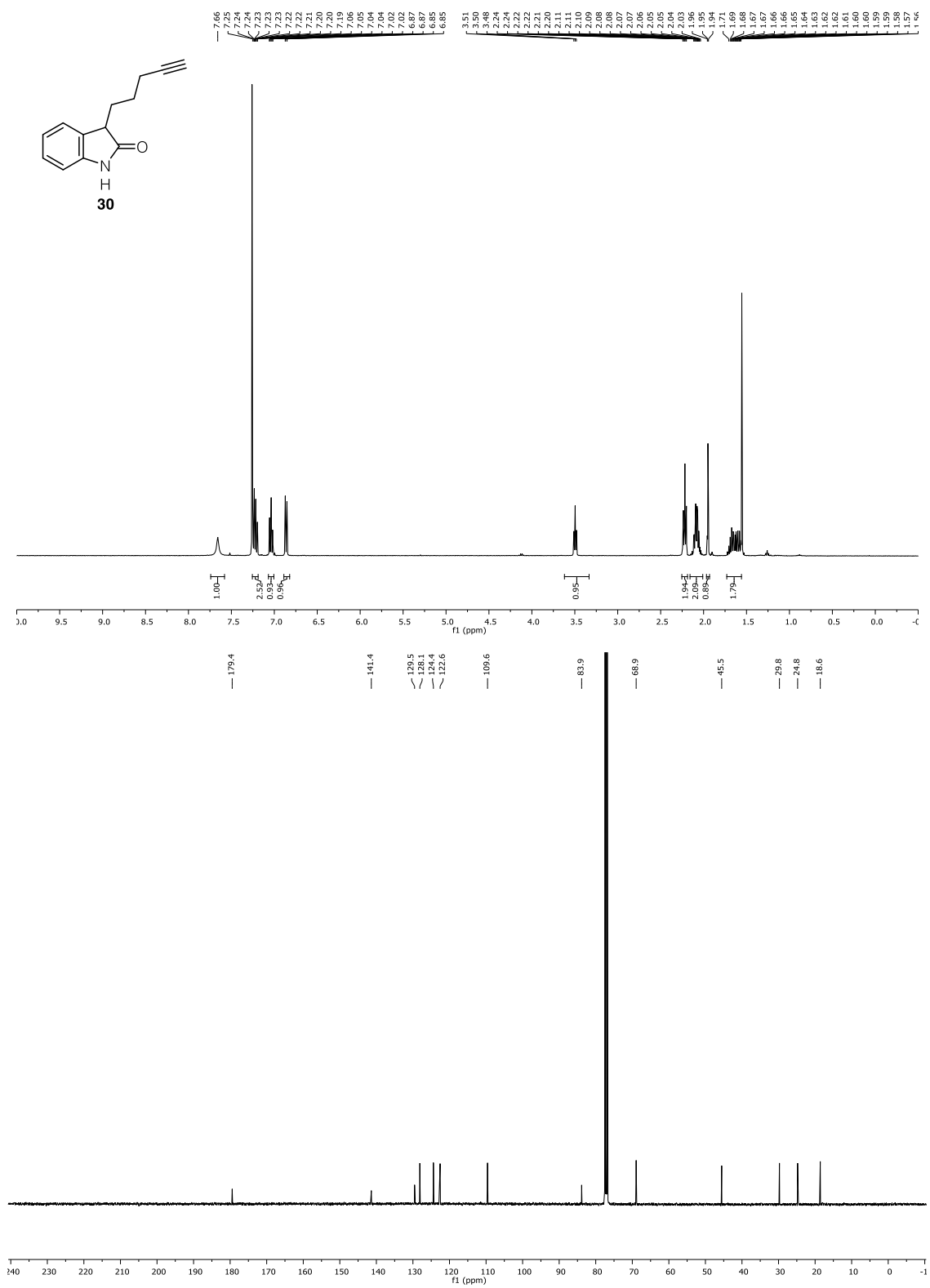


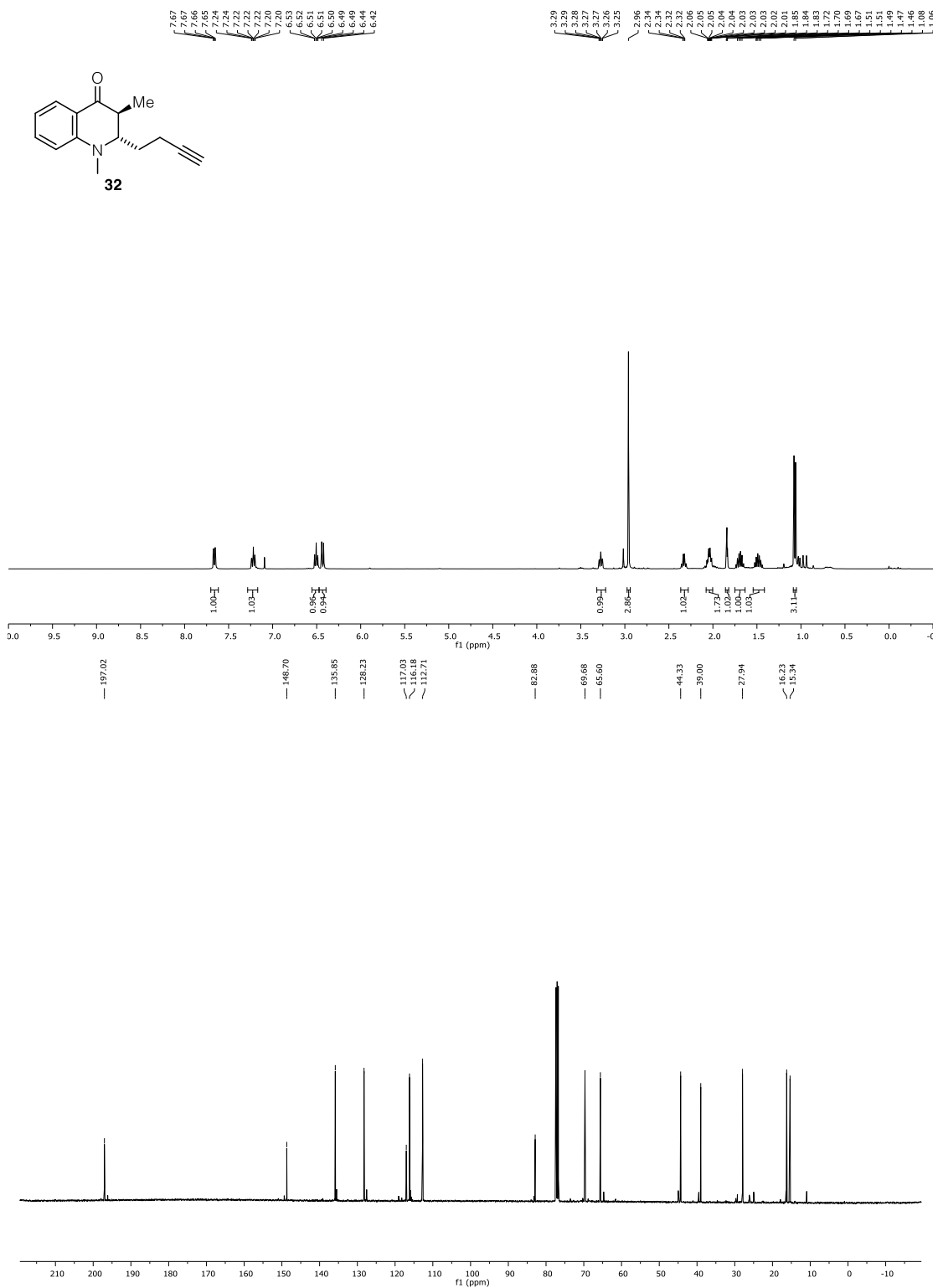
7.47
7.46
6.96
3.328
3.28
3.26
2.86
2.85
2.80
2.796
2.756
2.55
2.54
2.54
2.54
2.53
2.53
2.47
2.46
2.44
2.43
2.41
2.21
2.20
2.20
2.20
2.19
2.18
2.18
2.18
2.17
2.16
2.16
2.15
2.15
2.14
2.14
2.14
2.13
2.13
2.13
2.13
2.12
2.12
2.12
2.11
2.11
2.10
2.10
2.09
2.09
1.91
1.91
1.90
1.90
1.80
1.81
1.78
1.52
1.51
1.51
1.49
1.49
1.49
1.45
1.44
1.44
1.43
1.43
1.36
1.30
1.30
1.29
1.28
1.28

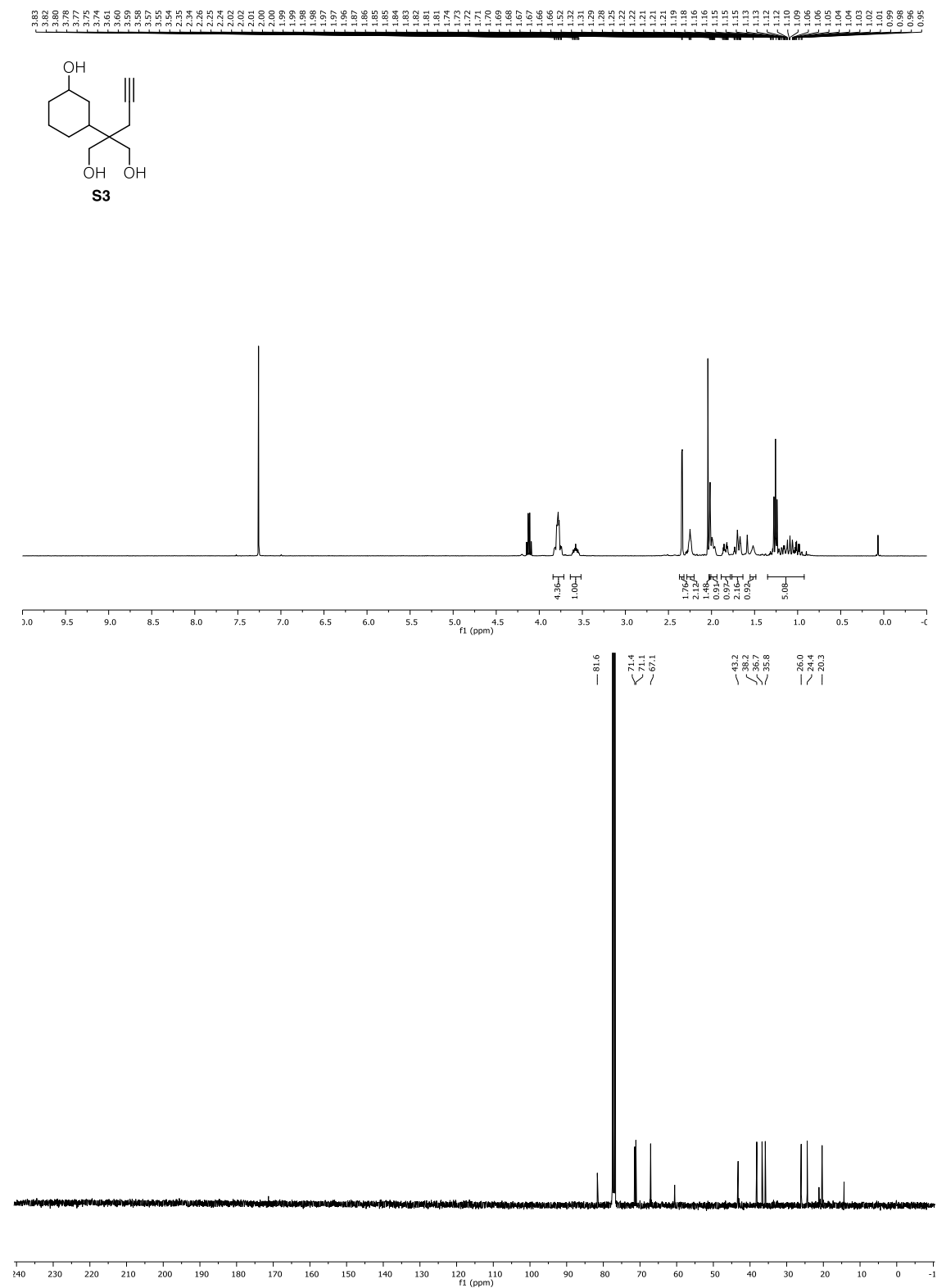


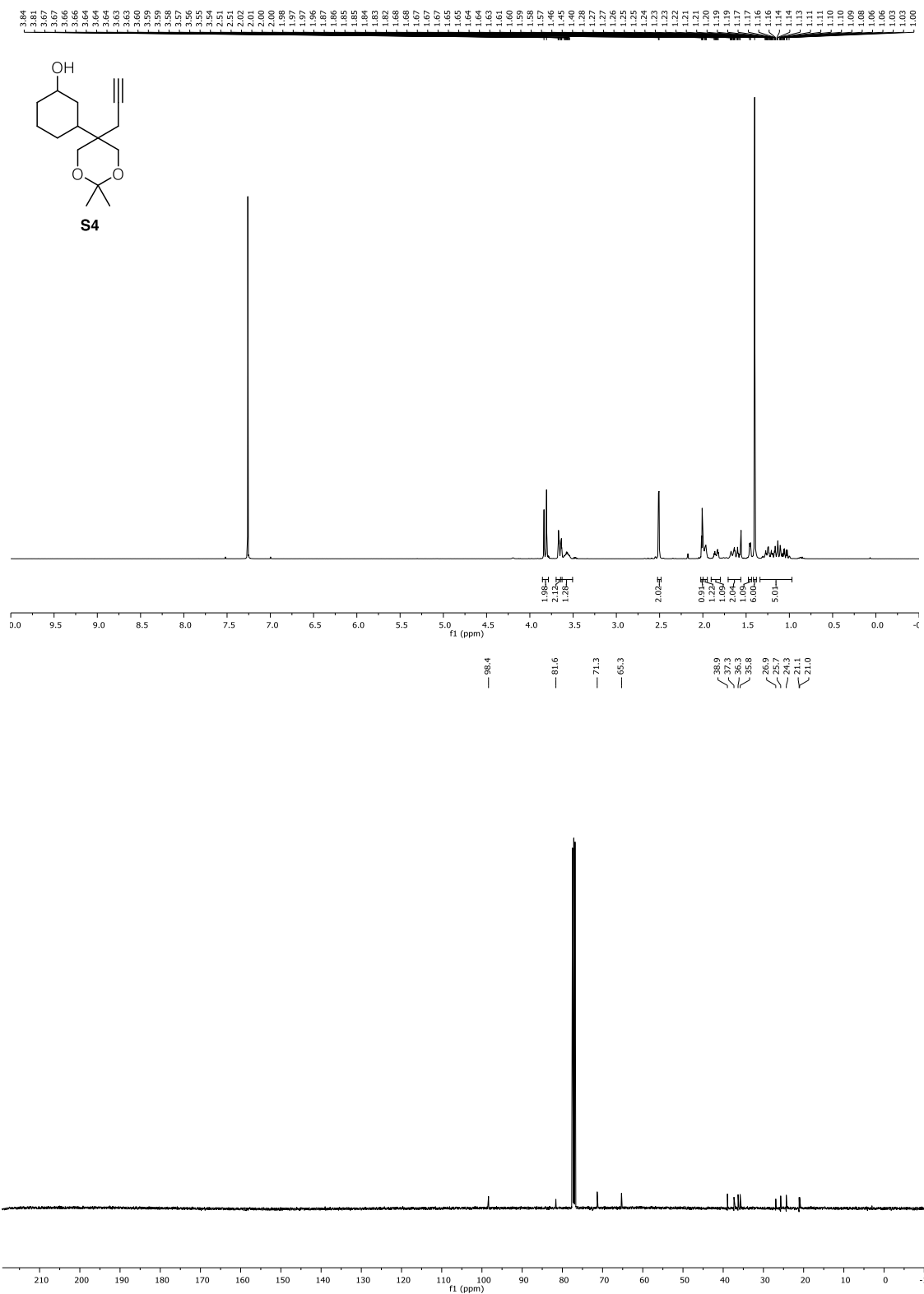
209.2
136.1
131.7
131.3
121.2
83.6
69.0
63.2
43.9
42.0
33.3
30.6
25.9
16.0



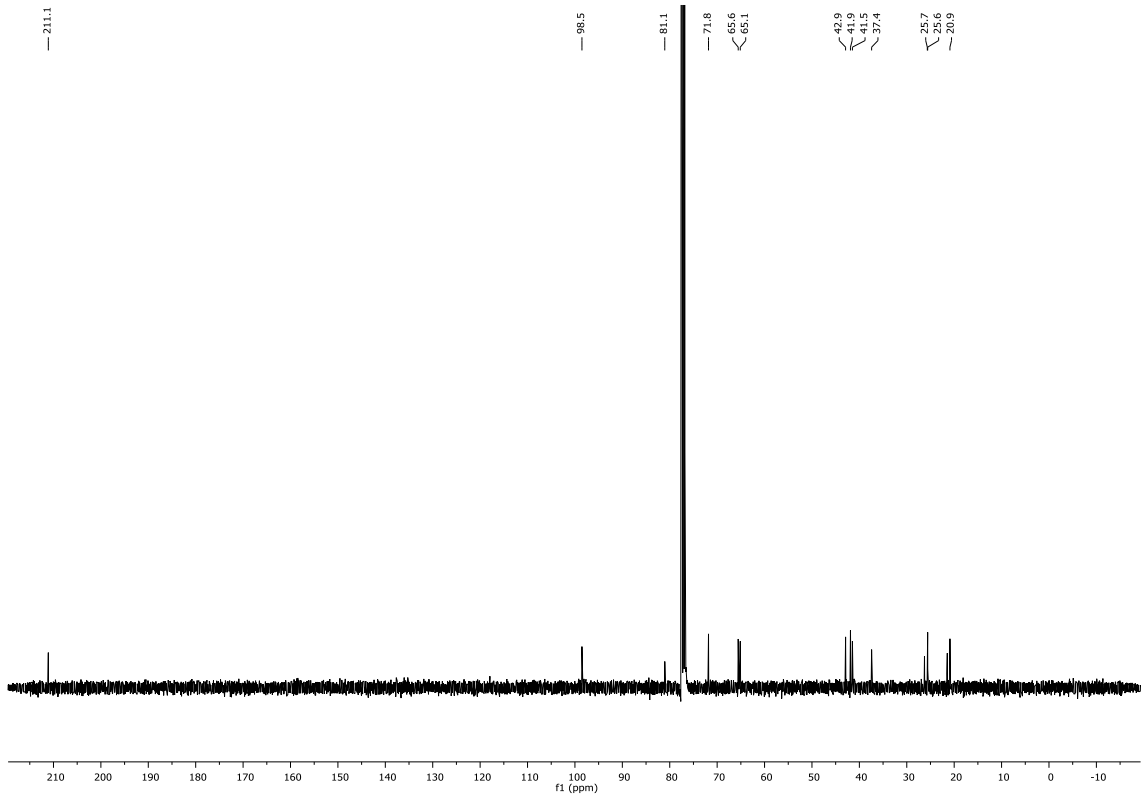
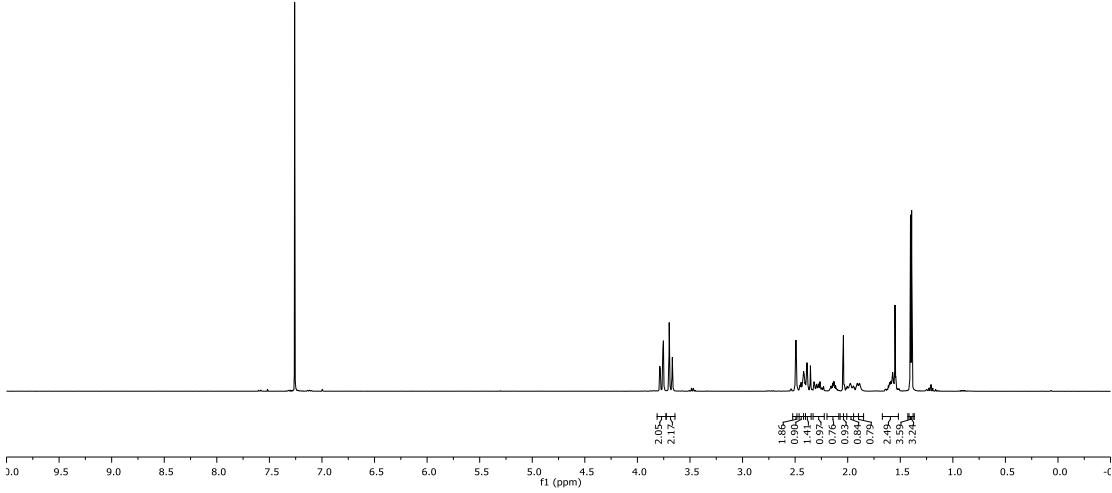
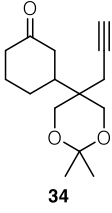


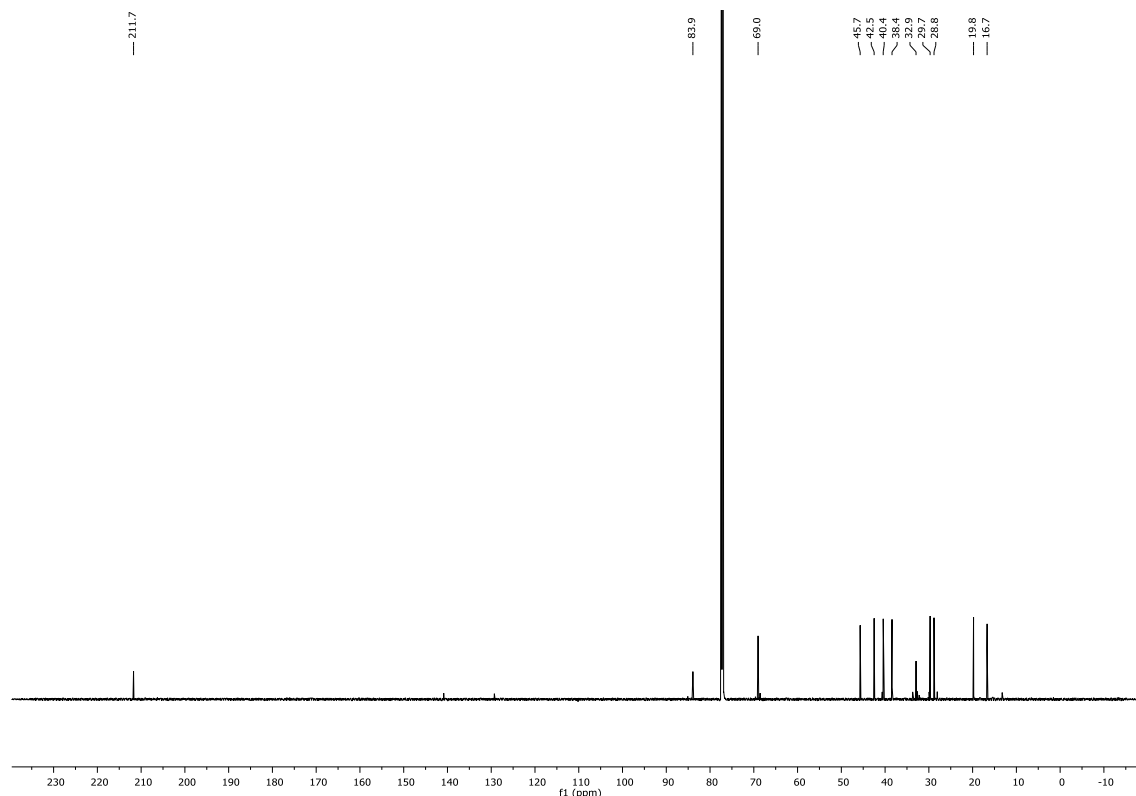
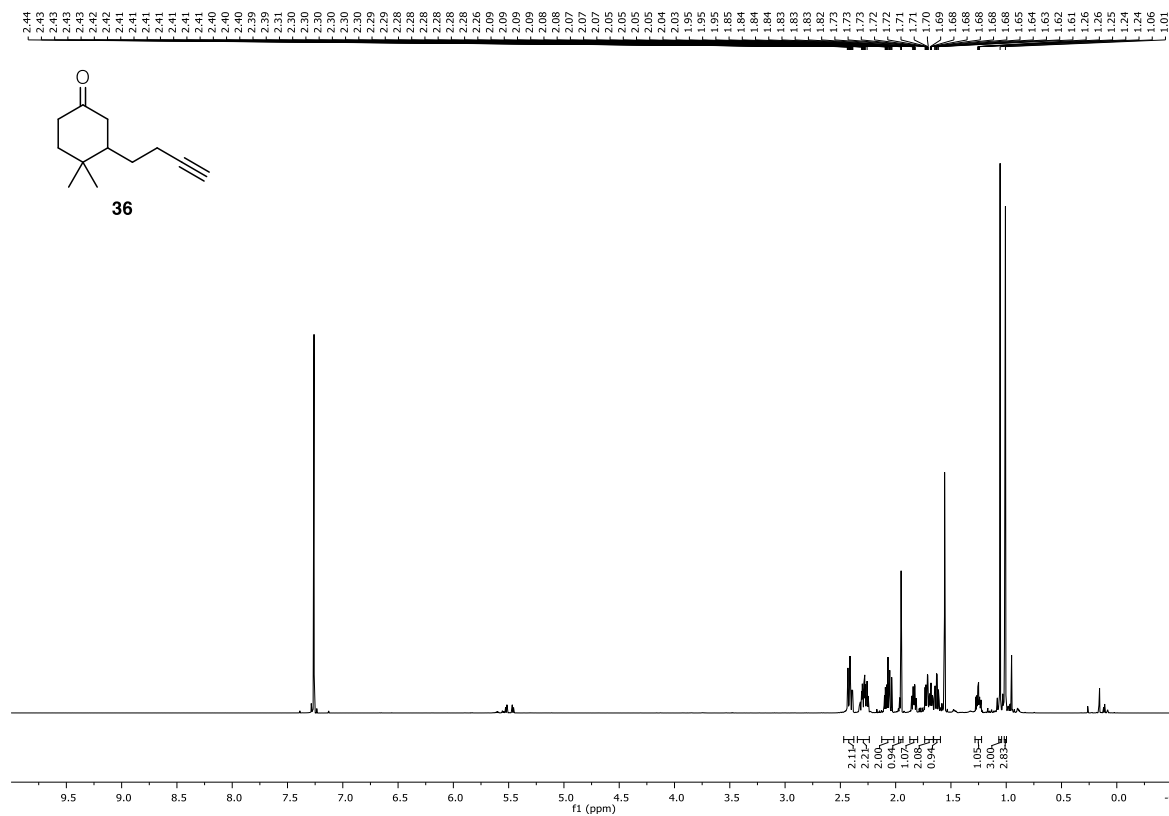


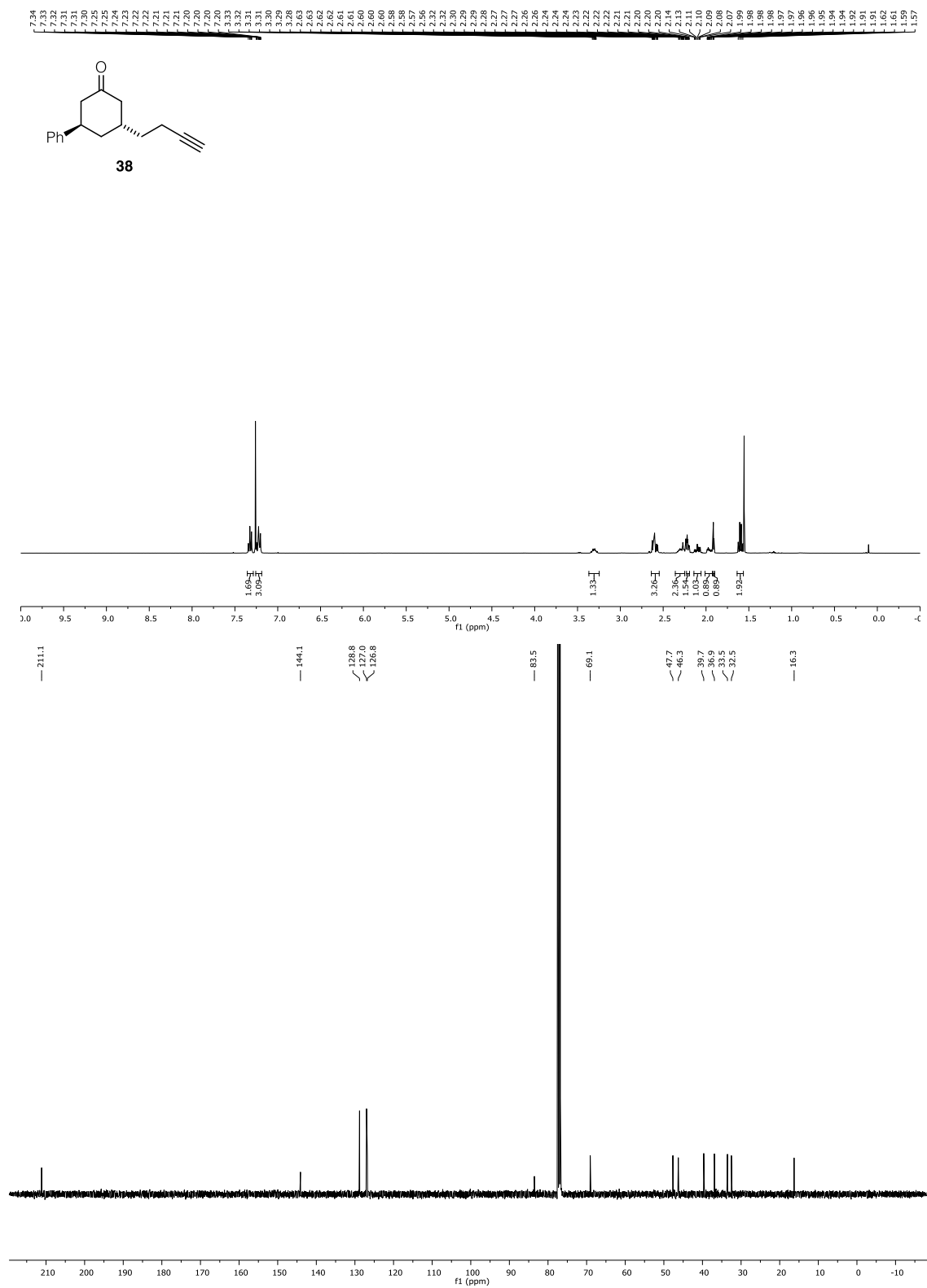


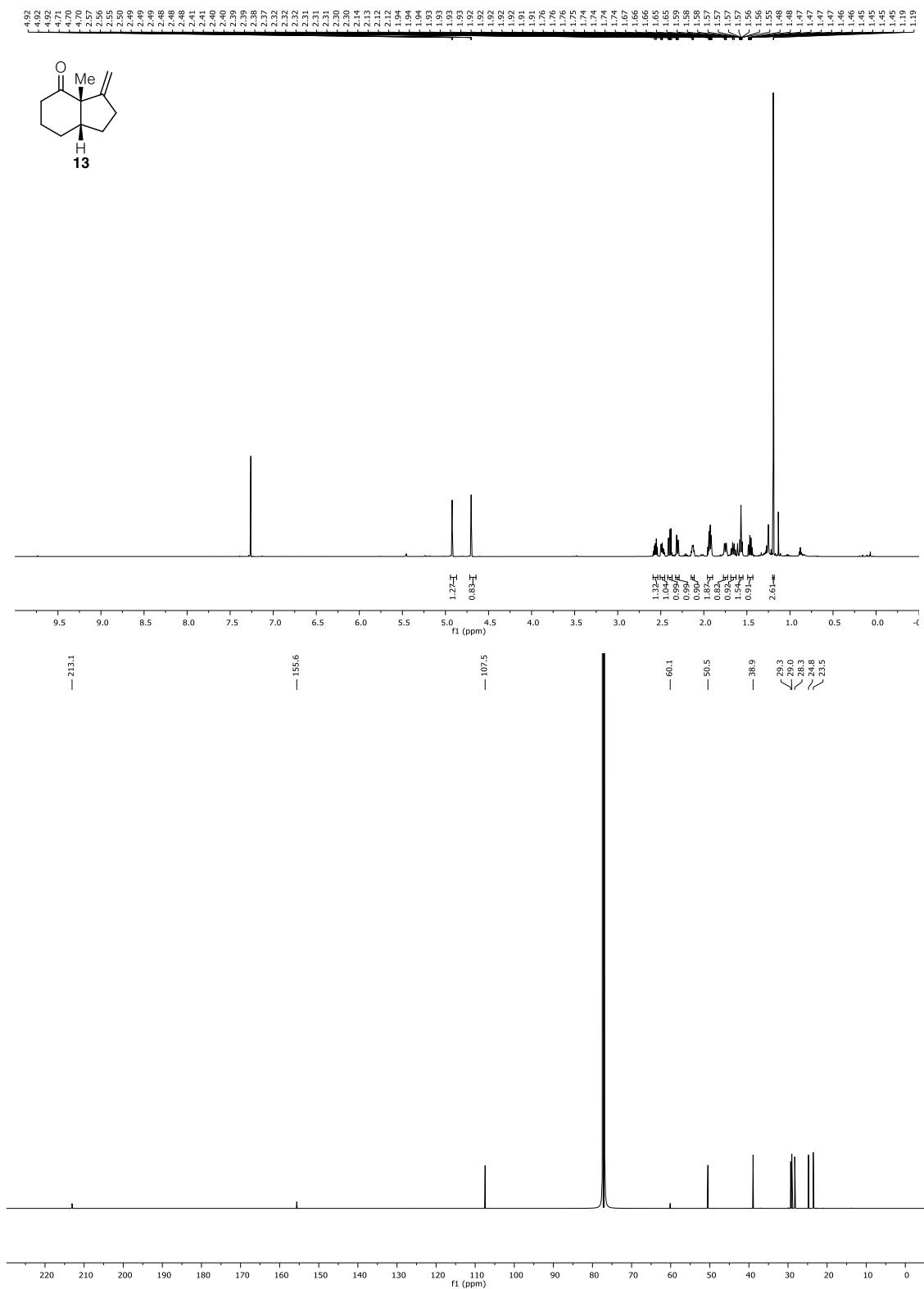


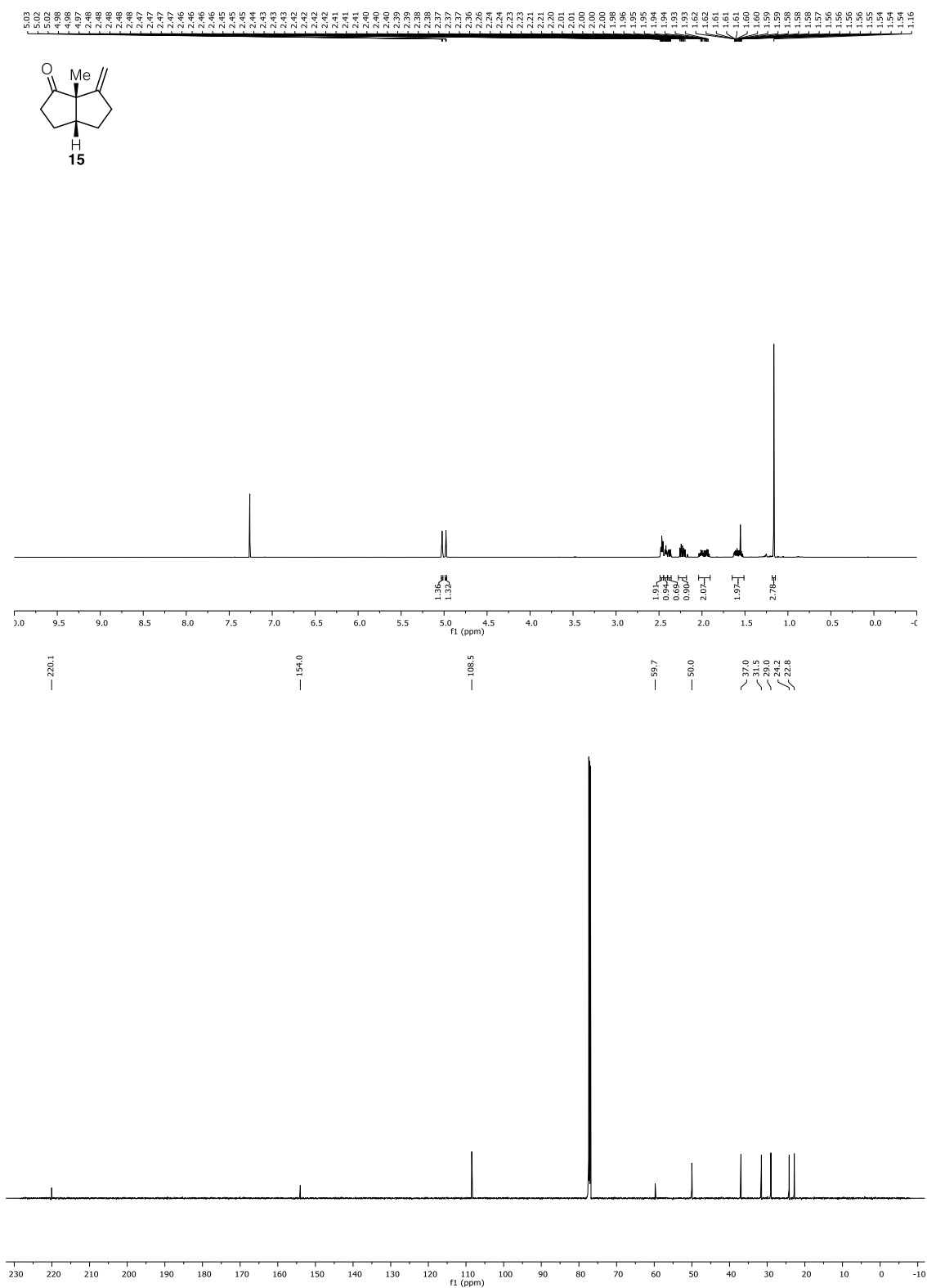
3.79 3.78 3.76 3.75 3.74 3.73 3.72 3.70 3.69 3.67 3.66 3.65 3.64 3.63 3.62 3.61 3.60 3.59 3.58 3.57 3.56 3.55 3.54 3.53 3.52 3.51 3.50 3.49 3.48 3.47 3.46 3.45 3.44 3.43 3.42 3.41 3.40 3.39 3.38 3.37 3.36 3.35 3.34 3.33 3.32 3.31 3.30 3.29 3.28 3.27 3.26 3.25 3.24 3.23 3.22 3.21 3.20 3.19 3.18 3.17 3.16 3.15 3.14 3.13 3.12 3.11 3.10 3.09 3.08 3.07 3.06 3.05 3.04 3.03 3.02 3.01 3.00 2.99 2.98 2.97 2.96 2.95 2.94 2.93 2.92 2.91 2.90 2.89 2.88 2.87 2.86 2.85 2.84 2.83 2.82 2.81 2.80 2.79

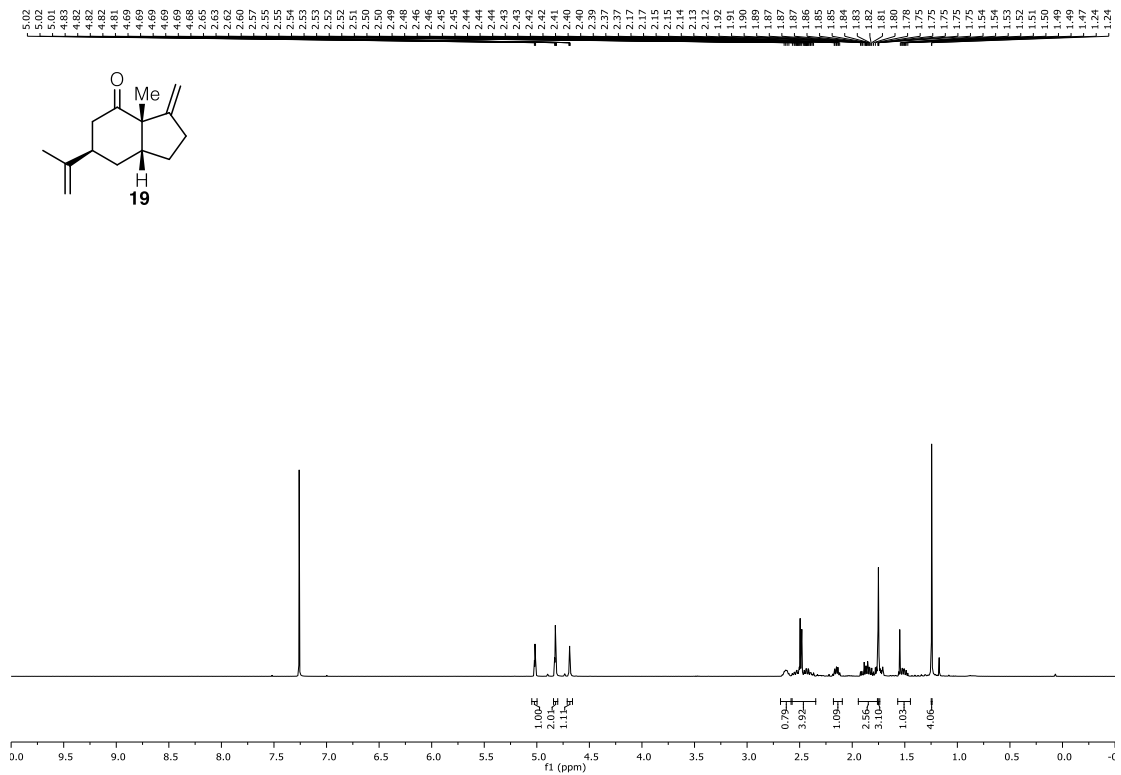




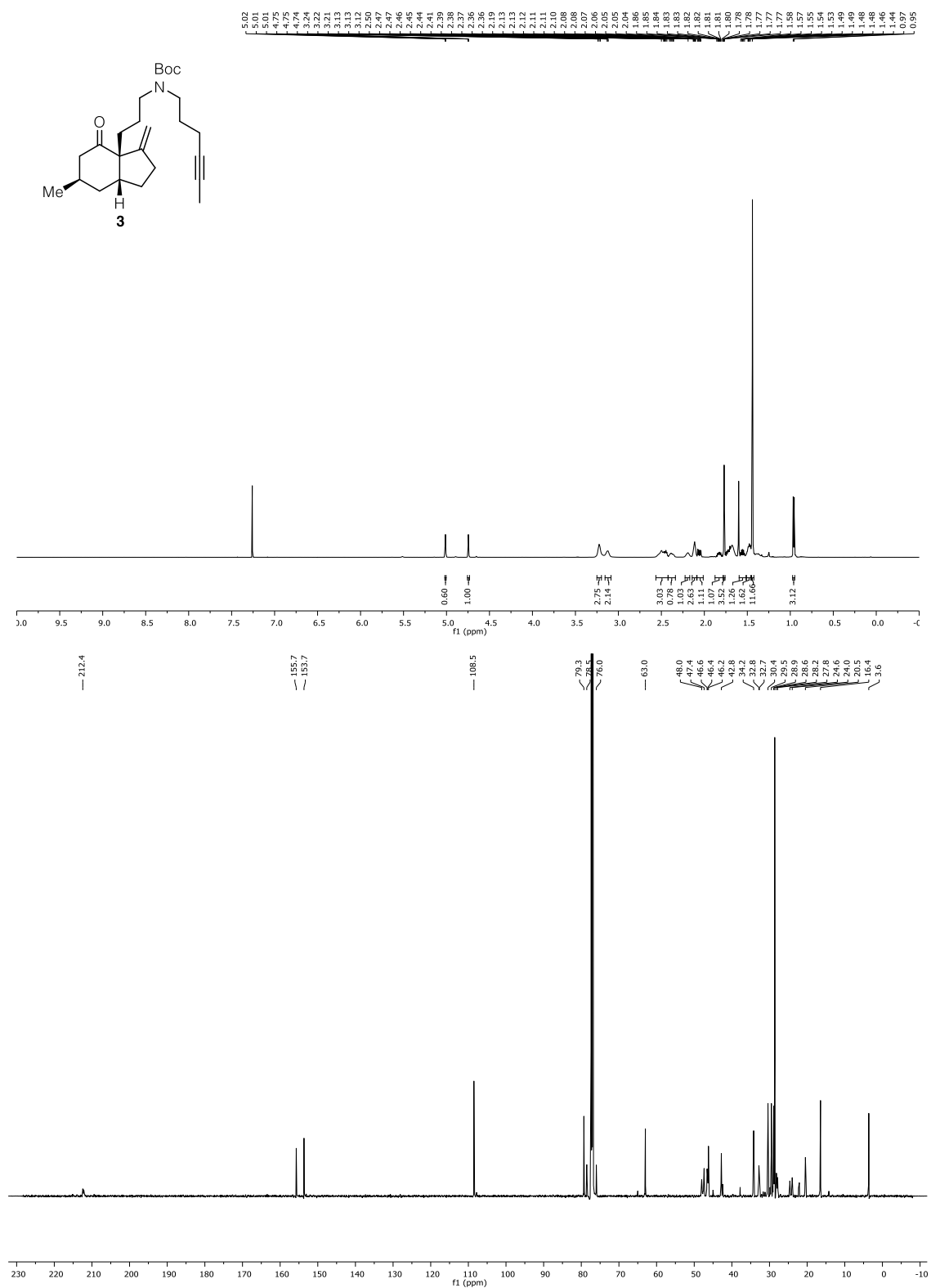


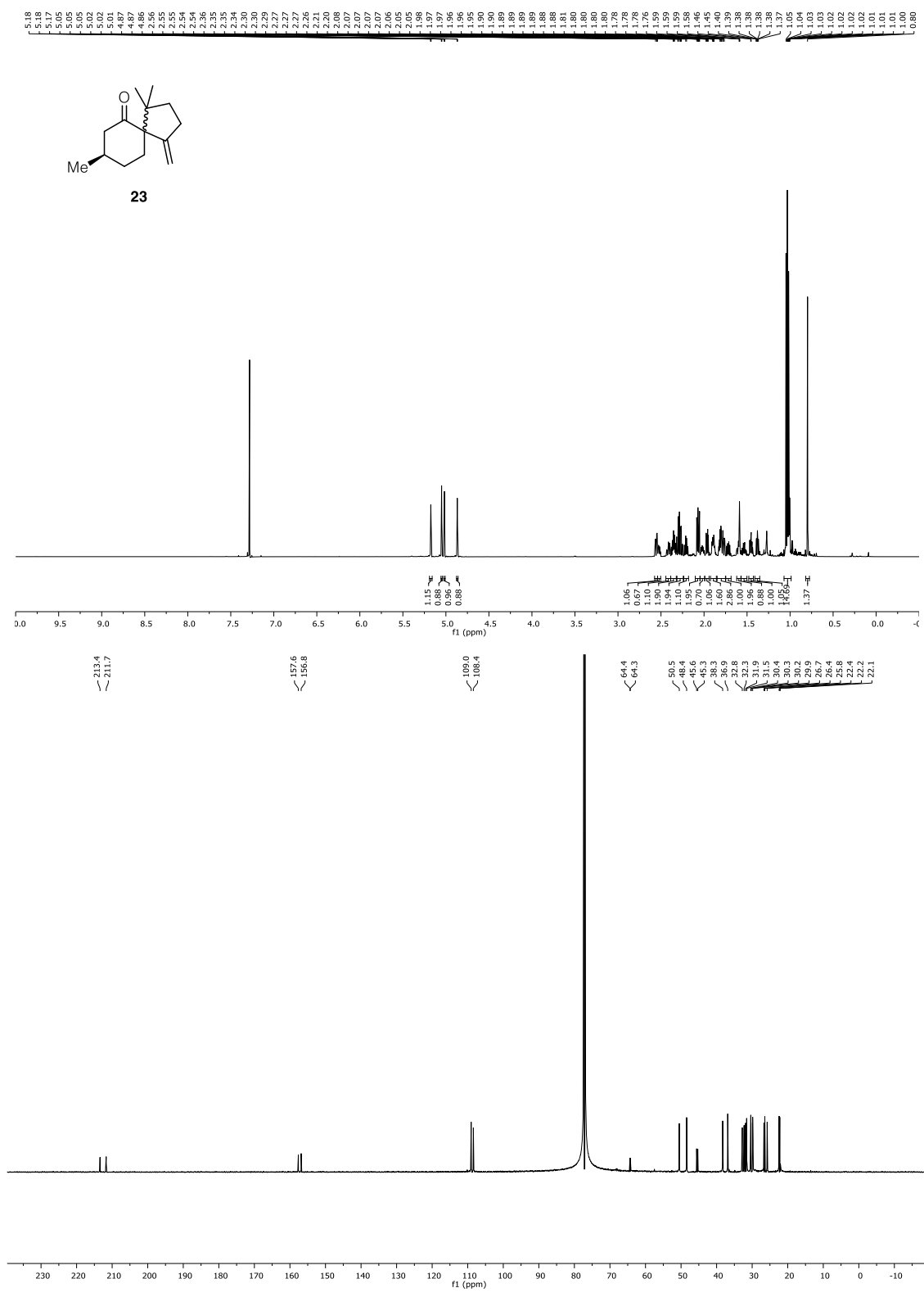


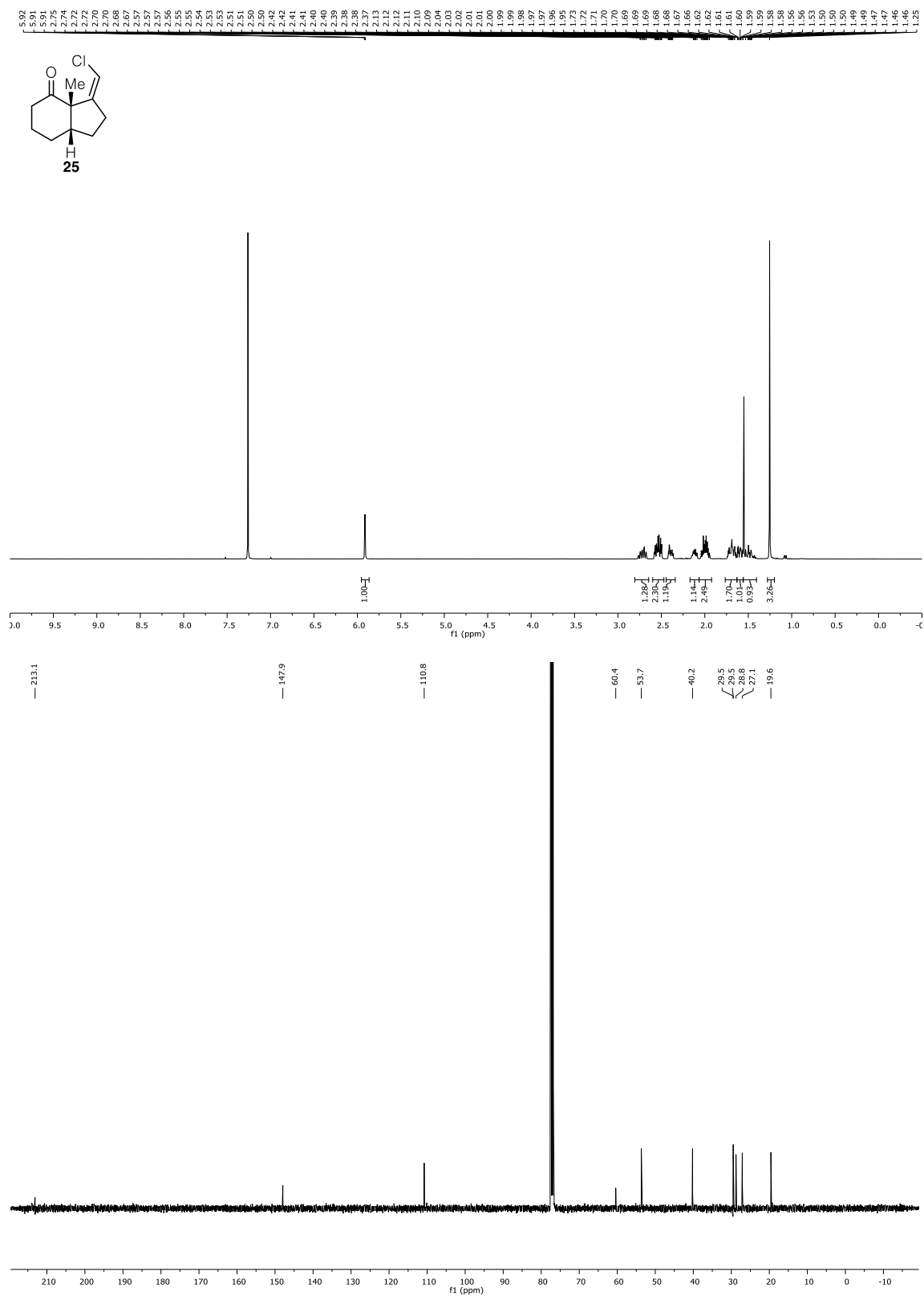


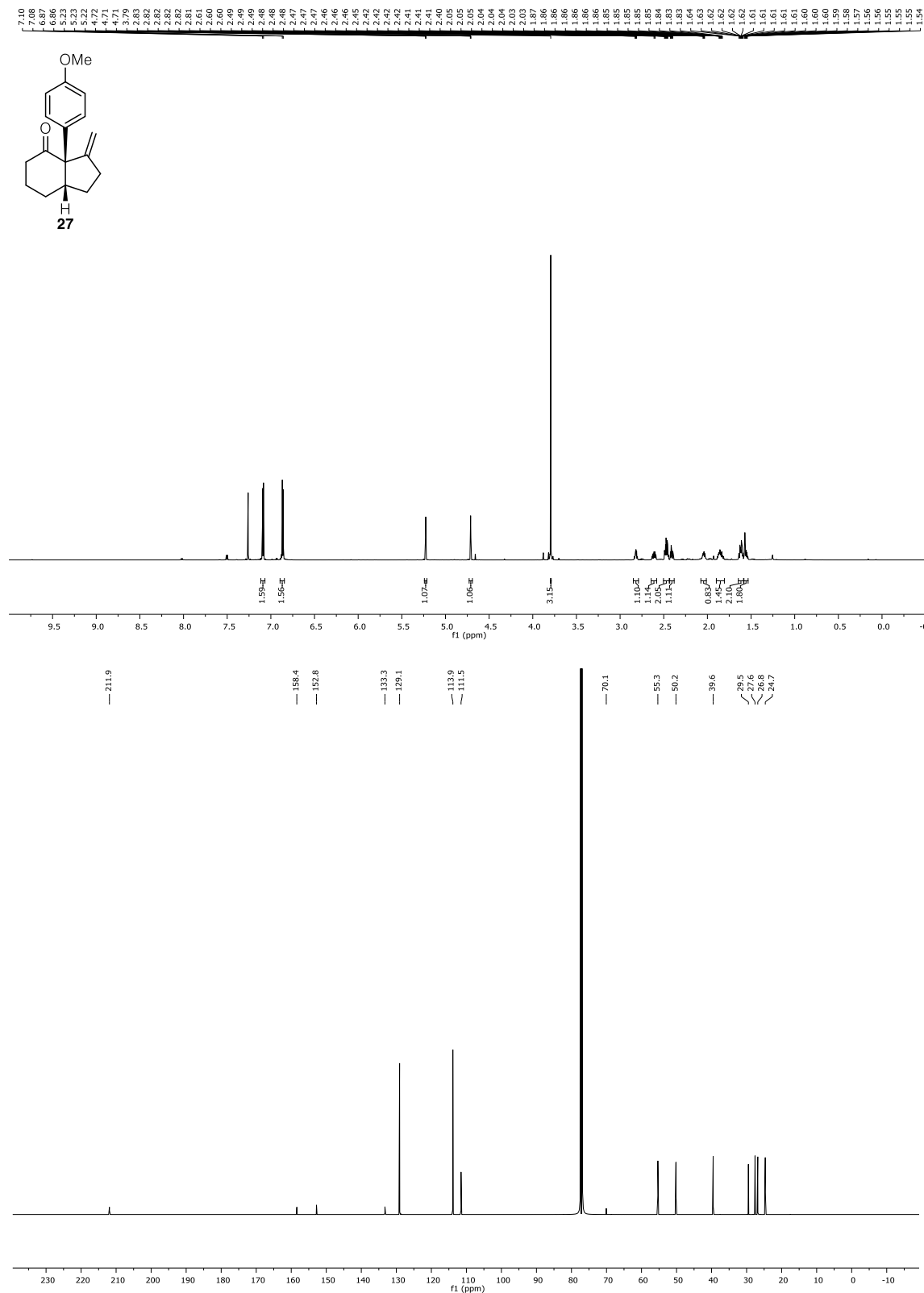


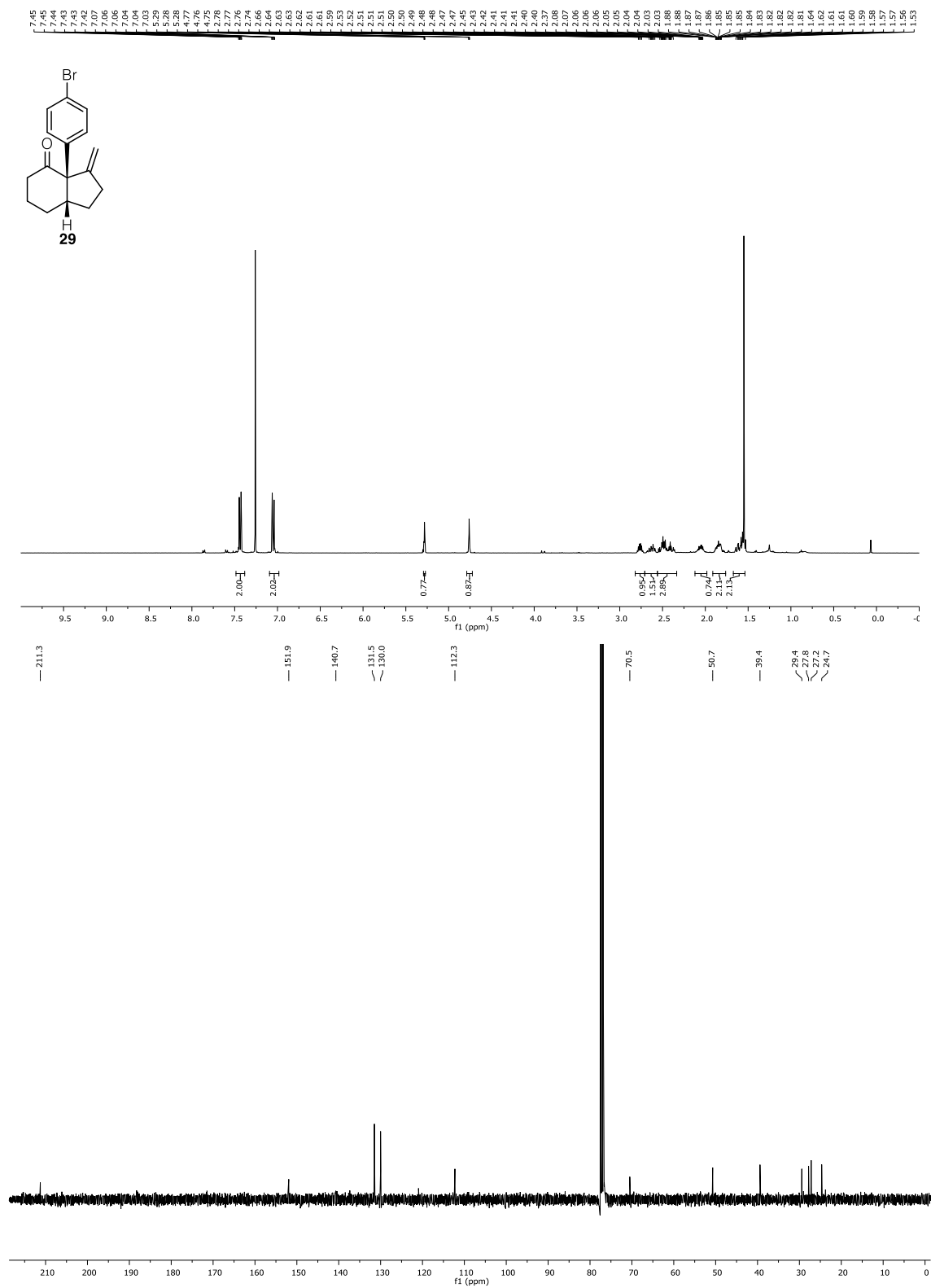
known compound

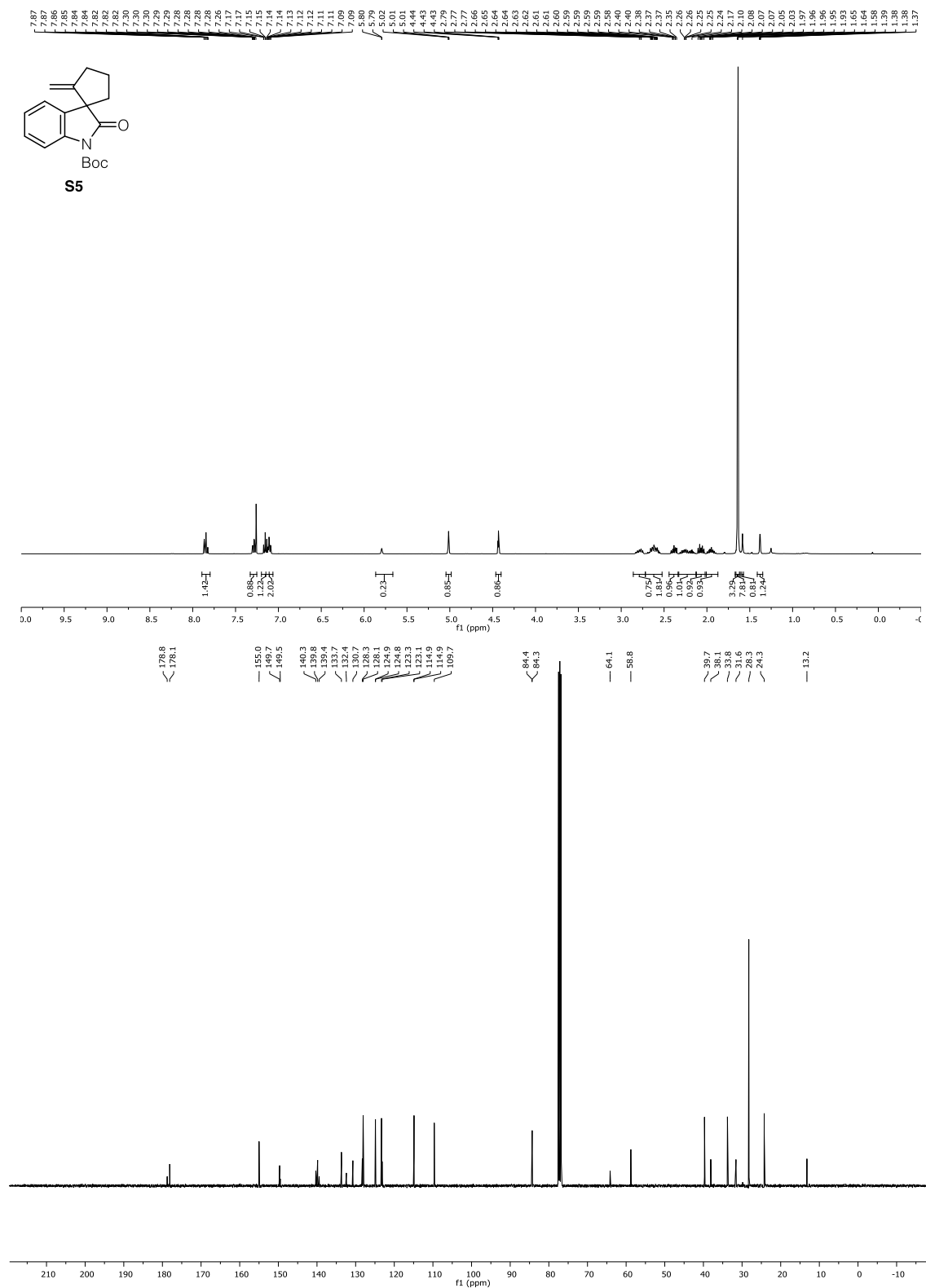


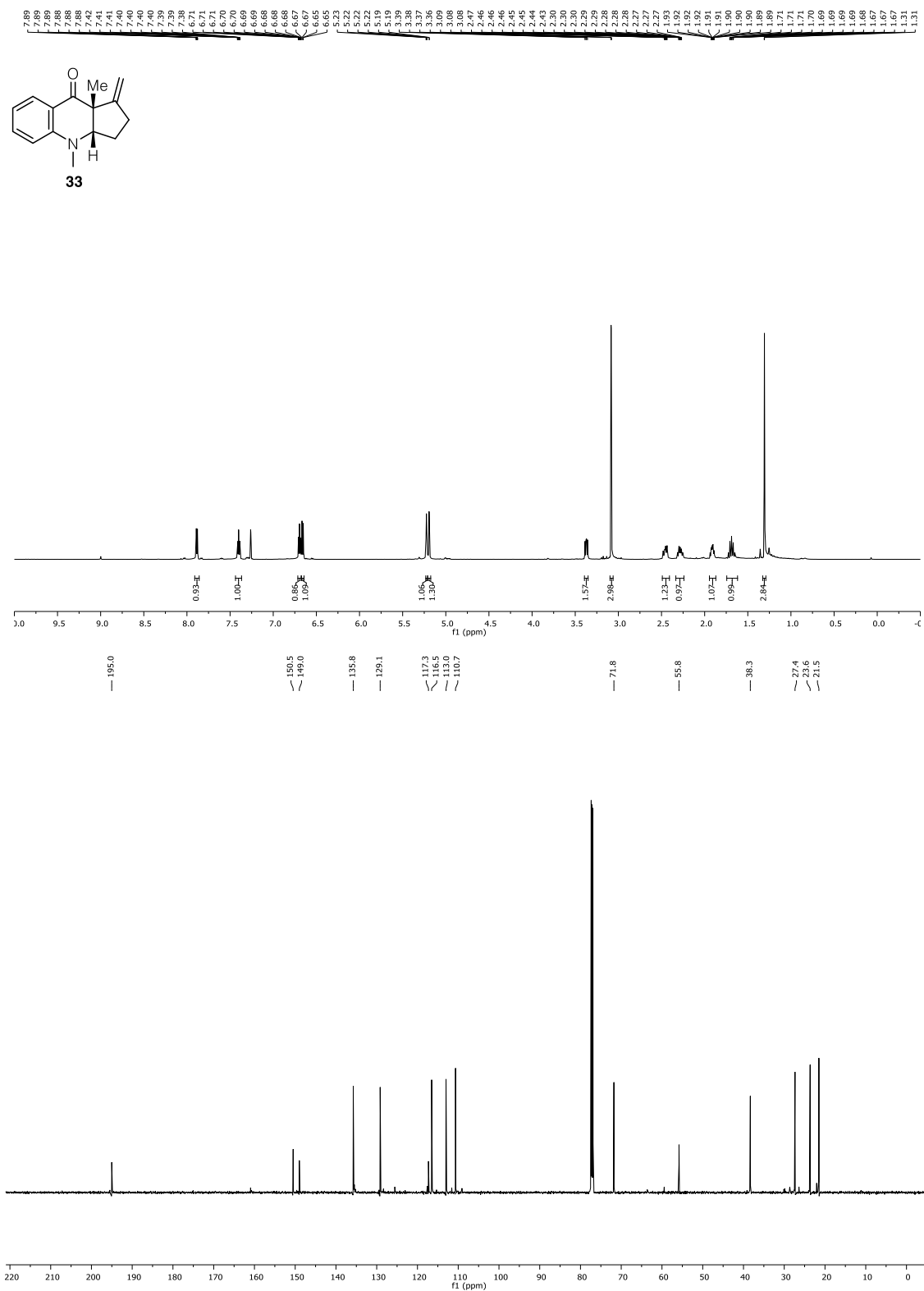




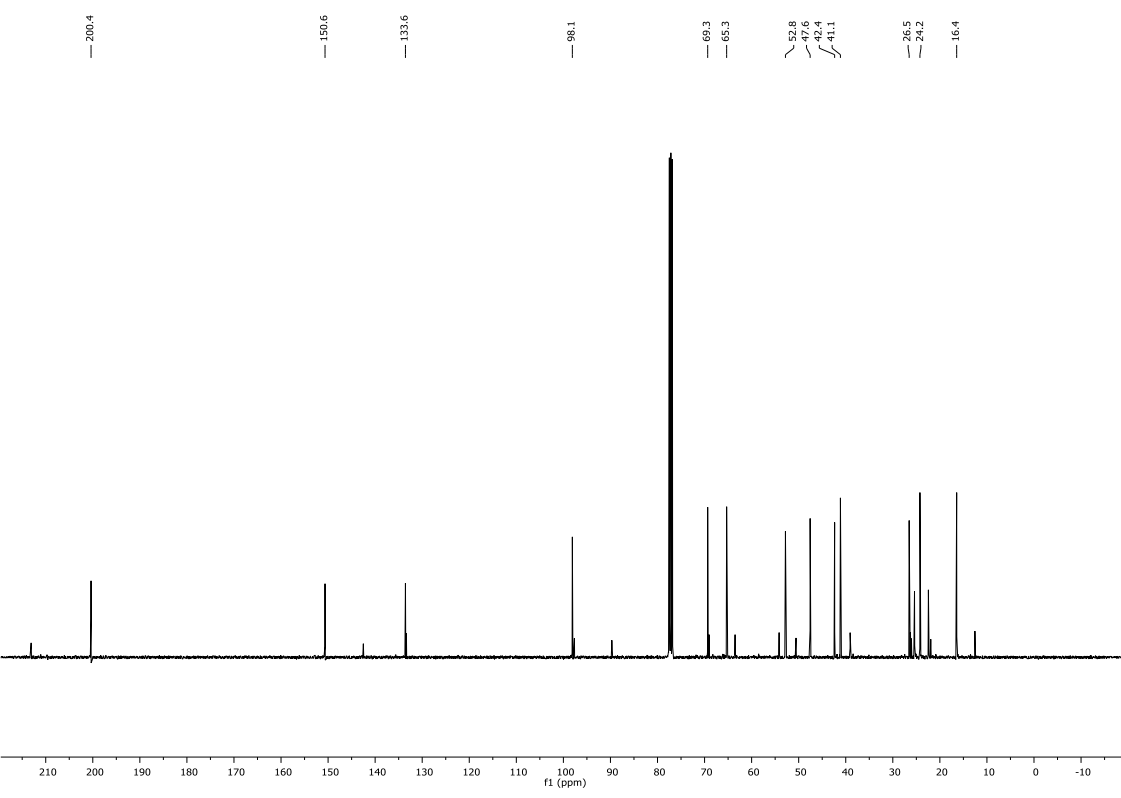
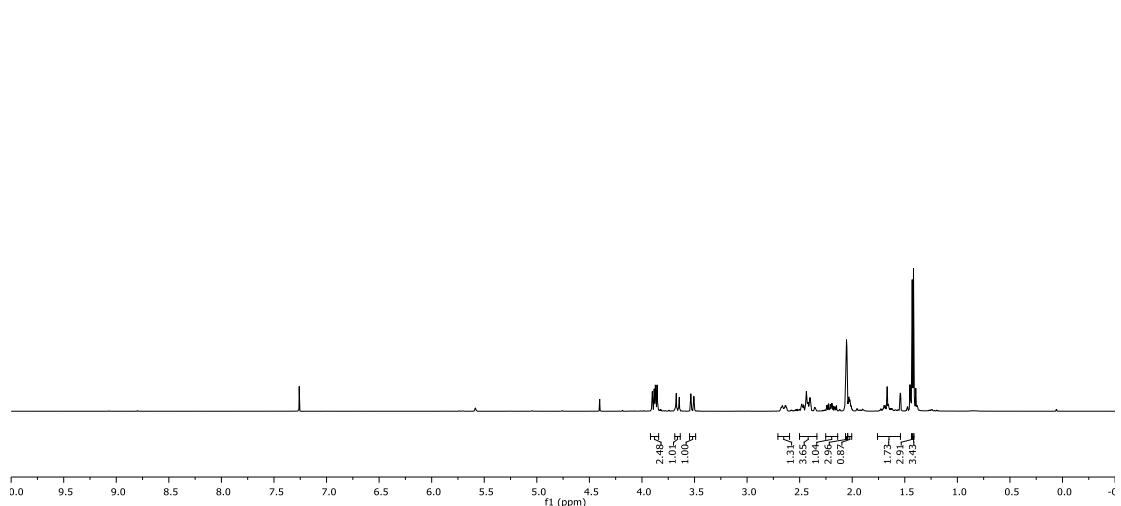
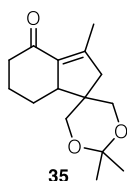


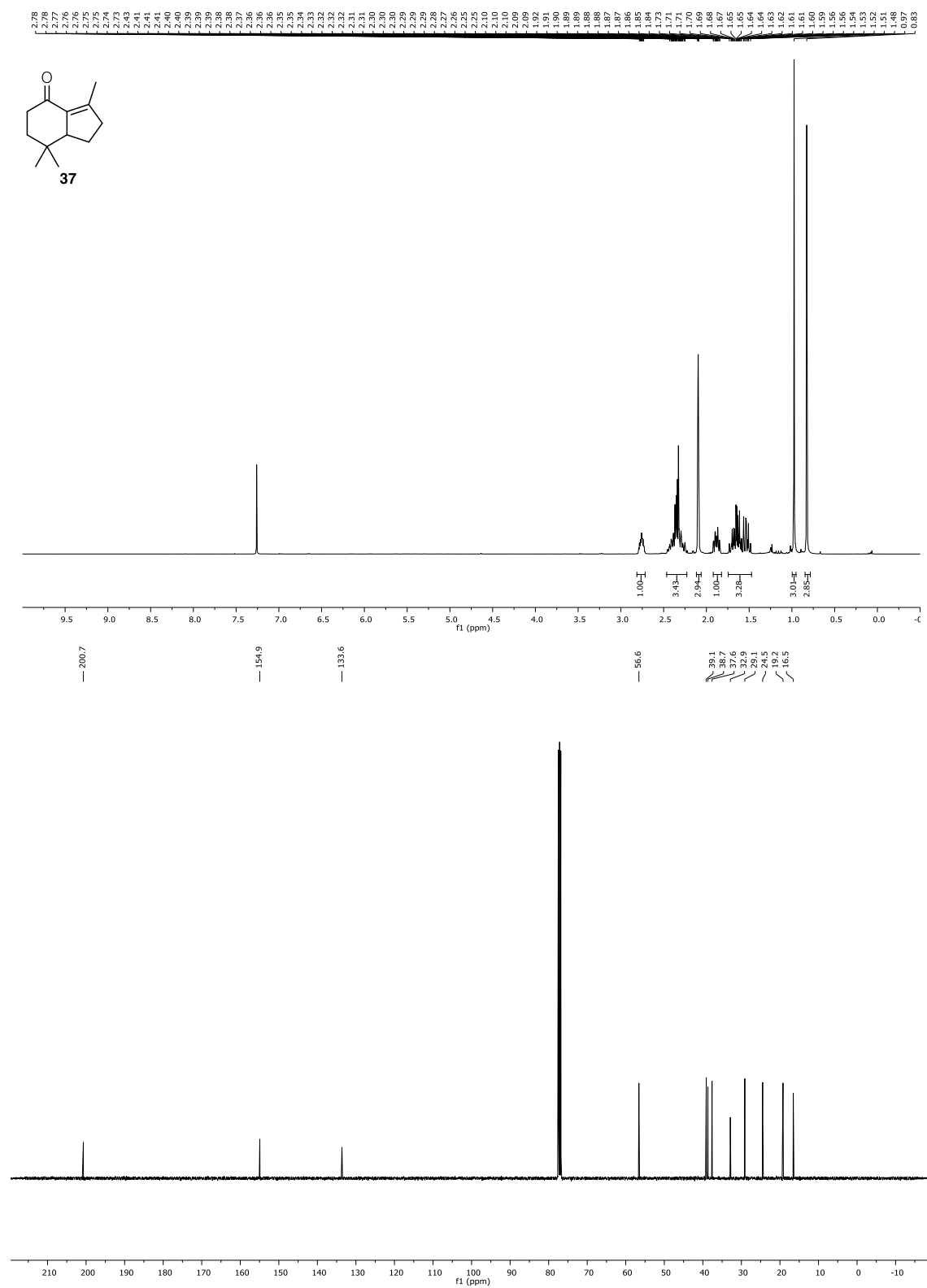


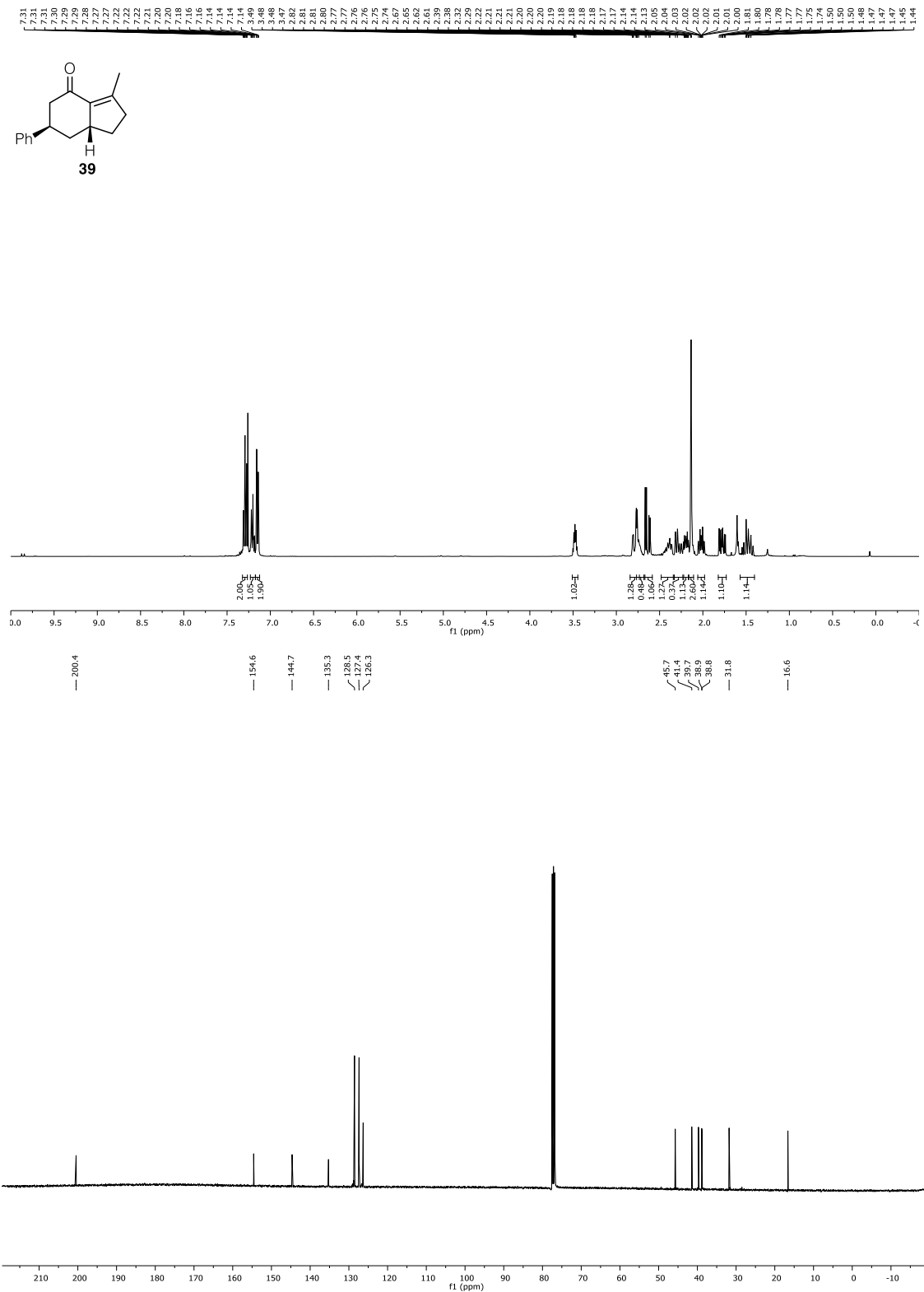
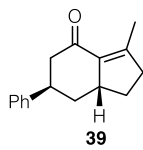


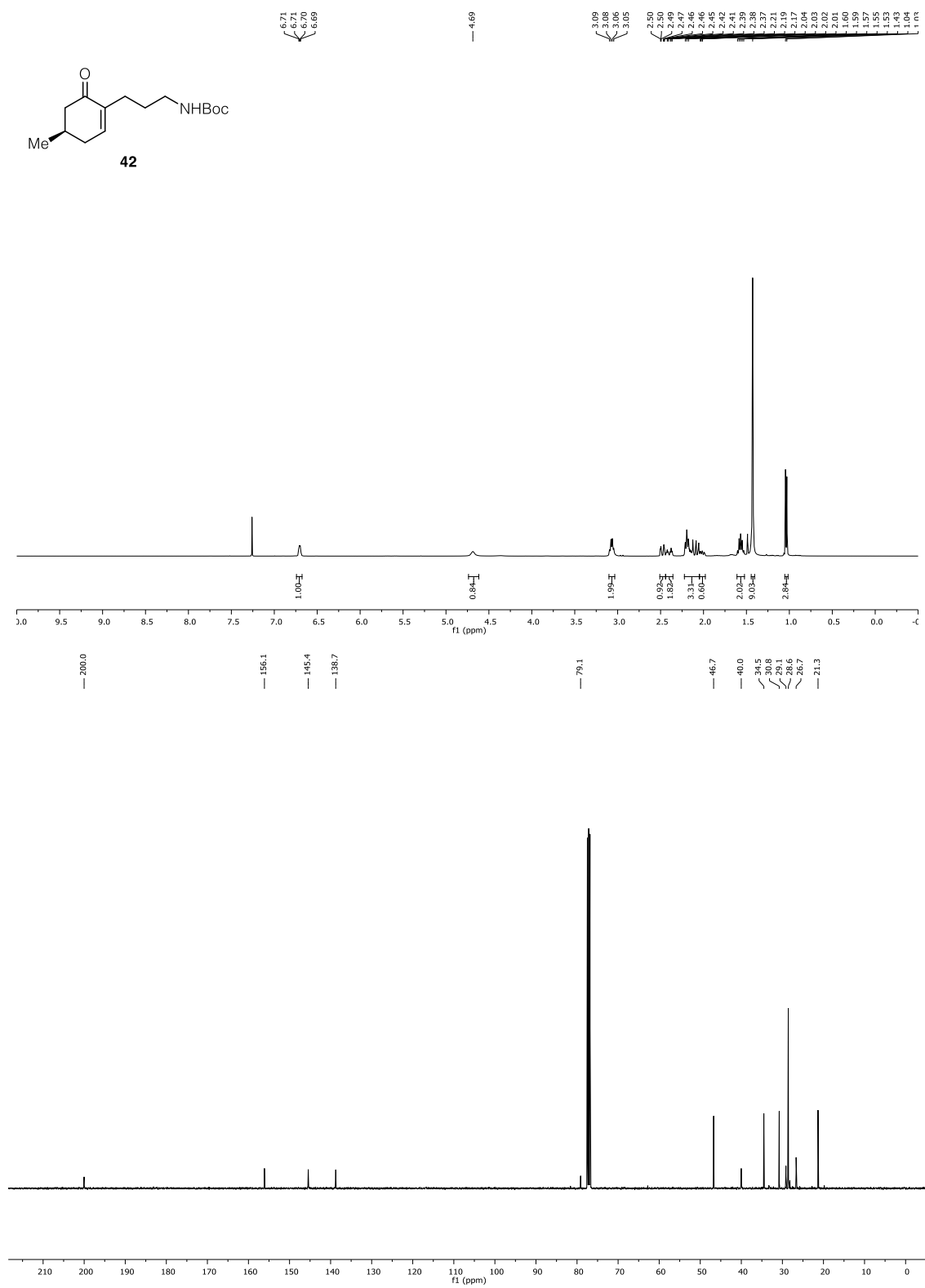


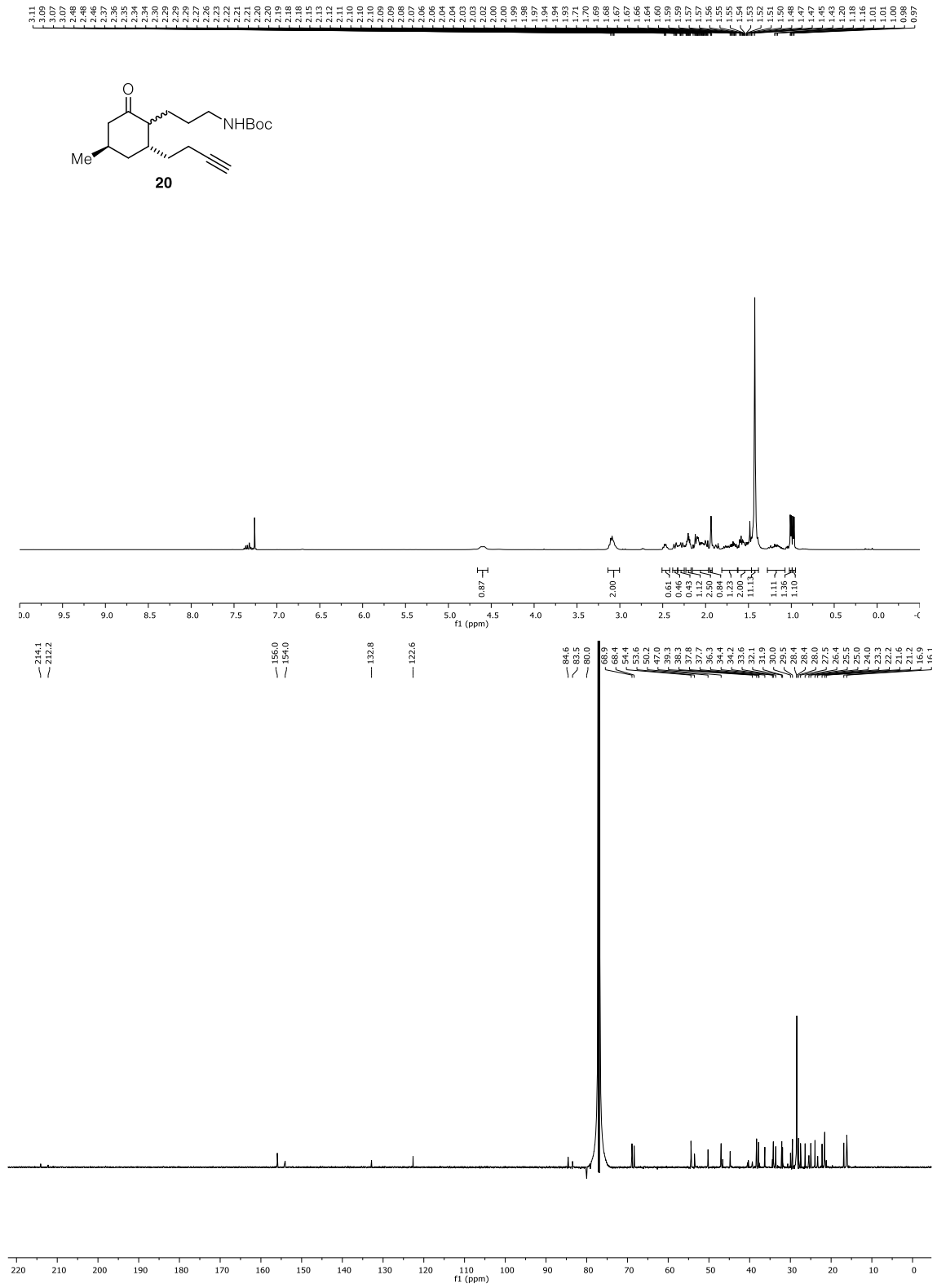
3.90
3.88
3.87
3.86
3.85
3.84
3.83
3.82
3.81
3.80
3.79
3.78
3.77
3.76
3.75
3.74
3.73
3.72
3.71
3.70
3.69
3.68
3.67
3.66
3.65
3.64
3.63
3.62
3.61
3.60
3.59
3.58
3.57
3.56
3.55
3.54
3.53
3.52
3.51
3.50
3.49
3.48
3.47
3.46
3.45
3.44
3.43
3.42
3.41
3.40
3.39
3.38
3.37
3.36
3.35
3.34
3.33
3.32
3.31
3.30
3.29
3.28
3.27
3.26
3.25
3.24
3.23
3.22
3.21
3.20
3.19
3.18
3.17
3.16
3.15
3.14
3.13
3.12
3.11
3.10
3.09
3.08
3.07
3.06
3.05
3.04
3.03
3.02
3.01
3.00
2.99
2.98
2.97
2.96
2.95
2.94
2.93
2.92
2.91
2.90
2.89
2.88
2.87
2.86
2.85
2.84
2.83
2.82
2.81
2.80
2.79
2.78
2.77
2.76
2.75
2.74
2.73
2.72
2.71
2.70
2.69
2.68
2.67
2.66
2.65
2.64
2.63
2.62
2.61
2.60
2.59
2.58
2.57
2.56
2.55
2.54
2.53
2.52
2.51
2.50
2.49
2.48
2.47
2.46
2.45
2.44
2.43
2.42
2.41
2.40
2.39
2.38
2.37
2.36
2.35
2.34
2.33
2.32
2.31
2.30
2.29
2.28
2.27
2.26
2.25
2.24
2.23
2.22
2.21
2.20
2.19
2.18
2.17
2.16
2.15
2.14
2.13
2.12
2.11
2.10
2.09
2.08
2.07
2.06
2.05
2.04
2.03
2.02
2.01
2.00
1.99
1.98
1.97
1.96
1.95
1.94
1.93
1.92
1.91
1.90
1.89
1.88
1.87
1.86
1.85
1.84
1.83
1.82
1.81
1.80
1.79
1.78
1.77
1.76
1.75
1.74
1.73
1.72
1.71
1.70
1.69
1.68
1.67
1.66
1.65
1.64
1.63
1.62
1.61
1.60
1.59
1.58
1.57
1.56
1.55
1.54
1.53
1.52
1.51
1.50
1.49
1.48
1.47
1.46
1.45
1.44
1.43
1.42

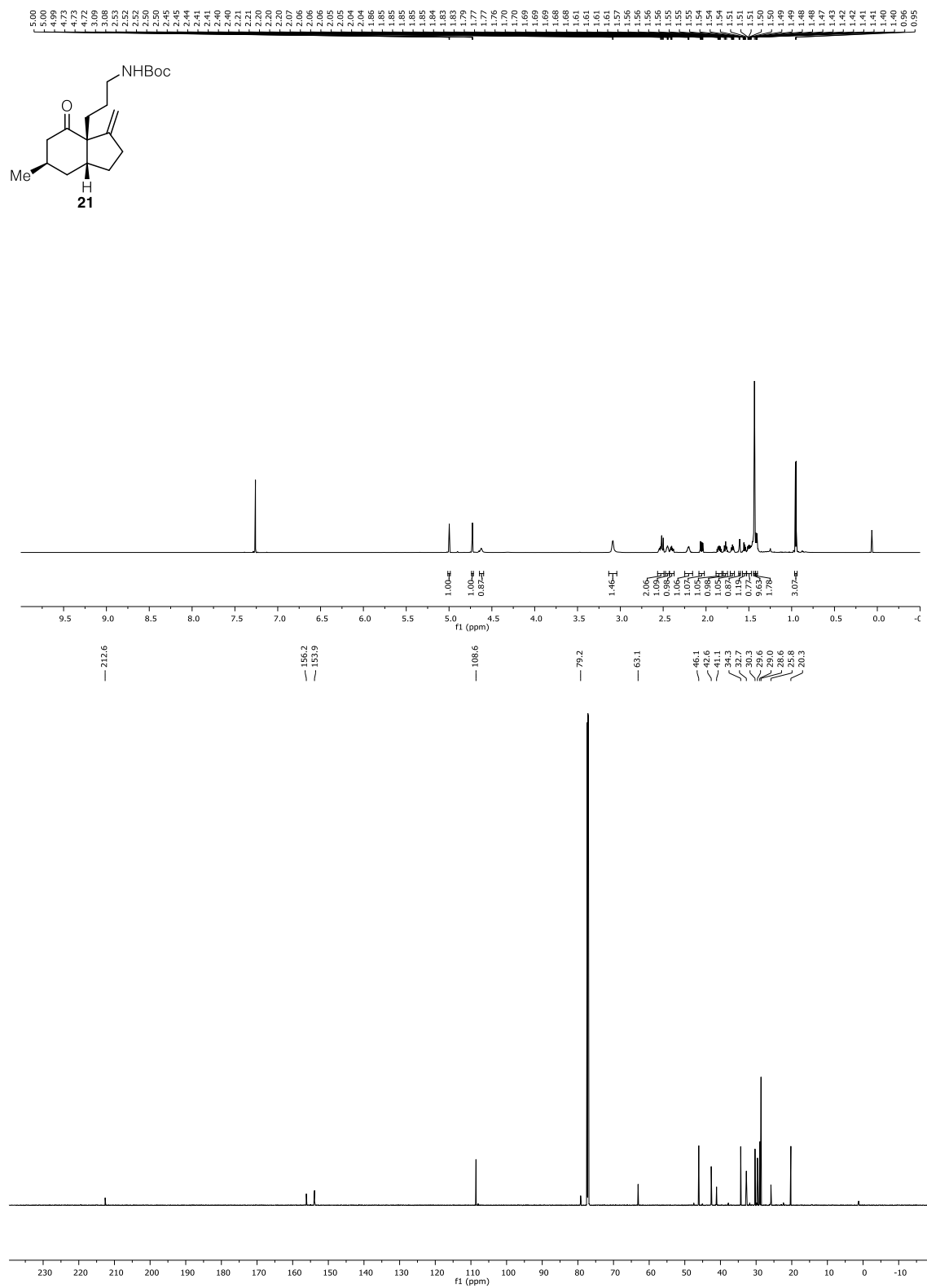


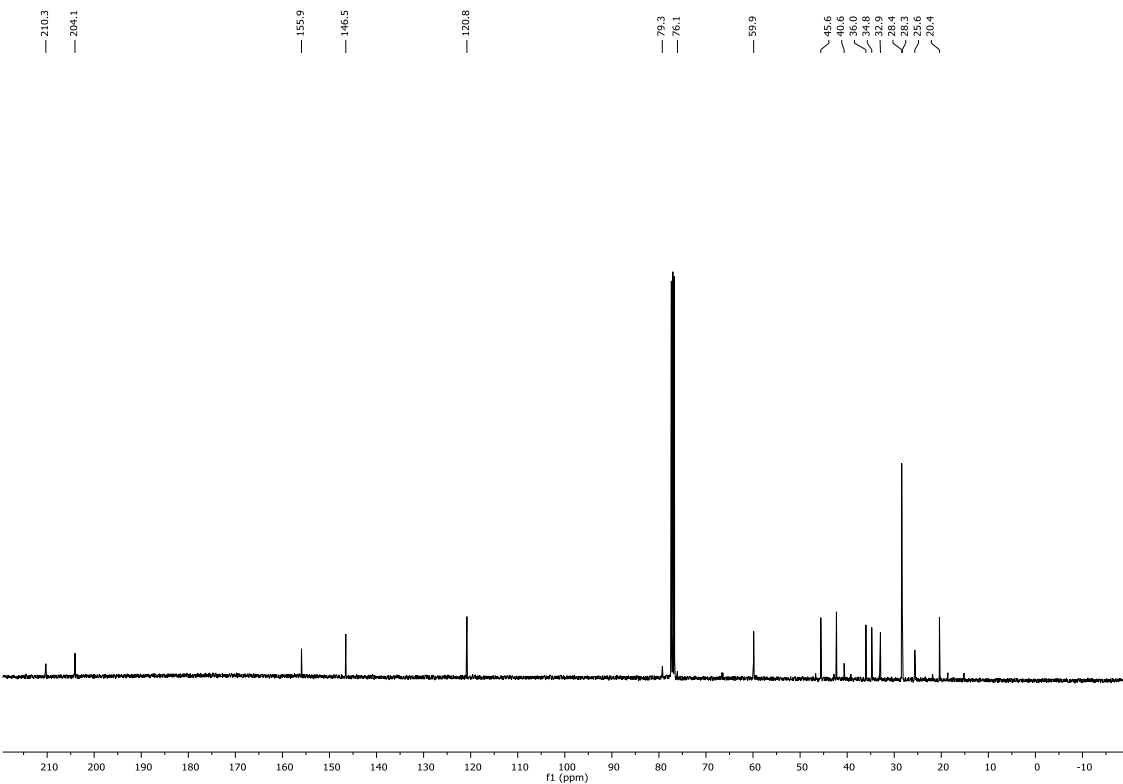
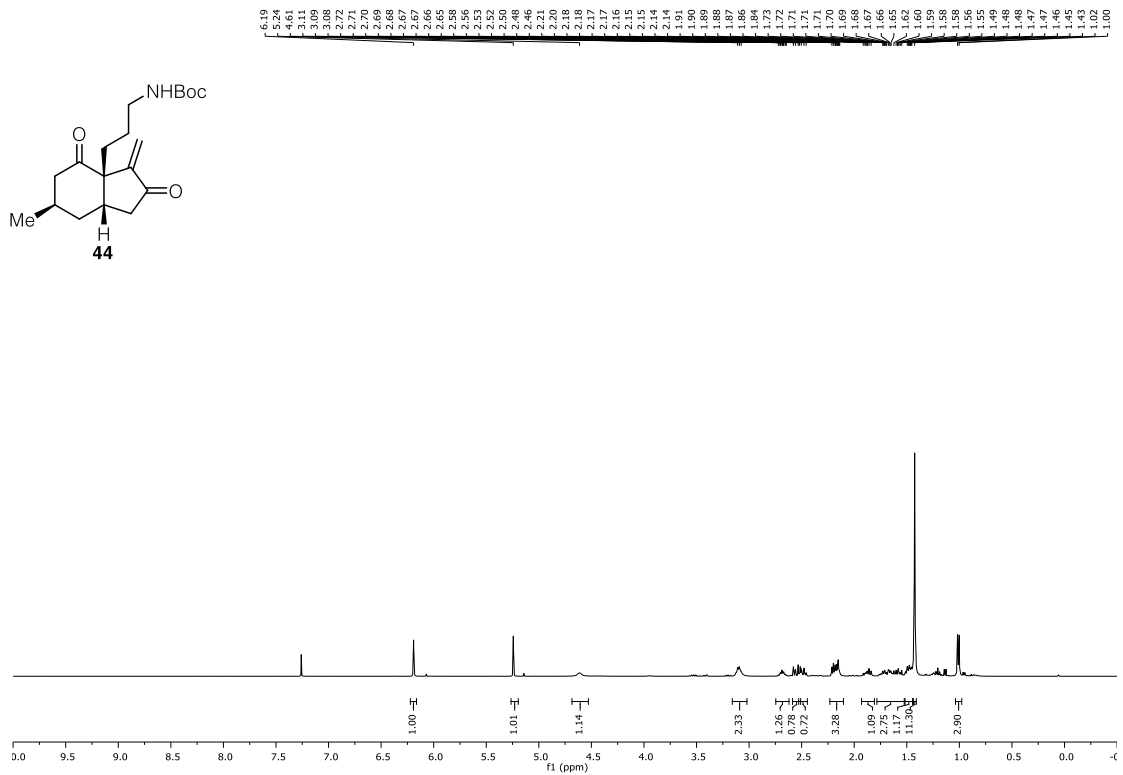
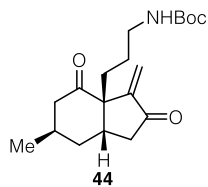


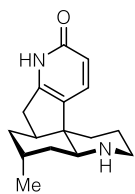




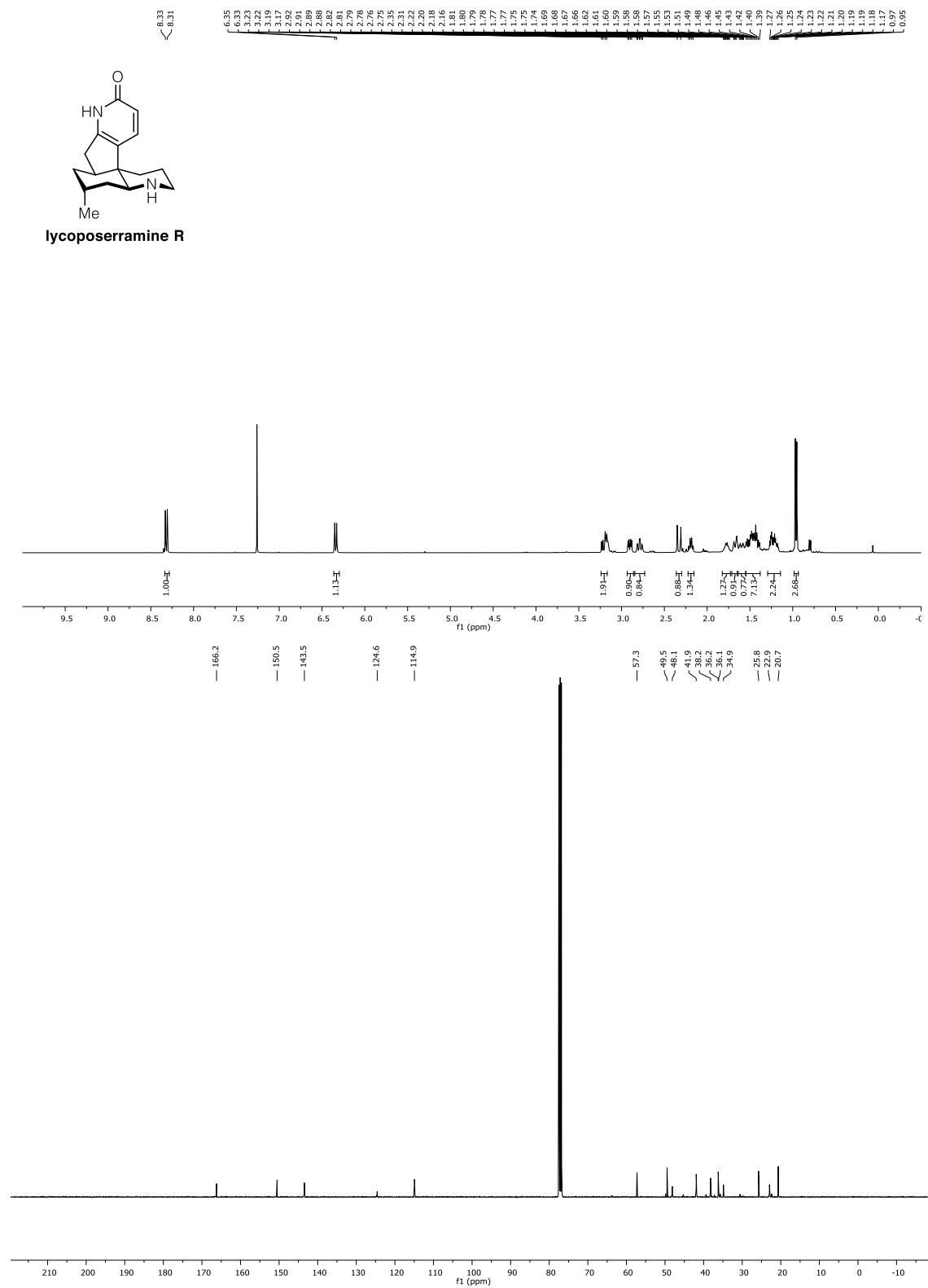


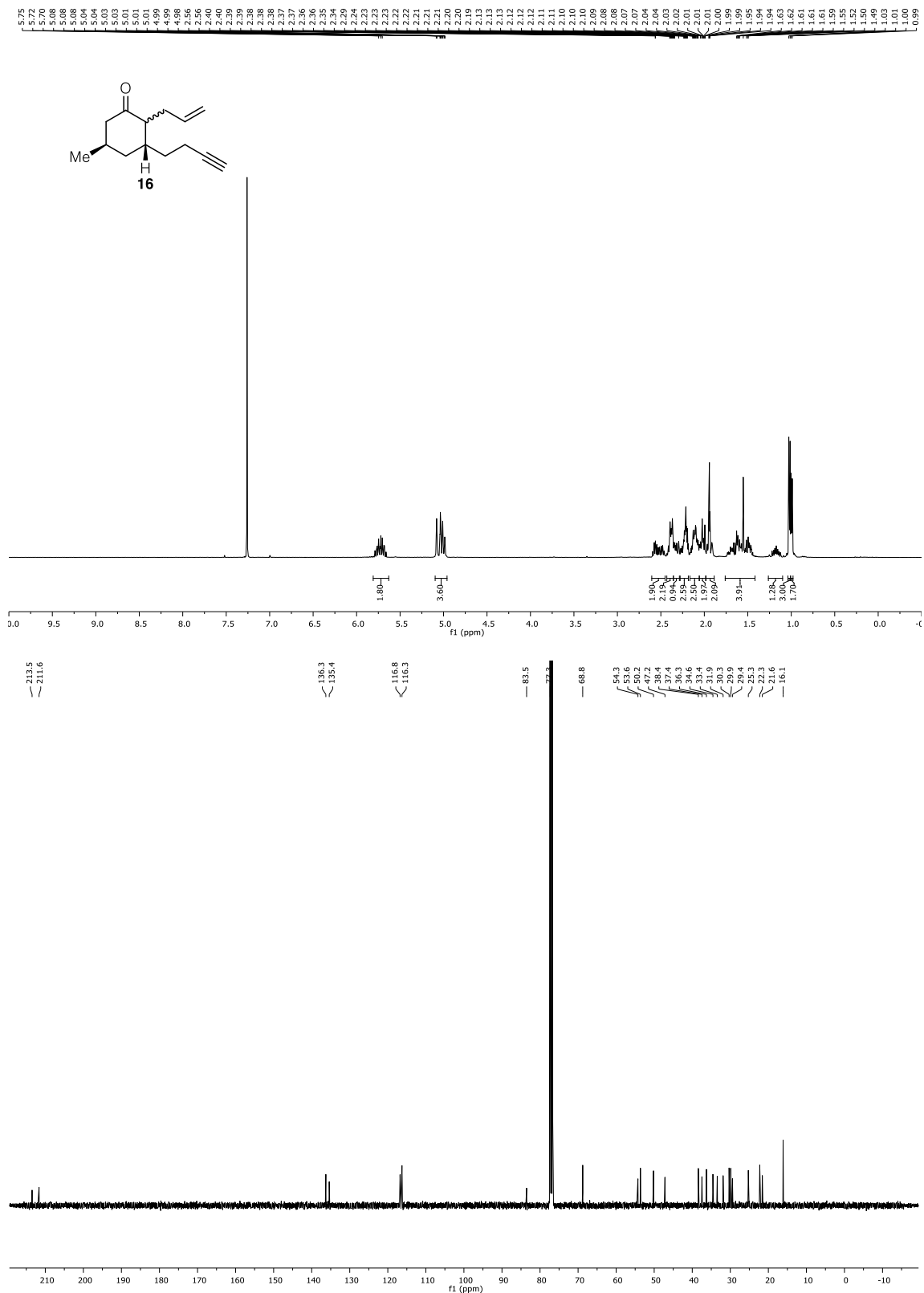


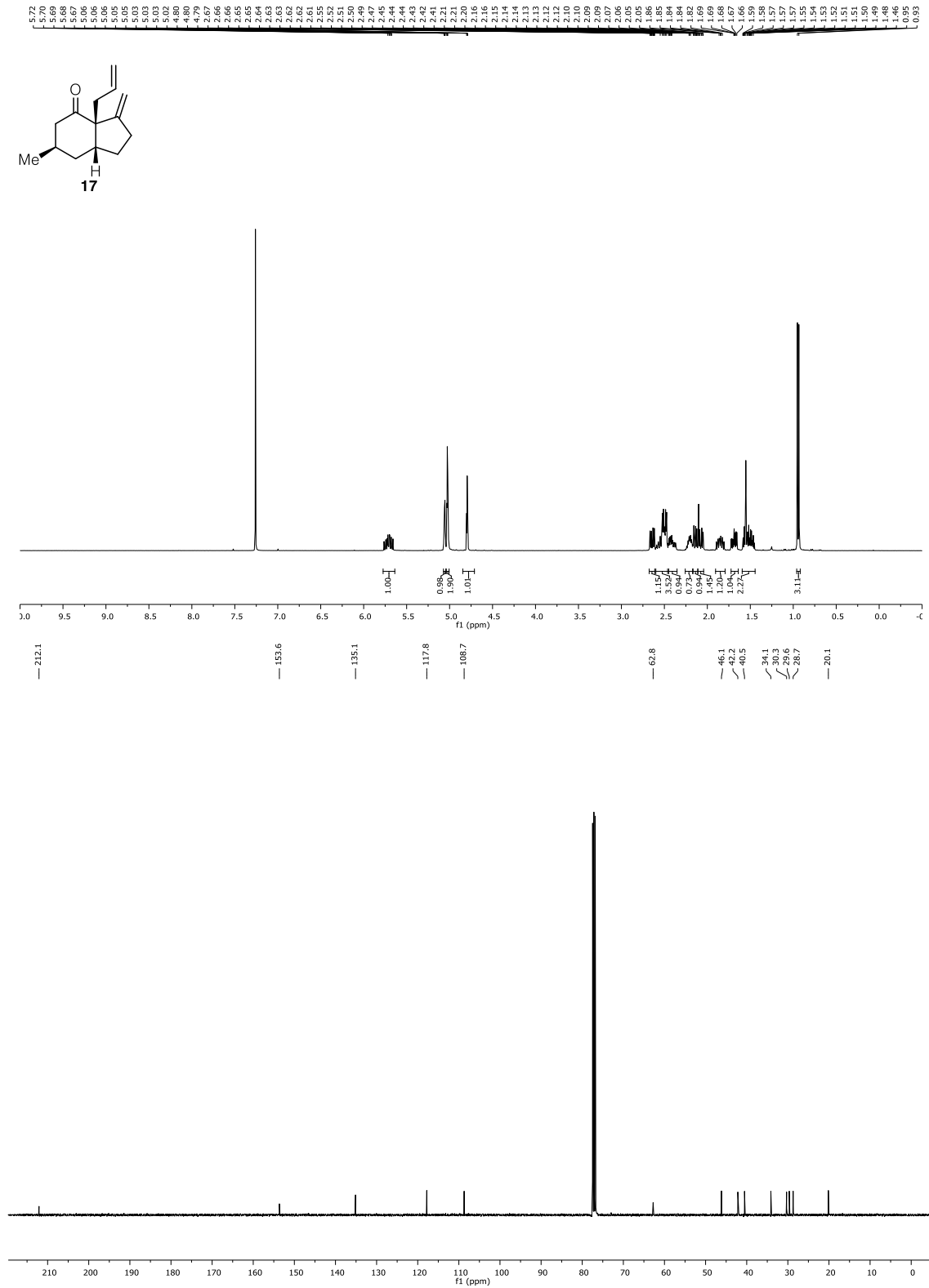


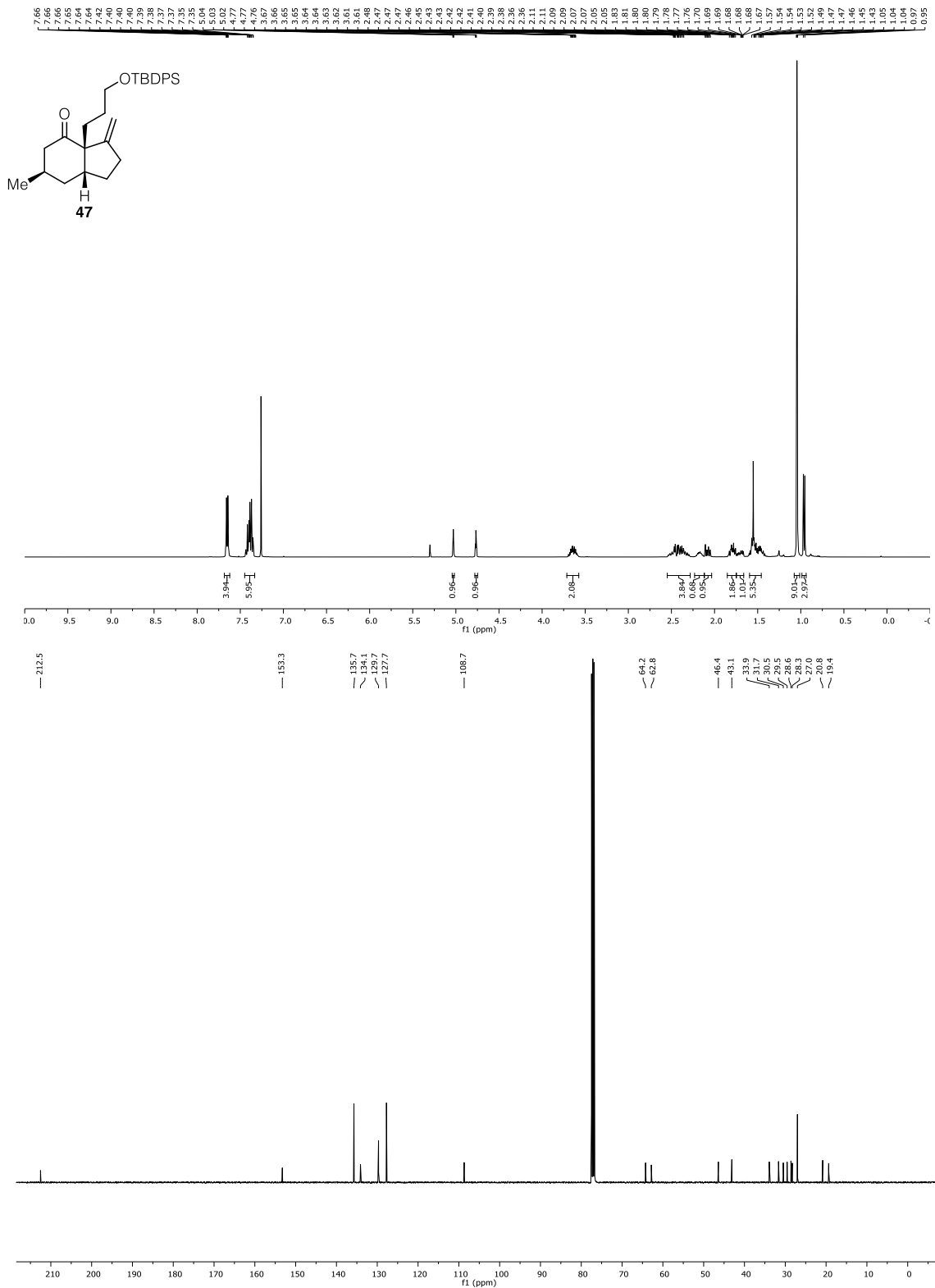


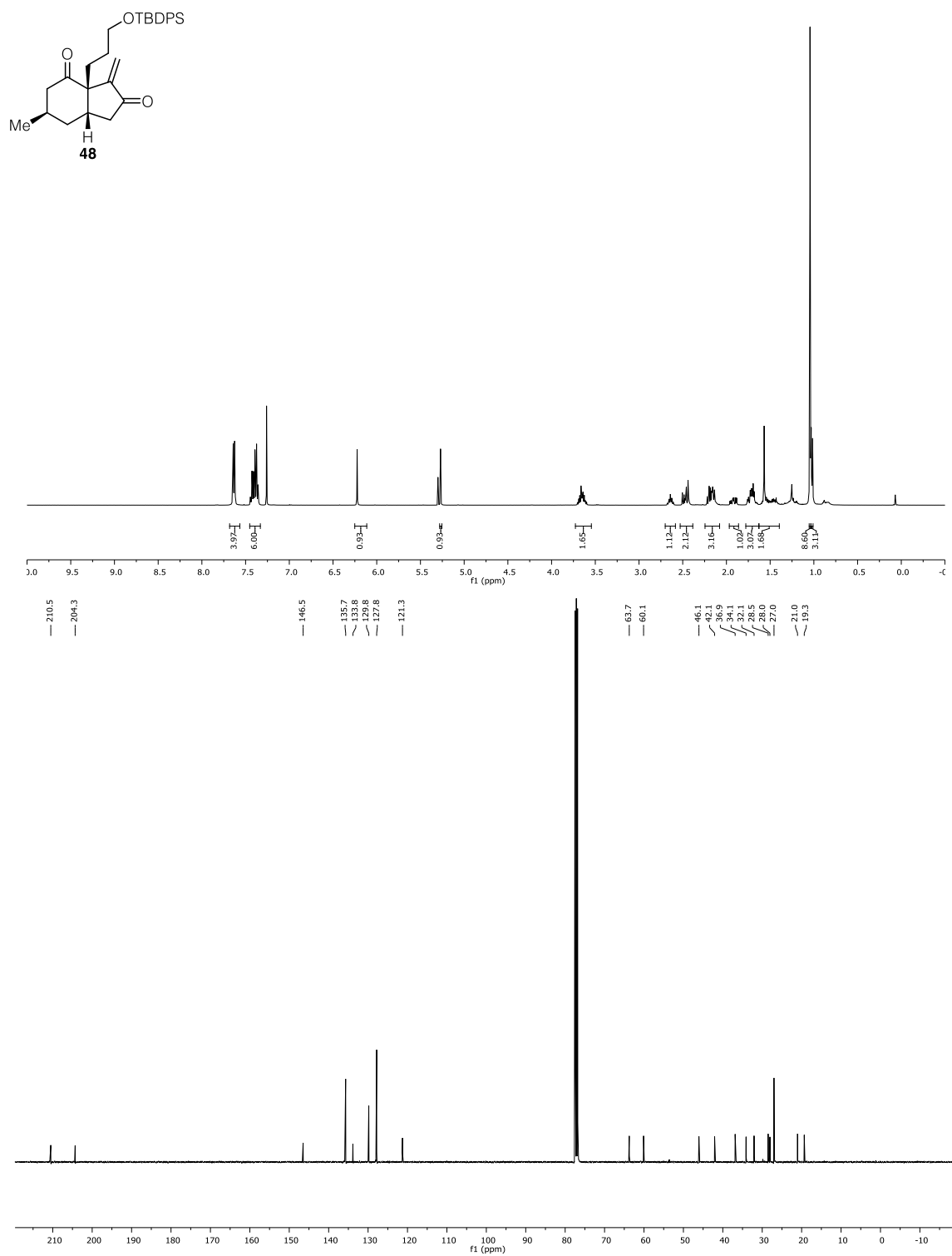
lycoserramine R



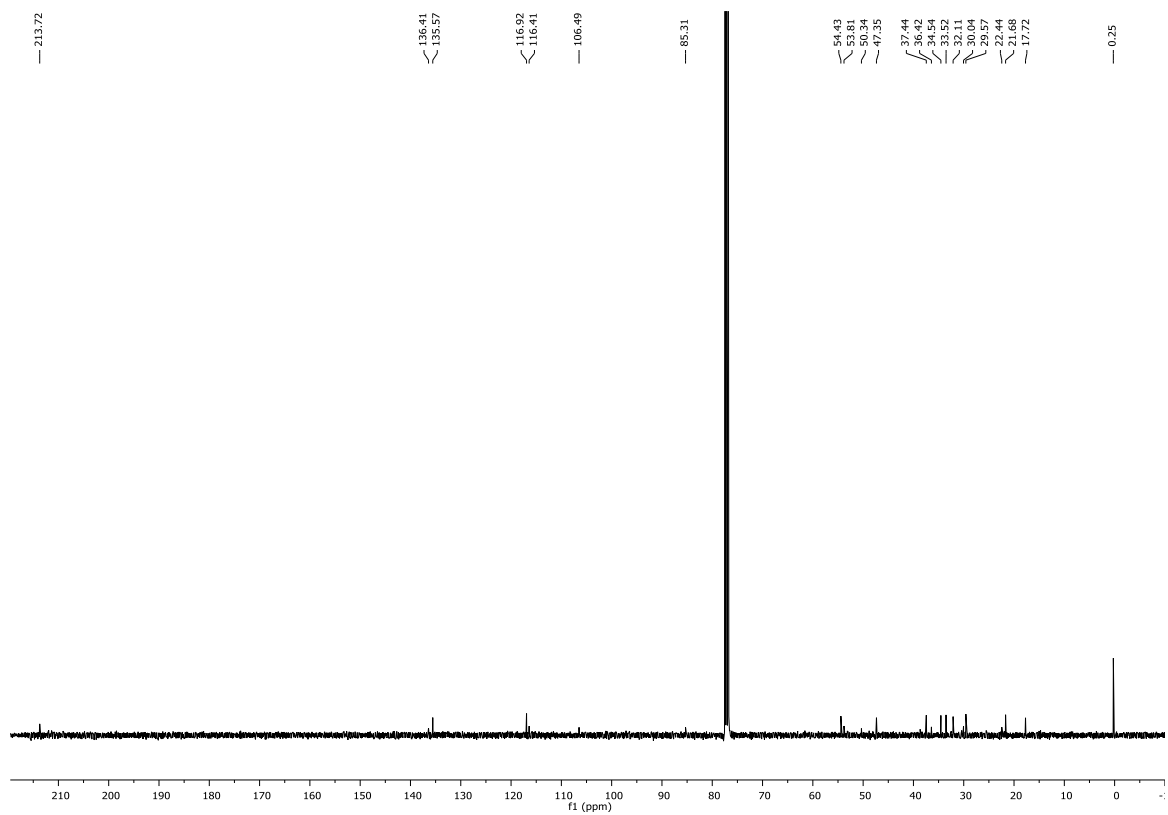
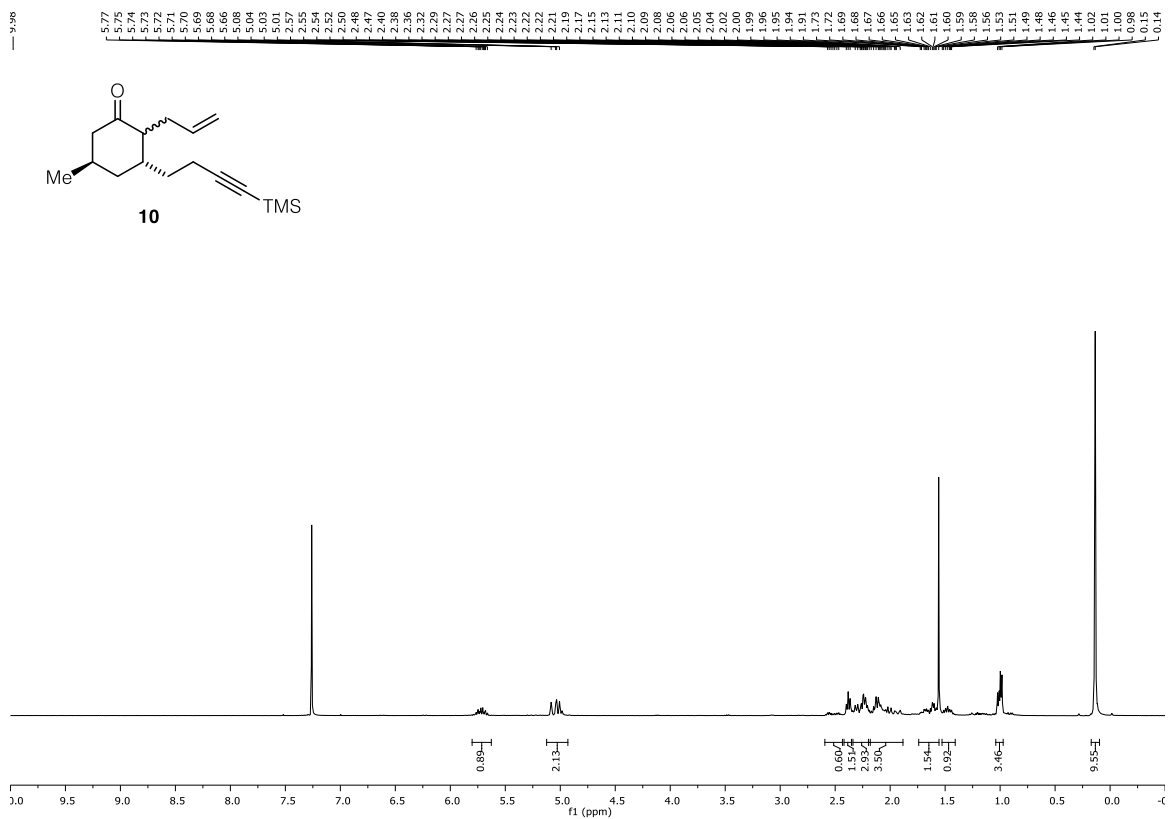


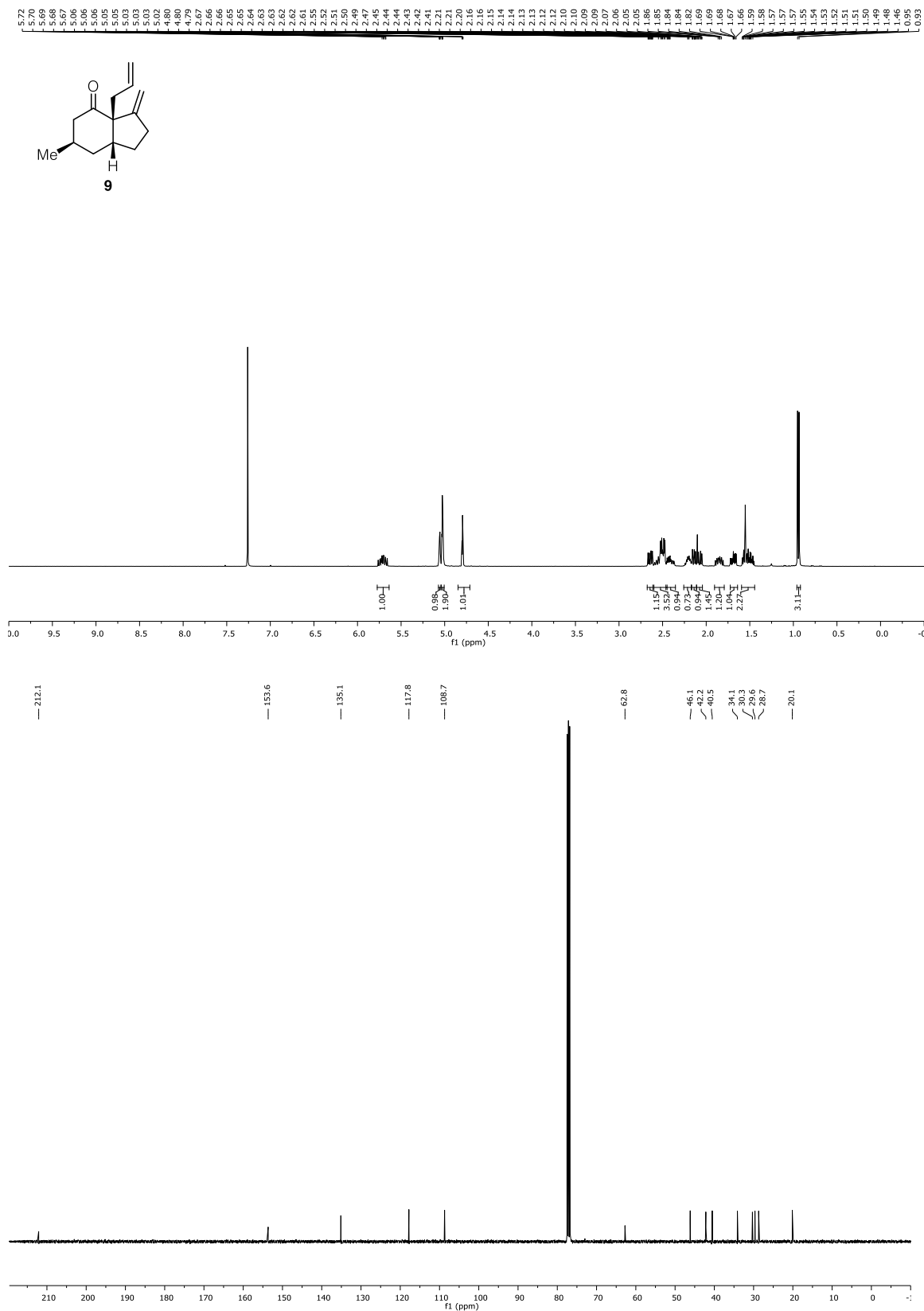


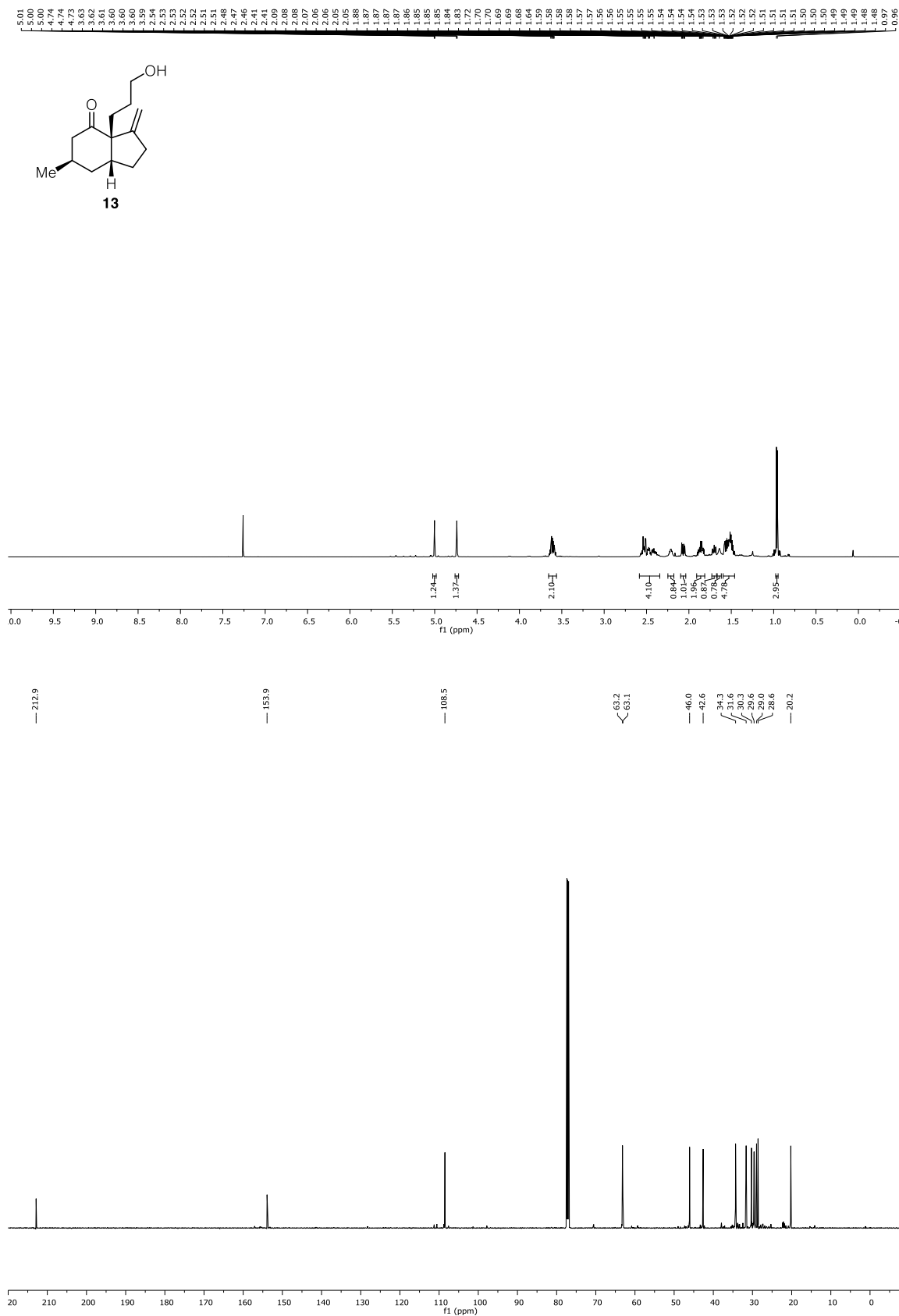


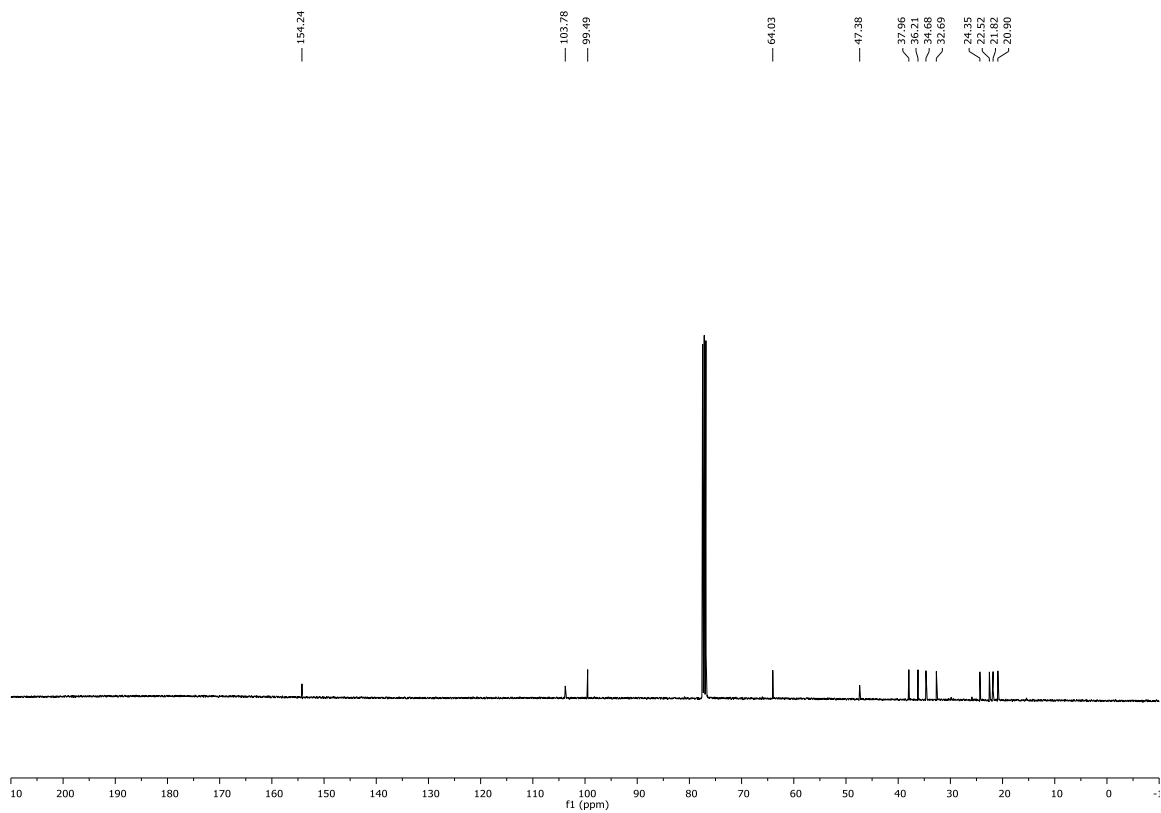
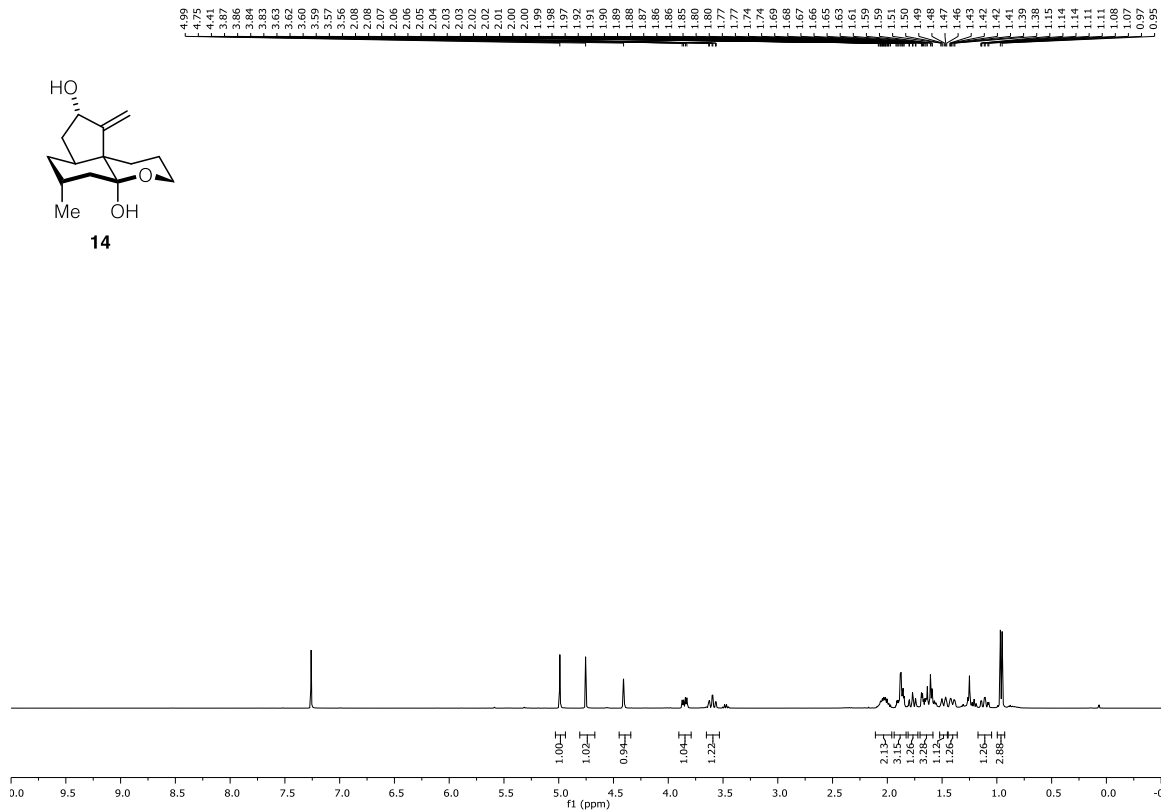
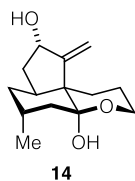


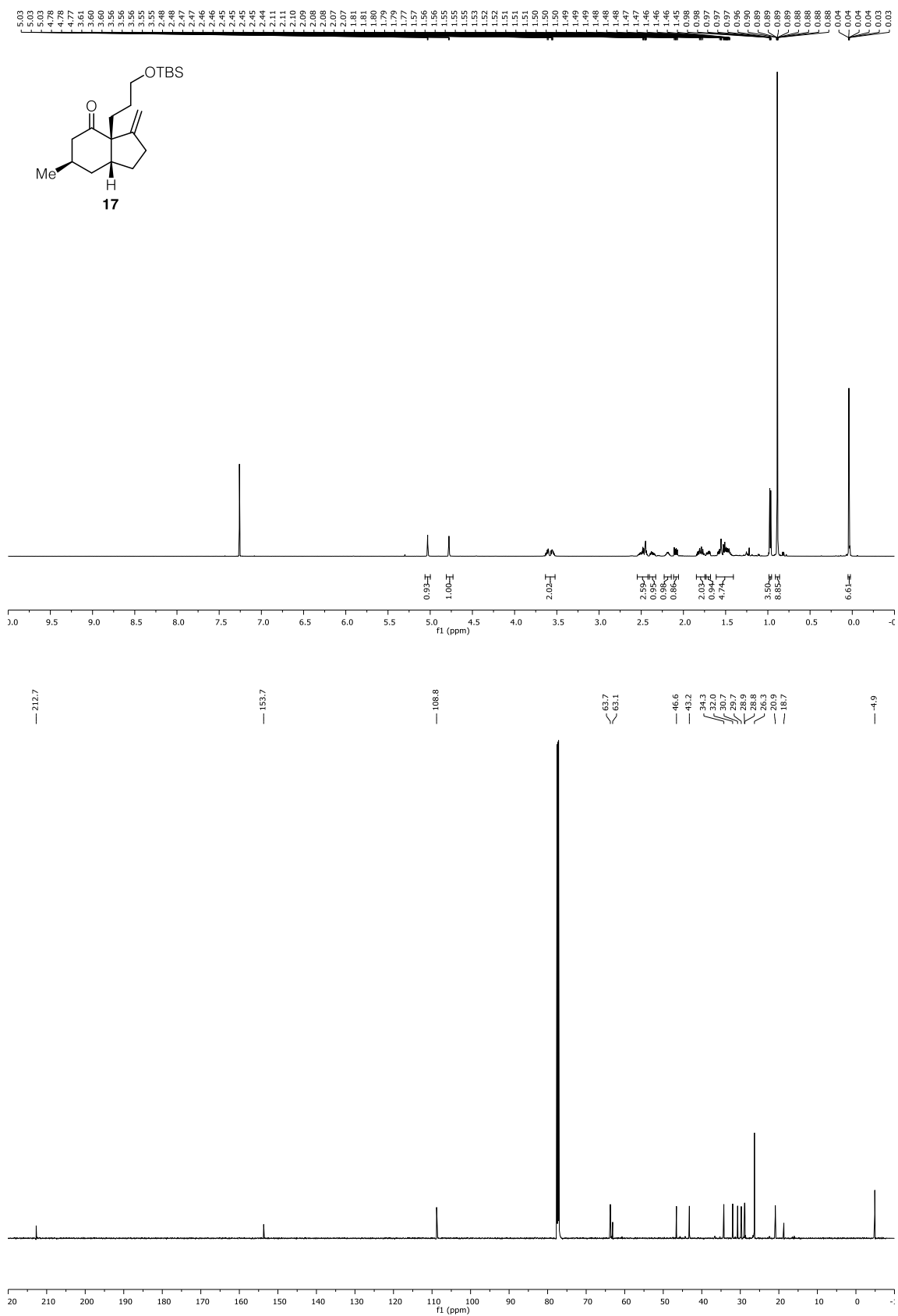
5.2 ^1H and ^{13}C NMR spectra for chapter 4.2.1.2

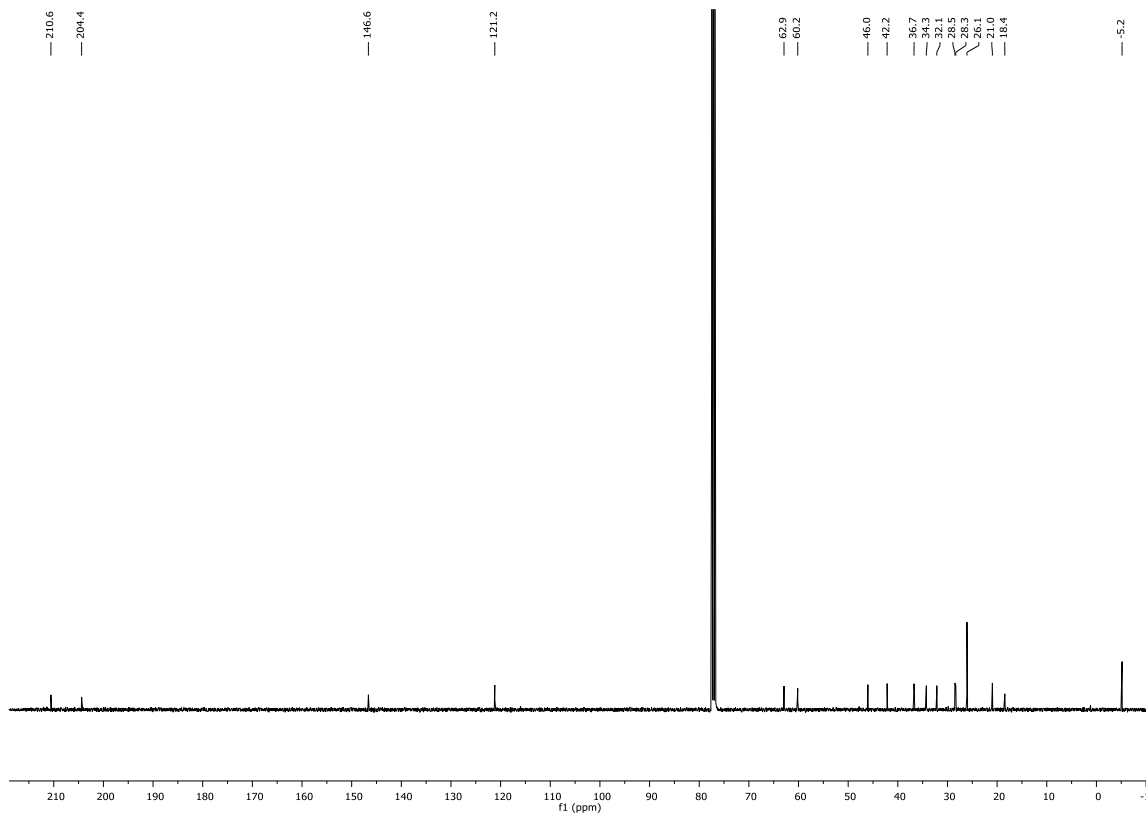
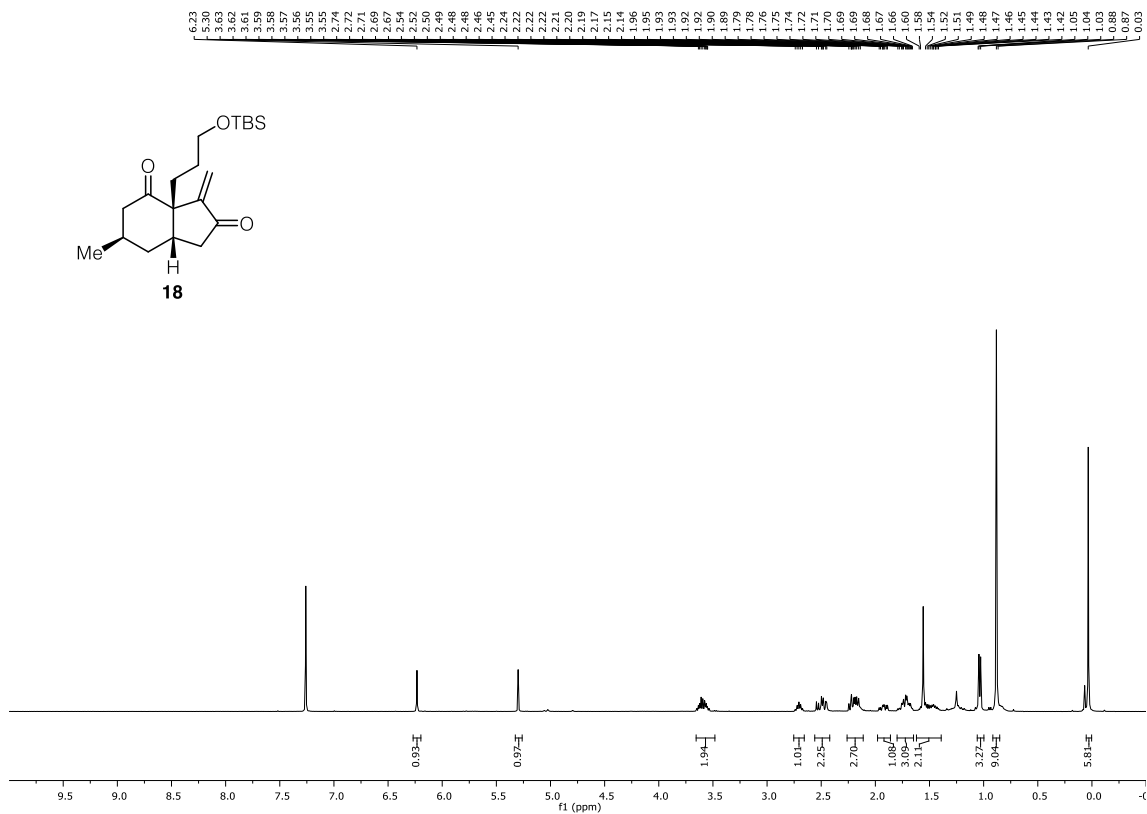
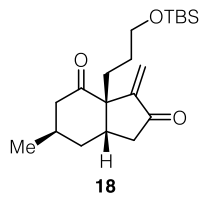


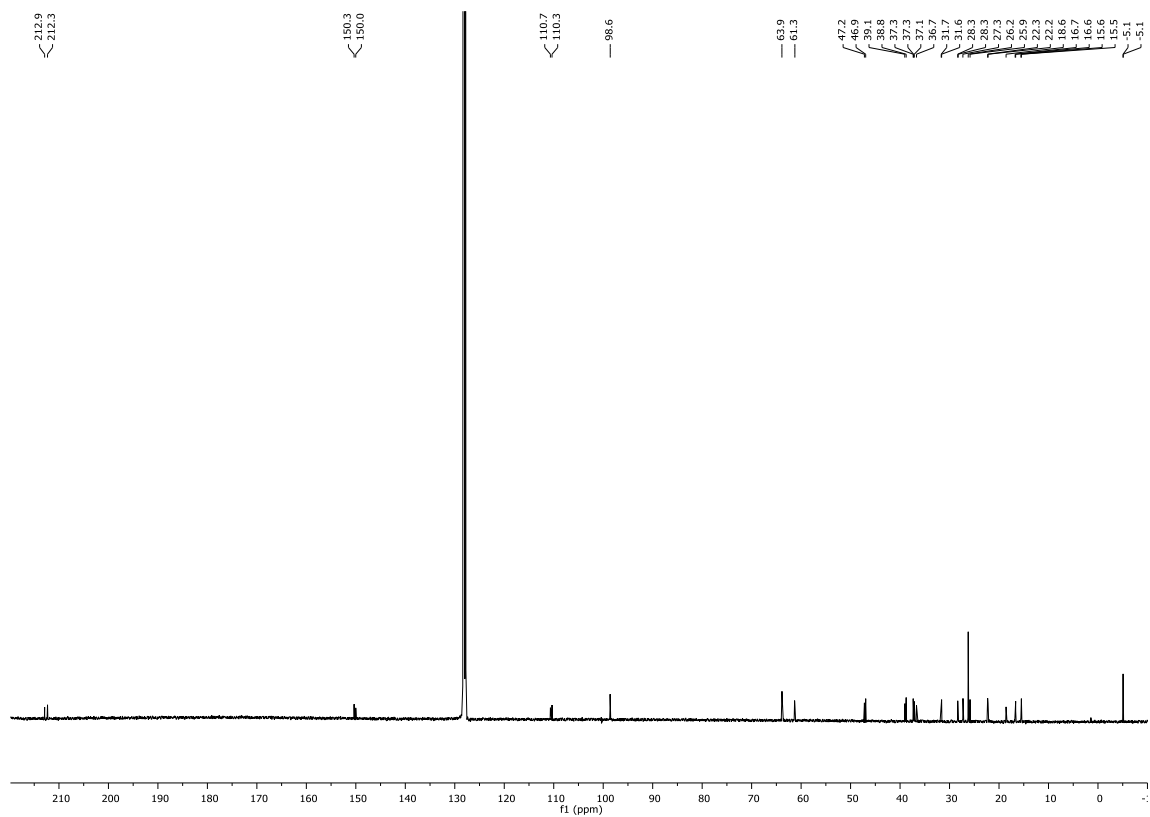
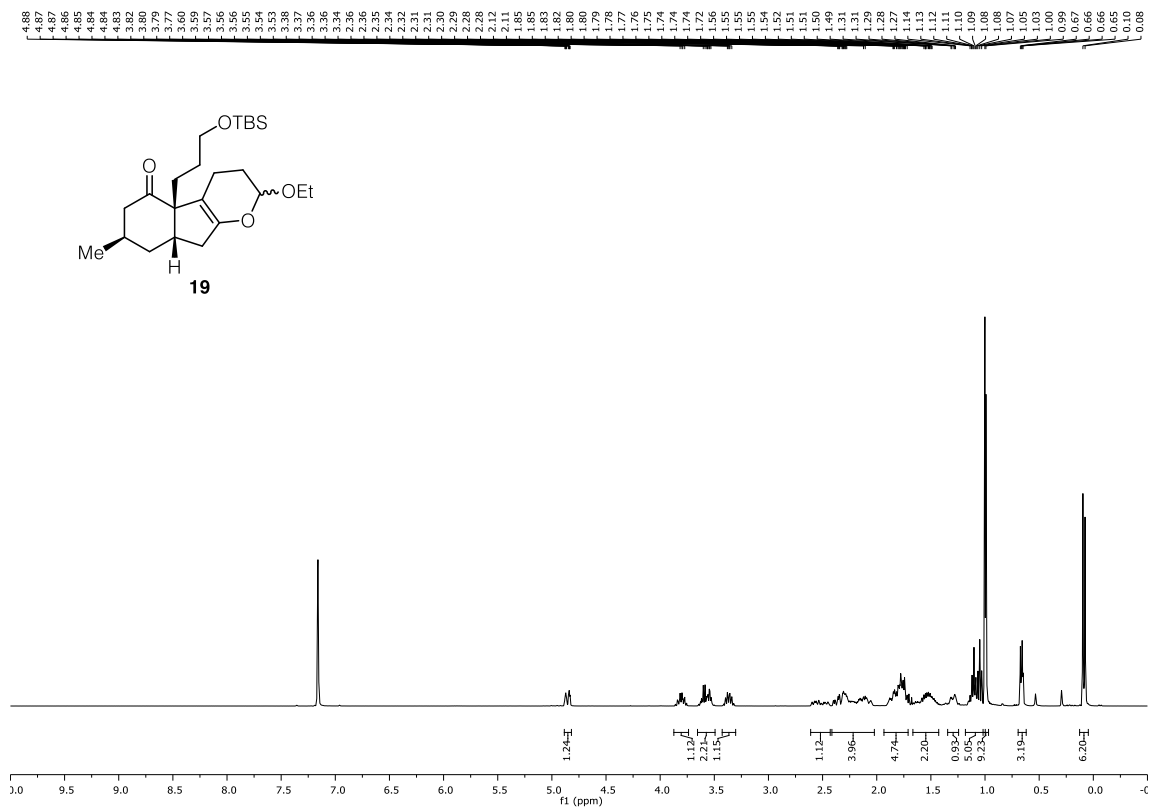


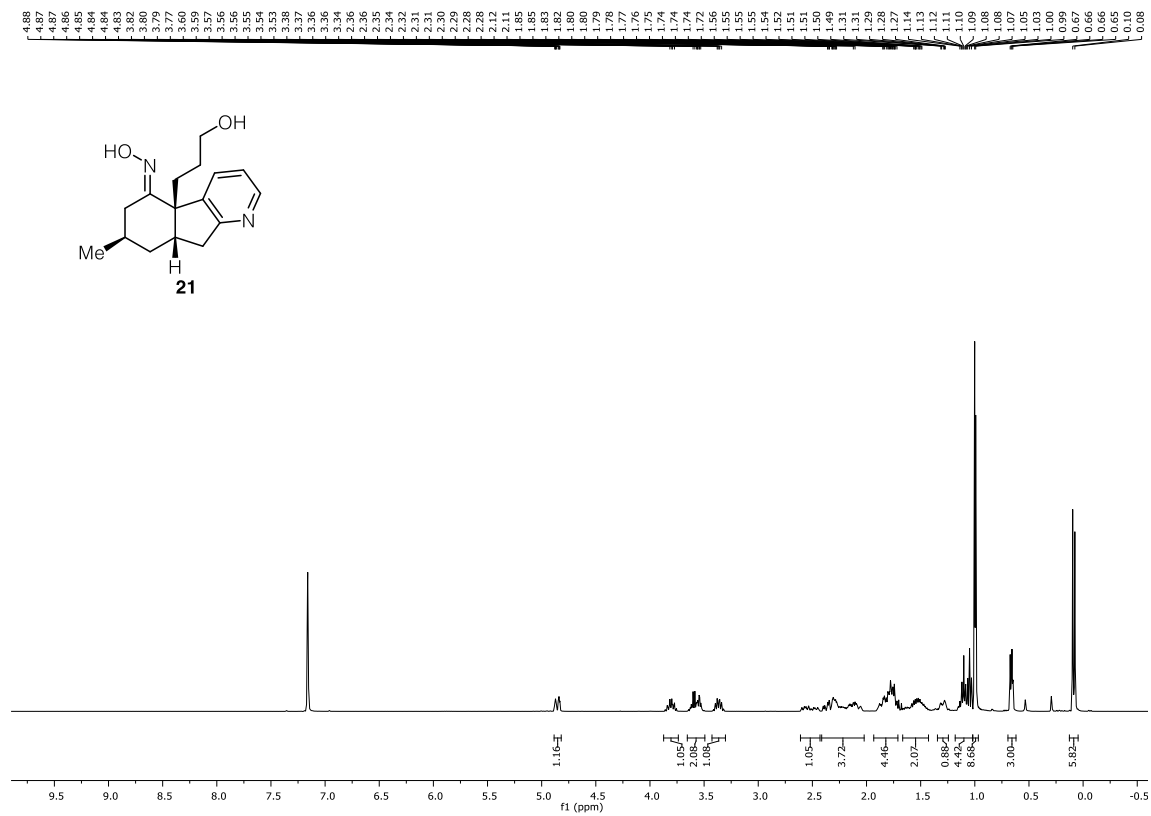




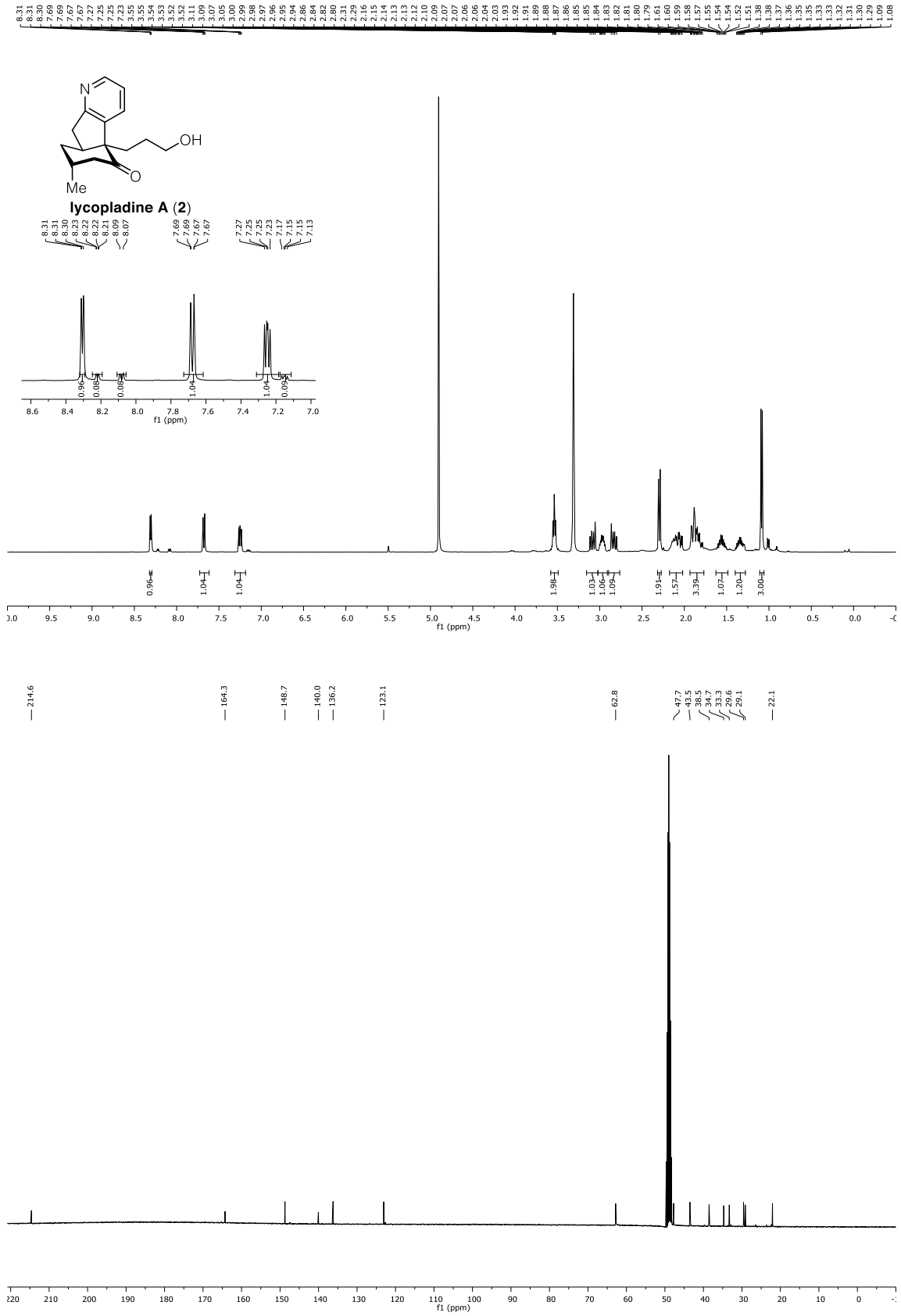


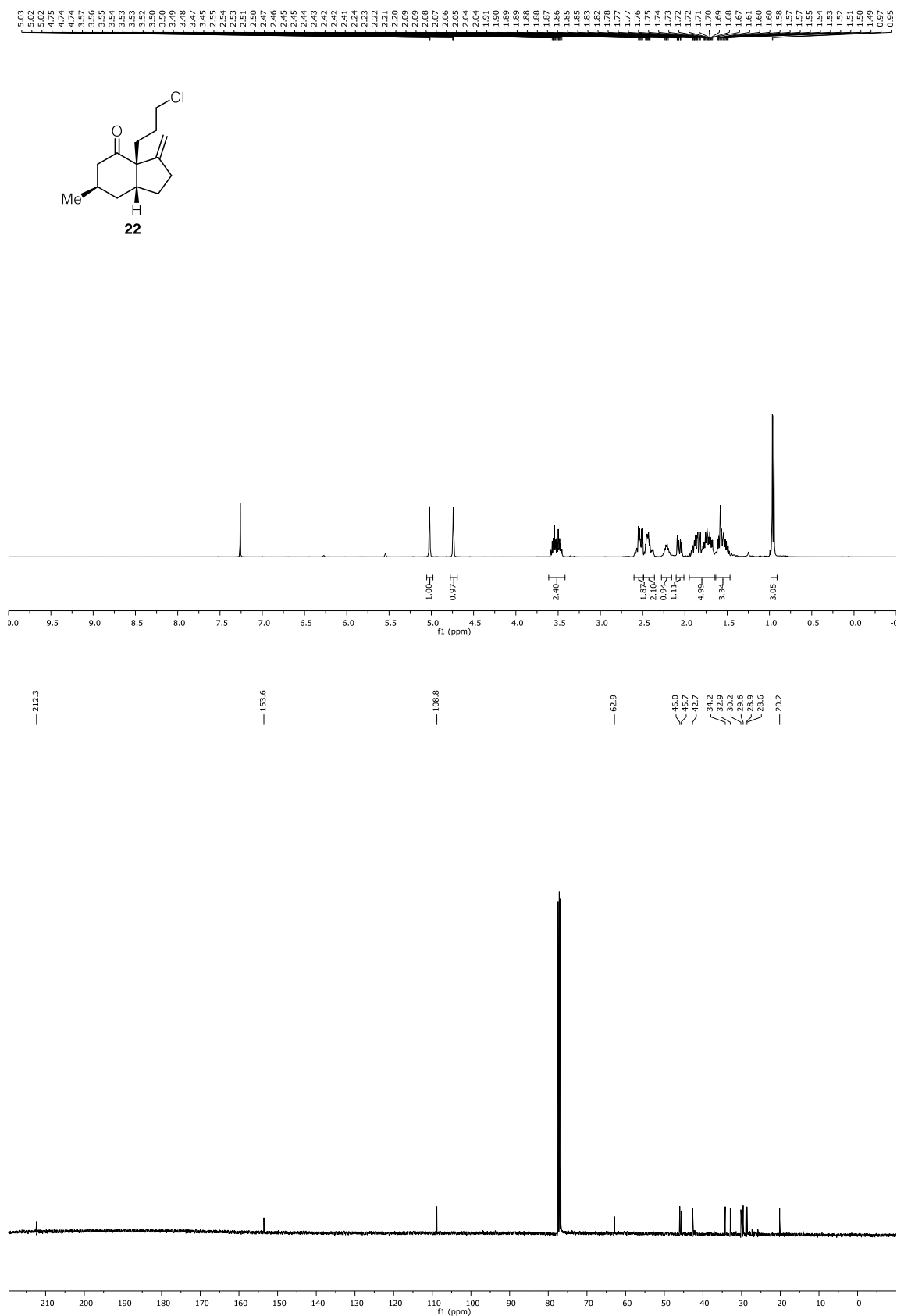


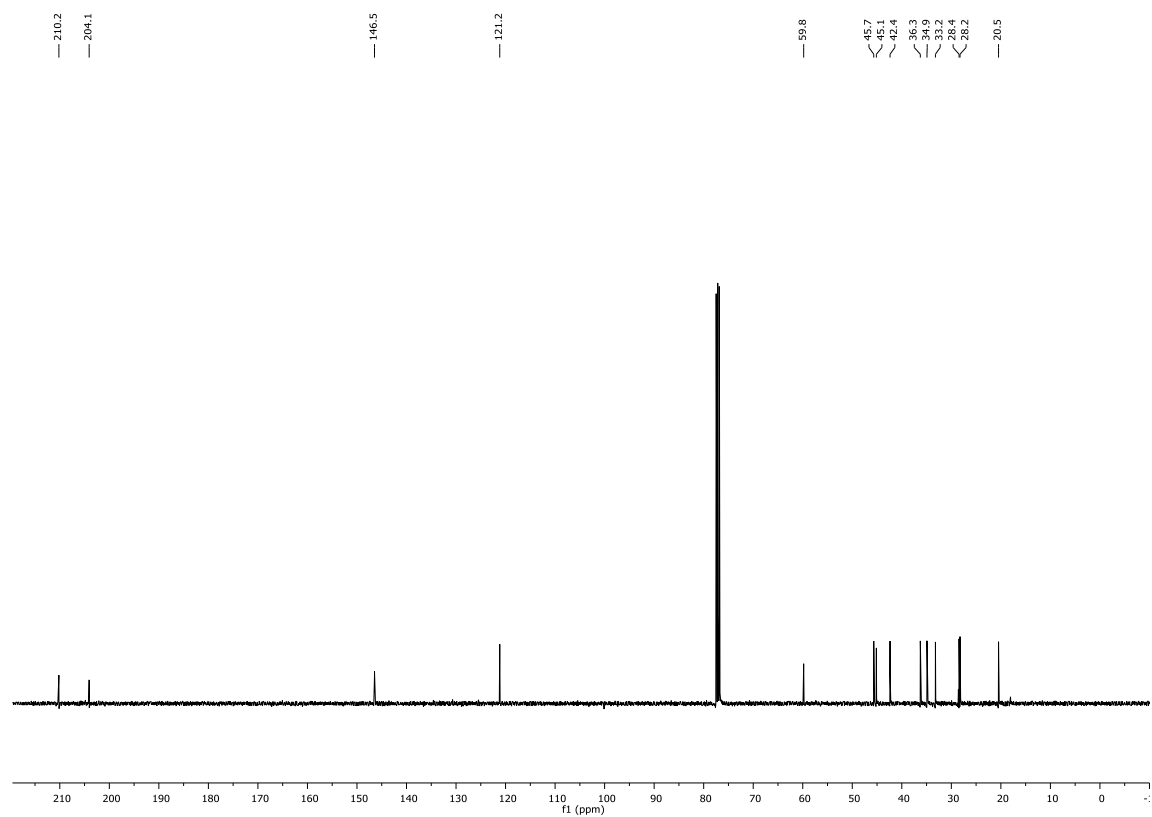
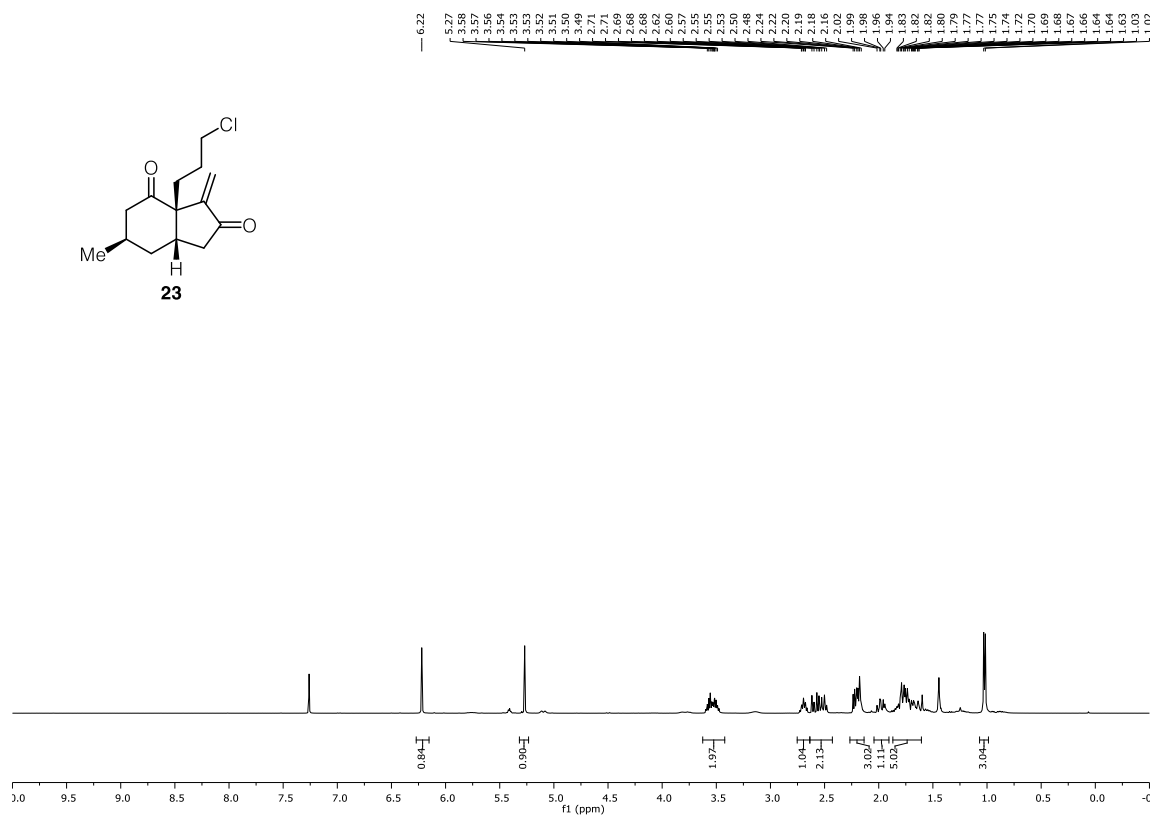
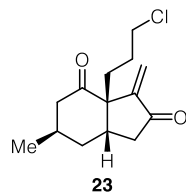


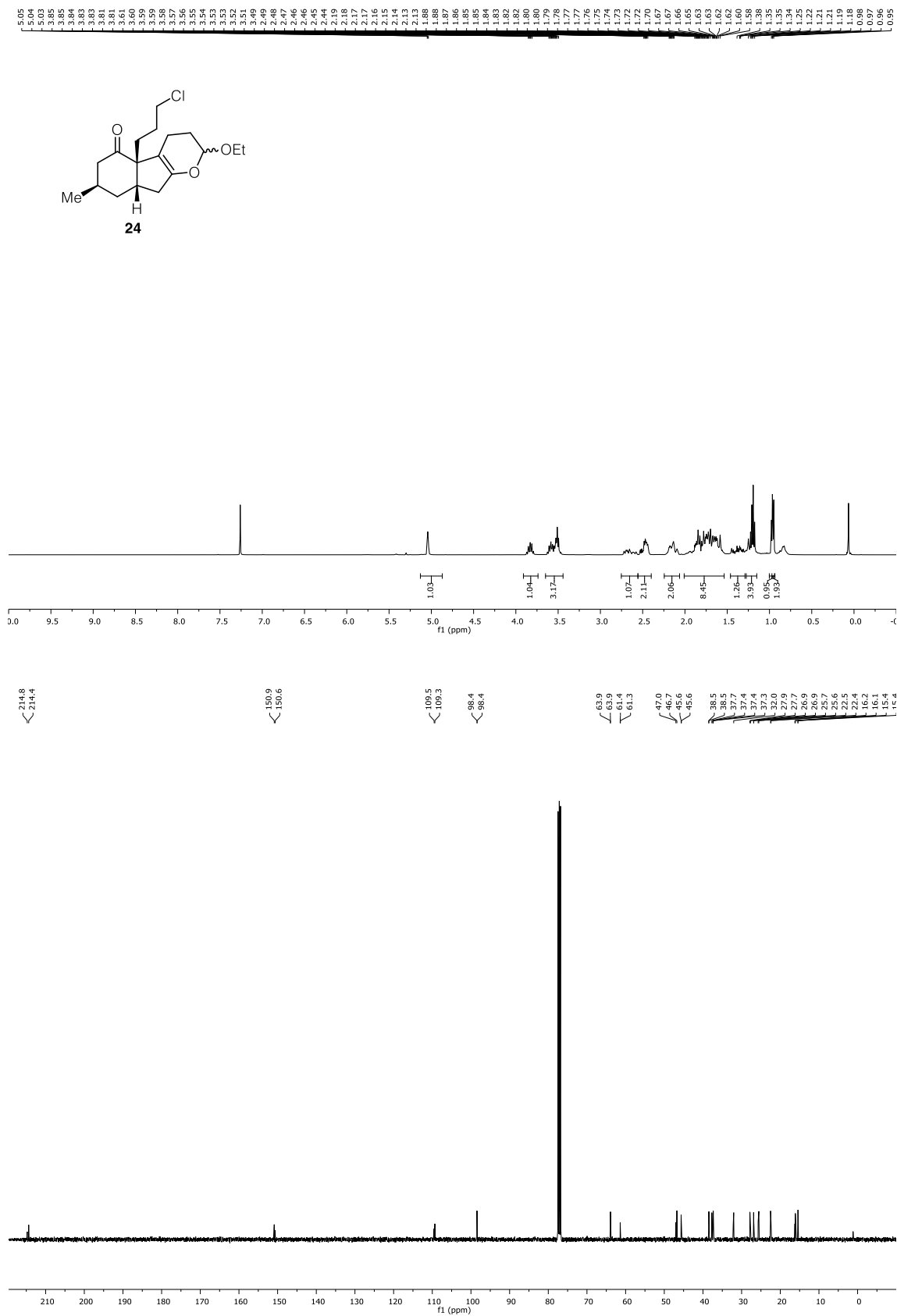


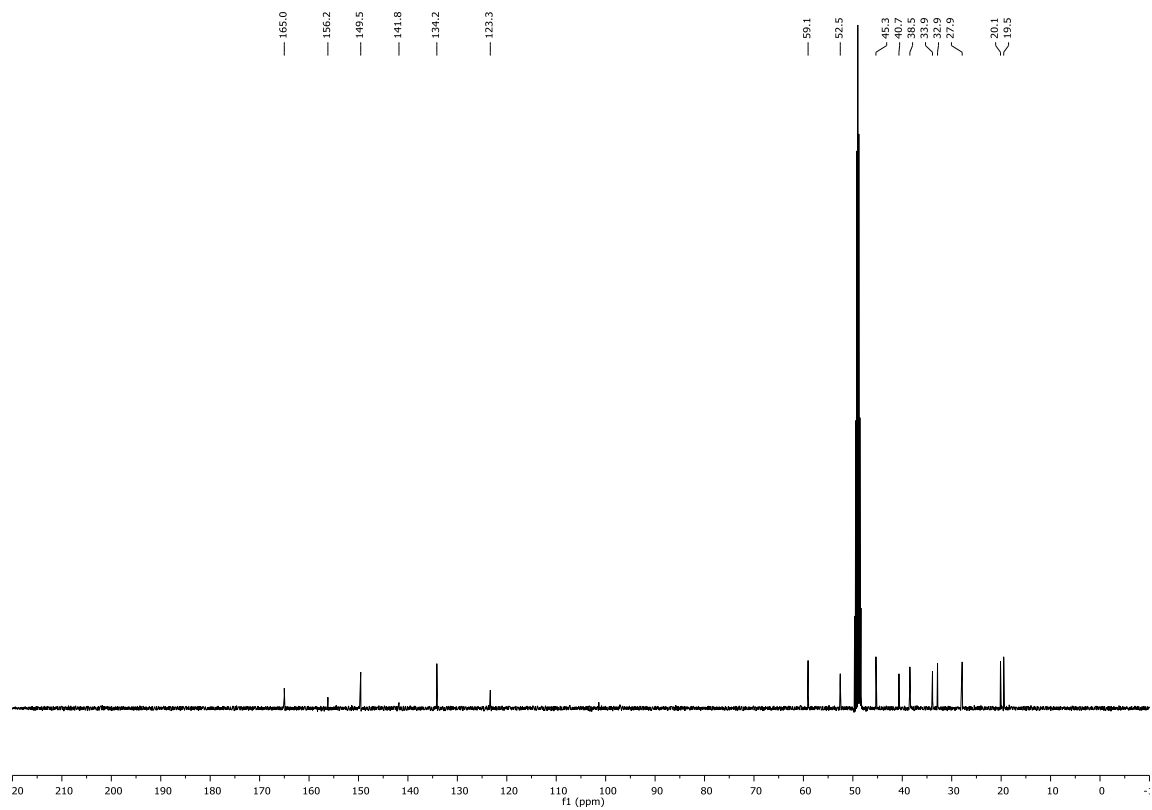
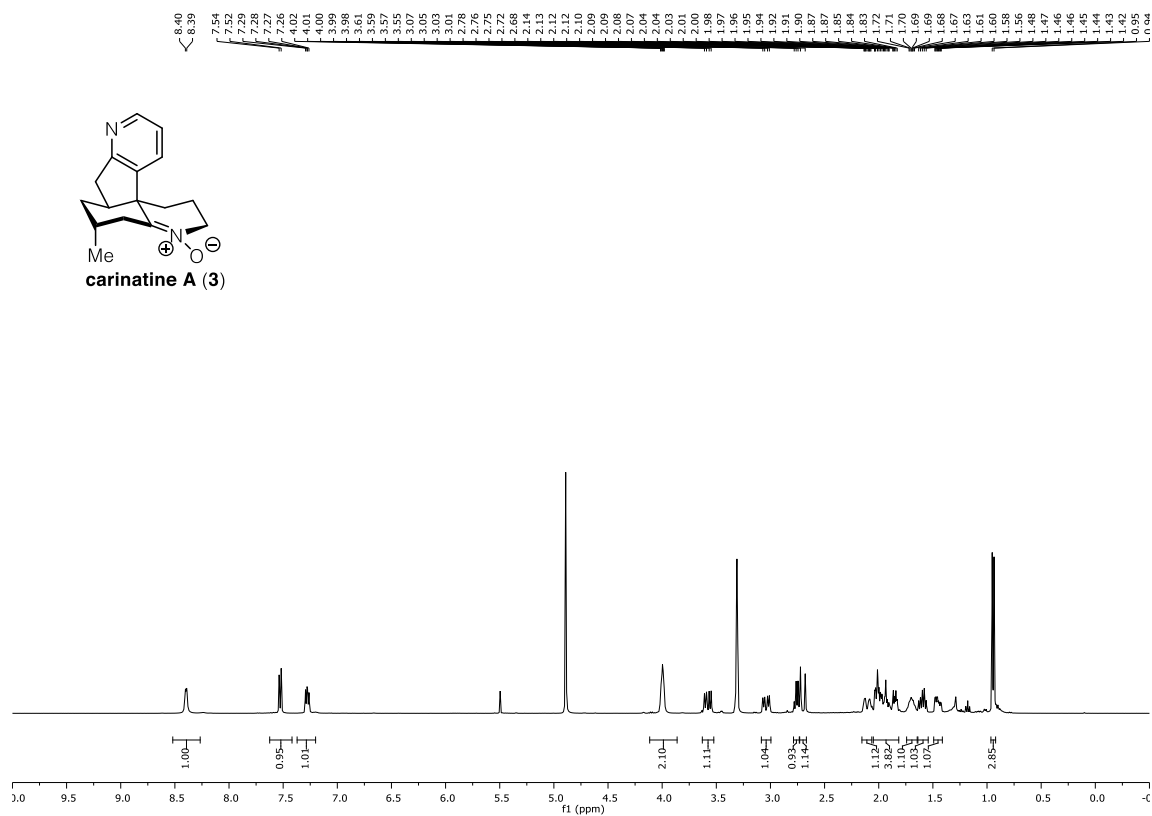
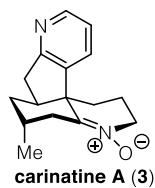
known compound



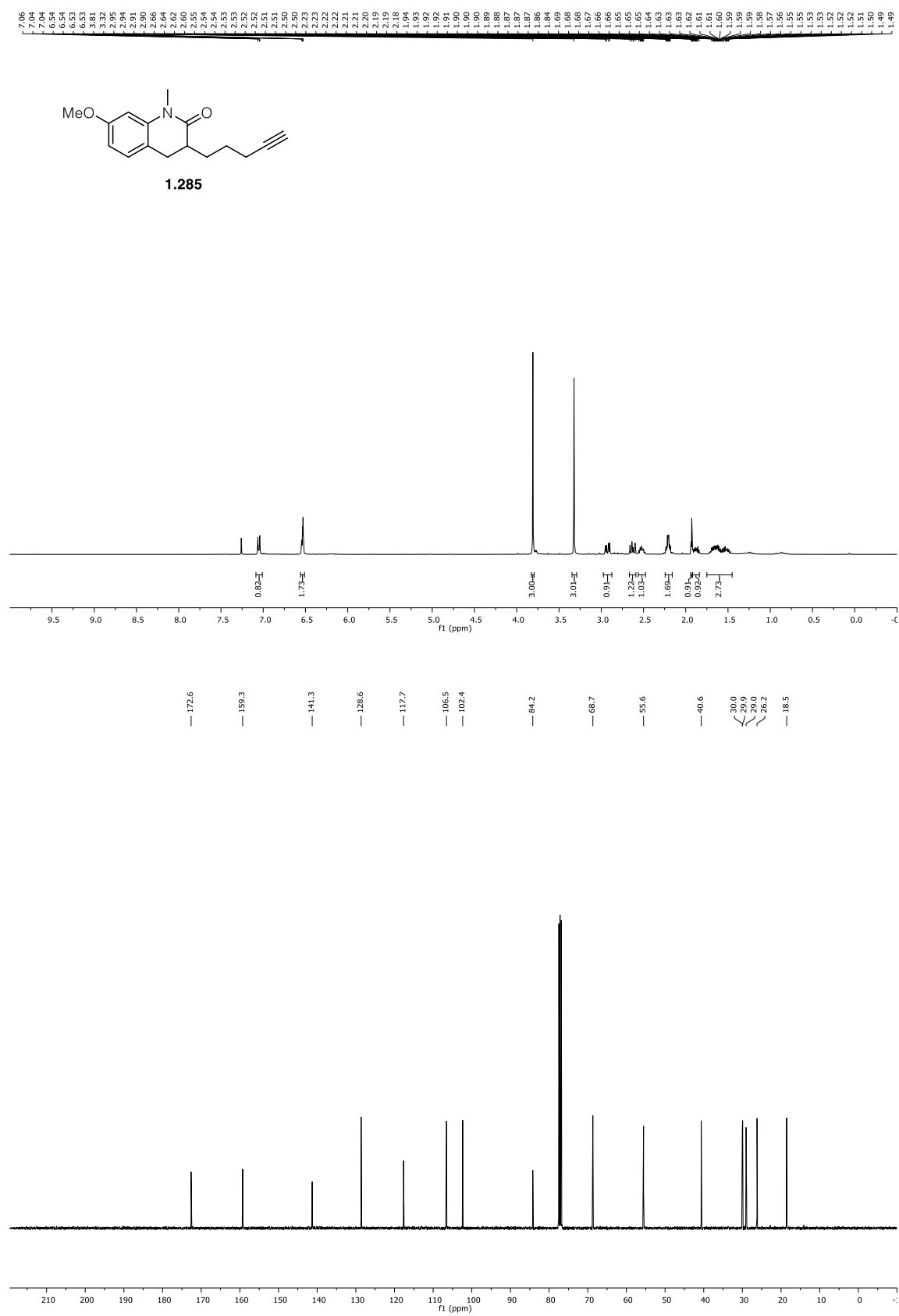


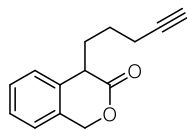




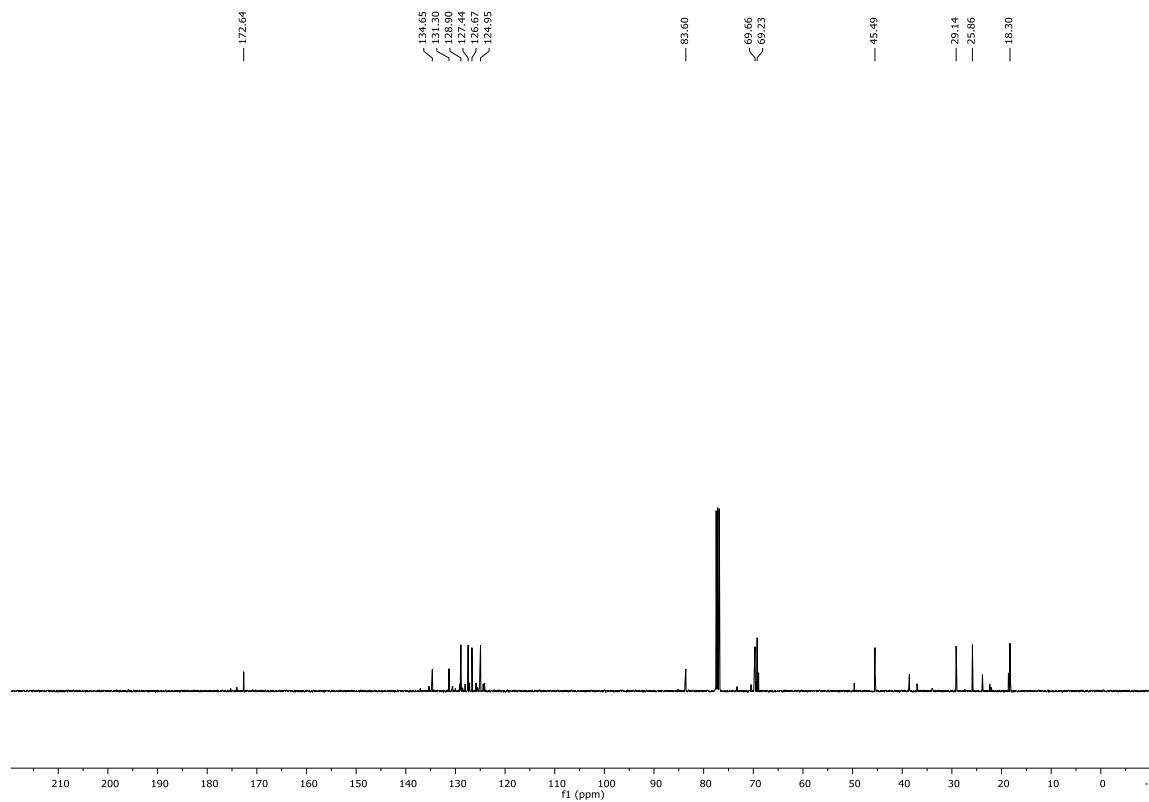
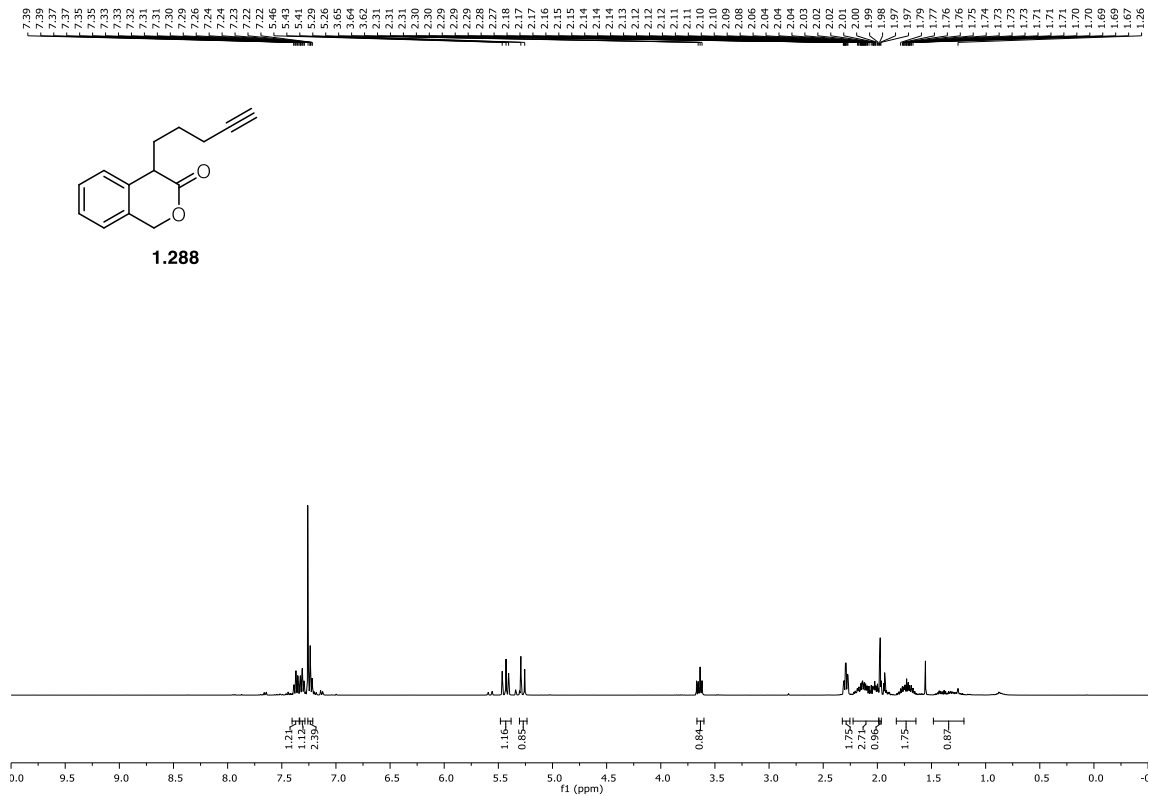


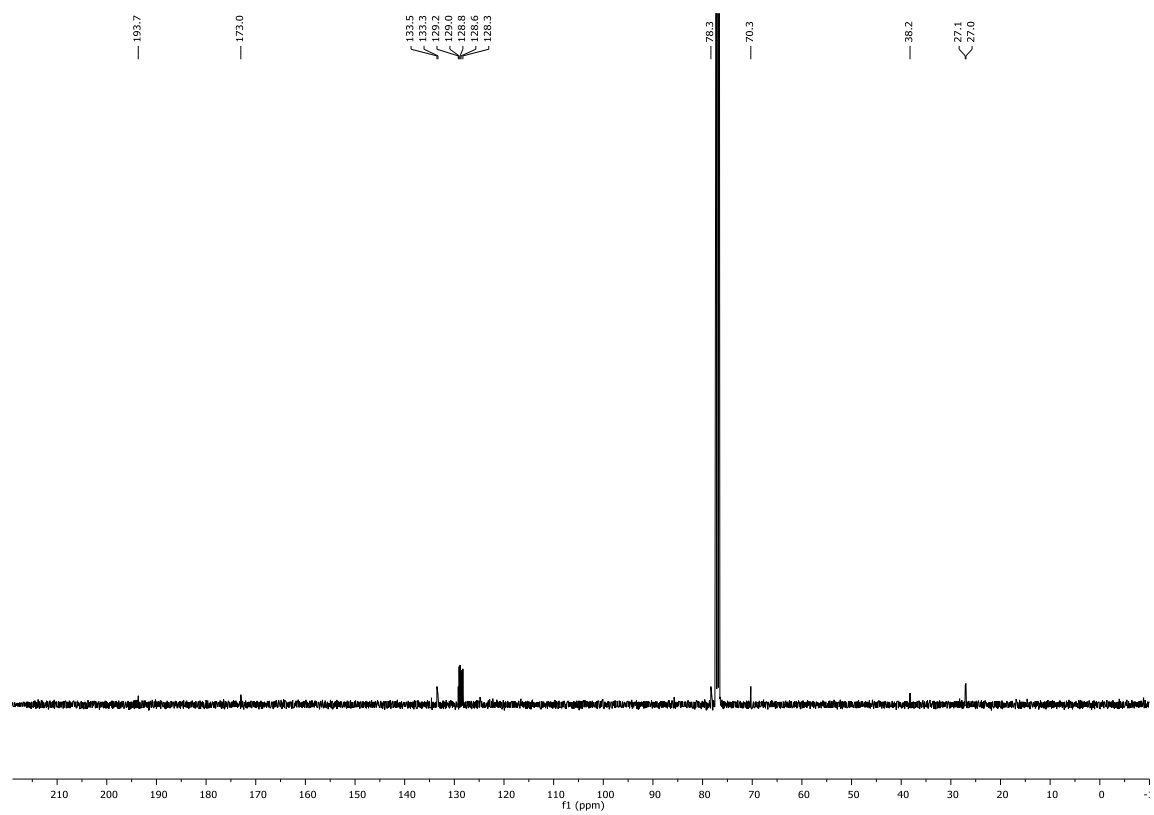
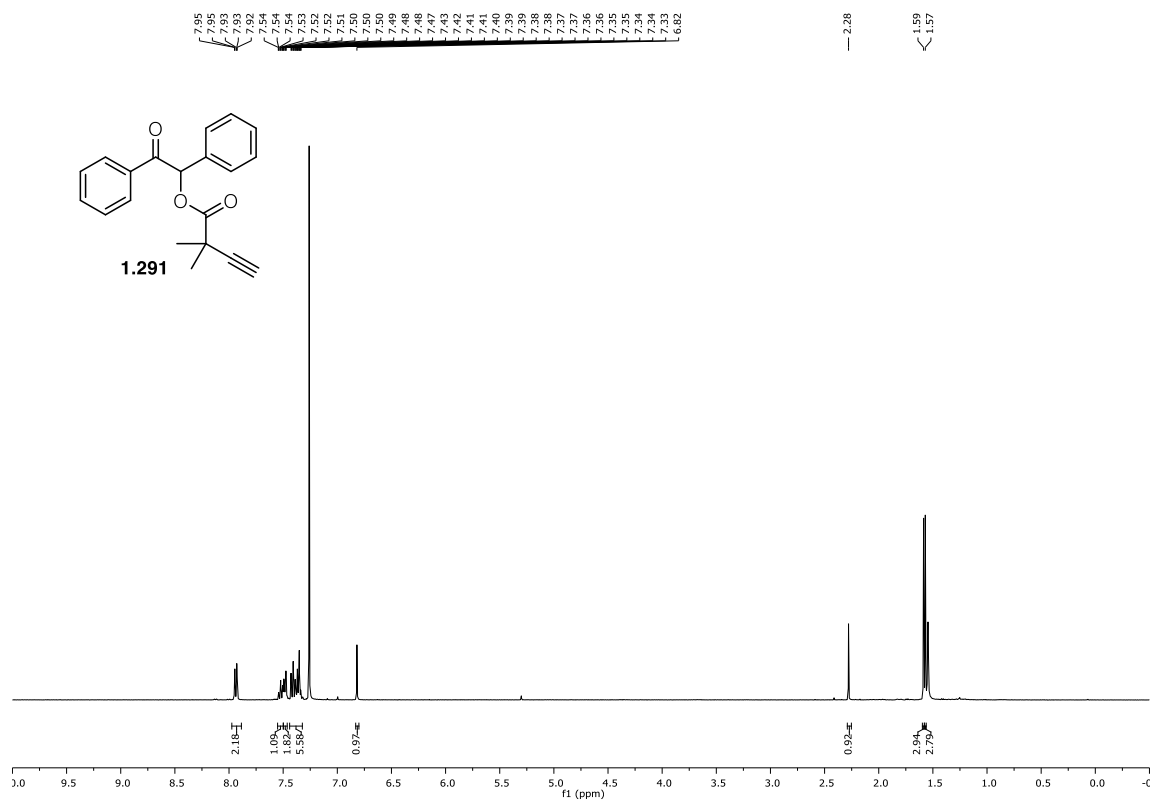
5.3 ^1H and ^{13}C NMR spectra for chapter 4.2.2

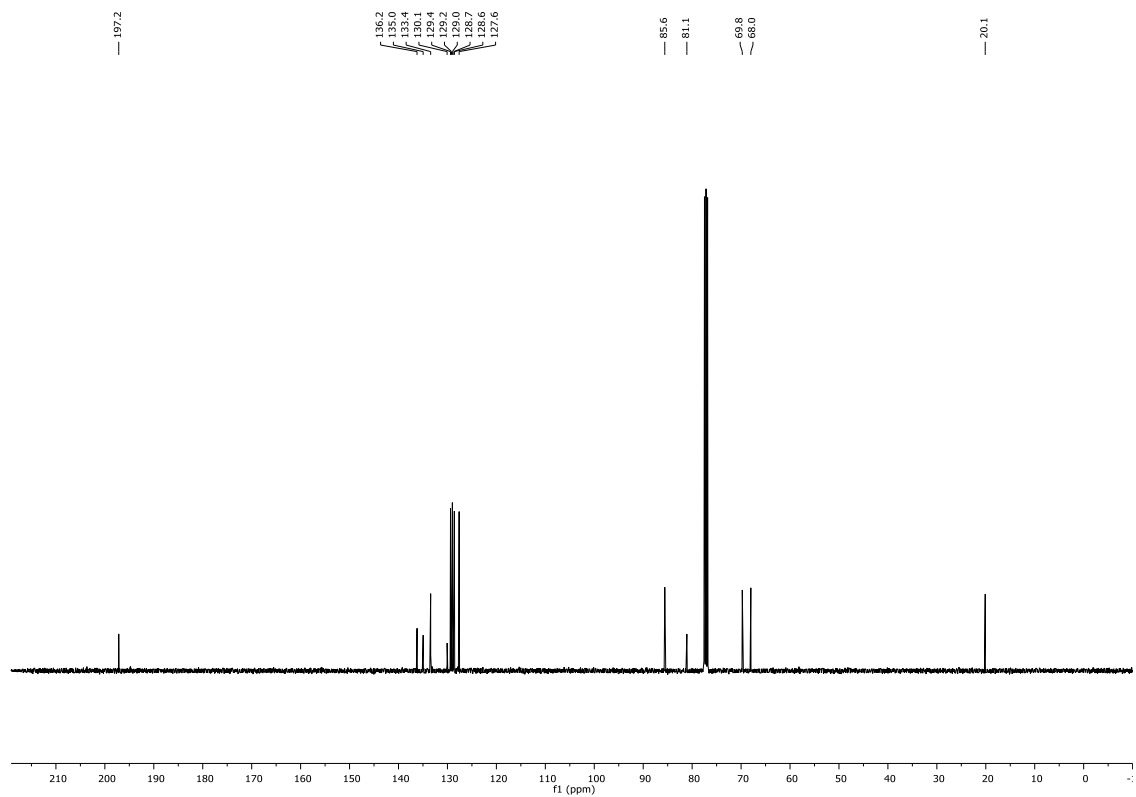
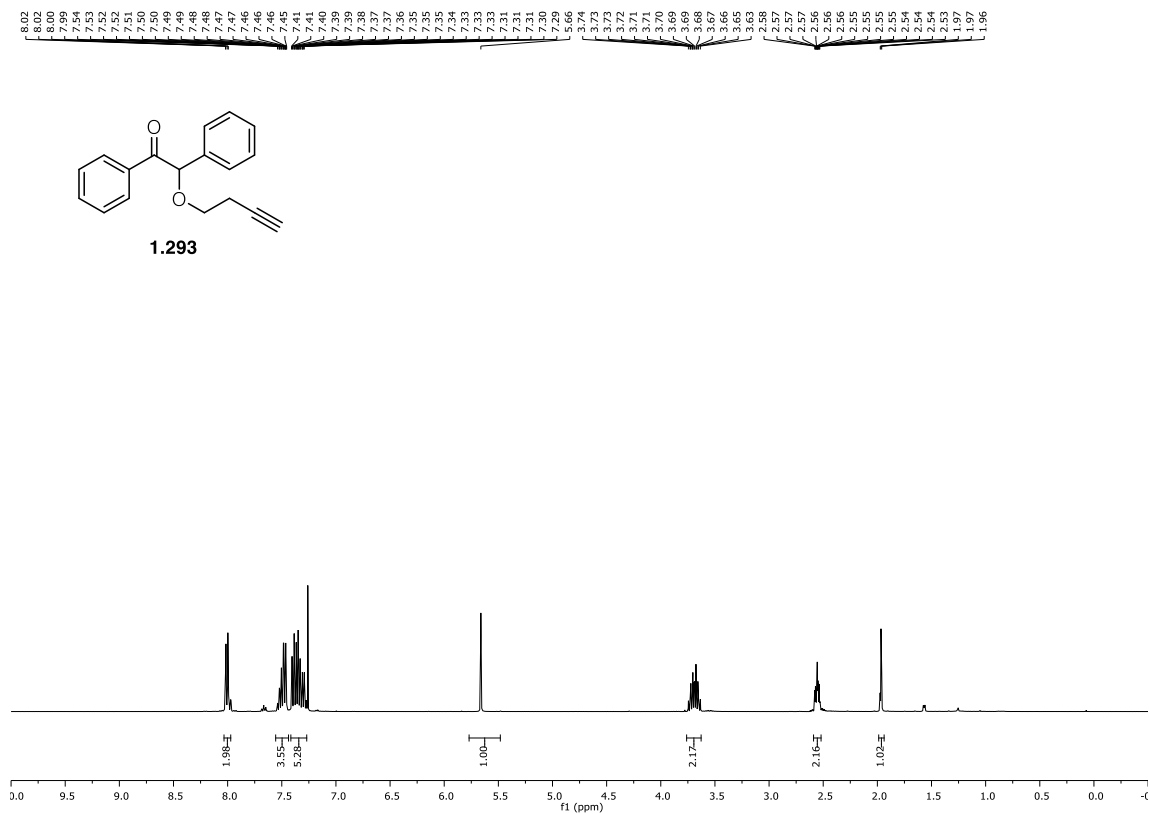


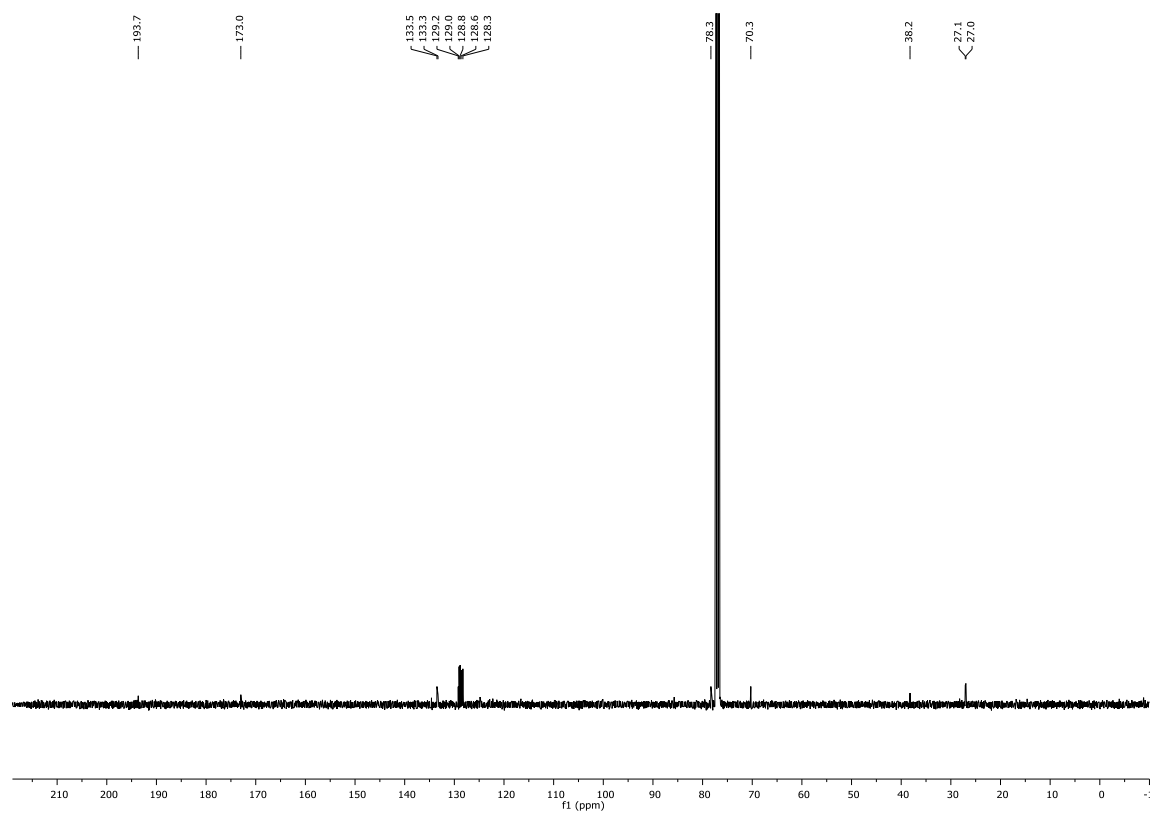
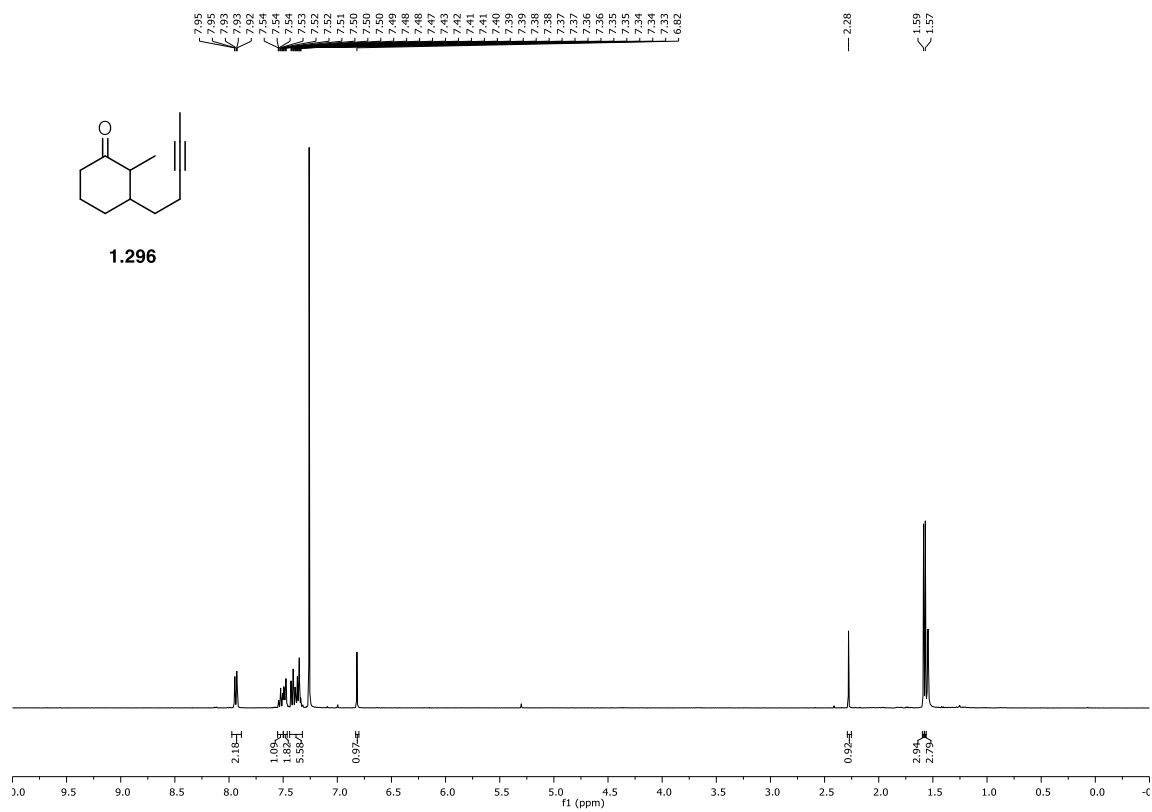


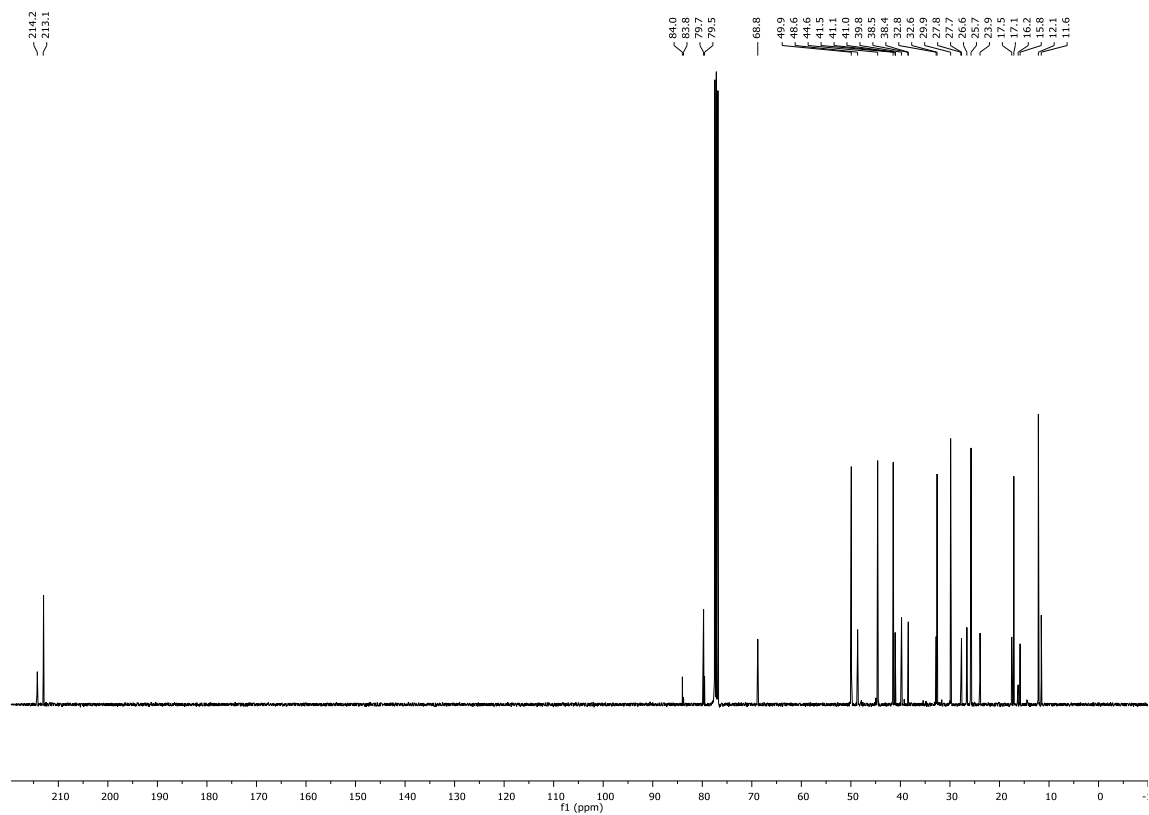
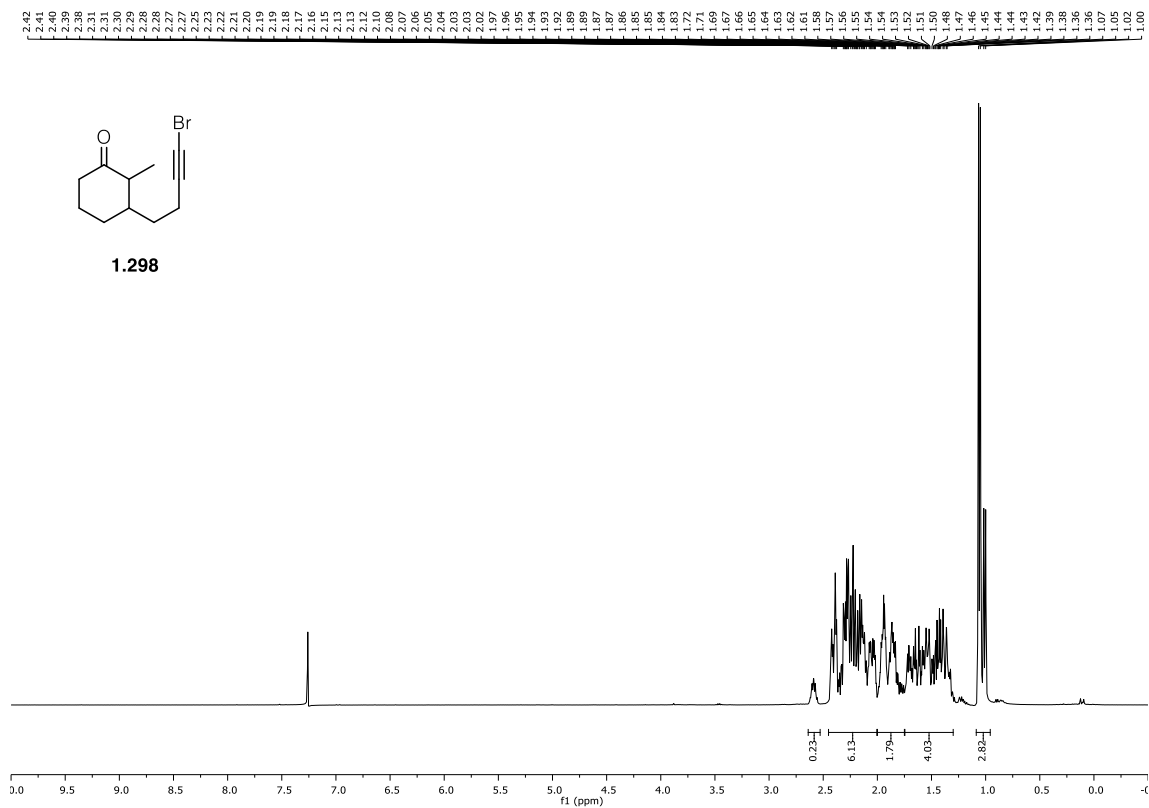
1.288

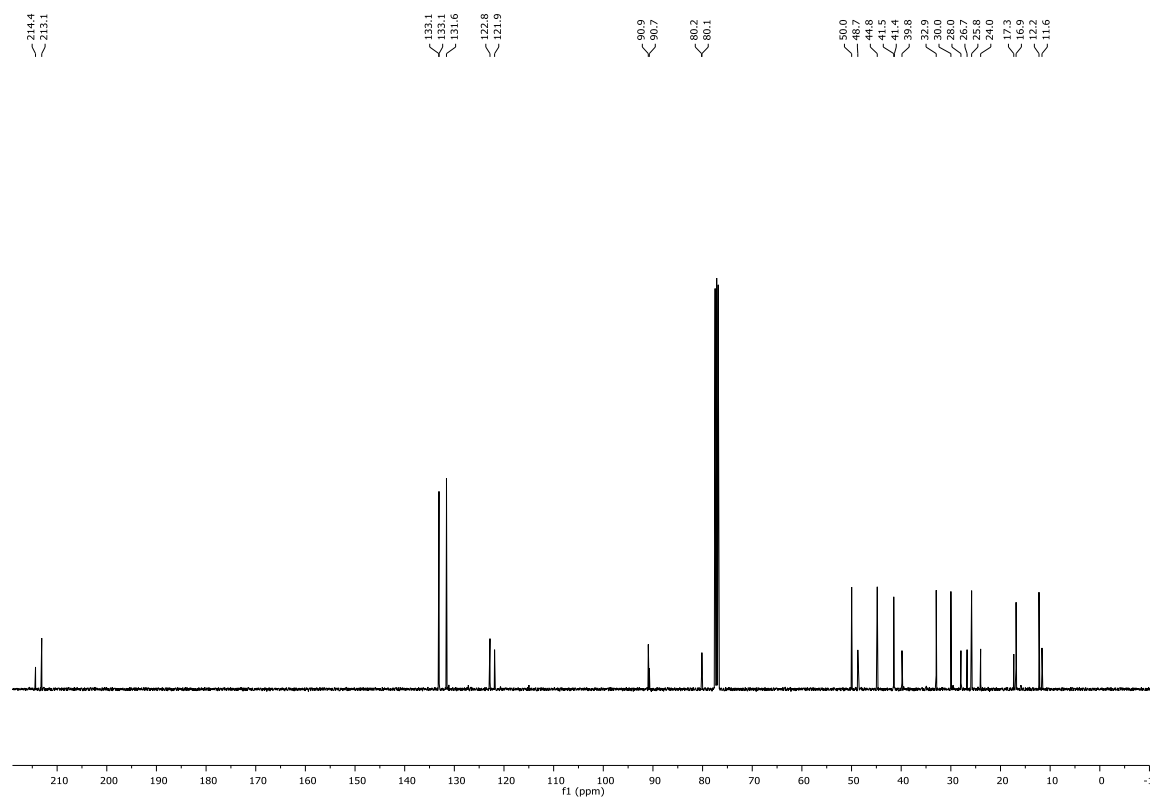
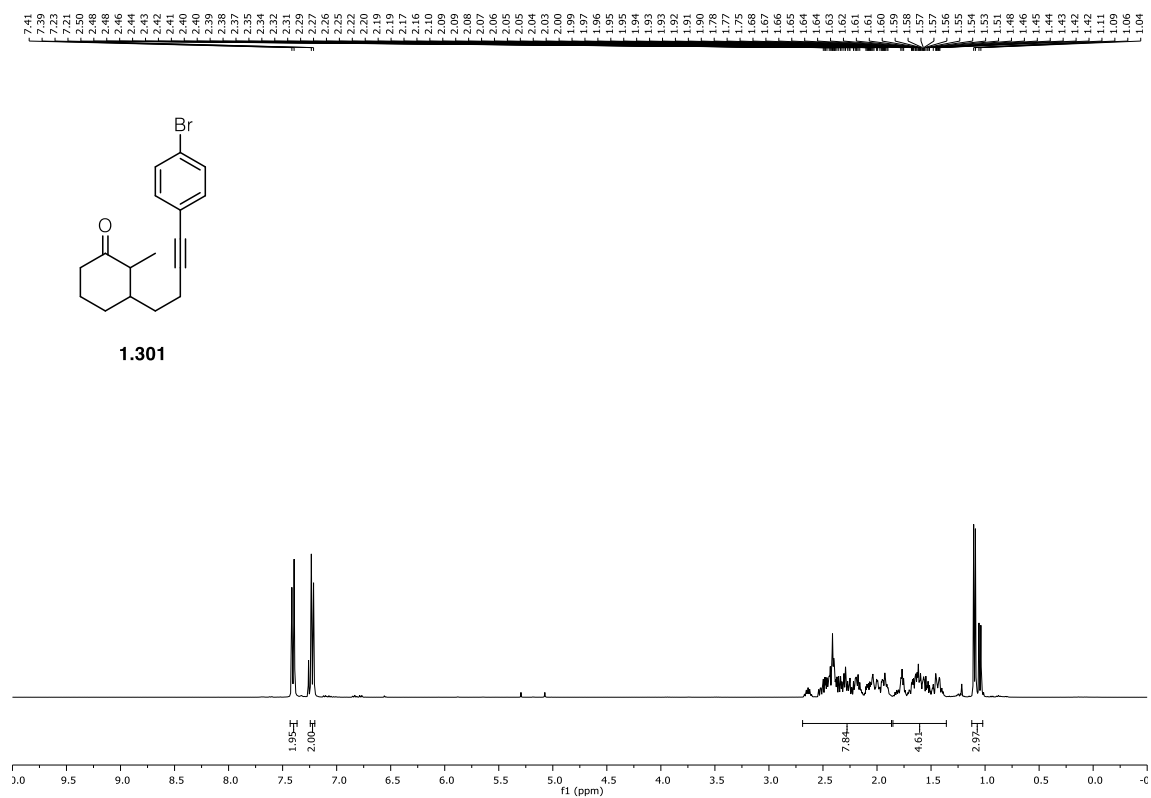


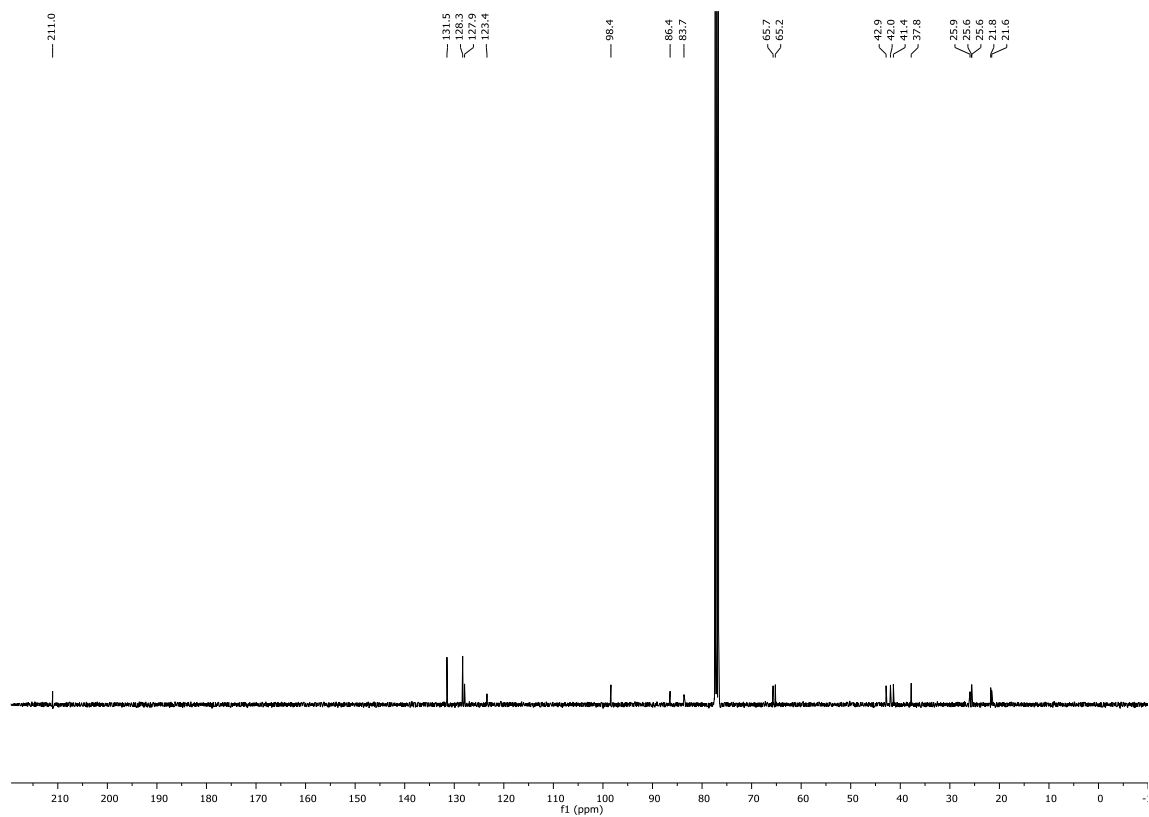


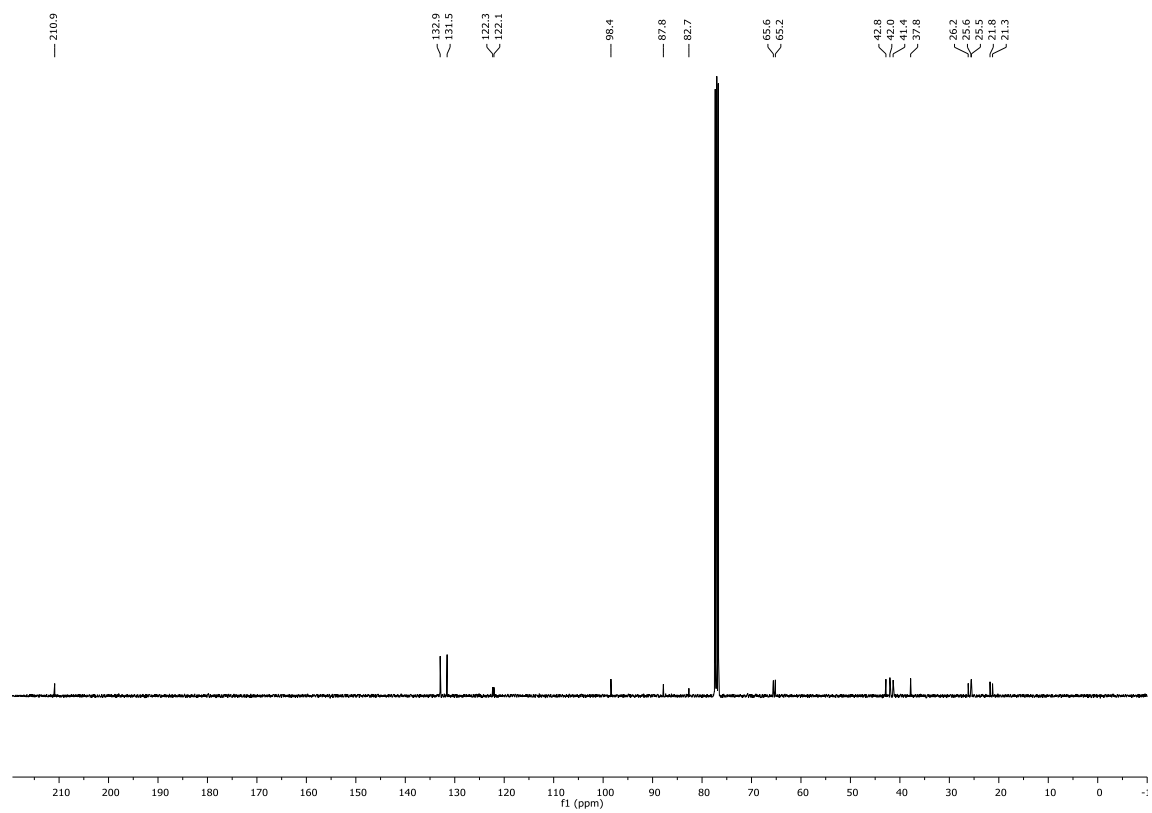
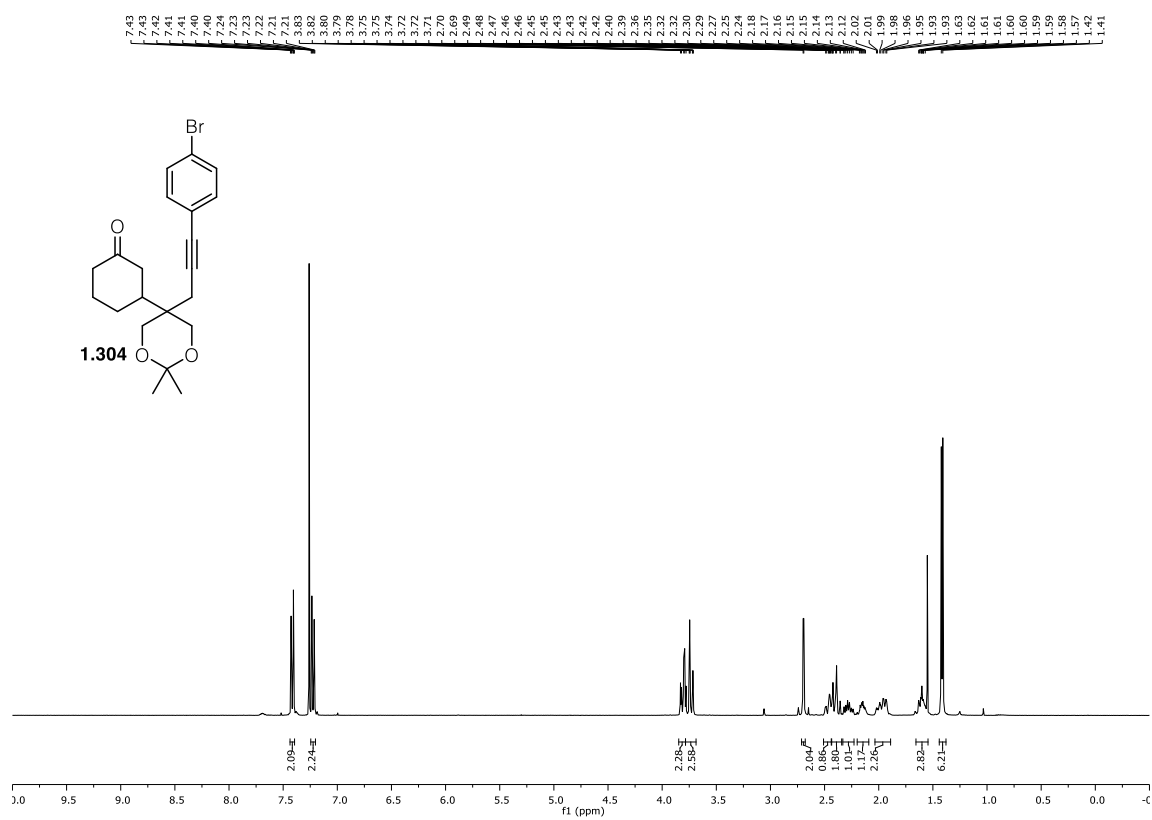


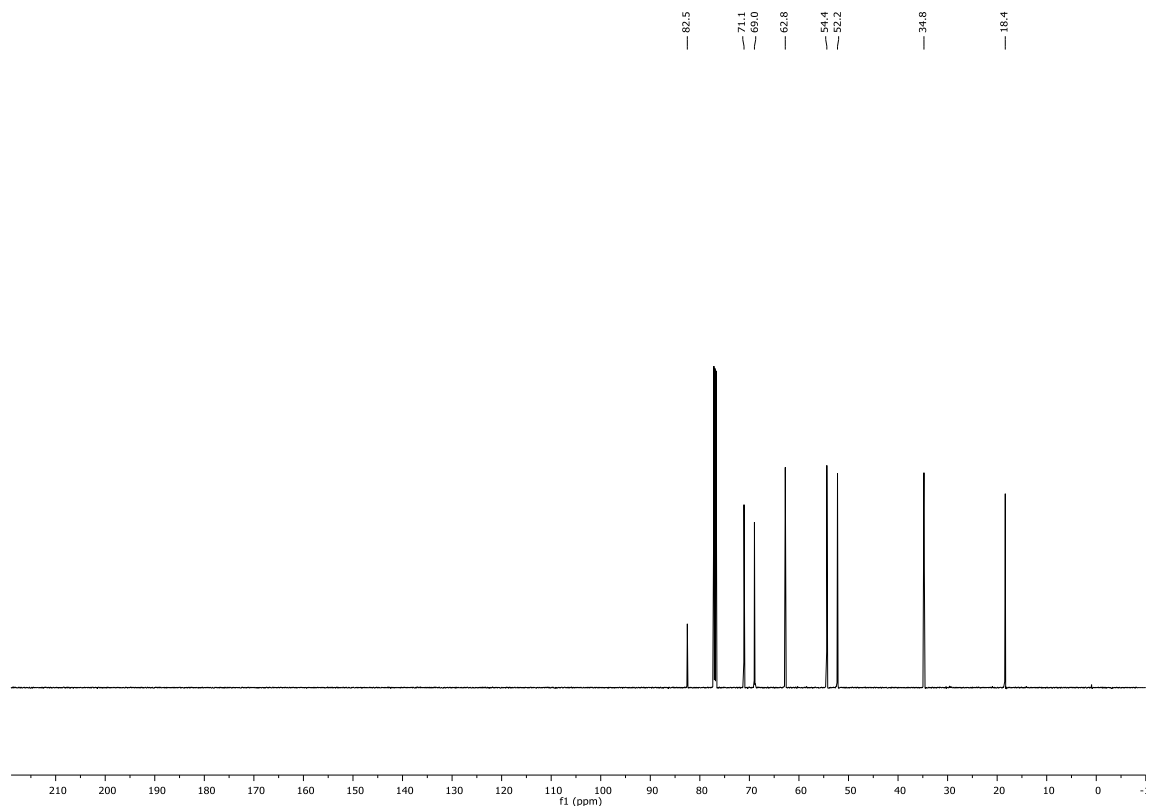
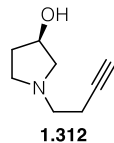
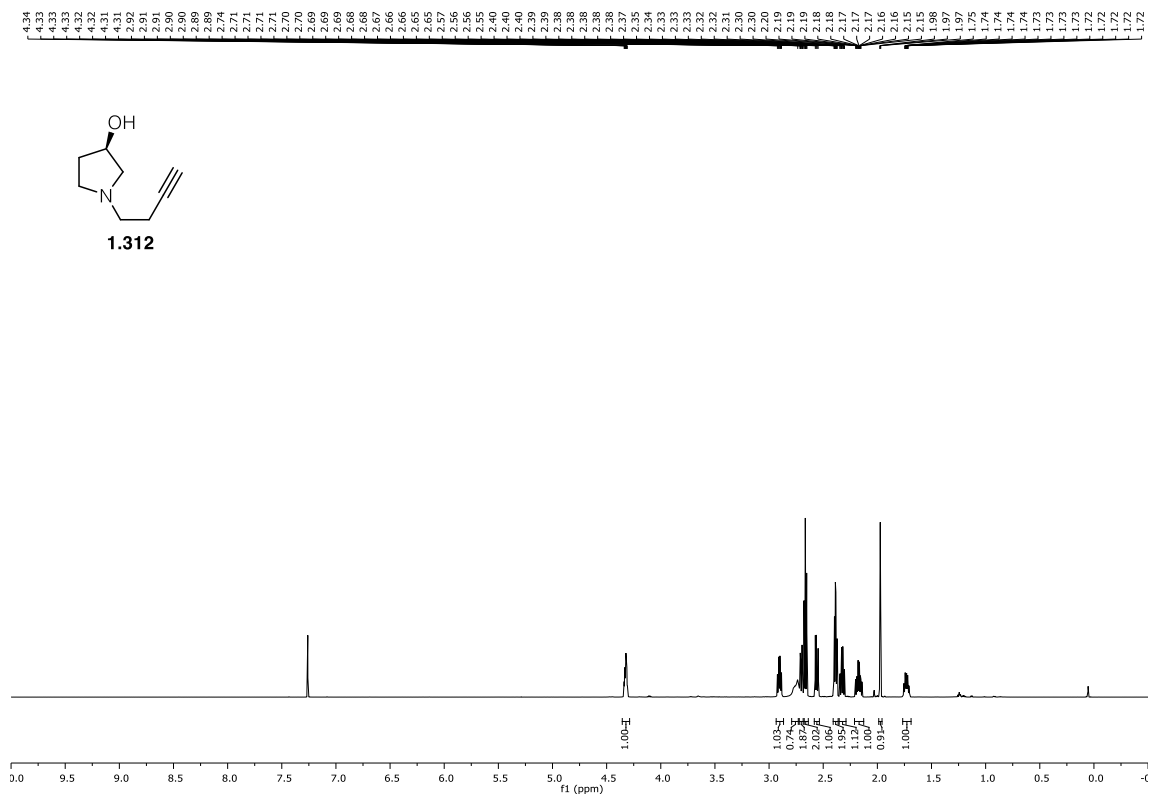


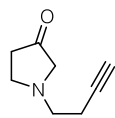




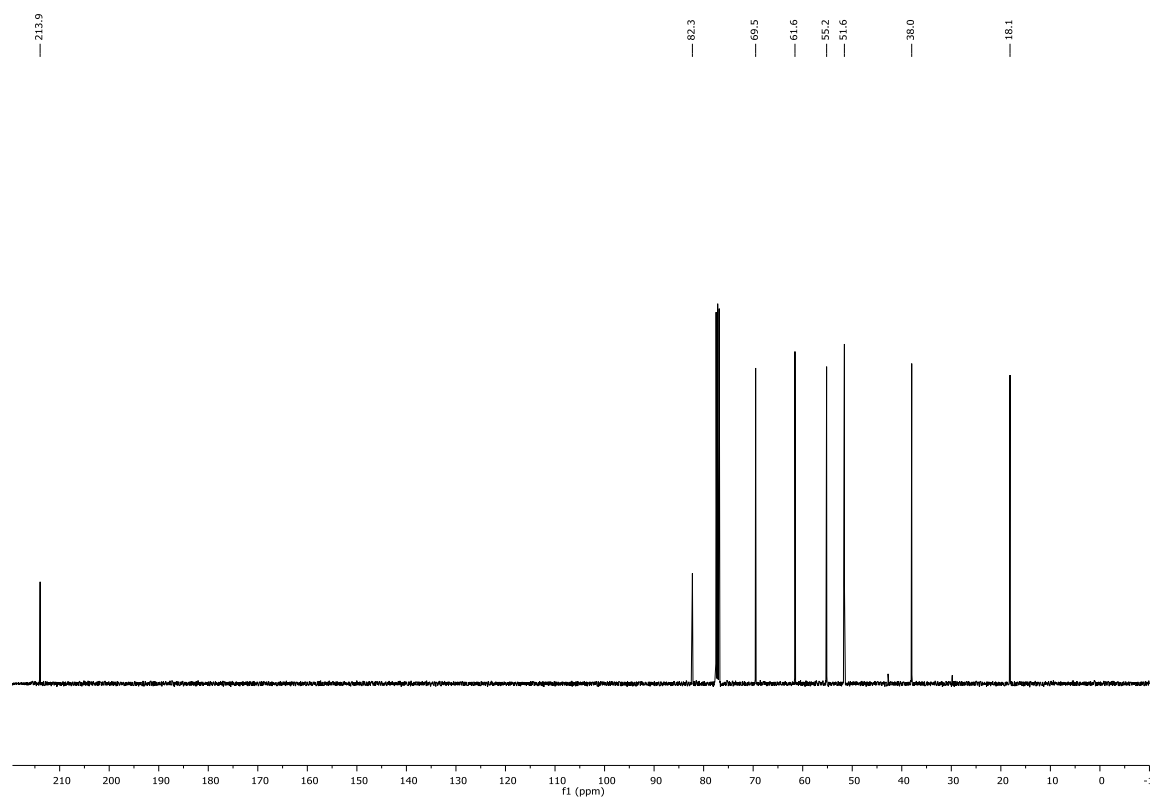
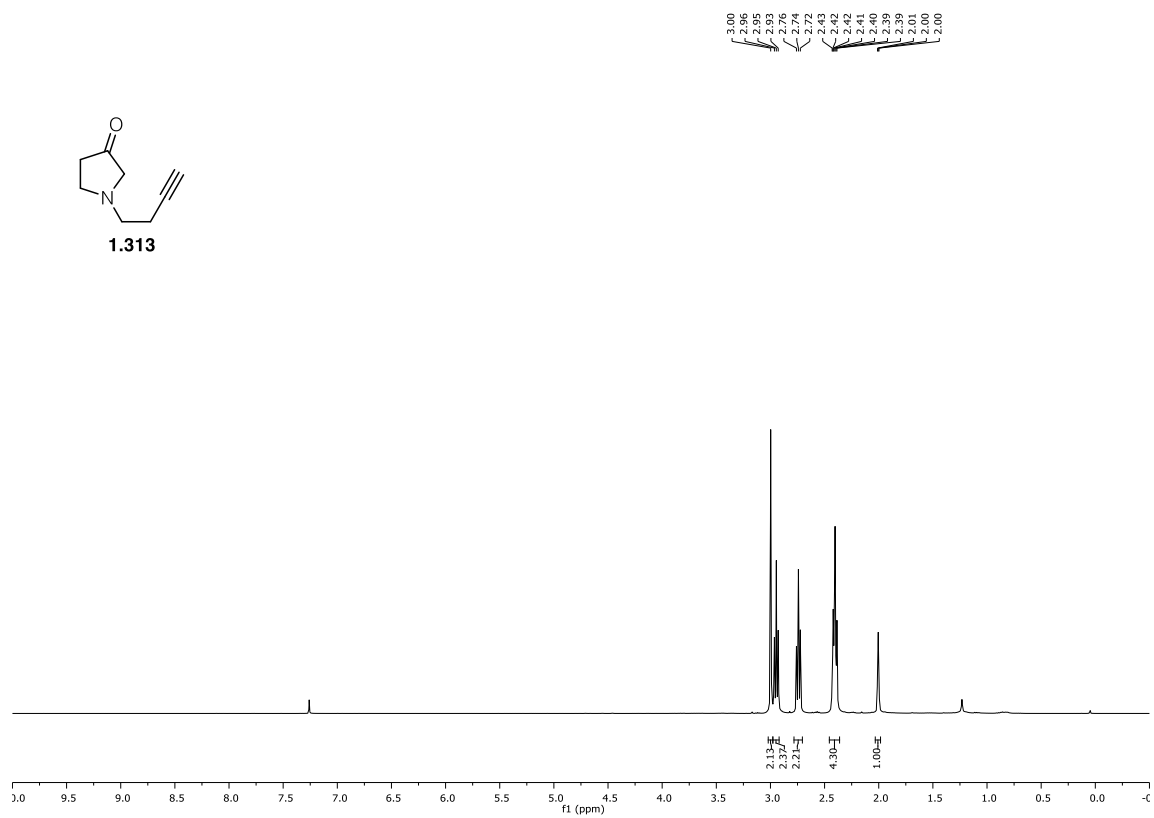


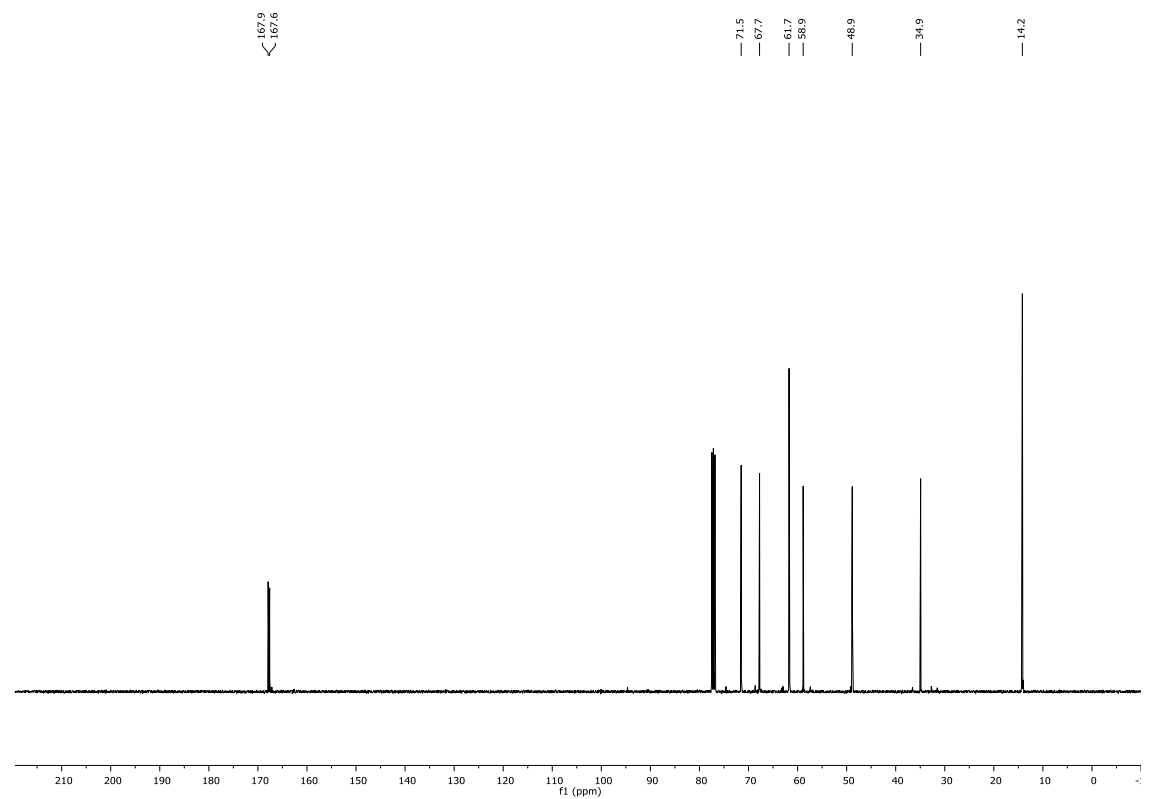
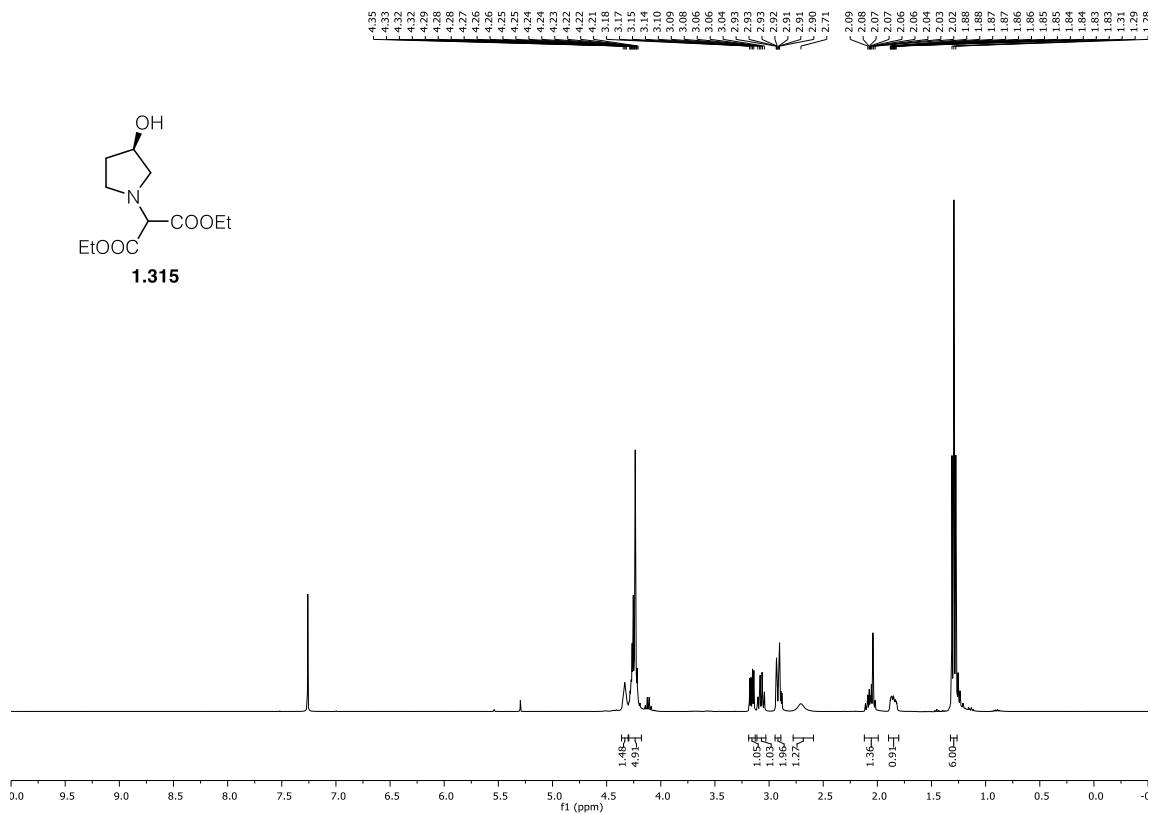
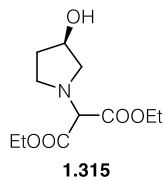


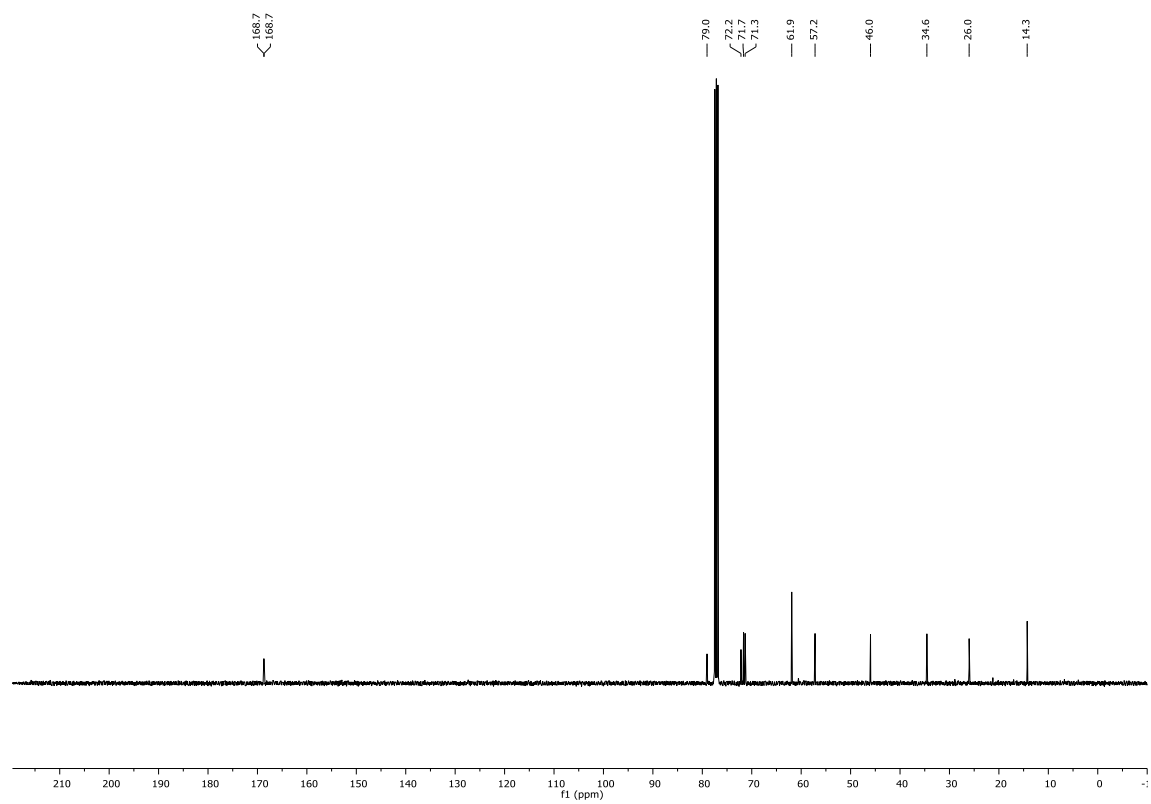
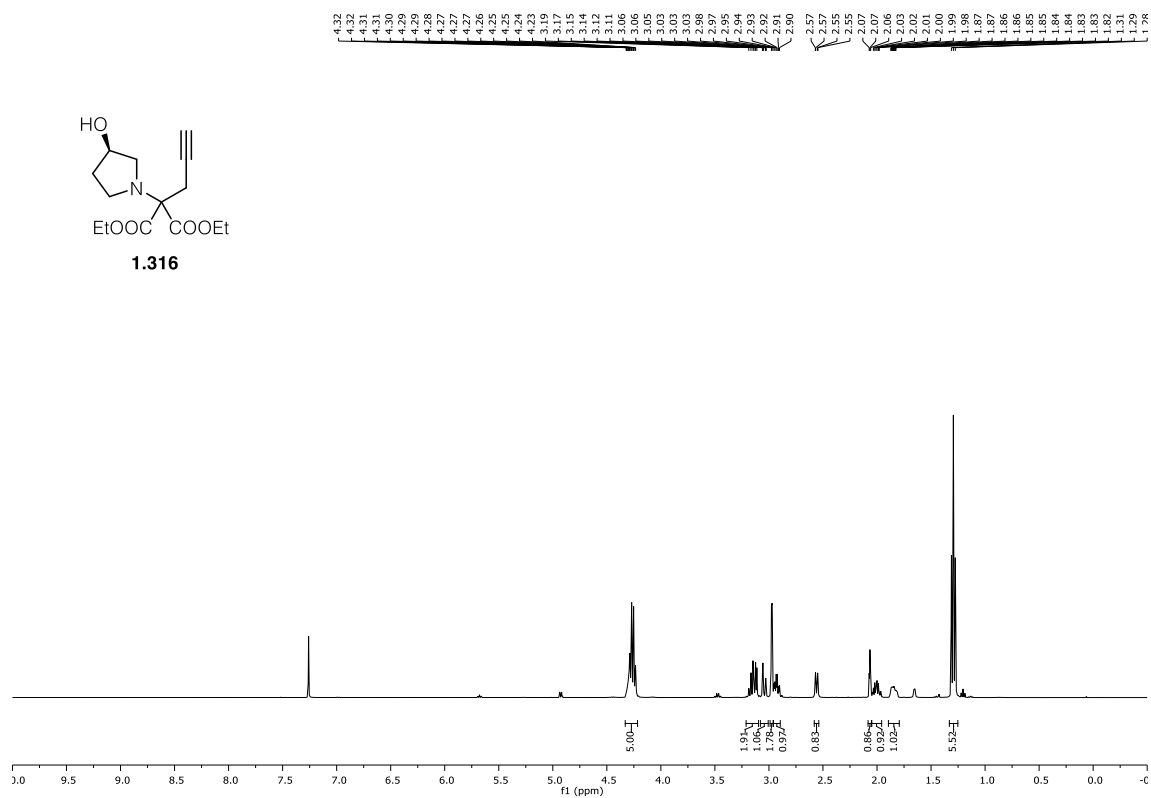
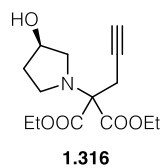


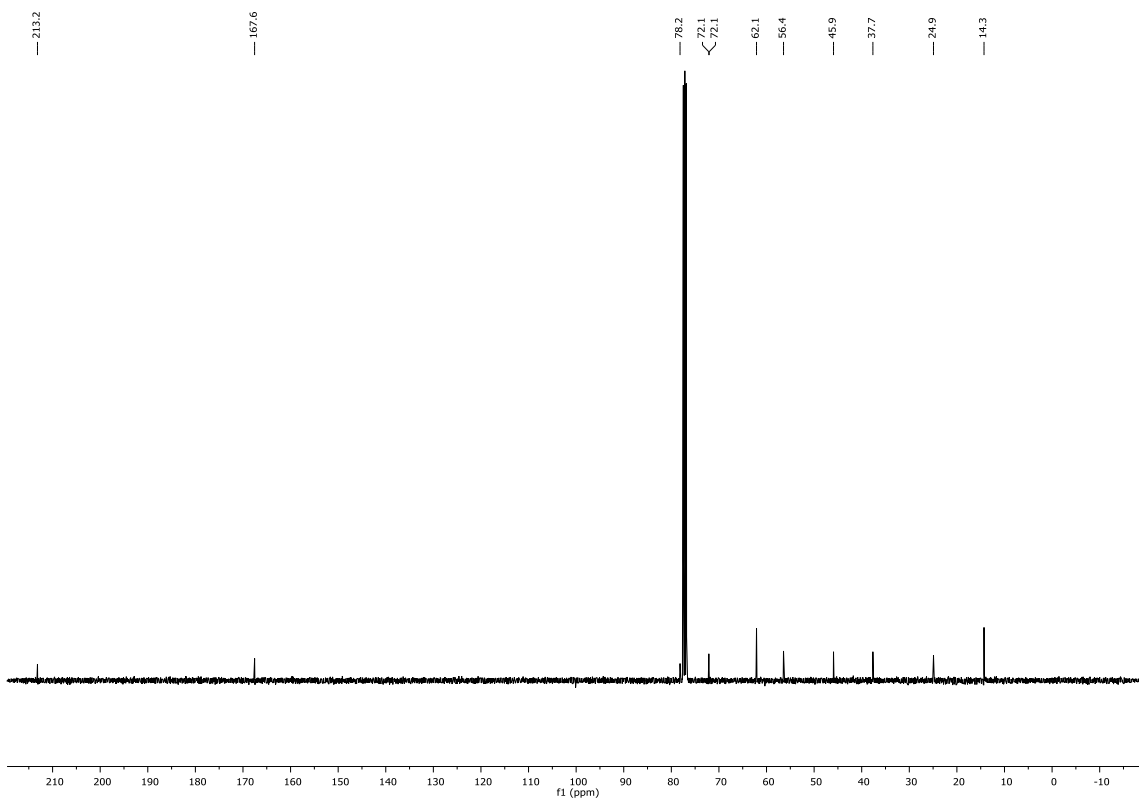
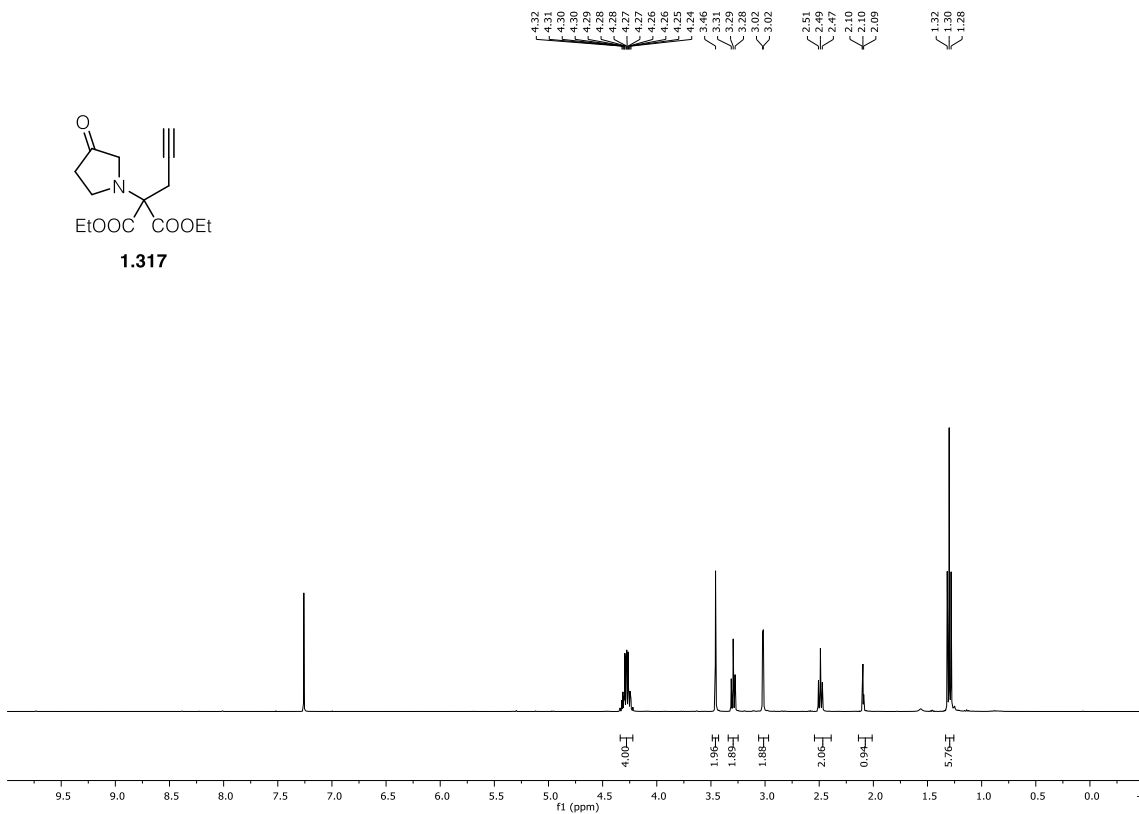
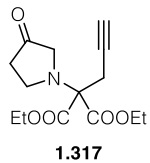


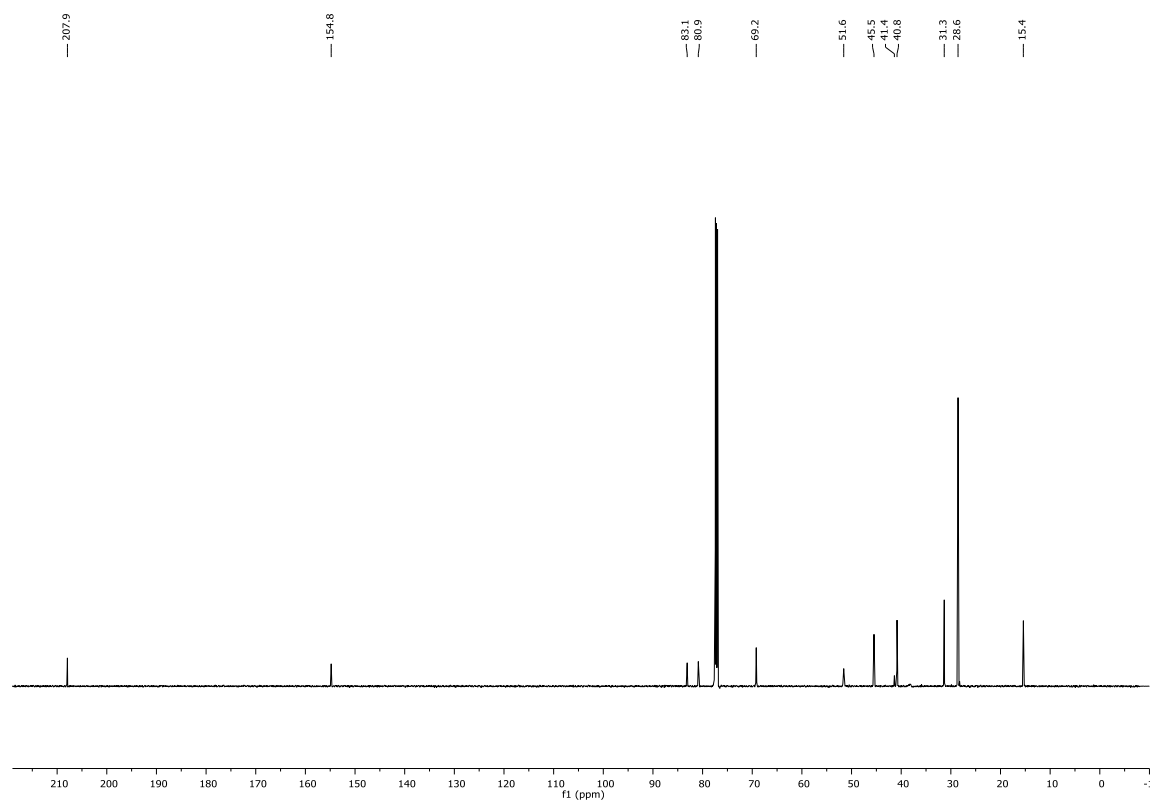
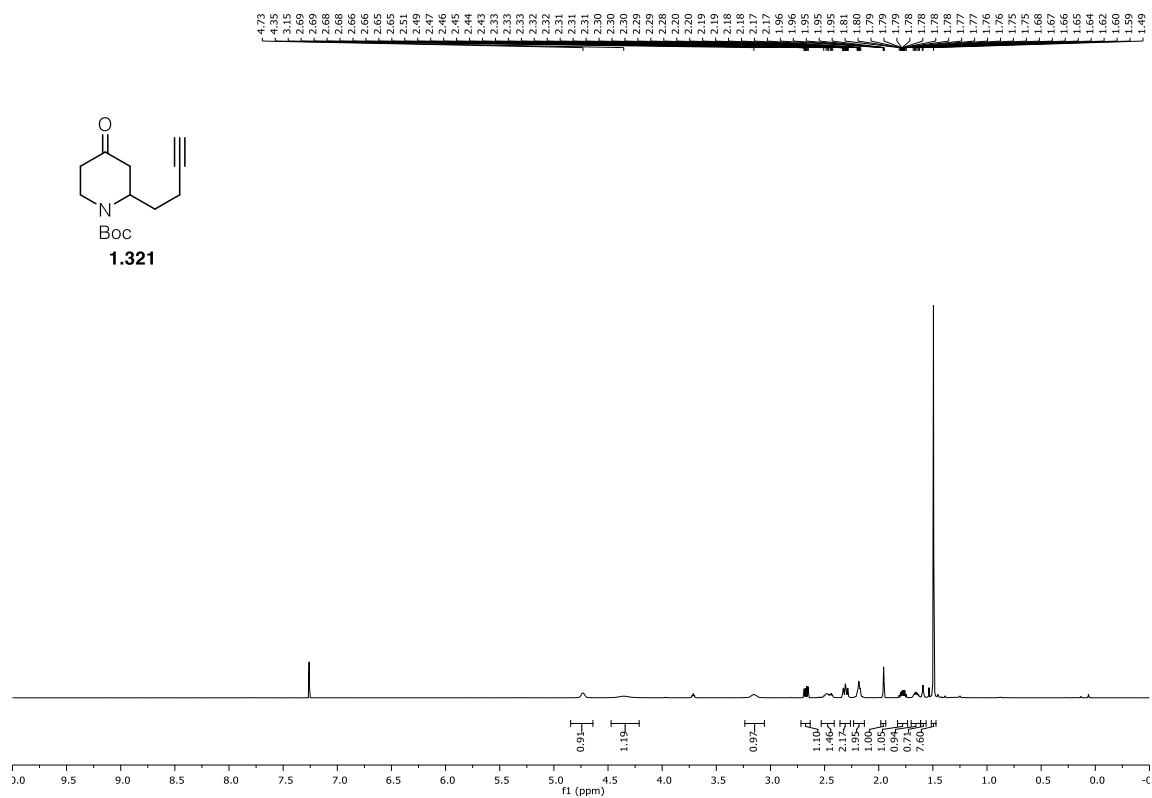
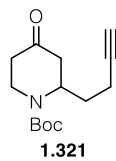
1.313

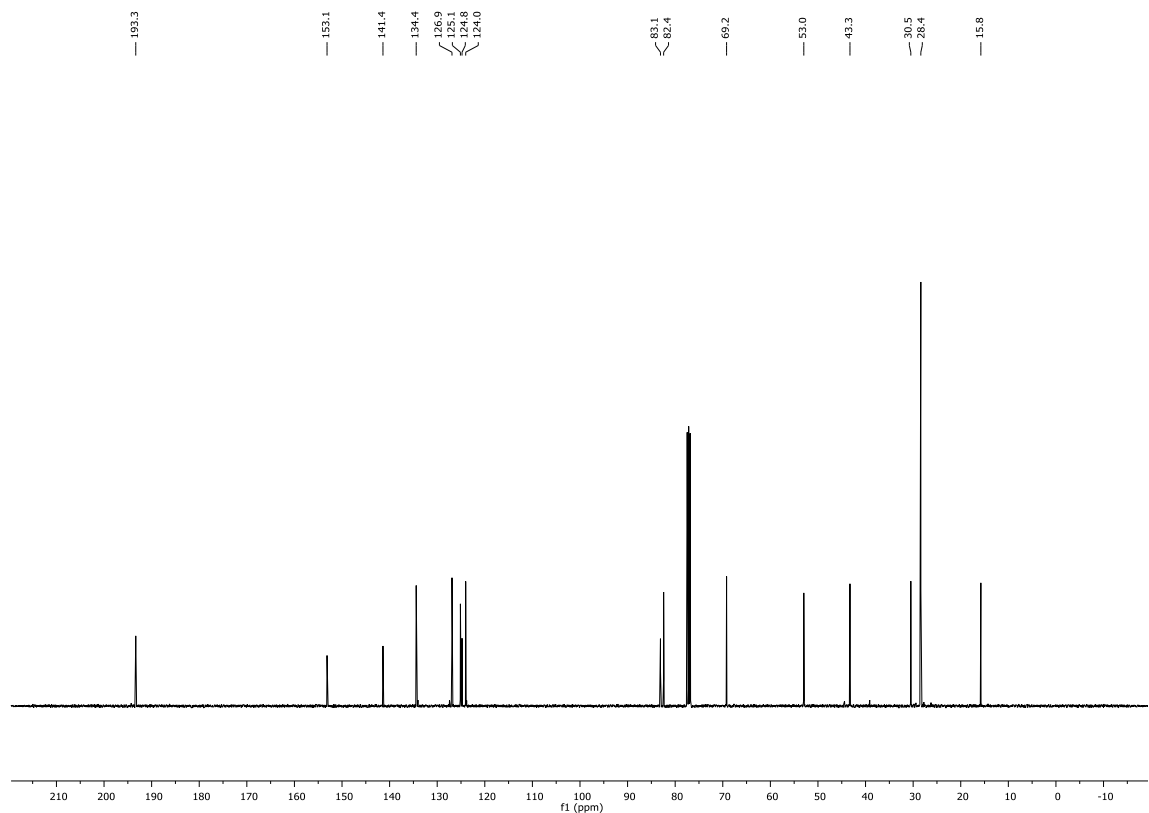
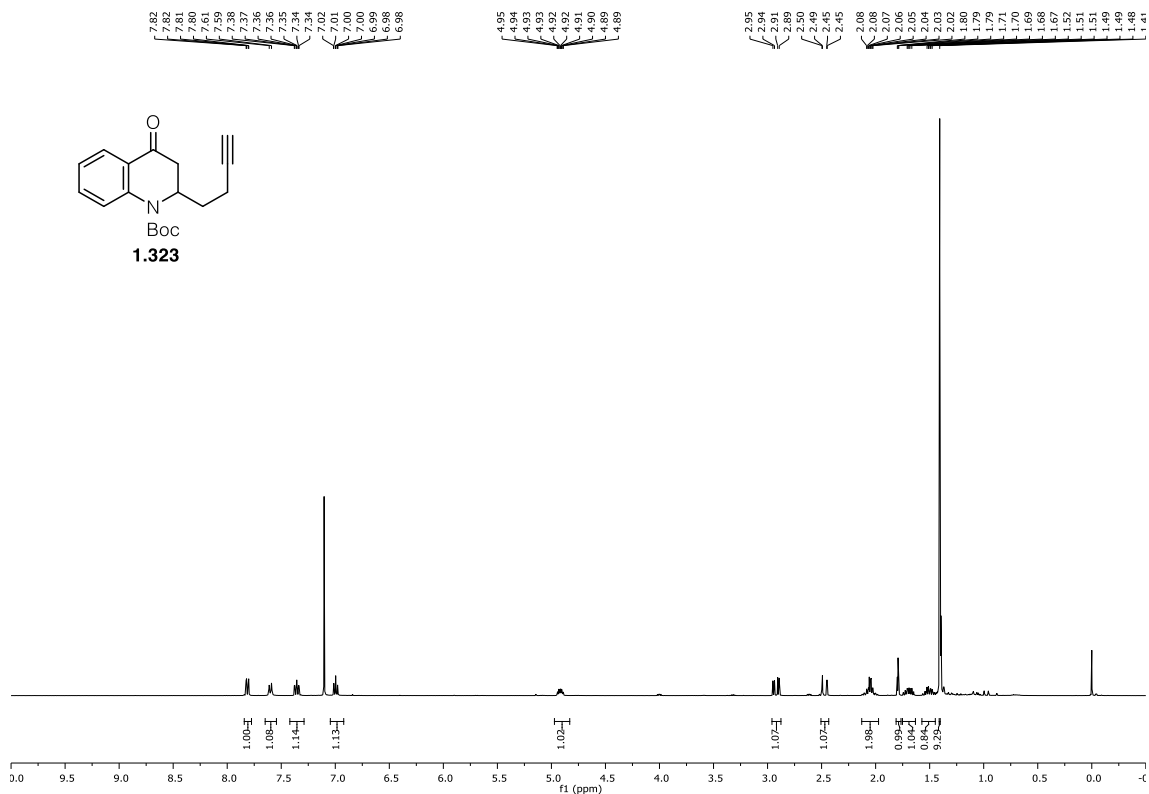
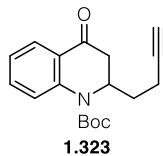


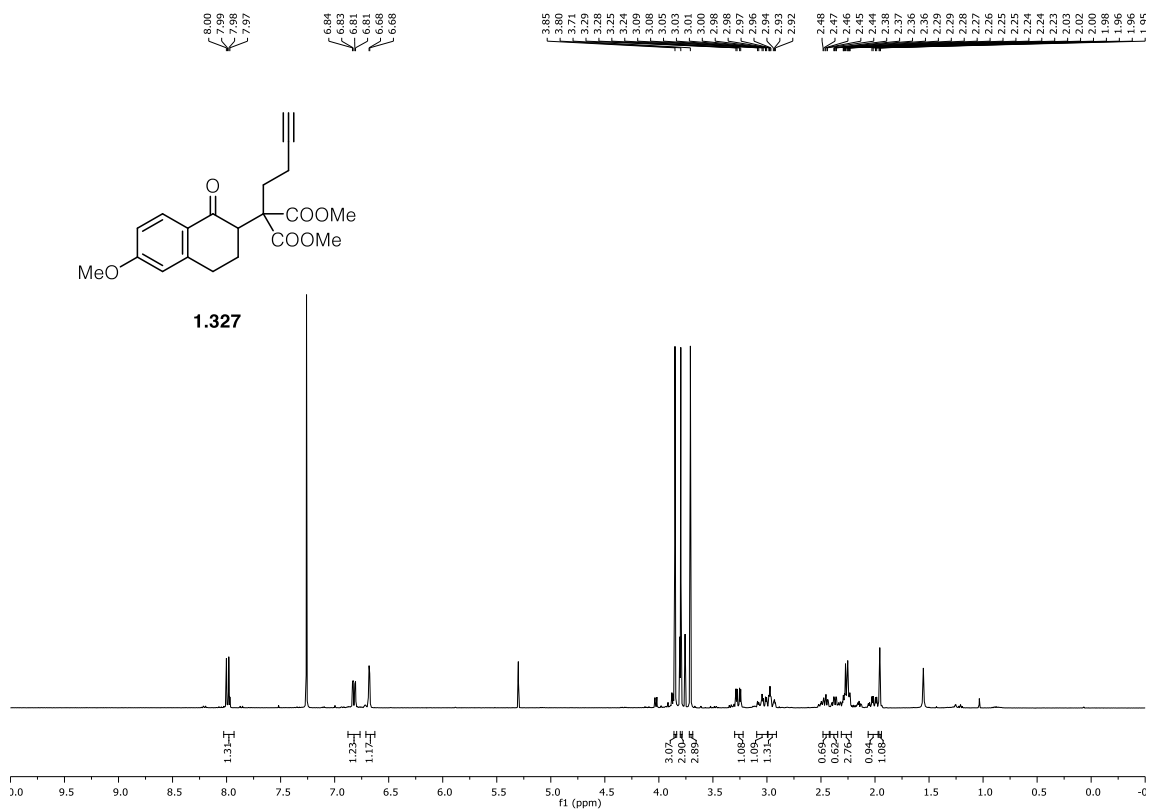


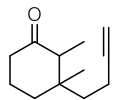




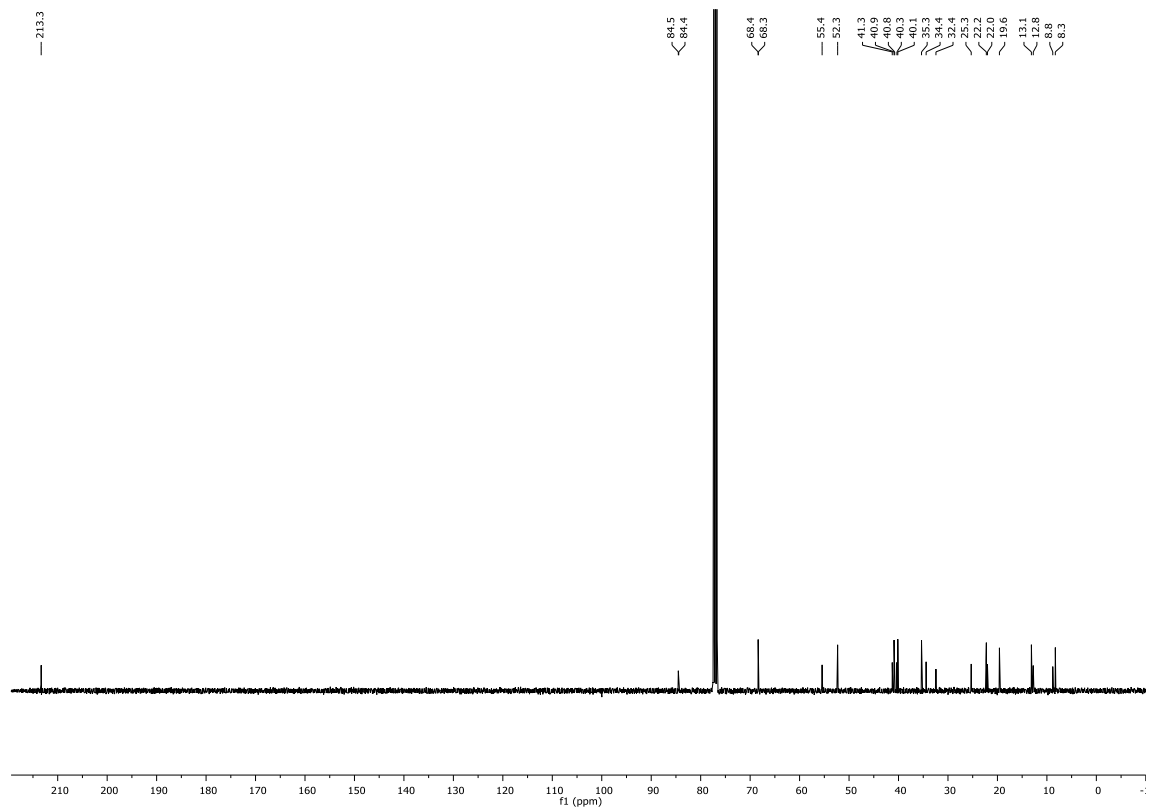
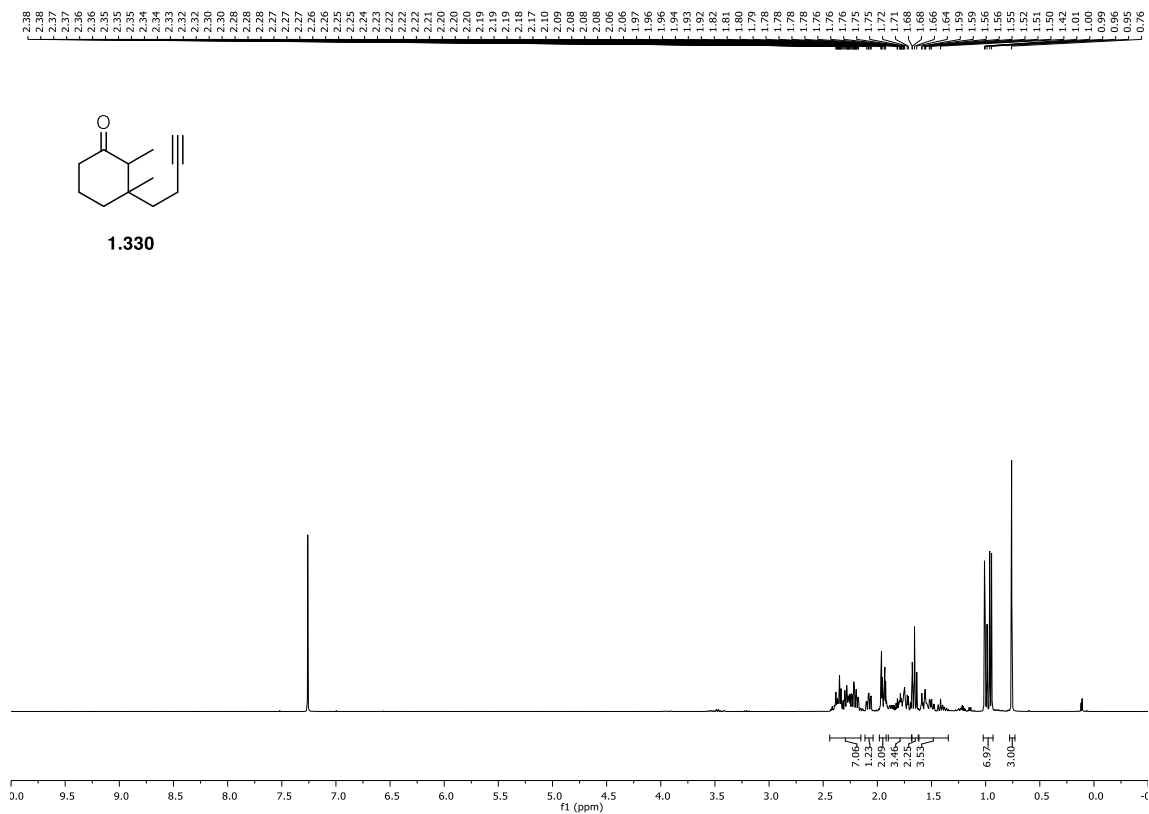


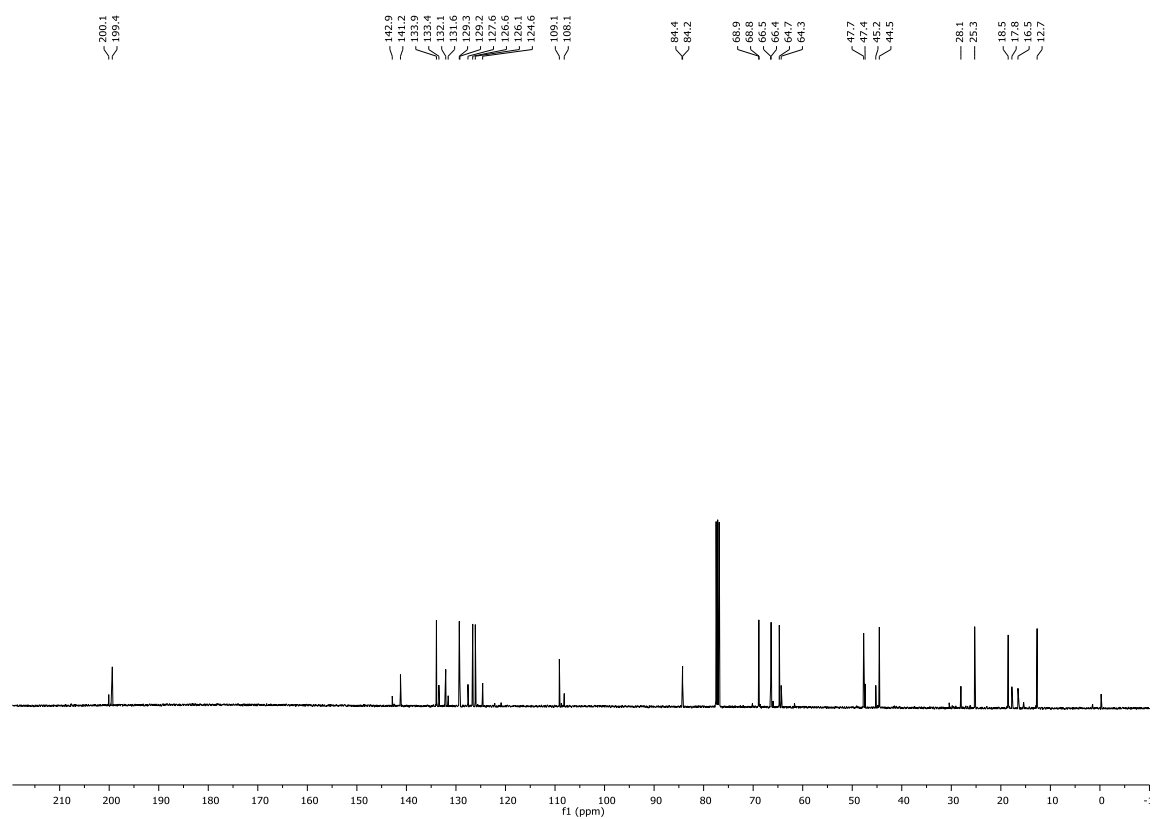
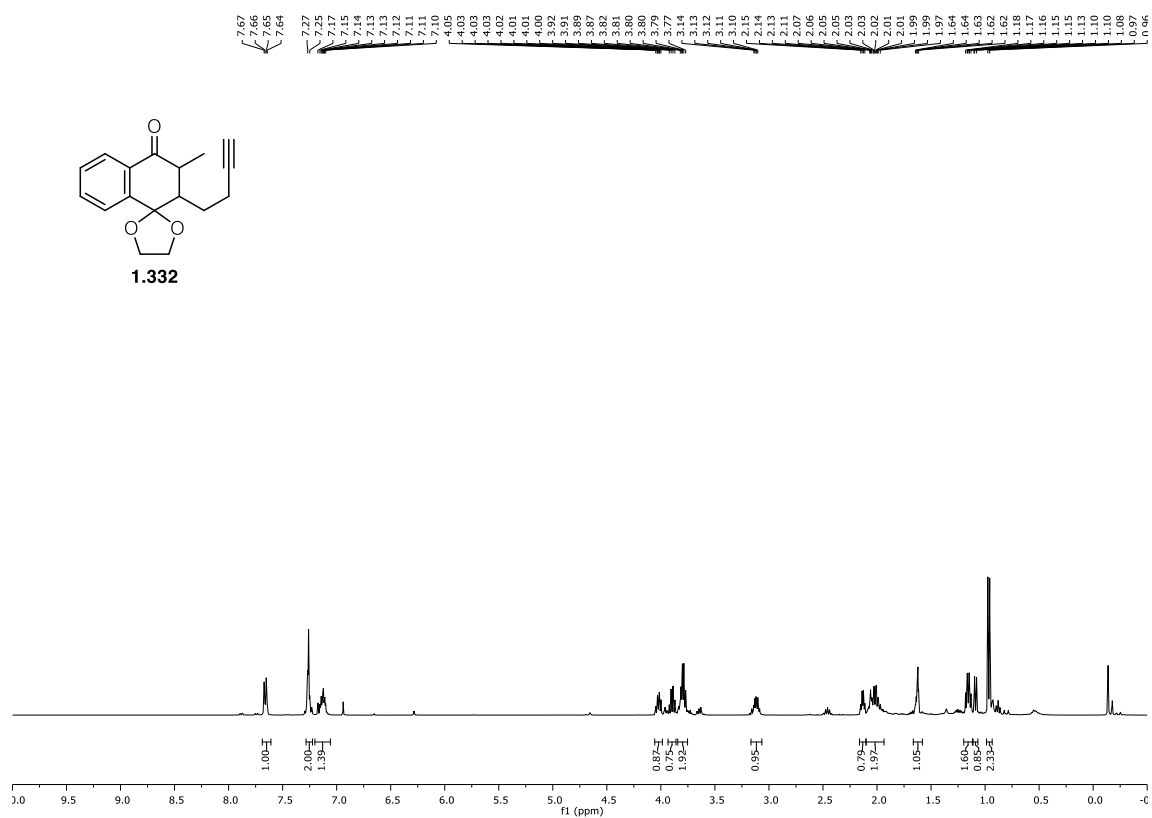
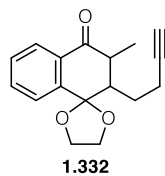




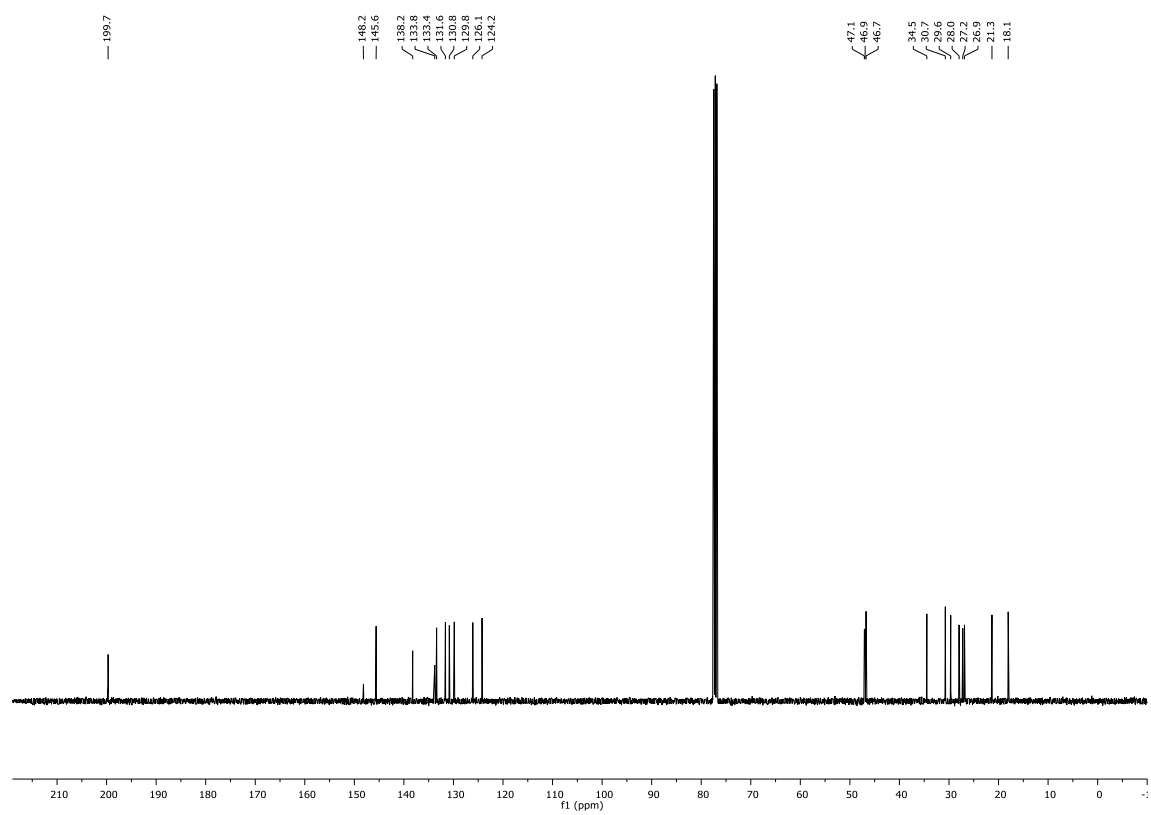
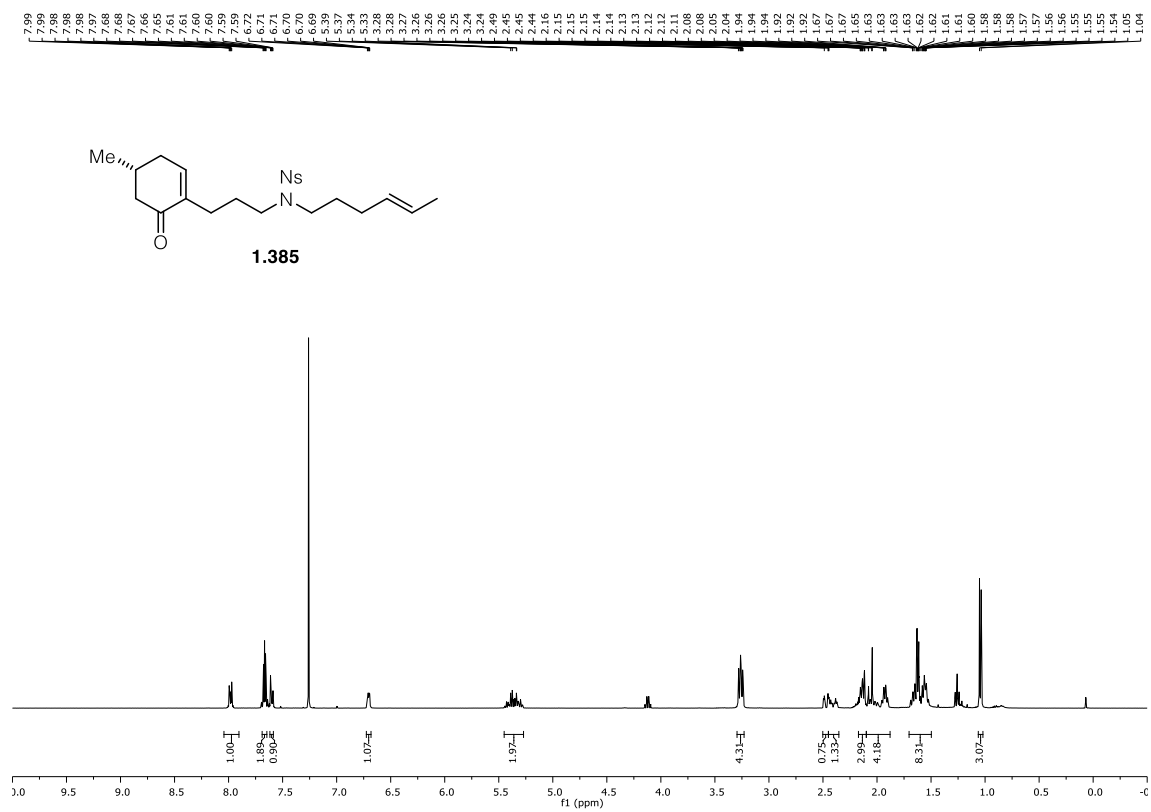


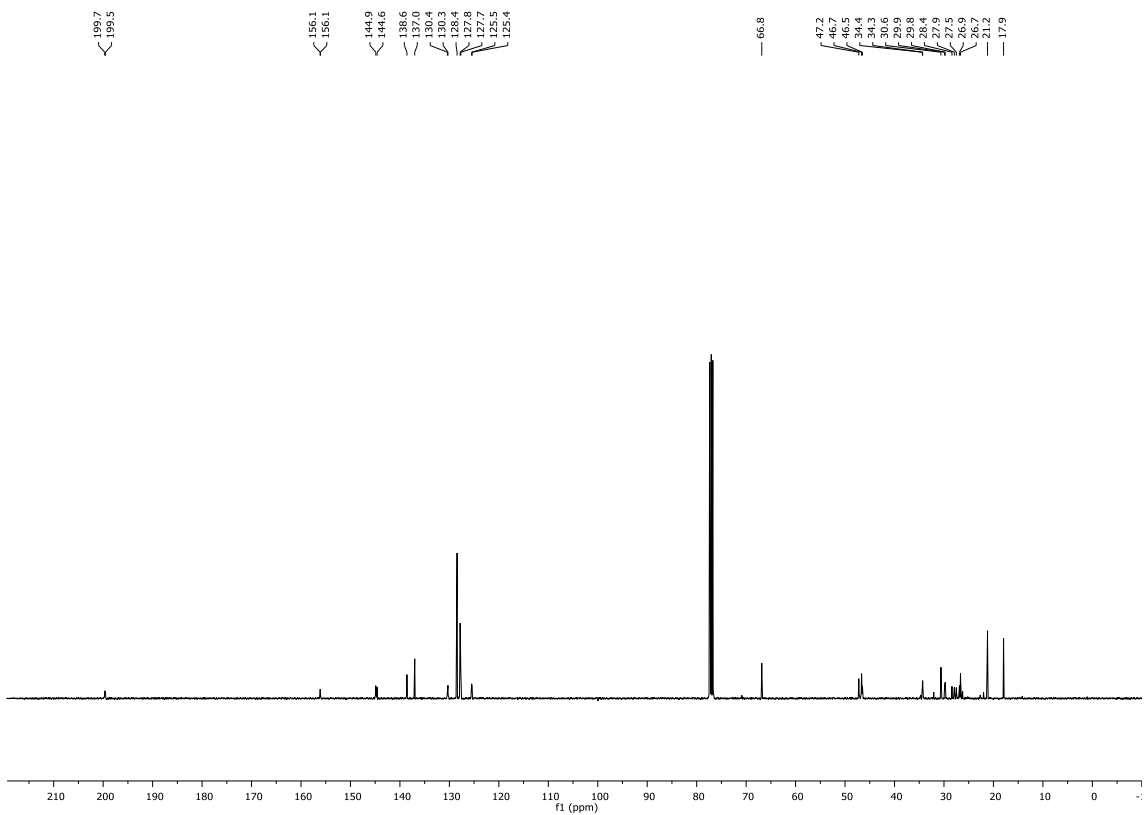
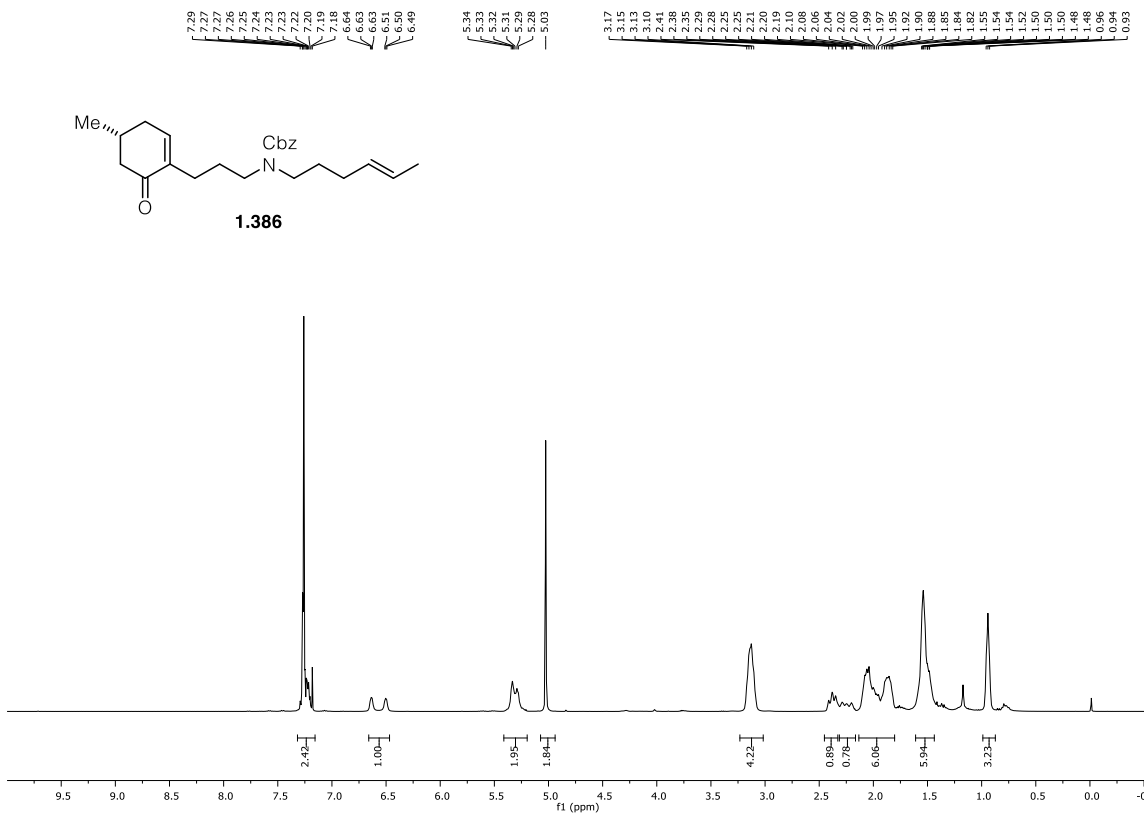
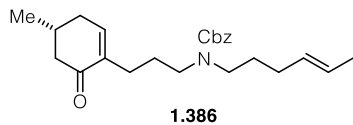
1.330

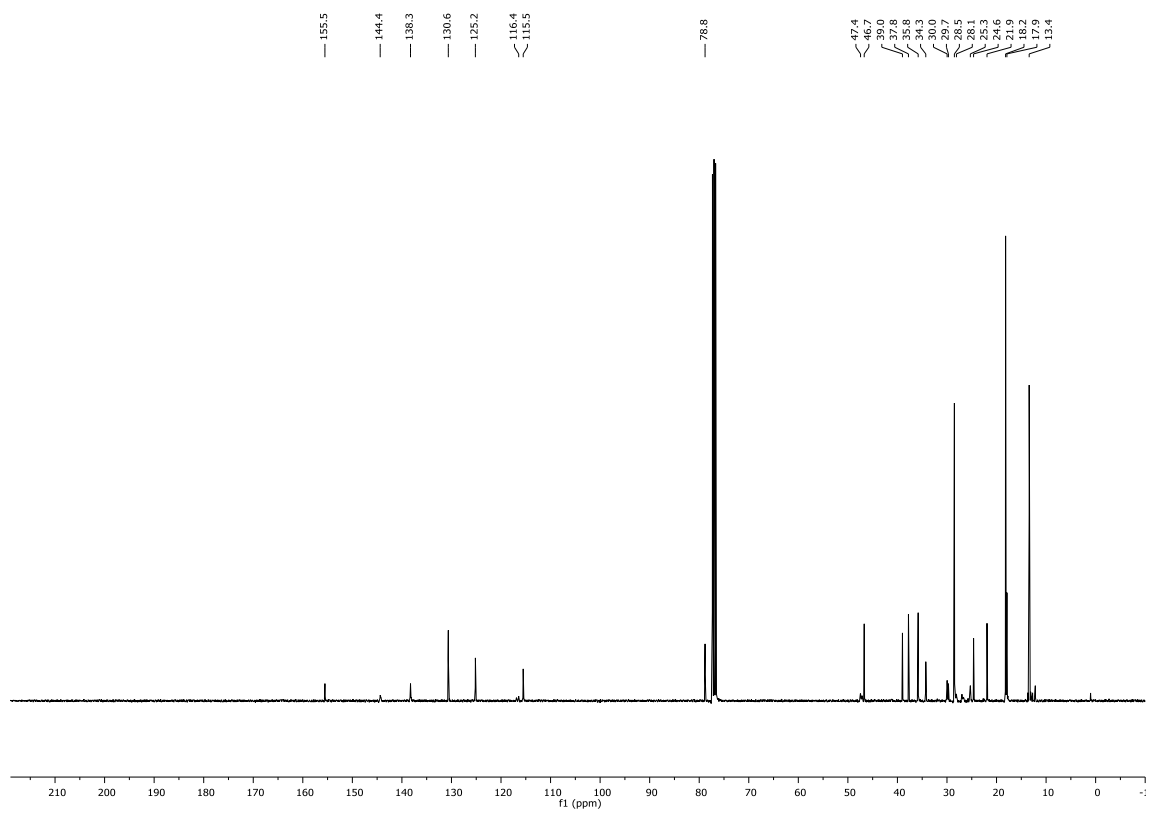
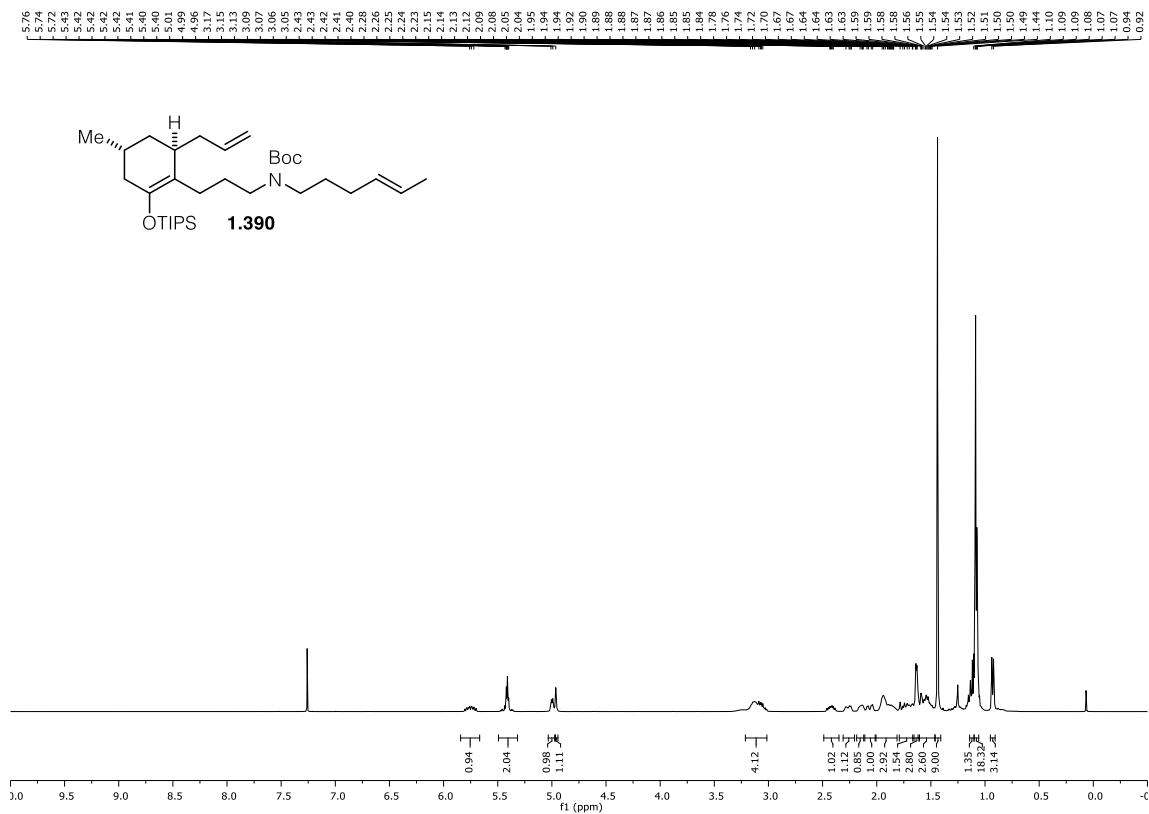


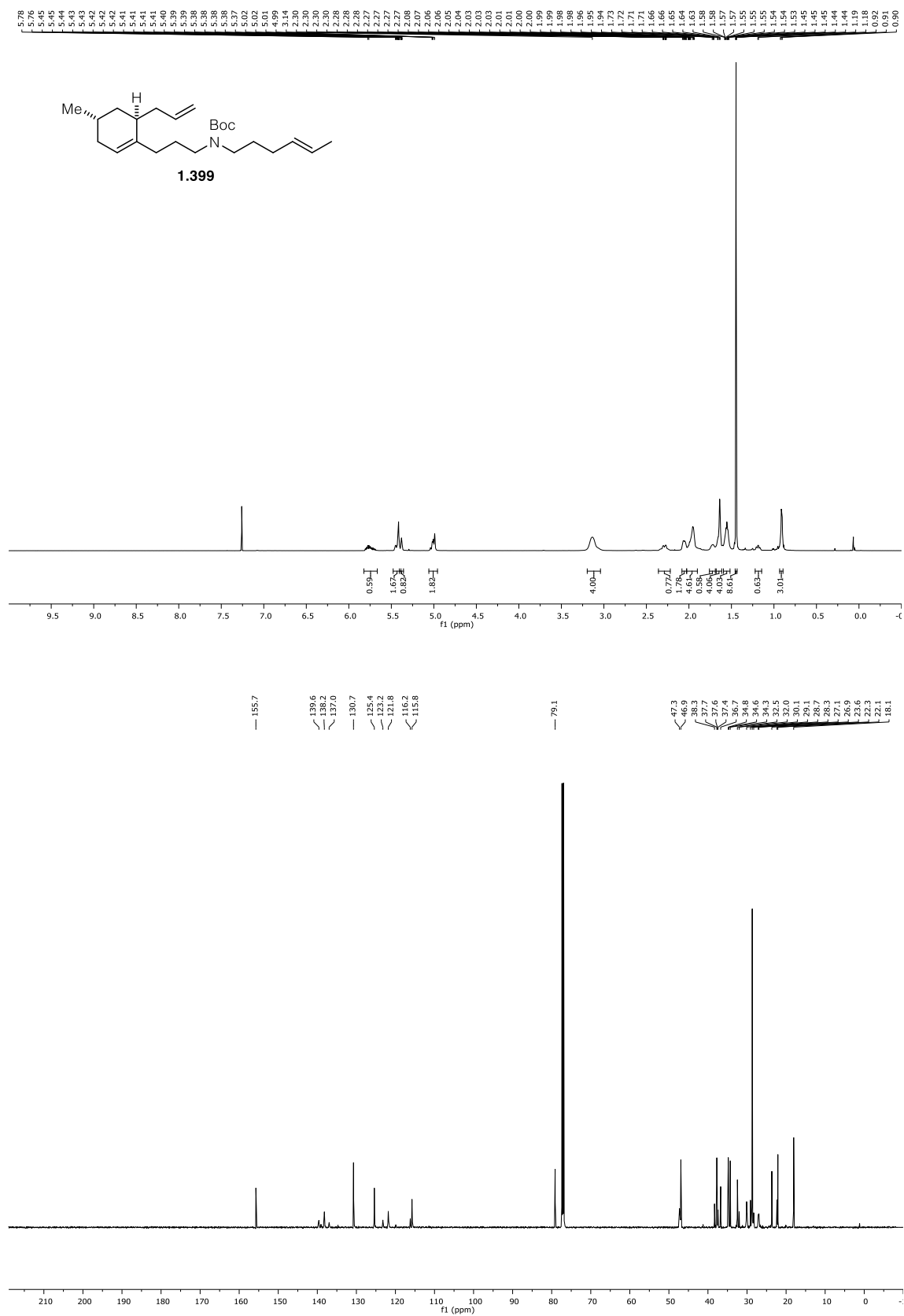


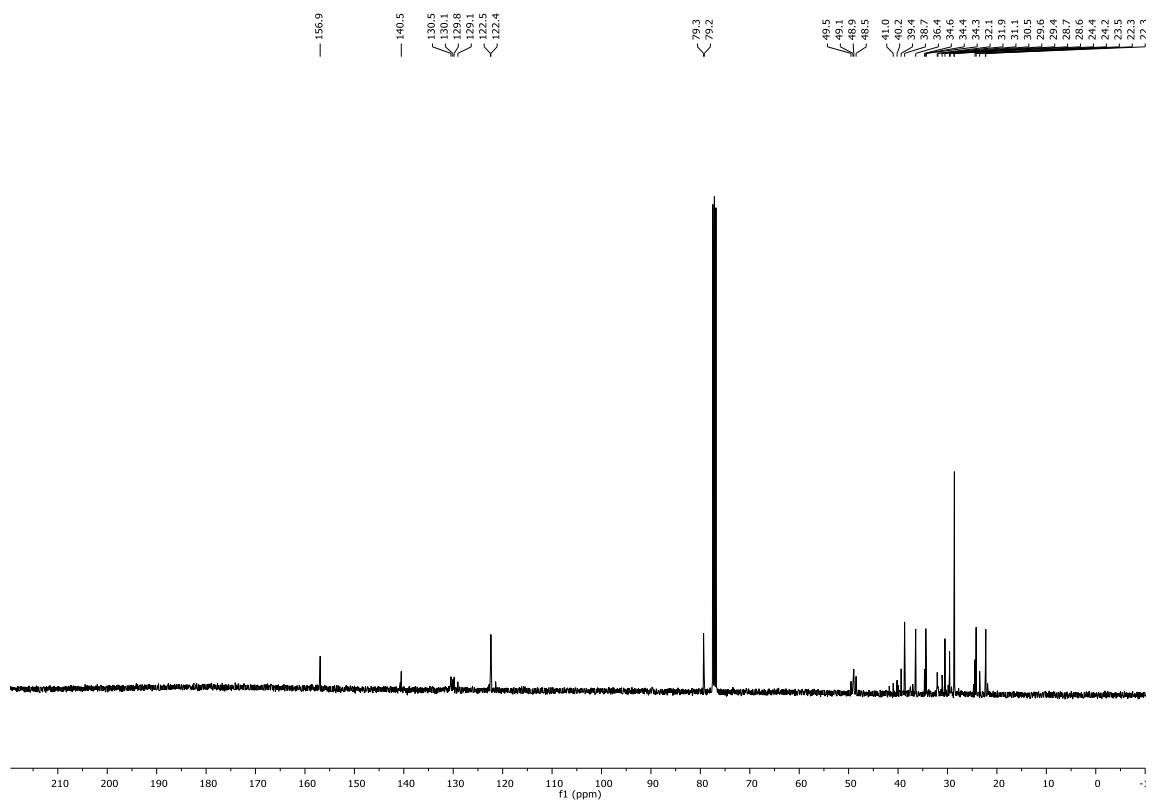
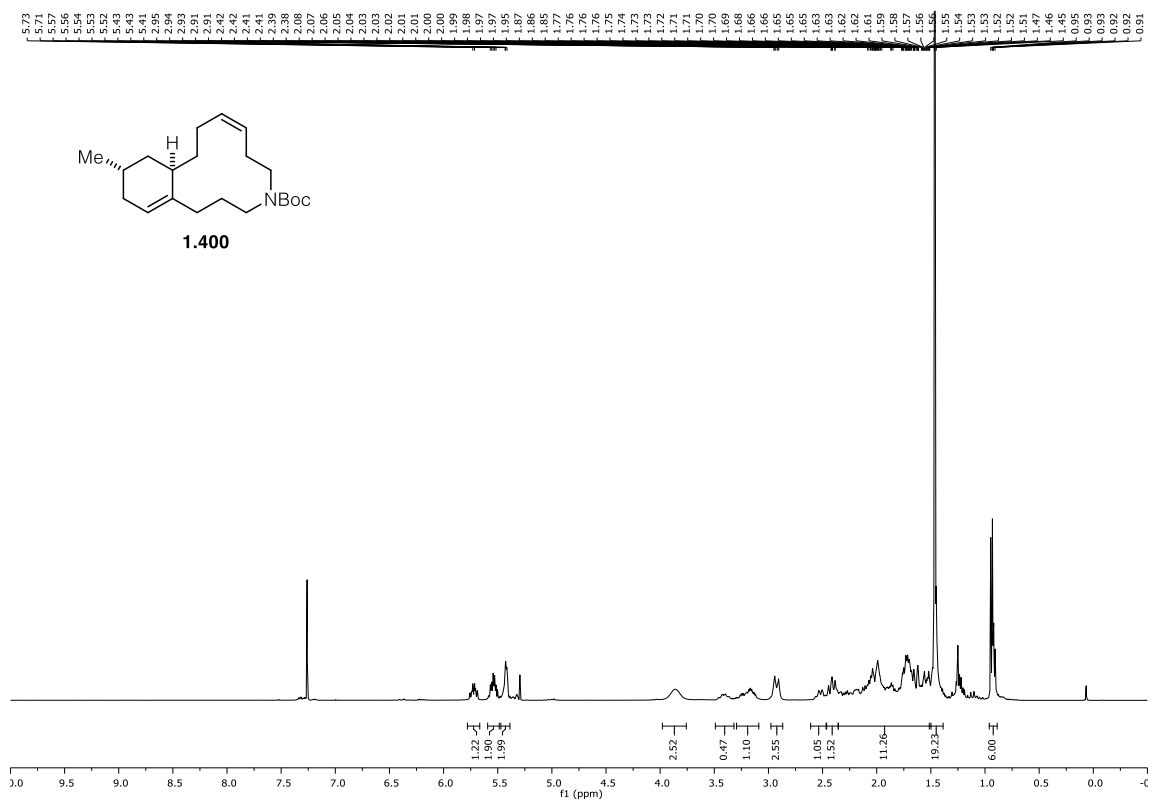
5.4 ^1H and ^{13}C NMR spectra for chapter 4.2.3

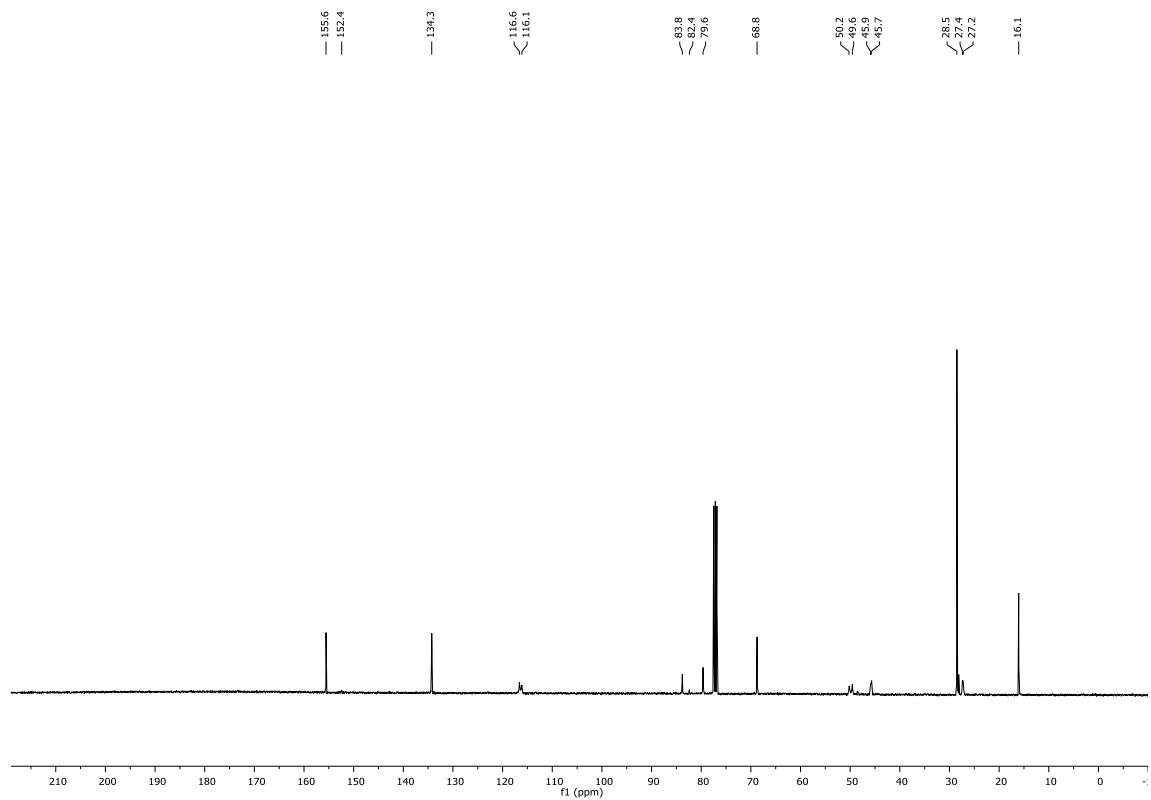
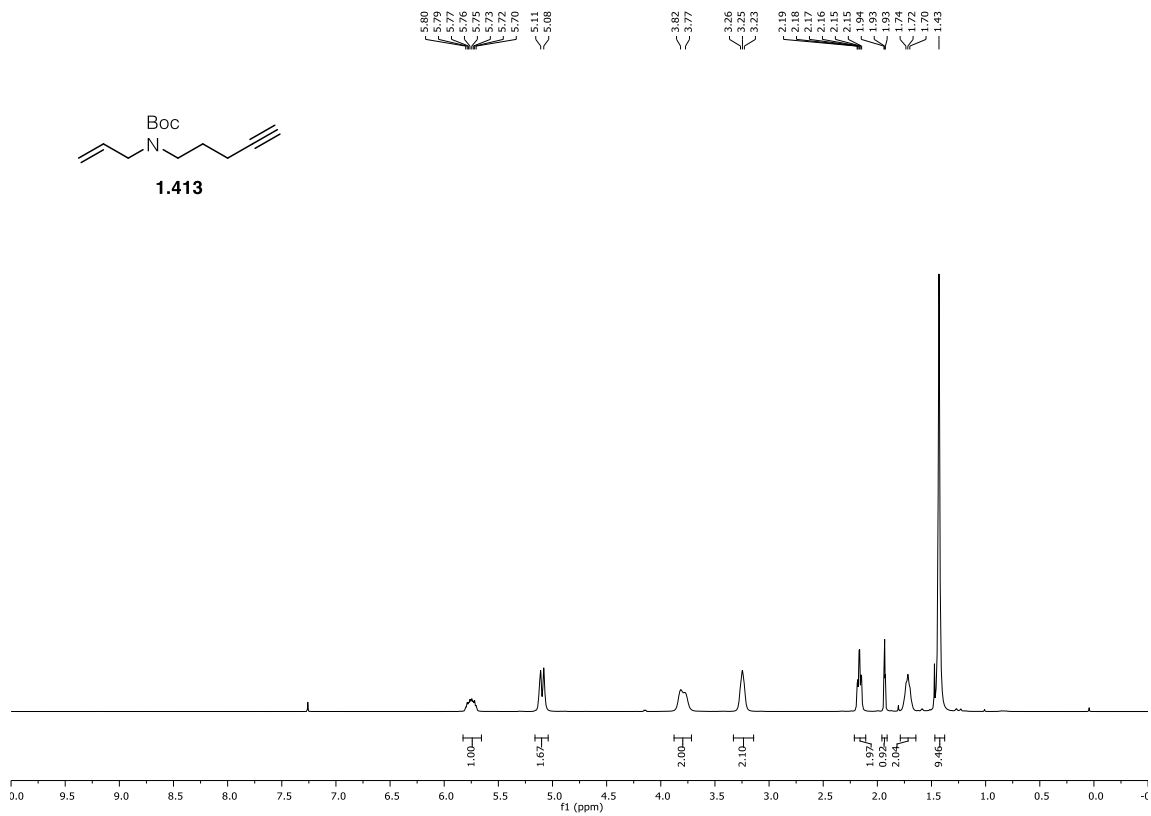
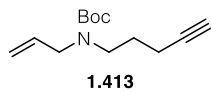


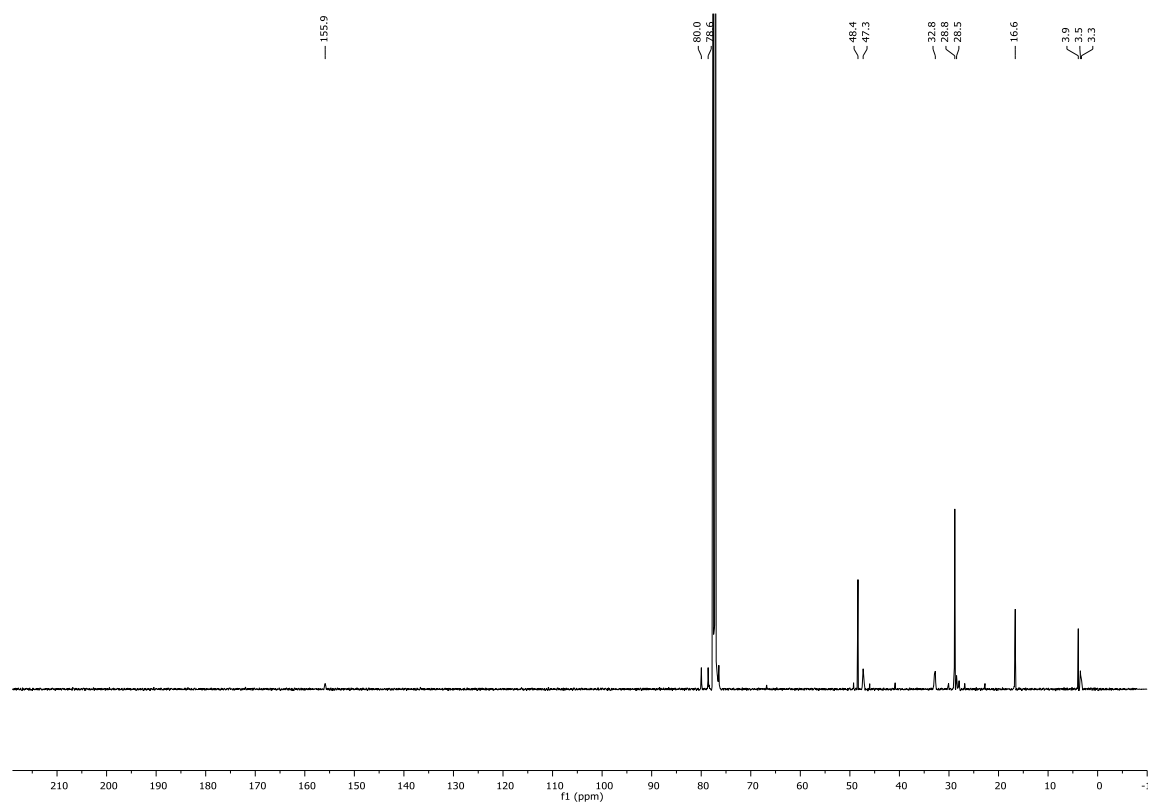
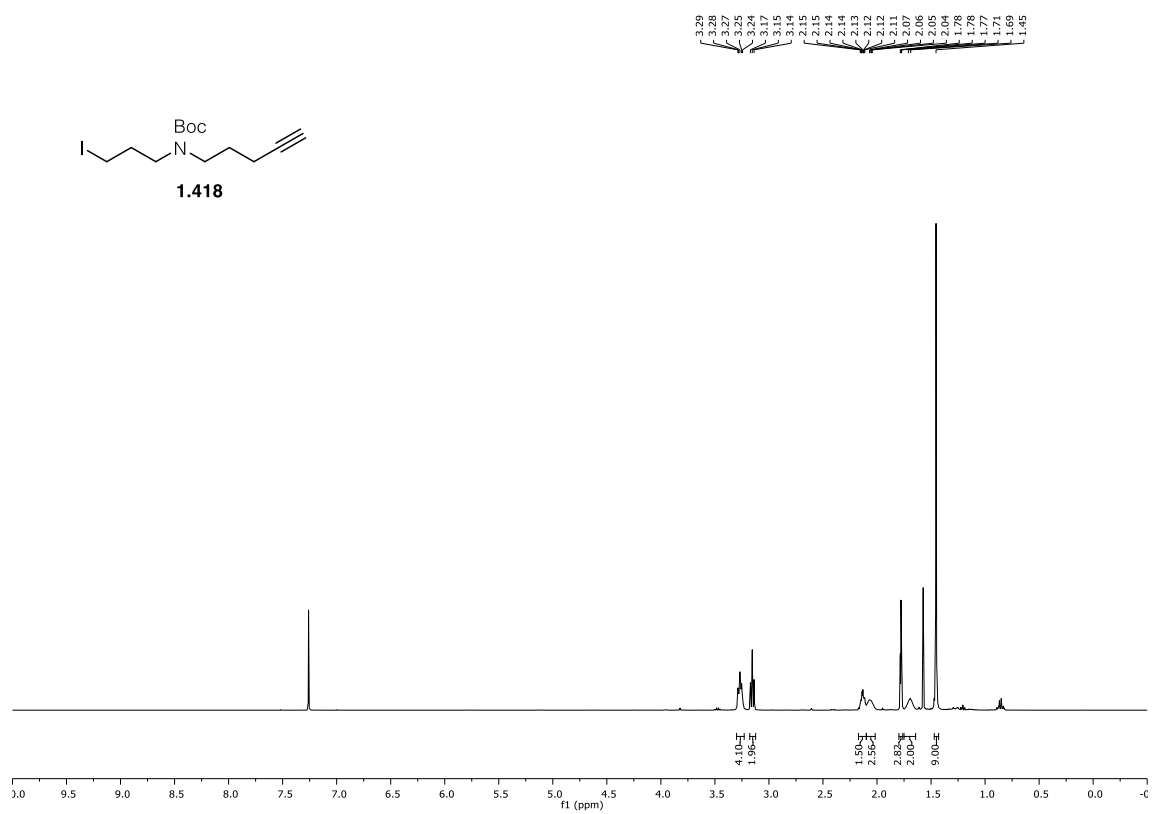


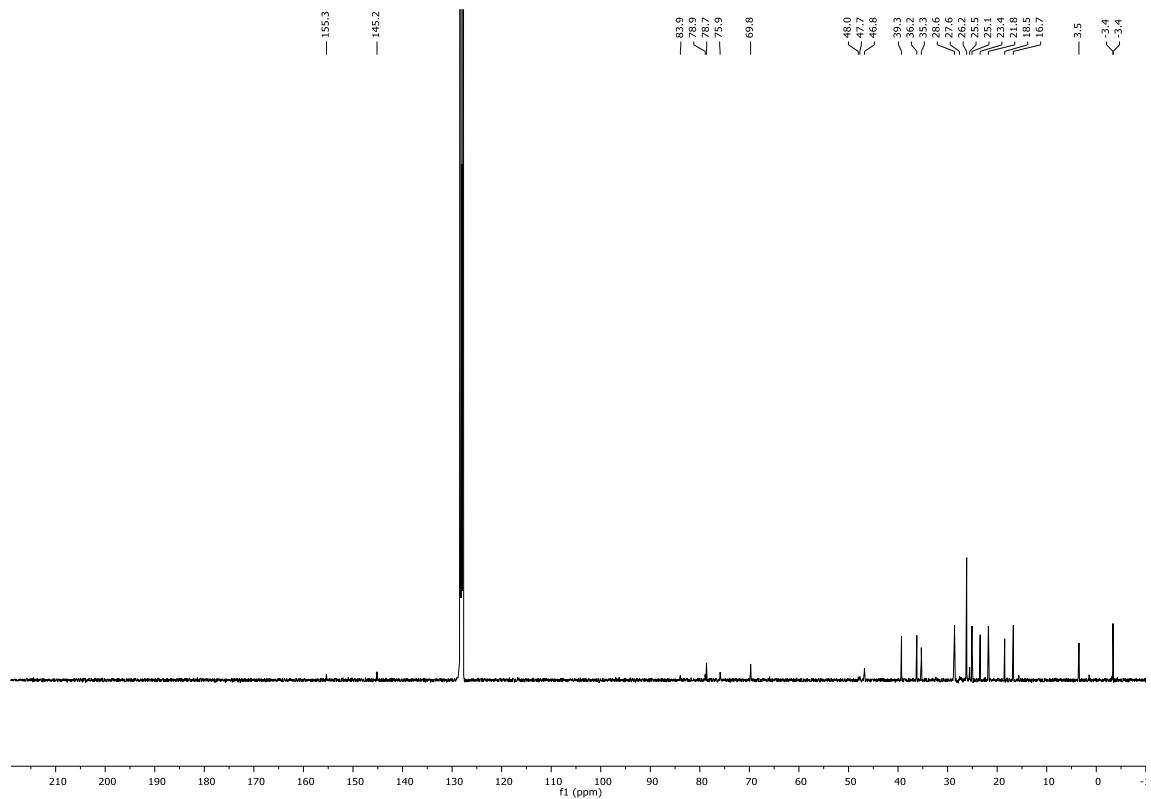
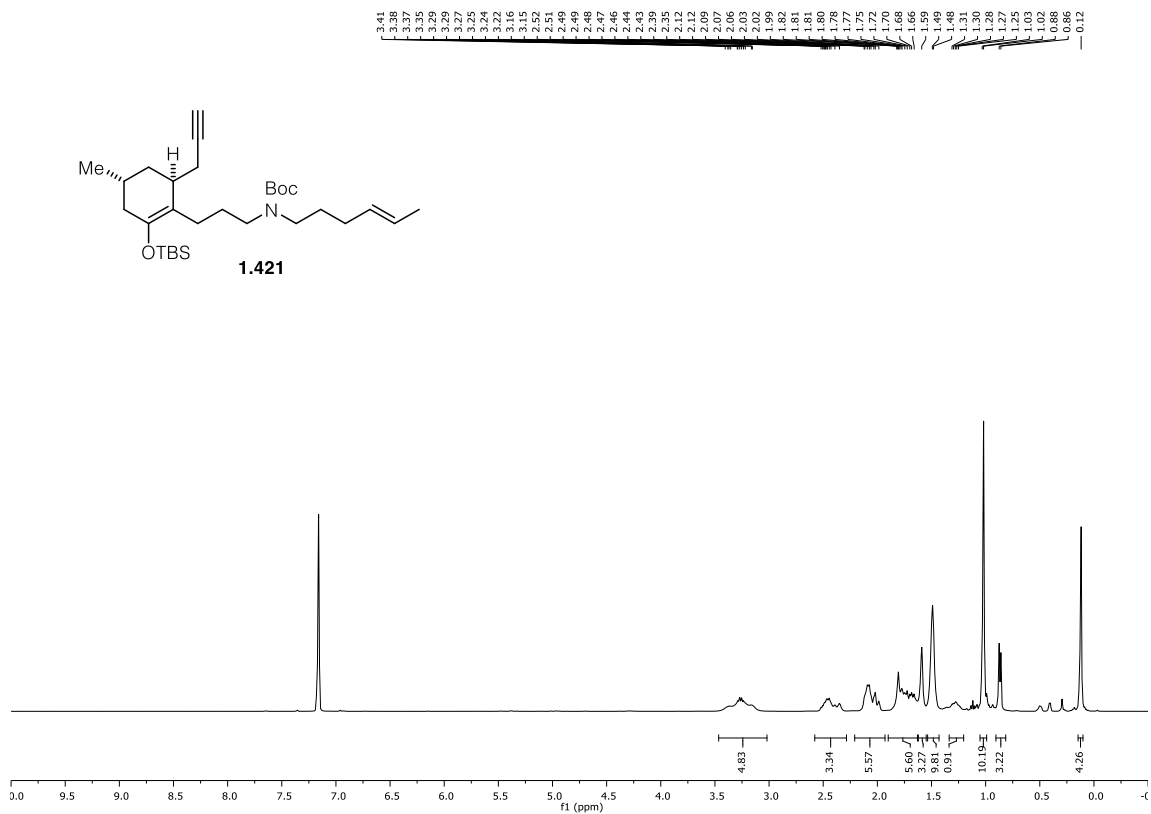
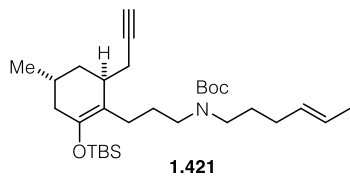


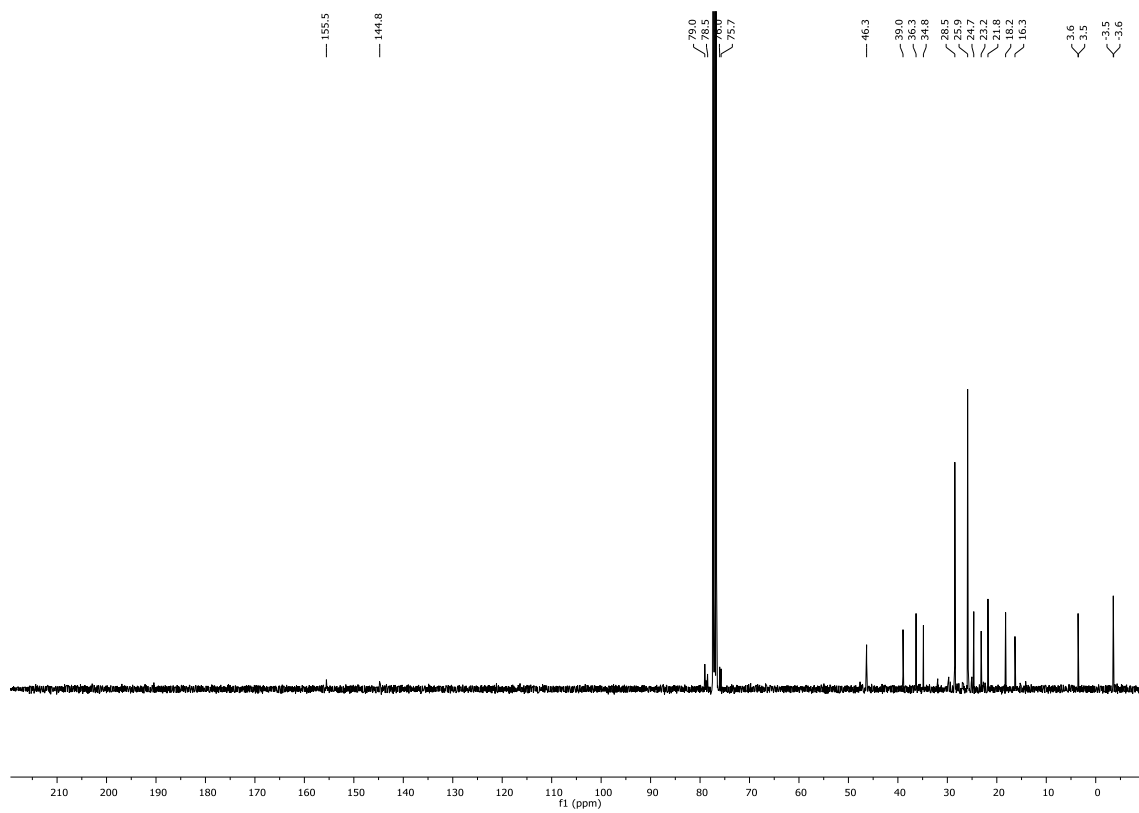
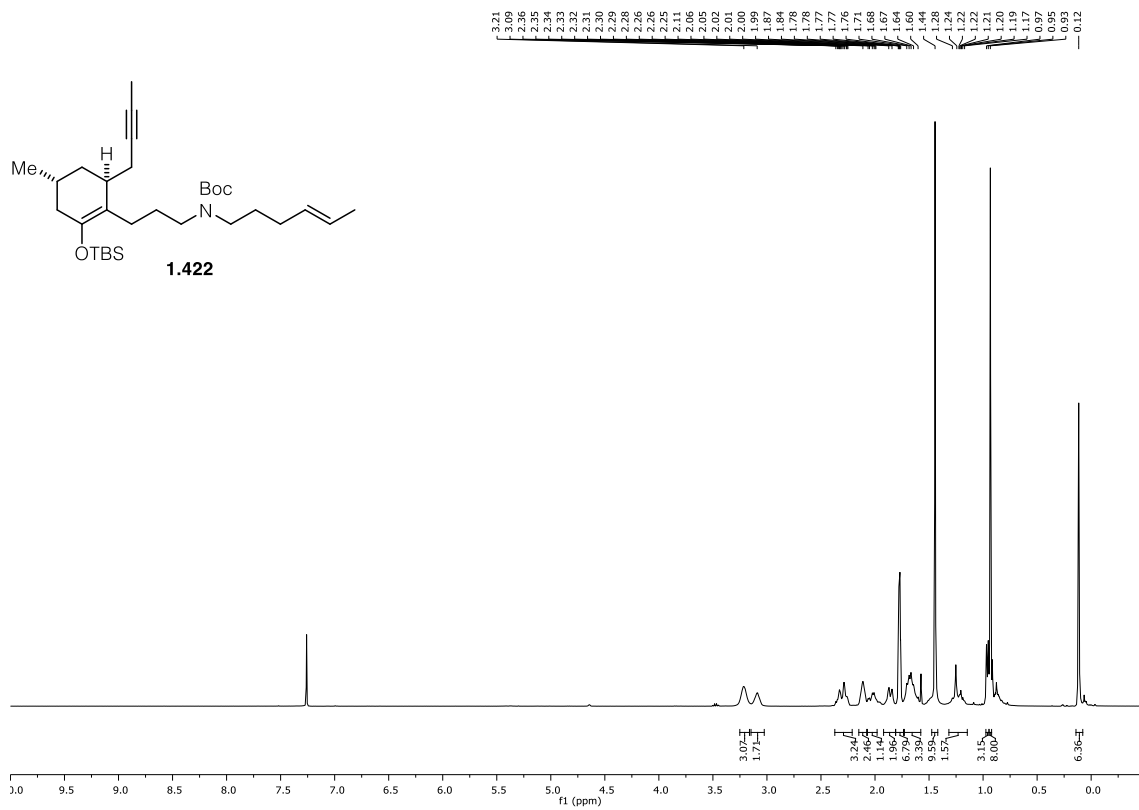
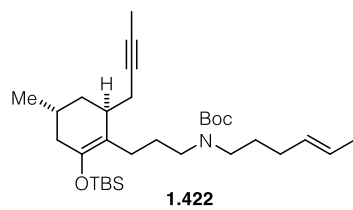


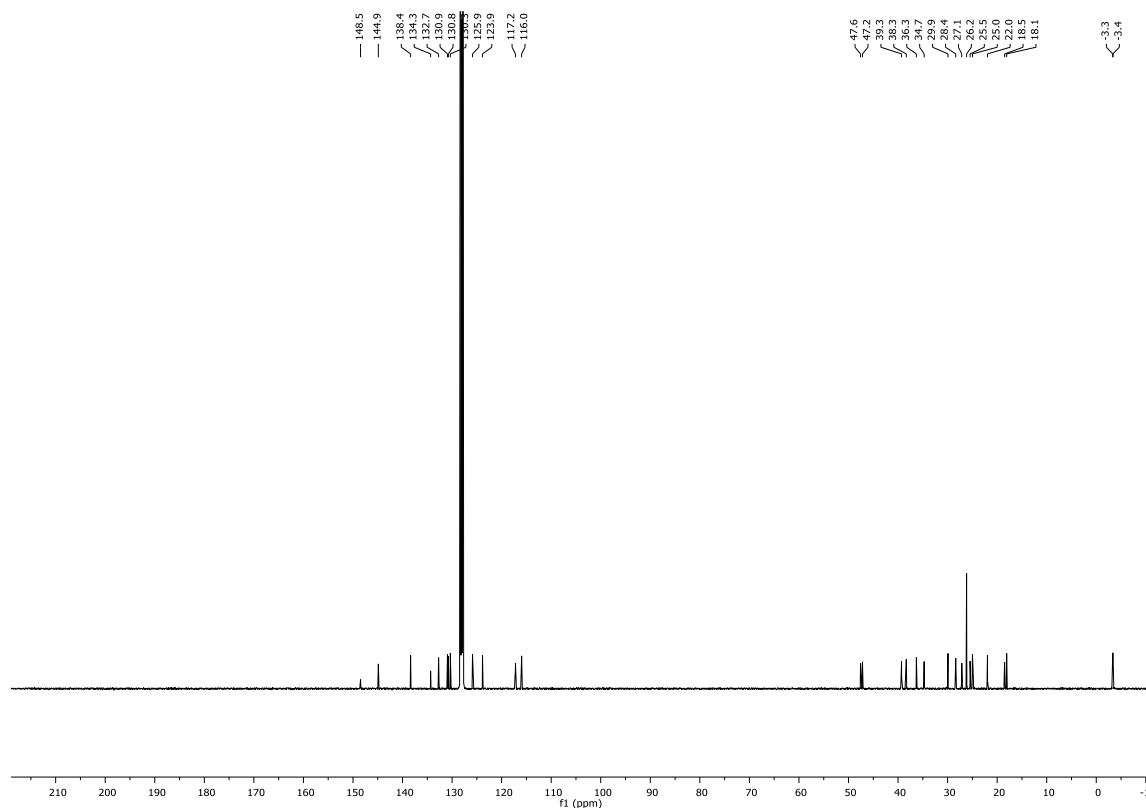
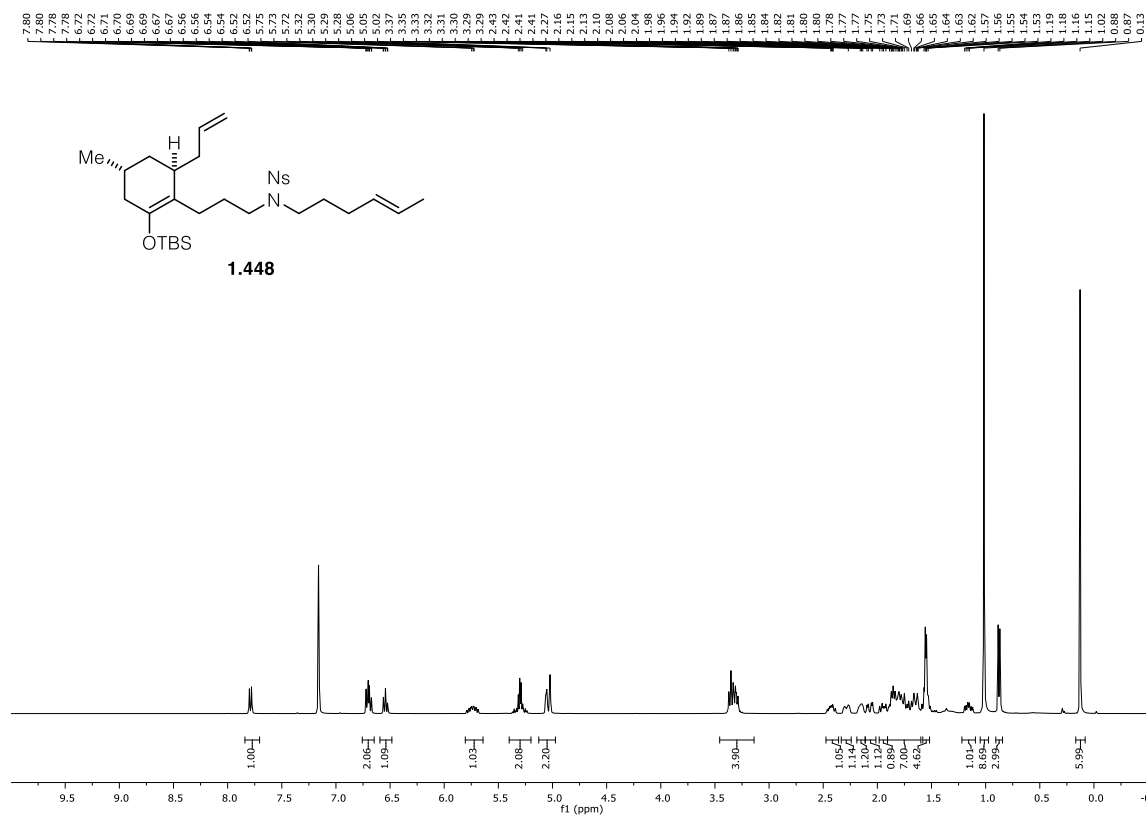




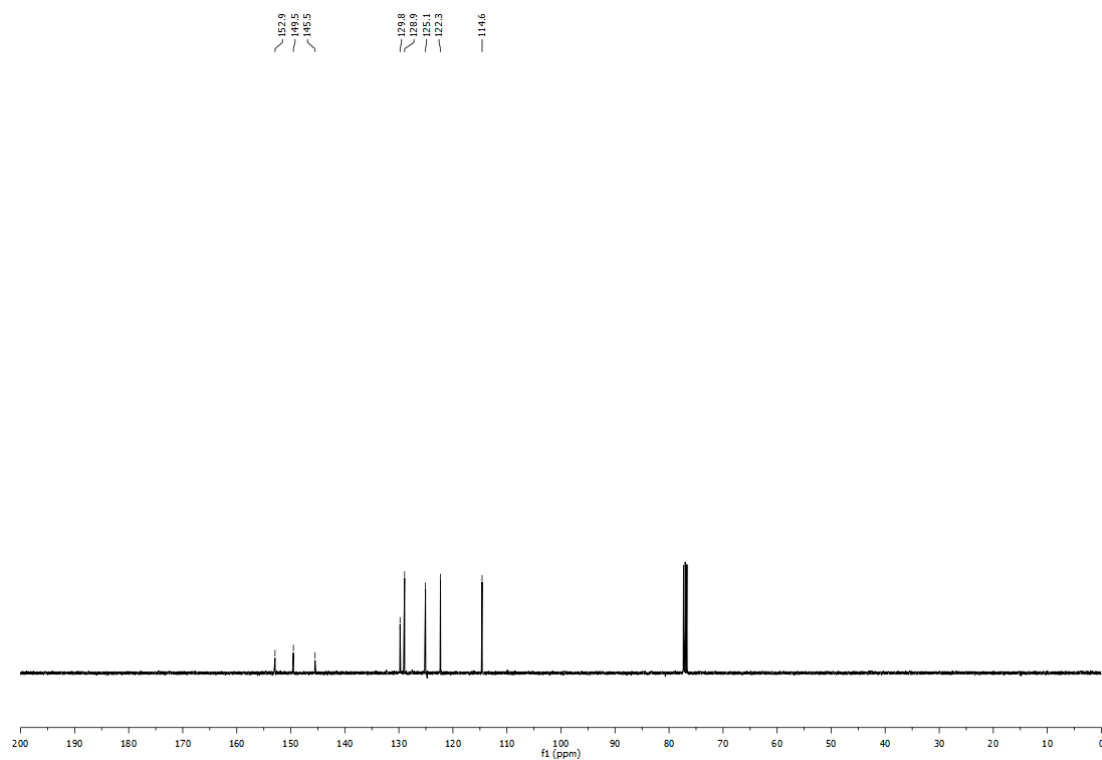
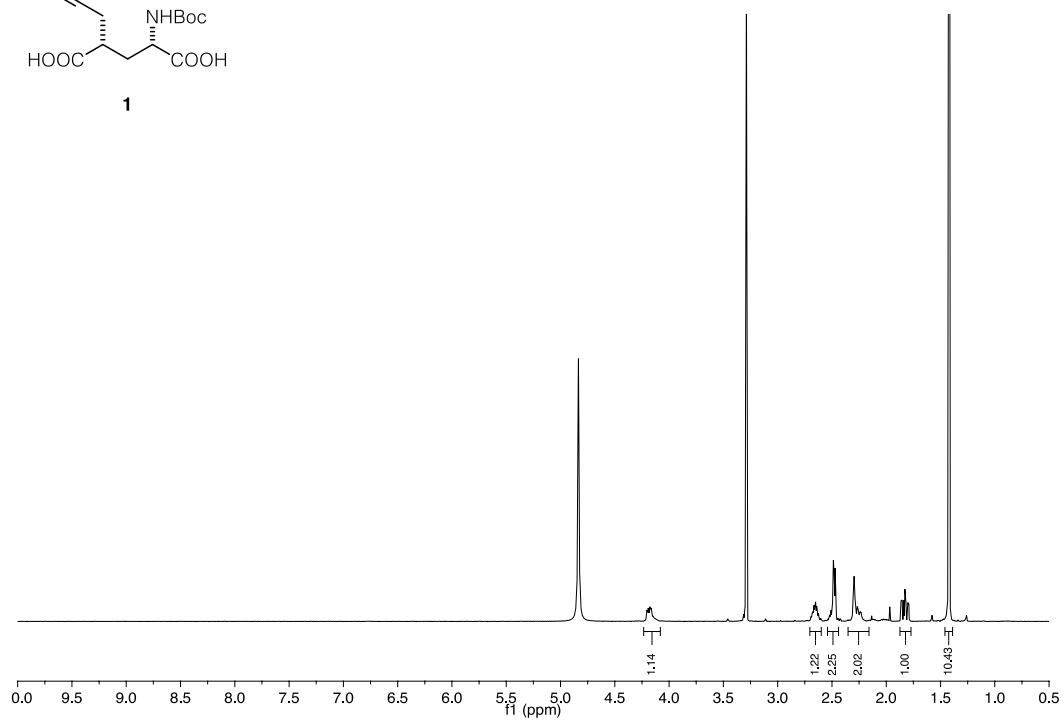
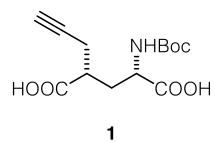


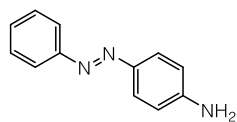
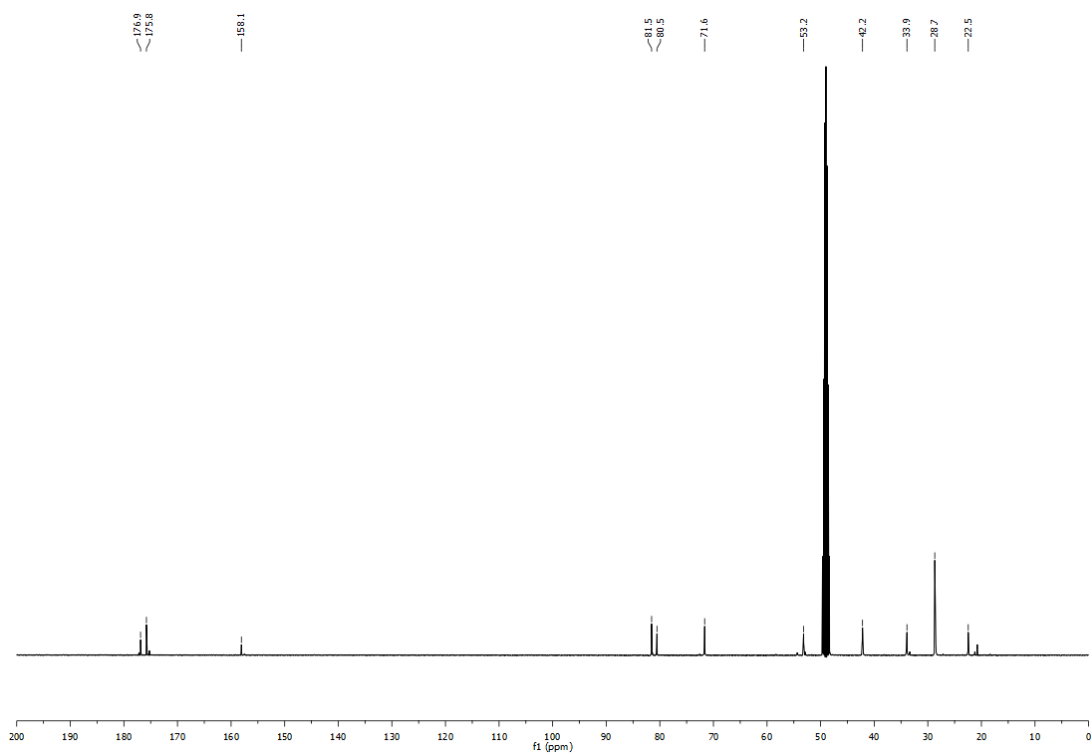
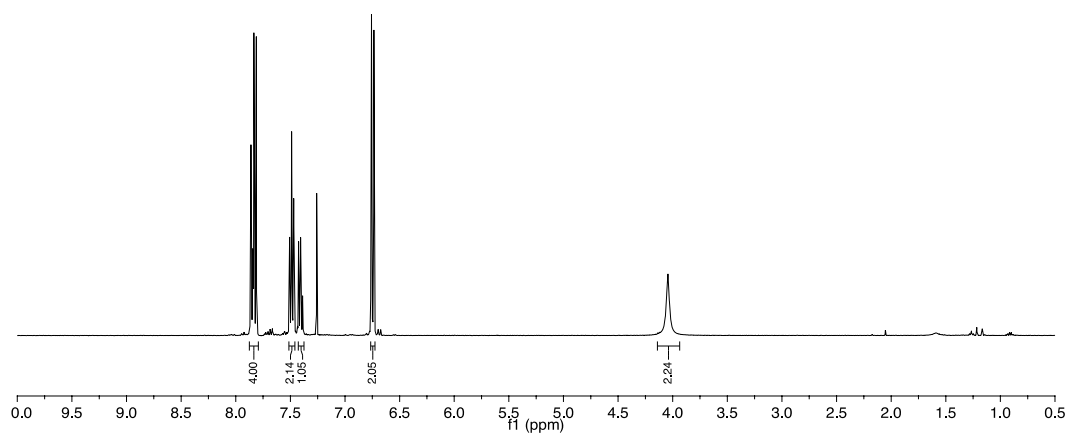


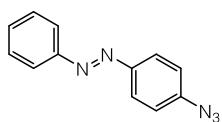
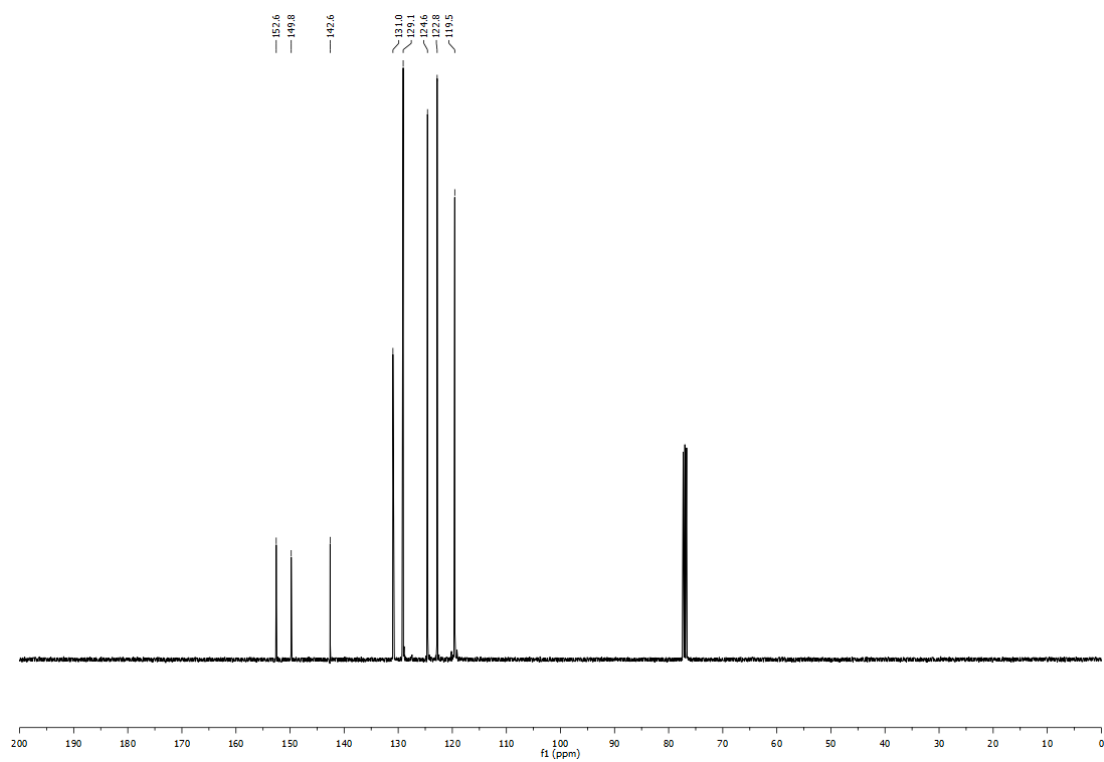
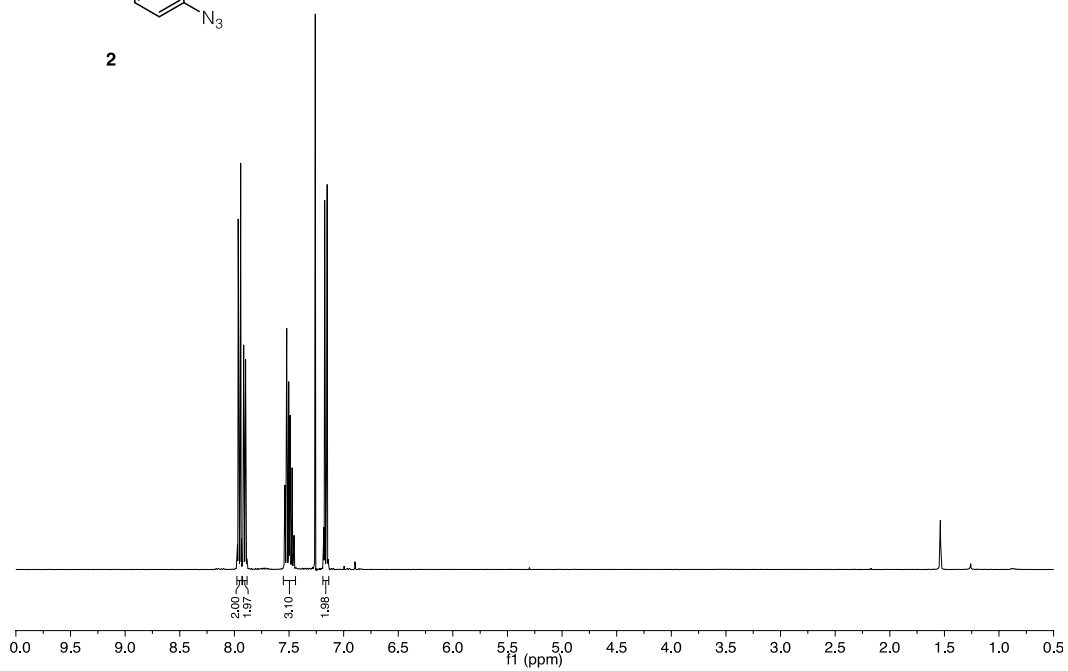


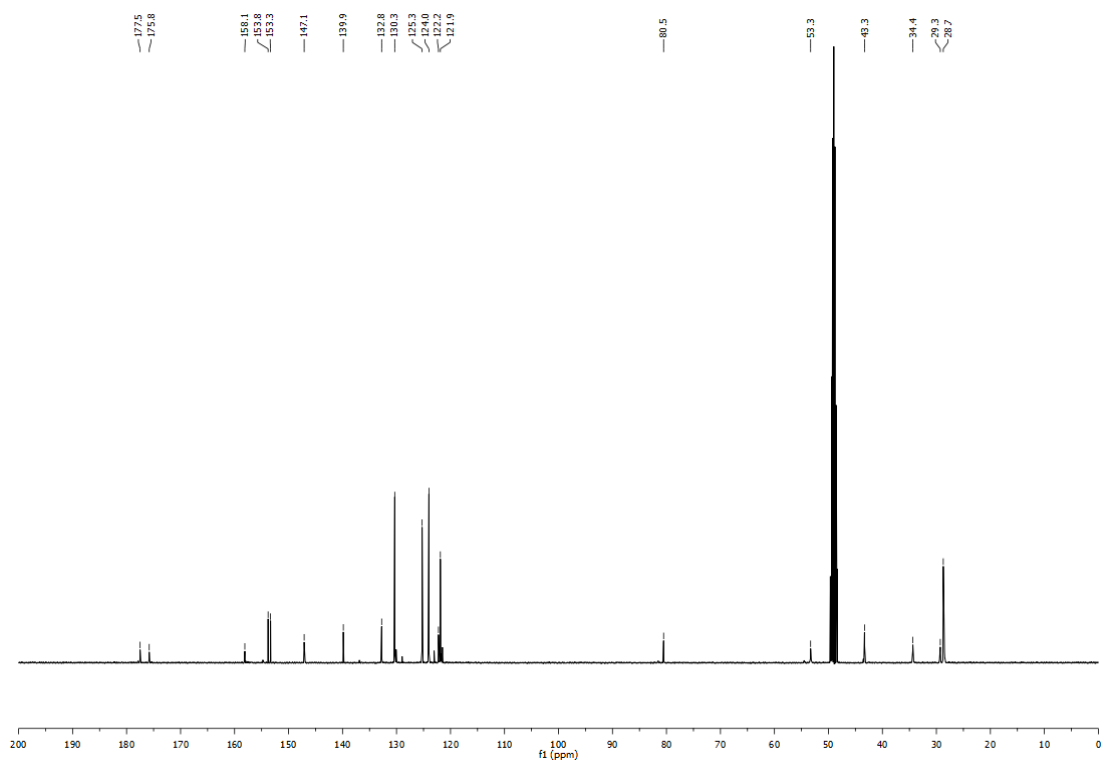
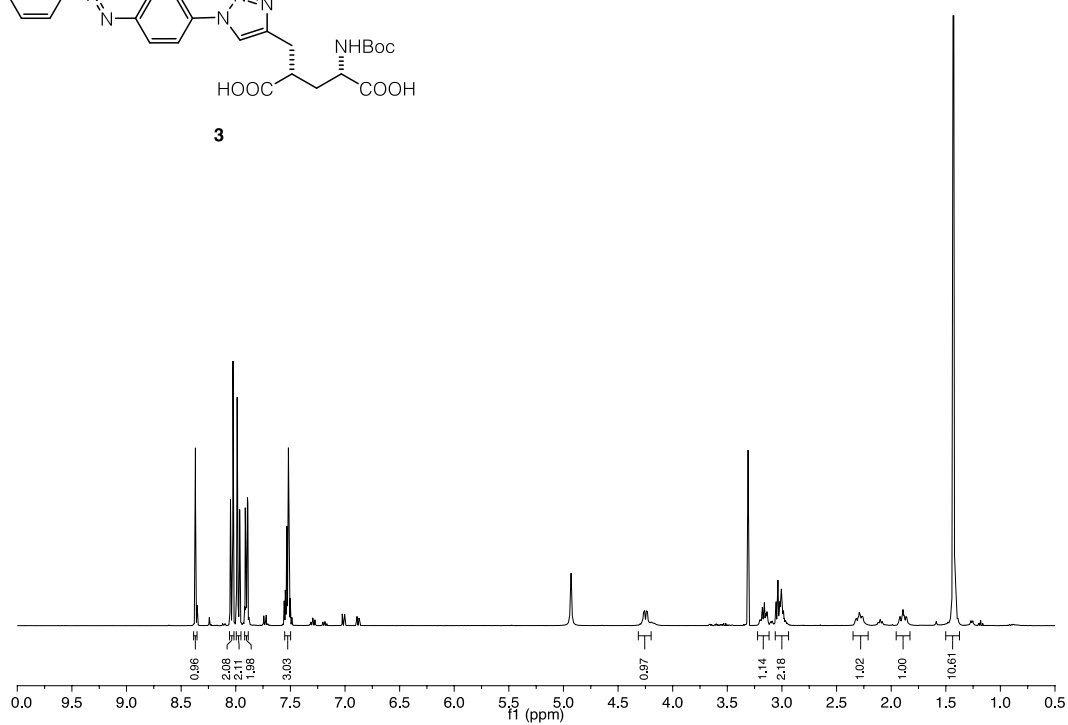
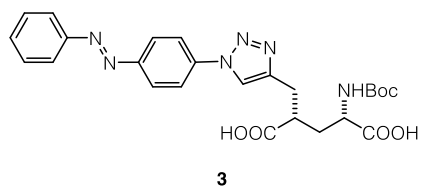


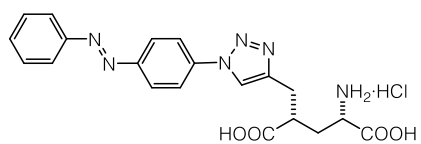
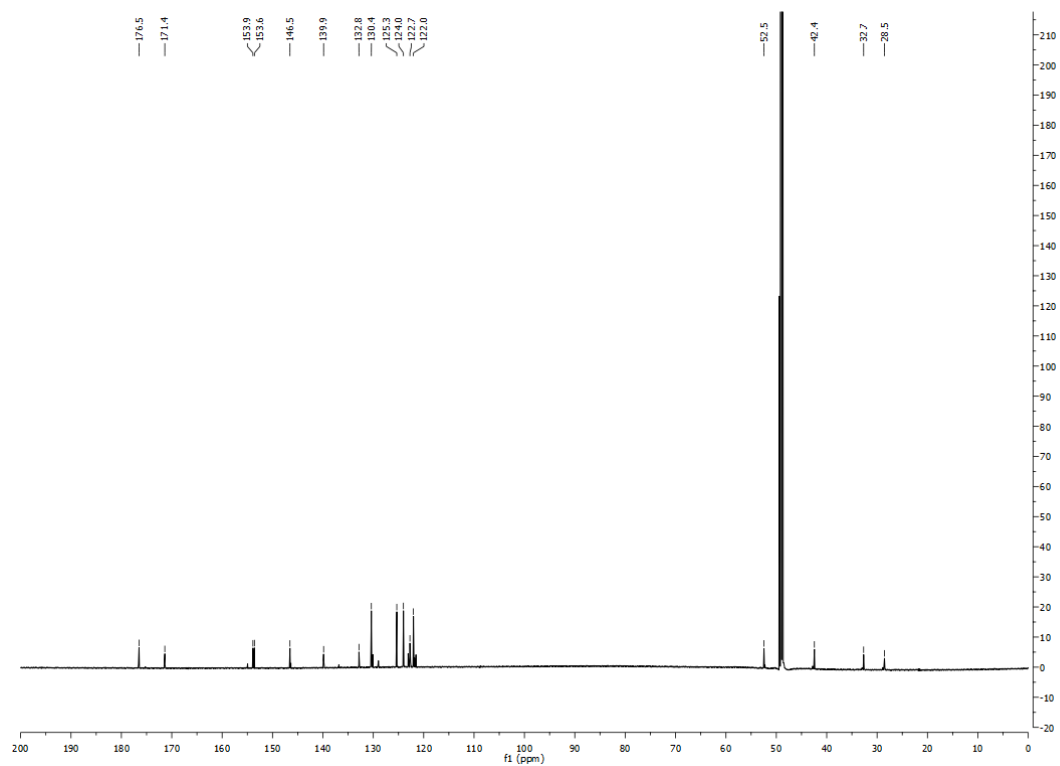
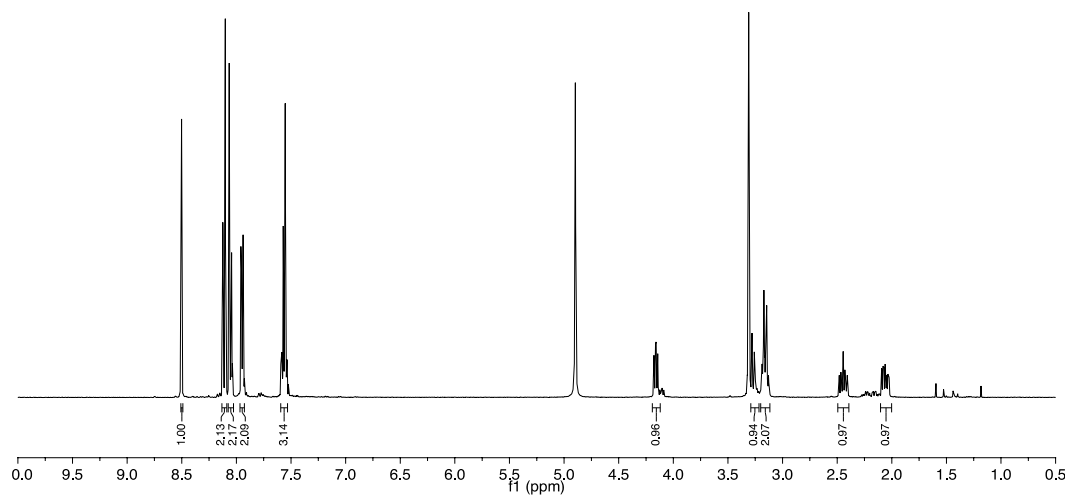
5.5 ^1H and ^{13}C NMR spectra for chapter 4.3.1

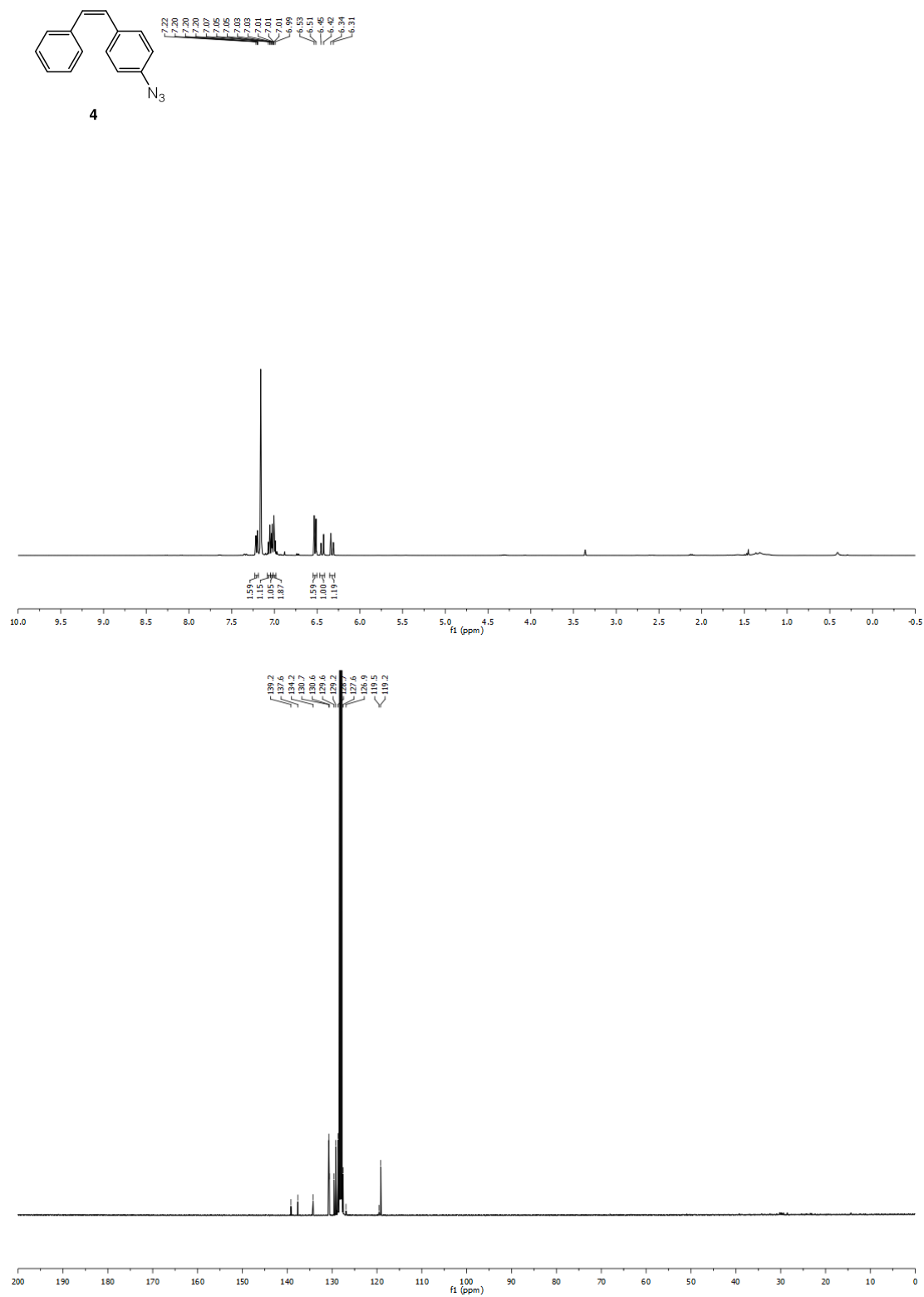


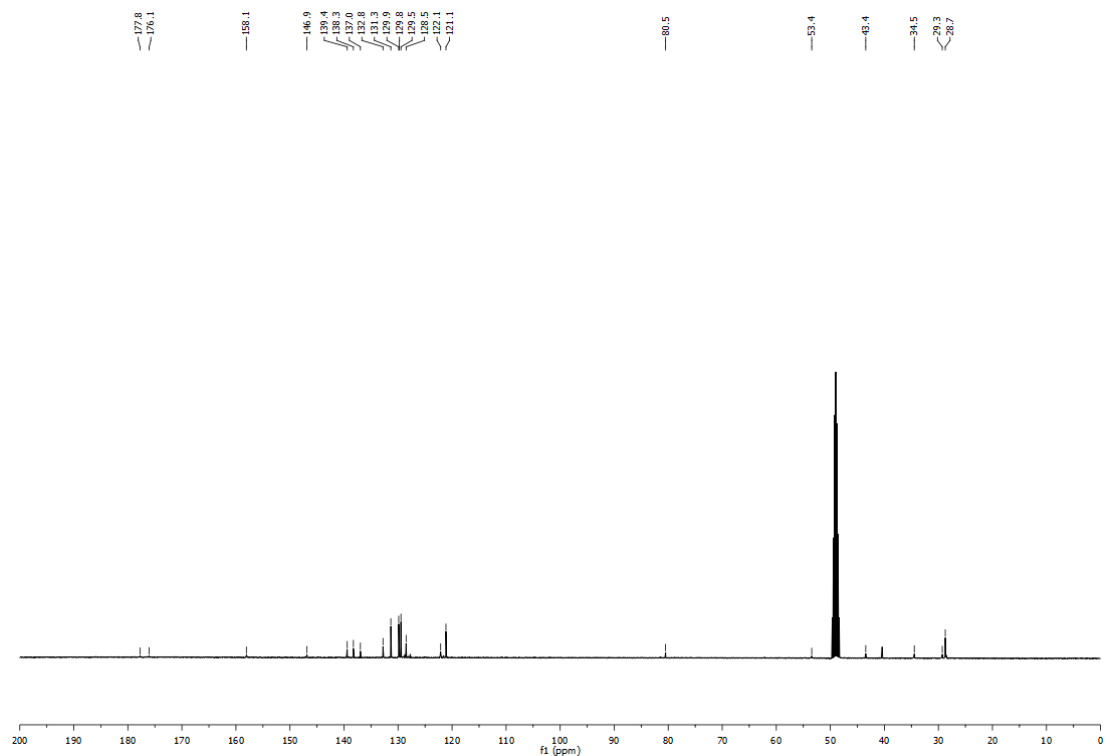
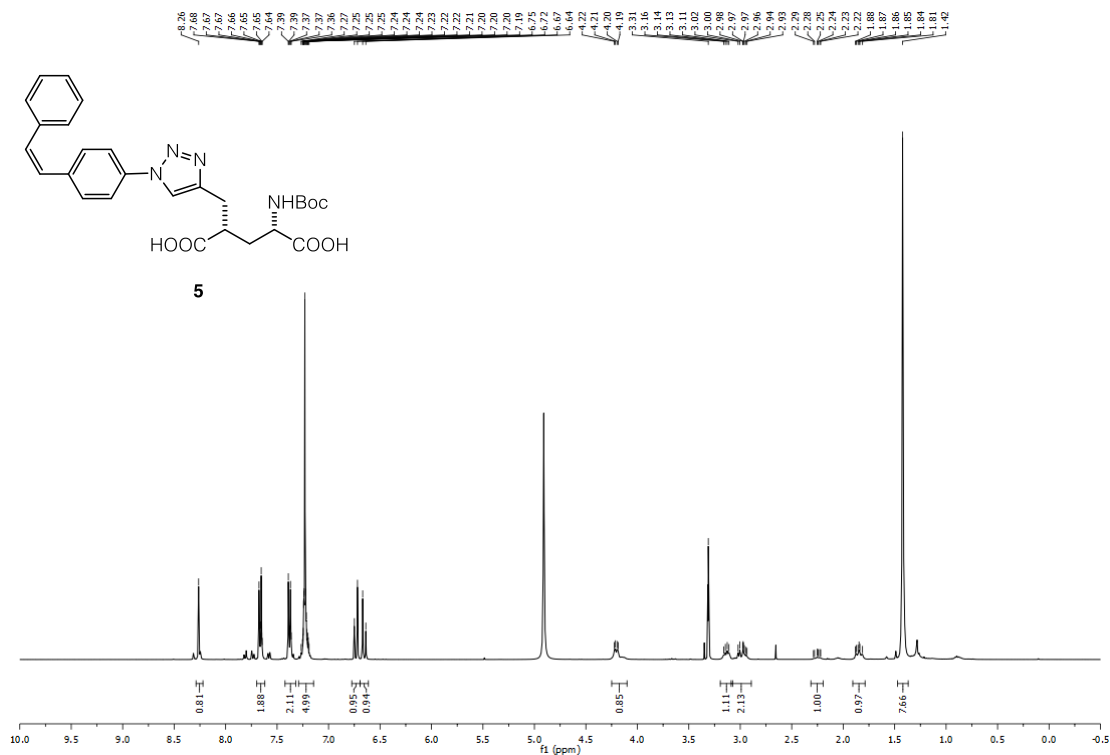
**S3**

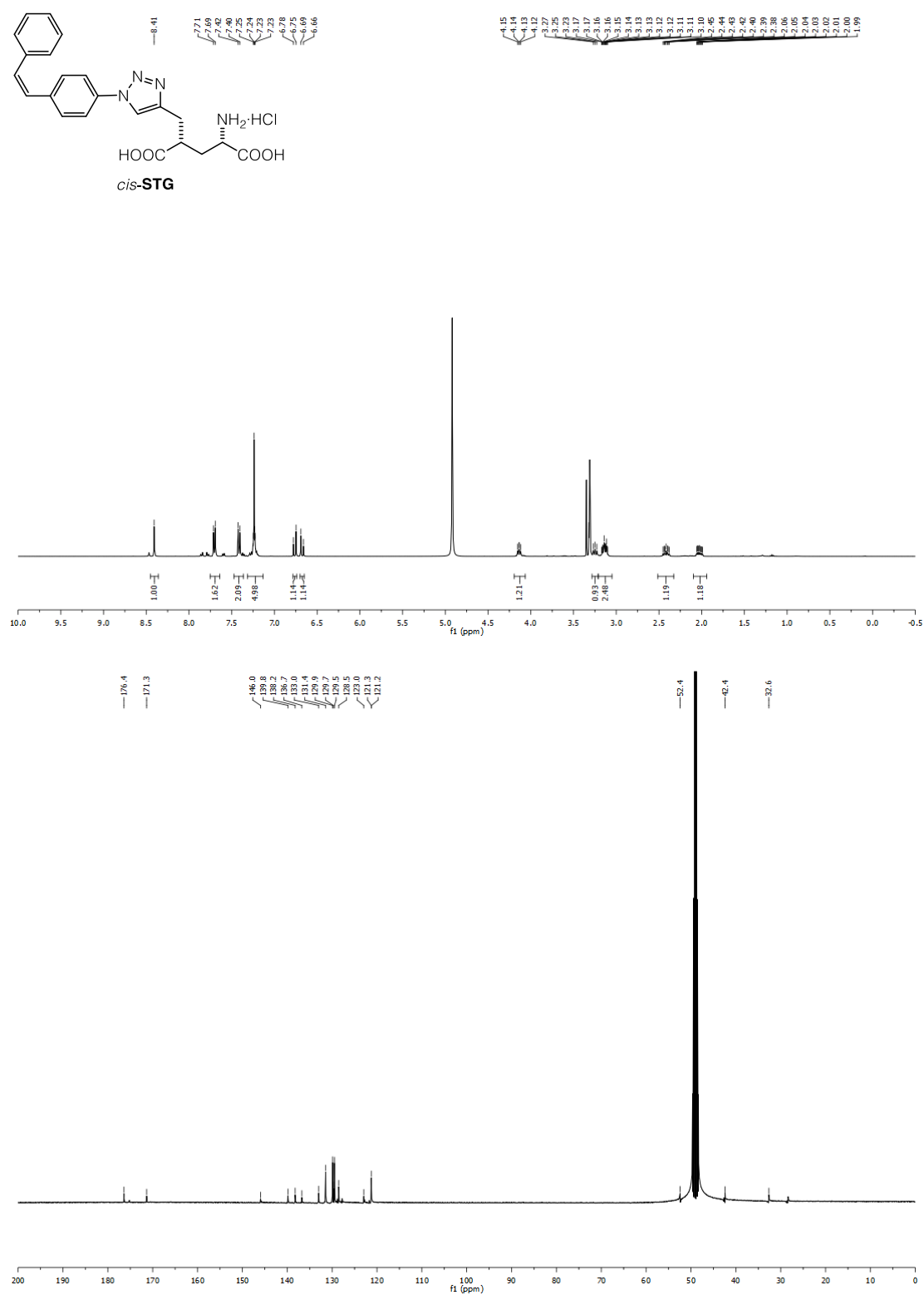
**2**



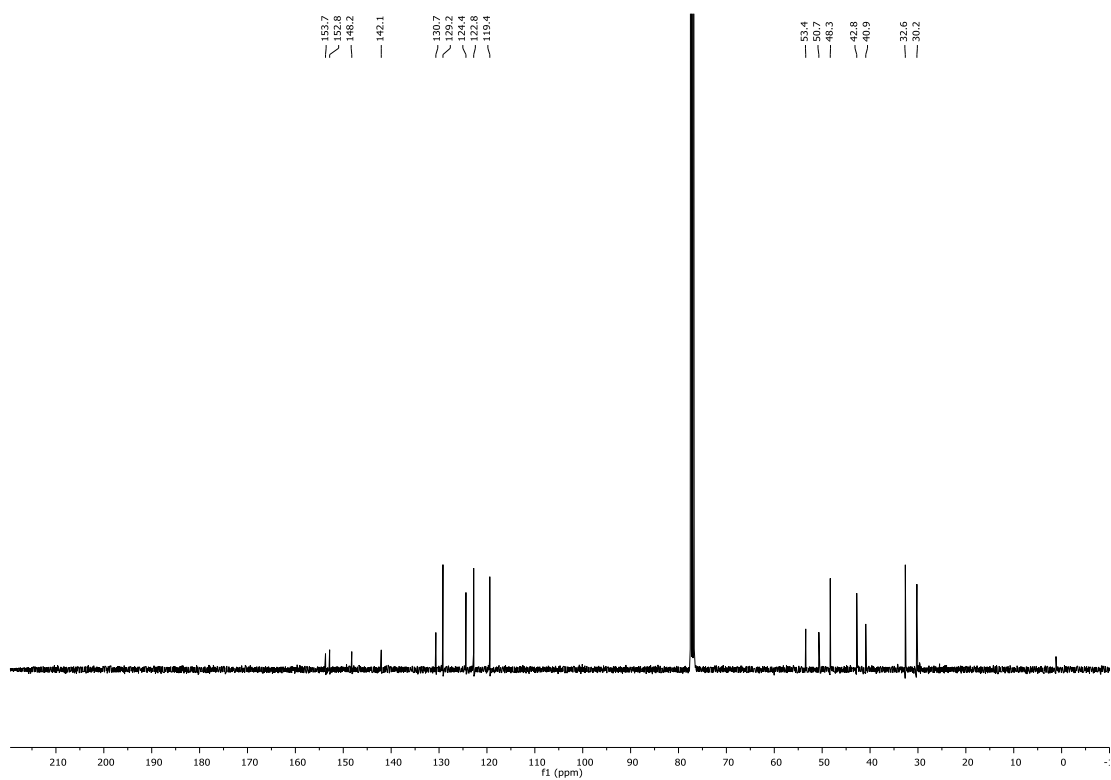
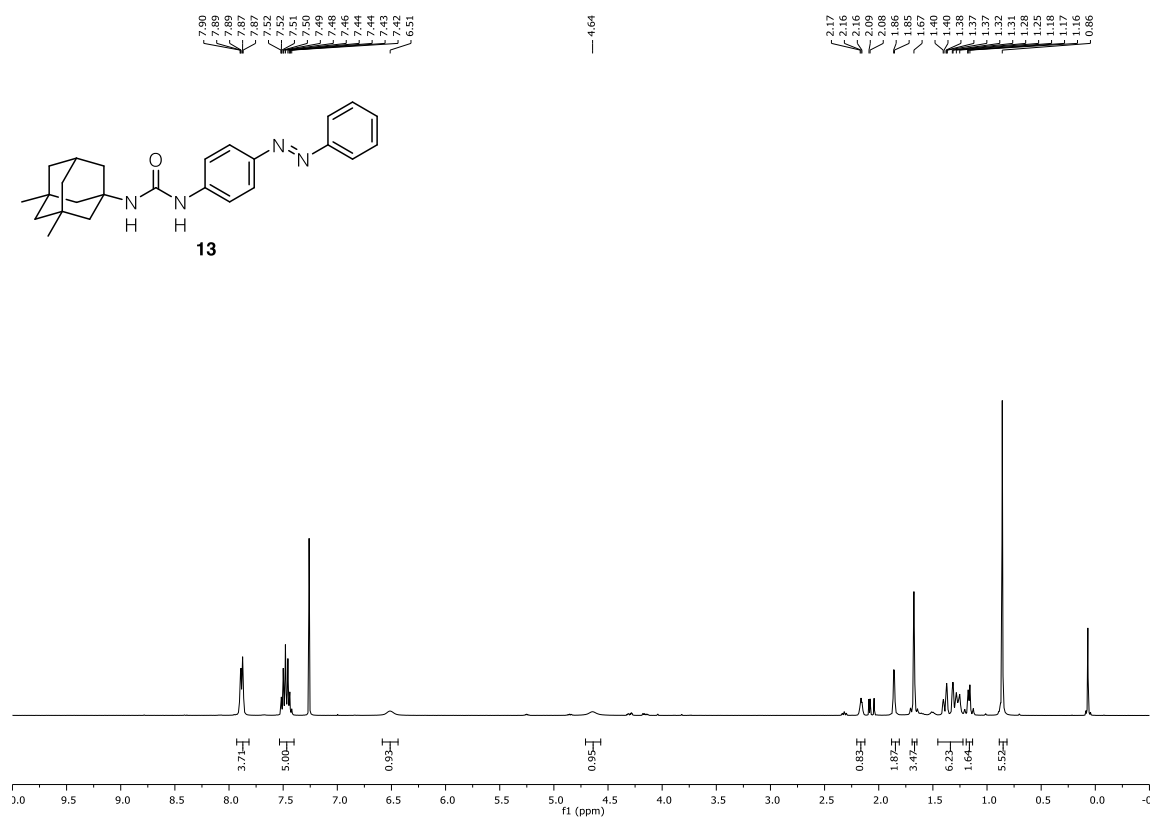
*trans-ATG*

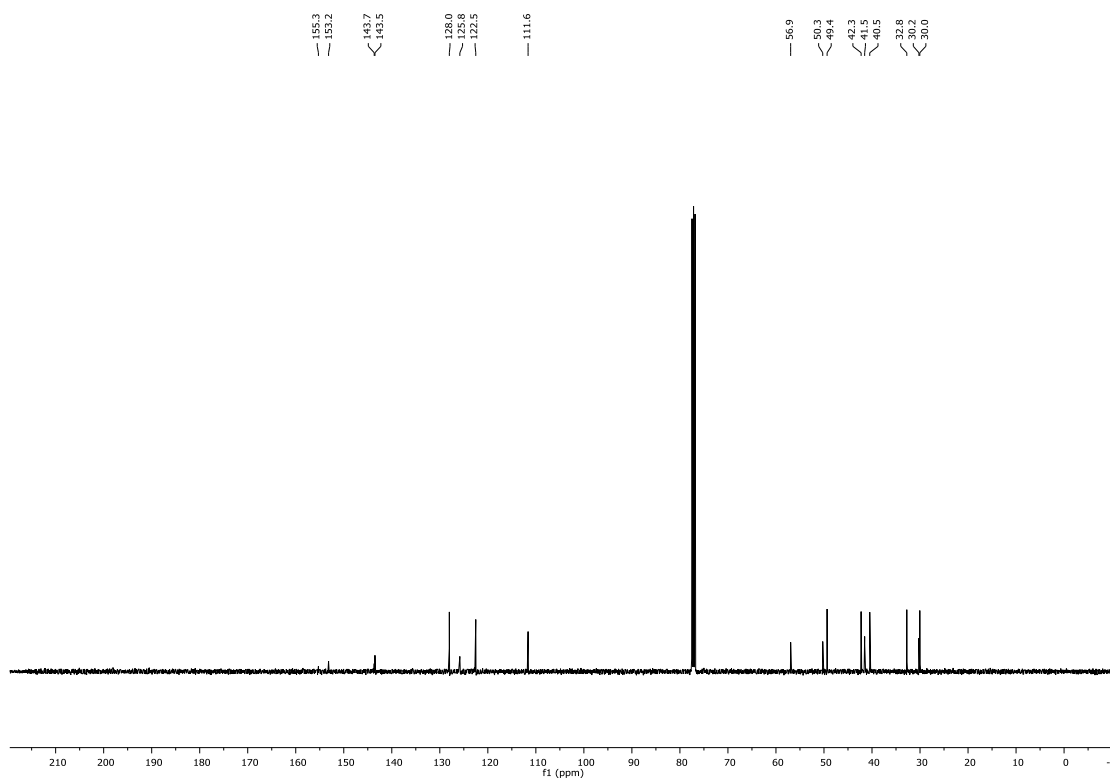


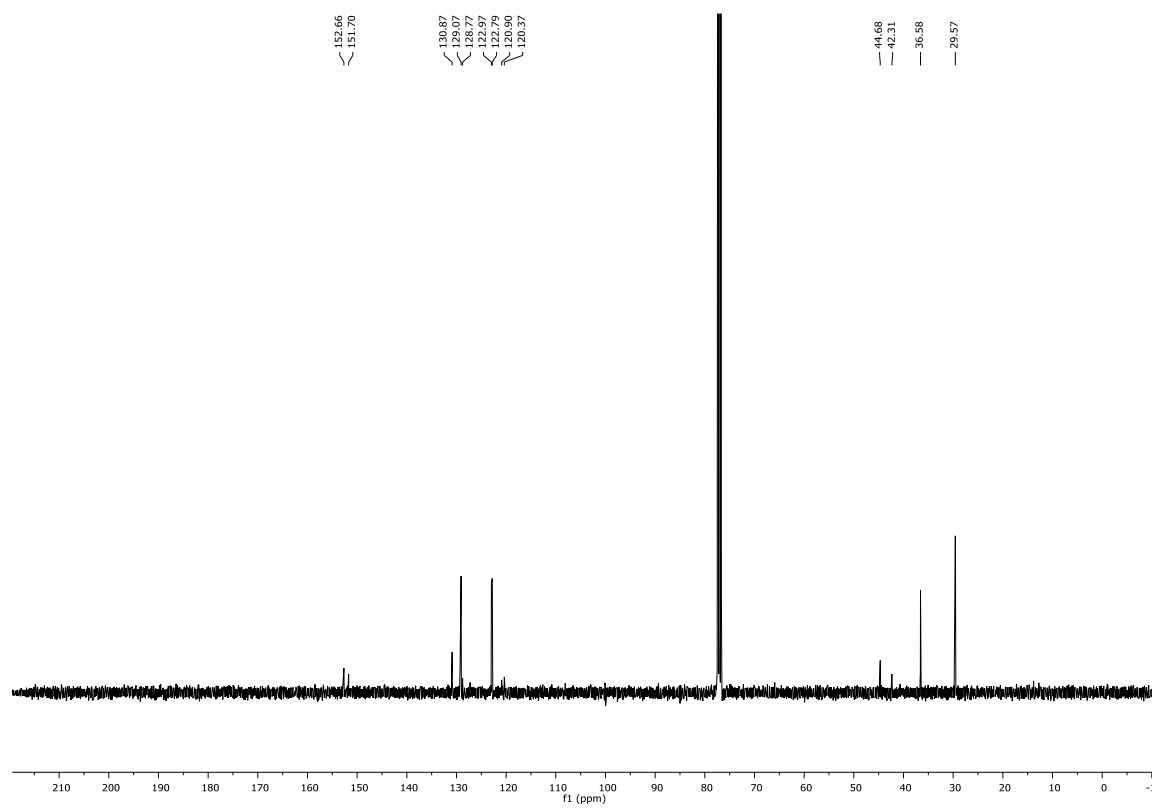
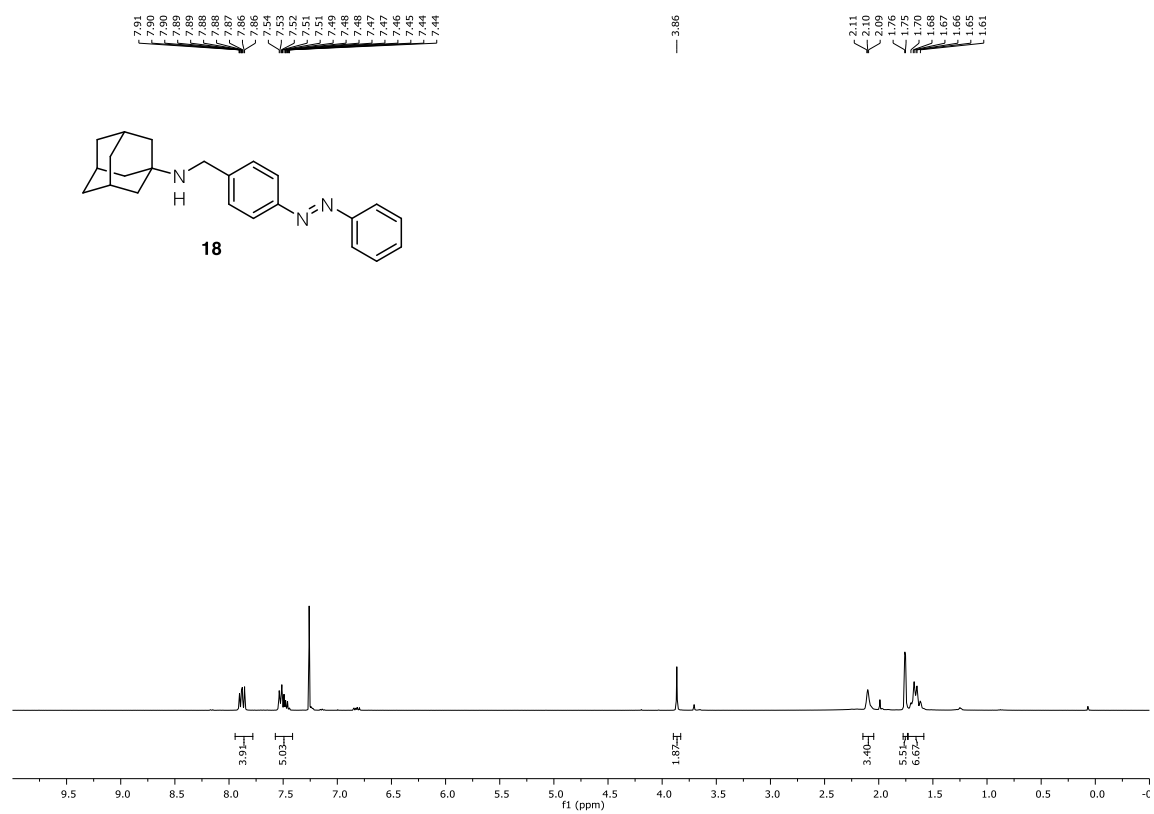


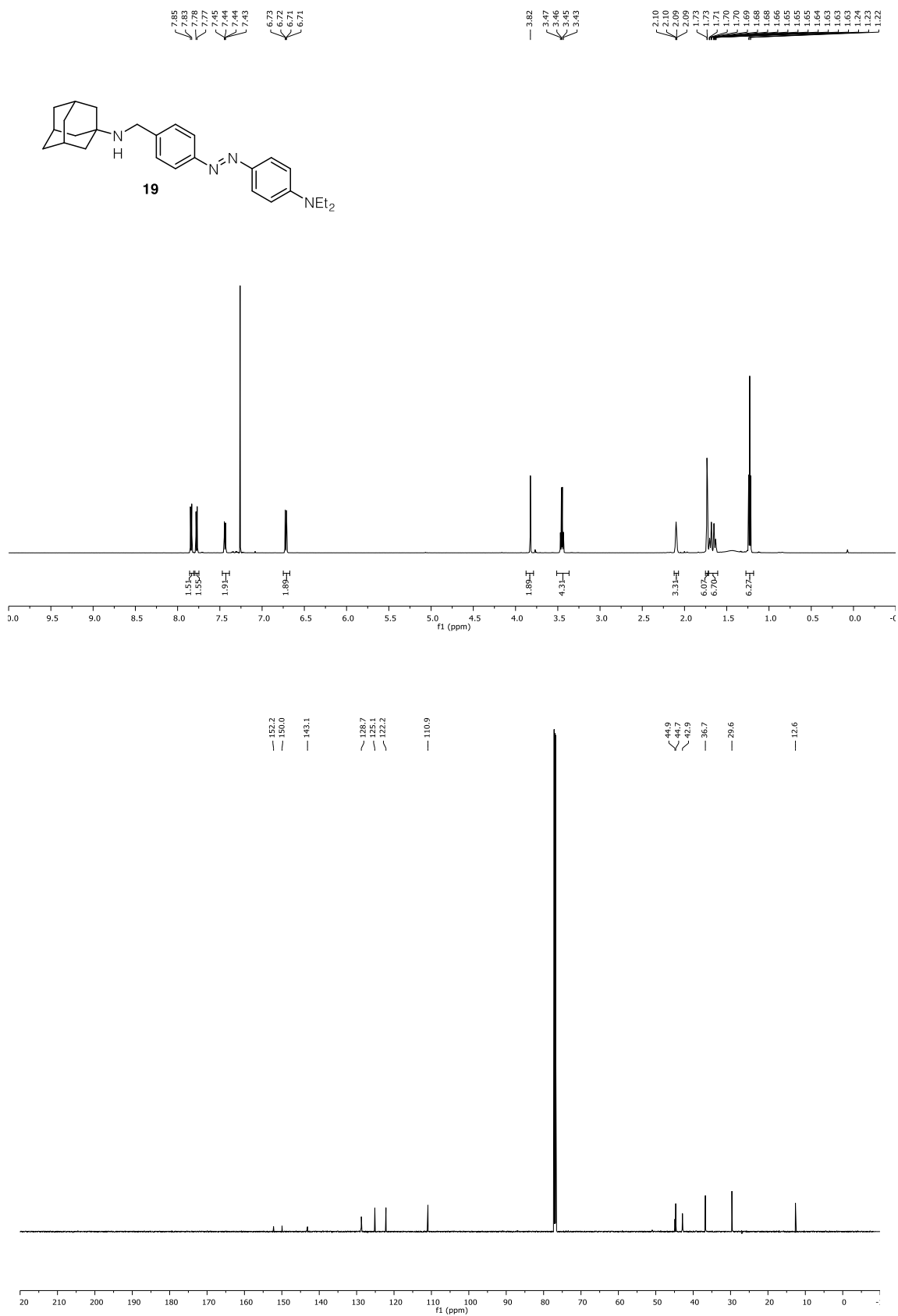


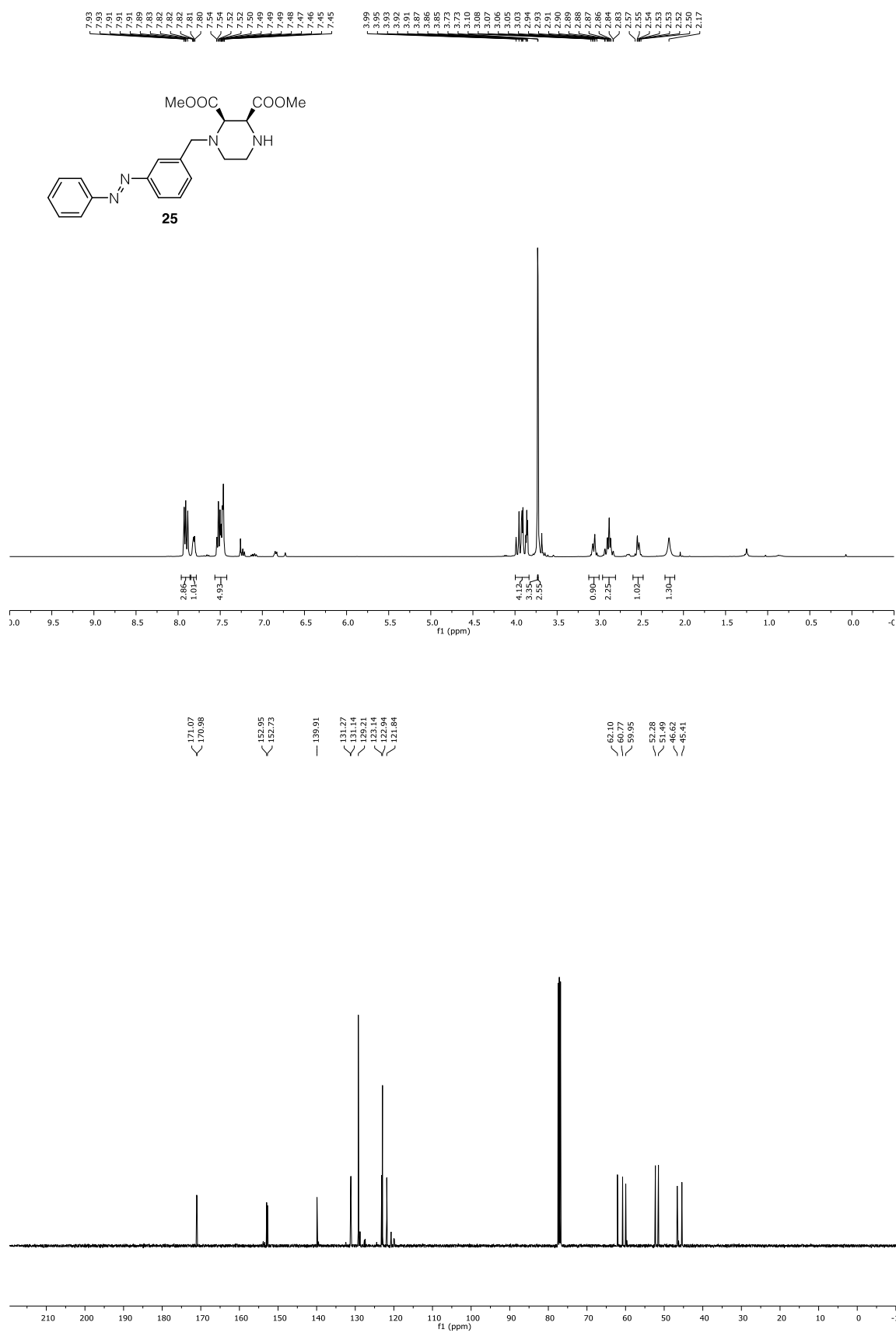
5.6 ^1H and ^{13}C NMR spectra and additional electrophysiology data for
chapter 4.3.2

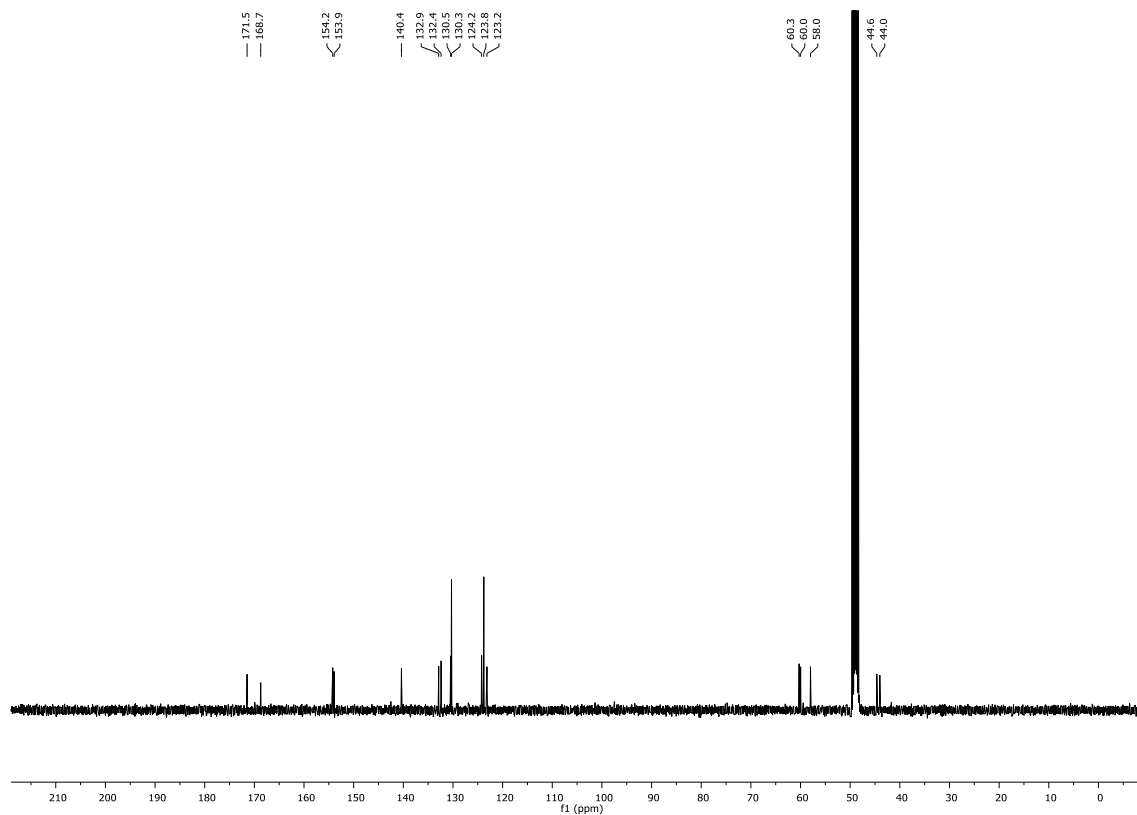
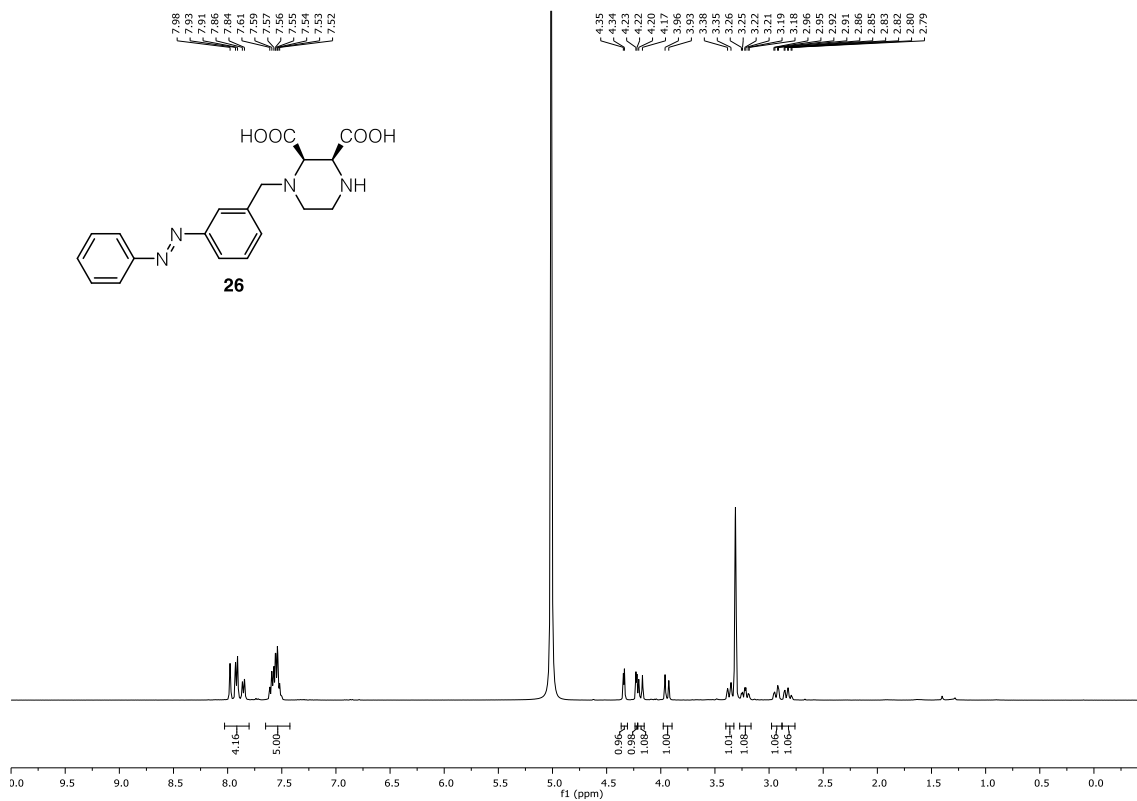


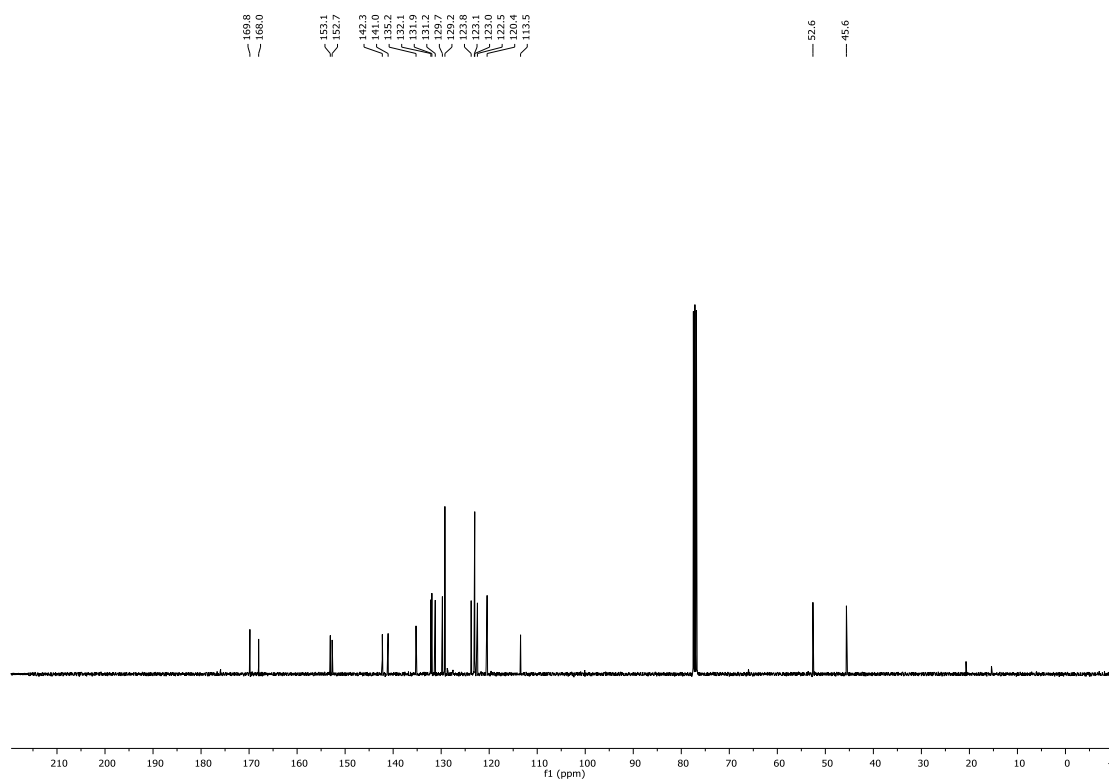
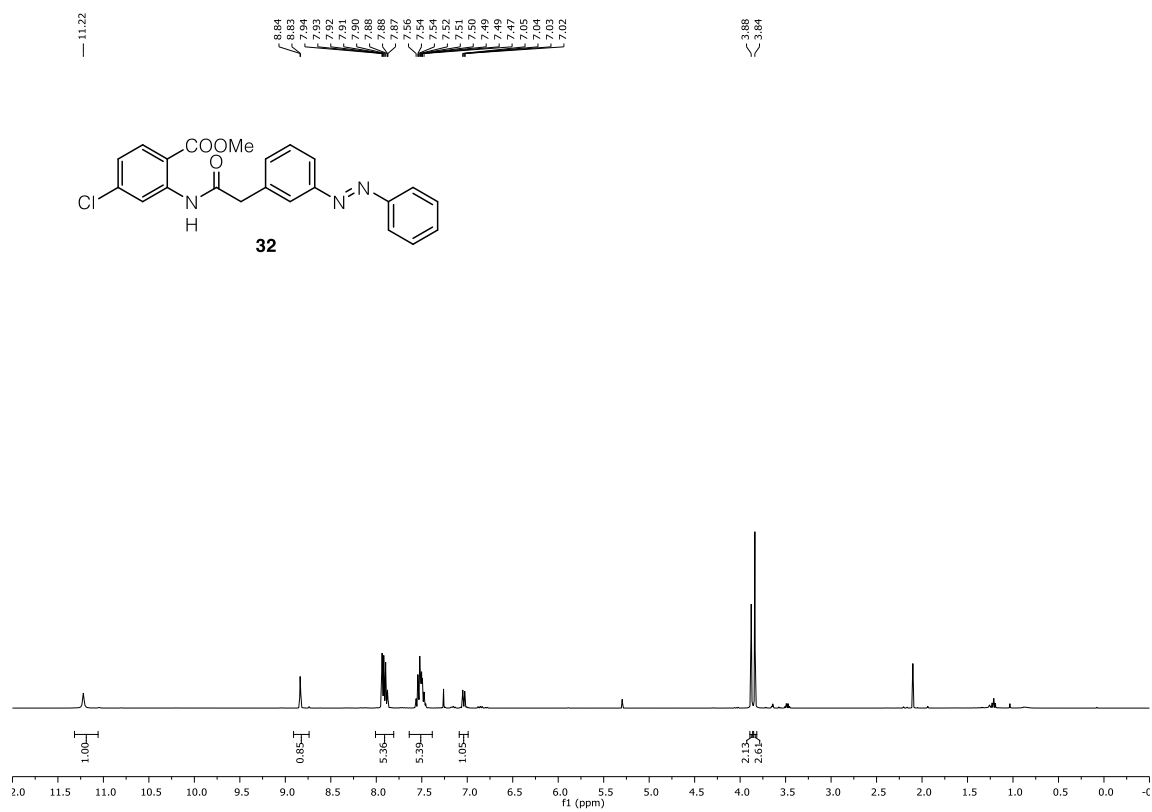


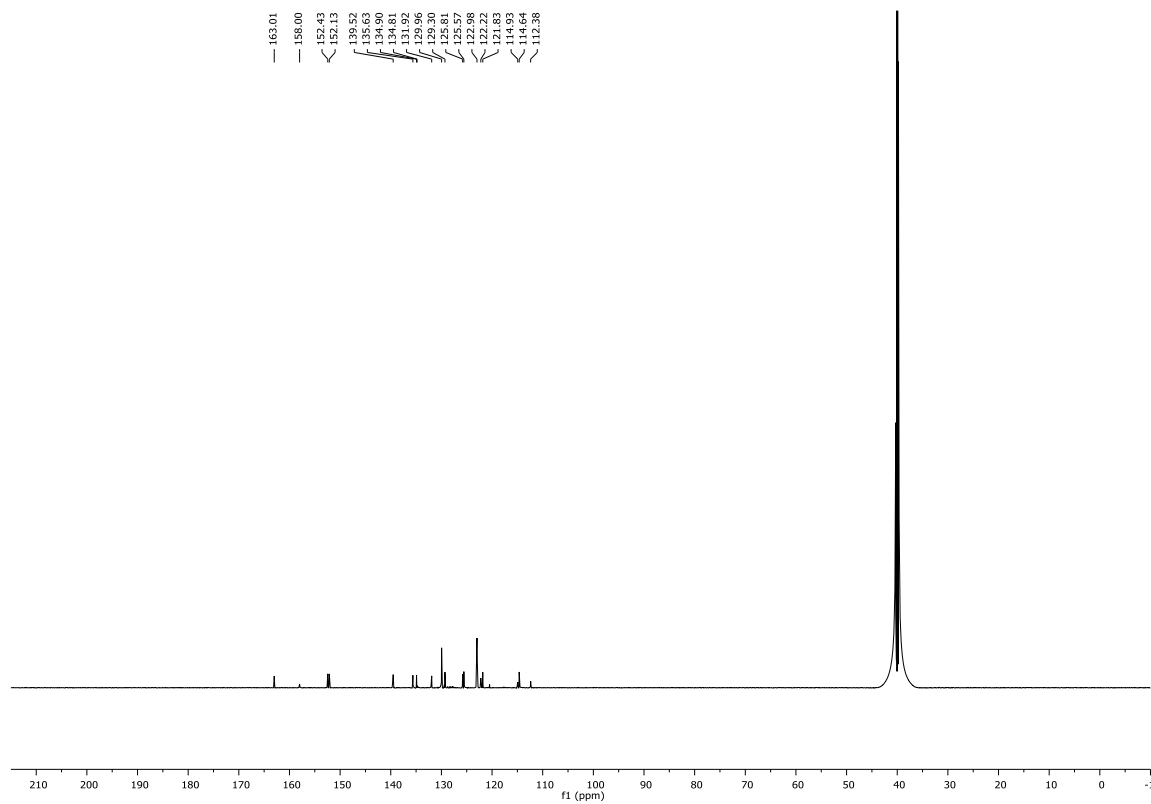
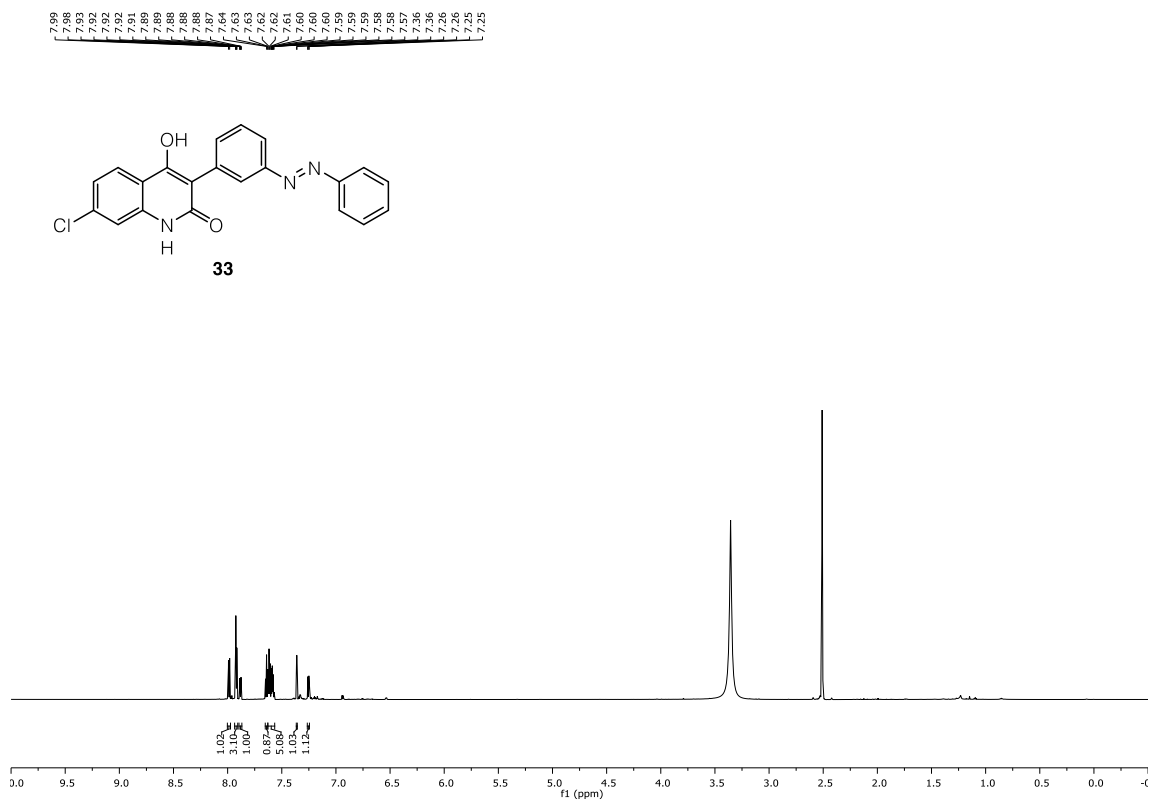












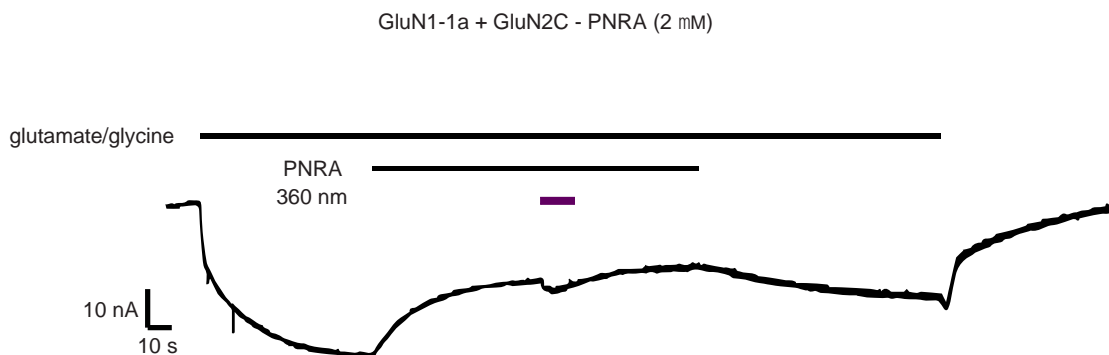
Two-electrode voltage clamp electrophysiology of *Xenopus* oocytes expressing GluN1-1a+GluN2B, GluN1-1a+GluN2C or GluN1-1a+GluN2D channels

Figure S1: Electrophysiological evaluation of PNRA with other NMDA receptor subunit combinations.

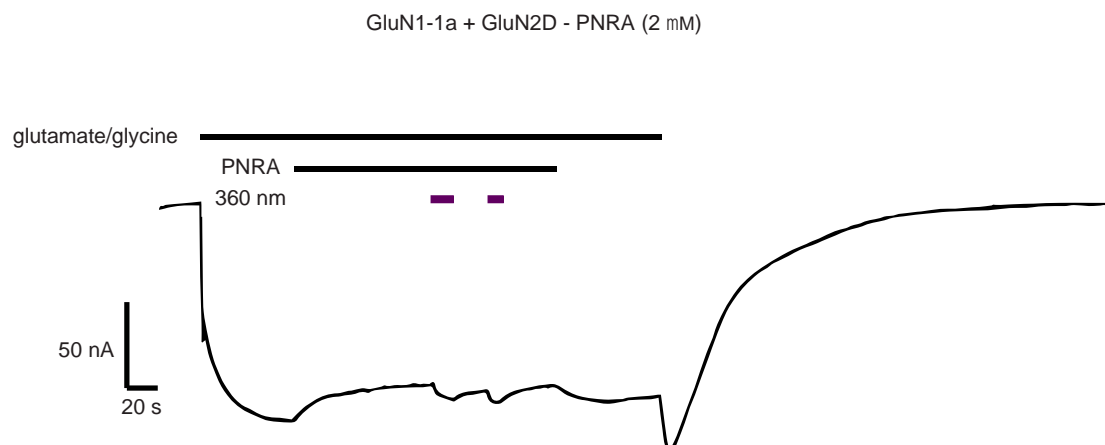
a)

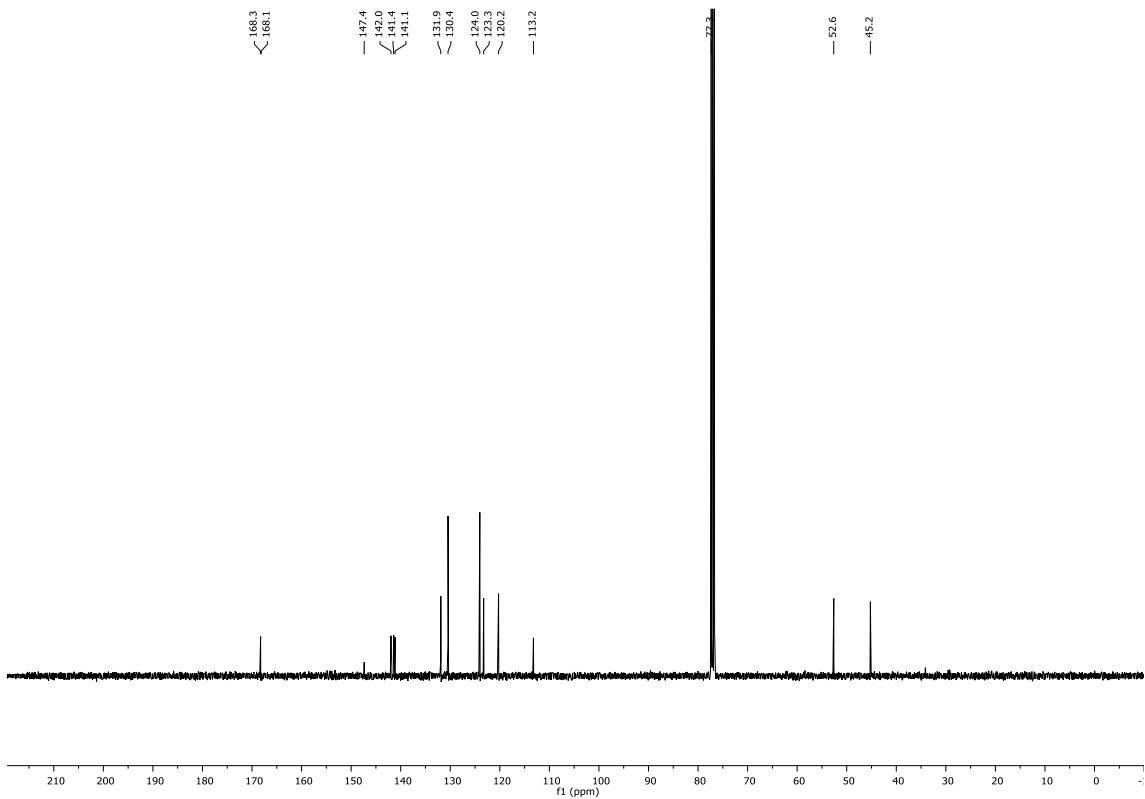
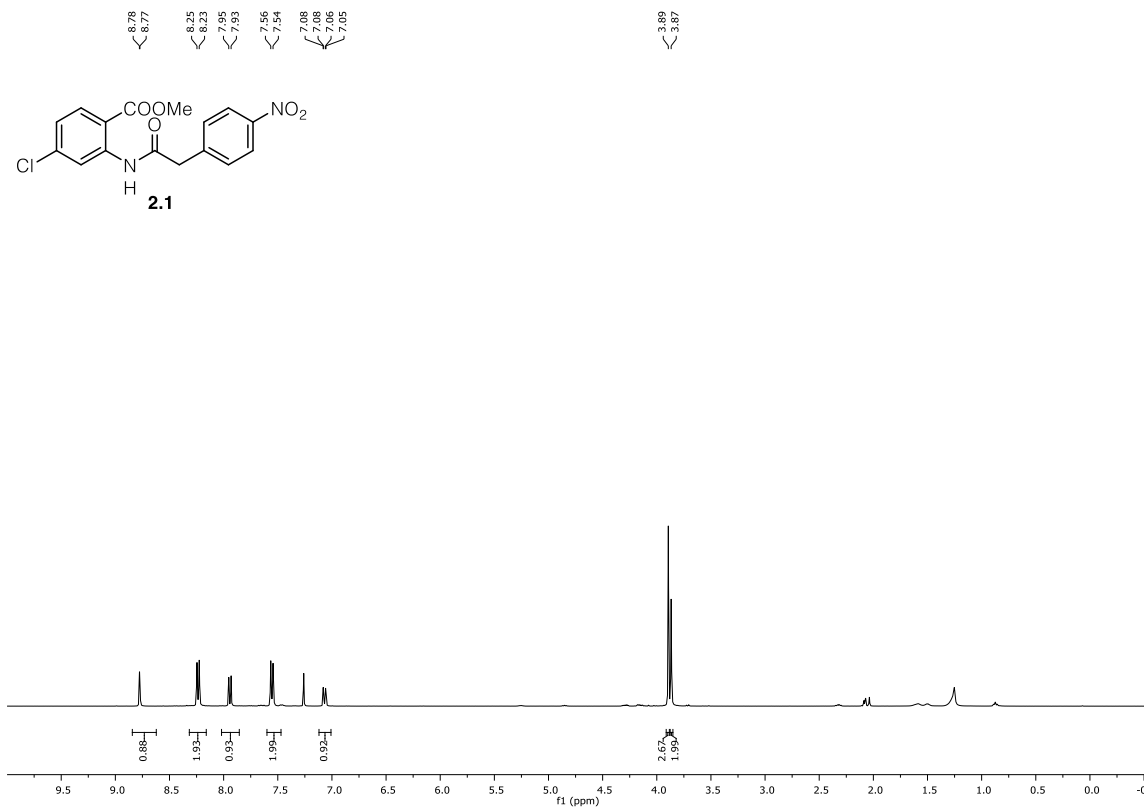
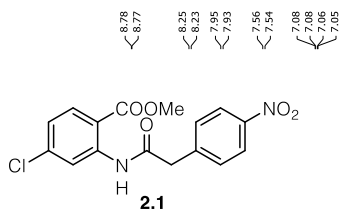


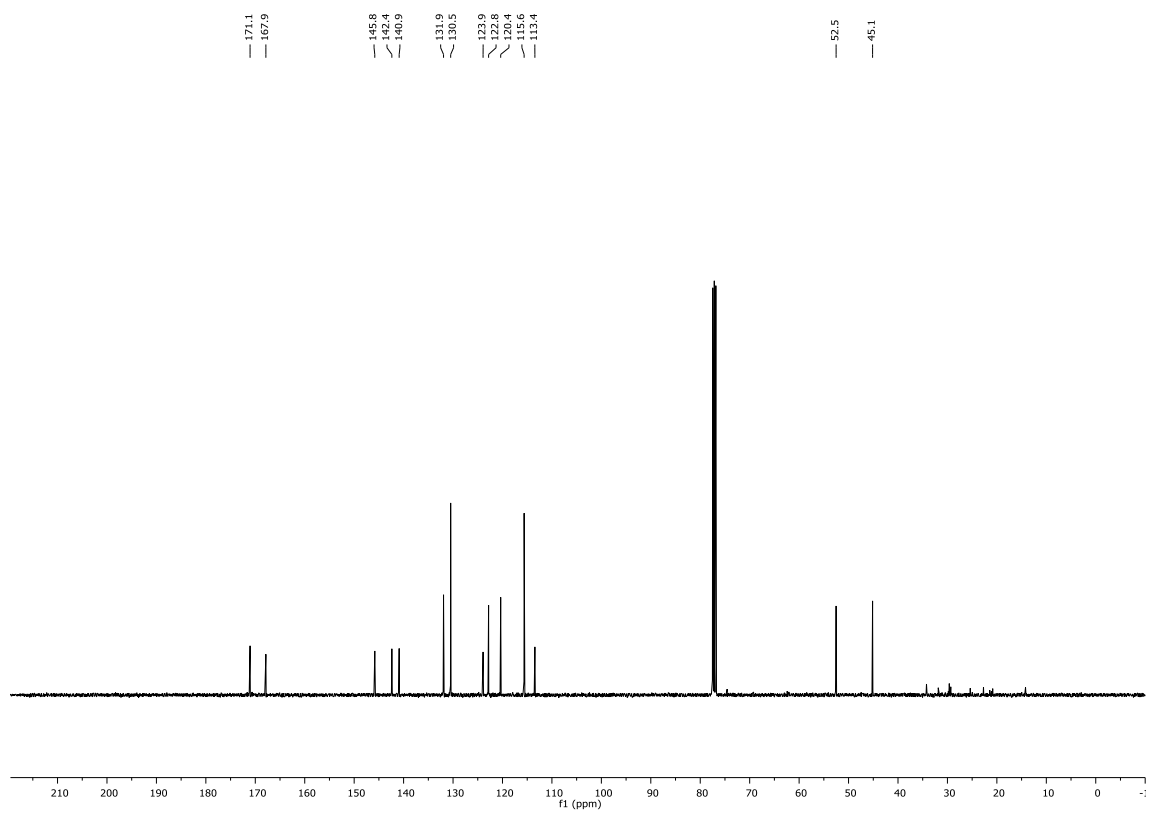
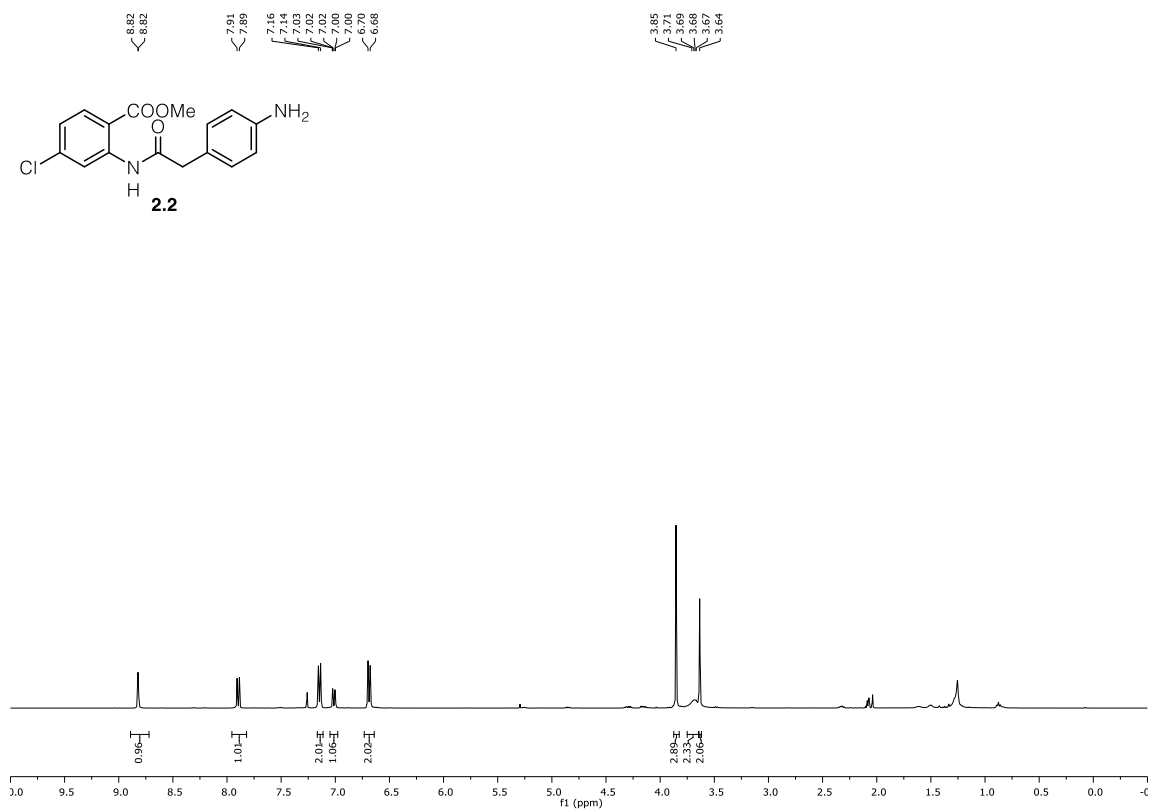
b)

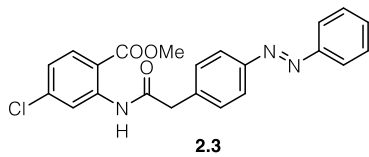
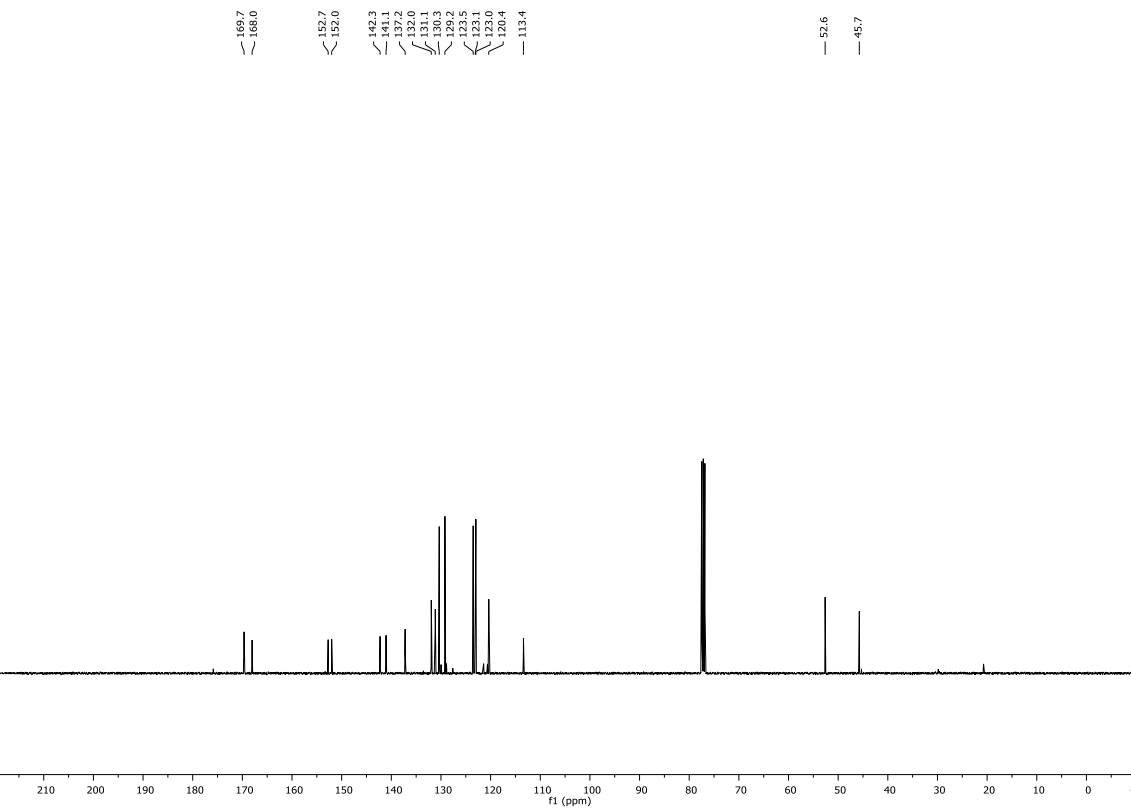
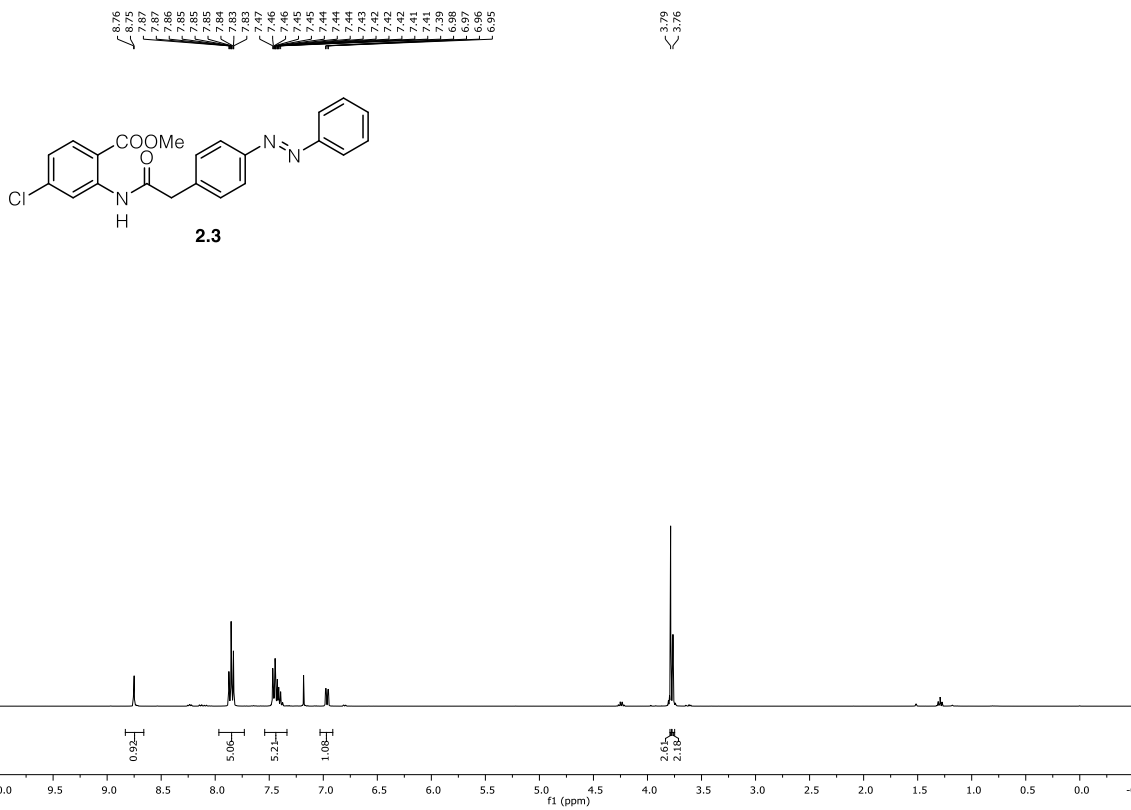


c)

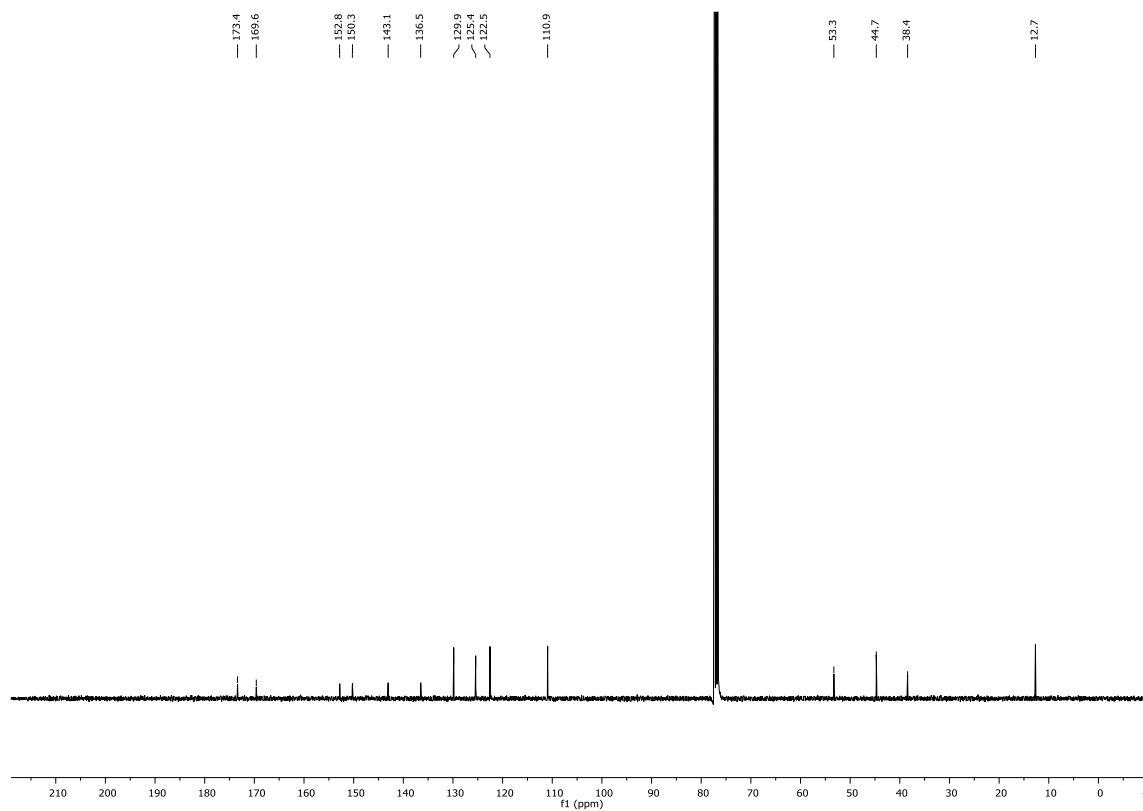
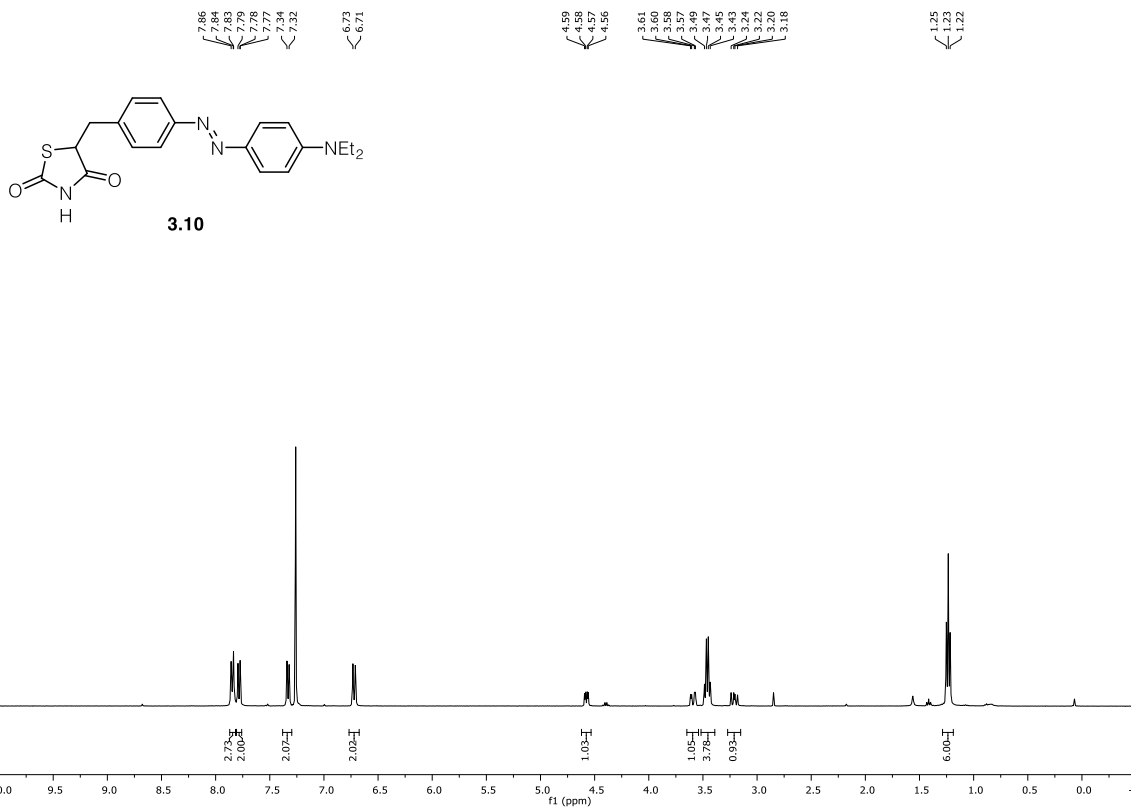


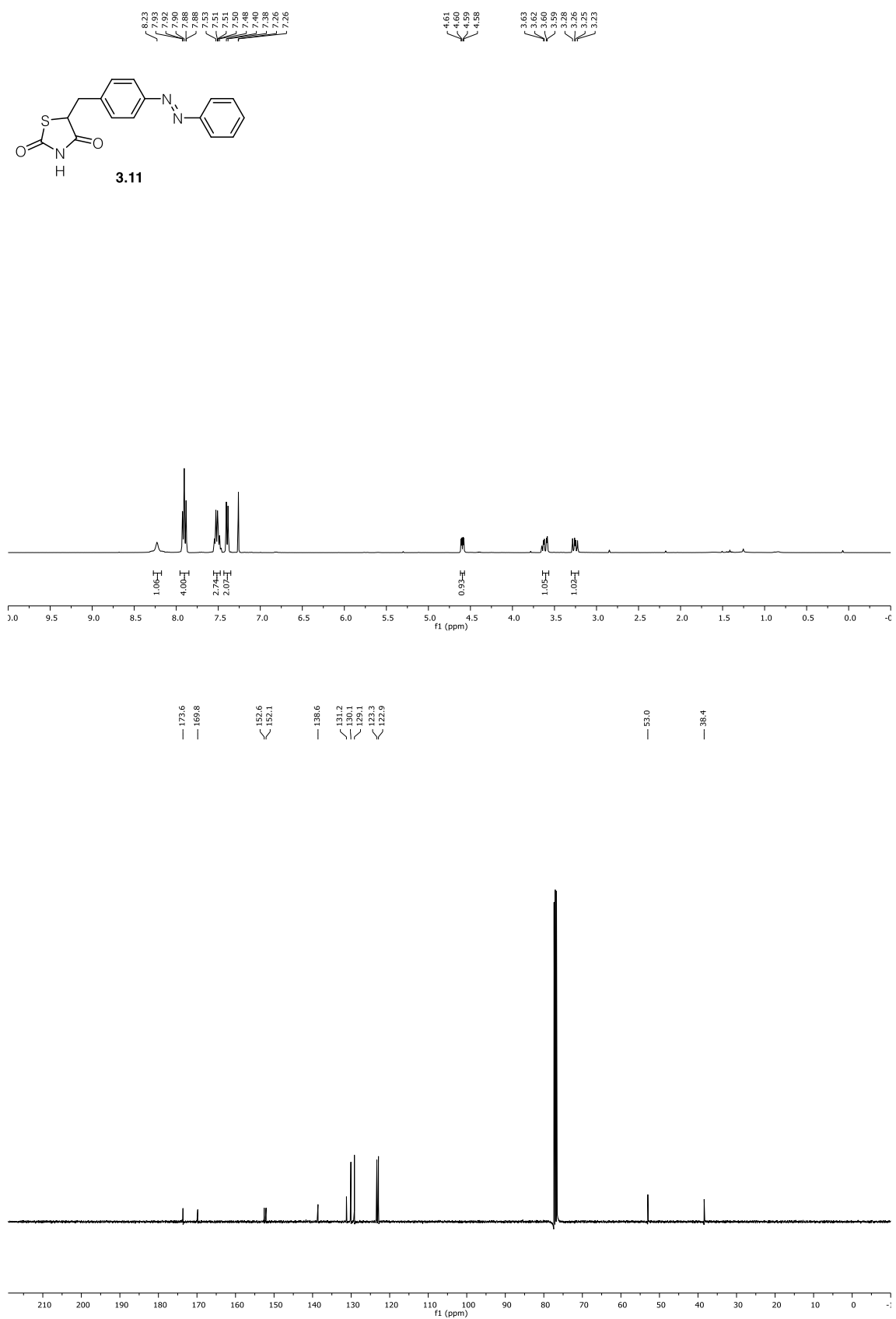


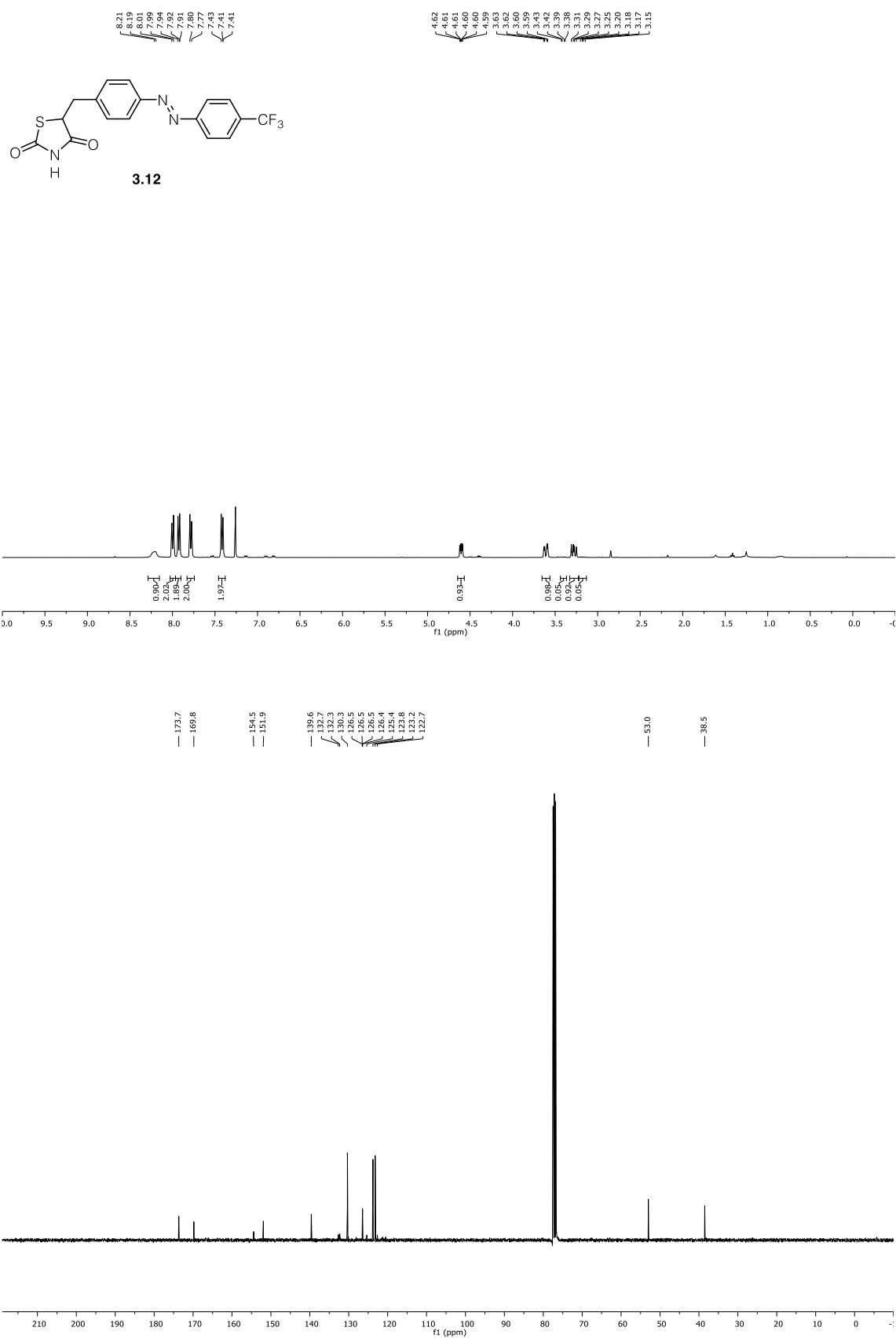




5.7 ^1H and ^{13}C NMR spectra for chapter 4.4







6 Bibliography

- [1] Z. Xie, X. Huang, *Dictionary of Traditional Chinese Medicine*, George Allen & Unwin, **1985**.
- [2] D. Bai, in *Pure Appl. Chem.*, Vol. 65, **1993**, p. 1103.
- [3] M. Wichtl, *Herbal Drugs and Phytopharmaceuticals: A Handbook for Practice on a Scientific Basis*, Medpharm, **2004**.
- [4] I. Orhan, E. Küpeli, B. Şener, E. Yesilada, *J. Ethnopharmacol.* **2007**, 109, 146–150.
- [5] S. K. Mandal, R. Biswas, S. S. Bhattacharyya, S. Paul, S. Dutta, S. Pathak, A. R. Khuda-Bukhsh, *Eur. J. Pharmacol.* **2010**, 626, 115–122.
- [6] K. Pan, X. Xia, W.-H. Guo, L.-Y. Kong, *J. Ethnopharmacol.* **2015**, 159, 17–22.
- [7] C. Armijos, G. Gilardoni, L. Amay, A. Lozano, F. Bracco, J. Ramirez, N. Bec, C. Larroque, P. V. Finzi, G. Vidari, *J. Ethnopharmacol.* **2016**, 193, 546–554.
- [8] J.-S. Liu, Y.-L. Zhu, C.-M. Yu, Y.-Z. Zhou, Y.-Y. Han, F.-W. Wu, B.-F. Qi, *Can. J. Chem.* **1986**, 64, 837–839.
- [9] J.-S. Liu, C.-M. Yu, Y.-Z. Zhou, Y.-Y. Han, B.-F. Qi, Y.-L. Zhu, *Acta Chim. Sinica* **1986**, 44, 1035–1040.
- [10] X. C. Tang, P. De Sarno, K. Sugaya, E. Giacobini, *J. Neurosci. Res.* **1989**, 24, 276–285.
- [11] R. Wang, H. Yan, X.-c. Tang, *Acta Pharmacol. Sin.* **2006**, 27, 1–26.
- [12] K. Bödeker, *Liebigs Ann. Chem.* **1881**, 208, 363–367.
- [13] A. Orechoff, *Arch. Pharm.* **1934**, 272, 673–691.
- [14] J. Muszyński, *Arch. Pharm.* **1935**, 273, 452–457.
- [15] R. H. F. Manske, in *The Alkaloids: Chemistry and Physiology*, Vol. 5 (Ed.: R. H. F. Manske), Academic Press, **1955**, pp. 295–300.
- [16] R. H. F. Manske, in *The Alkaloids: Chemistry and Physiology*, Vol. 7 (Ed.: R. H. F. Manske), Academic Press, **1960**, pp. 505–507.
- [17] D. B. Maclean, in *The Alkaloids: Chemistry and Physiology*, Vol. 10 (Ed.: R. H. F. Manske), Academic Press, **1968**, pp. 305–382.
- [18] D. B. MacLean, in *The Alkaloids: Chemistry and Physiology*, Vol. 14 (Ed.: R. H. F. Manske), Academic Press, **1973**, pp. 347–405.
- [19] D. B. Maclean, in *The Alkaloids: Chemistry and Pharmacology*, Vol. 26 (Ed.: B. Arnold), Academic Press, **1985**, pp. 241–298.
- [20] W. A. Ayer, L. S. Trifonov, in *The Alkaloids: Chemistry and Pharmacology*, Vol. 45 (Eds.: A. C. Geoffrey, B. Arnold), Academic Press, **1994**, pp. 233–266.
- [21] X. Ma, D. R. Gang, *Nat. Prod. Rep.* **2004**, 21, 752–772.
- [22] J. i. Kobayashi, H. Morita, in *The Alkaloids: Chemistry and Biology*, Vol. 61 (Ed.: G. A. Cordell), Academic Press, **2005**, pp. 1–57.
- [23] Y. Hirasawa, J. Kobayashi, H. Morita, *Heterocycles* **2009**, 77, 679–729.
- [24] T. Dwyer, A. S. Waegel, *Acta Horticulturae* **2004**, 181–185.

- [25] M. Castillo, R. N. Gupta, D. B. MacLean, I. D. Spenser, *Can. J. Chem.* **1970**, *48*, 1893–1903.
- [26] H. Conroy, *Tetrahedron Lett.* **1960**, *1*, 34–37.
- [27] T. Hemscheidt, I. D. Spenser, *J. Am. Chem. Soc.* **1992**, *114*, 5472–5473.
- [28] J. C. Braekman, R. N. Gupta, D. B. MacLean, I. D. Spenser, *Can. J. Chem.* **1972**, *50*, 2591–2602.
- [29] W. D. Marshall, T. T. Nguyen, D. B. MacLean, I. D. Spenser, *Can. J. Chem.* **1975**, *53*, 41–50.
- [30] T. Hemscheidt, I. D. Spenser, *J. Am. Chem. Soc.* **1990**, *112*, 6360–6363.
- [31] T. Hemscheidt, I. D. Spenser, *J. Am. Chem. Soc.* **1993**, *115*, 3020–3021.
- [32] T. Hemscheidt, I. D. Spenser, *J. Am. Chem. Soc.* **1996**, *118*, 1799–1800.
- [33] M. Castillo, R. N. Gupta, Y. K. Ho, D. B. MacLean, I. D. Spenser, *Can. J. Chem.* **1970**, *48*, 2911–2918.
- [34] A. Hager, N. Vrieling, D. Hager, J. Lefranc, D. Trauner, *Nat. Prod. Rep.* **2016**, *33*, 491–522.
- [35] R. H. Burnell, *J. Chem. Soc.* **1959**, 3091–3093.
- [36] Y. Inubushi, H. Ishii, T. Harayama, R. H. Burnell, W. A. Ayer, B. Altenkirk, *Tetrahedron Lett.* **1967**, *8*, 1069–1072.
- [37] K. Nishio, T. Fujiwara, K. Tomita, H. Ishii, Y. Inubushi, T. Harayama, *Tetrahedron Lett.* **1969**, *10*, 861–864.
- [38] T. Harayama, M. Takatani, Y. Inubushi, *Tetrahedron Lett.* **1979**, *20*, 4307–4310.
- [39] C. H. Heathcock, K. M. Smith, T. A. Blumenkopf, *J. Am. Chem. Soc.* **1986**, *108*, 5022–5024.
- [40] C. H. Heathcock, T. A. Blumenkopf, K. M. Smith, *J. Org. Chem.* **1989**, *54*, 1548–1562.
- [41] C. H. Heathcock, E. Kleinman, E. S. Binkley, *J. Am. Chem. Soc.* **1978**, *100*, 8036–8037.
- [42] P. Siengalewicz, J. Mulzer, U. Rinner, in *The Alkaloids: Chemistry and Biology*, Vol. 72 (Ed.: H.-J. Knölker), Academic Press, **2013**, pp. 1–151.
- [43] M. E. Jung, J. J. Chang, *Org. Lett.* **2010**, *12*, 2962–2965.
- [44] R. A. Murphy, R. Sarpong, *Chem. Eur. J.* **2014**, *20*, 42–56.
- [45] M. Kitajima, H. Takayama, in *Alkaloid Synthesis* (Ed.: H.-J. Knölker), Springer Berlin Heidelberg, Berlin, Heidelberg, **2012**, pp. 1–31.
- [46] A. Nakayama, M. Kitajima, H. Takayama, *Synlett* **2012**, *23*, 2014–2024.
- [47] X. Wang, H. Li, X. Lei, *Synlett* **2013**, *24*, 1032–1043.
- [48] J. Cassayre, F. Gagosz, S. Z. Zard, *Angew. Chem. Int. Ed.* **2002**, *41*, 1783–1785.
- [49] T. Kozaka, N. Miyakoshi, C. Mukai, *J. Org. Chem.* **2007**, *72*, 10147–10154.
- [50] Y. Otsuka, F. Inagaki, C. Mukai, *J. Org. Chem.* **2010**, *75*, 3420–3426.
- [51] A. Nakayama, N. Kogure, M. Kitajima, H. Takayama, *Angew. Chem. Int. Ed.* **2011**, *50*, 8025–8028.
- [52] N. Itoh, T. Iwata, H. Sugihara, F. Inagaki, C. Mukai, *Chem. Eur. J.* **2013**, *19*, 8665–8672.
- [53] B. M. Williams, D. Trauner, *Angew. Chem. Int. Ed.* **2016**, *55*, 2191–2194.
- [54] L.-R. Zhong, Z.-J. Yao, *Sci. China Chem.* **2016**, *59*, 1079–1087.

- [55] S. T. Staben, J. J. Kennedy-Smith, D. Huang, B. K. Corkey, R. L. LaLonde, F. D. Toste, *Angew. Chem. Int. Ed.* **2006**, *45*, 5991–5994.
- [56] X. Linghu, J. J. Kennedy-Smith, F. D. Toste, *Angew. Chem. Int. Ed.* **2007**, *46*, 7671–7673.
- [57] J. A. Kozak, G. R. Dake, *Angew. Chem. Int. Ed.* **2008**, *47*, 4221–4223.
- [58] D. Caine, K. Procter, R. A. Cassell, *J. Org. Chem.* **1984**, *49*, 2647–2648.
- [59] J. Ramharter, H. Weinstabl, J. Mulzer, *J. Am. Chem. Soc.* **2010**, *132*, 14338–14339.
- [60] W. A. Ayer, Y. Fukazawa, P. P. Singer, B. Altenkirk, *Tetrahedron Lett.* **1973**, *14*, 5045–5048.
- [61] J. Mulzer, *Nat. Prod. Rep.* **2014**, *31*, 595–603.
- [62] Y. Hirasawa, H. Morita, M. Shiro, J. i. Kobayashi, *Org. Lett.* **2003**, *5*, 3991–3993.
- [63] M. K. Abd El-Gaber, S. Yasuda, E. Iida, C. Mukai, *Org. Lett.* **2017**, *19*, 320–323.
- [64] S. M. Canham, D. J. France, L. E. Overman, *J. Am. Chem. Soc.* **2010**, *132*, 7876–7877.
- [65] S. M. Canham, D. J. France, L. E. Overman, *J. Org. Chem.* **2013**, *78*, 9–34.
- [66] For a very recent synthesis by Mukai that exploits his Pauson–Khand methodology, see *Org. Lett.* **2017**, *19*, 320–323
- [67] L. E. Overman, L. D. Pennington, *J. Org. Chem.* **2003**, *68*, 7143–7157.
- [68] A. Chandra, J. A. Pigza, J.-S. Han, D. Mutnick, J. N. Johnston, *J. Am. Chem. Soc.* **2009**, *131*, 3470–3471.
- [69] J. A. Pigza, J.-S. Han, A. Chandra, D. Mutnick, M. Pink, J. N. Johnston, *J. Org. Chem.* **2013**, *78*, 822–843.
- [70] H. Morita, M. Arisaka, N. Yoshida, J. i. Kobayashi, *J. Org. Chem.* **2000**, *65*, 6241–6245.
- [71] E. N. Prabhakaran, B. M. Nugent, A. L. Williams, K. E. Nailor, J. N. Johnston, *Org. Lett.* **2002**, *4*, 4197–4200.
- [72] R. W. Hoffmann, *Chem. Rev.* **1989**, *89*, 1841–1860.
- [73] G. Pan, R. M. Williams, *J. Org. Chem.* **2012**, *77*, 4801–4811.
- [74] C. Zeng, C. Zheng, J. Zhao, G. Zhao, *Org. Lett.* **2013**, *15*, 5846–5849.
- [75] K. Xu, B. Cheng, Y. Li, T. Xu, C. Yu, J. Zhang, Z. Ma, H. Zhai, *Org. Lett.* **2014**, *16*, 196–199.
- [76] H. Zaimoku, T. Taniguchi, *Chem. Eur. J.* **2014**, *20*, 9613–9619.
- [77] H. Li, X. Wang, X. Lei, *Angew. Chem. Int. Ed.* **2012**, *51*, 491–495.
- [78] M. Cakmak, P. Mayer, D. Trauner, *Nat. Chem.* **2011**, *3*, 543–545.
- [79] J. Zhang, J. Wu, B. Hong, W. Ai, X. Wang, H. Li, X. Lei, *Nat. Commun.* **2014**, *5*, 4614.
- [80] J. He, X.-Q. Chen, M.-M. Li, Y. Zhao, G. Xu, X. Cheng, L.-Y. Peng, M.-J. Xie, Y.-T. Zheng, Y.-P. Wang, Q.-S. Zhao, *Org. Lett.* **2009**, *11*, 1397–1400.
- [81] H. Li, X. Wang, B. Hong, X. Lei, *J. Org. Chem.* **2013**, *78*, 800–821.
- [82] B. Hong, H. Li, J. Wu, J. Zhang, X. Lei, *Angew. Chem. Int. Ed.* **2015**, *54*, 1011–1015.
- [83] X.-M. Zhang, Y.-Q. Tu, F.-M. Zhang, H. Shao, X. Meng, *Angew. Chem. Int. Ed.* **2011**, *50*, 3916–3919.

- [84] X.-M. Zhang, H. Shao, Y.-Q. Tu, F.-M. Zhang, S.-H. Wang, *J. Org. Chem.* **2012**, *77*, 8174–8181.
- [85] S.-H. Hou, Y.-Q. Tu, L. Liu, F.-M. Zhang, S.-H. Wang, X.-M. Zhang, *Angew. Chem. Int. Ed.* **2013**, *52*, 11373–11376.
- [86] M. Del Bel, A. Rovira, C. A. Guerrero, *J. Am. Chem. Soc.* **2013**, *135*, 12188–12191.
- [87] L.-B. Dong, J. Yang, J. He, H.-R. Luo, X.-D. Wu, X. Deng, L.-Y. Peng, X. Cheng, Q.-S. Zhao, *Chem. Commun.* **2012**, *48*, 9038–9040.
- [88] T. Hu, R. F. Chandler, A. W. Hanson, *Tetrahedron Lett.* **1987**, *28*, 5993–5996.
- [89] A. Nakayama, N. Kogure, M. Kitajima, H. Takayama, *Org. Lett.* **2009**, *11*, 5554–5557.
- [90] Y. Ochi, S. Yokoshima, T. Fukuyama, *Org. Lett.* **2016**, *18*, 1494–1496.
- [91] Y. Ochi, S. Yokoshima, T. Fukuyama, *Synthesis* **2017**, *49*, 96–114.
- [92] F.-W. Zhao, Q.-Y. Sun, F.-M. Yang, G.-W. Hu, J.-F. Luo, G.-H. Tang, Y.-H. Wang, C.-L. Long, *Org. Lett.* **2010**, *12*, 3922–3925.
- [93] L.-B. Dong, X. Gao, F. Liu, J. He, X.-D. Wu, Y. Li, Q.-S. Zhao, *Org. Lett.* **2013**, *15*, 3570–3573.
- [94] X.-J. Wang, L. Li, S.-S. Yu, S.-G. Ma, J. Qu, Y.-B. Liu, Y. Li, Y. Wang, W. Tang, *Fitoterapia* **2013**, *91*, 74–81.
- [95] X.-J. Wang, L. Li, S.-S. Yu, S.-G. Ma, J. Qu, Y.-B. Liu, Y. Li, Y. Wang, W. Tang, *Fitoterapia* **2016**, *114*, 194.
- [96] C. Zhao, H. Zheng, P. Jing, B. Fang, X. Xie, X. She, *Org. Lett.* **2012**, *14*, 2293–2295.
- [97] G. B. Zhang, F. X. Wang, J. Y. Du, H. Qu, X. Y. Ma, M. X. Wei, C. T. Wang, Q. Li, C. A. Fan, *Org. Lett.* **2012**, *14*, 3696–3699.
- [98] D. Gaugele, M. E. Maier, *Synlett* **2013**, *24*, 955–958.
- [99] N. Sizemore, S. D. Rychnovsky, *Org. Lett.* **2014**, *16*, 688–691.
- [100] S. Duan, D. Long, C. Zhao, G. Zhao, Z. Yuan, X. Xie, J. Fang, X. She, *Org. Chem. Front.* **2016**, *3*, 1137–1143.
- [101] F.-X. Wang, P.-L. Zhang, H.-B. Wang, G.-B. Zhang, C.-A. Fan, *Sci. China Chem.* **2016**, *59*, 1188–1196.
- [102] F. X. Wang, J. Y. Du, H. B. Wang, P. L. Zhang, G. B. Zhang, K. Y. Yu, X. Z. Zhang, X. T. An, Y. X. Cao, C. A. Fan, *J. Am. Chem. Soc.* **2017**, 4282–4285.
- [103] H. Niwa, K. Wakamatsu, T. Hida, K. Niiyama, H. Kigoshi, M. Yamada, H. Nagase, M. Suzuki, K. Yamada, *J. Am. Chem. Soc.* **1984**, *106*, 4547–4552.
- [104] K. Takasu, S. Mizutani, M. Ihara, *J. Org. Chem.* **2002**, *67*, 2881–2884.
- [105] V. Singh, S. Pal, S. M. Mobin, *J. Org. Chem.* **2006**, *71*, 3014–3025.
- [106] G. K. Murphy, T. Shirahata, N. Hama, A. Bedermann, P. Dong, T. C. McMahon, B. M. Twenter, D. A. Spiegel, I. M. McDonald, N. Taniguchi, M. Inoue, J. L. Wood, *J. Org. Chem.* **2013**, *78*, 477–489.

- [107] S. Harada, K. Li, R. Kino, T. Takeda, C.-H. Wu, S. Hiraoka, A. Nishida, *Chem. Pharm. Bull.* **2016**, *64*, 1474–1483.
- [108] T. Kan, T. Fukuyama, *Chem. Commun.* **2004**, 353–359.
- [109] T. Fukuyama, C.-K. Jow, M. Cheung, *Tetrahedron Lett.* **1995**, *36*, 6373–6374.
- [110] T. Fukuyama, M. Cheung, C.-K. Jow, Y. Hidai, T. Kan, *Tetrahedron Lett.* **1997**, *38*, 5831–5834.
- [111] J. P. Williams, D. Friedrich, E. Pinard, B. A. Roden, L. A. Paquette, D. R. St. Laurent, *J. Am. Chem. Soc.* **1994**, *116*, 4689–4696.
- [112] G. C. Hirst, T. O. Johnson, L. E. Overman, *J. Am. Chem. Soc.* **1993**, *115*, 2992–2993.
- [113] L. A. Paquette, D. Friedrich, E. Pinard, J. P. Williams, D. St. Laurent, B. A. Roden, *J. Am. Chem. Soc.* **1993**, *115*, 4377–4378.
- [114] C. F. Yen, C. C. Liao, *Angew. Chem. Int. Ed.* **2002**, *41*, 4090–4093.
- [115] M. Ishizaki, Y. Niimi, O. Hoshino, H. Hara, T. Takahashi, *Tetrahedron* **2005**, *61*, 4053–4065.
- [116] S.-Z. Jiang, T. Lei, K. Wei, Y.-R. Yang, *Org. Lett.* **2014**, *16*, 5612–5615.
- [117] K.-W. Lin, B. Ananthan, S.-F. Tseng, T.-H. Yan, *Org. Lett.* **2015**, *17*, 3938–3940.
- [118] P. McGee, G. Bétournay, F. Barabé, L. Barriault, *Angew. Chem. Int. Ed.* **2017**, *56*, 6280–6283.
- [119] H. Dugas, M. E. Hazenberg, Z. Valenta, K. Wiesner, *Tetrahedron Lett.* **1967**, 4931–4936.
- [120] K. Wiesner, V. Musil, K. J. Wiesner, *Tetrahedron Lett.* **1968**, 5643.
- [121] W. A. Ayer, W. R. Bowman, T. C. Joseph, P. Smith, *J. Am. Chem. Soc.* **1968**, *90*, 1648–1650.
- [122] G. Stork, R. A. Kretchmer, R. H. Schlessinger, *J. Am. Chem. Soc.* **1968**, *90*, 1647–1648.
- [123] C. H. Heathcock, E. F. Kleinman, E. S. Binkley, *J. Am. Chem. Soc.* **1982**, *104*, 1054–1068.
- [124] D. Schumann, H. J. Muller, A. Naumann, *Liebigs Ann. Chem.* **1982**, 1700–1705.
- [125] D. Schumann, H. J. Muller, A. Naumann, *Liebigs Ann. Chem.* **1982**, 2057–2061.
- [126] D. Schumann, A. Naumann, *Liebigs Ann. Chem.* **1983**, 220–225.
- [127] D. Schumann, A. Naumann, *Liebigs Ann. Chem.* **1984**, 1519–1528.
- [128] G. A. Kraus, Y. S. Hon, *J. Am. Chem. Soc.* **1985**, *107*, 4341–4342.
- [129] G. A. Kraus, Y. S. Hon, *Heterocycles* **1987**, *25*, 377–386.
- [130] for another lycopodine synthesis hinging on a cationic key step, see Grieco's synthesis featuring an ionic Diels–Alder reaction: *J. Am. Chem. Soc.* **1998**, *120*, 5128–5129.
- [131] W. Oppolzer, M. Petrzilka, *J. Am. Chem. Soc.* **1976**, *98*, 6722–6723.
- [132] W. Oppolzer, M. Petrzilka, *Helv. Chim. Acta* **1978**, *61*, 2755–2762.
- [133] H. Yang, R. G. Carter, L. N. Zakharov, *J. Am. Chem. Soc.* **2008**, *130*, 9238–9239.
- [134] H. Yang, R. G. Carter, *J. Org. Chem.* **2010**, *75*, 4929–4938.
- [135] M. Saha, X. Li, N. D. Collett, R. G. Carter, *J. Org. Chem.* **2016**, *81*, 5963–5980.
- [136] D. H. Ma, Z. L. Zhong, Z. M. Liu, M. J. Zhang, S. Y. Xu, D. Y. Xu, D. P. Song, X. G. Xie, X. G. She, *Org. Lett.* **2016**, *18*, 4328–4331.

- [137] S. Xu, J. Zhang, D. Ma, D. Xu, X. Xie, X. She, *Org. Lett.* **2016**, *18*, 4682–4685.
- [138] J.-T. Cheng, F. Liu, X.-N. Li, X.-D. Wu, L.-B. Dong, L.-Y. Peng, S.-X. Huang, J. He, Q.-S. Zhao, *Org. Lett.* **2013**, *15*, 2438–2441.
- [139] D. A. Evans, J. R. Scheerer, *Angew. Chem. Int. Ed.* **2005**, *44*, 6038–6042.
- [140] E. Wenkert, C. A. Broka, *J. Chem. Soc., Chem. Commun.* **1984**, 714–715.
- [141] K. M. Laemmerhold, B. Breit, *Angew. Chem. Int. Ed.* **2010**, *49*, 2367–2370.
- [142] K. Nakahara, K. Hirano, R. Maehata, Y. Kita, H. Fujioka, *Org. Lett.* **2011**, *13*, 2015–2017.
- [143] H.-Y. Lin, R. Causey, G. E. Garcia, B. B. Snider, *J. Org. Chem.* **2012**, *77*, 7143–7156.
- [144] C. Yuan, C.-T. Chang, A. Axelrod, D. Siegel, *J. Am. Chem. Soc.* **2010**, *132*, 5924–5925.
- [145] D. F. Fischer, R. Sarpong, *J. Am. Chem. Soc.* **2010**, *132*, 5926–5927.
- [146] T. Johnson, D. Siegel, *Bioorg. Med. Chem. Lett.* **2014**, *24*, 3512–3515.
- [147] J. i. Kobayashi, Y. Hirasawa, N. Yoshida, H. Morita, *Tetrahedron Lett.* **2000**, *41*, 9069–9073.
- [148] C. Yuan, C.-T. Chang, D. Siegel, *J. Org. Chem.* **2013**, *78*, 5647–5668.
- [149] J. N. Newton, D. F. Fischer, R. Sarpong, *Angew. Chem. Int. Ed.* **2013**, *52*, 1726–1730.
- [150] H. Morita, K. i. Ishiuchi, A. Haganuma, T. Hoshino, Y. Obara, N. Nakahata, J. i. Kobayashi, *Tetrahedron* **2005**, *61*, 1955–1960.
- [151] L. Zhao, C. Tsukano, E. Kwon, Y. Takemoto, M. Hirama, *Angew. Chem. Int. Ed.* **2013**, *52*, 1722–1725.
- [152] C. Tsukano, L. Zhao, Y. Takemoto, M. Hirama, *Eur. J. Org. Chem.* **2010**, *2010*, 4198–4200.
- [153] L. Zhao, C. Tsukano, E. Kwon, H. Shirakawa, S. Kaneko, Y. Takemoto, M. Hirama, *Chem. Eur. J.* **2017**, *23*, 802–812.
- [154] M. Azuma, T. Yoshikawa, N. Kogure, M. Kitajima, H. Takayama, *J. Am. Chem. Soc.* **2014**, *136*, 11618–11621.
- [155] R. V. Gerard, D. B. MacLean, R. Fagianni, C. J. Lock, *Can. J. Chem.* **1986**, *64*, 943–949.
- [156] B. B. Liao, M. D. Shair, *J. Am. Chem. Soc.* **2010**, *132*, 9594–9595.
- [157] A. S. Lee, B. B. Liao, M. D. Shair, *J. Am. Chem. Soc.* **2014**, *136*, 13442–13452.
- [158] J. Kobayashi, Y. Hirasawa, N. Yoshida, H. Morita, *J. Org. Chem.* **2001**, *66*, 5901–5904.
- [159] K. i. Ishiuchi, T. Kubota, H. Ishiyama, S. Hayashi, T. Shibata, J. i. Kobayashi, *Tetrahedron Lett.* **2011**, *52*, 289–292.
- [160] D. C. Beshore, A. B. Smith, *J. Am. Chem. Soc.* **2007**, *129*, 4148–4149.
- [161] D. C. Beshore, A. B. Smith, *J. Am. Chem. Soc.* **2008**, *130*, 13778–13789.
- [162] A. Bisai, S. P. West, R. Sarpong, *J. Am. Chem. Soc.* **2008**, *130*, 7222–7223.
- [163] S. P. West, A. Bisai, A. D. Lim, R. R. Narayan, R. Sarpong, *J. Am. Chem. Soc.* **2009**, *131*, 11187–11194.
- [164] T. Nishimura, A. K. Unni, S. Yokoshima, T. Fukuyama, *J. Am. Chem. Soc.* **2011**, *133*, 418–419.
- [165] X. Cheng, S. P. Waters, *Org. Lett.* **2013**, *15*, 4226–4229.

- [166] T. Nishimura, A. K. Unni, S. Yokoshima, T. Fukuyama, *J. Am. Chem. Soc.* **2013**, *135*, 3243–3247.
- [167] Y. Yang, C. W. Haskins, W. Zhang, P. L. Low, M. Dai, *Angew. Chem. Int. Ed.* **2014**, *53*, 3922–3925.
- [168] R. A. Samame, C. M. Owens, S. D. Rychnovsky, *Chem. Sci.* **2016**, *7*, 188–190.
- [169] K. Katakawa, N. Kogure, M. Kitajima, H. Takayama, *Helv. Chim. Acta* **2009**, *92*, 445–452.
- [170] K. Katakawa, M. Kitajima, K. Yamaguchi, H. Takayama, *Heterocycles* **2006**, *69*, 223–229.
- [171] W.-Y. Gao, Y.-M. Li, S.-H. Jiang, D.-Y. Zhu, *Helv. Chim. Acta* **2008**, *91*, 1031–1035.
- [172] W. A. Ayer, G. C. Kasitu, *Can. J. Chem.* **1989**, *67*, 1077–1086.
- [173] V. Bisai, R. Sarpong, *Org. Lett.* **2010**, *12*, 2551–2553.
- [174] H. Ishida, S. Kimura, N. Kogure, M. Kitajima, H. Takayama, *Tetrahedron* **2015**, *71*, 51–56.
- [175] H. Ishida, S. Kimura, N. Kogure, M. Kitajima, H. Takayama, *Org. Biomol. Chem.* **2015**, *13*, 7762–7771.
- [176] S. A. Bal, A. Marfat, P. Helquist, *J. Org. Chem.* **1982**, *47*, 5045–5050.
- [177] Y.-R. Yang, Z.-W. Lai, L. Shen, J.-Z. Huang, X.-D. Wu, J.-L. Yin, K. Wei, *Org. Lett.* **2010**, *12*, 3430–3433.
- [178] Y.-R. Yang, L. Shen, J.-Z. Huang, T. Xu, K. Wei, *J. Org. Chem.* **2011**, *76*, 3684–3690.
- [179] K. i. Ishiuchi, T. Kubota, H. Morita, J. i. Kobayashi, *Tetrahedron Lett.* **2006**, *47*, 3287–3289.
- [180] J. J. Kennedy-Smith, S. T. Staben, F. D. Toste, *J. Am. Chem. Soc.* **2004**, *126*, 4526–4527.
- [181] S. T. Staben, J. J. Kennedy-Smith, F. D. Toste, *Angew. Chem. Int. Ed.* **2004**, *43*, 5350–5352.
- [182] J. E. DeLorbe, M. D. Lotz, S. F. Martin, *Org. Lett.* **2010**, *12*, 1576–1579.
- [183] K. Hiroya, Y. Suwa, Y. Ichihashi, K. Inamoto, T. Doi, *J. Org. Chem.* **2011**, *76*, 4522–4532.
- [184] K. Hiroya, Y. Ichihashi, Y. Suwa, T. Ikai, K. Inamoto, T. Doi, *Tetrahedron Lett.* **2010**, *51*, 3728–3731.
- [185] X. Wang, Z. Yao, S. Dong, F. Wei, H. Wang, Z. Xu, *Org. Lett.* **2013**, *15*, 2234–2237.
- [186] L. Meng, *J. Org. Chem.* **2016**, *81*, 7784–7789.
- [187] F. Liu, Y.-C. Liu, W.-W. Jiang, J. He, X.-D. Wu, L.-Y. Peng, J. Su, X. Cheng, Q.-S. Zhao, *Nat. Prod. Bioprospect.* **2014**, *4*, 221–225.
- [188] X.-J. Liu, S.-L. You, *Angew. Chem. Int. Ed.* **2017**, *56*, 4002–4005.
- [189] M. A. Schexnayder, P. S. Engel, *J. Am. Chem. Soc.* **1975**, *97*, 4825–4836.
- [190] S. P. Bew, G. D. Hiatt-Gipson, J. A. Lovell, C. Poullain, *Org. Lett.* **2012**, *14*, 456–459.
- [191] K. i. Ishiuchi, T. Kubota, S. Hayashi, T. Shibata, J. i. Kobayashi, *Tetrahedron Lett.* **2009**, *50*, 6534–6536.
- [192] J. R. Sacher, S. M. Weinreb, *Tetrahedron* **2011**, *67*, 10203–10207.
- [193] J. R. Sacher, S. M. Weinreb, *Org. Lett.* **2012**, *14*, 2172–2175.
- [194] P. S. Chauhan, J. R. Sacher, S. M. Weinreb, *Org. Lett.* **2015**, *17*, 806–808.
- [195] W.-C. Liu, C.-C. Liao, *Synlett* **1998**, *1998*, 912–914.
- [196] M. Vertorano, University at Albany, State University of New York (ProQuest), **2016**.

- [197] X.-J. Wang, Y.-B. Liu, L. Li, S.-S. Yu, H.-N. Lv, S.-G. Ma, X.-Q. Bao, D. Zhang, J. Qu, Y. Li, *Org. Lett.* **2012**, *14*, 5688–5691.
- [198] Shortly before the completion of this thesis, a very creative approach toward lycodoline was disclosed by Fan and coworkers (*J. Am. Chem. Soc.* **2017**, *139*, 7095–7103). As part of a collective synthesis of C-12-hydroxylated Lycopodium alkaloids, lycojaponicum D was synthesized via the transannular Mannich reaction discussed in the biosynthetic proposal.
- [199] A. Deiters, S. F. Martin, *Chem. Rev.* **2004**, *104*, 2199–2238.
- [200] A. Gradillas, J. Pérez-Castells, *Angew. Chem. Int. Ed.* **2006**, *45*, 6086–6101.
- [201] G. C. Vougioukalakis, R. H. Grubbs, *Chem. Rev.* **2010**, *110*, 1746–1787.
- [202] S. R. Chemler, D. Trauner, S. J. Danishefsky, *Angew. Chem. Int. Ed.* **2001**, *40*, 4544.
- [203] F. W. W. Hartrampf, Ludwig-Maximilians-Universität München **2013**.
- [204] A. Hosomi, H. Sakurai, *J. Am. Chem. Soc.* **1977**, *99*, 1673–1675.
- [205] T. A. Blumenkopf, C. H. Heathcock, *J. Am. Chem. Soc.* **1983**, *105*, 2354–2358.
- [206] L. W. Xu, M. S. Yang, H. Y. Qiu, G. Q. Lai, J. X. Jiang, *Synth. Commun.* **2008**, *38*, 1011–1019.
- [207] J. S. Yadav, B. V. S. Reddy, K. Sadasiv, G. Satheesh, *Tetrahedron Lett.* **2002**, *43*, 9695–9697.
- [208] Z.-L. Shen, H.-L. Cheong, T.-P. Loh, *Tetrahedron Lett.* **2009**, *50*, 1051–1054.
- [209] B. H. Lipshutz, E. L. Ellsworth, S. H. Dimock, R. a. J. Smith, *J. Am. Chem. Soc.* **1990**, *112*, 4404–4410.
- [210] B. H. Lipshutz, C. Hackmann, *J. Org. Chem.* **1994**, *59*, 7437–7444.
- [211] S. Kim, J. M. Lee, *Synth. Commun.* **1991**, *21*, 25–29.
- [212] M. A. Grundl, D. Trauner, *Org. Lett.* **2006**, *8*, 23–25.
- [213] M. A. Grundl, A. Kaster, E. D. Beaulieu, D. Trauner, *Org. Lett.* **2006**, *8*, 5429–5432.
- [214] E. D. Beaulieu, L. Voss, D. Trauner, *Org. Lett.* **2008**, *10*, 869–872.
- [215] G. M. Rubottom, M. A. Vazquez, D. R. Pelegrina, *Tetrahedron Lett.* **1974**, *15*, 4319–4322.
- [216] A. G. Brook, D. M. Macrae, *J. Organomet. Chem.* **1974**, *77*, C19–C21.
- [217] A. Hassner, R. H. Reuss, H. W. Pinnick, *J. Org. Chem.* **1975**, *40*, 3427–3429.
- [218] B.-C. Chen, P. Zhou, F. A. Davis, E. Ciganek, in *Organic Reactions*, John Wiley & Sons, Inc., **2004**.
- [219] F. A. Davis, B. C. Chen, *Chem. Rev.* **1992**, *92*, 919–934.
- [220] F. A. Davis, A. C. Sheppard, *J. Org. Chem.* **1987**, *52*, 954–955.
- [221] W. Yu, Z. Jin, *Tetrahedron Lett.* **2001**, *42*, 369–372.
- [222] J. N. Gardner, F. E. Carlon, O. Gnoj, *J. Org. Chem.* **1968**, *33*, 3294–3297.
- [223] J. P. McCormick, W. Tomasik, M. W. Johnson, *Tetrahedron Lett.* **1981**, *22*, 607–610.
- [224] T. P. Lebold, J. L. Wood, J. Deitch, M. W. Lodewyk, D. J. Tantillo, R. Sarpong, *Nat. Chem.* **2013**, *5*, 126–131.
- [225] S. Stanković, J. H. Espenson, *J. Org. Chem.* **1998**, *63*, 4129–4130.

- [226] Y. Zhu, T. Yong, Y. Hongwu, S. Yian, *Tetrahedron Lett.* **1998**, *39*, 7819–7822.
- [227] D. Limnios, C. G. Kokotos, *J. Org. Chem.* **2014**, *79*, 4270–4276.
- [228] R. M. Moriarty, H. Hu, S. C. Gupta, *Tetrahedron Lett.* **1981**, *22*, 1283–1286.
- [229] R. M. Moriarty, K.-C. Hou, *Tetrahedron Lett.* **1984**, *25*, 691–694.
- [230] Y.-F. Liang, N. Jiao, *Angew. Chem. Int. Ed.* **2014**, *53*, 548–552.
- [231] G. Illuminati, L. Mandolini, *Acc. Chem. Res.* **1981**, *14*, 95–102.
- [232] S. J. Bamford, K. Goubitz, H. L. van Lingen, T. Luker, H. Schenk, H. Hiemstra, *J. Chem. Soc. Perkin Trans. I* **2000**, 345–351.
- [233] M. E. Maier, *Angew. Chem. Int. Ed.* **2000**, *39*, 2073–2077.
- [234] K. Grela, S. Harutyunyan, A. Michrowska, *Angew. Chem. Int. Ed.* **2002**, *41*, 4038–4040.
- [235] S. B. Garber, J. S. Kingsbury, B. L. Gray, A. H. Hoveyda, *J. Am. Chem. Soc.* **2000**, *122*, 8168–8179.
- [236] M. Scholl, S. Ding, C. W. Lee, R. H. Grubbs, *Org. Lett.* **1999**, *1*, 953–956.
- [237] I. C. Stewart, C. J. Douglas, R. H. Grubbs, *Org. Lett.* **2008**, *10*, 441–444.
- [238] I. C. Stewart, T. Ung, A. A. Pletnev, J. M. Berlin, R. H. Grubbs, Y. Schrodi, *Org. Lett.* **2007**, *9*, 1589–1592.
- [239] V. VanRheenen, R. C. Kelly, D. Y. Cha, *Tetrahedron Lett.* **1976**, *17*, 1973–1976.
- [240] R. Ray, D. S. Matteson, *Tetrahedron Lett.* **1980**, *21*, 449–450.
- [241] W. Yu, Y. Mei, Y. Kang, Z. Hua, Z. Jin, *Org. Lett.* **2004**, *6*, 3217–3219.
- [242] J. Eames, H. J. Mitchell, A. Nelson, P. O'Brien, S. Warren, P. Wyatt, *Tetrahedron Lett.* **1995**, *36*, 1719–1722.
- [243] K. Morikawa, J. Park, P. G. Andersson, T. Hashiyama, K. B. Sharpless, *J. Am. Chem. Soc.* **1993**, *115*, 8463–8464.
- [244] H. C. Kolb, M. S. VanNieuwenhze, K. B. Sharpless, *Chem. Rev.* **1994**, *94*, 2483–2547.
- [245] T. K. M. Shing, E. K. W. Tam, *Tetrahedron Lett.* **1999**, *40*, 2179–2180.
- [246] D. B. Dess, J. C. Martin, *J. Org. Chem.* **1983**, *48*, 4155–4156.
- [247] M. Frigerio, M. Santagostino, *Tetrahedron Lett.* **1994**, *35*, 8019–8022.
- [248] J. M. Khurana, B. M. Kandpal, *Tetrahedron Lett.* **2003**, *44*, 4909–4912.
- [249] J. K. Joseph, S. L. Jain, B. Sain, *Eur. J. Org. Chem.* **2006**, *2006*, 590–594.
- [250] S. L. Jain, V. B. Sharma, B. Sain, *Tetrahedron Lett.* **2004**, *45*, 1233–1235.
- [251] S. Verma, R. Singh, D. Tripathi, P. Gupta, G. M. Bahuguna, S. L. Jain, *RSC Adv.* **2013**, *3*, 4184–4188.
- [252] J. M. Bobbitt, C. Brückner, N. Merbouh, in *Organic Reactions*, John Wiley & Sons, Inc., **2004**.
- [253] X.-F. Zhao, C. Zhang, *Synthesis* **2007**, *2007*, 551–557.
- [254] M. G. Banwell, V. S. Bridges, J. R. Dupuche, S. L. Richards, J. M. Walter, *J. Org. Chem.* **1994**, *59*, 6338–6343.
- [255] Z. Ma, J. M. Bobbitt, *J. Org. Chem.* **1991**, *56*, 6110–6114.

- [256] J. M. Bobbitt, *J. Org. Chem.* **1998**, *63*, 9367–9374.
- [257] J. D. More, N. S. Finney, *Org. Lett.* **2002**, *4*, 3001–3003.
- [258] B. Das, A. S. Kumar, B. R. Kanth, *Synth. Commun.* **2009**, *39*, 3111–3118.
- [259] W. Ren, Y. Xia, S.-J. Ji, Y. Zhang, X. Wan, J. Zhao, *Org. Lett.* **2009**, *11*, 1841–1844.
- [260] A. Furstner, P. W. Davies, *Chem. Commun.* **2005**, 2307–2320.
- [261] A. Fürstner, *Angew. Chem. Int. Ed.* **2013**, *52*, 2794–2819.
- [262] X. Wu, M. Tamm, *Beilstein J. Org. Chem.* **2011**, *7*, 82–93.
- [263] M. Bindl, R. Stade, E. K. Heilmann, A. Picot, R. Goddard, A. Fürstner, *J. Am. Chem. Soc.* **2009**, *131*, 9468–9470.
- [264] J. Heppekausen, R. Stade, R. Goddard, A. Fürstner, *J. Am. Chem. Soc.* **2010**, *132*, 11045–11057.
- [265] P. Persich, J. Llaveria, R. Lhermet, T. de Haro, R. Stade, A. Kondoh, A. Fürstner, *Chem. Eur. J.* **2013**, *19*, 13047–13058.
- [266] S. Schaubach, K. Gebauer, F. Ungeheuer, L. Hoffmeister, M. K. Ilg, C. Wirtz, A. Fürstner, *Chem. Eur. J.* **2016**, *22*, 8494–8507.
- [267] J. Haruta, K. Nishi, S. Matsuda, S. Akai, Y. Tamura, Y. Kita, *J. Org. Chem.* **1990**, *55*, 4853–4859.
- [268] O. Coutelier, G. Nowogrocki, J.-F. Paul, A. Mortreux, *Adv. Synth. Catal.* **2007**, *349*, 2259–2263.
- [269] B. Haberlag, M. Freytag, C. G. Daniliuc, P. G. Jones, M. Tamm, *Angew. Chem. Int. Ed.* **2012**, *51*, 13019–13022.
- [270] R. Lhermet, A. Fürstner, *Chem. Eur. J.* **2014**, *20*, 13188–13193.
- [271] J. Willwacher, A. Fürstner, *Angew. Chem. Int. Ed.* **2014**, *53*, 4217–4221.
- [272] S. Hötling, C. Bittner, M. Tamm, S. Dähn, J. Collatz, J. L. M. Steidle, S. Schulz, *Org. Lett.* **2015**, *17*, 5004–5007.
- [273] M. Lakhrissi, Y. Chapleur, *J. Org. Chem.* **1994**, *59*, 5752–5757.
- [274] K. Lehr, S. Schulthoff, Y. Ueda, R. Mariz, L. Leseurre, B. Gabor, A. Fürstner, *Chem. Eur. J.* **2015**, *21*, 219–227.
- [275] A. Krief, B. Kenda, P. Barbeaux, E. Guittet, *Tetrahedron* **1994**, *50*, 7177–7192.
- [276] B. M. Trost, C. B. Lee, *J. Am. Chem. Soc.* **1998**, *120*, 6818–6819.
- [277] N. Miyaura, T. Ishiyama, M. Ishikawa, A. Suzuki, *Tetrahedron Lett.* **1986**, *27*, 6369–6372.
- [278] T. Shigeyama, K. Katakawa, N. Kogure, M. Kitajima, H. Takayama, *Org. Lett.* **2007**, *9*, 4069–4072.
- [279] N. Miyaura, T. Ishiyama, H. Sasaki, M. Ishikawa, M. Sato, A. Suzuki, *J. Am. Chem. Soc.* **1989**, *111*, 314–321.
- [280] Y. Yamamoto, R. Fujikawa, T. Umemoto, N. Miyaura, *Tetrahedron* **2004**, *60*, 10695–10700.
- [281] M. D. Charles, P. Schultz, S. L. Buchwald, *Org. Lett.* **2005**, *7*, 3965–3968.

- [282] T. E. Barder, S. D. Walker, J. R. Martinelli, S. L. Buchwald, *J. Am. Chem. Soc.* **2005**, *127*, 4685–4696.
- [283] T. Kinzel, Y. Zhang, S. L. Buchwald, *J. Am. Chem. Soc.* **2010**, *132*, 14073–14075.
- [284] K. Speck, R. Wildermuth, T. Magauer, *Angew. Chem. Int. Ed.* **2016**, *55*, 14131–14135.
- [285] H. C. Brown, M. W. Rathke, M. M. Rogic, N. R. De Lue, *Tetrahedron* **1988**, *44*, 2751–2762.
- [286] V. I. Bykov, T. A. Butenko, E. B. Petrova, E. S. Finkelshtein, *Tetrahedron* **1999**, *55*, 8249–8252.
- [287] E. Llàcer, F. Urpí, J. Vilarrasa, *Org. Lett.* **2009**, *11*, 3198–3201.
- [288] H. Tanaka, A. K. M. A. Hai, H. Ogawa, S. Torii, *Synlett* **1993**, *1993*, 835–836.
- [289] P. H. Lee, H. Kim, K. Lee, D. Seomoon, S. Kim, H. Kim, H. Kim, M. Lee, E. Shim, S. Lee, M. Kim, M. Han, K. Noh, M. Sridhar, *Bull. Korean Chem. Soc.* **2004**, *25*, 1687–1691.
- [290] K. Lee, H. Kim, T. Miura, K. Kiyota, H. Kusama, S. Kim, N. Iwasawa, P. H. Lee, *J. Am. Chem. Soc.* **2003**, *125*, 9682–9688.
- [291] A. Mortreux, M. Blanchard, *J. Chem. Soc., Chem. Commun.* **1974**, 786–787.
- [292] L. Kloppenburg, D. Song, U. H. F. Bunz, *J. Am. Chem. Soc.* **1998**, *120*, 7973–7974.
- [293] N. G. Pschirer, U. H. F. Bunz, *Tetrahedron Lett.* **1999**, *40*, 2481–2484.
- [294] G. Brizius, U. H. F. Bunz, *Org. Lett.* **2002**, *4*, 2829–2831.
- [295] R. K. Bly, K. M. Dyke, U. H. F. Bunz, *J. Organomet. Chem.* **2005**, *690*, 825–829.
- [296] K. Grela, J. Ignatowska, *Org. Lett.* **2002**, *4*, 3747–3749.
- [297] V. Sashuk, J. Ignatowska, K. Grela, *J. Org. Chem.* **2004**, *69*, 7748–7751.
- [298] V. Huc, R. Weihofen, I. Martin-Jimenez, P. Oulie, C. Lepetit, G. Lavigne, R. Chauvin, *New J. Chem.* **2003**, *27*, 1412–1414.
- [299] V. Maraval, C. Lepetit, A.-M. Caminade, J.-P. Majoral, R. Chauvin, *Tetrahedron Lett.* **2006**, *47*, 2155–2159.
- [300] A. Bencheick, M. Petit, A. Mortreux, F. Petit, *J. Mol. Catal.* **1982**, *15*, 93–101.
- [301] J. Heppekausen, R. Stade, A. Kondoh, G. Seidel, R. Goddard, A. Fürstner, *Chem. Eur. J.* **2012**, *18*, 10281–10299.
- [302] J. H. Wengrovius, J. Sancho, R. R. Schrock, *J. Am. Chem. Soc.* **1981**, *103*, 3932–3934.
- [303] R. R. Schrock, M. L. Listemann, L. G. Sturgeoff, *J. Am. Chem. Soc.* **1982**, *104*, 4291–4293.
- [304] A. Fürstner, C. Mathes, C. W. Lehmann, *J. Am. Chem. Soc.* **1999**, *121*, 9453–9454.
- [305] A. Fürstner, C. Mathes, C. W. Lehmann, *Chem. Eur. J.* **2001**, *7*, 5299–5317.
- [306] V. Hickmann, A. Kondoh, B. Gabor, M. Alcarazo, A. Fürstner, *J. Am. Chem. Soc.* **2011**, *133*, 13471–13480.
- [307] C. M. Neuhaus, M. Liniger, M. Stieger, K.-H. Altmann, *Angew. Chem. Int. Ed.* **2013**, *52*, 5866–5870.
- [308] M. Fuchs, A. Fürstner, *Angew. Chem. Int. Ed.* **2015**, *54*, 3978–3982.
- [309] S. M. Rummelt, J. Preindl, H. Sommer, A. Fürstner, *Angew. Chem. Int. Ed.* **2015**, *54*, 6241–6245.

- [310] A. Ahlers, T. de Haro, B. Gabor, A. Fürstner, *Angew. Chem. Int. Ed.* **2016**, *55*, 1406–1411.
- [311] L.-D. Guo, X.-Z. Huang, S.-P. Luo, W.-S. Cao, Y.-P. Ruan, J.-L. Ye, P.-Q. Huang, *Angew. Chem. Int. Ed.* **2016**, *55*, 4064–4068.
- [312] E. F. De Medeiros, J. M. Herbert, R. J. K. Taylor, *Tetrahedron Lett.* **1990**, *31*, 5843–5844.
- [313] C. F. Thompson, T. F. Jamison, E. N. Jacobsen, *J. Am. Chem. Soc.* **2000**, *122*, 10482–10483.
- [314] J. Chan, T. F. Jamison, *J. Am. Chem. Soc.* **2004**, *126*, 10682–10691.
- [315] F. W. W. Hartrampf, T. Furukawa, D. Trauner, *Angew. Chem. Int. Ed.* **2017**, *56*, 893–896.
- [316] R. A. Bradshaw, E. A. Dennis, *Handbook of Cell Signaling*, 2nd ed., Elsevier Science, **2009**.
- [317] M. A. Clark, R. A. Harvey, R. Finkel, J. A. Rey, K. Whalen, *Pharmacology*, Wolters Kluwer Health, **2011**.
- [318] W. A. Velema, W. Szymanski, B. L. Feringa, *J. Am. Chem. Soc.* **2014**, *136*, 2178–2191.
- [319] J. Broichhagen, J. A. Frank, D. Trauner, *Acc. Chem. Res.* **2015**, *48*, 1947–1960.
- [320] M. M. Lerch, M. J. Hansen, G. M. van Dam, W. Szymanski, B. L. Feringa, *Angew. Chem. Int. Ed.* **2016**, *55*, 10978–10999.
- [321] P. Gorostiza, E. Y. Isacoff, *Science* **2008**, *322*, 395–399.
- [322] W. Szymański, J. M. Beierle, H. A. V. Kistemaker, W. A. Velema, B. L. Feringa, *Chem. Rev.* **2013**, *113*, 6114–6178.
- [323] R. Weissleder, V. Ntziachristos, *Nat. Med.* **2003**, *9*, 123–128.
- [324] F. Zhang, M. Prigge, F. Beyriere, S. P. Tsunoda, J. Mattis, O. Yizhar, P. Hegemann, K. Deisseroth, *Nat. Neurosci.* **2008**, *11*, 631–633.
- [325] Y. Takeda, S. Okumura, S. Minakata, *Angew. Chem. Int. Ed.* **2012**, *51*, 7804–7808.
- [326] J. Y. Lin, P. M. Knutsen, A. Muller, D. Kleinfeld, R. Y. Tsien, *Nat. Neurosci.* **2013**, *16*, 1499–1508.
- [327] S. Samanta, A. A. Beharry, O. Sadoyski, T. M. McCormick, A. Babalhavaeji, V. Tropepe, G. A. Woolley, *J. Am. Chem. Soc.* **2013**, *135*, 9777–9784.
- [328] S. Okumura, C.-H. Lin, Y. Takeda, S. Minakata, *J. Org. Chem.* **2013**, *78*, 12090–12105.
- [329] A. Rullo, A. Reiner, A. Reiter, D. Trauner, E. Y. Isacoff, G. A. Woolley, *Chem. Commun.* **2014**, *50*, 14613–14615.
- [330] H. K. Inagaki, Y. Jung, E. D. Hoopfer, A. M. Wong, N. Mishra, J. Y. Lin, R. Y. Tsien, D. J. Anderson, *Nat. Meth.* **2014**, *11*, 325–332.
- [331] M. Dong, A. Babalhavaeji, S. Samanta, A. A. Beharry, G. A. Woolley, *Acc. Chem. Res.* **2015**, *48*, 2662–2670.
- [332] J. Broichhagen, J. A. Frank, N. R. Johnston, R. K. Mitchell, K. Smid, P. Marchetti, M. Bugliani, G. A. Rutter, D. Trauner, D. J. Hodson, *Chem. Commun.* **2015**, *51*, 6018–6021.
- [333] M. J. Hansen, M. M. Lerch, W. Szymanski, B. L. Feringa, *Angew. Chem. Int. Ed.* **2016**, *55*, 13514–13518.
- [334] D. B. Konrad, J. A. Frank, D. Trauner, *Chem. Eur. J.* **2016**, *22*, 4364–4368.
- [335] G. C. R. Ellis-Davies, *Nat. Meth.* **2007**, *4*, 619–628.

- [336] L. M. Palmer, A. S. Shai, J. E. Reeve, H. L. Anderson, O. Paulsen, M. E. Larkum, *Nat. Neurosci.* **2014**, *17*, 383–390.
- [337] G. C. R. Ellis-Davies, M. Matsuzaki, M. Paukert, H. Kasai, D. E. Bergles, *J. Neurosci.* **2007**, *27*, 6601–6604.
- [338] T. Fehrentz, M. Schönberger, D. Trauner, *Angew. Chem. Int. Ed.* **2011**, *50*, 12156–12182.
- [339] M. Schoenberger, A. Damijonaitis, Z. Zhang, D. Nagel, D. Trauner, *ACS Chem. Neurosci.* **2014**, *5*, 514–518.
- [340] M. Decker, *Design of Hybrid Molecules for Drug Development*, Elsevier Science, **2017**.
- [341] D. M. Barber, M. Schonberger, J. Burgstaller, J. Levitz, C. D. Weaver, E. Y. Isacoff, H. Baier, D. Trauner, *Chem. Sci.* **2016**, *7*, 2347–2352.
- [342] M. Volgraf, P. Gorostiza, R. Numano, R. H. Kramer, E. Y. Isacoff, D. Trauner, *Nat. Chem. Biol.* **2006**, *2*, 47–52.
- [343] J. Levitz, C. Pantoja, B. Gaub, H. Janovjak, A. Reiner, A. Hoagland, D. Schoppik, B. Kane, P. Stawski, A. F. Schier, D. Trauner, E. Y. Isacoff, *Nat. Neurosci.* **2013**, *16*, 507–516.
- [344] B.-Q. Shen, K. Xu, L. Liu, H. Raab, S. Bhakta, M. Kenrick, K. L. Parsons-Reponte, J. Tien, S.-F. Yu, E. Mai, D. Li, J. Tibbitts, J. Baudys, O. M. Saad, S. J. Scales, P. J. McDonald, P. E. Hass, C. Eigenbrot, T. Nguyen, W. A. Solis, R. N. Fuji, K. M. Flagella, D. Patel, S. D. Spencer, L. A. Khawli, A. Ebens, W. L. Wong, R. Vandlen, S. Kaur, M. X. Sliwowski, R. H. Scheller, P. Polakis, J. R. Junutula, *Nat. Biotechnol.* **2012**, *30*, 184–189.
- [345] J. Kalia, R. T. Raines, *Bioorg. Med. Chem. Lett.* **2007**, *17*, 6286–6289.
- [346] J. Broichhagen, A. Damijonaitis, J. Levitz, K. R. Sokol, P. Leippe, D. Konrad, E. Y. Isacoff, D. Trauner, *ACS Cent. Sci.* **2015**, *1*, 383–393.
- [347] D. L. Fortin, M. R. Banghart, T. W. Dunn, K. Borges, D. A. Wagenaar, Q. Gaudry, M. H. Karakossian, T. S. Otis, W. B. Kristan, D. Trauner, R. H. Kramer, *Nat. Meth.* **2008**, *5*, 331–338.
- [348] N. Caporale, K. D. Kolstad, T. Lee, I. Tochitsky, D. Dalkara, D. Trauner, R. Kramer, Y. Dan, E. Y. Isacoff, J. G. Flannery, *Mol. Ther.* **2011**, *19*, 1212–1219.
- [349] A. Polosukhina, J. Litt, I. Tochitsky, J. Nemargut, Y. Sychev, I. De Kouchkovsky, T. Huang, K. Borges, D. Trauner, Russell N. Van Gelder, Richard H. Kramer, *Neuron* **2012**, *75*, 271–282.
- [350] I. Tochitsky, A. Polosukhina, Vadim E. Degtyar, N. Gallerani, Caleb M. Smith, A. Friedman, Russell N. Van Gelder, D. Trauner, D. Kaufer, Richard H. Kramer, *Neuron* **2014**, *81*, 800–813.
- [351] Y. Zhang, F. Erdmann, G. Fischer, *Nat. Chem. Biol.* **2009**, *5*, 724–726.
- [352] W. A. Velema, J. P. van der Berg, M. J. Hansen, W. Szymanski, A. J. M. Driessen, B. L. Feringa, *Nat. Chem.* **2013**, *5*, 924–928.
- [353] D. Lemoine, C. Habermacher, A. Martz, P.-F. Méry, N. Bouquier, F. Diverchy, A. Taly, F. Rassendren, A. Specht, T. Grutter, *Proc. Natl. Acad. Sci. U. S. A.* **2013**, *110*, 20813–20818.

- [354] A. A. Beharry, G. A. Woolley, *Chem. Soc. Rev.* **2011**, *40*, 4422–4437.
- [355] R. W. Gereau, G. Swanson, *The Glutamate Receptors*, Humana Press, New York, **2008**.
- [356] B. L. Chenard, J. Bordner, T. W. Butler, L. K. Chambers, M. A. Collins, D. L. De Costa, M. F. Ducat, M. L. Dumont, C. B. Fox, *J. Med. Chem.* **1995**, *38*, 3138–3145.
- [357] S. F. Traynelis, L. P. Wollmuth, C. J. McBain, F. S. Menniti, K. M. Vance, K. K. Ogden, K. B. Hansen, H. Yuan, S. J. Myers, R. Dingledine, *Pharmacol. Rev.* **2010**, *62*, 405–496.
- [358] P. Stawski, H. Janovjak, D. Trauner, *Bioorg. Med. Chem.* **2010**, *18*, 7759–7772.
- [359] E. Karakas, H. Furukawa, *Science* **2014**, *344*, 992–997.
- [360] D. M. Bannerman, R. Sprengel, D. J. Sanderson, S. B. McHugh, J. N. P. Rawlins, H. Monyer, P. H. Seeburg, *Nat. Rev. Neurosci.* **2014**, *15*, 181–192.
- [361] X.-x. Dong, Y. Wang, Z.-h. Qin, *Acta Pharmacol. Sin.* **2009**, *30*, 379–387.
- [362] A. Faden, P. Demediuk, S. Panter, R. Vink, *Science* **1989**, *244*, 798–800.
- [363] J. A. Kemp, R. M. McKernan, *Nat. Neurosci.* **2002**, *5*, 1039–1042.
- [364] A. Biegon, P. A. Fry, C. M. Paden, A. Alexandrovich, J. Tsenter, E. Shohami, *Proc. Natl. Acad. Sci. U. S. A.* **2004**, *101*, 5117–5122.
- [365] P. Paoletti, C. Bellone, Q. Zhou, *Nat. Rev. Neurosci.* **2013**, *14*, 383–400.
- [366] B. a. Desvergne, W. Wahli, *Endocrine Reviews* **1999**, *20*, 649–688.
- [367] L. Michalik, J. Auwerx, J. P. Berger, V. K. Chatterjee, C. K. Glass, F. J. Gonzalez, P. A. Grimaldi, T. Kadowaki, M. A. Lazar, S. Rahilly, C. N. A. Palmer, J. Plutzky, J. K. Reddy, B. M. Spiegelman, B. Staels, W. Wahli, *Pharmacol. Rev.* **2006**, *58*, 726.
- [368] S. A. Kliewer, K. Umesono, D. J. Noonan, R. A. Heyman, R. M. Evans, *Nature* **1992**, *358*, 771–774.
- [369] I. Issemann, S. Green, *Nature* **1990**, *347*, 645–650.
- [370] P. Tontonoz, E. Hu, B. M. Spiegelman, *Cell* **1994**, *79*, 1147–1156.
- [371] E. D. Rosen, P. Sarraf, A. E. Troy, G. Bradwin, K. Moore, D. S. Milstone, B. M. Spiegelman, R. M. Mortensen, *Mol. Cell* **1999**, *4*, 611–617.
- [372] J. R. Jones, C. Barrick, K.-A. Kim, J. Lindner, B. Blondeau, Y. Fujimoto, M. Shiota, R. A. Kesterson, B. B. Kahn, M. A. Magnuson, *Proc. Natl. Acad. Sci. U. S. A.* **2005**, *102*, 6207–6212.
- [373] J. M. Lehmann, L. B. Moore, T. A. Smith-Oliver, W. O. Wilkison, T. M. Willson, S. A. Kliewer, *J. Biol. Chem.* **1995**, *270*, 12953–12956.
- [374] C. Pirat, A. Farce, N. Lebègue, N. Renault, C. Furman, R. Millet, S. d. Yous, S. Speca, P. Berthelot, P. Desreumaux, P. Chavatte, *J. Med. Chem.* **2012**, *55*, 4027–4061.
- [375] P. Shah, S. Mudaliar, *Expert Opinion on Drug Safety* **2010**, *9*, 347–354.
- [376] M. Ferwana, B. Firwana, R. Hasan, M. H. Al-Mallah, S. Kim, V. M. Montori, M. H. Murad, *Diabetic Medicine* **2013**, *30*, 1026–1032.
- [377] R. T. Nolte, G. B. Wisely, S. Westin, J. E. Cobb, M. H. Lambert, R. Kurokawa, M. G. Rosenfeld, T. M. Willson, C. K. Glass, M. V. Milburn, *Nature* **1998**, *395*, 137–143.

- [378] N. Zidar, T. Tomašić, R. Šink, V. Rupnik, A. Kovač, S. Turk, D. Patin, D. Blanot, C. Contreras Martel, A. Dessen, M. Müller Premru, A. Zega, S. Gobec, L. Peterlin Mašič, D. Kikelj, *J. Med. Chem.* **2010**, *53*, 6584–6594.
- [379] G. C. Mueller, J. A. Miller, *J. Biol. Chem.* **1949**, *180*, 1125–1136.
- [380] S. Garcia-Vallvé, L. Guasch, S. Tomas-Hernández, J. M. del Bas, V. Ollendorff, L. Arola, G. Pujadas, M. Mulero, *J. Med. Chem.* **2015**, *58*, 5381–5394.
- [381] M. Ahmadian, J. M. Suh, N. Hah, C. Liddle, A. R. Atkins, M. Downes, R. M. Evans, *Nat. Med.* **2013**, *99*, 557–566.
- [382] G. Derosa, A. E. Cicero, G. Bertone, M. N. Piccinni, L. Ciccarelli, D. E. Roggeri, *Clin. Ther.* **2004**, *26*, 1599–1607.
- [383] J. Wysocki, D. Belowski, M. Kalina, L. Kochanski, B. Okopien, Z. Kalina, *Int. J. Clin. Pharmacol. Ther.* **2004**, *42*, 212–217.
- [384] G. Steiner, *Diab. Vasc. Dis. Res.* **2007**, *4*, 368–374.
- [385] M. Jun, C. Foote, J. Lv, B. Neal, A. Patel, S. J. Nicholls, D. E. Grobbee, A. Cass, J. Chalmers, V. Perkovic, *The Lancet* **2010**, *375*, 1875–1884.
- [386] J. M. Thorp, W. S. Waring, *Nature* **1962**, *194*, 948–949.
- [387] D. Haigh, G. Allen, H. C. Birrell, D. R. Buckle, B. C. C. Cantello, D. S. Eggleston, R. C. Haltiwanger, J. C. Holder, C. A. Lister, I. L. Pinto, H. K. Rami, J. T. Sime, S. A. Smith, J. D. Sweeney, *Bioorg. Med. Chem.* **1999**, *7*, 821–830.
- [388] B. Hulin, L. S. Newton, D. M. Lewis, P. E. Genereux, E. M. Gibbs, D. A. Clark, *J. Med. Chem.* **1996**, *39*, 3897–3907.
- [389] C.-H. Lin, Y.-H. Peng, M. S. Coumar, S. K. Chittimalla, C.-C. Liao, P.-C. Lyn, C.-C. Huang, T.-W. Lien, W.-H. Lin, J. T. A. Hsu, J.-H. Cheng, X. Chen, J.-S. Wu, Y.-S. Chao, H.-J. Lee, C.-G. Juo, S.-Y. Wu, H.-P. Hsieh, *J. Med. Chem.* **2009**, *52*, 2618–2622.
- [390] D. J. Parks, N. C. O. Tomkinson, M. S. Villeneuve, S. G. Blanchard, T. M. Willson, *Bioorg. Med. Chem. Lett.* **1998**, *8*, 3657–3658.